Nouvelles preuves de concept pour la chélatothérapie contre la maladie d'Alzheimer : études spectroscopiques des interactions entre les ions cuivre et zinc

Amandine Conte-Daban

Université de Toulouse

THÈSE

En vue de l'obtention du

DOCTORAT DE L'UNIVERSITÉ DE TOULOUSE

Délivré par :

Université Toulouse 3 Paul Sabatier (UT3 Paul Sabatier)

Présentée et soutenue par :
Amandine Conte-Daban
Le vendredi 1er décembre 2017
Titre :

New proofs of concept for chelatotherapy in Alzheimer's disease:
Spectroscopic investigations of the interplay between copper and zinc ions.

ED SDM : Chimie, Biologie, Santé - CO 042

Unité de recherche :

Laboratoire de Chimie de Coordination

Directeur(s) de Thèse :

Dr. Christelle Hureau
Dr. Peter Faller

Rapporteurs :

Dr. Catherine Belle, CIRE, Grenoble
Dr. Yves Le Mest, CEMCA, Brest

Autre(s) membre(s) du jury :

Dr. Eric Benoist, SPCMIB, Toulouse
Dr. Katell Sénéchal-David, ICMMO, Orsay
Dr. Stéphane Torelli, BIG, Grenoble,
Dr. Christelle Hureau, LCC, Toulouse, et Dr. Peter Faller, BCB, Strasbourg

Remerciements

Cette thèse a été pour moi une période très enrichissante tant scientifiquement que humainement. Je souhaite remercier toutes les personnes qui y ont contribué de près ou de loin, et qui ont permis de rendre ces trois années aussi riches que ce qu'elles ont été.

Je souhaite tout d'abord remercier le Dr. Azzedine Bousseksou de m'avoir accueillie au sein de son établissement.

Je remercie également tous les membres de mon jury pour avoir évalué mon travail : Dr. Catherine Belle et Dr. Yves Le Mest, merci d'avoir accepté d'être rapporteurs de ma thèse, Dr. Eric Benoist, Dr. Katell Sénéchal-David, et Dr. Stéphane Torelli, merci d'avoir accepté d'être examinateurs de ma thèse.

Je souhaite maintenant remercier la personne sans qui tout cela n'aurait pas été possible : Christelle. Merci pour ta confiance, merci pour ta patience, merci d'avoir cru en moi !!! Tu m'as transmis tellement de choses… Tu es un puits de connaissances et d'idées inépuisable ! Tu m'as permis de faire ce que j'avais envie, de tester, d'expérimenter, etc. même si parfois j'aurais pu m'abstenir… Tu m'as également laissé faire des enseignements, tu m'as fait découvrir le monde des congrès, j'ai pu avoir des stagiaires, j'ai pu aller en Argentine en collaboration, etc. (la liste est tellement longue que je vais m'arrêter là !) Je ne te remercierai jamais assez pour tout ça ! Cette thèse a été pour moi un super moment de ma vie (j'espère que pour toi, ça n'a pas été un trop long calvaire ;)) Il ne me reste plus qu'une chose à espérer…que tu tiennes ta promesse le 1er décembre…

Peter, un grand merci à toi d'être venu me proposer de joindre ton équipe. Mais surtout, je te remercie pour toutes ces discussions enrichissantes, ces conseils toujours très avisés, ta bonne humeur quotidienne, ton savoir, … A nouveau, la langue française n'est pas suffisamment riche pour te remercier de tout ce que je voudrais… Alors tout simplement, merci pour tout !

Je tiens également à remercier tous les collaborateurs qui m'ont gentiment donné leur ligand ! Pascale Delangle, Raphaël Tripier, Laurent Lisnard, Clotilde Policar, Claude Gros et Olga Iranzo, un grand merci, car sans vous, je serais encore (après ces 3 ans de thèse) au stade de la synthèse du premier ligand !! Merci aussi à Sabrina Noël pour avoir synthétiser suffisamment de L2 pour qu'il en reste pour moi !!!

Un grand merci à toutes les personnes des services scientifiques, sans qui, les manips auraient été plus que difficiles …
Tout d'abord, un immense merci à Lionel Rechignat pour m'avoir TRES patiemment expliqué la RPE, malgré mes milliards de questions tordues… pour avoir passé mes interminables séries de tubes et aussi pour avoir toujours été derrière moi, même une fois que j'ai presque pris mon indépendance en RPE !
Isabelle Kieffer, Olivier Proux et Denis Testemale, les sessions à l'ESRF sur FAME ont toujours été des moments plus qu'attendus ! Vous m'avez expliqué tellement de concepts scientifiques (mais pas que !!), vous avez toujours pris le temps pour moi, pour que je comprenne, pour nous faire visiter les lignes, pour nous montrer aussi la construction de la nouvelle ligne… sans parler des sessions bonbons, des sessions musiques pourries et quizz musical, des appels téléphoniques très étranges, etc… Merci pour tout à vous trois, et j'espère revenir sur FAME !! ☺
Merci à Emmanuel Guillon et Stéphanie Sayen pour les moments passés à l'ESRF, les explications sur le XAS et la « ballade course » pour aller voir le synchrotron d'en haut !

Merci aussi à Vanessa Soldan pour ton aide précieuse en TEM.
Merci également à Christian Bijani pour ton aide en RMN.
Enfin, je tiens à remercier chaleureusement le service informatique du LCC, Jérôme et Fabrice, pour avoir toujours su me sortir des « boulettes » et autres problèmes informatiques (la plupart du temps occasionnés par moi-même !!), ainsi que le service administratif, Béatrice et Florence, pour votre aide si précieuse et votre gentillesse.

Je souhaite maintenant remercier toutes les personnes de l'équipe F. Manu, merci à toi pour ta bonne humeur, et la bonne ambiance que tu mets au sein de cette équipe !! Ça a été un réel plaisir de te connaitre. Fabrice, merci pour ta joie de vivre, pour les moments (comment les appeler ???) « délires » ou « pétage de plomb » à l'ESRF. On y a vraiment passé de supers séjours !!! James Bond, kidnapper de Petit Poney demandant une rançon restera quand même dans mes souvenirs !!! ☺ Béa, merci à toi pour tes conseils, ta gentillesse et tes bonnes adresses ! Viviane, je te remercie pour ton oreille toujours attentive, ta douceur et ta gentillesse. Je te remercie également pour tout le temps que tu m'as consacré : les heures incalculables à synthétiser mes ligands pourris, mais aussi et surtout le fameux mois où j'ai essayé d'être une chimiste organicienne !!! Même avec toute ta bonne volonté, et ton enthousiasme, je n'arriverai pas à faire de la « vraie chimie » Viviane, et je pense que c'est plus sécuritaire pour tout le monde !! ;) Merci aussi à toi Laurent, pour avoir remis en bon fonctionnement tout le labo !!! Ton aide a été très précieuse et m'a fait gagner un temps fou !! Merci aussi pour les découvertes de films « cultes » à l'ESRF, et je n'oublierai pas que tu « adores le pognon » !!! Je souhaite maintenant remercier tous les étudiants/post docs de l'équipe, en commençant par Adam. Tu m'as très gentiment et rapidement intégrée au sein de l'équipe et je t'en remercie. Ta maladresse légendaire restera gravée dans ma mémoire !! Marie, merci à toi d'avoir toujours su m'écouter et me conseiller. Clémence, Valentina et Elena, trop de choses à dire alors voir ci-dessous !! Omar, merci pour ta patience avec mon anglais (oui oui, Jacques Chirac restera ton meilleur ami, j'ai tout compris !!) et surtout merci pour tous ces bons moments passés ensemble, sans oublier tes « supers » conseils (les bombes par exemple !! ;)). Alex, merci à toi pour toutes ces conversations de pause-café plus tordues les unes que les autres, mais tellement drôles !! Sara, merci pour ta gentillesse et tes conseils et explications sur la biologie !! Olena, merci également à toi pour ta présence, pour nos échanges culturels, pour toutes ces découvertes culinaires, … Merci aussi à Sylvain et Valerii (pas de l'équipe F, mais on vous accepte quand même !!). Merci également à Olivia, Daniel, Melisa, Mireia, Carine, Inga et Simon, et toutes les personnes qui sont venues participer au bon fonctionnement et à la bonne ambiance de cette équipe !! Je tiens aussi à remercier « mes » 3 stagiaires qui m'ont fait confiance (oui vous n'aviez pas le choix, mais quand même !!) : Claudia, Tiriana et Agnès, ça a été un réel plaisir de travailler avec vous, et je ne vous oublierai pas. Merci du fond du cœur à toute l'équipe F, les week ends d'équipe, les Noël, etc., J'ai passé presque 4 superbes années avec vous !

Je voudrais maintenant remercier toute l'équipe pédagogique et notamment Jean-Luc et Barbora, pour m'avoir permis d'être presque une prof pendant 2 ans !! J'ai beaucoup appris, et c'est une super expérience que vous m'avez fait vivre. Merci pour votre confiance.

Ahora, quisiera agradecer a las personas de Argentina. Sandra, gracias por tu acogida tan cálida en tu equipo. Gracias también por tu gentileza y tus explicaciones sobre todo!! Claudia, fuiste quasi como una mama argentina para mí. Me hiciste descubrir muchas cosas científicas, pero también cosas argentinas y humanas. Siempre eres muy linda conmigo, y te lo agradezco. Espero que podamos vernos pronto, en Rosario, o aquí, en Francia. Nunca te olvidare… Gracias también a todo el equipo que fue muy lindo conmigo. Un gracias especial para mis amigos colombianos de Argentina!! Angel, mi compañera de habitación, tantas cosas por decir pero no hay bastante palabras… Nos veremos

pronto, y espero que podrás leer más que la primera página de este libro !!! Gracias por todo… Felipe, Pilar, Juan, Angelito, fueron tan cariñosos conmigo… Esas tres semanas quedaran por siempre en mi corazón !! Les extraño un montón…

Le club jeune de la SCF en Midi-Pyrénées a été aussi un bel investissement au cours de ma thèse. J'ai fait de belles rencontres, appris beaucoup… Merci particulièrement à toi Claudia, à toi Morgane et à toi Jérémy !! J'ai beaucoup aimé travailler avec vous !! Lydie, je te remercie également pour tout ce que tu as fait pour le club de jeunes, mais surtout pour moi !! J'espère que nos routes se recroiseront à Chimie et Terroir ou ailleurs !

Maintenant, je veux remercier mes amis, toujours présents pour moi, en toutes circonstances ! Lilia et Muriel, un immense merci à toutes les deux. Vous m'avez toujours motivée, toujours écoutée dans les bons mais aussi les moins bons moments… Toujours présentes, bien qu'à l'autre bout de la France (voire du monde par moments), cette thèse n'aurait jamais pu aussi bien se passer sans vous… Merci du fond du cœur pour tout les filles !! Bien sûr, Antoine, Louis (alias Titou et Loulou) merci à vous aussi pour tous ces bons moments passés ensemble !!! Vivement les prochains.

Clémence, à mon tour de te remercier… Et comme tu me l'as si bien dit, les mots sont ternes à côté de ce que mon cœur voudrait dire… (et oui, même avec tous mes mots du sud-ouest, je n'y arrive pas !!!) On a formé une chouette équipe… à reformer en collaboration à l'ESRF ou ailleurs !! ;) Grace à toi, ma thèse a été une super expérience !! Beaucoup de travail, mais aussi beaucoup de rigolades, de moments inoubliables (hein ma Clem Blonde !!), etc. etc. Tu as toujours été de bons conseils, toujours de bonne humeur, toujours là, tout simplement…Bref, un immense merci du fond du cœur pour tout !!

Valentina, ma coinquilina, grazie mille !! Je suis réellement heureuse que nos chemins se soient croisés (j'en deviendrai presque poète !!). Tellement de bons moments passés ensemble (et comme tu dis : la vie quoi !!)… et nos to do lists interminables de choses à faire après la journée… ☺ nos sessions ralages vont aussi me manquer je crois… Et oui, bien que tu ne sois pas d'accord avec ça, tu es devenue une vraie française !!! Un gros bisou à la française pour te remercier !! Et surtout, prends soin d'Ounette et de mon bureau !! ;)

Elena, muchas gracias por todo !! Toujours de bonne humeur, toujours à voir le bon côté des choses … Tu es l'oreille attentive de l'équipe et je ne t'en remercierai jamais assez… Tu m'as également apporté une grande aide, merci beaucoup !!! J'ai passé un super moment au LCC (et à Toulouse ou ailleurs!!), et c'est en partie grâce à toi ! Merci d'être toi, et d'être toujours là pour moi…

Julie, à mon tour d'évoquer les fameux zumbapéros… C'est quand même une superbe invention !!! Sans oublier les parties de Just Dance ! On aura bien rigolé ! Toi aussi, tu as toujours été présente pour moi. Merci pour tout et à très vite j'espère…

Emilie ma tikou, et Eloise, merci les filles de m'avoir accompagnée tout au long de ces trois/quatre années (et de ma vie, mais ce n'est pas le sujet !!! ;)) Vivement de vous revoir !!

Maintenant, je souhaite remercier mes parents chéris, sans qui, rien n'aurait pu être possible. Vous m'avez toujours poussée pour que je réalise mes rêves, pour que je donne le meilleur… Vous êtes des parents en or, toujours là pour moi. Et j'espère qu'avec tout ce que j'ai pu vous saouler, le peptide amyloide β n'a plus de secret pour vous !!! Un immense merci pour tout… Je vous aime…

Ahhhhh Emilie et Eva, mes frangines d'amour !! Si quand on était petites, on nous avait dit qu'on serait incapables de vivre les unes sans les autres, on aurait bien ri !!! Mais qu'est-ce qu'on aurait rrrrri ! Et pourtant… Je ne serai jamais arrivée à faire tout ça sans vous ! Vous m'êtes

indispensables !! Merci d'être toujours là, pour tout et pour rien, sérieusement ou en déconnant, mais toujours là !!! Rémi et Adrien, mes beaux-frères préférés, je ne vous oublie pas non plus ! Qu'est-ce qu'ils font du bien ces moments passés tous ensemble ! Vivement les prochains… Merci à vous quatre du fond du cœur… Je vous zaimeuhh…

Je ne vous oublie pas non plus, Papi Max, Mamie Solange et Mamie Jeannette ! Toujours là, toujours le sourire, toujours une oreille attentive pour une session papotage. C'est si bon d'être aussi bien entourée ! Merci également à papi Maurice et Dany et merci aussi pour les supers vacances détente à Marseillan qui m'ont permis de me ressourcer !

Un grand merci également à Dédé, Annie et Denis pour les bons moments passés ensemble !

Et comme on dit, le meilleur pour la fin…Laurent ! Tout d'abord, je voudrais saluer ton courage et ta patience sans limite (enfin, presque !! ;)), parce que oui, je me rends bien compte que je n'ai pas toujours été facile avec toi… Tu as toujours su me rassurer, me réconforter, me changer les idées quand ce n'était pas très facile. Et bonus, tu connais toutes mes présentations par cœur (hihihi merci public !!). Tu es ma source d'inspiration au quotidien, la force qui me fait avancer. Sans toi, tout tournerait à l'envers, rien ne serait possible. Merci de faire de moi celle que je suis. Tout simplement, merci… Je t'aime tellement mon cœur !

List of abbreviations

7-OH-CCA: 7-hydroxycoumarin carboxylic acid

ACh: acethylcholine
AChE: acetylcholine esterase
AFM: atomic force microscopy
APP: amyloid precursor protein
Asc: ascorbate
Asp: aspartate
Aβ: Amyloid-β

B: β-alanine
BBB: blood brain barrier
BHE : barrière hémato-encéphalique

CCA: coumarin carboxylic acid
CQ: clioquinol
CSF: cerebrospinal fluid

Fz: ferrozine

EPR: electronic paramagnetic resonance
Equiv.: equivalent
EXAFS: extended X-ray absorption fine structure

Glu: glutamic acid

HEPES: 4-(2-hydroxyethyl)-1-piperazineethanesulfonic acid
His: histidine
H6A: mutation of the amino acid H, in the position 6, to the amino acid A

M: molar
MPAC: metal protein attenuating compound

NMDA: *N*-methyl-D-aspartate
NMR: nuclear magnetic resonance

PiB: Pittsburgh compound B
PET: positron emission tomography

ROS: reactive oxygen species
RPE : résonance paramagnétique électronique

SOD: superoxide dismutase

TEM: transmission electron microscopy
ThT: Thioflavin T

XANES: X-ray absorption near edge structure
XAS: X-ray absorption spectroscopy

Table of contents

Résumé en français

I- Contexte général

I-A. La maladie d'Alzheimer

La maladie d'Alzheimer (MA) est une maladie neurodégénérative découverte en 1906 par Alois Alzheimer. Elle touche plus de 35 millions de personnes à travers le monde et est la première forme de démence. Les symptômes de la MA sont relativement bien connus par le public : perte de mémoire pouvant devenir très importants, perte de la notion d'espace et de temps, parfois agressivité, etc. Cette maladie difficile pour le patient l'est également pour son entourage. Malheureusement, il n'existe à ce jour aucun traitement curatif. Seuls des traitements symptomatiques sont disponibles, visant à améliorer la vie des patients et à ralentir la progression de la maladie.

La MA est caractérisée notamment par la présence d'enchevêtrements neurofibrillaires intra-neuronaux de protéine Tau hyperphosphorylée (Figure I-1). La protéine Tau, nécessaire à l'assemblage et à la stabilisation des microtubules, est hyperphosphorylée dans le cas de la MA. Elle s'agrège et s'accumule en enchevêtrements neurofibrillaires. Elle n'est donc plus apte à remplir son rôle, entraînant la mort des neurones. Un autre marqueur important est la présence de plaques séniles ou plaques amyloïdes dans le cerveau (Figure I-1). Ces plaques se situent dans les fentes synaptiques, notamment dans l'hippocampe et le cortex, empêchant les connexions neuronales. Ma thèse s'intéresse aux peptides Aβ, principaux composants de ces plaques séniles ; il n'y a pas d'études concernant la protéine Tau.

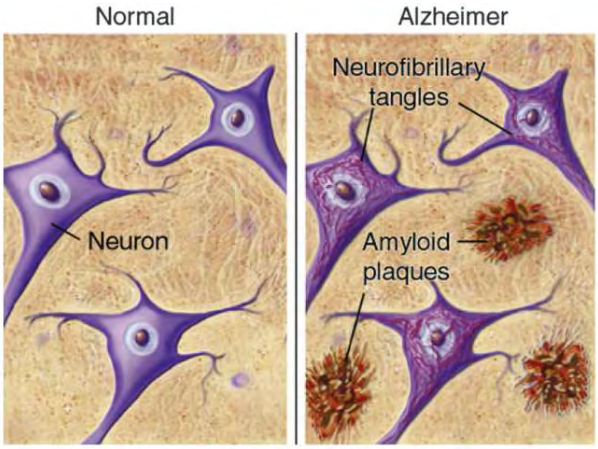

Figure I-1. Schéma représentant les deux évènements importants de la MA : les enchevêtrements neurofibrillaires ainsi que les plaques séniles.

I-B. Le peptide Aβ et les ions métalliques

Les plaques séniles sont majoritairement constituées de peptide Amyloïde-β (Aβ). Le peptide Aβ provient du double clivage de la protéine précurseur de l'amyloïde (APP pour Amyloid Precursor Protein) par deux enzymes, la β et la γ-sécrétase et est excrété extra-cellulairement. Aβ est un peptide d'une quarantaine d'acides aminés. Les seize premiers forment la partie hydrophile du peptide, capable de coordiner des ions métalliques. La partie C-terminale du peptide est hydrophobe et impliquée dans l'agrégation du peptide en plaques séniles. Des ions métalliques tels que les ions Cu et les ions Zn sont également présents dans ces plaques. Il y aurait 1 mM d'ions Zn et 400 µM d'ions Cu dans les plaques. Une dyshoméostasie en ions métalliques tels que les ions Cu et les ions Zn est aussi reportée dans les cerveaux atteints de la MA, les ions Cu étant déficients intra-cellulairement et en excès extra-cellulairement. Concernant les ions Zn, la tendance n'est pas claire : des concentrations supérieures mais aussi inférieures à celles dans les cerveaux sains sont détectées. Il est donc biologiquement pertinent d'étudier les interactions entre le peptide Aβ et ces ions métalliques.

I-A.i Coordination et constantes d'affinité

La coordination de ces ions métalliques avec le peptide Aβ monomérique a été très étudiée, ainsi que les constantes d'affinité associées. Les résultats présentés ici ont été effectués avec le peptide Aβ16, i.e. le peptide modèle de la séquence impliquée dans la coordination, et ce pour des raisons de solubilités restreintes du peptide entier. Concernant le Cu(II), différentes techniques spectroscopiques ont été utilisées. La coordination du Cu(II) au peptide dépend du pH. Les modes de coordination des composés 1 et 2 présentés en Figure I-2 sont ceux autour de pH 7,4 ; avec un pK_a entre les deux composés à 7.7. Le composé I coordine le Cu(II) dans une géométrie plan carré : l'amine terminale, l'atome O de la liaison peptidique entre l'Asp1 et l'Ala2, l'His6 et une autre His (His13 ou His14 en équilibre). Un carboxylate venant de l'Asp1, du Glu3, de l'Asp7 ou encore du Glu11 vient compléter la sphère de coordination en position apicale. Le composé 1 est en équilibre avec le composé 2 à pH 7.4. Le composé 2 a également une géométrie plan carré autour du Cu(II). L'amine terminale est toujours impliquée dans la coordination. Ensuite, l'atome N de la liaison peptidique entre l'Asp1 et l'Ala2, l'atome O de la liaison peptidique entre l'Ala2 et le Glu3 ainsi qu'une des trois His coordine Cu(II). Il y a également un équilibre dynamique entre les trois His. Un carboxylate provenant des mêmes chaines latérales que pour le composé I vient à nouveau compléter la sphère de coordination en position apicale. Concernant la constante d'affinité d'Aβ pour Cu(II), beaucoup de valeurs très différentes ont été proposées, mais récemment un consensus a été obtenu sur la valeur de 10^{10} M^{-1} à pH 7.4. Au cours de cette thèse, une nouvelle méthode de détermination de la constante d'affinité du Cu(II) pour l'Aβ

et des peptides mutants par UV-vis est proposée, en collaboration avec Dr Laurent Lisnard (Université Pierre et Marie Curie, à Paris). Cette méthode est une étude par compétition, permettant un accès relativement aisé à la valeur de la constante d'affinité. Une fois que la constante d'affinité du compétiteur a été déterminée, la constante d'affinité du peptide peut être mesurée par compétition entre l'Aβ et le compétiteur. Une valeur de 1.6 10^9 M^{-1} à pH 7.1 a été déterminée. Cette valeur est en accord avec le consensus proposé de 10^{10} M^{-1} à pH 7.4 mais également avec la valeur obtenue par potentiométrie par un autre groupe. Notons que les études réalisées au cours de cette thèse sont à pH 7.1 pour des raisons de constantes d'affinité (Cu(II) et Zn(II)) de certains ligands données seulement à pH 7.1. Ensuite, différents mutants d'Aβ16 ont été étudiés par la même méthode. L'idée est ici de vérifier le mode de coordination du Cu(II) par l'Aβ par cette méthode : si un mutant a une constante d'affinité égale à celle d'Aβ, alors l'acide aminé qui a été muté n'est pas impliqué dans la coordination, alors que si la valeur de l'affinité diminue, alors l'acide aminé avant mutation était impliqué dans la coordination. Les résultats obtenus sont en accord avec les coordinations proposées en Figure I-2. Cette étude a permis de confirmer la valeur de la constante d'affinité d'Aβ pour Cu(II), mais surtout de proposer une méthode robuste de détermination de constante d'affinité (pour des molécules d'affinité comparable à celle du compétiteur).

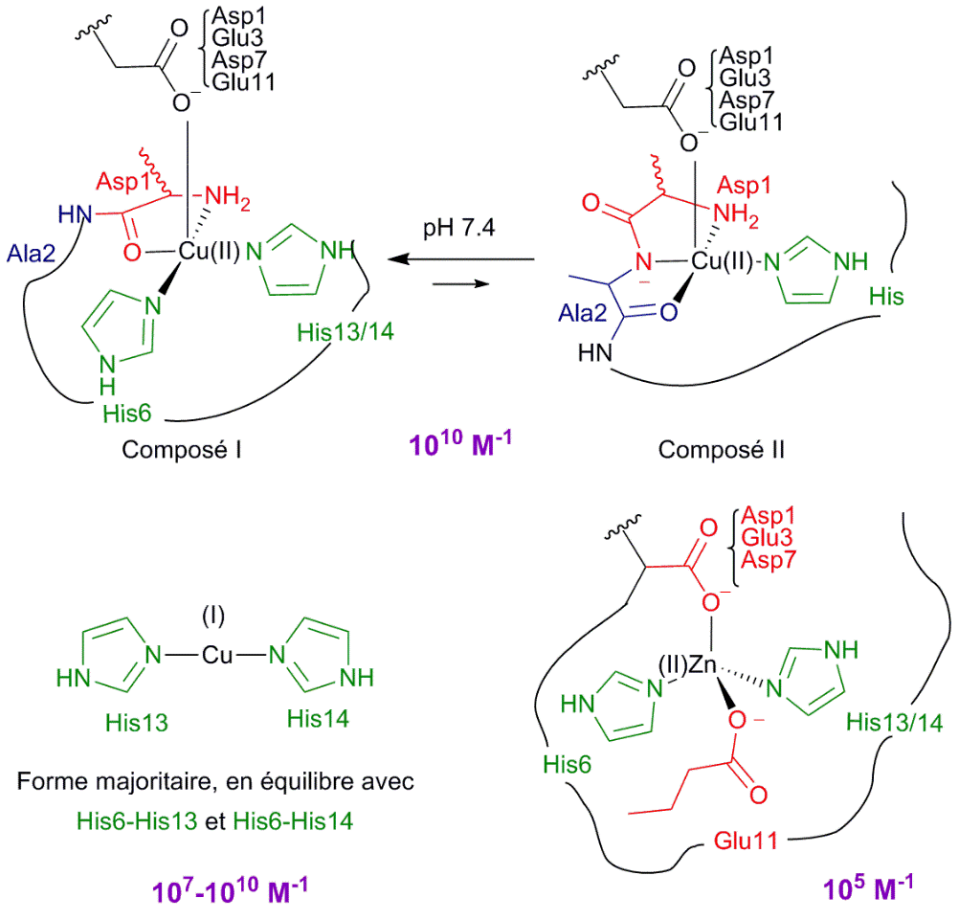

Figure I-2. Figure représentant les différentes coordinations des ions métalliques avec Aβ ainsi que les constantes d'affinité correspondantes, à pH 7.4.

Concernant le Cu(I), il est lié au peptide Aβ de façon linéaire entre deux résidus His (Figure I-2). A pH 7.4, la forme majoritaire est celle impliquant les His13 et His14. La constante d'affinité d'Aβ pour Cu(I) a été déterminée via une compétition avec la Ferrozine. Cependant, la constante d'affinité du Cu(I) pour la Ferrozine est controversée. Ainsi, deux valeurs sont proposées pour Aβ à pH physiologique, dépendant de la valeur choisie pour la Ferrozine : $10^{10.4}$ M^{-1} et $10^{6.9}$ M^{-1}.

L'ion Zn(II) est lié au peptide Aβ dans une géométrie tétraédrique. Dans la littérature, de nombreuses coordinations sont proposées, impliquant souvent l'amine terminale. Cependant, au cours de cette thèse, un nouveau mode de coordination a été proposé, n'impliquant pas l'amine terminale. Cette étude a été réalisée en mettant en parallèle les résultats obtenus par EXAFS, XANES et RMN. La première étape fut la détermination du nombre de ligands coordinant le Zn(II), ainsi que leur nature. Les résultats EXAFS et RMN ont permis de proposer un environnement tétraédrique. Ensuite, une série de mutants d'Aβ a été étudié par XANES et RMN en vue de déterminer quels acides aminés sont impliqués dans la coordination du Zn(II). En effet, si le signal obtenu pour le complexe Zn(II)-mutant est identique à celui obtenu pour Zn(II)-Aβ, alors l'acide aminé (avant mutation) n'est pas un ligand du Zn(II) ; au contraire, si le signal est modifié par rapport à celui de Zn(II)-Aβ, alors l'acide aminé avant mutation est impliqué dans la coordination du Zn(II). La Figure I-2 illustre le mode de coordination à pH physiologique proposé pour Zn(II) dans cette étude : l'His6, le carboxylate du Glu11, l'His13 ou l'His14, un carboxylate venant de l'Asp1, du Glu3 ou de l'Asp7. Concernant la constante d'affinité d'Aβ pour Zn (II), la valeur proposée est de 10^5 M^{-1} à pH 7.4.

I-A.ii Production d'ERO

Comme montré précédemment, le peptide Aβ peut coordiner le Zn(II), mais également le Cu dans ses deux degrés redox. Ainsi, le complexe Cu-Aβ est capable de catalyser la production d'espèces réactives de l'oxygène (ERO). Les ERO sont les produits de la réduction incomplète de l'oxygène par un réducteur, généralement l'ascorbate (Figure I-3). L'anion superoxyde ($O_2^{\bullet -}$) est formé, puis le peroxyde d'hydrogène (H_2O_2) et ensuite le radical hydroxyle ($HO^{\bullet}$). Ces ERO, lorsqu'elles ne sont pas régulées peuvent être très délétères pour les molécules environnantes, y compris celles constituant les parois neuronales. Dans les cerveaux atteints de la MA, les concentrations en ERO ne sont plus régulées en particulier à cause d'une surproduction catalytique d'ERO.

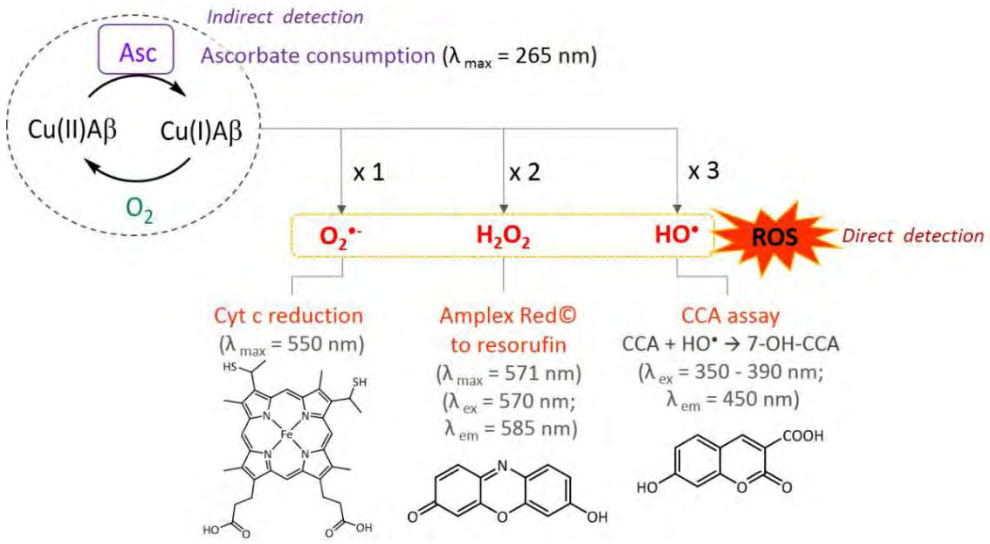

Figure I-3. Schéma représentant la production d'ERO par le complexe Cu-Aβ ainsi que les différentes techniques utilisées pour leur étude

Il existe différentes techniques spectroscopiques pour étudier la production d'ERO. Au cours de cette thèse, deux d'entre elles ont été utilisées. Le suivi de la consommation d'ascorbate par UV-vis à 265 nm (ε = 14 500 $cm^{-1}.M^{-1}$) est corrélé à la production d'ERO. En effet, si la concentration d'ascorbate diminue, alors l'ascorbate réagit avec le complexe Cu-Aβ et déclenche la production d'ERO. Au contraire, si cette concentration est constante, alors l'ascorbate ne réagit plus/pas et donc il n'y a pas de production d'ERO. La seconde méthode utilisée ici est une étude par fluorescence détectant les ions $HO^{\bullet}$. L'acide coumarine 3-carboxylique (CCA) est ajouté au milieu réactionnel, et en présence de radicaux hydroxyles, forme le 7-OH-CCA. Le 7-OH-CCA est une molécule fluorescente. Ainsi, une détection de fluorescence est corrélée à une production de 7-OH-CCA, et donc au relargage de radicaux hydroxyles par le système de Cu. Ainsi, une production d'ERO est traduite par une détection de fluorescence.

I-A.iii L'agrégation du peptide Aβ

L'agrégation du peptide Aβ en plaques séniles est un autre évènement de la MA. Elle est décrite dans le cadre de l'hypothèse de la cascade amyloïde qui place ce phénomène au centre de la MA. Cette hypothèse est relativement bien acceptée par la communauté scientifique, bien que controversée par certains groupes. Le peptide Aβ, qui est présent sous forme monomérique dans un cerveau sain, s'agrège dans un cerveau atteint de la MA en oligomères puis en fibres, s'assemblant ensuite en plaques séniles. Les fibres sont des structures riches en feuillet β. De nombreuses études cherchent à déterminer l'impact des ions métalliques dans l'agrégation du peptide. Les résultats obtenus jusqu'à présent ne convergent pas. Avec les conditions utilisées au cours de cette thèse, les ions Cu(II)

stabilisent les agrégats de faibles poids moléculaires supposés être les plus toxiques, alors que les ions Zn stabilisent des espèces fibrillaires. L'étude de l'agrégation du peptide Aβ en présence ou non d'ions métalliques se fait couramment *via* l'intermédiaire d'un fluorophore : la thioflavine T (ThT) (Figure I-4). La ThT est une molécule constituée de deux motifs aromatiques reliés par une simple liaison. Lorsque la ThT s'intercale dans les feuillets β, ce qui empêche la libre rotation autour de la simple liaison, on observe alors une très forte exaltation de la fluorescence à 490 nm (excitation à λ = 440 ± 15 nm). Par conséquent, les suivis cinétiques de l'agrégation du peptide Aβ sont effectués par fluorescence de la ThT. Lorsque la fluorescence est détectée, il y a présence de feuillets β et donc de fibres. Ces courbes d'agrégation ont une forme sigmoïdale, corrélée aux trois étapes de l'agrégation. La première est une étape de nucléation pendant laquelle les oligomères se forment. Ensuite, une seconde étape correspond à l'élongation des oligomères et protofibres en fibres. Enfin, le plateau de la sigmoïde traduit un équilibre.

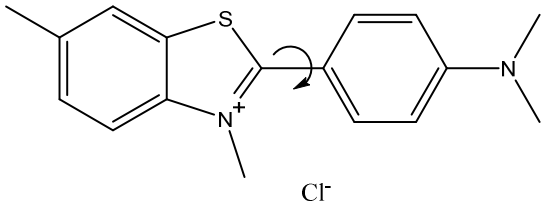

Figure I-4. Représentation de la Thioflavine T, ainsi que de la libre rotation entre les deux parties de la molécule.

I-C. Objectifs de la thèse

En résumé, le peptide Aβ agrège en oligomères, espèces désignées comme les plus toxiques des espèces présentes dans le processus d'agrégation, puis en fibres, elles-mêmes formant ensuite les plaques séniles observées dans les fentes synaptiques. Des ions métalliques tels que le Cu et le Zn interagissent avec le peptide. Les ions Cu catalysent la production d'ERO même lorsqu'ils sont liés au peptide. De plus, dans les conditions utilisées dans cette thèse, ils stabiliseraient les oligomères ou les agrégats de faible poids moléculaire, alors que les ions Zn, inertes d'un point de vue redox, semblent stabiliser des espèces fibrillaires. Ces ions Cu liés au peptide Aβ, pouvant catalyser la production d'ERO et stabilisant les agrégats de faible poids moléculaire sont par la suite appelés les « Cu toxiques ». La chélatothérapie est devenue une voie thérapeutique pour lutter contre la MA. Utiliser des ligands pour retirer les ions Cu toxiques semble prometteur et est une stratégie très étudiée. Les différents critères que doit remplir le chélateur sont : sa capacité à passer la Barrière Hémato-Encéphalique (BHE), une affinité pour les ions Cu supérieure à celle d'Aβ mais pas trop élevée pour ne pas retirer les ions Cu des

métalloprotéines. Dans cette thèse, différentes preuves de concept visant à mettre en lumière de nouveaux critères sont proposées. Dans une première partie, une étude bibliographique sur les ligands pour le Cu déjà existants et visant la MA est rapportée, ainsi que leur impact sur la production d'ERO et sur l'agrégation du peptide. Ensuite, une première preuve de concept concerne l'importance de la cinétique de captation du Cu(II) par le chélateur. En effet, il ne suffit pas que le chélateur ait une affinité pour le Cu supérieure à celle d'Aβ. Nous montrerons que la chélation doit être rapide. Une deuxième preuve de concept décrit une stratégie reposant sur le ciblage des deux états redox du Cu. En effet, le degré d'oxydation du Cu dans les fentes synaptiques n'étant pas connu à ce jour, cibler l'un des deux états redox pourrait s'avérer inefficace. La seconde partie de cette thèse s'attarde sur l'impact des ions Zn sur la chélation des ions Cu. En effet, puisqu'une concentration élevée en Zn(II) est retrouvée dans les plaques séniles et surtout dans la fente synaptique (respectivement 1 mM et 10 à 100 fois plus concentré que les ions Cu), il est pertinent de prendre en considération cet ion. D'abord, une étude bibliographique sur les interférences mutuelles entre les ions Zn, Cu et le peptide Aβ, en présence ou non de chélateurs, est rapportée. Leurs impacts sur la coordination, la production d'ERO et l'agrégation sont décrits. Ensuite, une preuve de concept concernant l'aspect thermodynamique de l'interaction des ions Zn dans la chélation des ions Cu est détaillée. Le chélateur doit pouvoir retirer sélectivement le Cu du peptide tout en laissant les ions Zn essentiels dans la fente synaptique. Enfin, la dernière preuve de concept propose une idée originale de chélatothérapie, le « pull-push ». Certains ligands ont une affinité pour le Cu et pour le Zn dans une gamme qui est telle que le Zn(II) devient nécessaire à la chélation des ions Cu. En absence de Zn(II), ces ligands ne sont pas efficaces dans le retrait du Cu du peptide, mais en présence de Zn(II), ils le deviennent. Le Zn(II) « tire » les ions Cu hors du peptide et les pousse dans le ligand, le Zn(II) étant alors coordiné par le peptide.

II. La chélation du Cu

II-A. Etat de l'art sur les ligands du Cu(II) contre la MA

Comme expliqué précédemment, puisque la dyshoméostasie des ions Cu est considérée comme un aspect important de la MA, l'approche de chélatothérapie et de redistribution des ions Cu contre la MA a été très étudiée. Elle consiste à utiliser des ligands capables de retirer les ions Cu du peptide ou d'interagir avec le complexe Cu-Aβ pour en changer les propriétés. Il existe à ce jour différents critères que doit respecter un ligand pour être utilisé dans le cadre de la MA. Il doit avoir une constante d'affinité pour les ions Cu supérieure à celle d'Aβ pour pouvoir les retirer du peptide. Cependant, cette

affinité ne doit pas être trop élevée pour ne pas retirer les ions Cu « utiles », présents dans les métalloprotéines essentielles. Ceci pourrait en effet être délétère, augmentant la dyshoméostasie déjà existante. Il est à noter que dans cette étude bibliographique, seuls les ligands capables de retirer les ions Cu d'Aβ1-x sont pris en considération. En effet, les peptides tronqués Aβ4-x et Aβ11-x commençant en positions 4 et 11, biologiquement présents dans les cerveaux de la MA, ont une constante d'affinité pour les ions Cu supérieures à celle d'Aβ1-x. Il existe deux types de ligands : les chélateurs, qui peuvent retirer le Cu du peptide et sont ensuite excrétés sous forme de complexes, ou les métallophores, qui sont des chélateurs redistribuant les ions Cu intra-cellulairement. Un autre critère important à considérer dans la conception des ligands contre la MA est que la BHE doit être perméable aux ligands, c'est-à-dire qu'ils doivent respecter au minimum les règles de Lipinski, puisque les ions Cu cibles se situent dans le cerveau. Différents paramètres doivent être respectés pour cela : le ligand ne doit pas être trop hydrophile (attention à ce qu'il ne soit pas trop hydrophobe non plus car il ne pourrait plus chélater les ions Cu), il ne doit pas avoir un poids moléculaire trop élevé, etc.

Des composés « multi-cibles » sont développés dans le cadre de la MA. Il existe deux stratégies : la partie « chélateur » peut être soit incorporée dans une seconde partie ou accrochée *via* un lien à cette seconde partie. Cette seconde partie peut être une partie anti-oxydante permettant de capter les ERO, peut être une partie qui cible les agrégats d'Aβ, ou encore une partie qui permet de modifier l'agrégation du peptide. On peut également trouver des parties qui permettent de passer la barrière hématoencéphalique, comme des glucoses ou des nanoparticules. Enfin, il existe aussi des « pro-chélateurs » qui sont des ligands qui ont leur partie « chélatrice » masquée. Elles sont « libérées » par une action extérieure (comme celle des sécrétases).

Il existe différentes catégories de ligands contre la MA. Il est possible de les regrouper en différentes familles, en fonction de leur structure. Une de ces familles regroupe les hydroxy/aminoquinolines, comme le clioquinol et le PBT2 (Figure II-1, en haut à gauche). Ces deux derniers sont connus pour avoir été testés en études cliniques, mais ne sont pas passés en phase III. Une raison possible de cet échec serait le manque de sélectivité pour le Cu par rapport au Zn(II). En effet, ces ligands formant des complexes 2 : 1 (ligand : ion métallique) peuvent adopter la géométrie plan carré (préférée par le Cu(II)) et tétraédrique (préférée par le Zn(II)). De nouveaux ligands basés sur le clioquinol et le PBT2 sont synthétisés, avec des modifications permettant de former des ligands 1 : 1, dont l'affinité du ligand pour le Cu(II) et la géométrie du complexe sont plus facilement contrôlables.

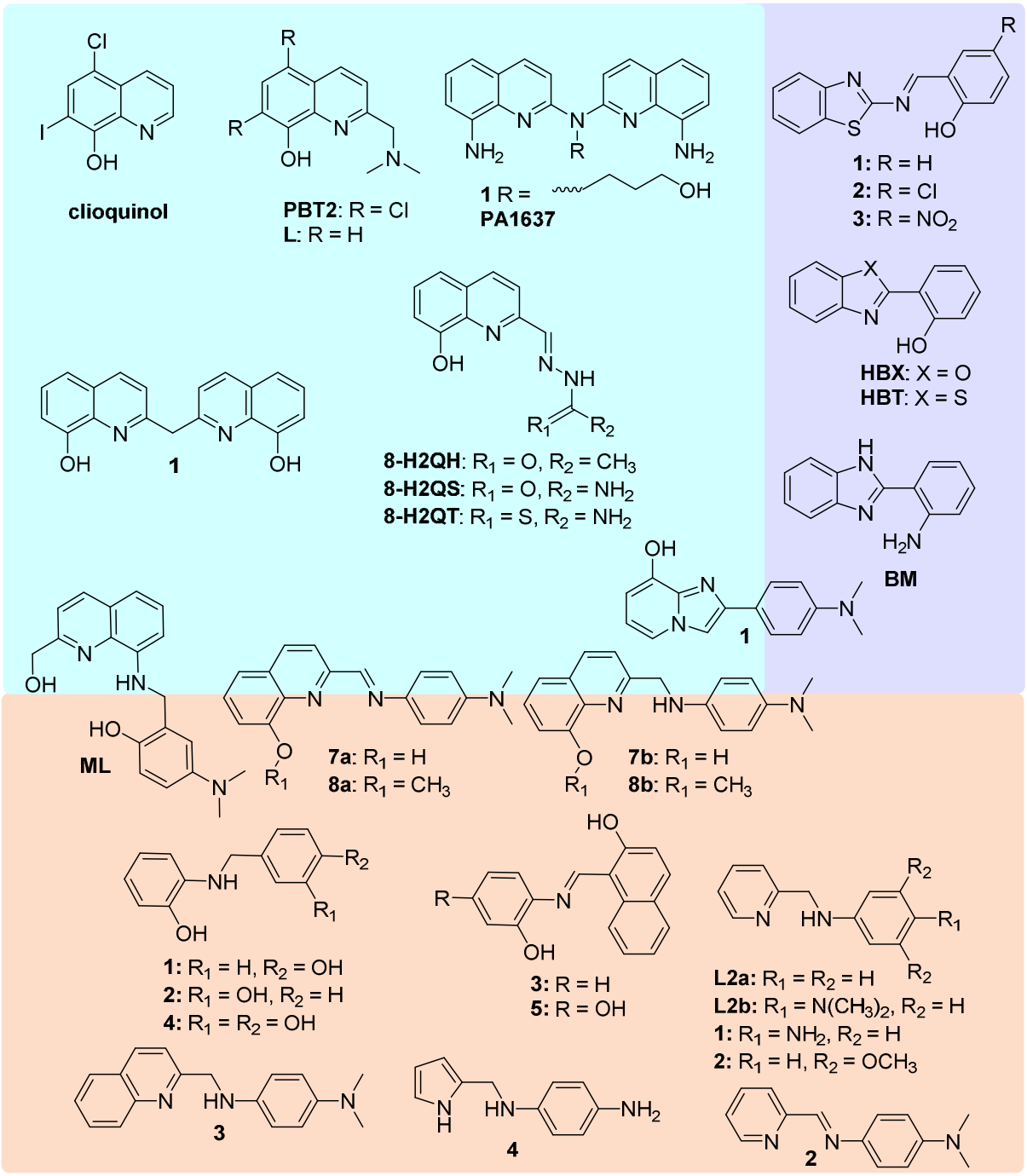

Figure II-1. Schéma regroupant les ligands étudiés dans la bibliographie dans le cadre de la MA : les hydroxy/aminoquinolines (en haut à gauche), les ligands basés sur les benzothiazoles (en haut à droite) et les ligands homologues azotés des stilbènes (en bas).

Une autre catégorie regroupe les ligands incorporant des motifs benzothiazoles et les ligands homologues azotés des stilbènes (Figure II-1, en haut à droite et en bas, respectivement). Ces motifs peuvent s'insérer dans les feuillets-β des fibres d'Aβ. Ceci permet de cibler la chélation : si les molécules interagissent avec les fibres, alors les ions Cu ne devraient être retirés que dans les zones proches des fibres. Notons qu'avec ces ligands, des complexes 2 : 1 et 1 : 1 peuvent être formés.

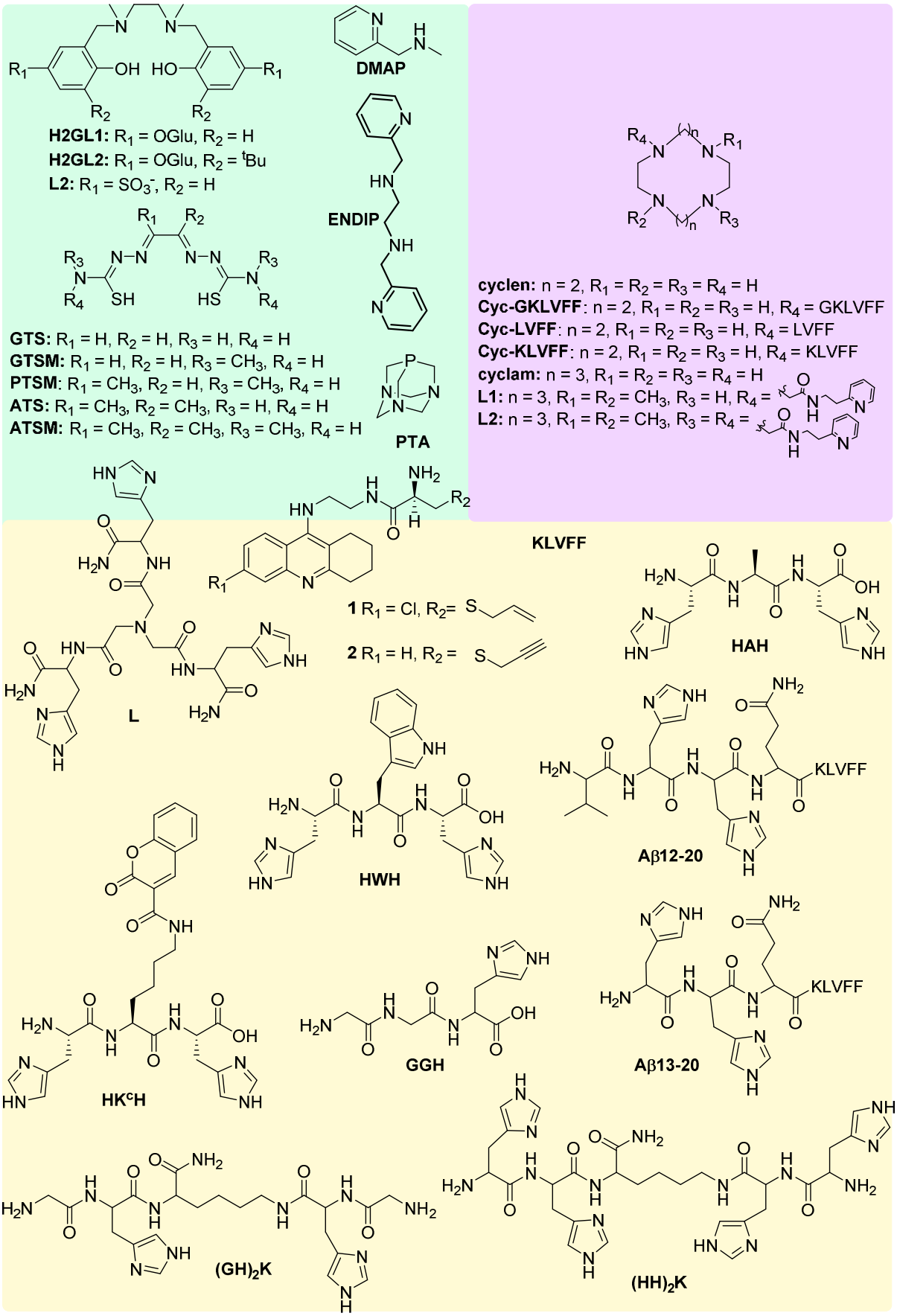

Figure II-2. Schéma regroupant le deuxième groupe de ligands étudiés dans la bibliographie dans le cadre de la MA : les structures de type salen, bispicen et bis(thiosemicarbazonato) (en haut à gauche), les ligands macrocycliques (en haut à droite) et les ligands peptidiques (en bas).

Une troisième catégorie est la famille des ligands macrocycliques ou peptidiques (Figure II-2, en haut à droite et en bas). En effet, en général, ces ligands chélatent les ions Cu(II) avec une forte affinité, dans une géométrie relativement stable, empêchant la réduction du Cu(II) et la catalyse de production d'ERO. On forme majoritairement des complexes 1 : 1 avec ces ligands.

La dernière catégorie regroupe les ligands de type salen, bis(thiosemicarbazonato) ou encore les bispicen (Figure II-2, en haut à gauche). Ils chélatent les ions Cu(II) et forment des complexes 1 :1.

Tous ces ligands peuvent retirer les ions Cu du peptide Aβ et en général peuvent au moins stopper la production d'ERO ou induire une agrégation du type « apo » et non Cu-induite. Concernant les complexes ternaires, il est probablement plus difficile pour eux d'arrêter la production d'ERO puisque la géométrie autour des ions Cu est plus flexible, accommodant les ions Cu(II) et Cu(I) et permettant le cycle rédox Cu(II)/Cu(I). Ainsi, les complexes ternaires sont peut-être plus efficaces dans la modification de l'agrégation que dans l'arrêt de la production d'ERO. De plus, pour pouvoir concevoir un métallophore, il semble plus simple d'utiliser des complexes 1 : 1. La littérature est riche d'études de chélateurs ou métallophores contre la MA, avec des structures et actions différentes. La suite de cette thèse propose différentes preuves de concept qui constituent de nouveaux critères à prendre en compte dans la conception de ligands dans le cadre de la MA. Il faut noter que les ligands étudiés dans cette thèse ne remplissent pas, dans un premier temps, tous les critères évoqués précédemment pour des raisons de solubilité et d'études *in vitro*. Cependant, la sophistication de ces ligands sera à envisager dans un second temps.

II-B. Impact de la cinétique de chélation

La première preuve de concept détaillée dans cette thèse concerne l'importance de la cinétique de captation des ions Cu(II) par un ligand. Les paramètres thermodynamiques ont souvent été étudiés : le chélateur a besoin d'une constante d'affinité pour le Cu(II) supérieure à celle d'Aβ, mais pas trop élevée pour ne pas retirer les ions Cu d'autres protéines. Pour illustrer l'importance des paramètres cinétiques, deux séries de ligands macrocycliques (en collaboration avec Dr. Raphaël Tripier, Laboratoire Chimie Electrochimie Moléculaires et Chimie Analytique, Brest) basés sur les 1,4,7,10-tetraazacyclododecan (cyclen) et 1,4,8,11-tetrazacyclotetradecane (cyclam) sont étudiées (Figure II-3). Les ligands cyclen et cyclam sont connus pour leur forte affinité pour les ions Cu(II) et pour l'inertie cinétique de leur complexe.

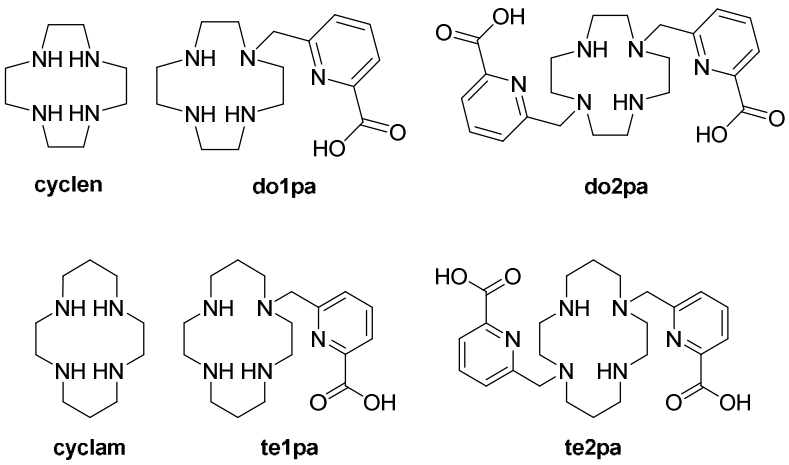

Figure II-3. Schéma des six ligands étudiés dans cette partie.

La première étude a concerné les ligands non substitués des séries, c'est-à-dire le cyclen et le cyclam. Les expériences de suivi de production d'ERO ont été réalisées et les résultats de la consommation d'ascorbate ainsi que ceux obtenus par suivi de fluorescence du 7-OH-CCA sont en accord. Si les ligands cyclen et cyclam sont ajoutés sur Cu(II)-Aβ avant l'ajout d'ascorbate, c'est-à-dire si l'on dispose d'un temps suffisamment long pour former les complexes Cu(II)-cyclen et Cu(II)-cyclam, alors il n'y a pas de production d'ERO. Cependant, si les ligands sont ajoutés en cours de production d'ERO par Cu-Aβ, alors ils ne peuvent plus retirer les ions Cu du peptide suffisamment rapidement, ne pouvant donc arrêter la production d'ERO. Il faut noter ici que la géométrie du complexe a un impact sur la cinétique de captation. En absence d'Aβ, on observe que le cyclen, mais pas le cyclam, arrive à chélater le Cu pendant la production d'ERO. Ceci est à mettre en relation avec la position du Cu(II) hors de la cavité macrocyclique dans le cas du cyclen contrairement au cyclam.

Ensuite, les ligands substitués par un ou deux bras méthylpicolinate ont été étudiés (Figure II-3). Les mêmes expériences que précédemment ont été réalisées. La Figure II-4 montre les résultats obtenus. Les panneaux A et B présentent les expériences avec temps d'incubation, c'est-à-dire avec possibilité de formation des complexes avant déclanchement de la production d'ERO. Comme pour les ligands non substitués, il n'y pas de production d'ERO, prouvant que les ligands ont retiré le Cu(II) du peptide Aβ et que les complexes formés ne forment pas d'ERO. Les panneaux C et D de la Figure II-4 présentent les expériences dans lesquelles les ligands sont ajoutés en cours de production d'ERO par le complexe Cu-Aβ. Ici, contrairement aux ligands non substitués, les ligands substitués chélatent suffisamment rapidement les ions Cu pour stopper la production d'ERO associée.

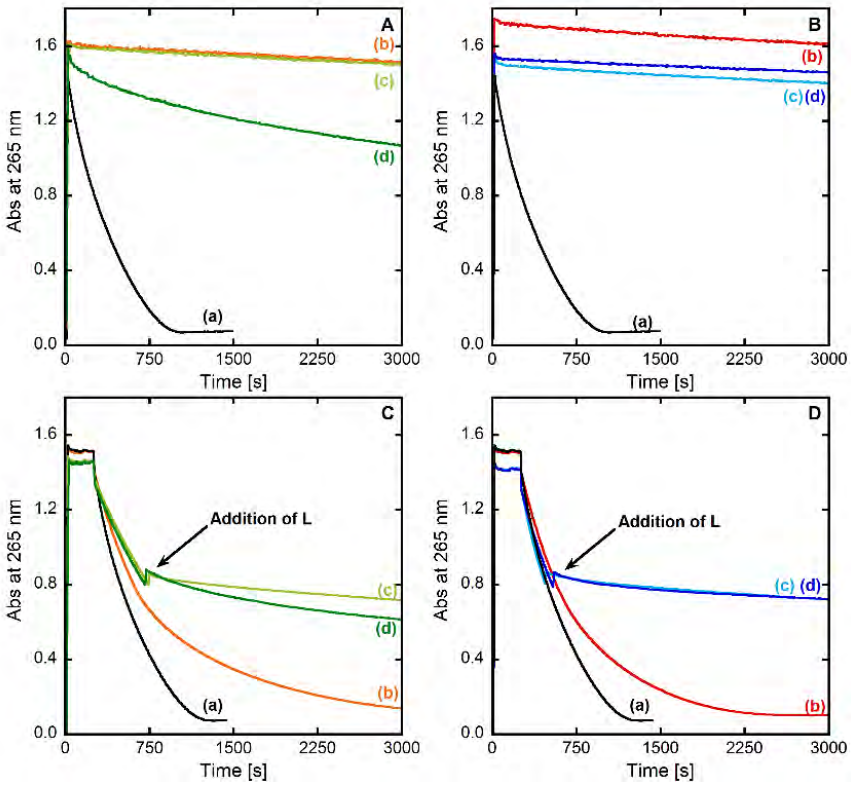

Figure II-4. Cinétiques de consommation d'ascorbate suivie par UV-Vis à 265 nm avec une correction à 800 nm. Panneau A. *(a) Aβ16 + Cu(II) + Asc, (b) Aβ16 + Cu(II) + cyclen + Asc, (c) Aβ16 + Cu(II) + do1pa + Asc, (d) Aβ16 + Cu(II) + do2pa + Asc.* Panneau B. *(a) Aβ16 + Cu(II) + Asc, (b) Aβ16 + Cu(II) + cyclam + Asc, (c) Aβ16 + Cu(II) + te1pa + Asc, (d) Aβ16 + Cu(II) + te2pa + Asc.* Panneau C. *(a) Asc + Aβ16 + Cu(II), (b) Asc + Aβ16 + Cu(II) + cyclen, (c) Asc + Aβ16 + Cu(II) + do1pa, (d) Asc + Aβ16 + Cu(II) + do2pa.* Panneau D. *(a) Asc + Aβ16 + Cu(II), (b) Asc + Aβ16 + Cu(II) + cyclam, (c) Asc + Aβ16 + Cu(II) + te1pa, (d) Asc + Aβ16 + Cu(II) + te2pa. [L] = [Aβ16] = 12 µM, [Cu(II)] = 10 µM, [Asc] = 100 µM, [HEPES] = 100 mM, pH 7.1.*

Ces expériences prouvent que l'effet cinétique de captation de Cu(II) est un paramètre très important dans des approches de chélatothérapie contre la MA. En effet, bien que les ligands macrocycliques non substitués aient une très forte constante d'affinité pour les ions Cu(II), leur cinétique de captation est lente par rapport à la vitesse de production d'ERO par Cu-Aβ. Ainsi, dans le cas le plus proche de ce qui se passe *in vivo*, *i.e.* lorsque les ligands sont ajoutés en cours de production d'ERO, cyclen et cyclam ne sont pas capables de retirer Cu d'Aβ et d'arrêter la production d'ERO associée. L'ajout de bras chélateurs permet d'accélérer la captation des ions Cu(II). Ainsi, le Cu n'est plus lié à Aβ et la production d'ERO est stoppée. Cette première preuve de concept met l'accent sur l'impact de la cinétique de captation des ions Cu par des ligands sur la production d'ERO catalysée par Cu-Aβ.

II-C. Choix de la cible : Cu(I) et/ou Cu(II) ?

La deuxième preuve de concept concerne le choix de la cible du chélateur. En effet, nombreux sont les ligands du Cu(II) développés pour la MA, alors que très peu de ligands ciblant le Cu(I) sont décrits dans la bibliographie. Pourtant, en théorie, hormis les difficultés pratiques à étudier les ions Cu(I), il n'y a pas d'explication à cela. En effet, à ce jour, le degré d'oxydation des ions Cu dans la fente synaptique n'est pas connu. Ainsi, comment choisir entre un ligand pour le Cu(II) et un ligand pour le Cu(I), sachant que dans les deux cas, il y a risque d'inefficacité dans la chélation ? C'est pourquoi le ligand **L** ciblant les deux états redox du Cu a été étudié, en collaboration avec Dr Pascale Delangle, Institut Nanosciences et Cryogénie, Grenoble. Trois résidus Histidine sont greffés sur un squelette nitrilotriacétique (Figure II-5).

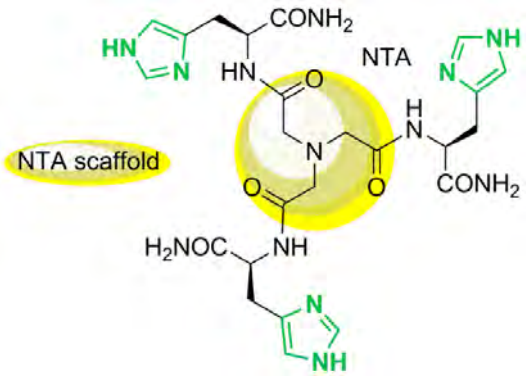

*Figure II-5. Schéma représentant le ligand **L** étudié comme chélateur du Cu(I) et du Cu(II). Un squelette nitrilotriacétique sert de support au greffage de trois résidus Histidine.*

Après avoir déterminé les constantes d'affinité des complexes Cu(II)-L et Cu(I)-L, la caractérisation de ces complexes par RPE et XANES respectivement, a permis de proposer un mode de coordination pour ces complexes, en fonction du pH. A pH 7.1, le Cu(II) est coordiné en géométrie plan carré par les trois Histidines du ligand ainsi que par un amide déprotoné (Figure II-6). Le Cu(I), lui, est coordiné par les trois Histidines ainsi que par un ligand extérieur, le solvant par exemple, dans une géométrie tétraédrique (Figure II-6). Les deux modes de coordination sont bien distincts.

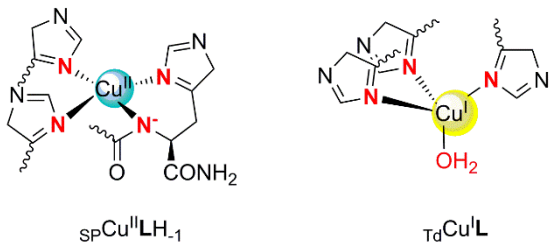

$_{SP}Cu^{II}LH_{-1}$ $_{Td}Cu^{I}L$

*Figure II-6. Schéma représentant les modes de coordination du Cu(II) et du Cu(I) par le ligand **L** à pH 7.1.*

Ensuite, une étude par voltamétrie cyclique a permis de caractériser le système. Un schéma carré ECEC (Electrochimie-Chimie-Electrochimie-Chimie) permet de le décrire. Le complexe Cu(II)-**L**, en

géométrie plan carré, est réduit en Cu(I)-**L**, en géométrie plan carré (E) suivi d'un réarrangement pour obtenir une géométrie tétraédrique (C). Dans l'autre sens, le complexe Cu(I)-**L** tétraédrique est oxydé en Cu(II)-**L** tétraédrique (E), suivi d'un réarrangement en Cu(II)-**L** plan carré (C). Il est à noter que les espèces intermédiaires, i.e. Cu(II)-**L** tétraédrique et Cu(I)-**L** plan carré ne sont pas visibles dans les conditions expérimentales utilisées. De plus, d'après les valeurs de réduction et d'oxydation de ces complexes, ils semblent être résistants à la réduction par l'ascorbate et à l'oxydation par le dioxygène.

Une fois la caractérisation des complexes effectuée, la première question a été de savoir si **L** pouvait retirer le Cu(II) du peptide Aβ. Pour cela, une étude par RPE a été réalisée. Il en résulte que au moins 95 % du Cu(II) est chélaté par **L**, laissant seulement moins de 5 % de Cu(II) sur Aβ. Ensuite, une étude par XANES a permis de déterminer que **L** retire également plus de 80 % de Cu(I) d'Aβ. Ces résultats sont en accord avec les valeurs de constante d'affinité mesurées. Ainsi, **L** est capable de retirer le Cu(I) et le Cu(II) d'Aβ. L'impact de ce chélateur sur la production d'ERO a ensuite été étudié. Le suivi de la consommation d'ascorbate a été utilisé pour cette étude, et la détection des radicaux $HO^{\bullet}$ par fluorescence a permis de confirmer les résultats. Les résultats présentés ci-après sont les mêmes en présence ou non d'Aβ. Dans un premier temps, le ligand est incubé avec le Cu(II)-Aβ et une fois le complexe Cu(II)-L formé, l'ascorbate est ajouté (Figure II-7A). L'ascorbate n'est pas consommé, ainsi il n'y a pas de production d'ERO. Ensuite, le complexe Cu(I) est préparé sous Argon en présence d'ascorbate et d'Aβ (Figure II-7B). Après ouverture à l'air, il n'y a pas non plus de production d'ERO. Finalement, lorsque L est ajouté pendant la production d'ERO, c'est-à-dire pendant que les ions Cu cyclent entre l'état d'oxydation +I et +II, la production d'ERO est très fortement ralentie (Figure II-7C). Ainsi, L est capable de fortement réduire la production d'ERO que ce soit en départ Cu(II), départ Cu(I) ou un mélange des deux degrés d'oxydation.

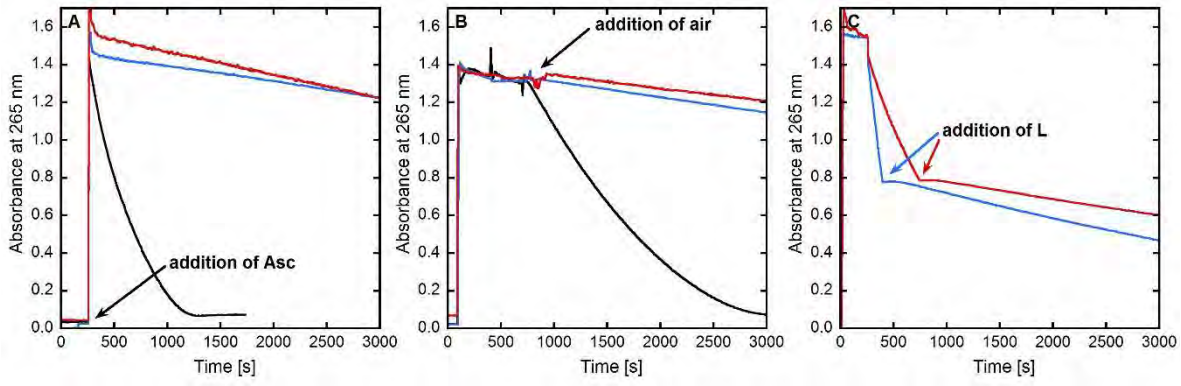

Figure II-7. Suivi de la production d'ERO par consommation d'ascorbate, par UV-Vis à 265 nm, avec une correction de la ligne de base à 800 nm. Panneau A. Aβ + Cu(II) + Asc (courbe noire), L + Cu(II) + Asc (courbe bleue), Aβ + Cu(II) + L + Asc (courbe rouge). Panneau B. Cu(II) + Asc + Aβ + air (courbe noire), Cu(II) + Asc + L + air (courbe bleue), Cu(II) + L + Asc + Aβ + L (courbe rouge). Panneau C. Asc + Cu(II) + L (courbe bleue), Asc + Aβ + Cu(II) + L (courbe rouge). [L] = [Aβ] = 12 µM, [Cu(II)] = 10 µM, [Asc] = 100 µM, [HEPES] = 100 mM, pH 7.1. Pour les expériences du panneau B, toutes les solutions ont été déoxygénées en bullant de l'Argon et ont été ajoutées sous une légère surpression d'Argon pour garder le Cu sous son état d'oxydation +I.

Cette deuxième preuve de concept décrit donc un ligand capable de chélater le Cu(II) et le Cu(I) et de produire très peu d'ERO (comparativement au peptide Aβ). Ceci semble être dû à la différence de géométrie et de coordination entre Cu(I)-L et Cu(II)-L. Ce changement est très important, empêchant le Cu de cycler et donc de produire des ERO. Cibler les deux états d'oxydation dans ce contexte est important puisque, actuellement, le degré d'oxydation du Cu dans les fentes synaptiques reste inconnu.

III. Impact des ions Zn sur la chélation des ions Cu

La première partie de ma thèse s'est focalisée sur la chélation des ions Cu dans le contexte de la MA. Après une étude de la bibliographie sur ces chélateurs, une première preuve de concept décrit l'impact de la cinétique de captation du Cu sur la production d'ERO. Ensuite, une deuxième preuve de concept détaille l'intérêt de cibler les deux états d'oxydation du Cu et propose un ligand répondant à ce critère. Bien entendu, les complexes formés ne doivent pas produire d'ERO. La seconde partie de cette thèse se concentre sur l'impact des ions Zn(II) sur la chélation du Cu(II). Ces études sont biologiquement pertinentes puisqu'il y aurait 10 à 100 fois plus de Zn(II) que d'ions Cu dans la fente synaptique.

III-A. Etat de l'art sur les interactions mutuelles entre Cu, Zn et Aβ

L'état de l'art concernant les études sur les effets des interactions mutuelles entre les ions Cu et Zn et le peptide Aβ est rapporté dans la première section de la dernière partie de la thèse. Dans les cerveaux atteints de la MA, il y a une mauvaise régulation des concentrations des ions Cu et Zn. Les ions Cu seraient trop concentrés extra-cellulairement, et déficients intra-cellulairement. Concernant les ions Zn, il est difficile de savoir si leur concentration est trop élevée ou trop faible, car ces deux résultats ont été obtenus par différents groupes. Les ions Cu et Zn ont également été retrouvés dans les plaques séniles et *in vitro*, les deux ions métalliques interagissent avec le peptide Aβ. Il a été montré que, séparément, ces ions pouvaient moduler l'agrégation du peptide, mais à nouveau, la tendance de cette modulation *in vitro* n'est pas claire. Cependant, toutes les études convergent vers l'importance du ratio métal : peptide et vers le fait que les effets des ions Cu et ceux des ions Zn sur l'agrégation sont différents. De plus, le complexe Cu(II)-Aβ catalyse la production d'ERO qui peuvent attaquer les biomolécules environnantes. C'est pour cela que la chélation des ions Cu(II) est une partie importante des recherches sur la MA depuis plusieurs années. Il existe deux grandes catégories de ligands : les

chélateurs et les métallophores. Les chélateurs sont des molécules capables de retirer les ions Cu du peptide ; les métallophores sont des chélateurs qui peuvent ensuite redistribuer les ions Cu intra-cellulairement. Certains de ces métallophores, comme le clioquinol et PBT2, ont été jusqu'aux tests cliniques, mais ont finalement échoué. Une des différentes hypothèses concernant ces échecs sont le manque de sélectivité des ions Cu par rapport aux ions Zn de ces ligands. En effet, ils peuvent chélater aussi bien les ions Cu que les ions Zn. Ceci met l'accent sur le fait que cibler seulement les ions Cu comme approche thérapeutique ne semble pas être suffisant et qu'il faille prendre en compte l'environnement des ions Cu. La première étape de cette approche plus réaliste est l'étude de l'impact des ions Zn(II). Premièrement, l'impact des ions Zn(II) sur la coordination des ions Cu est reporté, puis sur la production d'ERO et sur l'agrégation, et enfin sur la chélation des ions Cu.

La première partie de cet état de l'art se concentre sur les coordinations hétéro-bimétalliques. Elles ont été étudiées par différentes techniques spectroscopiques et potentiométriques. Concernant la coordination des ions Cu(II), les ions Cu(II) et Zn(II) déplacent mutuellement le site de coordination de l'autre ion (Figure III-1). Par exemple, le Zn(II) garde l'Histidine 6 comme ligand (ligand commun aux deux ions métalliques dans les complexes homo-métalliques) et le Cu(II) garde les deux autres Histidines à pH 7.1. Ainsi, le Zn(II) pousse le Cu(II) dans la coordination du composé 2 et le Cu(II) pousse le Zn(II) dans une coordination différente de celle du complexe homo-métallique, avec une seule Histidine. Concernant le Cu(I), il impose son mode de coordination, laissant une seule Histidine et non deux comme ligand pour le Zn(II) (Figure III-1). En résumé, Cu(I/II) et Zn(II) ont des interactions mutuelles sur leur site de coordination au peptide Aβ. Cependant, des études sont maintenant nécessaires pour déterminer l'impact mutuel de ces ions sur les constantes d'affinité.

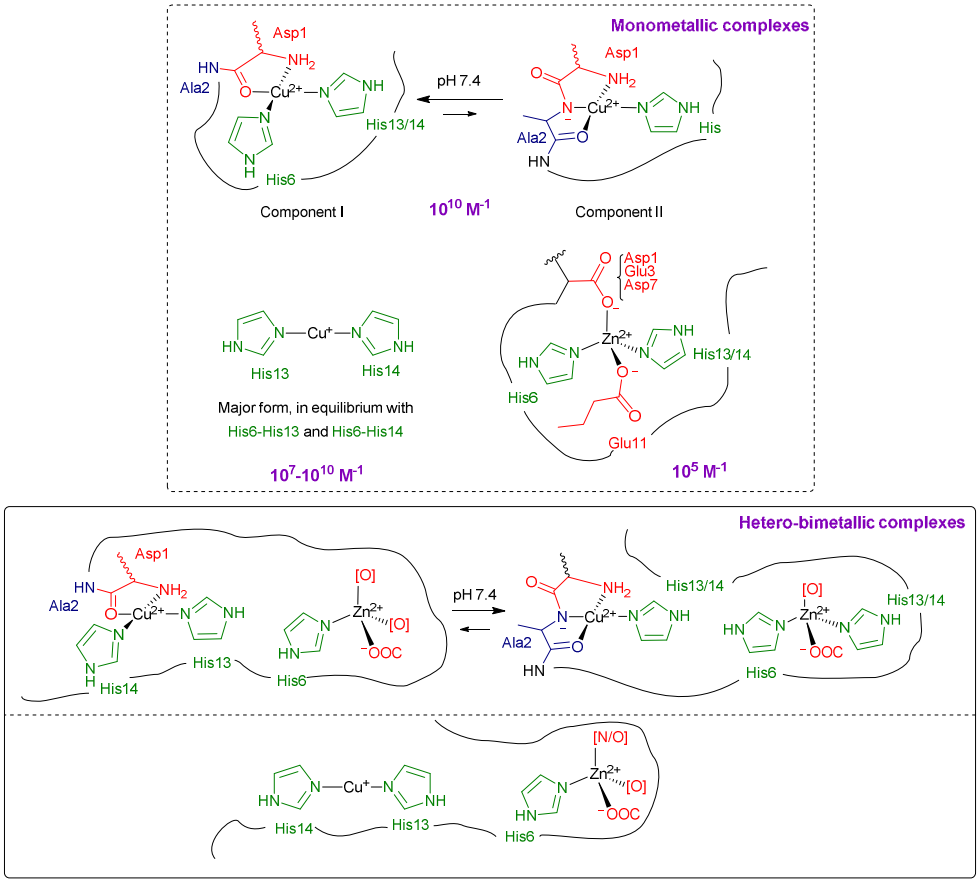

Figure III-1. Représentations des différents sites de coordination des ions Cu(I/II) et Zn(II) avec le peptide Aβ à pH physiologique, ainsi que des ceux des complexes hétéro-bimétalliques.

La seconde partie de cet état de l'art est concentrée sur l'impact des ions Zn sur l'agrégation du peptide et sur la production d'ERO. D'abord, l'agrégation du peptide est modulée par les ions Cu et Zn. Elle est également très dépendante du ratio métal : peptide, du pH, de la température, etc. Dans le cas de l'agrégation du complexe Cu-Aβ, le ratio métal : peptide est très important. En effet, avec des ratios sous-stœchiométriques en ions Cu comparés au peptide, des fibres sont formées, alors qu'avec des ratios au moins stœchiométriques, ce sont les oligomères toxiques qui sont formés. Les ions Zn impactent également l'agrégation du peptide, même à des stœchiométries très faibles. A des ratios stœchiométriques, des fibres sont formées mais seraient différentes des fibres apos. L'agrégation en présence des ions Cu(II) et Zn(II) serait la même que celle en présence de Zn(II) : les ions Zn, semblent imposer la morphologie des espèces formées. La production de ROS en fonction de ces deux ions métalliques est également détaillée. Cependant, il n'y a à ce jour pas suffisamment d'études pour proposer une tendance. Certains proposent une diminution de la production d'ERO en présence de Zn(II) alors que d'autres ne voient pas d'effet. Ensuite, la production d'ERO par les espèces agrégées est rapportée. A nouveau, il n'y a pas assez d'études pour pouvoir affirmer une tendance, mais il

semblerait que les espèces agrégées produisent moins d'ERO que les espèces monomériques. De plus, la présence de Zn semblerait diminuer les ERO produites par les agrégats.

La dernière partie de cette revue s'est concentrée sur l'impact du Zn(II) sur la chélation des ions Cu. Un ligand dans le contexte de la MA doit avoir une constante d'affinité pour le Cu supérieure à celle pour Aβ, mais pas trop forte non plus, pour ne pas retirer les ions Cu non toxiques d'autres métalloprotéines. Puisque les ions Zn ont un impact sur la coordination du Cu, sur la production d'ERO ainsi que sur l'agrégation du peptide, il est pertinent d'étudier son impact sur la chélation des ions Cu. Les premières études ont été réalisées avec les métallothionéines Zn_7-MT-3 puis MT-2A. Il se produit un échange d'ions métalliques Cu et Zn entre les MT et le peptide Aβ. Il se forme un cluster Cu(I) 4-thiolate stable à l'air, stoppant ainsi la production d'ERO. Ensuite, ces études ont été réalisées avec des ligands synthétiques L2 et Lc. Les deux ligands, ayant une constante d'affinité pour le Cu(II) supérieure à celle de Aβ, retirent Cu(II) du peptide et diminuent voire stoppent la production d'ERO. Cependant, en présence de Zn(II), seul le ligand L2 peut toujours retirer Cu(II). La thermodynamique permet d'expliquer ceci. En effet, la sélectivité, c'est-à-dire la différence entre la constante d'affinité pour le Cu et celle pour le Zn, est un paramètre important dans la chélation des ions Cu. Elle est supérieure à celle d'Aβ dans le cas de L2 alors qu'elle est inférieure dans le cas de Lc. Il est donc nécessaire d'avoir une constante d'affinité pour Cu supérieure à celle d'Aβ mais également une sélectivité (Cu *versus* Zn) supérieure à celle d'Aβ.

Ainsi, cette revue décrit les interactions mutuelles entre les ions Cu et Zn et le peptide Aβ. Zn(II) déplace le Cu(II) de son site de coordination, a un impact sur la production d'ERO ainsi que sur l'agrégation. Il impacte également la chélation du Cu(II), pouvant aller jusqu'à l'empêcher. Enfin, puisque le Zn(II) a un impact sur la chélation du cuivre, il faudrait également étudier l'impact d'autres ions biologiquement pertinents tels que les ions Ca(II) ou Fe(II/III) sur la chélation des ions Cu dans le cadre de la MA.

III-B. Effet thermodynamique de la présence des ions Zn

La première étape de la chélatothérapie contre la MA a été de comprendre et d'étudier comment un ligand pouvait retirer le Cu(II) du peptide Aβ et stopper la production d'ERO. De nombreuses études ont proposé des ligands organiques et peptidiques dans ce sens. Cependant, jusqu'à ce jour, les quelques ligands qui ont pu arriver en essais cliniques ont échoués. Ceci serait surement dû au fait que les ions Cu sont dans un environnement *in vivo* trop simplifié dans les études *in vitro*. Par exemple, la forte concentration en ions Zn n'est pas représentée dans ces études. Les ligands comme le clioquinol peuvent également chélater les ions Zn(II) avec une forte affinité, entrainant ainsi une possible

chélation *in vivo* des ions Zn(II) et laissant les ions Cu toxiques dans la fente synaptique. De plus, il a été montré que les ions Zn interfèrent dans la coordination des ions Cu au peptide, dans la production d'ERO par le complexe Cu-Aβ et sur l'agrégation de ce complexe peptidique. Ainsi, la seconde étape de ces études est de mimer cet environnement riche en Zn(II) et de déterminer son impact sur la chélation des ions Cu. Un système à quatre partenaires, c'est-à-dire Aβ, le ligand, le Cu(II) et le Zn(II), est ainsi étudié.

Rappelons qu'un « bon » ligand a besoin d'une constante d'affinité pour les ions Cu supérieure à celle d'Aβ pour pouvoir retirer les ions Cu du peptide. Cependant, en présence de Zn(II), ceci n'est plus suffisant. Deux ligands, L2 et Lc (Figure III-2), sont étudiés pour illustrer ce problème thermodynamique. Les deux ont une affinité pour les ions Cu et Zn supérieure à celle d'Aβ et les deux retirent les ions Cu(II) du peptide en absence de Zn(II).

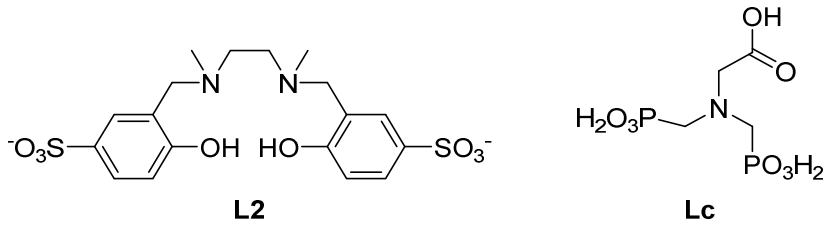

Figure III-2. Schéma des ligands L2 et Lc.

Avant de regarder l'impact de ces ligands sur la production d'ERO et sur l'agrégation, il est nécessaire d'étudier l'impact que peut avoir le Zn(II) sur ce retrait du Cu(II) d'Aβ. Pour cela, des études spectroscopiques par UV-visible, RPE et XANES ont été réalisées. Concernant le L2, la présence de Zn(II) n'a pas d'impact sur la chélation des ions Cu. Cependant, Lc n'est plus capable de chélater Cu(II) en présence de Zn(II) ; le Cu(II) reste lié au peptide, et Lc coordine Zn(II). Ceci semble contre-intuitif puisque les deux ligands ont une constante d'affinité pour Cu(II) supérieure à celle d'Aβ. Une explication thermodynamique est proposée. En effet, la différence qui existe entre ces deux ligands est leur sélectivité. La sélectivité est le rapport entre la constante d'affinité pour le Cu(II) et celle pour le Zn(II). Notons qu'une forte constante d'affinité pour le Cu(II) n'implique pas une grande sélectivité et inversement, une grande sélectivité n'est pas forcément due à une forte constante d'affinité pour le Cu(II). L'important est vraiment le rapport entre l'affinité du Cu(II) et celle du Zn(II). Ainsi, pour retirer le Cu(II) d'Aβ en présence de Zn(II), le ligand a besoin non seulement d'une affinité pour Cu(II) supérieure à celle d'Aβ mais aussi une sélectivité supérieure à celle d'Aβ. Cette sélectivité pour Aβ est déjà élevée, $10^{4.2}$ à pH 7.1. L2 a une sélectivité supérieure à celle d'Aβ alors que pour Lc, elle est

inférieure, $10^{7.7}$ et $10^{2.0}$ respectivement. Ainsi, thermodynamiquement, seul L2 est capable de retirer le Cu(II) d'Aβ en présence de Zn(II).

La deuxième partie de l'étude s'est centrée sur l'efficacité de ces deux ligands à arrêter la production d'ERO. Ceci a été réalisé *via* deux expériences différentes : le suivi de la consommation d'ascorbate par production d'ERO par spectroscopie UV-Vis (Figure III-3) et le suivi de la cinétique de fluorescence du 7-OH-CCA, molécule fluorescente formée suite à la réaction entre le CCA et le radical $HO^{\bullet}$. En absence de Zn(II), les deux ligands sont capables de réduire très fortement voire stopper la production d'ERO. Cependant, en présence de Zn(II), seul L2 arrête toujours la production d'ERO. Ceci s'explique par le fait qu'en présence de Zn(II), Cu(II) est chélaté par L2 capable d'arrêter la production d'ERO, alors que Cu(II) est chélaté par Aβ dans le cas de Lc, catalysant ainsi la production d'ERO.

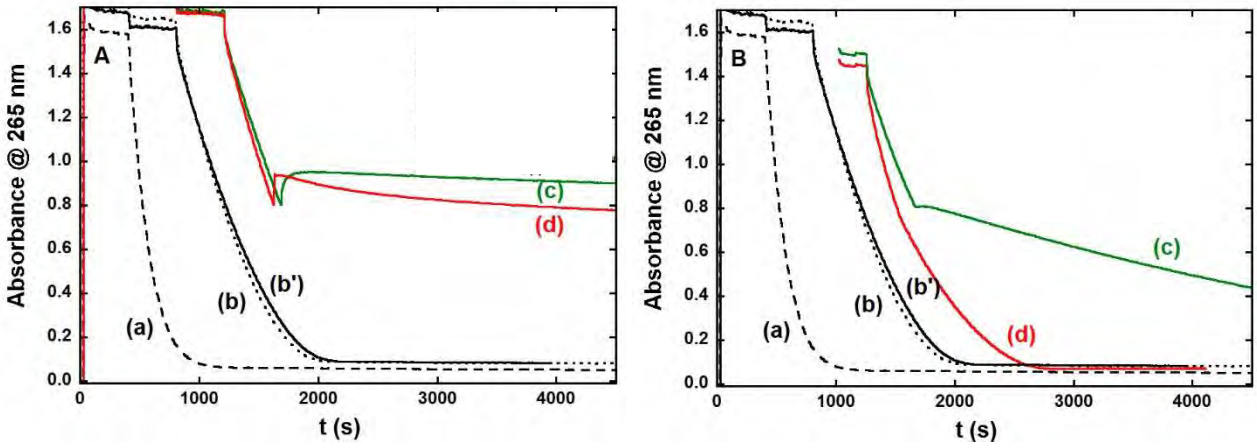

Figure III-3. Suivi de la consommation d'Ascorbate à 265 nm avec une correction de la ligne de base à 800 nm. Le t_0 des expériences a été arbitrairement décalé pour une meilleure visibilité. (a) Cu; (b, b') Cu(II)-Aβ ou Cu(II),Zn(II)-Aβ, (c) Cu(II)-Aβ + L, (d) Cu(II)-Aβ + Zn(II)-L, avec L = L2 (panneau A) et L = Lc (panneau B). L'Ascorbate est ajout en premier, et le ligand est ajouté à A = 0.8. [Aβ] = [L] = 12 µM, [Zn] = 12 µM; [Cu] = 10 µM, [Asc] = 100 µM, [HEPES] = 0.1 M, pH 7.1, T = 25°C.

La dernière étude de cette partie concerne l'agrégation du peptide Aβ. Elle a seulement été réalisée pour L2 et non pas pour Lc puisque en présence de Zn(II), le Cu(II) est chélaté par Aβ et donc la présence de Lc n'a pas d'impact sur l'agrégation. Le suivi de l'agrégation a été réalisé par suivi de fluorescence de la ThT et les échantillons ont été imagés par AFM. Rappelons que les conditions utilisées dans cette thèse permettent d'observer que le peptide apo ainsi que le complexe Zn(II)-Aβ agrègent en fibres, alors que Cu(II)-Aβ agrège en oligomères ou protofibres. Les résultats obtenus montrent que si L2 est ajouté à Cu(II)-Aβ, alors l'agrégation est la même que celle de Aβ apo. De plus, si Zn(II)-L2 est ajouté à Cu(II)-Aβ, l'agrégation est la même que celle de Zn(II)-Aβ. Ainsi, même en présence de Zn(II), l'ajout de L2 empêche la formation des oligomères qui sont définis comme étant les espèces les plus toxiques de l'agrégation du peptide. Cette étude prouve à nouveau qu'il y a un échange des ions métalliques entre Aβ et L2.

Cette troisième preuve de concept propose un nouveau critère pour la conception de ligand pour la chélatothérapie des ions Cu dans le cadre de la MA : la sélectivité des ions Cu versus Zn(II). En effet, il est important de prendre en considération la présence des ions Zn(II) en haute concentration dans la fente synaptique. L'étude des ligands L2 et Lc a permis d'illustrer ce problème. Ainsi, un ligand a besoin d'avoir une sélectivité, c'est-à-dire un rapport entre l'affinité pour Cu et celle pour Zn, supérieure à celle d'Aβ pour pouvoir retirer le Cu(II) du peptide dans un environnement riche en Zn(II). Ainsi, L2 arrête la production d'ERO par Cu-Aβ et empêche le Cu(II) de stabiliser des oligomères toxiques.

Cette étude est un premier pas vers une complexification du système. En effet, les ions Zn(II) ont été ici pris en compte pour la chélation des ions Cu. Cependant, il serait intéressant d'étudier également l'impact des autres biomolécules présentes dans les fentes synaptiques ainsi que les autres ions métalliques. De plus, ce concept peut également être appliqué pour la chélation des ions Cu(I).

III-C. Le concept du «pull-push»

Le concept du «pull-push» se place dans le contexte de la chélatothérapie des ions Cu contre la MA. Si les ligands ont une constante d'affinité pour les ions Cu inférieure à celle d'Aβ, ils ne pourront pas retirer le Cu du peptide ; une affinité du même ordre de grandeur que celle d'Aβ entraine un équilibre entre les espèces Cu-Aβ et Cu-L ; une affinité supérieure à celle d'Aβ permet un retrait total du Cu d'Aβ. Rappelons que ceci est vrai en absence de Zn. La présence de Zn, comme expliqué précédemment, perturbe ces équilibres. Il est nécessaire que la sélectivité du ligand soit supérieure à celle d'Aβ pour qu'il puisse retirer Cu d'Aβ (Table III-1, L >> Aβ). Ainsi, un ligand ayant une affinité de l'ordre de celle d'Aβ, ne retire qu'environ la moitié du Cu d'Aβ, alors qu'en présence de Zn, la totalité du Cu peut être retirée par le ligand si la sélectivité est suffisamment grande. Aβ attire le Zn(II) qui à son tour pousse le Cu(II) dans le ligand. Voici quelques exemples pour illustrer ce concept du «pull-push». Considérons les équilibres suivants.

Equilibre 1:

$Cu(II) - A\beta + L \leftrightarrow A\beta + Cu(II) - L$, avec

$$K_1 = \frac{[A\beta].[Cu(II) - L]}{[Cu(II) - A\beta].[L]} = \frac{K_{Cu}^{L}}{K_{Cu}^{A\beta}}$$

Equilibre 2:

$Cu(II) - A\beta + Zn(II) - L \leftrightarrow Zn(II) - A\beta + Cu(II) - L$, avec

$$K_2 = \frac{[Zn(II) - A\beta].[Cu(II) - L]}{[Cu(II) - A\beta].[Zn(II) - L]} = \frac{K_{Zn}^{A\beta}.K_{Cu}^{L}}{K_{Cu}^{A\beta}.K_{Zn}^{L}}$$

$K_M^{L'}$ représente la constant d'affinité de L' pour M, avec L' = Aβ ou L et M = Cu ou Zn.

Les équilibres 1 et 2 décrivent donc l'équilibre de retrait du Cu d'Aβ par L en absence et en présence de Zn, respectivement. La Table III-1 montre différents exemples d'affinité et de sélectivité ainsi que leur impact sur les équilibres 1 et 2, à pH 7.1.

Table III-1. Table montrant différents exemples différents exemples d'affinité et de sélectivité d'un ligand et leur impact sur les équilibres 1 et 2.

Constante d'affinité de L	**K_1**	**% Cu(II)-L**	**Sélectivité de L**	**K_2**	**% Cu(II)-L**
L >> Aβ $10^{11} >> 10^9$	10^2	90 %	10^1	10^{-3}	3 %
			10^4	1	50 %
			10^7	10^3	97 %
L = Aβ $10^9 = 10^9$	1	50 %	10^1	10^{-3}	3 %
			10^4	1	50 %
			10^7	10^3	97 %
L << Aβ $10^7 << 10^9$	10^{-2}	10 %	10^1	10^{-3}	3 %
			10^4	1	50 %
			10^7	10^3	97 %

Le concept du «pull-push» concerne deux catégories de ligands. La première correspond aux ligands avec une affinité pour le Cu de l'ordre de celle d'Aβ (10^9 M^{-1} à pH 7.1) (Table III-1, L = Aβ) et une sélectivité très supérieure à celle d'Aβ (~ 10^4). Ainsi, le ligand doit avoir les affinités suivantes : $K_{Cu}^{L} = 10^{8-9}$ M^{-1} et $K_{Zn}^{L} = 10^{1-2}$ M^{-1} à pH 7.1 pour pouvoir passer de 50 % de Cu(II) chélaté par L en absence de Zn(II) à 97 % en présence de Zn(II). La seconde correspond aux ligands qui ont une affinité pour le Cu(II) très faible (Table III-1, L << Aβ). Notons que si l'affinité pour Cu est faible, il faut une affinité pour le Zn très petite, sachant que 10^{1-2} est déjà très faible, pour avoir une sélectivité relativement forte (le cas de l'affinité à 10^7 et de la sélectivité à 10^7 est très probablement impossible

à avoir). Cette catégorie de ligands permet de passer de 10 % de Cu chélaté au ligand en absence de Zn(II) à 50 % en présence de Zn(II).

Pour illustrer le concept du «pull-push», trois ligands ont été étudiés (Figure III-4). Les constantes d'affinité pour le Cu(II) de ces ligands sont 3.2 10^9 M^{-1}, 3.0 10^8 $M^{-}1$ et 3.7 10^9 M^{-1} à pH 7.1 pour L, ABH et BAH respectivement. Les constantes d'équilibre en absence de Zn valent respectivement 2.0, 0.2 et 2.3. Ceci signifie qu'en absence de Zn, L et BAH retirent ~ 60 % d'Aβ et ABH 30 % de Cu(II) d'Aβ. Les constantes d'affinité pour le Zn(II) ne sont pas connues, ainsi il n'est pas possible de déterminer les constantes de l'équilibre 2. Différentes expériences spectroscopiques ont été réalisées pour illustrer la première catégorie de ligands « pull-push ».

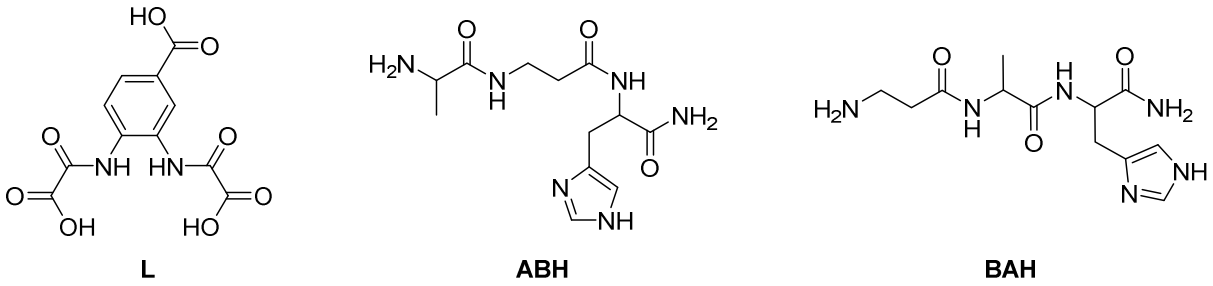

Figure III-4. Schéma des trois ligands L, ABH et BAH utilisés pour le «pull-push». B correspond à une β-alanine.

Des études par RPE ont été réalisées (Figure III-5). Une compétition entre Aβ, les ligands, le Cu(II), avec ou sans Zn(II) a été étudiée. Les résultats montrent qu'en absence de Zn, L retire 60 % de Cu(II) d'Aβ, ABH 25 % et BAH 50 %. Ceci est en accord avec les données thermodynamiques. En présence de Zn, L retire 80 % de Cu(II) d'Aβ, ABH 45 % et BAH 70 %. Ces expériences montrent bien l'effet «pull-push» : le Zn tire le Cu hors du peptide et le pousse dans le ligand.

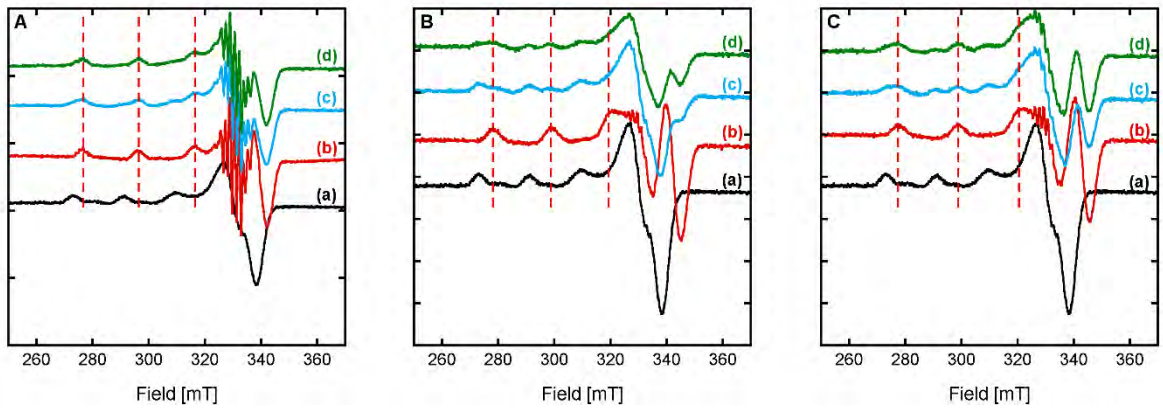

Figure III-5. Expériences RPE de compétition entre Aβ et L (Panneau A), ABH (Panneau B) ou BAH (Panneau C). (a) Aβ + Cu(II), (b) L + Cu(II), (c) Aβ + Cu(II) + L*, (d) Aβ + Cu(II) + Zn(II)-L*. (L* = L, ABH ou BAH). [L*] = [Aβ] = [Zn(II)] = 200 µM, [^{65}Cu(II)] = 190 µM, [HEPES] = 50 mM. pH = 7.1. T = 110 K. 10 % de glycérol est utilisé comme cryoprotecteur. Le temps d'incubation des échantillons pour L et ABH est de 64 h au frigo et 7 h à température ambiante pour BAH.*

Ensuite une étude par UV-Vis a également permis de mettre en évidence l'effet «pull-push» avec le ligand L. En effet, seul L a pu être étudié par UV-vis car il est le seul à avoir une intense bande d'absorption en présence de Cu(II) à 330 nm. Ainsi, le complexe Cu(II)-Aβ est formé puis L est ajouté. Lorsque l'équilibre thermodynamique est atteint, un équivalent de Zn(II) est ajouté, et ainsi de suite jusqu'à 5 équivalents de Zn(II). Les valeurs d'absorbance de Cu(II)-L en fonction du nombre d'équivalents de Zn(II) sont regroupées dans la Table III-2, ainsi que les pourcentages de Cu(II) lié à L. Notons qu'en absence de Zn(II), la quantité de Cu(II)-L est un peu élevée comparée aux données thermodynamiques, peut-être à cause d'une quantité initiale en L plus importante que prévu. La quantité de Cu(II)-L augmente à chaque ajout de Zn(II), pour atteindre 100 % du Cu(II) lié à L en présence de 5 équivalents de Zn(II). Cette expérience par UV-Vis permet de bien pouvoir visualiser le concept du «pull-push».

Table III-2. Tableau regroupant les valeurs d'absorbance à 330 nm de Cu(II)-L en fonction du nombre d'équivalents de Zn(II) ajoutés ainsi que les pourcentages de Cu(II)-L correspondants.

Nombre d'équivalents	0	1	2	3	4	5
Abs (330 nm)	0,28	0,30	0,32	0,34	0,35	0,36
% Cu(II)-L	78 %	83 %	89 %	94 %	97 %	100 %

Cette dernière preuve de concept repose donc sur l'utilisation des ligands de relativement faible affinité pour le Cu(II), de l'ordre de celle d'Aβ, pour retirer le Cu(II) d'Aβ. Cependant, il n'est possible de retirer qu'environ la moitié du Cu(II). La présence de Zn(II) est ici primordiale : le Zn(II) va tirer le Cu(II) hors du peptide et le pousser dans le ligand. Notons que pour cela, le ligand doit avoir une sélectivité bien supérieure à celle d'Aβ. Trois ligands ont été étudiés pour illustrer ce concept. Un équivalent de Zn(II) permet d'augmenter la quantité de Cu(II)-ligand. Concernant L, 5 équivalents de Zn(II) sont nécessaires pour retirer la totalité de Cu(II) d'Aβ. Cependant, *in vivo*, ceci ne devrait pas poser de problème puisque la concentration en Zn(II) dans la fente synaptique serait 10 à 100 fois supérieure à celle en Cu.

Un ligand «pull-push» dans le cadre de la MA est intéressant. En effet, puisqu'il a une relativement faible affinité pour Cu(II), il ne pourra pas retirer les ions Cu essentiels des métalloprotéines, sauf dans un environnement riche en Zn comme dans les fentes synaptiques. Ainsi, le concept du « pull-push » est une stratégie de prodrogue.

IV. Conclusion

Cette thèse s'est focalisée sur l'étude de nouvelles preuves de concept concernant la chélatothérapie du Cu dans le cadre de la MA. Quatre nouveaux critères à prendre en compte dans la conception de ligands contre la MA sont proposés et regroupés dans la Figure IV-1.

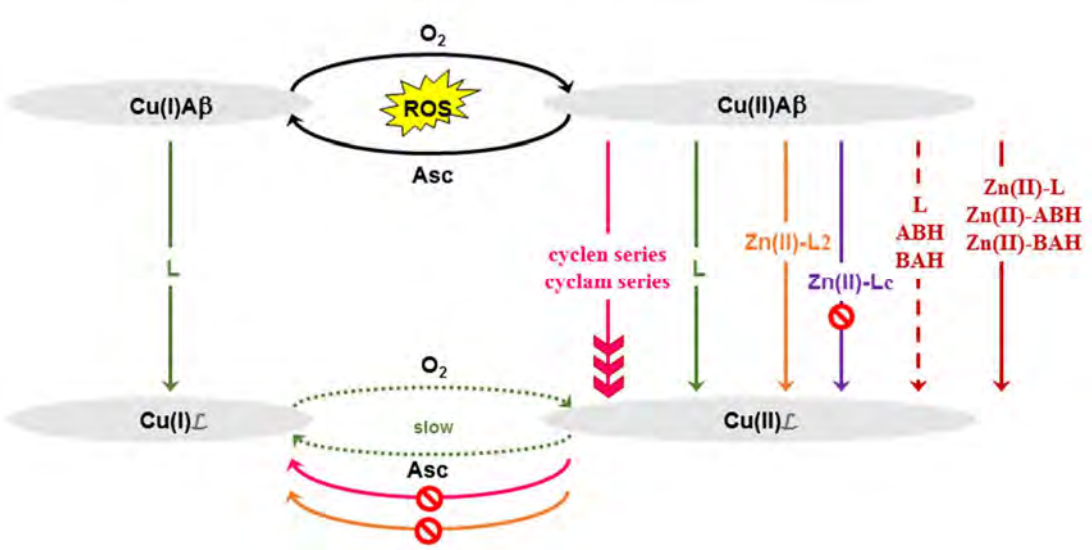

Figure IV-1. Schéma synthétisant les différents ligands et concepts étudiés au cours de cette thèse.

Le premier concerne la cinétique de captation des ions Cu par le ligand (Figure IV-1, rose). Deux séries de ligands macrocycliques sont étudiées. Il en découle que la géométrie du complexe a un impact sur la cinétique de chélation. En effet, un des macrocyles, le cyclam, a une cinétique de chélation du Cu(II) très lente dans nos conditions comparée à celle du cyclen. De plus, le cyclam chélate le Cu(II) dans sa cavité macrocyclique, alors que le cyclen le chélate hors de sa cavité. Ainsi, la géométrie du complexe est un paramètre important pour le design du ligand. De plus, en vue d'améliorer la cinétique de captation, des bras picolinates ont été greffés sur les macrocyles. Les expériences menées ont montré que ces bras accéléraient la captation des ions Cu par le ligand. Ainsi, cette première preuve de concept met en avant l'impact de la cinétique de captation, mais également l'importance du design du ligand.

Le second critère proposé ici est le fait que le ligand puisse cibler à la fois le Cu(I) et le Cu(II) (Figure IV-1, vert). Ceci est important puisque le degré d'oxydation du Cu dans la fente synaptique n'est pas connu. Cependant, un tel ligand a la possibilité de chélater le Cu(I) et le Cu(II), il est donc possible qu'il cycle facilement entre ces deux états redox et donc qu'il produise des ERO. Le ligand étudié dans cette

partie est en effet capable de retirer Cu(I) et Cu(II) d'Aβ. Cependant, il ne produit pas d'ERO. Ceci serait dû au fait que les deux coordinations et géométries sont différentes, et donc le passage redox d'un complexe à l'autre est lent. A nouveau, ce critère est important à prendre en compte dans le design de ligands.

Le troisième critère concerne la thermodynamique, notamment l'impact que peut avoir le Zn(II) sur la chélation du Cu (Figure IV-1, orange et violet). En effet, pour qu'un ligand puisse retirer le Cu(II) d'Aβ en présence de Zn(II), il doit avoir une sélectivité, c'est-à-dire un rapport d'affinité entre le Cu et le Zn, supérieure à celle d'Aβ. Dans le cas contraire, comme l'a montré l'étude des deux ligands L2 et Lc, le Cu(II) reste lié au peptide entrainant la toxicité relative à Cu-Aβ.

Enfin, la dernière preuve de concept proposée ici est le concept du «pull-push» (Figure IV-1, rouge). Il s'agit d'un ligand avec une affinité pour le Cu de l'ordre de celle d'Aβ, mais avec une sélectivité supérieure. Trois ligands ont été étudiés pour illustrer ce concept. En absence de Zn(II), le ligand ne peut retirer qu'environ la moitié de Cu(II) d'Aβ. En présence de Zn(II), le ligand retire plus que la moitié de Cu, voire la totalité. Ce concept est intéressant dans la chélatothérapie du Cu contre la MA puisqu'il permet d'utiliser des ligands qui ne peuvent pas retirer le Cu des métalloprotéines, excepté en présence de Zn(II), comme dans les fentes synaptiques.

Ensuite, des études concernant l'impact des ions Zn(II) sur la cinétique de captation ont été commencées. Dans certains cas, les ions Zn(II) sont chélatés par le ligand en premier, et leur vitesse de dissociation étant très lente, empêchent le retrait du Cu(II) d'Aβ. Il serait intéressant d'étudier aussi des ligands permettant d'illustrer la deuxième catégorie de ligands du concept du « pull-push », les ligands avec une faible affinité pour Cu(II) ; de regarder l'impact du « pull-push » avec le Cu(I).

Plus tard, il sera intéressant de combiner ces critères avec ceux déjà existants (en particulier la capacité à passer la BHE, la toxicité intrinsèque du ligand et du complexe) dans un seul ligand et de tester la capacité de ce nouveau ligand dans le cadre de la MA. Sûrement, d'autres critères seront à ajouter pour enfin trouver LE ligand contre la MA. On pourrait penser à l'excrétion du complexe de Cu(II) et donc au passage du complexe de la BHE, mais également à d'autres critères tels que l'impact des autres biomolécules environnantes ou des autres ions métalliques présents dans la fente synaptique.

General introduction

Alzheimer's disease (AD) is the most common neurodegenerative disease. Elderly people are the most affected by this disease. Nowadays, there is no known cure and this is an important issue, especially since life expectancy continuously increases. There is an important need to discover drugs against AD. This disease is difficult for the patients but also for their families, friends and caregivers. The patient can exhibit memory losses, troubles in the spatio-temporal framework, troubles in speaking, etc. Sometimes, patients can become aggressive. In the late stage of AD, the deleterious effects on the brain lead to the death of the disease's sufferers.

In the AD brains, different events happen. This thesis focuses on the formation of the senile plaques, between the neurons, precluding the synaptic connexions. These plaques are mainly composed by the Amyloid-β (Aβ) peptide and metal ions such as Cu and Zn ions. The Aβ peptide aggregates into the senile plaques following different steps. Furthermore, there is a dyshomeostasis of the Cu and Zn ions. The most supported hypothesis is that Cu ion level is too low intra-cellulary, while in excess extra-cellulary. For Zn ions, the tendency is not clear. Another important parameter of AD and under focus in this thesis is the Reactive Oxygen Species (ROS) production catalysed by the Cu-Aβ complex. A too high concentration of ROS is deleterious for the surrounding biomolecules, such as the neuronal membranes. Cu(II)-Aβ can be reduced by a reductant such as ascorbate and re-oxidized by dioxygen, leading to the ROS production.

Different therapeutic approaches against AD exist. Cu chelatotherapy is one of them. The idea is to develop Cu(II) ligands, able to remove Cu ions from Aβ and to stop associated deleterious events (ROS, aggregation, etc.). Many ligands have already been studied, and the most developed ones are clioquinol and PBT2. They went through clinical trials but failed in Phase II. This failure can be due to a lack a selectivity (*i.e*. the ratio between the affinity constant for Cu(II) and the one for Zn(II)) of Cu over Zn ions: they are able to chelate Cu and Zn ions, with a high affinity constant. This thesis focuses on the Cu chelatotherapy and proposes new concepts regarding criteria that have to be fulfilled by the ligand in order to remove Cu ions from Aβ and stop ROS production.

In the first part of this thesis, general features of AD are described. The clinical signs, the risk factors, the histopathological hallmarks and the different diagnostic tools are presented. Then, the

different interactions between Aβ and the metal ions are detailed. The available symptomatic drugs as well as the therapeutic approaches against AD are reviewed.

In the second part of this thesis, the Cu chelation is under focus. After a description of the different ligands used in chelatotherapy, an unexplored study is shown aiming at answering the following questions:

- Does the kinetic of Cu chelation by a ligand have an impact on the ROS production catalysed by Cu-Aβ complex? Note that during the ROS production, Cu oscillates rapidly between Cu(II) and Cu(I) and most of the chelators described up to now target only Cu(II).

- How is it possible to avoid that the ligands fail in the removal of Cu ions due to kinetic reasons (despite thermodynamically favoured) when designing a ligand against AD?

- Does the complex geometry have an impact on the kinetic of the Cu chelation?

Finally, another point is addressed. The redox state of Cu ions in the synaptic cleft is not well known and during the ROS production, Cu ions do redox cycle.

- Which redox state of Cu ions should be targeted by the ligand to efficiently remove Cu ions from Aβ? Cu(I), Cu(II) or both?

- Is it possible to target both redox states?

- If yes, is there a risk that the Cu-complex formed with the ligand itself can produce efficiently ROS by cycling between Cu(I) and Cu(II)? What parameters have to be considered?

This part answers to these questions with a ligand able to chelate both redox states.

The last part of this thesis focuses on the impact of Zn ions on the Cu chelation by a ligand from Cu-Aβ complex. Indeed, the concentration of Zn ions in the synaptic cleft is often 10 to 100 times higher than the one of Cu ions in the synaptic cleft. There is a possibility for the ligand to chelate Zn ions instead of Cu ions. Therefore, the “healthy” Zn(II) will be removed from the synaptic cleft where it is essential, while the “toxic” Cu ion will stay bound to Aβ in the synaptic cleft, producing ROS. First, a state of the art regarding the mutual interactions of Cu and Zn ions with Aβ is reported. Coordination, ROS production, aggregation and chelation are the key points of this review of literature. Then, a first study illustrates the importance of thermodynamic equilibria in the Cu chelation therapy and addresses the following issues. In the absence of Zn(II), a higher affinity constant for Cu of the ligand than Aβ is sufficient to remove Cu ions from Aβ (if the kinetic is favourable)

- Is it also the case in the presence of Zn ions?

Finally, the last part of this section illustrates a last new concept: the “pull push” effect.

- Is a ligand with an affinity constant for Cu in the same range than Aβ able to remove totally Cu from Aβ?

- Can Zn(II) help the ligand to chelate Cu ions from Aβ in this case?

Finally, a general conclusion answers these questions and proposes some perspectives with respect to the Cu chelatotherapy against AD.

Chapter I: Context of the project

This chapter focuses on the description of Alzheimer's disease, with the prevalence, the different symptoms, the risk factors, the histopathological hallmarks and the different diagnostic tools. Then this first chapter details one of the hallmarks of the disease, the senile plaques which are made of the Amyloid-β (Aβ) peptide and the interactions of Aβ with different metal ions present in the brain. Later on, the current treatments and therapeutic approaches are reported. Finally, the objectives of the present study are described.

I-A Alzheimer's disease

I-A.i Prevalence and symptoms

Alzheimer's Disease (AD) has first been described by Alois Alzheimer in 1906 with the case of a 51-years old woman, dead after four and a half years of illness.[1] It is the most common neurodegenerative disease worldwide and represents 50 to 80 % of all dementia. More than 35 million people are affected by the disease and this prevalence is estimated to triple by 2050, due to the increase of life expectency.[2] Different stages of the disease have been identified.[3] In the early-stage, people are able to work, to drive, to have social relationships, etc. They are still independent. Nevertheless, they have some trouble memories, such as familiar words or the location of everyday objects. The middle-stage, is generally the longest stage of the disease. Patients are suffering from important memory loss. They can have, for example, troubles in the spatio-temporal framework. Difficulties in expressing or performing routine tasks are also common symptoms. In addition, AD persons can have some behavioural changes. In the late-stage, people have difficulties in speaking, walking, or doing everyday actions. Furthermore, their memory and cognitive skills are worsened.

I-A.ii Risk factors

The age of the population is the most important risk factor. The prevalence[a] of AD is estimated to be 4.4 % by people of 65 years-old and more in Europe.[4] Note that this figure has been given in 2000 and from our best knowledge, more recent studies don't exist. Only figures from the USA appear

[a] The prevalence is a percentage of the number of cases in the population.
[b] The incidence is the number of new cases in a given period in the population.

regularly.[5] For example, in 2017, in the USA, around 5.5 million people are affected by AD, where 4 % of AD patients are less than 65 years-old, 16 % between 65 and 74 years-old, 44 % between 75 and 84 years-old and 38 % are more than 85 years-old. Note that the total percentage is higher than 100 due to the rounding.[5] The annual incidence[b] rate of AD is given age by age in the Figure I-1. These figures are alarming due to the increasing life expectancy and the lack of cure.

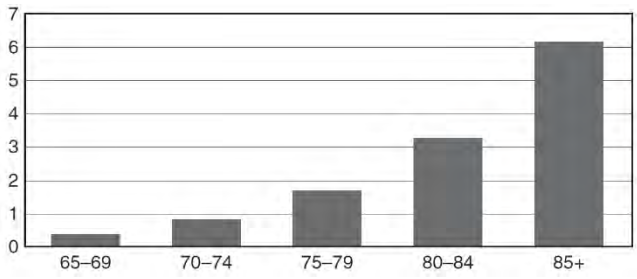

Figure I-1. Graphic illustrating the annual incidence rate by age of AD for 100 persons-years. Figure from ref.[6]

It is not well defined whether the gender is a risk factor of AD.[7] Indeed, estrogen seems to play a neuroprotective role, with an unknown mechanism.[7] After the menopause, woman serum contains less estrogen than man serum, the latter should have more neuroprotectors than woman serum. Some clinical trials of hormone replacement therapy have been performed, with no clear trend. Nevertheless, women are known to live longer than men. Therefore, they rich the "Alzheimer age" risk more often than men, and so they are more exposed to the disease than men (in this case, the age is the risk factor).

Other studies have demonstrated that the prevalence of the disease can decrease with a better way of life.[8-10] Indeed, diabetes mellitus, mid-life hypertension, depression, physical inactivity, smoking and cognitive inactivity are also risk factors of AD that can be prevented.[8-10] Moreover, the obesity is also a risk factor of Alzheimer's disease.[11] Chronic stress has been described as a potential accelerator of appearance of AD or as an effect that increases the incidence of the disease.[12] Hence, chronic stress is considered as an eventual risk factor for the disease.[12]

Some genetic modifications are also a risk factor of AD. For example, more than half of the AD patients have the APOE ε4 allele rather than the ε2/ε3 on the apolipoprotein E, the protein which transports lipids and which is responsible for the neuronal membrane care and remodelling.[13-14] Furthermore, other mutations on the Amyloid Precursor Protein (APP) for example and on Presenilin 1 and 2, which are a subunit of the γ-secretase, can be a risk factor for the disease[6, 15] (for more details on APP and γ-secretase, see § I-B.i). Table 1 summarises the different mutations found in AD patients. Other mutations on the Aβ peptide (for more details, see § I-B.i) are familial AD mutations,[16] other ones impact the amino acids involves in the metal ion coordination to Aβ.

Table 1- Table summarising the main alterations found in AD patients, from ref.[6]

Gene	Main alteration	Presumed mechanism
Amyloid precursor protein *(APP)*	Mutation	Autosomal dominant, mostly early onset
Presenilin 1 *(PSEN1)*	Mutation	Autosomal dominant, mostly early onset
Presenilin 2 *(PSEN2)*	Mutation	Autosomal dominant, mostly early onset
Apolipoprotein-E *(APOE)*	Common variant	Familial and sporadic, late onset
Sortilin-related receptor, L(DLR class) A repeats-containing *(SORL1)*	Common variant	Familial and sporadic, late onset
Clusterin *(CLU)*	Common variant	Sporadic, late onset
Phosphatidylinositol binding clathrin assembly protein *(PICALM)*	Common variant	Sporadic, late onset
Complement component (3b/4b) receptor 1 *(CR1)*	Common variant	Sporadic, late onset
Binding integrator 1 *(BIN1)*	Common variant	Sporadic, late onset

Some diseases can become a risk factor for AD. Periodontitis, among others, could be linked with sporadic late onset of AD.[17] Moreover, Traumatic Brain Injury (TBI) is also an important risk for the development of AD. Indeed, Amyloid β (Aβ) plaques have been found in the brain of 30 % of patient died of TBI.[18] Patients with Down's syndrome, or trisomy 21, have also a high risk to develop AD. This is attributed to the triplication and the over-expression of the APP gene located on chromosome 21.[19]

I-A.iii Histopathological hallmarks

There are three main histopathological hallmarks of AD. One of them is the loss of mass of the brain.[20-21] The size of the brain is diminished particularly in the brain regions involved in memory and in learning (Figure I-2). For example, the hippocampus suffers from a volume reduction of ~ 12 % each year.[22] This is due to the degeneration of the synapses and the death of the neurons.

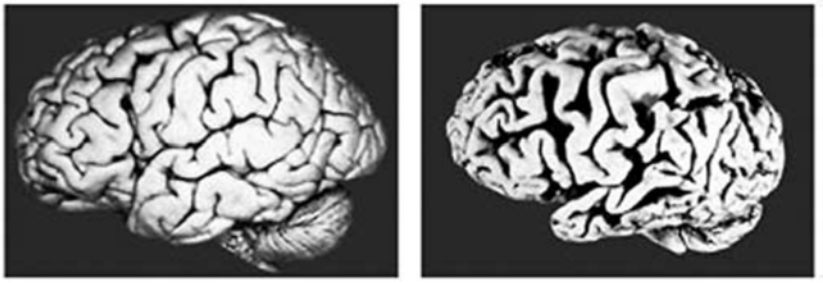

Figure I-2. Comparison between a normal brain (felt) and an AD brain. The loss of mass is easily notable on these pictures. Pictures adapted from ref.[21]

The neurofibrillary tangles of Tau protein are another histopathological hallmark of the disease.[23] This protein plays an important role in the stabilization of the microtubules as well as in the microtubule assembly. In the AD brain, this protein is hyperphosphorylated. Tau aggregates in the neuron into pair-helical filaments and then accumulates into neurofibrillary tangles.[23] The protein is not able to perform its roles and this leads to the apoptosis of the neurons. A scheme of this hallmark of AD is presented in Figure I-3.

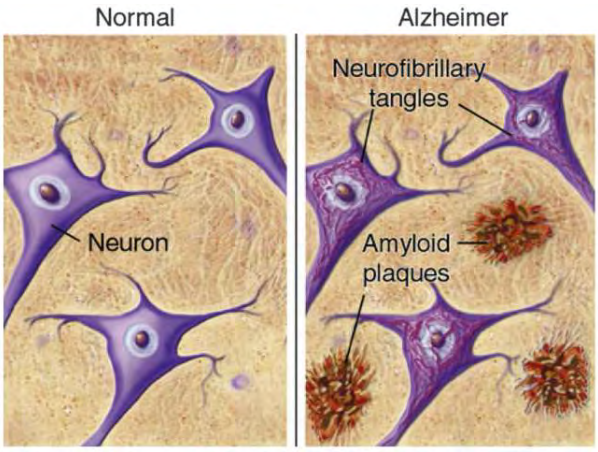

Figure I-3. Scheme representing the different hallmarks of the Alzheimer's disease. In an AD brain, neurofibrillary tangles of Tau protein and Amyloid plaques are present. Scheme from ref.[24]

The other important histopathological hallmark of AD is the senile plaques, also called amyloid plaques.[25] They mainly consist of the aggregated Amyloid-β (Aβ) peptide (for more details on the Aβ peptide and its aggregation, see § I-B). These aggregates are formed in the extracellular medium, between the neurons (Figure I-3). These plaques preclude the synaptic connection and thus can lead to the neuronal death. The research project presented here focuses on this aspect of the disease: the Aβ peptide and the senile plaques. There is no investigation on the Tau protein in this thesis.

I-A.iv Diagnostic tools

Diagnosing AD is not trivial: this disease has to be differentiated from other dementias. For an early detection, clinical tests are performed on the patients.[26-27] It exists the subjective memory complaint (SMC) test, the assessment of the late-onset depression, the speech testing, the olfactory testing, the eye testing, and the gait testing (there is a decrease about 50 % of the gait speed between a healthy people and an AD severe patient).[26] A blood test is also important in the diagnostic. Indeed, as about 500 mL of cerebrospinal fluid (CSF) is absorbed in the blood every day, biomarkers of AD could be detected in the blood.[26] Many biomarkers such as total cholesterol, plasma Aβ42/Aβ40 ratio, increased expression of inflammatory cytokines, etc., can be detected. The accuracy of blood test diagnostic is quite high: between 70 and 90 % depending on the biomarkers used. If the psychometric tests converge towards AD diagnostic, neuroimaging and CSF analyses are performed.[27] Indeed, not all

of these tests are sensitive for AD but for cognitive disorders in general.[26] They are not enough to diagnose AD with precision. For example, if these tests are performed on a neurodegenerative disease patient and on an AD patient, the diagnostic will not be clear on the nature of the dementia. More investigations towards a specific diagnostic are in progress.[26]

AD Neuroimaging Initiative (ADNI) has begun in 2005.[27] The neuroimaging of AD is divided in two main techniques: the Positron Emission Tomography (PET) and the Magnetic Resonance Imaging (MRI).[27] The functional MRI techniques are based on the functional integrity of brain networks involved in cognitive domains.[28] The structural MRI techniques are based on the progressive brain atrophy and/or on the changes of the tissue involved in AD.[28] These techniques allow for example to detect a change in the hippocampus volume or in the ventricular volume, or also in the integrity of the white matter.[28-29] Nevertheless, cerebral atrophy is not specific to AD. Therefore, MRI needs a complementary technique, such as PET imaging. PET is a nuclear medicine imaging technique, based on the detection of the gamma ray. A radionuclide emits positrons β^+ during its radioactive decay, the positron towards some distance before encountering an electron, causes an annihilation event, emitting two gamma rays in the opposite direction. In the examples given below, the radionuclides are ^{11}C, ^{18}F or ^{64}Cu. There are two main types of PET imaging methods for AD detection: the molecular imaging and the metabolic imaging.[27, 29] The first one is used in AD for the detection of Aβ deposits. The first human trial for the detection of Aβ plaques by PET is described by Klunk *et al.*[30] in 2004; it is the Pittsburgh compound B (PiB), a neutral 2-aryl-benzothiazole derivative labelled with the ^{11}C (Figure I-4). PiB compound was designed to bind the Aβ deposits.

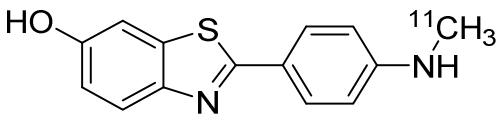

Figure I-4. Representation of the Pittsburgh compound B (PiB) used for the Aβ PET imaging.

The Figure I-5 top shows PiB-PET images of a healthy and an AD brains. In the control brain, there is no specific retention of PiB, whereas in the AD brain, there is a high PiB retention. This shows that Aβ deposits are present in the AD brain and not in the healthy brain, as expected. Note that in the regions of the brain which are not involved in AD, there is no retention of PiB both in the control brain and in the AD brain. PiB images should give quantitative information on the amyloid deposits. The limitation of this molecule is the short half-time of its radionuclide which is around 20 minutes. New molecules targeting Aβ deposits,[28, 31] such as ^{18}F-BAY94-9172,[32] ^{18}F-AV-45,[33-34] or also PiB ^{18}F derivatives[35-36] are emerging and have the radionuclide ^{18}F which has a longer life-time around 1.8 h. More recently, molecules targeting amyloid deposits with the radionuclide ^{64}Cu were developed.[37] The

half-time of the ^{64}Cu is much higher than the other two ones, around 12.7 h facilitating the PET imaging. Note that molecules targeting Tau deposits are currently under investigations as well.[28-29, 31] Other ^{64}Cu complexes for PET imaging are also developed for the detection of Cu ion deficiency, because Cu dyshomeostasis has been linked to AD.[38-39]

The metabolic imaging uses the Fluorodeoxyglucose PET (FDG-PET).[21, 28-29] It is a glucose molecule with a ^{18}F. The difference between both brains shown in Figure I-5 (bottom) regarding the ^{18}FDG uptake is tremendous: there is an important hypometabolism in the case of the AD brain. This technique is very sensitive,[29] but not specific enough. Indeed, the glucose retention in the brain can be altered by many phenomena. Therefore, performing PiB PET and ^{18}FDG PET allows a more accurate diagnostic of AD.

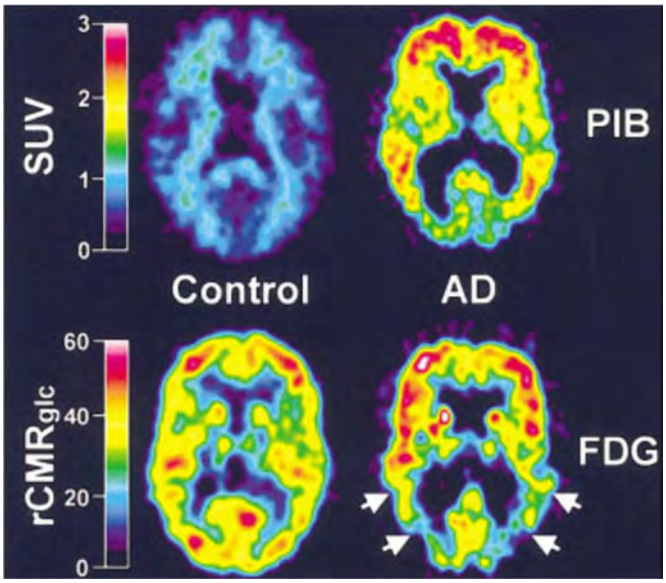

Figure I-5. PiB-PET images (top) and FDG-PET images (bottom) of a 67-years old healthy person as a control and of a 79-years old AD patient. A three-day delay exists between PiB and FDG-PET images. For the PiB-PET standardized uptake value (SUV) images (top), the images are summed over 40 to 60 minutes. In the healthy brain, there is no retention of PiB, contrary to the AD brain. This means that the healthy brain does not expose Aβ aggregates whereas the AD brain does. For the FDG-PET images (bottom), regional cerebral metabolic rate for glucose (rCMRglc) images (in mol.min^{-1}.100 ml) show a normal ^{18}FDG uptake for the healthy brain and a hypometabolism in the case of the AD brain (arrows). Figure from ref.[30]

Another technique can be performed: the CerebroSpinal Fluid (CSF) assay.[27, 29, 40-41] It consists in detecting CSF biomarkers such as Aβ42, Tau and phosphorylated Tau. Contrary to the PET imaging in which accumulation of Aβ could be detected, in the CSF assay, a decrease in the Aβ concentration is observed due to its aggregation in the synaptic clefts.[42] But CSF assay could be less reliable because Aβ levels can fluctuate.[29] The Aβ accumulation biomarkers used in PET imaging can also be used in the CSF assay. Biomarkers for neuronal injury or neurodegeneration are also developed.[42]

In brief, after the psychometric tests, the CSF assay, the MRI, the PET targeting Aβ such as PiB-PET, the Cu-PET and the FDG-PET are complementary tools and allows a quite accurate diagnostic of AD.[31]

I-B The Amyloid-β peptide and metal ions

I-B.i Aβ peptide

The Aβ peptide derives from the Amyloid Precursor Protein (APP).[25, 43-45] APP is a transmembrane protein with 695 amino acids in its predominant form.[44] The physiological role of the APP is still unclear. It was first described as a receptor at the cell-surface, but it is now considered as a cell adhesion biomolecule, involved in neuronal development and synaptogenesis.[46] APP can be cleaved by three enzymes. In the amyloidogenic pathway, APP is first cleaved by the β-secretase and then by the γ-secretase (Figure I-6). The residual extracellular peptide is the Aβ peptide.[25, 43-45] There is also a non amyloidogenic pathway, involving the α-secretase, avoiding the formation of the full length Aβ peptide.[44]

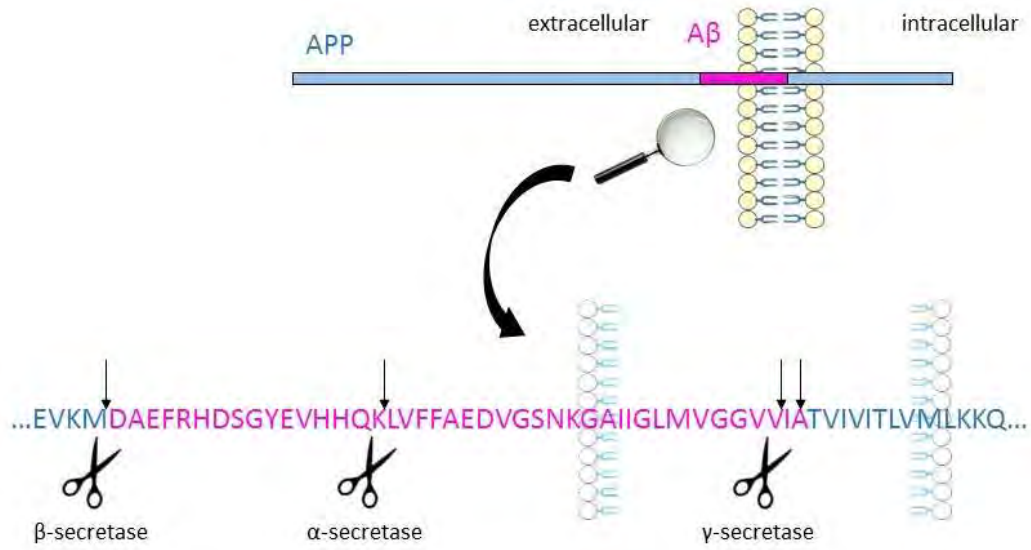

Figure I-6. Scheme representing the formation of the Aβ peptide. The APP protein is cleaved by two secretases, leading to the extracellular Aβ peptide. The sequence of the Aβ peptide is written in pink.

The Aβ peptide is a 38 to 43 amino acid residue sequence.[25] The first sixteen N-terminal amino acids form the hydrophilic part which is responsible for the metal ion coordination. The amino acids in the hydrophobic part of the peptide are responsible for the aggregation further leading to the so-called senile plaques. Note that the Aβ peptide can exhibit some mutations linked to the familial early-onset AD case,[25] and some truncations such as Aβ4-x or Aβ11-x.[47]

I-B.ii Metal ions

Many metal ions are present in the living beings. This study focuses only on the Cu and Zn ions. Copper is an essential metal ion.[48] In the human body, Cu is the catalytic centre in many enzymes.[48-50] For example, it is the catalytic centre of the Superoxide Dismutase, a (Cu, Zn) enzyme responsible for the regulation of the oxidative stress, *via* dismutation of the superoxide. Cu ions can also be found in proteins for their transport to the catalytic enzyme or also for their storage. Principally, Cu ions are involved in electron transfer processes or in the binding / activation / reduction of O_2 in human bodies.[49] On the other hand, Cu ions, due to their redox ability, are able to produce Reactive Oxygen Species (ROS).[51] ROS are very deleterious for the surrounding biomolecules and when they are over-produced, they contribute to oxidative stress. This is the reason why Cu ion concentration is tightly regulated. Many Cu-proteins exist: specific transporters which stabilize one redox state of Cu or the other as for example hCTR1[52] and ATP7A[53-54] involved in the Cu uptake and release into and from human neurons (Figure I-7); specific metal ion delivery proteins such as metallochaperones which protect Cu ions from scavengers, etc.[51] Cu ions play also an important role in neurotransmission.[55] Their tight regulation is also required for the neuronal health. In AD brains, the Cu homeostasis is deregulated.[56-60] Cu levels in the CSF are higher,[61] while they are lower in the hippocampus and in the intracellular medium[55, 62] in AD brains compared to healthy brains. This Cu ion dyshomeostasis may be one of the key event of AD.

Zn(II) is also an essential ion. It plays many roles, including regulatory, structural and enzymatic fonctions.[63] Moreover, it is the most abundant “trace metal” in the brain.[60] Its concentration in the synaptic cleft is high but not precise, depending the synaptic transmissions. It can reach 10 to 100 µM during its release from the vesicles into the synaptic cleft.[56] Zn homeostasis is well regulated, by several Zn transporter families. Intracellular concentrations of Zn(II) are decreased by the ZnT family whereas the ZIP family brings Zn ions from the extracellular medium to the cytoplasm (Figure I-7).[60, 64] Zn(II) is a modulator of the neurotransmittion. For example, it is released in the synaptic cleft, modulating receptors for the regulation of the activity of the glutamatergic synapses, like Cu ions.[59-60] In AD brains, there is also a Zn(II) dyshomeostasis. [56, 59-60] However, the tendency of the modification of Zn(II) concentrations is not clear: both decreased and increased concentrations are found in the hippocampus, in the serum and also in the CSF of AD patients.[60] Hence Zn(II) dyshomeostasis is linked to AD, but it is not clear how and to which extent.

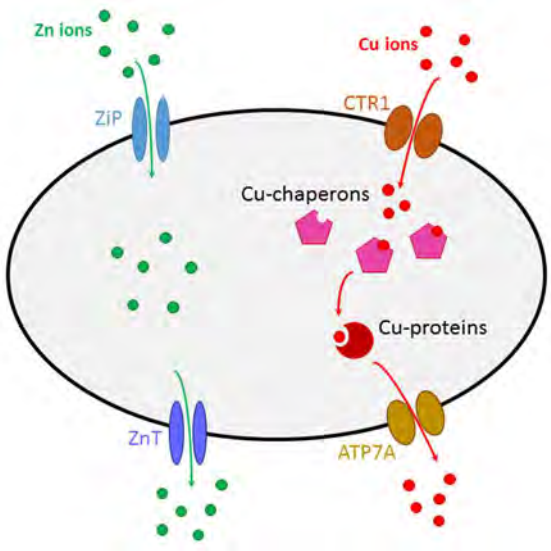

Figure I-7. Scheme illustrating the Cu and Zn ions regulation/uptake in neurones.

I-B.iii Interaction between Aβ and the metal ions Cu(I/II) and Zn(II)

As previously explained, Aβ peptide and dyshomeostasis of metal ions such as Cu(II), Cu(I) and Zn are linked to the aetiology of AD. The study of their interaction is thus biologically relevant. Indeed, metal ions have been detected in the senile plaques at high concentration: about 1 mM of Zn and about 400 µM of Cu ions and Aβ contains amino-acid residues able to bind metal ions.[65]

I-B.iii.1 Coordination and affinity constants

The first step in the study of the interaction between Aβ and Cu and Zn ions is the metal ion coordination and the determination of their affinity constants. Note that these studies have been mostly performed on the monomeric and C-terminally truncated Aβ. Indeed, as explained previously, the metal ion coordination involves the first sixteen N-terminal amino acids of Aβ. Therefore, the Aβ16 encompassing the first sixteen amino acids is a good model[58] and is used for these investigations.

Cu(II) coordination to Aβ monomers has been studied by many groups and reviewed.[58, 60, 66-68] Many spectroscopic techniques have been used. Depending on the pH, different Cu(II) coordination sites exist. Only those present around the physiological pH are described here. Figure I-8 (top) describes the main components of Cu(II)-Aβ near physiological pH. In Component I, Cu(II) has five ligands: the N-terminal amine, the O atom from the first peptidic bond and two N atoms from His6 and His13 or His14. There is a dynamic exchange between His13 and His14. On the apical position, there is one carboxylate group from the side chain of Asp1, Asp7, Glu3 or Glu11, with a preference for Asp1 *via* a H-bond and a water molecule.[69] In Component II, the five ligands are: the N-terminal amine, the

N^- from the first peptidic bond, the O atom from the second peptidic bond and a N atom of an imidazole side chain from one of three His residues. There is also a dynamic exchange between those three His. On the apical position, one of the 4 carboxylate groups from the side chain of Asp1, Asp7, Glu3 or Glu11 completes the coordination sphere of Cu(II). At pH 7.4, the affinity constant for Cu(II) of Aβ is about 10^{10} M^{-1}.[70-72] The evaluation of this affinity constant has been investigated by different groups. This is an important parameter for the design of ligands for chelation therapy approach because they need an affinity constant for Cu(II) higher than Aβ. Many works had been carried out and the affinity constant values ranged from 10^6 M^{-1} to 10^{19} M^{-1} at pH 7.4. But more recently, a consensual value was proposed near 10^{10} M^{-1} at pH 7.4. Most of these studies used potentiometric titrations, isothermal calorimetry, and fluorescence or competition experiments.

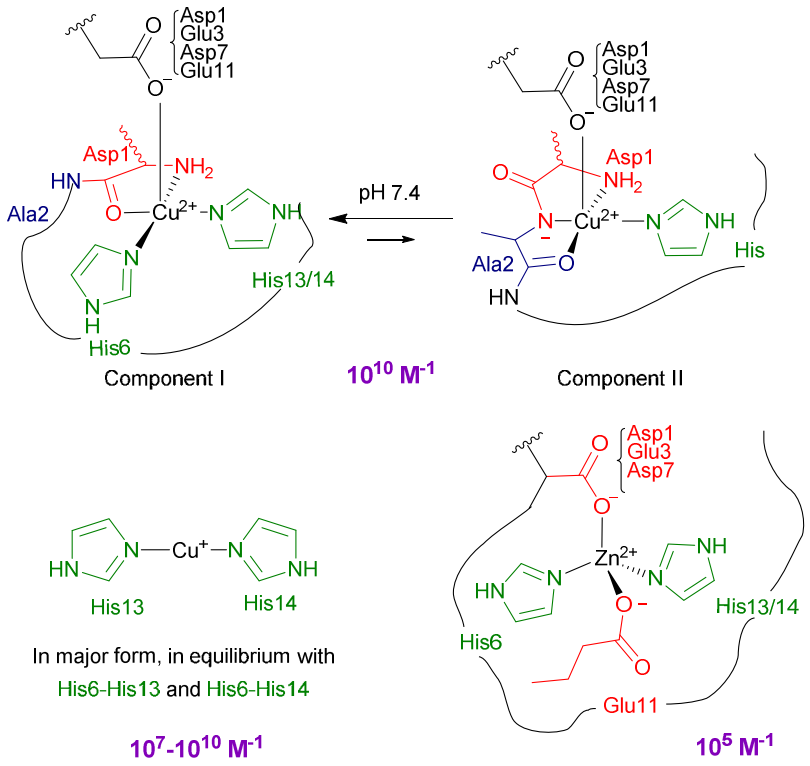

Figure I-8. Representations of the different metal ion coordination to the Aβ peptide at physiological pH 7.4. The affinity constants are given at pH 7.4. Figure adapted from ref.[73]

During this PhD work, a competition experiment with an UV-Visible competitor **L**, a 3,4-bis(oxamato)benzoic acid ligand, has been investigated.[74] This technique is easy to handle and to perform due to the intense absorption of Cu(II)-**L** at 330 nm, and it rapidly gives a value for the affinity constant of the target molecule. Once the affinity constant for Cu(II) of the used competitor **L** has been determined, the affinity constant of Aβ for Cu(II) can be measured by a competition for Cu(II) between Aβ and **L**. Using a home-made fitting of the competition data, an affinity constant of Aβ for Cu(II) of 1.6 x 10^9 M^{-1} at pH 7.1 has been obtained in line with value obtained by potentiometry by another group[71]

and in line with the value of 10^{10} M^{-1} reported at pH 7.4. Then, the affinity constant for the entire peptide Aβ40 is determined by the same way, and the value is closed to the Aβ16 peptide. The same experiment has been performed on a wide series of Aβ16 mutants; the mutations focusing on the amino acids involved in the Cu(II) coordination. The affinity constants obtained for each mutant are in line with the Cu(II) binding site of Aβ determined by spectroscopic studies. These experiments also show that **L** is a good competitor to determine the affinity constant of peptides or proteins with a moderate affinity constant for Cu(II). This study is given in Annexe A of this manuscript.

Cu(I) coordination to Aβ peptide has also been studied by several groups.[75-79] All converge towards a linear coordination (see Figure I-8, bottom left) between two His residues. The predominant form involves the N atoms from His13 and His14, in equilibrium with the coordination by His6 and His13 or His6 and His14. The affinity constant of Aβ for Cu(I) has also been determined by competition experiment assay with Ferrozine (Fz).[72, 80-81] Two values at physiological pH are found: $10^{10.4}$ M^{-1} [72, 81] and $10^{6.9}$ M^{-1}.[80] Such difference is due to the two different values of the affinity constant of the reference $Cu(I)(Fz)_2$ used for the competition studies. More studies have to be performed to determine the precise value of the affinity constant for Cu(I) of Aβ.

Regarding the Zn(II) coordination by Aβ peptide, different models have been proposed and in most of them, the N-terminal amine was involved.[82-84] Nevertheless, our recent multi-technical study[85] demonstrates that the N-terminal amine is not in the Zn(II) coordination sphere at pH 7.4 (see Figure I-8). This study has been divided in two main parts. The first one describes an EXAFS study paralleled to a NMR study used for the determination of the number and the nature of the ligands. Zn(II) is a 4-coordinated ion in the Aβ peptide, with a tetrahedral geometry. Then, XANES and NMR investigations have been performed on a wide series of Aβ16 mutants in order to determine which amino acid residue is involved in the coordination of Zn(II). If the complex Zn(II)-mutant exhibits the same XANES and NMR signals than the Zn(II)-Aβ complex, the amino acid mutated is not involved in the coordination, whereas if the signals are different, the amino acid mutated can be involved in the coordination. The ligands involved in the Zn(II) coordination are the N atom from His6, the carboxylate from the Glu11, a N atom from His13 or His14 and a carboxylate from Asp1, Glu3 or Asp7. This study is given in Annexe B of this manuscript.

The affinity constant of Aβ for Zn(II) has also been determined and the value is about 10^5 M^{-1} at pH 7.4.[86-87]

I-B.iii.2 ROS production

As previously explained, Cu ion homeostasis is essential for health. Indeed, a too weak concentration is lethal as well as a too high concentration. In the AD brains, there is a dyshomeostasis of Cu ions. Aβ peptide is able to coordinate both redox state of Cu ions: Cu(II) and Cu(I). Cu ions are able to catalyse ROS production. ROS are the products of the incomplete reduction of dioxygen by a reductant, a biologically pertinent being ascorbate.[88-91] First, superoxide ($O_2^{\bullet-}$) is produced,[92] then hydrogen peroxide (H_2O_2)[88-91] and then hydroxyl radical ($HO^{\bullet}$).[88-91] ROS are deleterious species, due to their high reactivity. Protein oxidation and lipid peroxidation are well known damages of this oxidative stress.[93-96] Figure I-9 reminds this ROS production and some methods used for their detection *in vitro*.

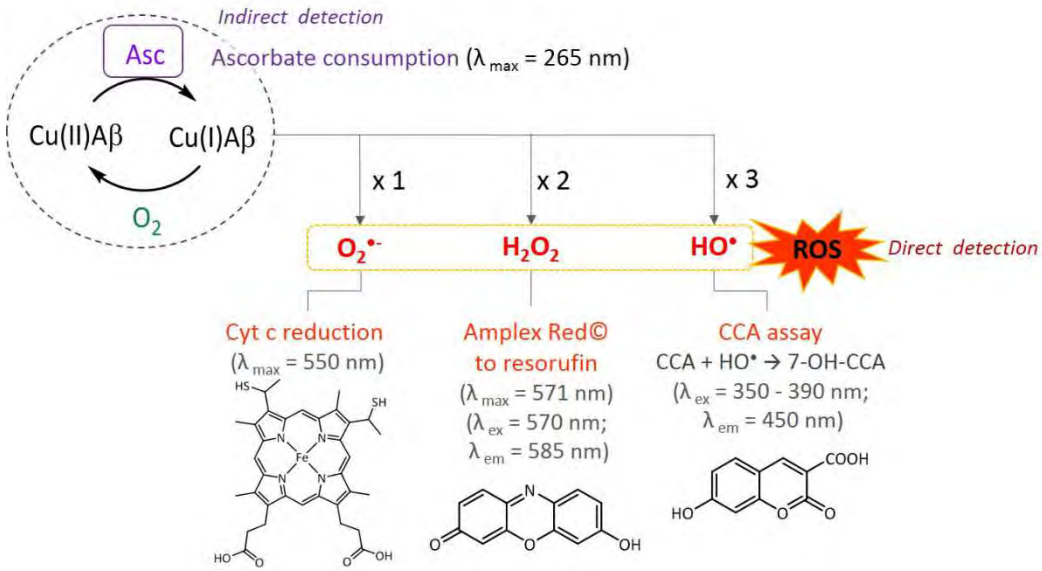

Figure I-9. Scheme representing the ROS production catalysed by the Cu-Aβ complex. The different detection methods are also reminded. Scheme from [73].

In this work, only Ascorbate consumption and 3-Coumarin Carboxylic Acid (CCA) assays were performed. The first assay consists in following the consumption of the Ascorbate, which exhibits an intense absorption at 265 nm (ε = 14 500 $cm^{-1}.M^{-1}$). The decrease in the concentration mirrors the ROS formation. The CCA assay consists in the detection of the $HO^{\bullet}$.[97] Hydroxyl radical reacts with the CCA, forming the 7-OH-CCA which is a fluorescent molecule. Under an excitation at 390 nm, 7-OH-CCA emits a fluorescence light at 450 nm. The detection of such a fluorescence is correlated to the $HO^{\bullet}$ production by the Cu-Aβ complex and O_2 in reductive conditions.

I-B.iii.3 Aggregation

The senile or amyloid plaques are one of the hallmarks of the disease. They are mainly present in or around the synaptic clefts of glutamatergic synapses of the cortex and of the hippocampus,[60] the loci of the highest Cu concentrations in the brain.[60] As previously explained in part I-A.iii, these plaques are mainly composed by the Aβ peptide and contain other molecules and metal ions such as Cu and Zn ions. Aβ is a monomeric and soluble peptide in healthy brains, and aggregates in AD brains. This aggregation process is part of the so-called amyloid cascade hypothesis.[98-103] Nowadays, this hypothesis is one of the most accepted, although still discussed.[104-107] The amyloid cascade hypothesis describes the aggregation of Aβ as the central event of the disease. This aggregation is an auto-catalytic self-assembly phenomenon.[108] Figure I-10 illustrates the aggregation process of the Aβ peptide. The kinetic of Aβ aggregation is mathematically described by a sigmoidal curve.[47, 108] The following equation is the model for this kinetic:[109] $F(t) = F_0 + \frac{A}{1+e^{-k(t-t_{1/2})}}$, where F_0 is the baseline level before the aggregation, k is the elongation rate constant, A is the amplitude and $t_{1/2}$ is the time at half of the aggregation process.

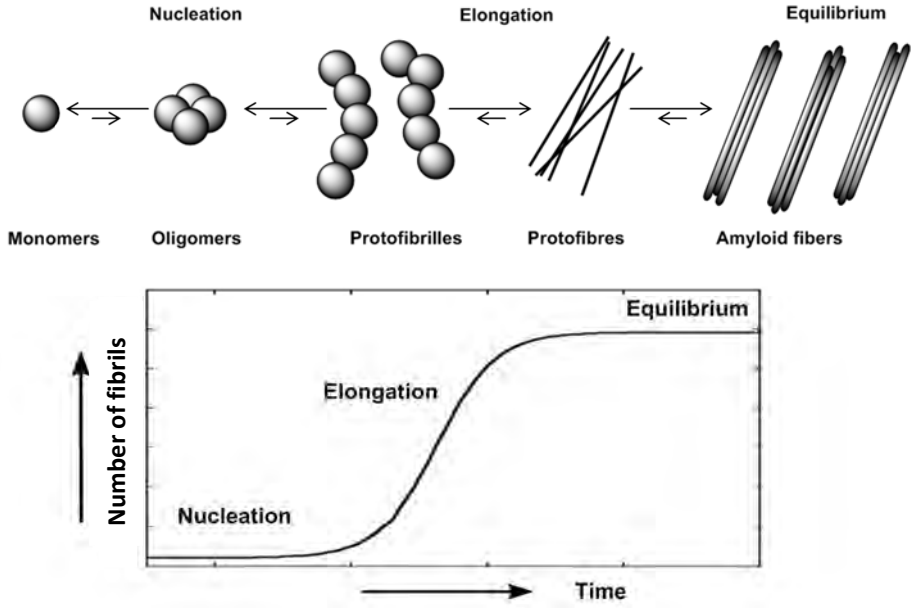

Figure I-10. Scheme describing the aggregation process and the ThT fluorescence kinetic shape for the associated experiment. Scheme adapted from [110].

The nature of the species during the aggregation process changes. The nucleation phase during which low molecular weight species such as oligomers are formed is the first phase of the aggregation. Note that oligomers have proposed to be the most toxic species of the aggregation due to their size and interaction with the membranes.[111-112] Then, there is the elongation phase during which the oligomers elongates into protofibrils and fibrils. The "plateau" or equilibrium phase is the

thermodynamic equilibrium. [47, 108] At a molecular level, the hydrophilic N-terminal part of the peptide may be involved in the aggregation process but remains mainly disordered in the fibrils. The 12 to 24 amino acid residues and 30 to 40 amino acid residues adopt β-strand conformation with electrostatic interaction between D23 and K28 in the loop of the β-strand.[113] Interaction between β-strands has been observed forming the β-sheet structure, *i.e.* there are hydrogen bonds between the peptide bonds of the hydrophobic part of the peptide along the fibril axis (β-sheet). It also exists interactions between the peptidic side chains perpendicular to the fibril axis.[108, 113] Note that in this thesis, the term aggregates defines either amorphous species or fibril species (*i.e.* amyloid species made of β-sheets).

Metal ions such as Cu and Zn ions have an impact on the aggregation of the peptide.[58, 108, 114] With the working conditions used during this thesis, Cu ions stabilize oligomers and other small aggregates which are proposed to be the most toxic species, while Zn ions lead to the fibril formation. The aggregation process depends on many conditions that is why different groups find different results.

In this work, in order to follow the aggregation of Aβ, a classical fluorescence assay is used.[115] The Thioflavin T, called ThT (see Figure I-11), is a fluorophore with a free rotation of the bond between the two aromatic moieties. ThT is able to interact with β-sheets, leading to preclusion of the free rotation. This phenomenon enhances its fluorescence. Therefore, during an aggregation experiment, the formation of β-sheets is monitored by the detection of the fluorescence. Hence, ThT fluorescence is used to monitor fibril formation. A particular caution is needed to not over-interpret the results obtained. After the aggregation experiment, different microscopies can be used, including the Atomic Force Microscopy (AFM) and the Transmission Electron Microscopy (TEM), in order to probe the morphologies of the aggregates formed.

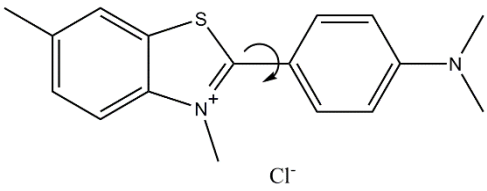

Figure I-11. Representation of the Thioflavin T dye or ThT, with the free rotation around the bond between the two aromatic rings.

I-C Current treatments and therapeutic approaches

Nowadays, there is no known cure for AD. It exists only symptomatic treatments, improving the way of life of the patients. There are few drugs available. One of the categories is acetycholine esterase inhibitors. Indeed, acetylcholine (ACh) is a neurotransmitter involved in the memory and in the learning and it is hydrolysed by the acetylcholinesterase (AChE). ACh is deficient in the AD brains.

Inhibiting the action of the AChE enzyme should increase the concentration of ACh. One of the first AChE inhibitors was Tacrine (Figure I-12) which is rarely used today due to its side effects.[116] Donepezil, Rivastigmine and Galantamine (Figure I-12) are the three AChE inhibitors currently available.[116-118] The other group of symptomatic treatment is the antagonist of the N-methyl-D-aspartate (NMDA) receptor, involved for example in the memory. When NMDA receptors are activated by glutamate for example, NMDA receptors open their channel and Ca^{2+} can enter into the neuron. Nevertheless, in AD brains, there is an excitotoxity, meaning that NMDA receptors are over activated and the concentration of Ca^{2+} that enters into the neuron is too high, leading to the degradation of the neuron.[119] The antagonists of the NMDA receptors block the channel and reduce the concentration of Ca^{2+} entering into the neuron.[119] The actual available drug is the Memantine (Figure I-12).[116-120] Some studies also propose high doses of vitamin E which is an antioxidant capable of improving the cognitive impairments,[116] but clinical trials showed no benefit.

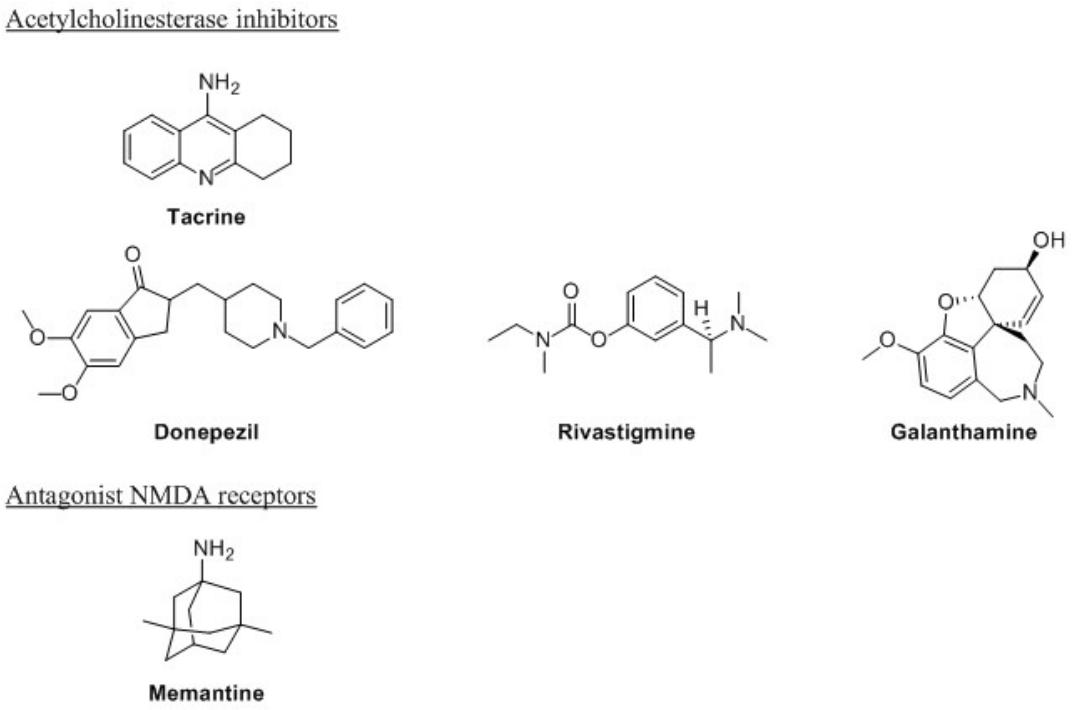

Figure I-12. The different structures of the available symptomatic drugs against AD.

Many other therapeutic approaches are currently under investigation.[121-122] Some of them concern the degradation and clearance of Aβ aggregates.[102] The immunotherapy is also highly under study.[107, 123-124] The use of antibodies targeting Aβ peptide can allow the clearance of Aβ by the immune system. The most notable immunotherapies are Bapineuzumab which is a humanized monoclonal antibody and Solanezumab which is a monoclonal antibody.[123] The first one has a high affinity for the 5 first amino acids of Aβ, and preferentially when Aβ is aggregated; the second one targets the center

of Aβ (amino acids from 13 to 28) preferentially when Aβ is monomeric. Both of them have failed in clinical trials. Another human monoclonal antibody for the clearance of Aβ which is under clinical trials and show promising results is the Aducanumab.[125] Another example of immunotherapy is the use of Interleukins 2 (IL2).[126-127] Their concentration in the hippocampus in AD brains is lower than in healthy brains. Treatment with IL2 in AD mice shows improvement in the memory.[126] This result is encouraging for the next immunotherapy investigations.

Some studies are developing small compounds to prevent the Aβ aggregation.[107] Other ones focus on the inhibition of the Aβ production via the stimulation of the α-secretase,[122] the modulation or inhibition of the γ-secretase in order to inhibit Aβ production or to induce the production of smaller Aβ peptides, not able to aggregate.[107, 122, 128] The inhibition of β-secretase is also a way to prevent the Aβ production.[107, 128] Furthermore, since the dyshomeostasis of Cu ions has been considered as a key event in the AD aetiology, the metal chelation approach is highly studied.[116, 129-132] Multi-target compounds are also developed.[122, 129, 131] The chelation moiety is linked to a moiety able to cross the BBB, or able to target Aβ aggregates, etc. It exists also therapeutic approaches concerning Tau protein, such as the inhibition of the aggregation of the protein.[121-122] Another therapeutic approach focuses on the APOE ε4 allele on the apolipoprotein E (see I-A.ii).[13] For example, using small molecules interfering with the domain interactions in APOE ε4, this apolipoprotein can be functionally and structurally converted to the APOE ε2 or 3.[13]

Many therapeutic approaches are under investigations. In this thesis, we have focused on the chelatotherapy targeting selectively Cu ions, since Cu ions are redox active and might stabilize small aggregates. Note that as Zn ions are essential in the neurotransmission and as they should be less toxic than Cu ions, they are to be kept in the synaptic cleft.

I-D Objectives of the study

Within the AD framework, Cu ion bound to Aβ in the synaptic cleft is currently considered as one of the target of choice due to its high toxicity: it is able to alter the aggregation of the Aβ peptide, leading to smaller more toxic aggregates and it is also able to catalyse ROS production. Note that these Cu ions bound to Aβ are then called “toxic Cu”. Many Cu(II) ligands have been studied, some of them have been tested in clinical trials, but failed to go through Phase III.[130, 133] One of the hypothesis explaining this failure could be the lack of Cu ion selectivity of the ligands since they are also (and mainly) able to coordinate Zn ions. Up to now, the criteria for a Cu chelator against AD are the Blood Brain Barrier (BBB) permeability, the higher affinity constant for Cu ions than the Aβ, the affinity constant for Cu ions not too high in order to not remove Cu ions from other metalloproteins, leading

to a more important dyshomeostasis (for more details, see § II-A). This study focuses on the Cu ion chelation. It is divided into two main parts.

The first part focuses on different Cu ion chelation strategies. First, a state of the art regards the strategy of using ligands, chelators or metallophores, in order to remove Cu ions from the Aβ peptide. In this thesis, a chelator is a ligand able to remove the metal ion from Aβ, while a metallophore is a chelator that redistribute metal ions into the cells where they are deficient. Their impacts on the ROS production, on the aggregation as well as their cell toxicity are reviewed. Then, two new concepts are developed. The first one detailed is the impact of the kinetic of Cu(II) removal from the Aβ peptide. Indeed, in order to remove Cu ions from the Aβ peptide, Cu ligands need a higher affinity constant for Cu ions than the one of Aβ. Nevertheless, this is a pre-requisite and could not be enough if the Cu chelation is too slow. To the best of our knowledge, this is the first time that this kinetic issue is studied in the AD context. The other proof of concept sheds light on the use of a Cu(I) and Cu(II) chelator. Indeed, nowadays, the redox state of Cu ions in the synaptic cleft is not well defined. This means that we do not know which Cu(I) or Cu(II) chelator will be the most efficient in the removal of Cu ions from Aβ. Therefore, a chelator able to remove both Cu(I) and Cu(II) is investigated in this context.

The second part focuses on the impact of Zn ions in the Cu ion chelation. This is biologically relevant since the concentration of Zn ions in the synaptic cleft should be 10 to 100 times higher than the concentration of Cu ions.[58-59] Due to this high concentration, the ligands could chelate first Zn ions, leading to an inhibition of the Cu chelation, where Cu ions are the toxic target. First, a state of the art details the different studies about the mutual interactions between Cu ions and Zn ions with the Aβ peptide, as well as in the presence of a Cu-chelator to remove Cu ions from Aβ. The coordination of these metal ions with the peptide, their affinity constants, the impact of this interaction on the ROS production and on the aggregation as well as the impact on the Cu chelation are reported. Then, the first new concept of this part is the thermodynamic issue on the Cu chelation regarding Zn ions. The impact of the selectivity for Cu ions over Zn ions of the ligand compared to the one of the Aβ peptide is described and proved experimentally. The second new concept is a “pull-push” effect, demonstrating that, with a special category of ligands, Zn ions can trigger the Cu ion removal from the Aβ peptide. In other words, the presence of Zn(II) pulls Cu ion out of the Aβ peptide and pushes it inside the ligand, Zn(II) being bound to Aβ.

In brief, the investigations reported in the manuscript show new concepts required to develop more efficient ligand in the removal of Cu ions from the Aβ peptide.

References

1. Stelzma, R. A.; Schnitwlein, H. N.; Muriiagh, F. R., An English I'ranslation of Alzheimer's 1907 Paper, "ijber eine eigenartige Erlranliung der Hirnrinde". *Clinical Anatomy* **1995,** *8*, 429-431.
2. Ising, C.; Stanley, M.; Holtzman, D. M., Current Thinking on the Mechanistic Basis of Alzheimer's and Implications for Drug Development. *Clin. Pharmacol. Ther.* **2015,** *98* (5), 469-471.
3. AlzheimerAssociation, *Basics of Alzheimer's disease* **2016**.
4. Qiu, C.; Kivipelto, M.; von Strauss, E., Epidemiology of Alzheimer's disease: occurrence, determinants, and strategies toward intervention. *Dialogues Clin. Neurosci.* **2009,** *11* (2), 111-128.
5. 2017 alzheimer's disease facts and figures. *alz.org* **2017**.
6. Mayeux, R.; Stern, Y., Epidemiology of Alzheimer Disease. *Cold Spring Harb. Perspect. Med.* **2012**, 2:a006239.
7. Janicki, S. C.; Schupf, N., Hormonal Influences on Cognition and Risk for Alzheimer's Disease. *Curr. Neurol. Neurosci. Rep.* **2010,** *10*, 359-366.
8. Barnes, D. E.; Yaffe, K., The projected effect of risk factor reduction on Alzheimer's disease prevalence. *Lancet Neurol.* **2011,** *10* (9), 819-828.
9. Norton, S.; Matthews, F. E.; Barnes, D. E.; Yaffe, K.; Brayne, C., Potential for primary prevention of Alzheimer's disease: an analysis of population-based data. *Lancet Neurol.* **2014,** *13* (8), 788-794.
10. Daviglus, M. L.; Plassman, B. L.; Pirzada, A.; Bell, C. C.; Bowen, P. E.; Burke, J. R.; Connolly, E. S. J.; Dunbar-Jacob, J. M.; Granieri, E. C.; McGarry, K.; Patel, D.; Trevisan, M.; Williams, J. W. J., Risk factors and preventive interventions for Alzheimer disease: state of the science. *Arch. Neurol.* **2011,** *68* (9), 1185-1190.
11. Letra, L.; Santana, I.; Seiça, R., Obesity as a risk factor for Alzheimer's disease: the role of adipocytokines. *Metab. Brain Dis.* **2014,** *29* (3), 563-568.
12. Machado, A.; Herrera, A. J.; de Pablos, R. M.; Espinosa-Oliva, A. M.; Sarmiento, M.; Ayala, A.; Venero, J. L.; Santiago, M.; Villarán, R. F.; Delgado-Cortés, M. J.; Argüelles, S.; Cano, J., Chronic stress as a risk factor for Alzheimer's disease. *Nat. Rev. Neurosci.* **2014,** *25* (6), 785-804.
13. Michaelson, D. M., APOE ε4: the most prevalent yet understudied risk factor for Alzheimer's disease. *Alzheimers Dement.* **2014,** *10* (6), 861-868.
14. Imtiaz, B.; Tolppanen, A. M.; Kivipelto, M.; Soininen, H., Future directions in Alzheimer's disease from risk factors to prevention. *Biochem. Pharmacol.* **2014,** *88* (4), 661-670.
15. Bilbul, M.; Schipper, H. M., Risk profiles of Alzheimer disease. *Can. J. Neurol. Sci.* **2011,** *38* (4), 580-592.
16. Barber, R. C., The genetics of Alzheimer's disease. *Scientifica (Cairo)* **2012,** *2012*, 246210.
17. Cerajewska, T. L.; Davies, M.; West, N. X., Periodontitis: a potential risk factor for Alzheimer's disease. *Br. Dent. J.* **2015,** *218* (1), 29-34.
18. Sivanandam, T. M.; Thakur, M. K., Traumatic brain injury: a risk factor for Alzheimer's disease. *Neurosci. Biobehav. Rev.* **2012,** *36* (5), 1376-1381.
19. Schupf, N., Genetic and host factors for dementia in Down's syndrome. *Br. J. Psychiatry.* **2002,** *180*, 405-410.
20. Soto-Rojas, L. O.; de la Cruz-López, F.; Ontiveros Torres, M. A.; Viramontes-Pintos, A.; Cárdenas-Aguayo, M. C.; Meraz-Ríos, M. A.; Salinas-Lara, C.; Florán-Garduño, B.; Luna-Muñoz, J., Neuroinflammation and Alteration of the Blood-Brain Barrier in Alzheimer´s Disease. In *Alzheimer's Disease - Challenges for the Future*, Intech, Ed. 2015.
21. Mattson, M. P., Pathways towards and away from Alzheimer's disease. *Nature* **2004,** *430*, 631-639.
22. Jahn, H., Memory loss in Alzheimer's disease. *Dialogues Clin. Neurosci.* **2013,** *15* (4), 445-454.
23. Grundke-Iqbal, I.; Iqbal, K.; Tung, Y. C.; Quinlan, M.; Wisniewski, H. M.; Binder, L. I., Abnormal phosphorylation of the microtubule-associated protein tau (tau) in Alzheimer cytoskeletal pathology. *PNAS* **1986,** *83*, 4913-4917.

24. Silbert, L. C., Does statin use decrease the amount of Alzheimer disease pathology in the brain? *Neurology* **2007,** *69*, 8-11.
25. Holtzman, D. M.; Morris, J. C.; Goate, A. M., Alzheimer's Disease: The Challenge of the Second Century. *Sci. Transl. Med.* **2011,** *3* (77), 77sr1.
26. Laske, C.; Sohrabi, H. R.; Frost, S. M.; López-de-Ipiña, K.; Garrard, P.; Buscema, M.; Dauwels, J.; Soekadar, S. R.; Mueller, S.; Linnemann, C.; Bridenbaugh, S. A.; Kanagasingam, Y.; Martins, R. N.; O'Bryant, S. E., Innovative diagnostic tools for early detection of Alzheimer's disease. *Alzheimers Dement.* **2015,** *11* (5), 561-578.
27. Weiner, M. W.; Veitch, D. P.; Aisen, P. S.; Beckett, L. A.; Cairns, N. J.; Green, R. C.; Harvey, D.; Jack, C. R. J.; Jagust, W.; Morris, J. C.; Petersen, R. C.; Saykin, A. J.; Shaw, L. M.; Toga, A. W.; Trojanowski, J. Q., Recent publications from the Alzheimer's Disease Neuroimaging Initiative: Reviewing progress toward improved AD clinical trials. *Alzheimers Dement.* **2017,** *13* (4), 1-85.
28. Johnson, K. A.; Fox, N. C.; Sperling, R. A.; Klunk, W. E., Brain imaging in Alzheimer disease. *Cold Spring Harb. Perspect. Med.* **2012,** *2* (4), a006213.
29. Caselli, R. J.; Beach, T. G.; Knopman, D. S.; Graff-Radford, N. R., Alzheimer Disease: Scientific Breakthroughs and Translational Challenges. *Mayo Clin. Proc.* **2017,** *92* (6), 978-994.
30. Klunk, W. E.; Engler, H.; Nordberg, A.; Wang, Y.; Blomqvist, G.; Holt, D. P.; Bergström, M.; Savitcheva, I.; Huang, G. F.; Estrada, S.; Ausén, B.; Debnath, M. L.; Barletta, J.; Price, J. C.; Sandell, J.; Lopresti, B. J.; Wall, A.; Koivisto, P.; Antoni, G.; Mathis, C. A.; Långström, B., Imaging brain amyloid in Alzheimer's disease with Pittsburgh Compound-B. *Ann. Neurol.* **2004,** *55* (3), 306-319.
31. Kantarci, K., Molecular imaging of Alzheimer disease pathology. *Am. J. Neuroradiol.* **2014,** *35* (6), 12-17.
32. Rowe, C. C.; Ackerman, U.; Browne, W.; Mulligan, R.; Pike, K. L.; O'Keefe, G.; Tochon-Danguy, H.; Chan, G.; Berlangieri, S. U.; Jones, G.; Dickinson-Rowe, K. L.; Kung, H. P.; Zhang, W.; Kung, M. P.; Skovronsky, D.; Dyrks, T.; Holl, G.; Krause, S.; Friebe, M.; Lehman, L.; Lindemann, S.; Dinkelborg, L. M.; Masters, C. L.; Villemagne, V. L., Imaging of amyloid β in Alzheimer's disease with ^{18}F-BAY94-9172, a novel PET tracer: proof of mechanism. *Lancet Neurol.* **2008,** *7* (2), 129-135.
33. Wong, D. F.; Rosenberg, P. B.; Zhou, Y.; Kumar, A.; Raymont, V.; Ravert, H. T.; Dannals, R. F.; Nandi, A.; Bražić, J. R.; Ye, W.; Hilton, J.; Lyketsos, C.; Kung, H. F.; Joshi, A. D.; Skovronsky, D. M.; Pontecorvo, M. J., In Vivo Imaging of Amyloid Deposition in Alzheimer Disease Using the Radioligand ^{18}F-AV-45 (Flobetapir F 18). *J. Nucl. Med.* **2010,** *51* (6), 913-920.
34. Clark, C. M.; Schneider, J. A.; Bedell, B. J.; Beach, T. G.; Bilker, W. B.; Mintun, M. A.; Pontecorvo, M. J.; Hefti, F.; Carpenter, A. P.; Flitter, M. L.; Krautkramer, M. J.; Kung, H. F.; Coleman, R. E.; Doraiswamy, P. M.; Fleisher, A. S.; Sabbagh, M. N.; Sadowsky, C. H.; Reiman, E. M.; Zehntner, S. P.; Skovronsky, D. M., Use of florbetapir-pet for imaging β-amyloid pathology. *JAMA* **2011,** *305* (3), 275-283.
35. Nelissen, N.; Van Laere, K.; Thurfjell, L.; Owenius, R.; Vandenbulcke, M.; Koole, M.; Bormans, G.; Brooks, D. J.; Vandenberghe, R., Phase 1 Study of the Pittsburgh Compound B Derivative ^{18}F-Flutemetamol in Healthy Volunteers and Patients with Probable Alzheimer Disease. *J. Nucl. Med.* **2009,** *50* (8), 1251-1259.
36. Vandenberghe, R.; Laere, K. V.; Ivanoiu, A.; Salmon, E.; Bastin, C.; Triau, E.; Hasselbalch, S.; Law, I.; Andersen, A.; Korner, A.; Minthon, L.; Garraux, G.; Nelissen, N.; Bormans, G.; Buckley, C.; Owenius, R.; Thurfjell, L.; Farrar, G.; Brooks, D. J., ^{18}F-flutemetamol amyloid imaging in Alzheimer disease and mild cognitive impairment: A phase 2 trial. *Ann. Neurol.* **2010,** *68* (3), 319-329.
37. Bandara, N.; Sharma, A. K.; Krieger, S.; Schultz, J. W.; Han, B. H.; Rogers, B. E.; Mirica, L. M., Evaluation of 64Cu-Based Radiopharmaceuticals that Target Abeta Peptide Aggregates as Diagnostic Tools for Alzheimer's Disease. *J. Am. Chem. Soc.* **2017,** *139* (36), 12550-12558.
38. Fodero-Tavoletti, M. T.; Villemagne, V. L.; Paterson, B. M.; White, A. R.; Li, Q.-X.; Camakaris, J.; O'Keefe, G. J.; Cappai, R.; Barnham, K. J.; Donnelly, P. S., Bis(thiosemicarbazonato) Cu-64 complexes for positron emission tomography imaging of Alzheimer's disease. *J. Alzheimers Dis.* **2010,** *20* (1), 49-55.

39. Torres, J. B.; Andreozzi, E. M.; Dunn, J. T.; Siddique, M.; Szanda, I.; Howlett, D. R.; Sunassee, K.; Blower, P. J., PET Imaging of Copper Trafficking in a Mouse Model of Alzheimer Disease. *J. Nucl. Med.* **2016,** *57* (1), 109-114.
40. Jellinger, K. A., Alzheimer 100 – highlights in the history of Alzheimer research. *J. Neural. Transm.* **2006,** *113*, 1603–1623.
41. Olsson, B.; Lautner, R.; Andreasson, U.; Öhrfelt, A.; Portelius, E.; Bjerke, M.; Hölttä, M.; Rosén, C.; Olsson, C.; Strobel, G.; Wu, E.; Dakin, K.; Petzold, M.; Blennow, K.; Zetterberg, H., CSF and blood biomarkers for the diagnosis of Alzheimer's disease: a systematic review and meta-analysis. *Lancet Neurol.* **2016,** *15* (7), 673-684.
42. Sperling, R.; Johnson, K., Biomarkers of Alzheimer disease: current and future applications to diagnostic criteria. *Continuum (Minneap Minn)* **2013,** *19* (2), 325-338.
43. Chen, G.-f.; Xu, T.-h.; Yan, Y.; Zhou, Y.-r.; Jiang, Y.; Melcher, K.; Xu, H. E., Amyloid beta: structure, biology and structure-based therapeutic development. *Acta Pharmacologica Sinica* **2017**, 1-31.
44. O'Brien, R. J.; Wong, P. C., Amyloid Precursor Protein Processing and Alzheimer's Disease. *Annu. Rev. Neurosci.* **2011,** *34* (1), 185-204.
45. Nicolas, M.; Hassan, B. A., Amyloid precursor protein and neural development. *Development* **2014,** *141* (13), 2543-2548.
46. Sosa, L. J.; Caceres, A.; Dupraz, S.; Oksdath, M.; Quiroga, S.; Lorenzo, A., The physiological role of the Amyloid Precursor Protein (APP) as an adhesion molecule in the developing nervous system. *J. Neurochem.* **2017**, In press.
47. Borghesani, V.; Alies, B.; Hureau, C., Cu(II) binding to various forms of amyloid-β peptides. Are they friends or foes ? *Eur. J. Inorg. Chem.* **2017**, Accepted Manuscript.
48. Solomon, E. I.; Heppner, D. E.; Johnston, E. M.; Ginsbach, J. W.; Cirera, J.; Qayyum, M.; Kieber-Emmons, M. T.; Kjaergaard, C. H.; Hadt, R. G.; Tian, L., Copper Active Sites in Biology. *Chem. Rev.* **2014,** *114* (7), 3659-3853.
49. Messerschmidt, A., Copper Metalloenzymes. In *Comprehensive Natural Products II*, Elsevier: Oxford, 2010; pp 489-545.
50. Elwell, C. E.; Gagnon, N. L.; Neisen, B. D.; Dhar, D.; Spaeth, A. D.; Yee, G. M.; Tolman, W. B., Copper–Oxygen Complexes Revisited: Structures, Spectroscopy, and Reactivity. *Chem. Rev.* **2017,** *117* (3), 2059-2107.
51. Kozlowski, H.; Janicka-Klos, A.; Brasun, J.; Gaggelli, E.; Valensin, D.; Valensin, G., Copper, iron, and zinc ions homeostasis and their role in neurodegenerative disorders (metal uptake, transport, distribution and regulation). *Coord. Chem. Rev.* **2009,** *253* (21), 2665-2685.
52. Eisses, J. F.; Kaplan, J. H., Molecular characterization of hCTR1, the human copper uptake protein. *J. Biol. Chem.* **2002,** *277* (32), 29162-29171.
53. D'Ambrosi, N.; Rossi, L., Copper at synapse: Release, binding and modulation of neurotransmission. *Neurochem. Int.* **2015,** *90*, 36-45.
54. Scheiber, I. F.; Mercer, J. F.; Dringen, R., Metabolism and functions of copper in brain. *Prog. Neurobiol.* **2014,** *116*, 33-57.
55. Hung, Y. H.; Bush, A. I.; Cherny, R. A., Copper in the brain and Alzheimer's disease. *J. Biol. Inorg. Chem.* **2010,** *15*, 61–76.
56. Ayton, S.; Lei, P.; Bush, A. I., Metallostasis in Alzheimer's disease. *Free Radical Biol. Med.* **2013,** *62*, 76-89.
57. Donnelly, P. S.; Xiao, Z.; Wedd, A. G., Copper and Alzheimer's disease. *Curr. Opin. Chem. Biol.* **2007,** *11* (2), 128-133.
58. Hureau, C., Coordination of redox active metal ions to the amyloid precursor protein and to amyloid-β peptides involved in Alzheimer disease. Part 1: An overview. *Coord. Chem. Rev.* **2012,** *256* (19), 2164-2174.
59. Barnham, K. J.; Bush, A. I., Metals in Alzheimer's and Parkinson's Diseases. *Curr. Opin. Chem. Biol.* **2008,** *12* (2), 222-228.

60. Kozlowski, H.; Luczkowski, M.; Remelli, M.; Valensin, D., Copper, zinc and iron in neurodegenerative diseases (Alzheimer's, Parkinson's and prion diseases). *Coord. Chem. Rev.* **2012,** *256*, 2129– 2141.
61. Hozumi, I.; Hasegawa, T.; Honda, A.; Ozawa, K.; Hayashi, Y.; Hashimoto, K.; Yamada, M.; Koumura, A.; Sakurai, T.; Kimura, A.; Tanaka, Y.; Satoh, M.; Inuzuka, T., Patterns of levels of biological metals in CSF differ among neurodegenerative diseases. *J. Neurol. Sci.* **2011,** *303* (1), 95-99.
62. Barnham, K. J.; Bush, A. I., Biological metals and metal-targeting compounds in major neurodegenerative diseases. *Chem. Soc. Rev.* **2014,** *43* (19), 6727-6749.
63. Frederickson, C. J.; Suh, S. W.; Silva, D.; Frederickson, C. J.; Thompson, R. B., Importance of Zinc in the Central Nervous System: The Zinc-Containing Neuron. *J. Nutr.* **2000,** *130* (5), 1471S-1483S.
64. Kambe, T.; Tsuji, T.; Hashimoto, A.; Itsumura, N., The Physiological, Biochemical, and Molecular Roles of Zinc Transporters in Zinc Homeostasis and Metabolism. *Physiol. Rev.* **2015,** *95* (3), 749-784.
65. Lovell, M. A.; Robertson, J. D.; Teesdale, W. J.; Campbell, J. L.; Markesbery, W. R., Copper, iron and zinc in Alzheimer's disease senile plaques. *J. Neurol. Sci.* **1998,** *158*, 47–52.
66. Hureau, C.; Dorlet, P., Coordination of redox active metal ions to the amyloid precursor protein and to amyloid-β peptides involved in Alzheimer disease. Part 2: Dependence of Cu(II) binding sites with Aβ sequences. *Coord. Chem. Rev.* **2012,** *256* (19), 2175-2187.
67. Migliorini, C.; Porciatti, E.; Luczkowski, M.; Valensin, D., Structural characterization of Cu2+, Ni2+ and Zn2+ binding sites of model peptides associated with neurodegenerative diseases. *Coord. Chem. Rev.* **2012,** *256* (1), 352-368.
68. Rowinska-Zyrek, M.; Salerno, M.; Kozlowski, H., Neurodegenerative diseases – Understanding their molecular bases and progress in the development of potential treatments. *Coord. Chem. Rev.* **2015,** *284*, 298-312.
69. Kim, D.; Kim, N. H.; Kim, S. H., 34 GHz Pulsed ENDOR Characterization of the Copper Coordination of an Amyloid β Peptide Relevant to Alzheimer's Disease. *Angew. Chem. Int. Ed.* **2013,** *52* (4), 1139-1142.
70. Alies, B.; Renaglia, E.; Rózga, M.; Bal, W.; Faller, P.; Hureau, C., Cu(II) Affinity for the Alzheimer's Peptide: Tyrosine Fluorescence Studies Revisited. *Anal. Chem.* **2013,** *85* (3), 1501-1508.
71. Kowalik-Jankowska, T.; Ruta, M.; Wiśniewska, K.; Łankiewicz, L., Coordination abilities of the 1–16 and 1–28 fragments of β-amyloid peptide towards copper(II) ions: a combined potentiometric and spectroscopic study. *J. Inorg. Biochem.* **2003,** *95* (4), 270-282.
72. Young, T. R.; Kirchner, A.; Wedd, A. G.; Xiao, Z., An integrated study of the affinities of the Aβ16 peptide for Cu(i) and Cu(ii): implications for the catalytic production of reactive oxygen species. *Metallomics* **2014,** *6* (3), 505-517.
73. Atrián-Blasco, E.; Conte-Daban, A.; Hureau, C., Mutual interference of Cu and Zn ions in Alzheimer's disease: perspectives at the molecular level. *Dalton Trans.* **2017,** *46* (38), 12735–13146.
74. Conte-Daban, A.; Borghesani, V.; Sayen, S.; Guillon, E.; Journaux, Y.; Gontard, G.; Lisnard, L.; Hureau, C., Link between Affinity and Cu(II) Binding Sites to Amyloid-beta Peptides Evaluated by a New Water-Soluble UV-Visible Ratiometric Dye with a Moderate Cu(II) Affinity. *Anal. Chem.* **2017,** *89* (3), 2155-2162.
75. Hureau, C.; Balland, V.; Coppel, Y.; Solari, P. L.; Fonda, E.; Faller, P., Importance of dynamical processes in the coordination chemistry and redox conversion of copper amyloid-β complexes. *J. Biol. Inorg. Chem.* **2009,** *14* (7), 995-1000.
76. Shearer, J.; Szalai, V. A., The Amyloid-β Peptide of Alzheimer's Disease Binds CuI in a Linear Bis-His Coordination Environment: Insight into a Possible Neuroprotective Mechanism for the Amyloid-β Peptide. *J. Am. Chem. Soc.* **2008,** *130* (52), 17826-17835.
77. Himes, R. A.; Park, G. Y.; Siluvai, G. S.; Blackburn, N. J.; Karlin, K. D., Structural Studies of Copper(I) Complexes of Amyloid-β Peptide Fragments: Formation of Two-Coordinate Bis(histidine) Complexes. *Angew. Chem. Int. Ed.* **2008,** *47* (47), 9084-9087.
78. Himes, R. A.; Park, G. Y.; Barry, A. N.; Blackburn, N. J.; Karlin, K. D., Synthesis and X-ray Absorption Spectroscopy Structural Studies of Cu(I) Complexes of HistidylHistidine Peptides: The Predominance of Linear 2-Coordinate Geometry. *J. Am. Chem. Soc.* **2007,** *129* (17), 5352-5353.

79. Lu, Y.; Prudent, M.; Qiao, L.; Mendez, M. A.; Girault, H. H., Copper(i) and copper(ii) binding to β-amyloid 16 (Aβ16) studied by electrospray ionization mass spectrometry. *Metallomics* **2010,** *2* (7), 474-479.
80. Alies, B.; Badei, B.; Faller, P.; Hureau, C., Reevaluation of Copper(I) Affinity for Amyloid-β Peptides by Competition with Ferrozine—An Unusual Copper(I) Indicator. *Chem. Eur. J.* **2012,** *18* (4), 1161-1167.
81. Xiao, Z.; Gottschlich, L.; van der Meulen, R.; Udagedara, S. R.; Wedd, A. G., Evaluation of quantitative probes for weaker Cu(i) binding sites completes a set of four capable of detecting Cu(i) affinities from nanomolar to attomolar. *Metallomics* **2013,** *5* (5), 501-513.
82. Danielsson, J.; Pierattelli, R.; Banci, L.; Graslund, A., High-resolution NMR studies of the zinc-binding site of the Alzheimer's amyloid beta-peptide. *FEBS Journal* **2007,** *274* (1), 46-59.
83. Rezaei-Ghaleh, N.; Giller, K.; Becker, S.; Zweckstetter, M., Effect of Zinc Binding on β–Amyloid Structure and Dynamics: Implications for Aβ Aggregation. *Biophys. J.* **2011,** *101* (5), 1202-1211.
84. Syme, C. D.; Viles, J. H., Solution ^{1}H NMR investigation of Zn^{2+} and Cd^{2+} binding to amyloid-beta peptide (Aβ) of Alzheimer's disease. *Biochimica et Biophysica Acta - Proteins and Proteomics* **2006,** *1764* (2), 246-256.
85. Alies, B.; Conte-Daban, A.; Sayen, S.; Collin, F.; Kieffer, I.; Guillon, E.; Faller, P.; Hureau, C., Zinc(II) Binding Site to the Amyloid-β Peptide: Insights from Spectroscopic Studies with a Wide Series of Modified Peptides. *Inorg. Chem.* **2016,** *55* (20), 10499-10509.
86. Noel, S.; Bustos Rodriguez, S.; Sayen, S.; Guillon, E.; Faller, P.; Hureau, C., Use of a new water-soluble Zn sensor to determine Zn affinity for the amyloid-β peptide and relevant mutants. *Metallomics* **2014,** *6* (7), 1220-1222.
87. Zawisza, I.; Rózga, M.; Bal, W., Affinity of copper and zinc ions to proteins and peptides related to neurodegenerative conditions (Aβ, APP, α-synuclein, PrP). *Coord. Chem. Rev.* **2012,** *256* (19), 2297-2307.
88. Chassaing, S.; Collin, F.; Dorlet, P.; Gout, J.; Hureau, C.; Faller, P., Copper and Heme-Mediated Abeta Toxicity: Redox Chemistry, Abeta Oxidations and Anti-ROS Compounds. *Curr. Top. Med. Chem.* **2012,** *12* (22), 2573-2595.
89. Hureau, C.; Faller, P., Aβ-mediated ROS production by Cu ions: Structural insights, mechanisms and relevance to Alzheimer's disease. *Biochimie* **2009,** *91* (10), 1212-1217.
90. Smith, D. G.; Cappai, R.; Barnham, K. J., The redox chemistry of the Alzheimer's disease amyloid β peptide. *Biochim. Biophys. Acta* **2007,** *1768* (8), 1976-1990.
91. Barnham, K. J.; Masters, C. L.; Bush, A. I., Neurodegenerative diseases and oxidative stress. *Nature Reviews* **2004,** *3*, 205-214.
92. Reybier, K.; Ayala, S.; Alies, B.; Rodrigues, J. V.; Bustos Rodriguez, S.; La Penna, G.; Collin, F.; Gomes, C. M.; Hureau, C.; Faller, P., Free Superoxide is an Intermediate in the Production of H2O2 by Copper(I)-Aβ Peptide and O2. *Angew. Chem. Int. Ed.* **2015,** *55* (3), 1085-1089.
93. Butterfield, D. A.; Lauderback, C. M., Lipid peroxidation and protein oxidation in Alzheimer's disease brain: potential causes and consequences involving amyloid β-peptide-associated free radical oxidative stress. *Free Radical Biol. Med.* **2002,** *32* (11), 1050-1060.
94. Butterfield, D. A.; Reed, T.; Newman, S. F.; Sultana, R., Roles of amyloid β-peptide-associated oxidative stress and brain protein modifications in the pathogenesis of Alzheimer's disease and mild cognitive impairment. *Free Radical Biol. Med.* **2007,** *43* (5), 658-677.
95. Markesbery, W. R., Oxidative Stress Hypothesis in Alzheimer's Disease. *Free Radical Biol. Med.* **1997,** *23* (1), 134-147.
96. Yatin, S. M.; Varadarajan, S.; Link, C. D.; Butterfield, D. A., In vitro and in vivo oxidative stress associated with Alzheimer's amyloid β-peptide (1–42). *Neurobiol. Aging* **1999,** *20* (3), 325-330.
97. Manevich, Y.; Held, K. D.; Biaglow, J. E., Coumarin-3-Carboxylic Acid as a Detector for Hydroxyl Radicals Generated Chemically and by Gamma Radiation. *Radiat. Res.* **1997,** *148* (6), 580-591.

98. Valensin, D.; Gabbiani, C.; Messori, L., Metal compounds as inhibitors of β-amyloid aggregation. Perspectives for an innovative metallotherapeutics on Alzheimer's disease. *Coord. Chem. Rev.* **2012,** *256* (19), 2357-2366.
99. Andreeva, T. V.; Lukiw, W. J.; Rogaev, E. I., Biological Basis for Amyloidogenesis in Alzheimer's Disease. *Biochemistry* **2017,** *82* (2), 122-139.
100. Minati, L.; Edginton, T.; Bruzzone, M. G.; Giaccone, G., Current Concepts in Alzheimer's Disease: A Multidisciplinary Review. *Am J Alzheimers Dis Other Demen.* **2009,** *24* (2), 95-121.
101. Hardy, J. A.; Higgins, G. A., Alzheimer's disease: the amyloid cascade hypothesis. *Science* **1992,** *256* (5054), 184-185.
102. Barage, S. H.; Sonawane, K. D., Amyloid cascade hypothesis: Pathogenesis and therapeutic strategies in Alzheimer's disease. *Neuropeptides* **2015,** *52*, 1-18.
103. Hardy, J.; Allsop, D., Amyloid deposition as the central event in the aetiology of Alzheimer's disease. *Trends Pharmacol. Sci.* **1991,** *12* (10), 383-388.
104. Kozlov, S.; Afonin, A.; Evsyukov, I.; Bondarenko, A., Alzheimer's disease: as it was in the beginning. In *Nat. Rev. Neurosci.*, 2017.
105. Herrup, K., The case for rejecting the amyloid cascade hypothesis. *Nature Neuroscience* **2015,** *18* (6), 794-799.
106. Armstrong, R. A., A critical analysis of the 'amyloid cascade hypothesis'. *Folia Neuropathol.* **2014,** *52* (3), 211-225.
107. Karran, E.; Strooper, B. D., The amyloid cascade hypothesis: are we poised for success or failure? *J. Neurochem.* **2016,** *139* (S2), 237-252.
108. Faller, P.; Hureau, C.; Berthoumieu, O., Role of Metal Ions in the Self-assembly of the Alzheimer's Amyloid-β Peptide. *Inorg. Chem.* **2013,** *52* (21), 12193-12206.
109. Hellstrand, E.; Boland, B.; Walsh, D. M.; Linse, S., Amyloid beta-protein aggregation produces highly reproducible kinetic data and occurs by a two-phase process. *ACS Chem. Neurosci.* **2010,** *1* (1), 13-18.
110. Viles, J. H., Metal ions and amyloid fiber formation in neurodegenerative diseases. Copper, zinc and iron in Alzheimer's, Parkinson's and prion diseases. *Coord. Chem. Rev.* **2012,** *256* (19), 2271-2284.
111. Kayed, R.; Lasagna-Reeves, C. A., Molecular mechanisms of amyloid oligomers toxicity. *J. Alzheimers Dis.* **2013,** *33*, S67-S78.
112. Fu, L.; Sun, Y.; Guo, Y.; Chen, Y.; Yu, B.; Zhang, H.; Wu, J.; Yu, X.; Kong, W.; Wu, H., Comparison of neurotoxicity of different aggregated forms of Aβ40, Aβ42 and Aβ43 in cell cultures. *J. Pept. Sci.* **2017,** *23* (3), 245-251.
113. Petkova, A. T.; Ishii, Y.; Balbach, J. J.; Antzutkin, O. N.; Leapman, R. D.; Delaglio, F.; Tycko, R., A structural model for Alzheimer's β-amyloid fibrils based on experimental constraints from solid state NMR. *PNAS* **2002,** *99* (26), 16742-16747.
114. Tiiman, A.; Palumaa, P.; Tougu, V., The missing link in the amyloid cascade of Alzheimer's disease – Metal ions. *Neurochem. Int.* **2013,** *62*, 367–378.
115. Khurana, R.; Coleman, C.; Ionescu-Zanetti, C.; Carter, S. A.; Krishna, V.; Grover, R. K.; Roy, R.; Singh, S., Mechanism of thioflavin T binding to amyloid fibrils. *J. Struct. Biol.* **2005,** *151* (3), 229-238.
116. Rowinska-Zyrek, M.; Salerno, M.; Kozlowski, H., Neurodegenerative diseases – Understanding their molecular bases and progress in the development of potential treatments. *Coord. Chem. Rev.* **2015,** *284*, 298–312.
117. Santos, M. A.; Chand, K.; Chaves, S., Recent progress in repositioning Alzheimer's disease drugs based on a multitarget strategy. *Future Med. Chem.* **2016,** *8* (17), 2113-2142.
118. Tan, C. C.; Yu, J. T.; Wang, H. F.; Tan, M. S.; Meng, X. F.; Wang, C.; Jiang, T.; Zhu, X. C.; Tan, L., Efficacy and safety of donepezil, galantamine, rivastigmine, and memantine for the treatment of Alzheimer's disease: a systematic review and meta-analysis. *J. Alzheimers Dis.* **2014,** *41* (2), 615-631.
119. Johnson, J. W.; Kotermanski, S. E., Mechanism of action of memantine. *Curr. Opin. Pharmacol.* **2006,** *6* (1), 61-67.
120. Matsunaga, S.; Kishi, T.; Iwata, N., Memantine monotherapy for Alzheimer's disease: a systematic review and meta-analysis. *PLoS One* **2015,** *10* (4), e0123289.

121. Hampel, H.; Schneider, L. S.; Giacobini, E.; Kivipelto, M.; Sindi, S.; Dubois, B.; Broich, K.; Nistico, R.; Aisen, P. S.; Lista, S., Advances in the therapy of Alzheimer's disease: targeting amyloid beta and tau and perspectives for the future. *Expert Rev. Neurother.* **2015,** *15* (1), 83-105.
122. Berk, C.; Paul, G.; Sabbagh, M., Investigational drugs in Alzheimer's disease: current progress. *Expert Opin. Investig. Drugs* **2014,** *23* (6), 837-846.
123. Tayeb, H. O.; Murray, E. D.; Price, B. H.; Tarazi, F. I., Bapineuzumab and solanezumab for Alzheimer's disease: is the 'amyloid cascade hypothesis' still alive? *Expert Opin. Biol. Ther.* **2013,** *13* (7), 1075-1084.
124. Morgan, D., Immunotherapy for Alzheimer's Disease. *J. Intern. Med.* **2011,** *269* (1), 54-63.
125. Sevigny, J.; Chiao, P.; Bussiere, T.; Weinreb, P. H.; Williams, L.; Maier, M.; Dunstan, R.; Salloway, S.; Chen, T.; Ling, Y.; O'Gorman, J.; Qian, F.; Arastu, M.; Li, M.; Chollate, S.; Brennan, M. S.; Quintero-Monzon, O.; Scannevin, R. H.; Arnold, H. M.; Engber, T.; Rhodes, K.; Ferrero, J.; Hang, Y.; Mikulskis, A.; Grimm, J.; Hock, C.; Nitsch, R. M.; Sandrock, A., The antibody aducanumab reduces Aβ plaques in Alzheimer's disease. *Nature* **2016,** *537* (7618), 50-56.
126. Alves, S.; Churlaud, G.; Audrain, M.; Michaelsen-Preusse, K.; Fol, R.; Souchet, B.; Braudeau, J.; Korte, M.; Klatzmann, D.; Cartier, N., Interleukin-2 improves amyloid pathology, synaptic failure and memory in Alzheimer's disease mice. *Brain* **2017,** *140* (3), 826-842.
127. Dansokho, C.; Ait Ahmed, D.; Aid, S.; Toly-Ndour, C.; Chaigneau, T.; Calle, V.; Cagnard, N.; Holzenberger, M.; Piaggio, E.; Aucouturier, P.; Dorothée, G., Regulatory T cells delay disease progression in Alzheimer-like pathology. *Brain* **2016,** *139* (4), 1237-1251.
128. Selkoe, D. J., Alzheimer's Disease: Genes, Proteins, and Therapy. *Physiol. Rev.* **2001,** *81* (2), 741–766.
129. Xia, N.; Liu, L., Metallothioneins and Synthetic Metal Chelators as Potential Therapeutic Agents for Removal of Aberrant Metal Ions from Metal-AB Species. *Mini Rev. Med. Chem.* **2014,** *14* (3), 271-281.
130. Robert, A.; Liu, Y.; Nguyen, M.; Meunier, B., Regulation of copper and iron homeostasis by metal chelators: a possible chemotherapy for Alzheimer's disease. *Acc. Chem. Res.* **2015,** *48* (5), 1332-1339.
131. Santos, M. A.; Chand, K.; Chaves, S., Recent progress in multifunctional metal chelators as potential drugs for Alzheimer's disease. *Coord. Chem. Rev.* **2016,** *327 –328*, 287–303.
132. Scott, L. E.; Orvig, C., Medicinal inorganic chemistry approaches to passivation and removal of aberrant metal ions in disease. *Chem. Rev.* **2009,** *109* (10), 4885-4910.
133. Sampson, E. L.; Jenagaratnam, L.; McShane, R., Metal protein attenuating compounds for the treatment of Alzheimer's dementia. *Cochrane Database Syst. Rev.* **2014,** (2), Cd005380.

Chapter II: Cu ion chelation

This chapter focuses on the Cu(I/II) chelation within the Alzheimer's disease context. This work might be biologically relevant since Cu ions might interact with the Aβ peptide in AD as previously explained an form toxic Cu-Aβ species. Thus, Cu ions bound to Aβ were considered as a therapeutic target of choice.

A first part reports the state of art regarding the Cu(II) chelation approach in AD. Different ligands are grouped in categories, depending on their structures. Their impact on the ROS production by Cu-Aβ, on the aggregation of Aβ and on the cell toxicities are reported. Then, a first proof-of-concept focuses on the kinetic issue regarding the Cu(II) removal. Two series of macrocyclic ligands are studied. It is demonstrated that, by measuring the ROS production by Cu-Aβ, a high affinity constant for Cu(II) is not enough to remove the Cu ions from the Aβ if the removal is slower than the redox cycling of Cu-Aβ. The second proof-of-concept detailed here describes the removal of both Cu(II) and Cu(I) from the Aβ peptide since the redox state of Cu ions bound to Aβ in the synaptic cleft is not defined. The ligand **L** and the corresponding Cu(I) and Cu(II) complexes are characterized. The ability of this chelator to remove both Cu ions from the peptide is demonstrated by EPR and XANES spectroscopies as well as its ability to stop Cu-Aβ mediated ROS production.

II-A Cu ion chelators: State of art

As previously explained, the dyshomeostasis of Cu ions is considered as an important event in the AD aetiology. The metal chelation approach is intensively studied.[1-5] One approach is preventing the coordination of Cu ions to Aβ using molecules able to occupy the binding site of Cu ions.[6] Nevertheless, Cu ions have several binding sites so it is difficult to block all of them.[6] Another approach is the use of ligands able to remove Cu ions from the Aβ peptide or to interfere with the Cu-Aβ complex in order to change its properties.[3, 6-10] Up to now, different criteria for a Cu ligand to fight against AD exist. The ligand needs an affinity constant for Cu ions higher than the one of Aβ in order to remove the metal ion from the peptide. Nevertheless, this affinity constant does not have to be too much higher. Indeed, a too high affinity constant will lead to a ligand able to remove "healthy" Cu ions from essential metalloproteins.[6, 11] This could exacerbate Cu ion dyshomeostasis in AD. Note that in this review, only ligands able to remove Cu ions from the Aβ1-x are reported. The N-terminally truncated peptides such as Aβ4-x and Aβ11-x are also present in AD brains and exhibit a higher affinity constant for Cu(II) than

the Aβ1-x (~ 10^{13}).[12-13] Hence, not all the ligands reported here are able to remove Cu(II) from the truncated peptides. Nevertheless, this should not be an issue since the Cu(II) complexes with the truncated peptides do not produce ROS.[12-13]

Another important criterion for the ligand in the AD context is its Blood Brain Barrier (BBB) permeability since the targeted Cu ions are localized in the brain.[14] The Lipinski's rules describes some criteria that have at least to be fulfilled for a passive diffusion: a low molecular weight, no more than 5 hydrogen bond donors, no more than 10 hydrogen bond acceptor and a log P < 5 (meaning a quite hydrophobic ligand).[15] Regarding the hydrophobicity of the ligand, a balance between the hydrophilicity and the hydrophobicity is needed.[2, 16-19] *Ab initio* studies propose a correlation between the metallo-aromaticity (*i.e. "manifestation of aromatic properties in the chelate metallacycle"*[20]) and the stability constant of the Cu(II)-ligand complex.[21] Another approach to go through the BBB is the addition of a moiety to the ligand that increases its BBB permeability.[14, 22] For example, ligands with a glucose moeity[23] or grafted on a nanoparticle[24-26] are developed.

Multi-target compounds are also developed in the AD chelatotherapy context.[2, 4, 16, 19, 22, 27-29] Two strategies exist: the chelation moiety can be included in the multi-functionality or it can be linked to the multi-functionality moiety. The multi-target moiety can be an radical scavenging moiety, a moiety targeting the Aβ aggregates, a moiety able to cross the BBB as previously explained, etc. These compounds have many advantages. For example, they can target Aβ and the ligand can chelate Cu ions bound to Aβ and not to another metalloprotein. Another strategy is the use of prochelators. The chelating moiety is hidden; a cleavage of the molecule releases the chelating moiety. For example, Franz's group has proposed a cleavage by H_2O_2[30] or by β-secretase.[31]

In this state of the art, only the Cu ion chelation is under focused: the multifunctional ligand will not be discussed, except if the chelator moiety is included inside the multi-functionality. First, the different structures of the ligands developed for the Cu chelatotherapy are described. The different ligands are gathered together in four categories: the hydroxyl/amino quinolones, the stilbene like and the benzothiazole (BzT) like ligands, the macrocyclic and peptidic ligands, and finally other structures. Then several aspects of the chelatotherapy in the AD context are discussed.

II-A.i The different categories of ligands

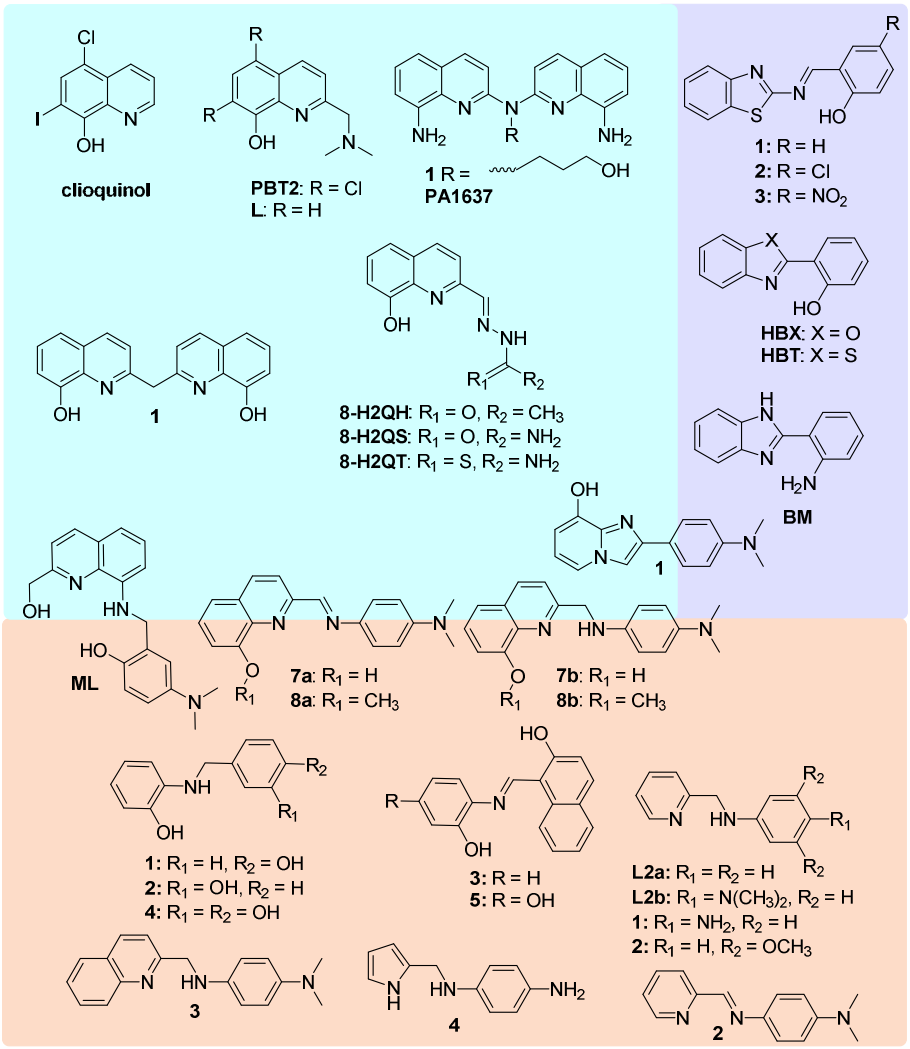

Figure II-1. Three categories of ligands studied in the literature: the hydroxyl/aminoquinolines (top left), the benzothiazole like ligands (top right) and the stilbene like ligands (bottom).

Hydroxy-Aminoquinolines

The hydroxyl-aminoquinolines are one of the different categories of ligands developed against AD (Figure II-1, top left). The most well-known are clioquinol and then PBT2.[6, 32 19, 33-40] Clioquinol (CQ) is a prototypical Metal Protein Attenuating Compound (MPAC). The MPAC are then called metallophores. Previously, it was tested against other diseases but was stopped due to its side effects. Nevertheless, it has been proposed and tested against AD.[41] Many *in vitro*,[42] such as structural characterizations of the Cu(II)-complex[43-45] as well as aggregation studies[46-47], studies on its capability to cross the BBB,[48] and *in vivo*[49-51] studies have been performed to determine its effects on the Aβ peptide and Cu ions. CQ was the first ligand against AD that has gone under clinical trials[52-56] but has failed before going through phase III. Different hypotheses have been proposed, as for example the lack of selectivity (*i.e.* the ratio between the affinity constant for Cu(II) and the one for Zn(II)) between Cu and Zn ions. Indeed,

CQ is able to chelate Cu and Zn ions with a very high affinity constant, meaning that in the synaptic cleft, it is able to chelate Zn(II) and to leave Cu ions bound to Aβ. Furthermore, it has also been stopped due to the issue in the scale-up of the fabrication. [57] Note that CQ is a metallophore, meaning that it is able to redistribute Cu ions inside the cells where they are deficient. Some studies on yeast for example have shown that CQ increases the intracellular concentration of Cu ions.[58] The second generation of metallophores[59] is the PBT2 synthetized by Barnham and collaborators.[60] It is also a hydroxyquinoline, similar to CQ, but it does not have the iodine, supposed to trigger safety concerns.[32] Some *in vitro* studies,[61] studies on the solubility and permeability to BBB,[57] *in vivo* tests and metallophoric capacities[62] have been performed. PBT2 has also gone to clinical trials[63-65] but failed in phase IIa. Then, other groups have developed hydroxyl/aminoquinolines based on the CQ moiety. The effect of these ligands are reminded in Table II-1. For the ROS production, two different effects are reported: redox silencing means that the ligand removes Cu ions from Aβ and stop the ROS production, radical scavenging means that the ligand itself captures the radical species. For the aggregation, the effect of the ligand by removing Cu ions from Aβ on the aggregation is reported as well as the effect of the ligand itself.

Note that the modifications, such as linking two CQ moieties (see Figure II-1, top left), performed on the CQ moiety allow to have 1:1 complexes (ligand:metal ratio) and not 2:1 complexes as for CQ.

Table II-1. Hydroxy/aminoquinolines reported from the literature as well as their impact on the ROS production, on the aggregation and on cellular toxicities. ✓ means that there is redox silencing or ROS scavenging, no Cu-induced aggregation or impact on the apo aggregation, no cell toxicity, metallophoric capabilities. ✗ means that there is no redox silencing or no ROS scavenging, Cu-induced aggregation or no impact on the apo aggregation, cell toxicity, no metallophoric capabilities. WB stands for Western Blot, ThT means a ThT assay, TEM is the microscopy performed to image the aggregates. Note that if the characteristic has not been studied, n.d. (not determined) is written. pCu is calculated for a Cu(II) concentration at 10 µM. Grey lines mean that the complex formed is not a 1:1 complex.
** = pH 7.1, ** = pH6.6, *** = pH 7.4. ⁺ = conditional value, ¤ = apparent value.*

	pCu	ROS production		Aggregation			Cell toxicity		Metallophore	Refs.	Entry
		Redox silencing	Radical scavenging	Cu removal effect	Ligand effect	Techn.	Without Asc	With Asc			
Hydroxy/amino quinoline											
clioquinol	9.5[66]	✓ 67	✗ 68	~68	✗ 46-47	ThT + AFM	✓	✓ 69	✓ 58	46-47, 58, 66-69	a
PBT2	n.d.	n.d.	n.d.	✓	✗	WB + ThT + TEM[61, 70]	✓	n.d.	✓ 71	61,70-71	b
1	10.8¤***	✓	n.d.	n.d.	n.d.	n.d.	n.d.	n.d.	✓	72-74	c
PA1637	10.9¤***	✓	n.d.	n.d.	n.d.	n.d.	n.d.	n.d.	✓	72, 75	d
1	15.7*+	✓	n.d.	✓	n.d.	Micro BCA Assay	n.d.	n.d.	n.d.	76	e

8-H2QH	n.d.	n.d.	✓	✓	✗	turb. + WB + TEM	✓	n.d.	n.d.	[70]	f
8-H2QS	n.d.	n.d.	✓	✓	✗	turb. + WB + TEM	✓	n.d.	n.d.	[70]	g
8-H2QT	n.d.	n.d.	✓	n.d.	n.d.	turb. + WB + TEM	n.d.	n.d.	n.d.	[70]	h
L	9.9*+	n.d.	n.d.	n.d.	n.d.	n.d.	n.d.	n.d.	n.d.	[59, 77]	i
1	n.d.	✓	n.d.	✗	~	ThT + WB + TEM	✗	~	n.d.	[67]	j

Stilbene like and benzothiazole like ligands

Stilbene and benzothiazole (BzT) like ligands form the same category due to their structures involved as Aβ targeting moieties (Figure II-1 top right and bottom). Indeed, BzT is the scaffold of the ThT and it is well known that ThT interacts with the β-sheets of the Aβ fibrils. Thus, ThT derivatives are developed as well as other planar structures such as the stilbene like. The effects of these ligands are reported in Table II-2. Regarding the ROS production, the impact of these ligands is not clear. Regarding the aggregation, BzT like ligands reported in Table II-2 do not have effect on the apo aggregation, apo meaning without any metal ions, while they have an effect on the metal-induced aggregation. Regarding the stilbene like ligands, some of them, meaning the ones with oxygen groups, have an impact on the apo-aggregation contrary to the other ones. The metal-induced aggregation is affected by these ligands, but again, the impact depends on the ligand. If cell toxicity has been studied, the results show that there is no cell toxicity for the ligand and/or the Cu(II)-complex in the presence or not of Aβ. No metallophore capability has been studied for these ligands.

*Table II-2. Stilbene like and Benzothiazole like ligands reported from the literature as well as their impact on the ROS production, on the aggregation and on cellular toxicities. ✓ means that there is redox silencing or ROS scavenging, no Cu-induced aggregation or impact on the apo aggregation, no cell toxicity, metallophoric capabilities. ✗ means that there is no redox silencing or no ROS scavenging, Cu-induced aggregation or no impact on the apo aggregation, cell toxicity, no metallophoric capabilities. WB stands for Western Blot, ThT means a ThT assay, Turb. means a turbidimetric assay, IM-MS for ion mobility-mass spectrometry, TEM and AFM are the microscopies performed to image the aggregates. Note that if the characteristic has not been studied, n.d. (not determined) is written. Grey lines mean that the complex formed is not a 1:1 complex. pCu is calculated for a Cu(II) concentration at 10 µM. Grey lines mean that the complex formed is not a 1:1 complex. * = pH 7.1, ** = pH6.6, *** = pH 7.4. + = conditional value, ¤ = apparent value.*

	pCu	ROS production		Aggregation			Cell toxicity		Metallophore	Refs.	Entry
		Redox silencing	Radical scavenging	Cu removal effect	Ligand effect	Techn.	Without Asc	With Asc			
Stilbene-like											
2	n.d.	~	n.d.	✗	n.d.	ThT +	✓	✓	n.d.	[67]	a

						WB + TEM					
1	8.9$^{+++¤}$	~	✓	✓	✓	ThT + Turb.	✓	n.d.	n.d.	[68]	b
2	9.0$^{+++¤}$	~	✓	✓	✓	ThT + Turb.	✓	n.d.	n.d.	[68]	c
3	9.5$^{+++¤}$	✓	✗	✓	✓	ThT + Turb.	✓	n.d.	n.d.	[68]	d
4	8.8$^{+++¤}$	~	✓	✓	✓	ThT + Turb.	✓	n.d.	n.d.	[68]	e
5	9.6$^{+++¤}$	✓	~	✓	✓	ThT + Turb.	✓	n.d.	n.d.	[68]	f
7a	n.d.	~	n.d.	✓	✓	ThT + TEM	n.d.	n.d.	n.d.	[61]	g
8a	n.d.	~	n.d.	✓	~	ThT + TEM	n.d.	n.d.	n.d.	[61]	h
7b	n.d.	✗	n.d.	✓	~	ThT + TEM	n.d.	n.d.	n.d.	[61]	i
8b	n.d.	✗	n.d.	✓	~	ThT + TEM	n.d.	n.d.	n.d.	[61]	j
L2a	n.d.	~	n.d.	✗	✗	WB + TEM	✓	n.d.	n.d.	[78]	k
L2b	1:1 : 7.8^{*+} 2:1 : 6.8^{*+}	✓	n.d.	~	✗	WB + TEM	✓	n.d.	n.d.	[78-79]	l
1	n.d.	~	✓	✗	✗	WB + TEM	✓	n.d.	n.d.	[80]	m
2	n.d.	~	✗	✓	✗	WB + TEM	✓	n.d.	n.d.	[80]	n
3	n.d.	~	✓	✗	✗	WB + TEM	✓	n.d.	n.d.	[80]	o
4	n.d.	n.d.	✓	✗	~	WB + TEM	✓	n.d.	n.d.	[80]	p
ML	8.8^{*+}	✓	✓	✓	✓	WB + TEM / IM-MS	✓	n.d.	n.d.	[81]	q
BzT-like											
1	6.0^{**+}	~	n.d.	✓	✗	Turb. + AFM	✓	~	n.d.	[82]	r
2	n.d.	~	n.d.	✓	✗	Turb. + AFM	✓	~	n.d.	[82]	s
3	n.d.	~	n.d.	✓	✗	Turb. + AFM	✓	~	n.d.	[82]	t
HBX	1:1 : 5.5^{*+} 2:1 : 9.4^{*+}	n.d.	n.d.	~	✗	Turb.	n.d.	n.d.	n.d.	[83]	u
HBT	8.4^{*+}	n.d.	n.d.	~	✗	Turb.	n.d.	n.d.	n.d.	[83]	v

BM	8.1^{*+}	n.d.	n.d.	~	✗	Turb.	n.d.	n.d.	n.d.	83	w

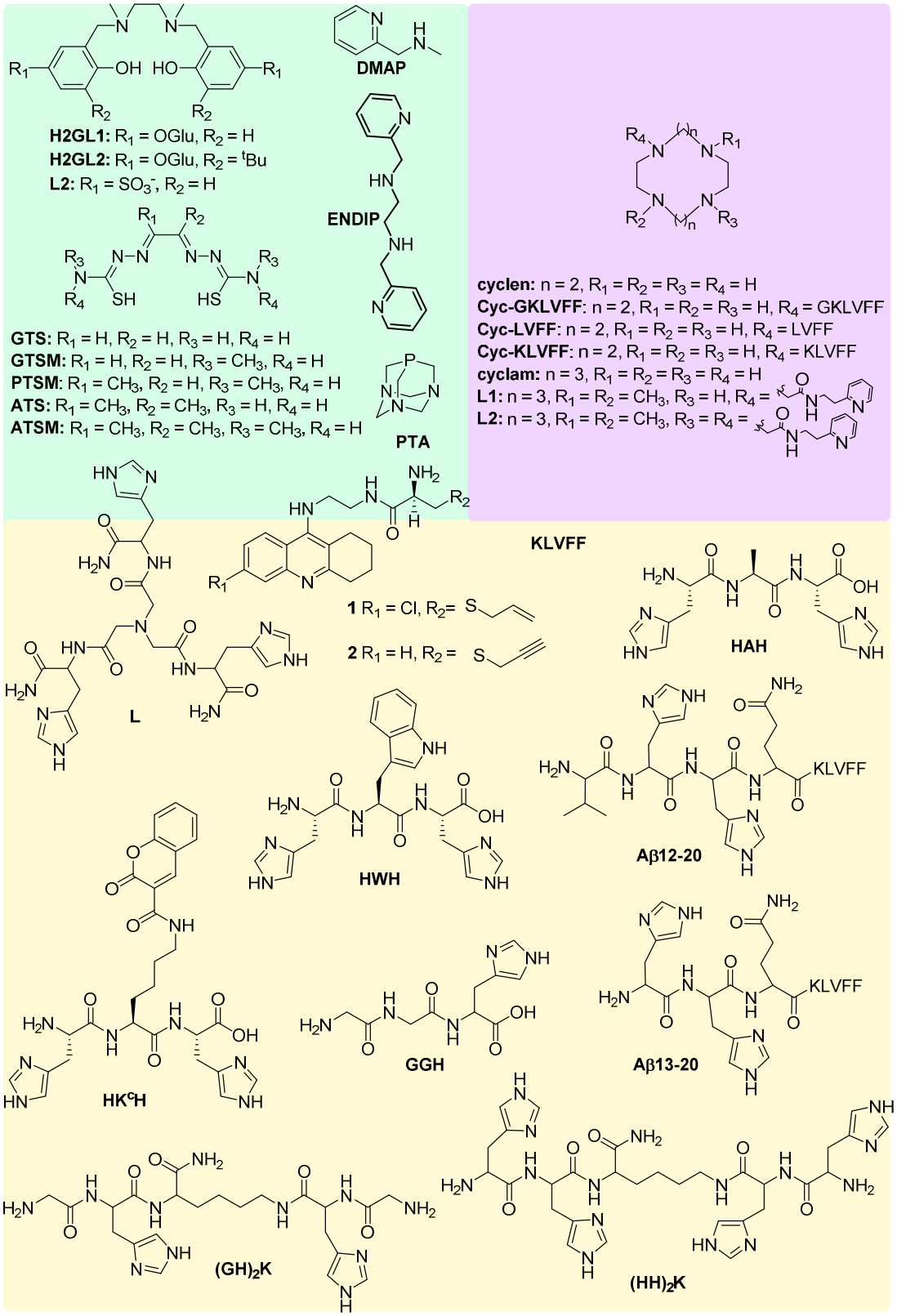

Figure II-2. Three other categories of ligands from the literature: salen, bispicen and bis(thiosemicarbazonato) (top left), macrocyclic ligands (top right) and peptidic ligands (bottom).

Peptidic and macrocyclic ligands

Peptidic and macrocyclic ligands can belong to the same group (Figure II-2 bottom and top right). Indeed, the peptidic ligands studied here are rich in Histidine residues and they often can form ATCUN complexes with Cu(II).[84] The ATCUN motif is a NH_2-Xxx-Yyy-His motif with a high affinity constant for Cu(II) (~ 10^{14}) and with a high stability of the complex, precluding the switch between Cu(II) and Cu(I). The macrocyclic ligand form also Cu(II) complexes of high affinity, that is why peptidic and macrocyclic ligands can be grouped in the same category. The effects of these ligands are reported in Table II-3. This category of ligands does not have radical scavenging capability and no impact on apo aggregation. They are more focused on the removal of Cu ions from Aβ, leading to an important decrease of the ROS production catalysed by Cu-Aβ and to apo-like fibril formation.

*Table II-3. Peptidic and macrocyclic ligands reported from the literature as well as their impact on the ROS production, on the aggregation. ✓ means that there is redox silencing or ROS scavenging, no Cu-induced aggregation or impact on the apo aggregation, no cell toxicity, metallophoric capabilities. ✗ means that there is no redox silencing or no ROS scavenging, Cu-induced aggregation or no impact on the apo aggregation, cell toxicity, no metallophoric capabilities. ThT means a ThT assay, Turb. means a turbidimetric assay, CD stands for circular dichroism, GFP stands for green fluorescent protein assay, TEM is the microscopy performed to image the aggregates. Note that if the characteristic has not been studied, n.d. (not determined) is written. pCu is calculated for a Cu(II) concentration at 10 µM. Grey lines mean that the complex formed is not a 1:1 complex. * = pH 7.1, ** = pH6.6, *** = pH 7.4. $^{+}$ = conditional value, $^{¤}$ = apparent value.*

	pCu	ROS production		Aggregation			Cell toxicity		Metallophore	Refs.	Entry
		Redox silencing	Radical scavenging	Cu removal effect	Ligand effect	Techn.	Without Asc	With Asc			
Peptidic ligands											
(GH)2K	9.3^{*+}	n.d.	n.d.	n.d.	n.d.	n.d.	n.d.	n.d.	n.d.	85	a
(HH)2K	10.1^{*+}	n.d.	n.d.	n.d.	n.d.	n.d.	n.d.	n.d.	n.d.	85	b
KLVFF	n.d.	✗	~	✗	✗	ThT	n.d.	✗	n.d.	86	c
L	8.8^{*+}	✓	n.d.	n.d.	n.d.	n.d.	n.d.	n.d.	n.d.	87	d
AB12-20	n.d.	✓	n.d.	✓	✓	ThT	n.d.	~	n.d.	86	e
AB13-20	n.d.	✓	n.d.	✓	✓	ThT	n.d.	✗	n.d.	86	f
HWH	7.3^{***+}	✓	n.d.	✓	✗	GFP ThT	n.d.	n.d.	n.d.	88	g
HK^{c}H	6.8^{***+}	✓	n.d.	✓	✗	GFP ThT	n.d.	n.d.	n.d.	88	h
HAH	n.d.	✓	n.d.	✓	✗	GFP ThT	n.d.	n.d.	n.d.	88	i
GGH	n.d.$^{***¤}$	✓ 4 eq	n.d.	n.d.	n.d.	n.d.	n.d.	~ (4eq)	n.d.	89	j
1	5.4^{*+}	n.d.	n.d.	~	✗	ThT	n.d.	n.d.	n.d.	90	k

2	5.3*+	n.d.	n.d.	~	✗	ThT	n.d.	n.d.	n.d.	90	l
Macrocyclic ligands											
cyclam	12.5*+	~	n.d.	✓	n.d.	Turb. + ThT	✓	n.d.	n.d.	91	m
cyclen	11.5*+	~	n.d.	✓	n.d.	Turb. + ThT	✓	n.d.	n.d.	91	n
cyc-KLVFF	n.d.	✓	n.d.	n.d.	✗	ThT + TEM	✓	n.d.	n.d.	92	o
cyc-LVFF	n.d.	✓	n.d.	n.d.	n.d.	n.d.	n.d.	n.d.	n.d.	92	p
cyc-GKLVFF	n.d.	✓	n.d.	n.d.	n.d.	n.d.	n.d.	n.d.	n.d.	92	q
L1 (Yang)	n.d.	~	n.d.	✓	✗	Turb. + CD + ThT	✓	~	n.d.	93	r
L2 (Yang)	n.d.	~	n.d.	✓	✗	Turb. + CD + ThT	✓	~	n.d.	93	s

Other organic ligands

In this last category, salen, bispicen and bis(thiosemicarbazonato) ligands are grouped (Figure II-2, top right). They mainly formed 1:1 complexes. The effects of these ligands are reported in Table II-4. They are able to remove Cu(II) (or Cu(I) for PTA ligand) from Aβ and to stop the associated deleterious events. The metallophoric capabilities have been studied only for the bis(thiosemicarbazonato) (btsc) ligands. [6,19, 34-35, 57, 94] Studies explain that some Cu(II)-btsc complexes, such as Cu(II)-gtsm, are able to cross the membrane of the cell and under the reductant intra-cellular conditions, Cu(II)-btsc is reduced. The "new" complex is not stable anymore and Cu(I) is released. Then, there is an activation of the Aβ degradation pathways.

*Table II-4. Other ligands reported from the literature as well as their impact on the ROS production, on the aggregation. ✓ means that there is redox silencing or ROS scavenging, no Cu-induced aggregation or impact on the apo aggregation, no cell toxicity, metallophoric capabilities. ✗ means that there is no redox silencing or no ROS scavenging, Cu-induced aggregation or no impact on the apo aggregation, cell toxicity, no metallophoric capabilities. ThT means a ThT assay, Turb. means a turbidimetric assay, DLS stands for diffusion light scattering assay, TEM and AFM are the microscopies performed to image the aggregates Note that if the characteristic has not been studied, n.d. (not determined) is written. pCu is calculated for a Cu(II) concentration at 10 µM. Grey lines mean that the complex formed is not a 1:1 complex. * = pH 7.1, ** = pH6.6, *** = pH 7.4. + = conditional value, ¤ = apparent value.*

	pCu	**ROS production**		**Aggregation**			**Cell toxicity**		**Metall-ophore**	**Refs.**	**Entry**
		Redox silencing	**Radical scave-nging**	**Cu remo-val effect**	**Ligand effect**	**Techn.**	**Wit-hout Asc**	**With Asc**			
Other structures											
H_2GL1	8.6*+	n.d.	✓	✓	n.d.	Turb.	n.d.	n.d.	n.d.	95	a

H_2GL2	8.3^{*+}	n.d.	✓	~	n.d.	Turb.	n.d.	n.d.	n.d.	95	b
L2	9.4^{*+}	✓	n.d.	✓	n.d.	ThT + AFM	n.d.	n.d.	n.d.	96-97	c
ENDIP	10.2^{*+}	n.d.	n.d.	✓	n.d.	DLS	n.d.	n.d.	n.d.	98	d
DMAP	7.0^{*+}	n.d.	n.d.	n.d.	n.d.	n.d.	n.d.	n.d.	n.d.	98	e
PTA	13.2	~	n.d.	✓ 20 equiv.	n.d.	ThT + AFM	n.d.	n.d.	n.d.	99	f
btsc	n.d.	n.d.	n.d.	n.d.	n.d.	n.d.	✓	n.d.	✓	100-101	h

Discussion

All of the reported ligands have been separated in different categories, depending on their structures. Their effects on the ROS production, on the aggregation and on the cell toxicities have been reported. Note that the assays performed for each ligand are not the same. Regarding the aggregation assays, ThT assay, Western Blot or turbidimetry assay have been performed. The accuracy of the techniques are not the same and it becomes difficult to comprare the results. For example, with the turbidimetry assay, only the heterogeneity of the sample is probed and not the type of aggregates. For the ThT assay, some studies are performed during 24 h and other ones during one week. Another important issue when comparing the results is that the effect of the Cu removal on the ROS production as well as their radical scavenging capability depend on the ligand itself and also on the experimental condition (*e.g.* ratio ligand:metal:Aβ, order of addition of the reactants, etc.).

The first group, with the hydroxyl/aminoquinolines derivatives, the Bzt like and the stilbene like ligands, are quite planar ligands, supposed to interact with the β-sheets of the Aβ fibrils. They are supposed to impact the apo aggregation of Aβ. They are able to form 2:1 or 1:1 complexes (ligand:metal), depending on the ligand. This can lead to a difficulty in stopping the ROS production. Indeed, in a ternary complex, Cu ions could be in a not rigid geometry and the switch between Cu(II) and Cu(I) could be possible. Nevertheless, this group of ligands have most of the time a good radical scavenging capability (*i.e*. radical scavenging). Furthermore, for a metallophore, a 2:1 complex might not be a good point. Indeed, as the geometry of the complex is not rigid, it is possible to chelate both Cu(II) and Cu(I) easier than for a 1:1 complex. Thus, the release of Cu(I) upon reduction in the cell might be compromised by the high Cu(I) affinity constant.

The other important group is the macrocyclic and peptidic ligands and other ligands such as the salen. They exhibit a very high stability of their associated Cu(II) complex and they mainly form 1:1 Cu complexes. They are able to remove Cu(II) ions from Aβ and to stop the associated deleterious events

such as the ROS production and the Cu-induced aggregation. Nevertheless, they are not designed to have radical scavenging capabilities or interactions with the Aβ peptide. The bis(thiosemicarbazonato) ligands, mainly gtsm, show interesting metallophoric capabilities. They are able to redistribute Cu intra-cellularly, leading to the activation of the Aβ degradation pathways and improving the cognitive performances of AD mice.[100-101]

This section has reported the different ligands already studied in the context of the chelatotherapy against AD with their impacts on the ROS production, on the aggregation, on the cell toxicity and on their metallophoric capability.

II-B The kinetic aspect of the Cu(II) removal

This session focused on the importance of the kinetic of the Cu(II) chelation from Cu-Aβ in the AD context. It is composed of a draft of an article which will be submitted and of the supplementary information. The synthesis of the ligand, the potentiometric and crystallographic studies have been performed by the Tripier's group in Brest. I have written the first draft.

We are currently waiting for EXAFS and EPR fitting data which should confirmed that the structures of the complexes studied are the same in solution than in crystals. Furthermore, the kinetic of the formation of the complexes will be performed later.

II-B.i Draft of the publication

Kinetic is the key when targeting copper ions to fight Alzheimer's disease: an illustration with azamacrocyclic ligands

Amandine Conte-Daban,[a,b] Maryline Beyler,[c] Raphaël Tripier [c] and Christelle Hureau [a,b]

a) CNRS, LCC (Laboratoire de Chimie de Coordination), 205 route de Narbonne, BP 44099 31077 Toulouse Cedex 4, France

b) University of Toulouse, UPS, INPT, 31077 Toulouse Cedex 4, France

c) Université de Bretagne Occidentale, UMR-CNRS 6521, IBSAM, UFR des Sciences et Techniques, 6 avenue Victor le Gorgeu, C.S. 93837, 29238 BREST Cedex 3, France

Abstract

Targeting copper ions to either remove or redistribute them is currently proposed as a possible therapeutic strategy in the context of Alzheimer's disease (AD). Thermodynamic parameters, as for instance the Cu(II) affinity of the drug candidate or the Cu(II) over Zn(II) selectivity, are often/always considered. In contrast, kinetic ones have been overlooked despite their high importance. In the present communication, we use a wide series of azamacrocyclic ligands to demonstrate that kinetic issues has to be taken into account when designing copper chelators or metallophores in the context of AD.

AD is the most common neurodegenerative disorder characterized by the formation of extracellular senile plaques.[102] They are detected in AD brains and contain high levels of Cu and Zn ions embedded with aggregates of the amyloid-β (Aβ) peptide.[103-104] Aggregates of Aβ can be of various size and morphologies with distinct cell toxicity.[105] While metal ions can effect aggregation pathways and final species, neither the mechanism nor the resulting aggregate types are clear-cut. Cu ions are essential and play key biological roles,[106] but due to their redox ability, they play a harmful role in AD.[107-108] Actually, Cu in the presence of a reductant such as ascorbate (Asc) present at 200-400 µM in the synaptic cleft, produces Reactive Oxygen Species (ROS) that participate in the oxidative stress observed in AD and damage neighboring biomolecules.[108] This is one of the main reason why molecules targeting copper ions, mainly Cu(II), have been developed as drug candidates within the context of AD. Such ligands can either remove Cu from Aβ (chelator) and redistribute it (metallophore) and many of them have been reported in the last years.[109-110] They fulfill several requirements, including having a higher affinity for Cu(II) than the Aβ peptide, the ability to redox silence the Cu(II) ion to stop the ROS production and a very high Cu over Zn selectivity.[111] Tetraazamacrocycles are ligands well known for the kinetic inertness and the thermodynamic stability of the complexes counterparts. In particular, 1,4,8,11-tetrazacyclotetradecane (cyclam) and 1,4,7,10-tetraazacyclododecan (cyclen) have been previously tested in the AD context with mitigate results.[112] They are also the scaffold of many chelators used for radiopharmaceutical purposes that bind $^{64/67}$Cu for positron emission tomography[113-115] and Gd for magnetic resonance imaging[116], for instance. As a general trend, Cu(II) complexation with unsubstituted tetraazamacrocycles is quite slow and pending arms are added to help improving the rate of Cu(II) complexation[117-118] as it was observed also with other metals as Gd(III).[119] Inspired by this observation, we report here the use of two families of tetraazamacrocycles based on the cyclen or cyclam scaffold as potential Cu(II) chelators against AD and illustrate the importance of kinetic issues in the removal of Cu(II) from the Aβ peptide.

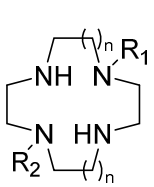

cyclen: n = 1, R_1 = R_2 = H
do1pa: n = 1, R_1 = H, R_2 = CH_2-picolinate
do2pa: n = 1, R_1 = R_2 = CH_2-picolinate
cyclam: n = 2, R_1 = R_2 = H
te1pa: n = 2, R_1 = H, R_2 = CH_2-picolinate
te2pa: n = 2, R_1 = R_2 = CH_2-picolinate

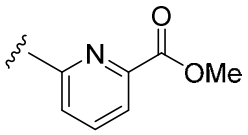

= picolinate

Scheme 1. Representation of the six different azaligands studied in this work.

Scheme 1 show the structure of the six ligands used in the present study. In addition to the non-functionalized cyclen and cyclam ligands, four macrocycles based on cyclen and cyclam ligands and bearing one (do1pa and te1pa, respectively) or two (do2pa and te2pa, respectively) methylpicolinate pendant arms are under study (Scheme S1). The last one is new and as for its three analogues, has been obtained following the regiospecific N-functionnalization of the macrocycle via the bisaminal chemistry (See synthetic scheme in the Supporting Information, Scheme S1). A view of the structure of the Cu(II) corresponding complex is shown in Figure 1, while bond distances and angles of the metal coordination environment are given in the caption (see also Tables S1 and S2). The central Cu(II) cation is six-coordinated in a highly elongated octahedral geometry, with the four nitrogen atoms of the macrocycle in the equatorial plane and the two nitrogen atoms of the picolinate arms at the apical positions. The Cu-NH bond are shorter than the Cu-Nalkylated bond ((1.9974(13) and 2.0462(13) Å, respectively) whereas the axial Cu-Nmethylpicolinate bonds are much longer (2.7910(16) Å). The carboxylate function does not participate to the coordination of the metal as it has already been observed with te1pa.[120] This six-coordinated Cu(II) complex adopts the usually observed trans-III configuration (R,R,S,S conformation). The thermodynamic protonation constants of te2pa and its stability constants with Cu(II) were determined in 0.10 M KNO_3 at 25°C using potentiometric titrations. The stepwise constants (log K) and the overall constants (log β) determined are collected in Table S3 while the speciation diagrams are presented in Figures S1-S2. Based on these values, the conditional affinity constant (corresponding to the absolute affinity constant at a given pH) has been calculated and equal $10^{14.9}$ at pH 7.1, a weaker value compared to affinity constants determined for the other two cyclam and te1pa analogues as well as for do2pa (Table 1).[120-121] XANES and EPR signatures of the six Cu(II)-macrocylic complexes in frozen solution are shown in Figure S3-S4 and corresponding EPR parameters are listed in Table 1. XANES fingerprints of Cu(II)-te2pa is reminiscent of those of the parent Cu(II)-cyclam complex in line with the X-ray structure (Figure 1) that indicates an extremely long apical distance. EPR signatures and parameters are consistent with an elongated octahedral geometry and a 4N binding set in the equatorial plane.[122]

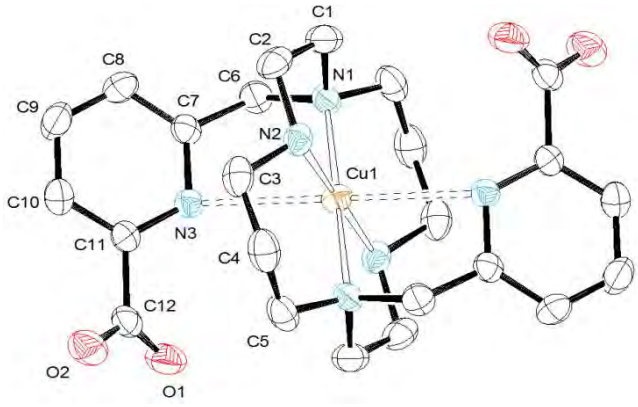

Figure 1. X-ray crystal structures of Cu(II)-**te2pa** with atom labelling; hydrogen atoms and water molecules are omitted for simplicity. The ORTEP plots is drawn at the 30% probability level. Cu-N(1) = 2.0604(15), Cu-N(2) = 1.9906(15), Cu-N(3) = 2.7910(16), N(1)-Cu-N(2) = 86.61(6), N(1)-Cu-N(2) = 93.39(6), N(1)-Cu-N(3) = 75.81(5), N(2)-Cu-N(3) = 87.90(6), N(3)-Cu-N(1) = 104.19. Symmetry transformations used to generate equivalent atoms: #1 –x+1, -y+1, -z+1

The cyclic voltammogramm of the six Cu(II) complexes (Figure S5) indicate the possibility of reduction but at very low redox potentials (below -0.5 V versus SCE). In addition, the electrochemical reversibility of the cathodic process depend on the complex, with Cu(II)-do1pa, Cu(II)-do2pa and Cu(II)-te1pa showing quasi-reversible reduction process. As a general trend, addition of methylpicolinate arm(s) makes the reduction easier, i.e. the reduction occurs at higher potential (Table 1). Given the value of the cathodic peak, reduction by Asc is thermodynamically disfavored.

Table 1. Thermodynamic, spectroscopic and electrochemical characteristics of the six studied Cu(II) complexes (recorded under the very same conditions).

		Cu(II)-cyclen	Cu(II)-do1pa	Cu(II)-do2pa	Cu(II)-cyclam	Cu(II)-te1pa	Cu(II)-te2pa
Coordination		4Neq 1Oap	5N 1O	5N 1O	4Neq	4 Neq 1Nap	4 Neq
$log\ K_a^{Cu}$ pH7.1		17.4 – 18.8	18.5	17.4	19.9 – 20.8	18.0	14.9
refs.		123-124	120	121	125-126	120	This work
$g_{//}$		2.20 ± 0.01	2.23 ± 0.01	2.23 ± 0.01	2.18 ± 0.01	2.19 ± 0.01	2.18 ± 0.01
$A_{//}(^{65}Cu)$ (10^{-4} cm^{-1})		202 ± 5	187 ± 5	181 ± 5	224 ± 5	211 ± 5	217 ± 5
E_{pc} (V vs. SCE)		- 0.85	- 0.82	- 0.67	- 0.98	- 0.88	- 0.76
Reversibility		Irrev.	Rev.	Rev.	Irrev.	Rev.	Irrev.
ROS	Incubation						
	Cu	✓	✓	✓	✓	✓	✓
	Cu(Aβ)	✓	✓	✓	✓	✓	✓
	No incubation						
	Cu	✓	✓	✓	×	✓	✓
	Cu(Aβ)	×	✓	✓	×	✓	✓

In line with the electrochemical measurements, once the Cu(II) complexes are formed (with any of the six ligands), they are not reduced by Asc as probed by the absence of Asc consumption

monitored by UV-Vis (Figure S6). Similarly, Asc consumption was not observed when Cu(II)-Aβ complex was pre-incubated with the ligand (Figure 2, panels A and B). This is in line with the higher Cu(II) affinity values of the ligands compared to Aβ (see Table 1) and the resistance to Asc reduction of the resulting Cu(II)-L complexes. Hence, the six macrocyclic ligands appear as good candidates for Cu(II) chelatotherapeutic purposes. In order to go further and challenge these ligands under more biologically relevant conditions, the Asc consumption assay was performed differently: Cu(II) (Figure S6) or Cu(II)-Aβ (Figure 2, Panels C and D) was first reacted with Asc and then the ligands were added. Such condition better mimics the brain environment, which is at the same time rich in Asc and dioxygen. Under such conditions, the arrest of Asc consumption depends on the ligand: the arrest is total with do1pa, te1pa and te2pa, quasi-total with do2pa and absent for both cyclam and cyclen. This may be linked to the rate of Cu(II) extraction from Cu(II)-Aβ during the redox cycling. Indeed, there is a competition between Cu(II)-Aβ reduction (and thus Asc consumption) and Cu(II) extraction by the ligands. If the Cu(II) extraction is not fast enough, the system Cu(II)-Aβ continue to redox cycle. Based on the properties of non-substituted and substituted ligands with respect to the rate of Cu(II) complexation, it is anticipated that the addition of the methylpicolinate arm(s) accelerates Cu(II) removal from Aβ.

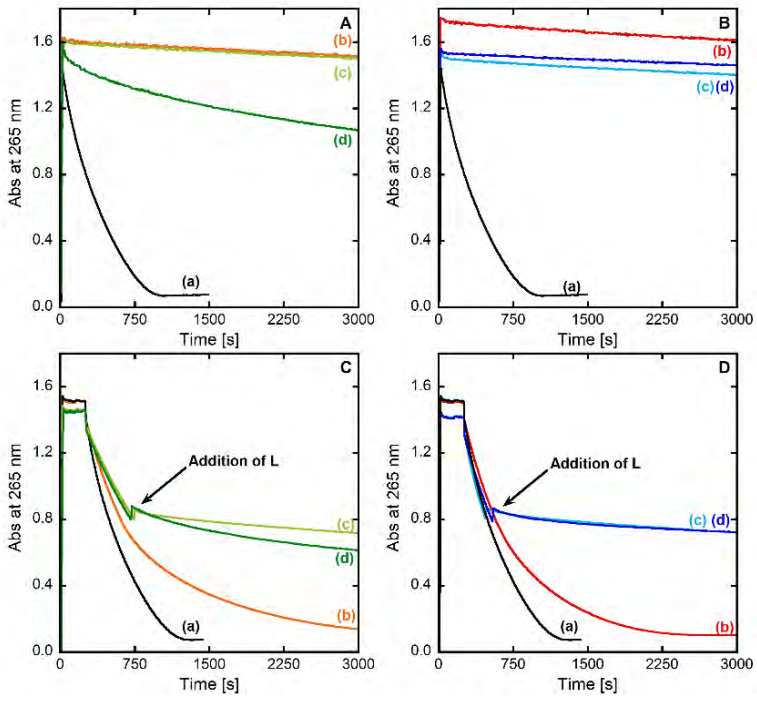

Figure 2. Kinetics of Ascorbate consumption, followed by UV-visible spectroscopy at 265 nm with a background correction at 800 nm. *Panel A*. (a) Aβ16 + Cu(II) + Asc, (b) Aβ16 + Cu(II) + cyclen + Asc, (c) Aβ16 + Cu(II) + do1pa + Asc, (d) Aβ16 + Cu(II) + do2pa + Asc. *Panel B*. (a) Aβ16 + Cu(II) + Asc, (b) Aβ16 + Cu(II) + cyclam + Asc, (c) Aβ16 + Cu(II) + te1pa + Asc, (d) Aβ16 + Cu(II) + te2pa + Asc. *Panel C*. (a) Asc + Aβ16 + Cu(II), (b) Asc + Aβ16 + Cu(II) + cyclen, (c) Asc + Aβ16 + Cu(II) + do1pa, (d) Asc + Aβ16 + Cu(II) + do2pa. *Panel D*. (a) Asc + Aβ16 + Cu(II), (b) Asc + Aβ16 + Cu(II) + cyclam, (c) Asc + Aβ16 + Cu(II) + te1pa, (d) Asc + Aβ16 + Cu(II) + te2pa. [L] = [Aβ16] = 12 µM, [Cu(II)] = 10 µM, [Asc] = 100 µM, [HEPES] = 100 mM, pH 7.1. Note that the experiments are performed under aerobic conditions.

It is worth noting the the Asc consumption experiments has previously been proved to mirror the formation of ROS, in particular H_2O_2 and HO°.[127] Here, we also directly monitor the formation HO° using the CCA Assay (Figure S7) and the results perfectly match those of the Asc consumption assay.

As modulation of Aβ aggregation by Cu ions could potentiate the toxicity of the Aβ aggregates, we also test the six ligands for the ability to prevent formation of Cu(II)-type fibrils and restore the formation of apo-like fibrils. All six ligands have the ability to do so, as evidenced either by the monitoring of kinetic of fibrils formation using the classical ThT assay and the morphologies of the Cu(II)-type or apo-type fibrils as imaged by TEM (Figures S8-S9). The identical activity of the six ligands observed here is linked to the time scale of the aggregation experiments (several hours), which allows Cu(II) to be removed from the Aβ peptide by any of them.

In the present communication, we report the study of six macrocyclic ligands to demonstrate how kinetic issues are important in the design of new chelator/metallophore within the AD context (Scheme 2). We in particular show that kinetic parameters can be as important as thermodynamic or structural one. This is particularly clear when comparing the te2pa and the parent cyclam ligand: While the Cu(II) environments are very close in both Cu(II) complexes and the affinity of the latter is higher by about 5 orders of magnitude, the te2pa can remove Cu(II) faster from Aβ and is active against ROS production in contrast to cyclam.

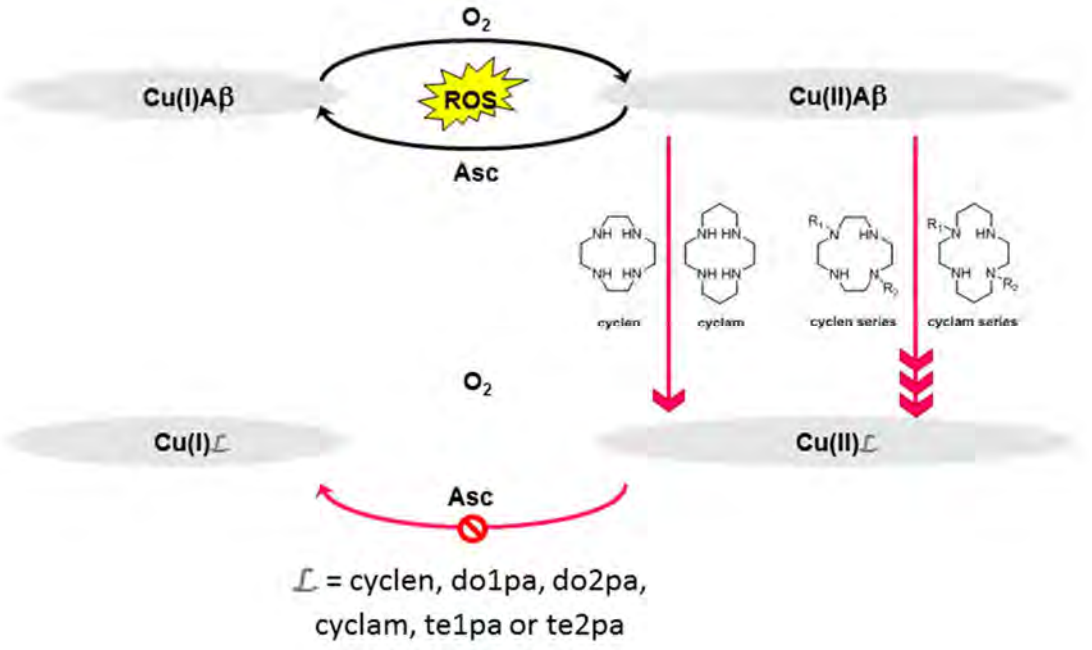

Scheme 2. Scheme representing the kinetic issues studied here, with the six macrocyclic ligands.

More generally, having ligands able to remove Cu from Aβ fast enough may be one new requirement to take into account in the design of drug-candidate against AD, which add to other

better-known requirement such as having an higher Cu affinity, being able to cross the blood brain barrier, not removing Cu ions form essential enzymes.

II-B.ii Supplementary information

SUPPORTING INFORMATION

1-Synthesis of Cu(te2pa) complex

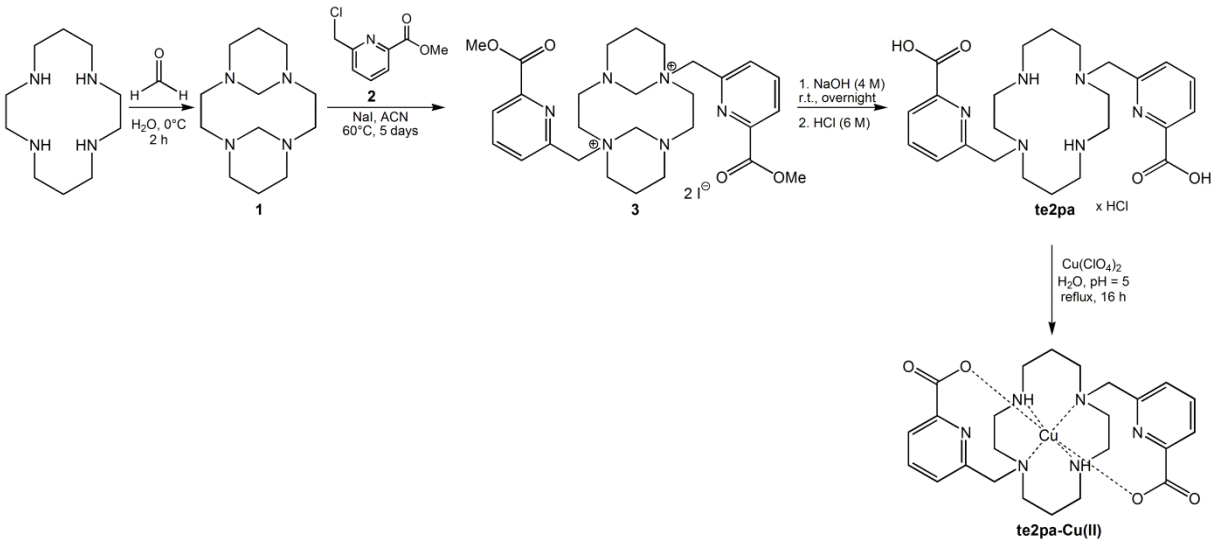

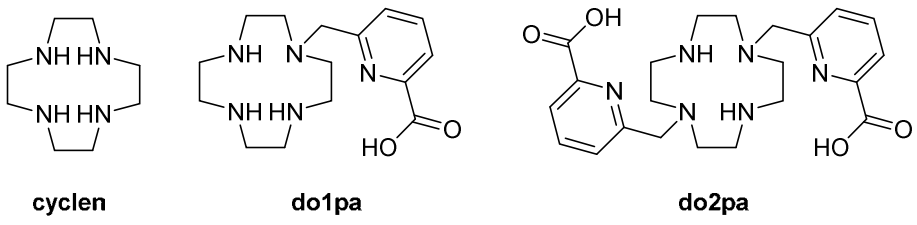

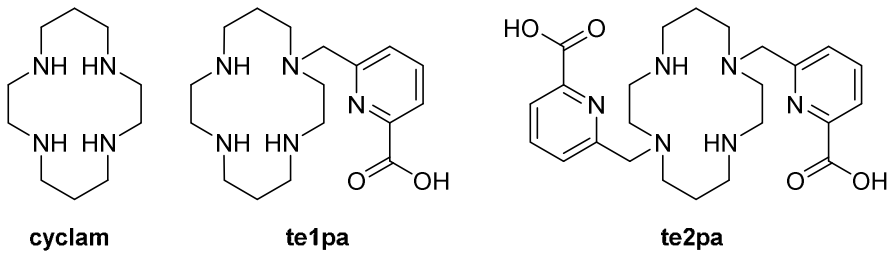

Scheme S1. (Top) Synthetic route to the te2pa ligand and its Cu(II) complex and (bottom) scheme of the six ligands under study.

Compound 3.

Bisformyl-cyclam (**1**) (200 mg, 0.89 mmol) and NaI (540 mg, 3.57 mmol) were dissolved in 10 mL of freshly distilled acetonitrile. Methyl 6-(chloromethyl)picolinate (**2**) (348 mg, 1.88 mmol) dissolved in 10 mL of acetonitrile was added dropwise to the previous solution and the mixture was stirred at reflux for 5 days. The precipitate was filtered and washed with acetonitrile to obtain compound **3** as a white insoluble salt (686 mg, 98 %) that was used without further purification.

Ligand te2pa

An aqueous solution of NaOH 4 M was added to compound **3** (686 mg, 0.88 mmol). The mixture was stirred at r.t. for 3 days. HCl 6 M was added until pH 2. A white precipitate appeared that was filtered and washed with acetone to give **te2pa** as a hydrochloride salt (491 mg, 80 %).

^{1}H NMR (300 MHz, $CDCl_3$): δ 8.05 (m, 4 H), 7.67 (dd, 2 H, ^{3}J = 6.9 Hz, ^{4}J = 2.1 Hz), 3.98 (s, 4H), 3.37 (bt, 4 H, ^{3}J = 5.1 Hz), 3.02 (m, 4 H), 2.86 (bt, 4 H, ^{3}J = 6.0 Hz), 1.97 (bq, 4 H, ^{3}J = 6.3 Hz).

^{13}C NMR (75.47 MHz, $CDCl_3$): 169.7, 160.0, 149.2, 130.6, 127.7, 60.1, 56.5, 52.1, 46.4, 46.2, 25.8

HR-MS: m/z: 236.1396 $[M + 2H]^{2+}$ calcd. 236.1394 for $C_{24}H_{34}N_6O_4$+ $2H^+$, 471.2718 $[M+ H]^+$ calcd. 471.2714 for $C_{24}H_{34}N_6O_4 + H^+$

Caution! *Although no problem was found during our experiments, salts of perchlorate and their metal complexes are potentially explosive and should be handled with great care and in small quantities.*

Cu(te2pa)

Te2pa.xHCl (50 mg, 0.081 mmol) was dissolved in H_2O (5 mL) and the pH adjusted to 5 with a solution of KOH 1 M. $Cu(ClO_4)_2.6H_2O$ (39 mg, 0.11 mmol) was added to the ligand solution. The mixture was refluxed overnight and then concentrated. Acetone was added to precipitate the salts which were removed by filtration. This operation was repeated twice to lead to a purple solid (40.8 mg, 95 %).

ESI-HR-MS (positive, H_2O) *m/z* 266.5967$[M + 2H]^{2+}$ calcd. 266.5963 for $[C_{24}H_{32}CuN_6O_4 + 2H]^{2+}$.

2-X-ray diffraction study of Cu(II)-te2pa.10H_2O

Table S1. Selected bond lengths (Å) and angles (°) of the metal coordination environment in Cu(II)-te2pa. See Figure 1 for labelling.

Cu(1)-N(1)	2.7910(16)
Cu(1)-N(2)	1.9974(13)
Cu(1)-N(3)	2.0462(13)
N(2)-Cu(1)-N(2)#1	180.00(8)
N(2)-Cu(1)-N(1) #1	92.95(6)
N(2)-Cu(1)-N(1)	87.05(6)

Symmetry transformations used to generate equivalent atoms: #1 –x+1, -y+1, -z+1

Table S2. Crystal data and refinement details for **Cu(II)-te2pa.10H_2O**

	Cu(II)-te2pa.10H_2O
formula	$C_{24}H_{52}CuN_6O_{14}$
MW	712.26
crystal system	Monoclinic
space group	$P2_1/c$
T/K	297(2)
a/Å	9.5261(2)
b/Å	12.2915(3)
c/Å	14.3849(4)
β/deg	101.102(2)
V/Å^3	1652.81(7)
F(000)	758
Z	2
λ, Å (MoK_α)	0.71073
D_{calc}/g cm^{-3}	1.431
μ/mm^{-1}	0.733
θ range/deg	3.26 to 30.50

R_{int}	0.0232
reflns measd	16365
unique reflns	4955
GOF on F^2	1.065
R_1[a]	0.0551
wR_2 (all data)[b]	0.1082
Largest differences peak and hole /eÅ^{-3}	0.456 and -0.283

[a] $R1 = \sum \left| \left| F_o \right| - \left| Fc \right| \right| / \sum \left| F_o \right|$. [b] $wR2 = \{\sum[w(\left| \left| F_o \right|^2 - \left| Fc \right|^2)^2] / \sum[w(F_o^4)]\}^{1/2}$

3-Potentiometric study

Table S3. Stepwise and overall protonation and stability constants of **te2pa**$^{2-}$ and its Cu(II) complex at 25.0 ºC and *I* = 0.10 M in KNO_3.

Equilibrium reaction[a]	**log β_{HiL} / log K_{HiL}**
$L + H^+ \rightleftarrows HL$	11.12 / 11.12 (2)
$HL + H^+ \rightleftarrows H_2L$	21.48 / 10.36 (1)
$H_2L + H^+ \rightleftarrows H_3L$	24.86 / 3.38 (2)
$H_3L + H^+ \rightleftarrows H_4L$	27.49 / 2.63 (1)
	log β_{MHiL} / log K_{MHiL}
$L + Cu(II) \rightleftarrows CuL$	23.5 / 23.5 (1)
$CuL + H^+ \rightleftarrows CuHL$	26.47 /2.97 (5)
$CuL \rightleftarrows CuLOH + H^+$	12.47 / -10.93 (6)
pCu[b]	16.8

[a] L denotes the ligand in general; charges of ligand and complex species were omitted for simplicity, [b] Calculated at pH = 7.4 for 100% excess of ligand with $[M^{2+}]_{tot} = 1.0\times10^{-5}$ M

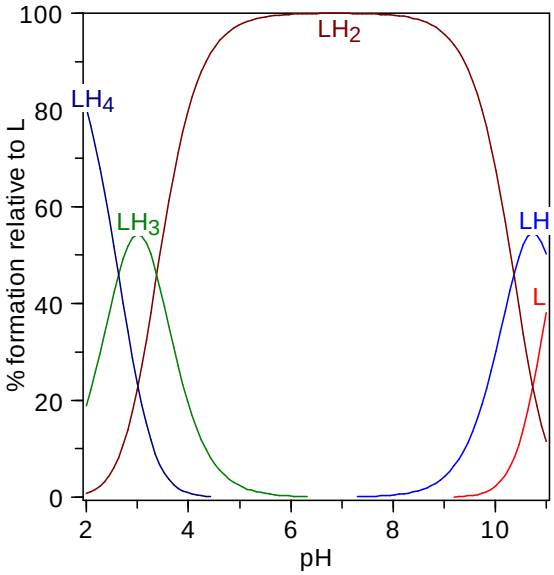

Figure S1. Speciation diagram of the protonated species of **te2pa** in aqueous solution at $[L]_{tot} = 10^{-3}$ M.

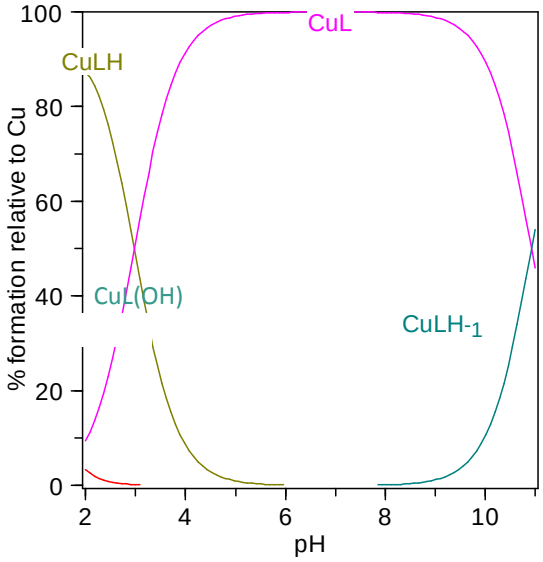

Figure S2. Speciation diagram of **te2pa** in presence of Cu(II) in aqueous solution at $[M^{2+}]_{tot} = [L]_{tot} = 10^{-3}$ M.

4-Spectroscopic signatures of the six Cu(II) complexes

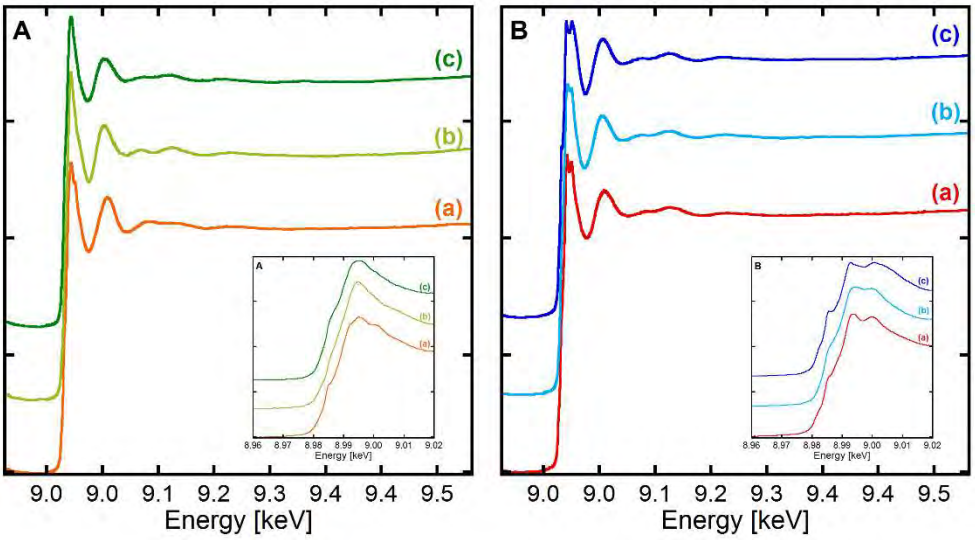

Figure S3. XANES spectra of the different Cu(II) complexes. *Panel A*. (a) Cu(II)-cyclen, (b) Cu(II)-do1pa, (c) Cu(II)-do2pa. *Panel B*. (a) Cu(II)-cyclam, (b) Cu(II)-te1pa, (c) Cu(II)-te2pa. [L] = 1 mM, [Cu(II)] = 0.9 mM, [HEPES] = 100 mM, pH 7.1. 10% of glycerol was used as cryoprotectant. *T* = 20 K.

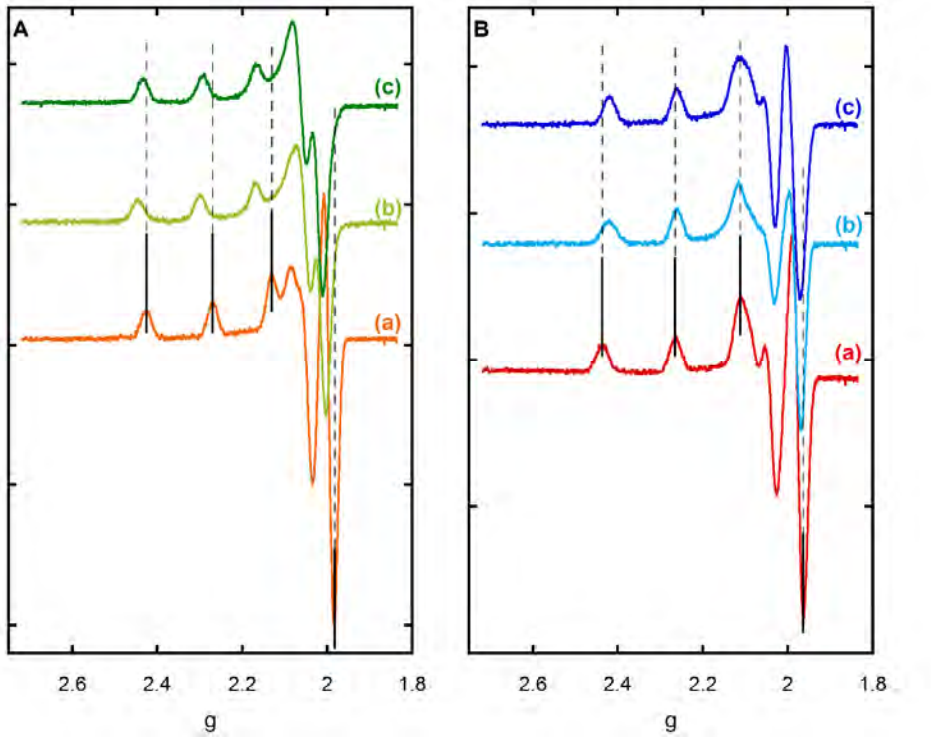

Figure S4. EPR signatures of the different Cu(II) complexes. *Panel A*. EPR experiments of (a) Cu(II)-cyclen, (b) Cu(II)-do1pa, (c) Cu(II)-do2pa. *Panel B*. EPR experiments of (a) Cu(II)-cyclam, (b) Cu(II)-te1pa, (c) Cu(II)-te2pa. [L] = 200 µM, [^{65}Cu(II)] = 190 µM, [HEPES] = 50 mM, pH 7.1. 10% of glycerol was used as cryoprotectant. *T* = 110 K.

5-Cyclic voltammetry signatures of the six Cu(II) complexes

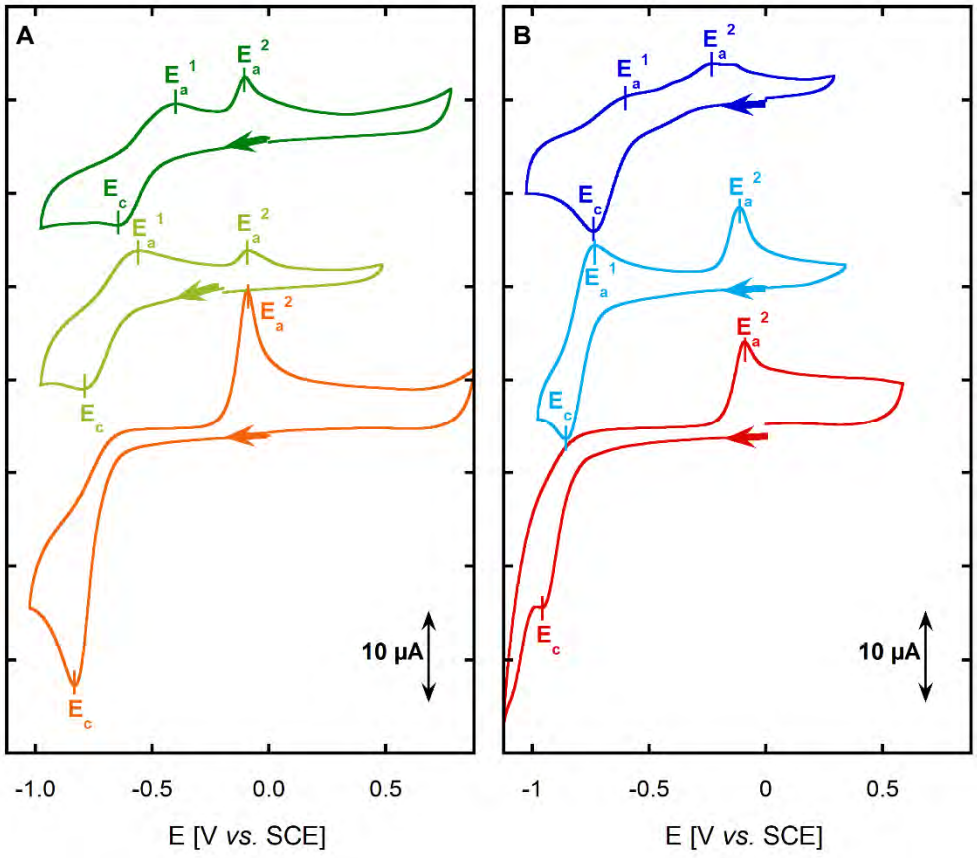

Figure S5. Cyclic voltamograms of the different Cu(II) complexes. *Panel A.* Cu(II)-cyclen (orange curve), Cu(II)-do1pa (light green curve) and Cu(II)-do2pa (dark green line). *Panel B*. Cu(II)-cyclam (red curve), Cu(II)-te1pa (light blue curve) and Cu(II)-te2pa (dark blue line). [L] = 1.00 mM, [Cu(II)] = 0.96 mM, [phosphate buffer] = 100 mM at pH 7.1. The scanning speed is 0.1 $V.s^{-1}$. Saturated Calomel Electrode was used as a reference.

6-ROS production studies

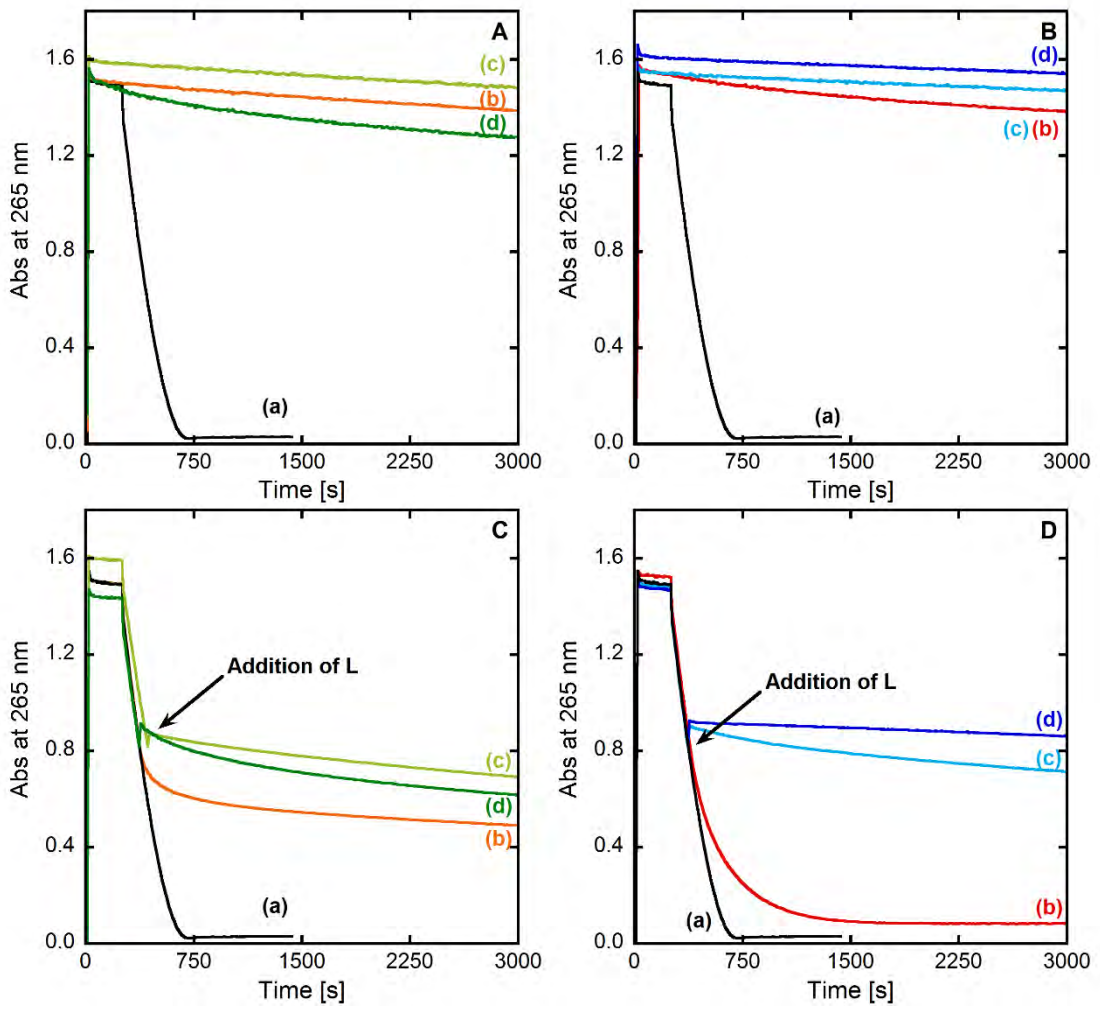

Figure S6. Kinetics of Ascorbate consumption, followed by UV-visible spectroscopy at 265 nm with a background correction at 800 nm. Panel A. (a) Asc + Cu(II), (b) cyclen + Cu(II) + Asc, (c) do1pa + Cu(II) + Asc, (d) do2pa + Cu(II) + Asc. Panel B. (a) Asc + Cu(II), (b) cyclam + Cu(II) + Asc, (c) te1pa + Cu(II) + Asc, (d) te2pa + Cu(II) + Asc. Panel C. (a) Asc + Cu(II), (b) Asc + Cu(II) + cyclen, (c) Asc + Cu(II) + do1pa, (d) Asc + Cu(II) + do2pa. Panel D. (a) Asc + Cu(II), (b) Asc + Cu(II) + cyclam, (c) Asc + Cu(II) + te1pa, (d) Asc + Cu(II) + te2pa. [L] = [Aβ16] = 12 µM, [Cu(II)] = 10 µM, [Asc] = 100 µM, [HEPES] = 100 mM, pH 7.1. Asc is added latter after the first reactants in order to reach the thermodynamic equilibrium.

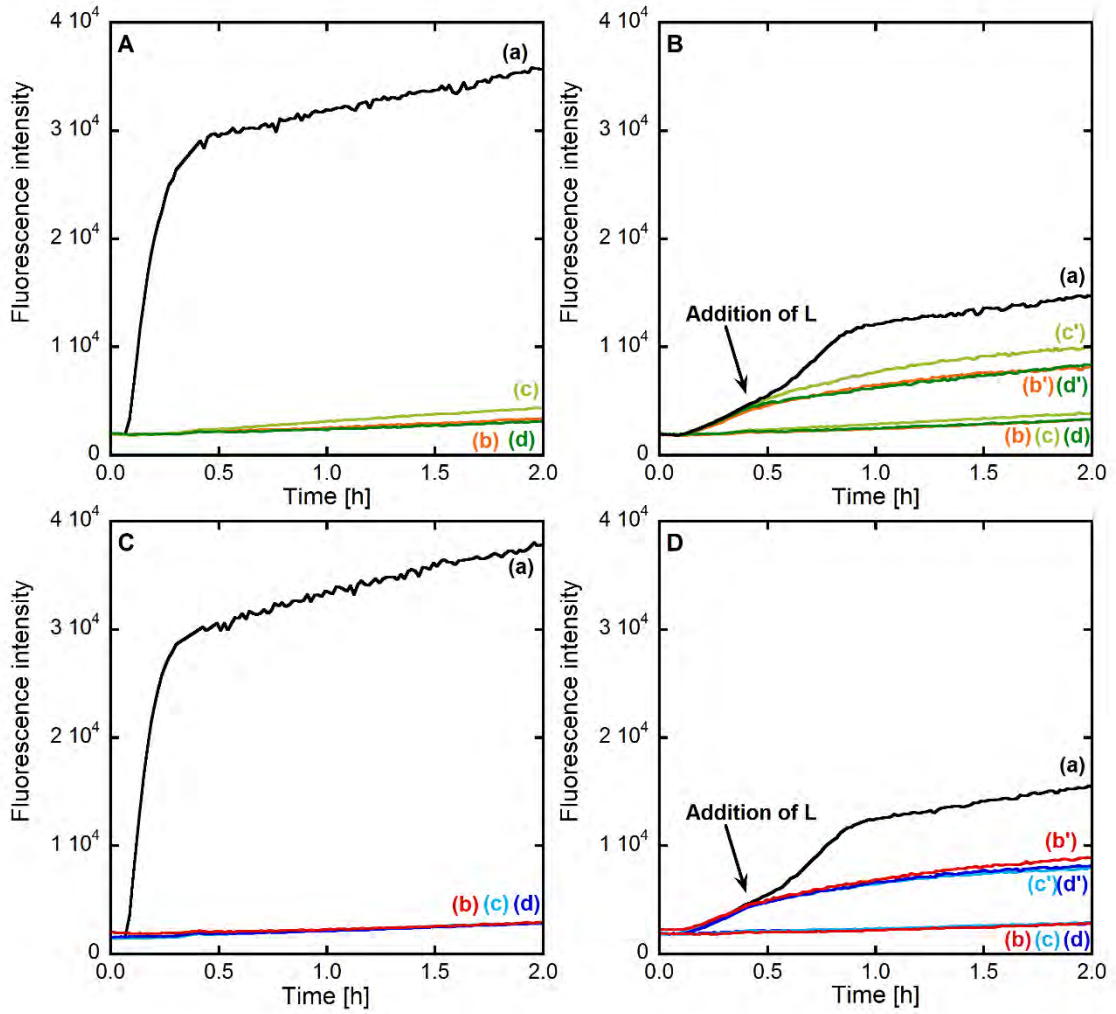

Figure S7. Fluorescence kinetics of CCA experiments. *Panel A*. (a) Cu(II) + Asc, (b) cyclen-Cu(II) + Asc, (c) do1pa-Cu(II) + Asc, (d) do2pa-Cu(II) + Asc. *Panel B*. (a) Aβ16 + Cu(II) + Asc, (b) Aβ16 + Cu(II) + cyclen + Asc, (b') Aβ16 + Cu(II) + Asc + cyclen, (c) Aβ16 + Cu(II) + do1pa + Asc, (c') Aβ16 + Cu(II) + Asc + do1pa, (d) Aβ16 + Cu(II) + do2pa + Asc, (d') Aβ16 + Cu(II) + Asc + do2pa. *Panel C*. (a) Cu(II) + Asc, (b) cyclam-Cu(II) + Asc, (c) te1pa-Cu(II) + Asc, (d) te2pa-Cu(II) + Asc. *Panel D*. (a) Aβ16 + Cu(II) + Asc, (b) Aβ16 + Cu(II) + cyclam + Asc, (b') Aβ16 + Cu(II) + Asc + cyclam, (c) Aβ16 + Cu(II) + te1pa + Asc, (c') Aβ16 + Cu(II) + Asc + te1pa, (d) Aβ16 + Cu(II) + te2pa + Asc, (d') Aβ16 + Cu(II) + Asc + te2pa. If Asc is the last reactant, it was added 5 min after the beginning of the measurement. For the experiments A(b), A(c), A(d), B(b), B(c), B(d), C(b) and D(b), the samples were prepared 1 to 2 days before the addition of Asc. [L] = [Aβ16] = 12 µM, [Cu(II)] = 10 µM, [CCA] = 500 µM, [Asc] = 500 µM, [phosphate buffer] = 50 mM, pH 7.3.

7-Aggregation study

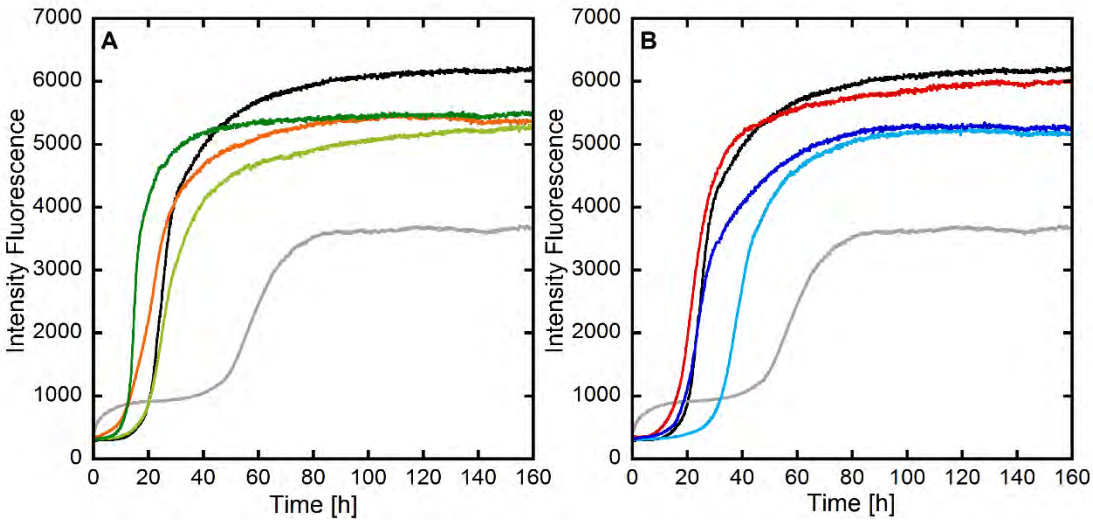

Figure S8. Aggregation curves of Aβ peptide. *Panel A*. Kinetics of ThT fluorescence of Aβ (black curve), Cu(II)-Aβ (grey curve), Cu(II)-Aβ + cyclen (orange curve), Cu(II)-Aβ + do1pa (light green curve), Cu(II)-Aβ + do2pa (dark green curve). *Panel B*. Kinetics of ThT fluorescence of Aβ (black curve), Cu(II)-Aβ (grey curve), Cu(II)-Aβ + cyclam (red curve), Cu(II)-Aβ + te1pa (light blue curve), Cu(II)-Aβ + te2pa (dark blue curve). [L] = [Aβ40] = 20 µM, [Cu(II)] = 18 µM, [ThT] = 10 µM, [HEPES] = 50 mM, pH 7.1, *T* = 37°C.

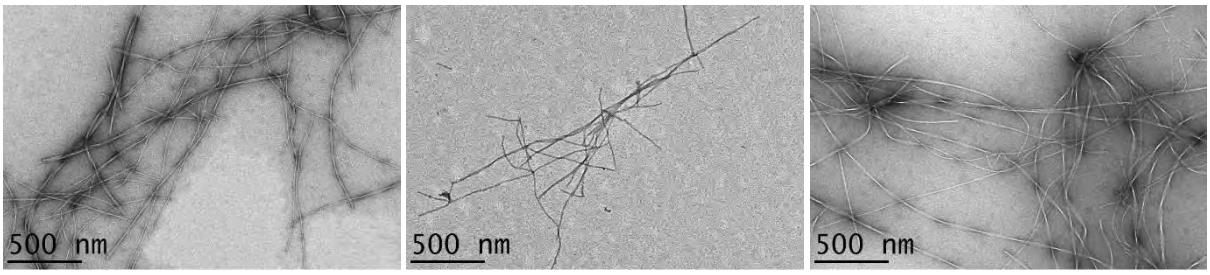

Figure S9. TEM images of Aβ40 (left image), Cu(II)-Aβ (central image) and Aβ40 + Cu(II) + te2pa (right image).

8-Experimental details

Synthesis. Reagents were purchased from ACROS Organics and from ALDRICH Chemical Co. Cyclam was purchased from Chematech (Dijon, France). Bisformyl-Cyclam (**1**)[128] and methyl 6-(chloromethyl)picolinate (**2**)[129] were synthesized as previously described. The solvents were freshly distilled prior to use and according to the standard methods. NMR spectra (^{1}H and ^{13}C) were recorded at the core facilities of the University of Brest, with Bruker Avance 500 (500 MHz) or Bruker AMX-3 300 (300 MHz) spectrometers. The HR-MS analyses were performed at the Institute of Analytic and Organic Chemistry, ICOA in Orléans.

Reagents, except the different ligands, were commercially available and were used as received. All the solutions were prepared in milliQ water (resistance: 18.2 MΩ.cm).

The Cu(II) ion source was $CuSO_4.5H_2O$, bought from Sigma-Aldrich.

HEPES buffer (sodium salt of 2-[4-(2-hydroxyethyl)piperazin-1-yl]ethanesulfonic acid) was bought from Sigma-Aldrich. A stock solution was prepared at 500 mM, pH = 7.1.

Phosphate buffer was bought from Sigma-Aldrich. Two stock solutions, K_2HPO_4 and KH_2PO_4, were prepared at 500 mM, and they were mixed until to reach a stock solution at pH = 7.1.

Sodium ascorbate was bought from Sigma-Aldrich. A stock solution was prepared at 5 mM each day because of the quick degradation of the ascorbate.

Coumarin-3-carboxilic acid (CCA) was bought from Acros Organics. A stock solution at 5 mM was prepared in phosphate buffer at 500 mM, pH = 7.1. The stock solution was stored at 4°C.

Thioflavin T (ThT) was bought from Acros Organics. A stock solution of ThT at 250 µM was prepared in water without any further purification.

Peptides. Aβ16 (DAEFRHDSGYEVHHQK) was bought from Genecust. A stock solution of about 10 mM was prepared and titrated using the Tyr chromophore, with ε = 1410 cm^{-1} M^{-1} at acidic pH. The stock solution was stored at 4°C.

Aβ40 (DAEFRHDSGYEVHHQKLVFFAEDVGSNKGAIIGLMVGGVV) was bought from Genecust. Around 6 mg were dissolved in approx. 400 µL of NaOH 50 mM. This solution was purified by FPLC, with a Superdex 75 column and NaOH 15 mM as eluent, with a flow rate at 0.9 mL min^{-1}. The collected fractions were titrated using the Tyr chromophore, with ε = 2400 cm^{-1} M^{-1} at basic pH. The stock solution was directly used for the ThT experiments.

Single crystal X-ray diffraction measurements. Single-crystal X-ray diffraction data were collected at 170 K on an X-CALIBUR-2 CCD 4-circle diffractometer (Oxford Diffraction) with graphite-monochromatized MoK_α radiation (λ = 0.71073). Crystal data and structure refinement details are given in Table 5. Unit-cell determination and data reduction, including interframe scaling, Lorentz, polarization, empirical absorption and detector sensitivity corrections, were carried out using attached programs of Crysalis software (Oxford Diffraction).[130] Structures were solved by direct methods and refined by full matrix least squares method on F^2 with the SHELXL[131] suites of programs. The hydrogen atoms were identified at the last step and refined under geometrical restraints and isotropic U-constraints.[132] CCDC number 1540075-1540076 contains the supplementary crystallographic data for this paper. These data can be obtained free of charge from the Cambridge Crystallographic Data Centre via www.ccdc.cam.ac.uk/data_request/cif.

Potentiometric studies.

Equipment and Work Conditions The potentiometric setup consisted of a 50 mL glass-jacketed titration cell sealed from the atmosphere and connected to a separate glass-jacketed reference electrode cell by a Wilhelm type salt bridge filled with 0.1 M KNO_3 electrolyte. An Orion 720A+ measuring instruments fitted with a Metrohm 6.0123.100 glass electrode and a Metrohm 6.0733.100 Ag/AgCl reference electrode was used for the measurements. Batch points were measured with a Metrohm 6.0233.100 combined glass electrode. The ionic strength of the experimental solutions was kept at 0.10 ± 0.01 M with KNO_3; temperature was controlled at 298.2 ± 0.1 K using a Huber CC3-K6 compact cooling and heating bath thermostat and a previously calibrated Orion 91-70-06 ATC-probe. Atmospheric CO_2 was excluded from the titration cell during experiments by slightly bubbling purified nitrogen on the experimental solution. Titrant solutions were added through capillary tips at the surface of the experimental solution by a Metrohm Dosimat 665 automatic buret. Titration procedure is automatically controlled by software after selection of suitable parameters, allowing for long unattended experimental runs. The titrant was a KOH solution prepared at *ca.* 0.1 M from a commercial ampule of analytical grade, and its accurate concentration was obtained by application of the Gran's method[133] upon titration of a standard HNO_3 solution. Ligand solution was prepared at *ca.* 2.0×10^{-3} M, and the Cu(II) solution was prepared at *ca.* 0.05 M from analytical grade nitrate salts and standardized by complexometric titrations with H_4edta (ethylenediaminetetraacetic acid).[134] Sample solutions for titration contained approximately 0.04 mmol of ligand in a volume of 30.00 mL. In complexation titrations metal cations were added at 0.9 equiv of the ligand amount. In competition titrations H_4edta was additionally added at 1.2 equiv. Batch titrations were prepared in a similar way with approximately 0.08 mmol of the ligand in a total volume of 3.00 mL, with Cu(II) and H_4edta added respectively at 1 and 2.3 equiv. of the ligand amount. Increasing amounts of standardized KOH solution at ca. 0.1 M were added to each one. Batch titration points were incubated in tightly closed vials at 25 °C until potential measurements attained complete stability.

Measurements. The electromotive force of the sample solutions was measured after calibration of the electrode by titration of a standard HNO_3 solution at 2.0×10^{-3} M in the work conditions. The $[H^+]$ of the solutions was determined by measurement of the electromotive force of the cell, $E = E^{\circ\prime} + Q \log [H^+] + E_j$. The term pH is defined as $-\log[H^+]$. $E^{\circ\prime}$ and Q were determined by acid region of the calibration curves. The liquid-junction potential, E_j, was found to be negligible under the experimental conditions used. The value of $K_w = [H^+][OH^-]$ was found to be equal to $10^{-13.78}$ by titrating a solution of known hydrogen-ion concentration at the same ionic strength in the alkaline pH region, considering $E^{\circ\prime}$ and Q valid for the entire pH range. The protonation constants of H_4edta and the thermodynamic stability

constants of its copper(II) complex used in competition titration refinements were taken from the literature.[135] Each titration consisted of 50–70 equilibrium points in the range pH 2.5-11.5, and at least two replicate titrations were performed for each particular system.

Calculations. The potentiometric data were refined with the HYPERQUAD software,[136] and speciation diagrams were plotted using the HySS software.[137] The overall equilibrium constants β_i^H and β_{MmHhLl} are defined by $\beta_{MmHhLl} = [M_mH_hL_l]/[M]^m[H]^h[L]^l$ ($\beta_i^H = [H_hL_l]/[H]^h[L]^l$ and $\beta_{MH-1L=}\ \beta_{ML(OH)} \times K_w$). Differences, in log units, between the values of protonated (or hydrolyzed) and nonprotonated constants provide the stepwise (log *K*) reaction constants (being $K_{MmHhLl} = [M_mH_hL_l]/[M_mH_{h-1}L_l][H]$). The errors quoted are the standard deviations calculated by the fitting program from all the experimental data for each system.

Electron Paramagnetic Resonance. Electron Paramagnetic Resonance (EPR) data were recorded using an Elexsys E 500 Bruker spectrometer, operating at a microwave frequency of approximately 9.5 GHz. Spectra were recorded using a microwave power of 5 mW across a sweep width of 120 mT (centred at 310 mT) with modulation amplitude of 1.0 mT. Experiments were carried out at 110 K using a liquid nitrogen cryostat.

EPR samples were prepared from stock solution of ligand diluted down to 0.2 mM in H_2O. 0.95 eq. of ^{65}Cu(II) was added from 25 mM $^{65}Cu(NO_3)_2$ stock solution home-made from a ^{65}Cu foil. If necessary, pH was adjusted with H_2SO_4 and NaOH solutions. Samples were frozen in quartz tube after addition of 10% glycerol as a cryoprotectant and stored in liquid nitrogen until used.

Electrochemistry. Cyclic voltamogram were recorded on an Autolab PGSTAT302N at 25°C. Saturated Calomel Electrode was used as a reference, Platine electrode was the counter electrode and the working electrode was a glassy carbon electrode. This last electrode was carefully polished before each measurement on a red disk NAP with 1 µm AP-A suspension under abundant distillate water flow during at least three minutes (Struers). The solution was deoxygenated by bubbling Argon before each measurement. Any support electrolyte was added because of the high concentration of phosphate buffer in the solution. The scanning speed was 0.1 $V.s^{-1}$. The samples were prepared from stock solutions of ligand and Cu(II) down to approx. 1 mM and 0.9 mM respectively in a buffered solution.

UV-Visible spectrophotometry. UV-vis kinetics were recorded on a spectrophotometer Agilent 8453 at 25°C in 1 cm path length quartz cuvette, with an 800 rpm stirring. The samples were prepared from stock solutions of ligand, peptide and Cu(II) diluted down to 12, 12 and 10 µM respectively in HEPES solution, pH = 7.1. Ascorbate is diluted down to 100 µM.

CCA experiments were recorded on a FLUOstar OPTIMA BMG LABTECH at 25°C in a 96-well plate bought from Dutscher SAS. CCA was excited at 390 nm and the fluorescence was recorded at 450 nm. The gain was 1350. The samples were prepared from stock solutions of ligand, peptide and Cu(II) diluted down to 12, 12 and 10 µM respectively in phosphate solution, pH = 7.1. CCA was added at a resulting concentration of 500 µM. Injector was used for the addition of ascorbate diluted down to 500 µM, 5 min after the beginning of the experiment.

ThT experiments were recorded on a FLUOstar OPTIMA BMG LABTECH at 37°C in a 384-well plate bought from Dutscher SAS. ThT was excited at 440 nm and the fluorescence was recorded at 490 nm. The gain was 1200. The samples were prepared from stock solutions of ligand, peptide and Cu(II) diluted down to 20, 20 and 18 µM respectively in HEPES buffer, pH = 7.1. ThT was added at a resulting concentration of 10 µM.

Transmission electron microscopy. Specimens were prepared for electron microscopy using the conventional negative staining procedure. 20 µL of solution was absorbed on Formvar-carbon-coated grids for 2 min, blotted, and negatively stained with uranyl acetate (1%) for 1 min. Grids were examined with a TEM (Jeol JEM-1400, JEOL Inc, Peabody, MA, USA) at 80 kV. Images were acquired using a digital camera (Gatan Orius, Gatan Inc, Pleasanton, CA, USA) at a x 25 000 magnification.

II-C A Cu(I) and Cu(II) chelator

This session focused on a chelator able to chelate Cu(II) but also Cu(I). It is composed of a summary of the article published in *Chemistry – A European Journal* in 2017, then the publication itself and finally the supporting information. The synthesis of the ligand, the potentiometric studies and the mass spectroscopy analyses have been performed by the Delangle's group in Grenoble.

II-C.i Summary

This article describes a chelator able to remove both Cu(II) and Cu(I) from the Aβ peptide within the context of Alzheimer's disease. In most cases of the literature, only Cu(II) chelators are studied, although the redox state of Cu ions bound to Aβ in the synaptic clefts is not known. Moreover, as previously detailed, the Cu-Aβ complex has the capability to produce ROS in presence of a reductant and O_2. This means that Cu ions cycle between the (+I) and the (+II) redox state during the ROS production. Mostly Cu(II) (or Cu(I)) chelators in the literature that are redox-silent have a coordination optimized for Cu(II) (or Cu(I)). Thus, Cu(II) ligands are classically poor Cu(I) ligands and *vice versa*. Thus, a ligand that binds Cu(II) and Cu(I) strongly is new and it is explained in the following why it is also redox-silent.

This ligand, noted **L**, is designed in order to chelate both redox states of Cu ions. As for the Aβ peptide, three Histidine residues are involved in the coordination of the metal ion. They are graft on a nitrilotriacetic platform. **L** has affinities higher than Aβ for Cu(II) and Cu(I) and should be able to remove Cu(II) and Cu(I) from the peptide.

The first step of this study is the synthesis of the ligand. Three Histidine residues are grafted on a nitrilotriacetic acid scaffold. The carboxylate groups of the Histidine residues are amidated to avoid their possible coordination to metal ions. Then, the protonation states are measured.

The next step was the characterization of the complex Cu(II)-**L**. ESI-MS has shown the existence of the complex 1:1 as the unique species. Then, potentiometric studies have been performed and demonstrated three predominant species between pH 3 and pH 8. This leads to a proposition of three binding modes depending on the pH. The first one, at pH around 4, involves two nitrogen atoms from Histidine residues, the third one staying protonated. Two molecules of solvent or O atoms from the CO groups complete the coordination sphere. Around pH 6, the predominant form involves the three Hisitine residues and a solvent molecule or an O atom. Finally, at pH around 7, the three Histidine residues and a deprotonated amide coordinate the Cu(II). The last characterization of the complex has

been performed by EPR. The deduced parameters confirm the three binding modes previously proposed at the different pH.

The third step of this study was the characterization of the Cu(I)-**L** complex. As for the Cu(II) complex, the ESI-MS has shown a 1:1 complex as the unique species. Then, EXAFS experiments have been performed. The intensity of the 1s → 4p transition of Cu(I) corresponds to a tri- or tetra-coordination. The fitting of the EXAFS data proposes three nitrogens (likely from the Histidine residues) and one oxygen as ligands for the Cu(I). Then, the affinity constant of **L** for Cu(I) has been determined by a competition experiment, with ferrozine as a competitor. As expected, for Cu(II) and for Cu(I), **L** shows a higher affinity constant than Aβ, due to its pre-organized scaffold.

The last step of the characterization of the complexes was their electrochemical study. The Cu(I)/Cu(II) redox process is characteristic of a ECEC (E = electrochemical, C = chemical) electrochemical process. Cu(II), under a square planar geometry, is reduced into Cu(I) under the same geometry (E), which reorganizes into a tetrahedral geometry (C). For the reverse oxidation process, the oxidation occurs on Cu(I) in the tetrahedral geometry (E), and then the species rearranges into a square planar geometry (C). Another important parameter is that the reduction of Cu(II)-**L** occurs at a lower potential than the oxidation of the Ascorbate, and the oxidation of Cu(I)-**L** occurs at higher potential than the reduction of O_2. This means that the complexes should resist to the reactions with ascorbate and O_2, *i.e.* if **L** removes Cu ions from the peptide, the ROS production would be slowed down significantly.

The ability of **L** to remove Cu(II) and Cu(I) from the Aβ peptide has been studied by EPR and XANES spectroscopies, respectively. The EPR experiments have shown that one equivalent of **L** is enough to remove almost all Cu(II) from Aβ. A linear combination of the signatures of Cu(II)-Aβ and Cu(II)-**L** proposes that less than 5 % of Cu(II) stays on Aβ. Based on the affinity constants, 0.2 % of Cu(II) should stay on the peptide. The XANES experiments have probed the removal of Cu(I). A linear combination of the spectra of Cu(I)-Aβ and Cu(I)-**L** shows that around 17 % ± 5 % of Cu(I) stay bound to Aβ. This value is also in good agreement with the affinity constants since 30 % of Cu(I) should stay bound to the peptide. These experiments have proved that **L** is able to fully remove Cu(II) and partly Cu(I) from the Aβ peptide, in line with the affinity constants.

The last part of this work was the study of the capability of **L** to stop the ROS production catalyzed by Cu-Aβ. Two indirect methods have been used: the consumption of ascorbate by UV-Vis spectroscopy and the following of 7-OH-CCA formation by fluorescence. The UV-Vis experiments have shown that **L** stops the ROS production in all the configurations: if the Cu(II) or Cu(I) complex is formed before the addition of ascorbate, as well as if **L** is added during the ROS production. The results

obtained by CCA fluorescence assay are consistent. Note that this is not intuitive. Indeed, if a ligand chelates Cu(I) and Cu(II), it may be able to catalyze the ROS production. The hypothesis for **L** is that the geometry and coordination modes for the Cu(I) and Cu(II) complexes are very different. Switching from one complex to another one should take too much time, leading to a strong decrease of the ROS production.

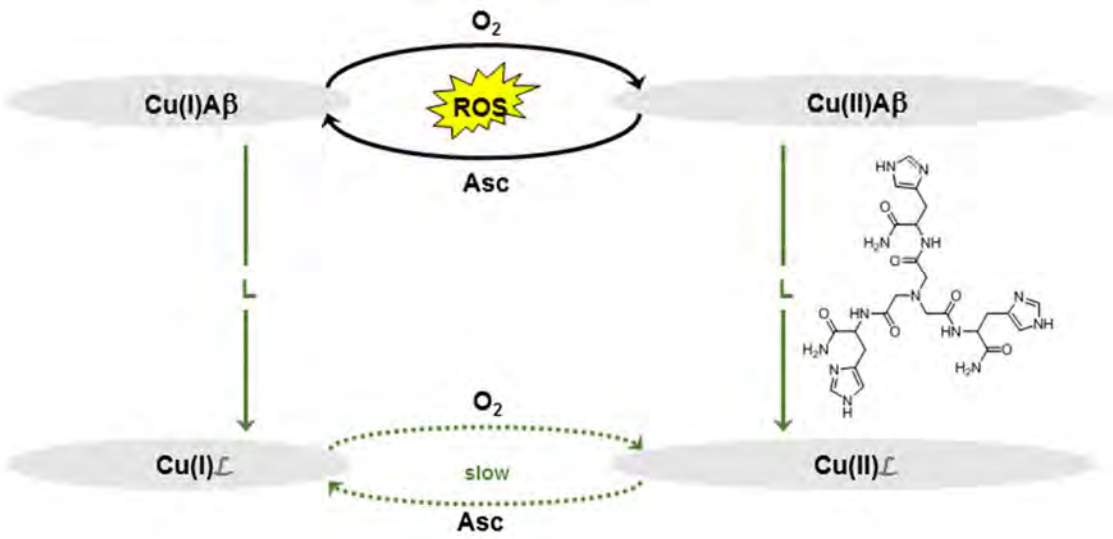

Figure II-3. Scheme representing the ligand L, able to remove both Cu(I) and Cu(II) from Aβ and stop the ROS production.

In summary, this article reports a ligand able to chelate Cu(II) and Cu(I) (Figure II-3). Different characterizations have been performed for both complexes. The binding modes have been proposed, depending on the pH. Affinity constants have been measured. The electrochemical properties of the complexes have shown that after the reduction or oxidation of the metal, a geometric reorganization occurs. In addition, the ability of **L** to remove Cu(II) and Cu(I) from Aβ has been probed by EPR and XANES, and 5 % of Cu(II) and 17 % of Cu(I) stay bound to the peptide. Then the capability of **L** to stop the ROS produced by Cu-Aβ has been proved. The strategy of targeting both Cu(I) and Cu(II) ions shows interesting properties in the context of the removal of Cu ions in the Alzheimer's disease. Furthermore, this could overcome the kinetic issue for a Cu(I) or Cu(II) ligand. Indeed, if the ligand takes more time to remove Cu ions from Aβ than the redox process of Cu-Aβ, the ligand will not be able to remove Cu from Aβ. If the ligand can chelate both metal ions, there is no more kinetic issue.

II-C.ii Article

ChemPubSoc Europe

DOI: 10.1002/chem.201703429

CHEMISTRY A European Journal Full Paper

Bioinorganic Chemistry

A Trishistidine Pseudopeptide with Ability to Remove Both Cu^{I} and Cu^{II} from the Amyloid-β Peptide and to Stop the Associated ROS Formation

Amandine Conte-Daban[+],[a, b] Bastien Boff[+],[c] Andreza Candido Matias,[c, d] Claudia N. Montes Aparicio,[a, b] Christelle Gateau,[c] Colette Lebrun,[c] Giselle Cerchiaro,[d] Isabelle Kieffer,[e, f] Stéphanie Sayen,[g] Emmanuel Guillon,[g] Pascale Delangle,*[c] and Christelle Hureau*[a, b]

Abstract: The pseudopeptide **L**, derived from a nitrilotriacetic acid scaffold and functionalized with three histidine moieties, is reminiscent of the amino acid side chains encountered in the Alzheimer's peptide (Aβ). Its synthesis and coordination properties for Cu^{I} and Cu^{II} are described. **L** efficiently complex Cu^{II} in a square-planar geometry involving three imidazole nitrogen atoms and an amidate–Cu bond. By contrast, Cu^{I} is coordinated in a tetrahedral environment. The redox behavior is irreversible and follows an ECEC mechanism in accordance with the very different environments of the two redox states of the Cu center. This is in line with the observed resistance of the Cu^{I} complex to oxidation by oxygen and the Cu^{II} complex reduction by ascorbate. The affinities of **L** for Cu^{II} and Cu^{I} at physiological pH are larger than that reported for the Aβ peptide. Therefore, due to its peculiar Cu coordination properties, the ligand **L** is able to target both redox states of Cu, redox silence them and prevent reactive oxygen species production by the CuAβ complex. Because reactive oxygen species contribute to the oxidative stress, a key issue in Alzheimer's disease, this ligand thus represents a new strategy in the long route of finding molecular concepts for fighting Alzheimer's disease.

[a] *A. Conte-Daban,[+] C. N. M. Aparicio, Dr. C. Hureau*
CNRS, LCC, Laboratoire de Chimie de Coordination
205 route de Narbonne, BP 44099
31077 Toulouse Cedex 4 (France)
E-mail: christelle.hureau@lcc-toulouse.fr

[b] *A. Conte-Daban,[+] C. N. M. Aparicio, Dr. C. Hureau*
University of Toulouse, UPS, INPT
31077 Toulouse Cedex 4 (France)

[c] *Dr. B. Boff,[+] Dr. A. Candido Matias, Dr. C. Gateau, C. Lebrun, Dr. P. Delangle*
Univ. Grenoble Alpes, CEA, CNRS, INAC, SyMMES, UMR 5819, CIBEST
17 rue des martyrs
F-38 000 Grenoble (France)
E-mail: pascale.delangle@cea.fr

[d] *Dr. A. Candido Matias, Prof. G. Cerchiaro*
Center for Natural Sciences and Humanities
Federal University of ABC-UFABC
09210-580, Santo André, SP (Brazil)

[e] *Dr. I. Kieffer*
BM30B/FAME beamline, ESRF
F-38043 Grenoble cedex 9 (France)

[f] *Dr. I. Kieffer*
Observatoire des Sciences de l'Univers de Grenoble, UMS 832 CNRS Université Grenoble Alpes
F-38041 Grenoble (France)

[g] *Dr. S. Sayen, Prof. E. Guillon*
Institut de Chimie Moléculaire de Reims, ICMR, UMR CNRS 7312
Université de Reims Champagne-Ardenne
F-51687 Reims Cedex 2 (France)

[+] *These authors contributed equally to this work.*

Supporting information and the ORCID identification number(s) for the author(s) of this article can be found under: https://doi.org/10.1002/chem.201703429.

Introduction

Copper enzymes play crucial role in biology, where copper ions exert structural and/or catalytic function(s).[1] However, the copper ions can also be detrimental, illustrated by two genetic disorders, namely Menkes and Wilson's disease, linked to a dysfunction of Cu homeostasis, which induces a depletion of Cu and an overload of Cu, respectively.[2] In Alzheimer's disease (AD), copper ions have been proposed to play a harmful role as well (for recent reviews, see Ref. [3]). Indeed, a high level of copper ions is found in the senile plaques, one of the neuropathological hallmark of AD brains.[4] Due to its redox ability, copper is involved in the production of reactive oxygen species (ROS), taking part in the oxidative stress linked to the etiology of the disease.[3b, 5] It has been shown that when bound to the amyloid-β (Aβ) peptide, the amyloidogenic peptide encountered in AD, copper ions are able to cycle between the +I and +II oxidation states.[6] The resulting CuAβ complex can catalyze the formation of ROS in the presence of dioxygen and of a physiological reductant such as ascorbate,[7] via a complex mechanism.[8] While AD is a multi-factorial disease, involving many biological actors and complex interactions between them (Aβ and Tau protein, secretases responsible of the production of the (non-)amyloidogenic forms of the Aβ, acetylcholine esterase etc.),[9] CuAβ associated ROS over-production is recognized as a key event.[10] Copper ions thus remain a pertinent target for a therapeutic approach,[3d, 5a, 10a, 11] although the

ChemPubSoc Europe

CHEMISTRY A European Journal Full Paper

first clinical trials along this approach failed to benefit patients.[3d,12] Targeting Cu ions requires well-defined coordination-based approaches and ligand design that is, in general, difficult to include in multi-targeted drug in a first-line strategy.[9a] Hence, we designed the chelating moiety of a drug candidate that could be further implemented towards a multi-targeted purpose.

Up to now, most of the synthetic ligands designed to remove copper ions from Aβ have targeted Cu^{II} (see Refs. [3d, 9a, 11, 13] for recent reviews), including peptide-based ligands.[14] Only few studies have focused on Cu^{I} synthetic chelators,[15] based on previous results using naturally occurring Cu^{I} proteins.[16] The reason for such a preference is not clear and has no real biological basis since the extracellular space of brain in which the senile plaques are observed mainly represents a reducing environment.[17]

In the present study, another more "pragmatic" approach is pursued: the ligand **L** (Scheme 1) was designed such as being able to remove either Cu^{II} or Cu^{I} from Aβ. Indeed, in contrast

Scheme 1. $NTA(HisNH_2)_3$, noted **L**. The protonation state and charge of the ligand is given only when necessary.

to other diseases for which the redox state of the targeted copper is quite well-defined—Cu^{II} for blood circulating Cu or Cu^{I} for the intracellular hepatic pool in Wilson's disease for instance[2a]—for neurodegenerative diseases, the situation is less clear although Cu^{II} has been considered as the therapeutic target of choice. The synaptic cleft where the CuAβ interaction occurs[18] is an ill-defined space[19] with a unknown redox potential. In addition, the redox potential might be subject to spacio and/or temporal changes. It has for instance been shown that the level of Aβ can induce a reductive shift of the extracellular potential.[20] In addition, although the redox cycle between Cu^{I} and Cu^{II} is the pre-requisite for ROS production implying that both redox states may be present, one redox state may be largely predominant and it is not known yet which one it is. Thus targeting either Cu^{II} or Cu^{I} might be a uncertain approach; chelators are, in general, specific for one given redox state,[3d,9a,11,13,15a] because Cu^{II} and Cu^{I} coordination requirements are very different[21] (distorted square-planar, with N/O ligands for Cu^{II} and tetrahedral with N,S ligands for Cu^{I}). Hence, the risk is to miss the good target since it has for instance been shown that although being able to remove Cu^{II} from Aβ and being redox inert, tetra-azamacrocycle ligands failed in stopping CuAβ induced ROS production.[22] Therefore, as the redox state of the Cu center in the brain regions has not been identified yet, targeting both Cu oxidation states may be considered as the safest approach.

The coordination sites of Cu^{I} and Cu^{II} to Aβ near physiological pH are reminded in Scheme 2. The Cu^{I} center lies in a digonal environment made by two imidazole groups from the histidine (His) residues at positions 6, 13, and 14, with no strong

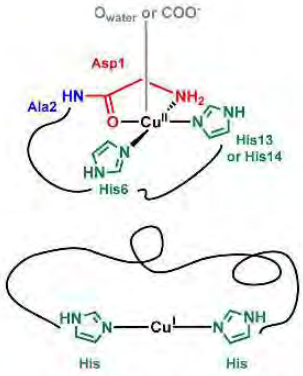

Scheme 2. Main coordination sites of Cu^{II} and Cu^{I} in Aβ at physiological pH.

preference for one His couple among the three possible ones.[3b,23] In the form mainly present at physiological pH, the Cu^{II} center is surrounded by the N-terminal amine, the adjacent carbonyl group from the peptide backbone, and two imidazole rings from the His in a square-planar geometry.[3b,24] To achieve removal of Cu^{I} or Cu^{II} from Aβ, the ligand was based on functional group reminiscent of the amino-acid side-chains encountered in the Aβ peptide, that is, three His.

To benefit from preorganization of metal-binding groups, a tripodal pseudopeptide based on a chemical scaffold was chosen to introduce the three His moieties. The nitrilotriacetic (NTA) scaffold is a perfect candidate to anchor three amino acids that can be grafted to the three acidic functions with peptide amide bonds. Moreover, bioinspired pseudopeptides built up on the NTA template and extended with three sulfur amino acids such as cysteines[25] D-penicillamine[26] or methionine,[27] have proven their capacity to tightly bind Cu^{I} in trigonal planar coordination sites, $Cu^{I}S_3$, with three sulfur donors in the first sphere. Therefore the novel ligand **L** (Scheme 1), based on a similar design with His is expected to make the N-donors of the three amino acids converge to the metal center. Regarding Cu^{I}, the preorganization of the chelating site due to the central amine anchor is expected to increase its affinity compared to that of Aβ by entropic effect. The entropic contribution may also help the ligand having a higher affinity for Cu^{II} compared to Aβ, although changes in the nature of the coordinating moieties are expected.

In the present paper, the structural, thermodynamic and redox characterizations of the Cu^{II} and Cu^{I} complexes with **L** are described. The ability of **L** to remove both Cu^{II} and Cu^{I} ions from $Aβ_{1-16}$ at physiological pH is probed by electronic paramagnetic resonance (EPR) and X-ray absorption near-edge structure (XANES) spectroscopies, respectively. Lastly, the ability

ChemPubSoc Europe

CHEMISTRY A European Journal Full Paper

of **L** to abolish the ROS produced by the CuAβ complex is also demonstrated, which makes the ligand **L** a good candidate for further therapeutic purposes.

Results and Discussion

Synthesis and characterization of L

Synthesis

The histidine moiety to be grafted to the nitrilotriacetic acid scaffold may be chosen among the free acid[28] or C-terminus protected His derivatives. The latter are preferred here over the free carboxylate, which can coordinate to metal ions and have been demonstrated to induce harmful electrostatic repulsions for the formation of the preorganized mononuclear metal complexes with cysteine tripods.[25a] Therefore, the histidine moiety was chosen as the C-terminus primary amide derivative of His (H-His-NH_2), which is neutral, highly soluble in water and stable in physiological conditions.

The synthetic procedure of the ligand **L** (Scheme S1) is similar to previously published procedures for thioether-based pseudopeptides.[27] The coupling reaction of the activated ester nitrilotriacetic acid tri(*N*-succinimidyl) (NTA(NHS)$_3$) with commercially available H-His-NH_2·2 HCl was carried out in presence of *N*,*N*-diisopropylethylamine (DIEA) as a base, leading to the desired pure compound in 11 % yield after RP-HPLC purification.

Protonation of the ligand

The potentiometric studies (Figure 1) have been performed in KCl 0.1 M at 298 K. The protonation constants of **L** could be obtained from the titrations of the free ligand with KOH and HCl and are listed in Table 1.

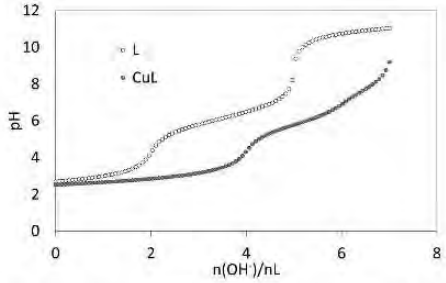

Figure 1. Alkalimetric titrations of solutions containing 10^{-3} M **L**·4 TFA + 10^{-3} M HCl with 0 and 1 equiv of $CuSO_4$ in water KCl 0.1 M at 298 K.

The titration shown in Figure 1 is indicative of three protonation sites with pK_a values characteristic of His nitrogen protonations.[29] The difference between two successive pK_a values is expected to be 0.48 (=log3) if the three His were non interacting and therefore independently deprotonated.[30] Here these differences are 0.62 (pK_{a2}−pK_{a1}) and 0.63 (pK_{a3}−pK_{a2}) and are significantly larger than 0.48, due to the charge repulsion between the protonated arms, which is expected considering their proximity in the tripodal architecture of ligand **L**. The apical nitrogen protonation is not detected because the corresponding pK_a value is too low, in accordance with previous studies with other pseudopeptides (p$K_a \leq 2.8$)[25a] or with the tripodal amide ligand N(CH_2CONH_2)$_3$ (pK_a = 2.6).[31] The three pK_a values of the imidazole nitrogen atoms (pK_a = 5.5–6.75) of the grafted histidine side-chains are consistent with values reported for trishistidyl peptides (pK_a = 5.4–6.9).[32]

Table 1. Protonation and complexation constants from potentiometric measurements in water KCl 0.1 M at 298 K.[a] The numbers *m*, *l* and *h* represent the numbers of metal, ligand and proton in the species, respectively.

	m	*l*	*h*	logβ_{mlh}	pK_a	
LH^+	0	1	1	6.75(3)	6.75(3)	$LH \rightleftharpoons L + H$
LH_2^{2+}	0	1	2	12.87(3)	6.12(6)	$LH_2 \rightleftharpoons LH + H$
LH_3^{3+}	0	1	3	18.42(7)	5.5(1)	$LH_3 \rightleftharpoons LH_2 + H$
$CuLH^{3+}$	1	1	1	16.65(5)	5.5(1)	$CuLH \rightleftharpoons CuL + H$
CuL^{2+}	1	1	0	11.15(5)		
$CuLH_{-1}^{+}$	1	1	−1	5.1(1)	6.0(1)	$CuL \rightleftharpoons CuLH_{-1} + H$
$CuLH_{-2}$	1	1	−2	−2.6(2)	7.7(3)	$CuLH_{-1} \rightleftharpoons CuLH_{-2} + H$

[a] The figures in brackets correspond to the standard deviations of the last figure in three independent titrations.

Cu^{II} complexes

ESI-MS

The formation of the Cu^{II} complex is clearly detected by electrospray-ionization mass spectrometry (ESI-MS). The spectrum recorded in the positive mode with 1 Cu^{II} equiv is shown in Figure S1. The complex Cu^{II}**L** is the unique species detected as the monocation $[L + Cu^{II} - H]^+$ (m/z = 661.1) and its sodium and potassium adducts, with only traces of the free ligand.

Potentiometric titrations

Potentiometric titrations also evidence the formation of Cu^{II} complexes. A typical titration curve is shown in Figure 1. Titrations with 0.5 and 1 equivalent of Cu^{II} could be fitted over the pH range 2.5–8 according to the formation of Cu**L** with various protonation states: Cu**L**H, Cu**L**, Cu**L**H_{-1} and Cu**L**H_{-2}. Titrations performed in excess of Cu^{II} showed some precipitation and therefore they were not included in the fitting process. The corresponding stability constants are given in Table 1. The comparison of the stability constants with literature data,[32] in particular those obtained with polyhistidine peptides leads us to propose the structures drawn in Scheme 3 for Cu**L**H, Cu**L** and Cu**L**H_{-1}.

The stability constant calculated for the Cu**L** complex (logβ_{110} = 11.15) is significantly larger than values reported for short peptides with three His: Ac-HxHxH-NH_2 or Ac-GHHPHG-NH_2 (logβ_{110} = 6.7–8.4),[32a,b] which evidences the greater preorganization of the tripodal pseudopeptide **L** in comparison to linear peptide sequences. The affinity of **L** for Cu^{II} is similar to that reported for a cyclodecapeptide bearing three His resi-

ChemPubSoc Europe

CHEMISTRY A European Journal Full Paper

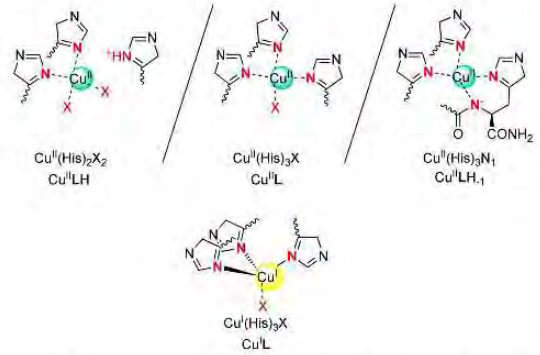

Scheme 3. Proposed coordination in the Cu^{II} and Cu^{I} complexes. X is the solvent or an O atom of an amide function of the ligand.

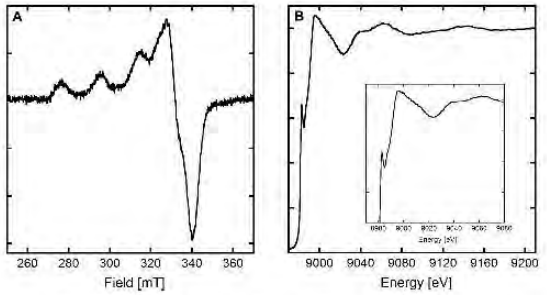

Figure 3. Panel A: EPR spectrum of $Cu^{II}LH_{-1}$, [L] = [$^{65}Cu^{II}$] = 200 μM, [HEPES] = 50 mM, pH 7.1. 10% of glycerol was used as cryoprotectant. T = 110 K. Panel B: Normalized XANES spectrum of Cu^{I}L; [L] = 1.0 mM, [Cu^{II}] = 0.95 mM, [dithionite] = 10 mM, [HEPES] = 100 mM, pH 7.1. 10% of glycerol was used as cryoprotectant. T = 20 K.

dues ($\log\beta_{110} = 11.44$).[32c] This type of peptide scaffold is indeed known to be preorganized in a β-sheet structure that orients the side-chains of several amino acids in the same half-space for metal coordination.[33] The speciation in an equimolar solution of the ligand **L** and Cu^{II} is presented in Figure 2 and shows that the Cu**L** complex protonates below pH 6 to give the Cu**L**H species with only two histidine coordinated to the metal center. The pKa value of Cu**L**H is 5.5 and is similar to literature data.[32a,b] Interestingly the major species at physiological pH is Cu**L**H$_{-1}$ with a pK_a value of the Cu**L** complex of 6.0 in accordance with amide deprotonation to afford a metallacycle involving an amidate and the proximal imidazole nitrogen atom. The coordination sites of Cu^{II} bound to **L** are summarized in Scheme 3 and are consistent with the potentiometric experiments and previously quoted literature data.

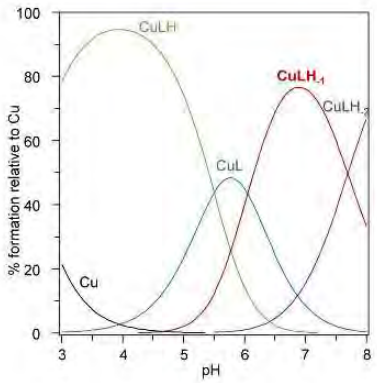

Figure 2. Speciation diagram of a solution containing 1 mM **L** and Cu^{II}. The stability constants tabulated in Table 1 were used to generate this diagram with the speciation program Hyss.[34]

Electron paramagnetic resonance

The EPR spectrum of the Cu**L**H$_{-1}$ species shown in Figure 3, panel A indicates that the Cu^{II} center lies in a distorted square-planar geometry with an elongated Jahn–Teller effect.

The EPR parameters deduced from the spectrum ($g_{\parallel} = 2.23$, $A_{\parallel}(^{65}Cu) = 198 \pm 5 \times 10^{-4}$ cm^{-1}) best fit with a [2N2O] equatorial environment of the Cu^{II} according to the Peisach and Blumberg correlation.[35] However divergences from this phenomenological correlation have previously been observed for imidazole containing ligands,[35,36] especially with constrained geometry.[36a] Such effect may be linked to an orientation of the imidazole rings that doesn't permit the best delocalization of the unpaired density on the Cu center, leading to a weaker covalent character of the N–Cu bond (thus resembling a "O–Cu" bond). In the present case in which a [4N] environment is proposed, this agrees well with the pre-organized and constrained Cu^{II} environment when bound to **L**H$_{-1}$ (Scheme 3).

The EPR spectra of the Cu^{II} complexes recorded as a function of pH are shown in Figure S2. For the Cu**L**H species, a $g_{\parallel} = 2.25$ and a $A_{\parallel}(^{65}Cu) = 202 \pm 5$ 10^{-4} cm^{-1} values are deduced in line with a [2N2O] Cu^{II} environment according to the Peisach and Blumberg correlation.[35] The Cu**L** species is not predominant enough (see the speciation diagram in Figure 2) to evaluate undoubtedly its EPR parameters. The close values observed for Cu**L**H and Cu**L**H$_{-1}$ complexes mirror the flexibility of the ligand when only two His are bound to the metal center and the rigid structure imposed by the same ligand when the three His and a deprotonated amide are folded around the Cu^{II}. In the former case, the imidazole rings may be positioned such as to maximize the covalent character of the Cu–N bond while in the latter case, this is not possible anymore.

Cu^{I} complex

ESI-MS

The ESI-MS spectrum of **L** with 1 Cu^{I} equiv (Figure S3 in the Supporting Information) shows the formation of the Cu^{I}**L** complex as a unique metal species. The detailed observation of the isotopic pattern of the Cu^{I}**L** complex reveals the presence of a small amount of the Cu^{II}**L** complex which may be formed when the solution is taken out the glovebox to perform the experiment. This is in accordance with the ability of this trishistidine ligand to also efficiently chelate Cu^{II} as shown above.

ChemPubSoc Europe

CHEMISTRY A European Journal Full Paper

Cu K-edge X-ray absorption spectroscopy (XAS)

The XANES spectrum of the Cu^{I}**L** complex is shown in Figure 3, panel B. It is characteristic of a Cu^{I} species and the intensity of the 1s→4p transition (approx. 0.65) agrees with a tri- or tetra-coordination of the Cu^{I} center.[1,37] Extended X-ray absorption fine structure data (Figure S4 and Table 2) are consistent with a coordination of Cu^{I} by the nitrogen atoms of the three histidine residues with Cu–N distances of 2.05 Å together with an extra O atom from the solvent/buffer at 1.92 Å, as proposed in Scheme 3. The relatively weak Debye–Waller values (< 0.003 $Å^2$) are consistent with a relatively low structural disorder.

Table 2. First coordination shell structural data obtained from *R* space fits of EXAFS spectra: *N* is the number of neighbors, *R* is the absorber–neighbor distance, σ is the Debye–Waller factor.

	Scattered–backscattered	*N* (± 20 %)	*R* [Å] (± 0.02 Å)	σ^2 [$Å^2$] (± 0.0005 $Å^2$)	*R* factor [%][a]
Cu^{I}**L**	Cu–N	2.57	2.05	0.0021	0.70
	Cu–O	1.24	1.92	0.0027	

[a] *R* factor represents the overall goodness-of-fit.

Affinity of L for Cu^{I}

The conditional stability constant of the Cu^{I}**L** complex was measured at pH 7.4 using ferrozine (Fz) as a competitor according to the reaction given in Equation (1). Indeed, bathocuproine disulfonate (BCS) or bicinchoninate anion (BCA) fully displace the Cu^{I} cation from the ligand even at low competitor concentration. Therefore Fz, which has a lower affinity for Cu^{I} was chosen as a competitor of appropriate affinity to conduct these experiments.[38]

$$CuL + 2\,Fz \rightarrow Cu(Fz)_2 + L \qquad (1)$$

The conditional stability constant of the Cu^{I}**L** complex was calculated using two models found in the literature for the $Cu^{I}(Fz)_2$ complex stability ($\beta_{210}^{pH\,7.4}$).[38] This gives $\log\beta_{110}^{pH\,7.4}$ values for the Cu^{I}**L** complex of 11.1 according to the model of Xiao et al.[38a] and 7.6 according to the model of Alies et al.[38b] Importantly, regardless the model chosen for $Cu^{I}(Fz)_2$, **L** exhibits an affinity for Cu^{I} slightly larger than that found for the $A\beta_{1-16}$ peptide, corresponding to the C-terminally truncated part of the $A\beta_{1-40/42}$ peptides.[38] The difference in the stability constants is $\Delta\log\beta_{110}^{pH\,7.4} = 0.7$ in favor of **L**. As expected, the preorganization of three His in the tripodal pseudopeptide **L** induces a larger affinity for the soft Cu^{I} cation than linear His-containing peptide sequences such as found in the Aβ peptides, which binds Cu^{I} with two His in a dynamic complex with digonal geometry. It is therefore expected that **L** is able to remove Cu^{I} from the $A\beta_{1-16}$ peptide.

In the pseudopeptide series derived from the nitrilotriacetic acid scaffold, the trishistidine ligand **L** displays an affinity for Cu^{I} in between that of the triscysteine[25a] and the tristhioether[27] derivatives, as predicted for peptide sequences with these amino acids at physiological pH.[39]

Redox properties of the Cu complex at physiological pH

The cyclic voltammogram of the $Cu^{II}LH_{-1}$ complex predominant at pH 7.1 is shown in Figure 4. It shows one irreversible cathodic peak at $E^{pc} = -0.65 \pm 0.02$ V versus SCE and an anodic peak on the reverse scan at $E^{pa} = 0.10$ V vs. SCE. The cathodic peak is attributed to reduction of $Cu^{II}LH_{-1}$ complex followed by a structural rearrangement thus explaining the absence of reversibility.

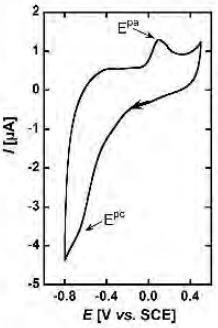

Figure 4. Cyclic voltamogram of $Cu^{II}LH_{-1}$. [L] = 0.2 mM, [Cu^{II}] = 0.18 mM in [phosphate buffer] = 100 mM at pH 7.1 under Ar. Scan rate = 100 mV s^{-1}, WE = Glassy carbon, Ref = SCE, CE = Pt wire.

The origins of such rearrangement may be the change in the copper center geometry from square-planar (SP) to tetrahedral (Td) and the protonation of the amide bond upon reduction (See Scheme 3 and previous paragraphs). The anodic peak then corresponds to the oxidation of the tetrahedral Cu^{I}**L** species, and the irreversibility is due to the inverse changes: tetrahedral to square-planar and deprotonation of the amide bond. The mechanism is thus a classical ECEC (electrochemical–chemical–electrochemical–chemical) square Scheme as shown in Scheme 4. Actually, the chemical reactions are double, that is, structural rearrangement plus protonation/deprotonation processes. Determining whether this protonation/deprotonation steps are concerted with the structural rear-

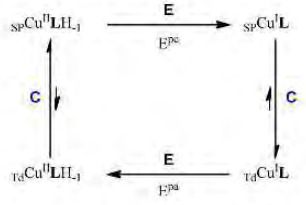

Scheme 4. Proposed ECEC square Scheme to explain the electrochemical data in Figure 4. E = Electrochemical process with the corresponding E^p of Figure 4; C = Chemical process, structural rearrangement and/or protonation/deprotonation events. SP indicates that the geometry of the complex is square-planar and Td that the geometry of the complex is tetrahedral.

ChemPubSoc Europe

CHEMISTRY A European Journal Full Paper

rangement is beyond the scope of the present paper. It is worth noting that the cyclic voltammetry features is strongly reminiscent of what has been previously reported in case of calixarene-based Cu species.[40] However, in the present case, neither the $_{Td}Cu^{II}$ nor the $_{SP}Cu^{I}$ has been observed.[41]

It is important to note that (i) the reduction potential of the Cu^{II} species is well beyond the oxidation potential of ascorbate and (ii) the oxidation of the Cu^{I} complex well above the reduction potential of dioxygen (recorded under the very same conditions, see supplementary Figure S5). Hence, the Cu^{II} complex is expected to resist to reduction by ascorbate and the Cu^{I} complex to oxidation by dioxygen.

Ability of L to remove Cu^{II} and Cu^{I} from the $A\beta_{1-16}$ peptide proved by competition experiments

The removal of the Cu^{II} and Cu^{I} ions from Aβ by the ligand **L** has been directly probed by EPR and XANES spectroscopy, respectively.

Figure 5 shows that 1 equivalent of **L** almost completely removes Cu^{II} from the Aβ peptide. Indeed, the EPR signature in the presence of equimolar concentrations of the ligand **L** and the $A\beta_{1-16}$ peptide is almost superimposable with the one of the $Cu^{II}LH_{-1}$ complex.

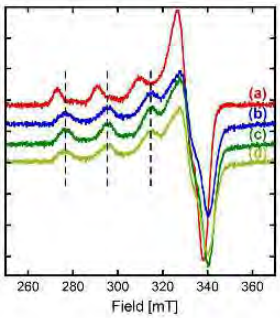

Figure 5. Competition experiments between the $A\beta_{1-16}$ peptide and the ligand **L**. EPR experiments of (a) $Cu^{II}A\beta_{1-16}$, (b) $Cu^{II}L$, (c) $A\beta_{1-16}+Cu^{II}+L$, (d) best linear combination representing (c): 5% (a) + 95% (b). [**L**] = $[A\beta_{1-16}] = [^{65}Cu^{II}] = 200$ μM, [HEPES] = 50 mM, pH 7.1. 10% of glycerol was used as cryoprotectant. $T = 110$ K.

The proportion of Cu^{II} remaining bound to Aβ was experimentally determined by linear combinations of the EPR spectra (see Figures 5 and S6) to be less than 5%. The corresponding theoretical proportion was estimated with the speciation program Hyss.[34] The conditional stability constants used for this calculation were 9.2 (pH 7.1) and 9.7 (pH 7.4) for $Cu^{II}A\beta_{1-16}$ reported in the literature,[42] and $\log\beta_{11} = 12.1$ (pH 7.1) or 12.6 (pH 7.4) for $Cu^{II}L$, obtained from the global protonation and complexation constants given in Table 1. Given the possible modification in equilibria between room temperature and frozen solution studies, the calculated 3.4% value is in total accordance with the 5% experimental value from EPR measurements.

The three orders of magnitude between the affinity constants of the peptide and **L** for Cu^{II} may be assigned to the preorganized tripodal chemical architecture of the pseudopeptide **L** and also to its ability to form an amidate bond with Cu^{II} at physiological pH. These data demonstrate that Cu^{II} can be removed from the N-terminally unmodified Aβ peptide, but not from the relatively abundant N-terminally truncated peptide at position 4 that forms a very high-affinity Cu^{II} site.[43]

A similar competition followed by XANES for Cu^{I} is shown in Figure 6. In the presence of 1 equivalent of **L**, Cu^{I} is removed from the $A\beta_{1-16}$ peptide but to a lesser extent than Cu^{II}. The proportion of Cu^{I} remaining bound to Aβ is evaluated to 17 ± 5% by linear combinations (see Figure 6 and Supporting Information Figure S7). This value agrees well with the log difference in the stability constants of 0.7 in favor of **L** obtained in a previous section. Indeed the speciation program Hyss[34] using the conditional stability constants measured for $Cu^{I}L$ in this paper and previously published for $Cu^{I}A\beta$[38] predicts 30% of Cu^{I} bound to Aβ in these conditions.

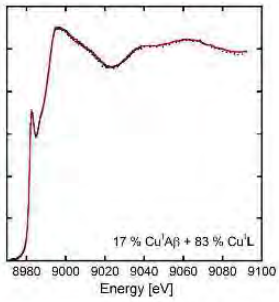

Figure 6. Competition experiments between the $A\beta_{1-16}$ peptide and the ligand **L**. XANES experiments for [**L**] = $[A\beta_{1-16}] = 1.0$ mM, $[Cu^{II}] = 0.95$ mM, [dithionite] = 10 mM, [HEPES] = 100 mM, pH 7.1. 10% of glycerol was used as cryoprotectant. The red line represents the experimental spectrum and black circles the best linear combination from Athena[44] (17% $Cu^{I}A\beta_{1-16}$ + 83% $Cu^{I}L$).

The trishistidine pseudopeptide **L** is thus able to remove Cu^{I} and/or Cu^{II} from the Aβ peptide at physiological pH.

Reactive oxygen species production

The impact of Cu removal from the monomeric CuAβ for both the $A\beta_{1-16}$ model peptide (used for solubility issue in previous spectroscopic studies) and the $A\beta_{1-40}$ peptide complex by the ligand **L** on ROS production was investigated by previously described methods in similar context.[45] We have focused our study on the monomeric peptidic complex, because it is the major form responsible for ROS production, fibrillary forms being less active by one order of magnitude.[46] ROS production corresponds to the incomplete reduction of dioxygen by ascorbate catalyzed by the $Cu^{I/II}A\beta$ complex leading to $O_2^{\bullet-}$, H_2O_2 and $HO^{\bullet}$. Thus, to probe ROS formation, either ascorbate consumption can be followed by UV/Vis at 265 nm or $HO^{\bullet}$ formation can be monitored by the detection of the fluorescent

ChemPubSoc Europe
CHEMISTRY A European Journal Full Paper

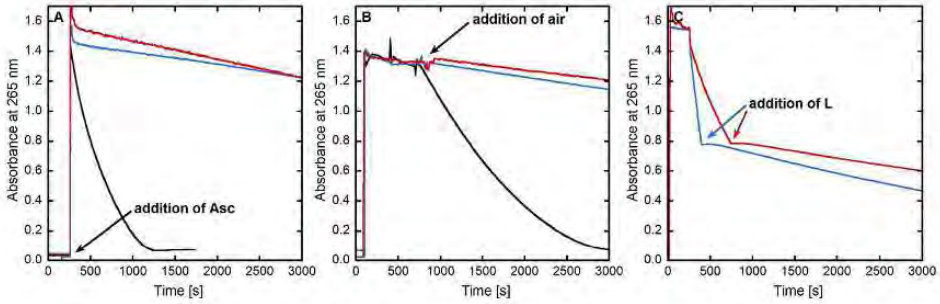

Figure 7. Kinetics of ascorbate consumption, followed by UV/Visible spectroscopy at 265 nm with subtraction of the background signal at 800 nm. Panel A: $A\beta_{1-40}+Cu^{II}+Asc$ (black curve), $L+Cu^{II}+Asc$ (blue curve), $A\beta_{1-40}+Cu^{II}+L+Asc$ (red curve). Panel B: $Cu^{II}+Asc+A\beta_{1-40}+air$ (black curve), $Cu^{II}+Asc+L+air$ (blue curve), $Cu^{II}+Asc+A\beta_{1-40}+L+air$ (red curve). Panel C: $Asc+Cu^{II}+L$ (blue curve), $Asc+A\beta_{1-40}+Cu^{II}+L$ (red curve). [L] = $[A\beta_{1-40}]$ = 12 μM, $[Cu^{II}]$ = 10 μM, [Asc] = 100 μM, [HEPES] = 100 mM, pH 7.1. For the experiments from Panel B, all the solutions were deoxygenated by bubbling argon and were added under a little overpressure of Argon in order to keep Cu under its +I oxidation state.

7-OH-CCA (7-hydroxy-coumarin-3-carboxylic acid) dye formed by reaction of HO$^{\bullet}$ with the CCA (coumarin-3-carboxylic acid) molecule.[7b] It has indeed been shown that the ascorbate consumption perfectly mirrors the H_2O_2 production.[7b,47] The results of ascorbate consumption experiments are shown in Figure 7 and Figure S8 with $A\beta_{1-40}$ and $A\beta_{1-16}$ peptides, respectively. Those of the CCA experiments are described in the Supporting Information (Figure S9). Three different ascorbate consumption experiments were performed representing three starting conditions for ROS production: (i) starting from Cu^{II}, (ii) starting from Cu^{I} and (iii) starting from a mixture of Cu^{I} and Cu^{II}. In the first experiment, the ligand **L** is added to Cu^{II} or $Cu^{II}A\beta$ under aerobic conditions and then ascorbate is added. In the second one, the ligand **L** is added to Cu^{I} or $Cu^{I}A\beta$ under anaerobic conditions and then air is added. In the last one, ascorbate and air are mixed, then either Cu^{II} or $Cu^{II}A\beta$ is added and after a while (typically 8 minutes) the ligand **L** is added. Whatever the experiments, the ligand **L** is able to preclude the production of ROS, in the presence of Cu bound to the buffer only or to Aβ. This mirrors the double ability of the ligand to remove rapidly Cu from the peptide and to redox silence it. These experiments are fully consistent with affinity values as well as with the redox properties of the $CuLH_{-1}$ previously described.

Conclusions

Pseudopeptides based on chemical scaffolds grafted with amino acids with a large affinity for Cu^{I}, such as cysteines, have proven their efficacy in chelating Cu^{I} with coordination properties similar to metallothioneins. Whereas these chelators are proposed as intracellular drugs to treat Cu overload in Wilson's disease, they are not appropriate for Alzheimer's disease (AD), which is not a classical metal overload disease. Such high affinity chelators could deplete the brain in essential metals, whereas AD requires chelating molecules with moderate affinities to not disturb Cu homeostasis. Therefore, the novel pseudopeptide **L** based on functional groups reminiscent of the amino-acid side-chains encountered in the Aβ peptide, that is, three histidines, was designed to get a moderate affinity for Cu^{I} and Cu^{II} and also to target both oxidation states of Cu.

The trishistidine ligand **L** promotes a tetrahedral (Td) geometry around Cu^{I} as suggested by EXAFS, with three nitrogen of the histidines and an extra O-donor from the solvent. Interestingly, the conditional stability constant of the $Cu^{I}L$ complex at physiological pH is significantly lower than those measured with thiolate derivatives, but slightly larger than the one of the $A\beta_{1-16}$ peptide that coordinates Cu^{I} with only two histidines. Potentiometric studies point to a $Cu^{II}LH_{-1}$ complex at physiological pH, with a metallacycle involving an amidate and the proximal imidazole nitrogen atom. According to the EPR parameters, **L** binds the Cu^{II} ion in a square-planar geometry (SP). The conditional stability constant of the Cu^{II} complex at physiological pH is three orders of magnitude larger than the one measured for the $Cu^{II}A\beta_{1-16}$ complex. This might arise from the pre-organized structure of the ligand **L** and also from its ability to form an amidate bond with Cu^{II} at low pH (pK_a of $Cu^{II}L$ = 6.0). **L** can therefore remove Cu^{II} from the N-terminally unmodified Aβ peptide. Other derivatives of the Aβ peptide, such as the abundant N-terminally truncated peptide at position 4 were not studied in this work.[43] The stability constants measured in the present paper indicate that the ligand **L** should not be able to remove Cu^{II} from such truncated peptides that exhibit high-affinity Cu^{II} sites. However, this is not a major issue since when Cu^{II} is bound in this high-affinity site, it is redox silent and doesn't produce ROS.[43b]

The pseudopeptide **L** has therefore a higher affinity than Aβ for both Cu^{I} and Cu^{II} ions enabling it to remove Cu from Aβ regardless of the redox state of the metal center. The very different coordination of Cu^{I} and Cu^{II} in complexes with ligand **L** account for the redox properties obtained by cyclic voltammetry where a ECEC mechanism is observed. It is indicative of a two steps (first the reduction, then a chemical reorganization) process going from $_{SP}Cu^{II}$ to $_{Td}Cu^{I}$ and of a second two steps (first the oxidation, then a chemical reorganization) process going back from $_{Td}Cu^{I}$ to $_{SP}Cu^{II}$. Such redox properties are in line with the resistance of $Cu^{II}LH_{-1}$ to reduction by ascorbate and of $Cu^{I}L$ to oxidation by oxygen and hence with an almost

ChemPubSoc Europe

CHEMISTRY A European Journal Full Paper

inactive CuL complex with respect to ROS production. They are due to the flexibility of the ligand and to its multi-site character. It actually reconciles what seems irreconcilable: (i) In the case of Cu^{II}/Cu^{I} complexes exhibiting redox processes, the possibility to not produce ROS relies on either a very low redox potential or very high potential of the Cu^{II}/Cu^{I} couple. This stabilizes only either the Cu^{II} or the Cu^{I} state of the complex, respectively. Hence, in such a case, only one redox state can be targeted, which is as described in the introduction not the safest option; (ii) in the case of ligands able to target both redox states, the formed complex is generally redox active. In our case, we can fulfil the two required properties (i.e. targeting both redox states and stopping ROS production) because the CuL complex undergoes sluggish redox process (Scheme 5).

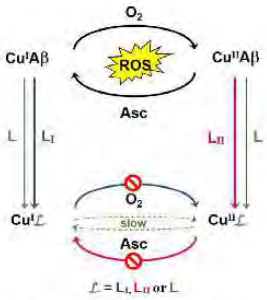

Scheme 5. Two possible approaches to stop CuAβ ROS production. On the one hand, Cu^{I} or Cu^{II} is targeted and the system $Cu^{I}L_{I}$ or $Cu^{II}L_{II}$ is inert toward O_2 or Asc reaction, respectively. Note that this is a prerequisite (see for instance[15a] and[45,48] for ligands L_I and L_{II} ligands) but may be not enough (see Ref. [22]). On the other hand, Cu^{I} ***and*** Cu^{II} are targeted and the associated redox couple is slow. This is what is observed with **L**.

In conclusion, due to its unique Cu coordination properties, the ligand **L** is able to target both redox states of the Cu center and redox silence them. The delivery of **L** and in particular its crossing through the blood brain barrier (BBB) is beyond the scope of the present paper. However, the pseudopeptide **L** structure is versatile enough to be grafted with various functions either to target BBB receptors or for encapsulation in biological vectors. Some of these strategies have been previously developed to target hepatic cells for localized Cu detoxification in Wilson's disease.[2a,49] This ligand thus represents a new strategy in the long route of finding new coordination concepts for fighting AD.

Experimental Section

Synthesis

General information

Solvents and starting materials were purchased from ALDRICH, FLUKA, ACROS ORGANICS, ALFA AESAR and BACHEM and used without further purification. $NTA(NHS)_3$ was obtained according to Jullien et al.[27]. Water solutions were prepared from ultrapure laboratory grade water that has been filtered and purified by reverse osmosis using a Millipore MILLIQ reverse-osmosis cartridge system (resistivity ~18 MΩ cm). The ^{1}H NMR and ^{13}C NMR spectra were recorded on a Bruker Avance 400 MHz spectrometer. The chemical shifts (δ) are reported in ppm with the solvent as the internal reference. The NMR coupling constants (J) are reported in Hz. The mass spectra were acquired with a FINIGAN LXQ-linear ion trap (THERMO Scientific, San Jose, USA) equipped with an electrospray source. Analytical and preparative HPLC were performed with a VWR system fitted with Chromolith RP-18e columns (L = 100 mm, Ø = 4.6 mm for analytical column; L = 100 mm, Ø = 25 mm for preparative column) with A = CH_3CN/H_2O/TFA (*v/v/v* = 90:10:0.1) and B = H_2O/TFA (*v/v* = 99.925:0.075) as solvents. Flow rates of 1 mL min^{-1} and 15 mL min^{-1} were used for analytical and preparative column, respectively.

To a suspension of $NTA(NHS)_3$ (250 mg, 0.518 mmol) in CH_3CN/DMF mixture (15:15 mL), H-His-NH_2·2 HCl (502 mg, 2.21 mmol) and DIEA (0.59 mL, 3.39 mmol) were successively added. After stirring for 48 h at 30 °C, the resulting mixture was concentrated in vacuo. The crude product was purified by preparative C18 reversed-phase HPLC (gradient from A/B: 0:100 to 50:50 in 15 min, Rt = 3.7 min) followed by lyophilisation to afford the desired compound **L**·4TFA (60 mg, Yield 11 %) as a white powder. The number of TFA per ligand in the solid was confirmed by potentiometric titrations. (+)ESI-MS calculated for $C_{24}H_{34}N_{13}O_6$: $[M+H]^+$ *m/z* 600.27, Experimental $[M+H]^+$ *m/z* 600.3. ^{1}H NMR (400 MHz, D_2O, 300 K): δ = 8.63 (s, 3 H, H_2), 7.32 (s, 3 H, H_5), 4.68 (dd, 3 H, ^3J = 6.7 Hz, CH_α), 3.52 (d_{AB}, 3 H, $^2J_{AB}$ = 16.6 Hz, NCH_2), 3.47 (d_{AB}, 3 H, $^2J_{AB}$ = 16.6 Hz, NCH_2), 3.24 ppm (ABX syst., 6 H, J_{AB} = 15.4, J_{AX} = 6.2, J_{BX} = 8.2, $CH_{2\beta}$). ^{13}C NMR (100 MHz, D_2O, 300 K): δ = 174.1 ($CONH_2$), 171.9 (CONH), 133.6 (C_2), 128.4 (C_4), 117.2 (C_5), 57.3 (NCH_2), 52.3 (CH_α), 26.5 ppm ($CH_{2\beta}$) (for ^{1}H NMR and ^{13}C NMR spectra, see Figures S10 and S11 respectively).

Complexation studies

Chemicals

Reagents, except the ligand **L**, were commercially available and were used as received. All the solutions were prepared in milliQ water (resistance: 18.2 MΩ). The Cu^{II} ion source was $CuSO_4{\cdot}5H_2O$ bought from Sigma–Aldrich. The Cu^{I} source, except for XAS samples, was $Cu(CH_3CN)_4PF_6$ bought from Sigma–Aldrich. The stock solution was prepared in acetonitrile and the exact concentration was determined by adding excess sodium bathocuproine disulfonate (BCS) and measuring the absorbance of $Cu(BCS)_2^{3-}$. HEPES buffer (sodium salt of 2-[4-(2-hydroxyethyl)piperazin-1-yl]ethanesulfonic acid) was bought from Sigma–Aldrich. A stock solution was prepared at 500 mM, pH 7.1. Phosphate buffer was bought from Sigma–Aldrich. Two stock solutions, K_2HPO_4 and KH_2PO_4, were prepared at 500 mM, and they were mixed until to reach a stock solution at pH 7.1. Sodium ascorbate was bought from Sigma–Aldrich. A stock solution was prepared at 5 mM each day because of the quick degradation of the ascorbate. Coumarin-3-carboxilic acid (CCA) was bought from Acros Organics. A stock solution at 5 mM was prepared in phosphate buffer at 500 mM, pH 7.1. The stock solution was stored at 4 °C. Sodium dithionite was bought from Sigma–Aldrich. Before each experiment, a stock solution at 1 M was prepared. Ferrozine was bought from Sigma–Aldrich. A stock solution was prepared 20 mM phosphate buffer, pH 7.4, and titrated with the Cu^{I} solution to determine the exact Fz concentration. Peptide. $A\beta_{1-16}$ (DAEFRHDSGYEVHHQK) was bought from Genecust. A stock solution was prepared around 10 mM and stored at 4 °C. Peptide concentration was determined by UV/Visible absorption of

ChemPubSoc Europe

CHEMISTRY A European Journal Full Paper

Tyr10 considered as free tyrosine (at pH 2, $(\varepsilon_{276}-\varepsilon_{296})=1410\ M^{-1}\ cm^{-1}$). $A\beta_{1-40}$ (DAEFRHDSGYEVHHQKLVFFAEDVGSNKGAIIGLMVGGVV) was bought from Genecust. Stock solution of the Aβ40 peptide was prepared by dissolving the powder in 50 mM NaOH at approx. 400 μM. Peptide concentration was then determined by UV/Vis absorption spectroscopy of Tyr10 considered as free tyrosine (at pH 13, $(\varepsilon_{296}-\varepsilon_{360})=2400\ M^{-1}\ cm^{-1}$). The solutions were diluted down to the appropriate concentration in peptide. All pH values are given with a ±0.2 pH unit error.

ESI-MS spectrometry

100 μM pseudopeptide solutions were prepared in ammonium acetate buffer (20 mM, pH 6.9). Cu was added to the peptide solution from stock solutions of $CuSO_4$ in water or $Cu(CH_3CN)_4PF_6$ in acetonitrile, for Cu^{II} and Cu^{I} samples, respectively. Mass spectra were recorded on a LXQ type THERMO SCIENTIFIC spectrometer equipped with an electrospray ionization source and a linear trap detector. Solutions were injected in the spectrometer at $10\ \mu L\ min^{-1}$ flow rate. Ionization voltage and capillary temperature were about 2 kV and 250 °C, respectively.

Potentiometry

All titrant solutions were prepared using water purified by passing through a Millipore Milli-Q reverse-osmosis cartridge system (resistivity 18 MΩ cm). Carbonate-free 0.1 $mol\ L^{-1}$ KOH and 0.1 $mol\ L^{-1}$ HCl were prepared from Fisher Chemicals concentrates. Potentiometric titrations were performed in 0.1 $mol\ L^{-1}$ aqueous KCl under an argon atmosphere, the temperature was controlled to ±0.1 °C with a circulating water bath. The pH (pH = −log[H^+], concentration in molarity) was measured in each titration with a combined pH glass electrode (Metrohm) filled with 3 $mol\ L^{-1}$ KCl and the titrant addition was automated by use of a 751 GPD titrino (Metrohm). The electrode was calibrated in hydrogen ion concentration by titration of HCl with KOH in 0.1 $mol\ L^{-1}$ KCl.[50] A plot of meter reading versus pH allows the determination of the electrode standard potential (E°) and the slope factor (f). Ligand's concentration was determined by potentiometric titrations and was in accordance with the formula $NTA(HisNH_2)_3{\cdot}4TFA$. Continuous potentiometric titrations with KOH 0.1 $mol\ L^{-1}$ were conducted on 20 mL of aqueous solutions containing 10^{-3} $mol\ L^{-1}$ of the ligand and 0, 0.5, 1, and 2 equiv of the Cu^{II} cation. Back titrations with HCl 0.1 $mol\ L^{-1}$ were systematically performed after each experiment to check whether equilibration had been achieved. In a typical experiment, 100 points were measured with a 2 min delay between the measurements for the free ligand, and a 5 min delay for metallic complexes. Experimental data were refined using the computer program Hyperquad 2000.[34,51] Some precipitation was detected in the experiments performed with 2 Cu^{II} equiv below pH 8. Therefore the latter titrations were not included in the fitting process. All equilibrium apparent constants are expressed as concentration ratio and not activities. The ionic product of water at 25 °C and 0.1 $mol\ L^{-1}$ ionic strength is $pK_w=13.78$.[29] The initial concentrations of ligand, metal and proton were fixed, as well as the ligand's pK_a values for the metallic complex stability constant determination. All values and errors (one standard deviation) reported represent the average of at least three independent experiments.

Affinity for Cu^I

The apparent affinity constants at pH 7.4 of the Cu^I complexes were measured by UV/Visible titrations in presence of ferrozine (Fz) as a competitor. The spectra were recorded with a Varian Cary50 spectrophotometer equipped with optical fibers connected to an external cell holder in the glove box. A solution of the Cu^I complex with L in 20 mM phosphate buffer/ MeCN (9:1, *v/v*), pH 7.4, in the UV cell was titrated with Fz. The spectra were then recorded and show the increase of the orange $Cu(Fz)_2^{3-}$ complex which absorbs at 470 nm with a molar extinction coefficient value $\varepsilon=4320\ M^{-1}\ cm^{-1}$. The stability of the absorbance at 470 nm was controlled before the addition of any other aliquots of competitor. The stability constants were then determined using the two models described in the literature: binding constant of the $Cu(Fz)_2^{3-}$ complex ($\log\beta_{12}=15.1$[38a] or $\log\beta_{12}=11.6$).[38b]

Electron paramagnetic resonance

Electron paramagnetic resonance (EPR) data were recorded using an Elexsys E 500 Bruker spectrometer, operating at a microwave frequency of approximately 9.5 GHz. Spectra were recorded using a microwave power of 20 mW across a sweep width of 150 mT (centered at 310 mT) with modulation amplitude of 0.5 mT. Experiments were carried out at 110 K using a liquid nitrogen cryostat. EPR samples were prepared from stock solution of ligand diluted down to 0.2 mM in H_2O. 0.9 equiv. of $^{65}Cu^{II}$ was added from 25 mM $^{65}Cu(NO_3)_2$ stock solution home-made from a ^{65}Cu foil. If necessary, pH was adjusted with H_2SO_4 and NaOH solutions. Samples were frozen in quartz tube after addition of 10% glycerol as a cryoprotectant and stored in liquid nitrogen until used.

X-ray absorption spectroscopy (XAS)

Cu *K*-edge XANES (X-ray absorption near-edge structure) and EXAFS (Extended X-ray absorption fine structure) spectra were recorded at the BM30B (FAME) beamline at the European synchrotron radiation facility (ESRF, Grenoble, France).[52] The storage ring was operated in 7/8+1 mode at 6 GeV with a 200 mA current. The beam energy was selected using a Si(220) N_2 cryo-cooled double-crystal monochromator with an experimental resolution close to that theoretically predicted (namely ≈0.5 eV FWHM at the Cu energy).[53] The beam spot on the sample was approximately 300× 100 μm^2 (H×V, FWHM). Because of the low Cu^I and Cu^{II} concentrations, spectra were recorded in fluorescence mode with a 30-element solid state Ge detector (Canberra) in frozen liquid cells in a He cryostat. The temperature was kept at 20 K during data collection. The energy was calibrated with a Cu metallic foil, such that the maximum of the first derivative was set at 8979 eV. EXAFS Cu data were collected from 8830 to 8970 eV using 2 eV step of 2 s, from 8970 to 9038.5 eV using 0.5 eV step of 3 s, and from 9038.5 to 9828.1 eV with a k-step of 0.05 $Å^{-1}$ and an increasing time 3–10 s per step. At least five scans recorded on different spots were averaged. XANES Cu data were collected from 8830 to 8970 eV using 2 eV step of 2 s, from 8970 to 9038.5 eV using 0.5 eV step of 2 s, and from 9038.5 to 9320 eV with a k-step of 0.05 $Å^{-1}$ and 2 s per step. At least three scans recorded on different spots were averaged. The data analysis was performed using the "Multi-Plateform Applications for X-ray absorption" package, including Cherokee and Roundmidnight programs,[54] according to the standard and previously reported data analysis procedures.[55] Spectra were background-corrected by a linear regression through the pre-edge region and a polynomial through the post-edge region. The back-scattering phase, Φi(k,Ri), and amplitude, Ai(k,Ri), functions were obtained using the ab initio FEFF7 code.[56] Since theoretical phase shifts were used, it is necessary to fit the energy threshold E_0 by adding an extra fitting parameter, ΔE_0. Moreover, the FEFF7 code was used to check if the multiple scattering of our reference compounds of known crystallographic structure is negligible in the 0–

ChemPubSoc Europe

CHEMISTRY A European Journal Full Paper

3 Å range. The estimated errors for distances and coordination numbers are ±0.02 Å and ±20%, respectively. XAS samples were prepared from stock solutions of ligand, peptide $A\beta_{1-16}$ and Cu^{II} diluted down to 1.0 mM in buffered solution (phosphate buffer, pH 7.1). Dithionite was used to reduce Cu^{II} in Cu^{I}. Samples were frozen in the sample holder after addition of 10% glycerol as a cryoprotectant and stored in liquid nitrogen until used. Cu^{II} photoreduction was controlled by recording successive scans at the same spot. It was considered that during the first 20 minutes of recording the photoreduction is insignificant.

Electrochemistry

Cyclic voltamograms were recorded on a Autolab PGSTAT302N at 25 °C. Saturated calomel electrode was used as a reference, platinum electrode was the counter electrode and the working electrode was a glassy carbon electrode. The working electrode was carefully polished before each measurement on a red disk NAP with 1 μm AP–A suspension under abundant distillate water flow during at least three minutes (Struers). The solution was deoxygenated by bubbling Argon before each measurement. Any support electrolyte was added because of the high concentration of phosphate buffer in the solution. The scanning speed was 0.1 $V s^{-1}$. The samples were prepared from stock solutions of ligand and Cu^{II} down to approx. 1 mM and 0.9 mM respectively in a buffered solution. pH was adjusted with H_2SO_4 and NaOH solutions.

Competitions

EPR samples were prepared from stock solutions of peptide $A\beta_{1-16}$ and ligand **L** in HEPES 50 mM pH 7.1 to reach 200 μM concentration of each compound. An aliquot of a 25 mM $^{65}Cu(NO_3)_2$ stock solution home-made from a ^{65}Cu foil was then added to reach a 200 μM Cu^{II} concentration. Samples were frozen in quartz tube after addition of 10% glycerol as a cryoprotectant and stored in liquid nitrogen until used. Remaining Cu^{II}-bound to the $A\beta_{1-16}$ peptide was evaluated by linear combinations of the spectra registered in the same conditions for the $Cu^{II}A\beta_{1-16}$ and Cu^{II}**L** complexes.

XAS samples were prepared from stock solutions of peptide $A\beta_{1-16}$ and ligand **L** in HEPES 100 mM pH 7.1 to reach 1 mM concentration of each compound. An aliquot of a stock solution of $CuSO_4$ was then added to reach a 0.95 mM Cu concentration. Excess dithionite was added (10 mM) to reduce Cu^{II} in Cu^{I}. Samples were frozen in the sample holder after addition of 10% glycerol as a cryoprotectant and stored in liquid nitrogen until used. Remaining Cu^{I}-bound to the $A\beta_{1-16}$ peptide was evaluated by linear combinations of the spectra registered in the same conditions for the $Cu^{I}A\beta_{1-16}$ and Cu^{I}**L** complexes with the program Athena.[44]

ROS formation

UV/Vis kinetics were recorded on a spectrophotometer Agilent 8453 at 25 °C in 1 cm path length quartz cuvette, with an 800 rpm stirring. The samples were prepared from stock solutions of ligand, peptide $A\beta_{1-40}$ or $A\beta_{1-16}$ and Cu^{II} diluted down to 12, 12 and 10 μM respectively in HEPES solution, pH 7.1. Ascorbate is diluted down to 100 μM.

CCA experiments were recorded on a FLUOstar OPTIMA BMG LABTECH at 25 °C in a 96-well plate bought from Dutscher SAS. CCA was excited at 390 nm and the fluorescence was recorded at 450 nm. The gain used was 1350. The samples were prepared from stock solutions of ligand, peptide and Cu^{II} diluted down to 12, 12 and 10 μM respectively in phosphate solution, pH 7.1. CCA was added at a resulting concentration of 500 μM. Injector was used for the addition of ascorbate diluted down to 500 μM, 5 min after the beginning of the experiment.

Acknowledgements

The authors thank Drs. Clémence Cheignon and Fabrice Collin for their contribution in the recording of XAS data and Prof. P. Faller for fruitful discussions. This research was supported by the ERC StG-638712 (C.H.) and Labex ARCANE (Grant ANR-11-LABX-0003-01, P.D.) and the "Fondation pour la Recherche Médicale" (grant DCM20111223043, P.D.). A.C.M. and G.C. thank FAPESP (Bepe 2012/06754-4). The ESRF is acknowledged for providing access to the beamline BM30B (experiments 30-02-1100).

Conflict of interest

The authors declare no conflict of interest.

Keywords: Alzheimer's disease · bioinorganic chemistry · copper · ligand design · peptides

[1] E. I. Solomon, D. E. Heppner, E. M. Johnston, J. W. Ginsbach, J. Cirera, M. Qayyum, M. T. Kieber-Emmons, C. H. Kjaergaard, R. G. Hadt, L. Tian, *Chem. Rev.* **2014**, *114*, 3659–3853.

[2] a) P. Delangle, E. Mintz, *Dalton Trans.* **2012**, *41*, 6359–6370; b) C. Gateau, E. Mintz, P. Delangle in *Rational design of Cu and Fe chelators to treat Wilson's disease and hemochromatosis* (Ed.: T. Storr), Wiley, Chicester, **2014**, pp. 287–319.

[3] a) A. Pal, M. Siotto, R. Prasad, R. Squitti, *J. Alzheimer's Dis.* **2015**, *44*, 343–354; b) C. Hureau, *Coord. Chem. Rev.* **2012**, *256*, 2164–2174; c) P. Faller, C. Hureau, G. La Penna, *Acc. Chem. Res.* **2014**, *47*, 2252–2259; d) S. Ayton, P. Lei, A. I. Bush, *Neurotherapeutics* **2015**, *12*, 109–120; e) A. Avan, T. U. Hoogenraad, *J. Alzheimer's Dis.* **2015**, *46*, 89–92; f) H. Kozlowski, M. Luczkowski, M. Remelli, D. Valensin, *Coord. Chem. Rev.* **2012**, *256*, 2129–2141.

[4] L. M. Miller, Q. Wang, T. P. Telivala, R. J. Smith, A. Lanzirotti, J. Miklossy, *J. Struct. Biol.* **2006**, *155*, 30–37.

[5] a) V. Chiurchiù, A. Orlacchio, M. Maccarrone, *Oxid. Med. Cell. Longevity* **2016**, *2016*, 7909380; b) K. A. Jellinger, *Int. Rev. Neurobiol.* **2013**, *110*, 1–47.

[6] a) V. Balland, C. Hureau, J.-M. Savéant, *Proc. Natl. Acad. Sci. USA* **2010**, *107*, 17113–17118; b) L. G. Trujano-Ortiz, F. J. González, L. Quintanar, *Inorg. Chem.* **2015**, *54*, 4–6.

[7] a) C. Hureau, P. Faller, *Biochimie* **2009**, *91*, 1212–1217; b) S. Chassaing, F. Collin, P. Dorlet, J. Gout, C. Hureau, P. Faller, *Curr. Top. Med. Chem.* **2012**, *12*, 2573–2595; c) D. G. Smith, R. Cappai, K. J. Barnham, *Biochim. Biophys. Acta Biomembr.* **2007**, *1768*, 1976–1990.

[8] a) L.-E. Cassagnes, V. Hervé, F. Nepveu, C. Hureau, P. Faller, F. Collin, *Angew. Chem. Int. Ed.* **2013**, *52*, 11110–11113; *Angew. Chem.* **2013**, *125*, 11316–11319; b) C. Cheignon, M. Jones, E. Atrián-Blasco, I. Kieffer, P. Faller, F. Collin, C. Hureau, *Chem. Sci.* **2017**, *8*, 5107–5118.

[9] a) M. A. Santos, K. Chand, S. Chaves, *Coord. Chem. Rev.* **2016**, *327*, 287–303; b) S. O. Bachurin, E. V. Bovina, A. A. Ustyugov, *Med. Res. Rev.* **2017**, *37*, 1186–1225; c) K. Wild, A. August, C. U. Pietrzik, S. Kins, *Front. Mol. Neurosci.* **2017**, *10*, 21.

[10] a) P. Faller, C. Hureau, *Chem. Eur. J.* **2012**, *18*, 15910–15920; b) M. Dumont, M. F. Beal, *Free Radicals Biol. Med.* **2011**, *51*, 1014–1026; c) K. Jomova, D. Vondrakova, M. Lawson, M. Valko, *Mol. Cell. Biochem.* **2010**, *345*, 91–104.

[11] a) N. Xia, L. Liu, *Mini-Rev. Med. Chem.* **2014**, *14*, 271–281; b) P. J. Crouch, K. J. Barnham, *Acc. Chem. Res.* **2012**, *45*, 1604–1611; c) K. J. Barnham, A. I. Bush, *Chem. Soc. Rev.* **2014**, *43*, 6727–6749; d) A. Robert, Y. Liu, M. Nguyen, B. Meunier, *Acc. Chem. Res.* **2015**, *48*, 1332–1339.

ChemPubSoc Europe

CHEMISTRY A European Journal Full Paper

[12] S. C. Drew, *Front. Neurosci.* **2017**, *11*, 317.
[13] a) Y. Wang, H. Wang, H. Z. Chen, *Curr. Neuropharmacol.* **2016**, *14*, 364–375; b) C. Rodríguez-Rodríguez, M. Telpoukhovskaia, C. Orvig, *Coord. Chem. Rev.* **2012**, *256*, 2308–2332; c) N. Guzior, A. Wieckowska, D. Panek, B. Malawska, *Curr. Med. Chem.* **2015**, *22*, 373–404.
[14] a) M. Jensen, A. Canning, S. Chiha, P. Bouquerel, J. T. Pedersen, J. Østergaard, O. Cuvillier, I. Sasaki, C. Hureau, P. Faller, *Chem. Eur. J.* **2012**, *18*, 4836–4839; b) A. B. Caballero, L. Terol-Ordaz, A. Espargaró, G. Vázquez, E. Nicolás, R. Sabaté, P. Gamez, *Chem. Eur. J.* **2016**, *22*, 7268–7280; c) X. Hu, Q. Zhang, W. Wang, Z. Yuan, X. Zhu, B. Chen, X. Chen, *ACS Chem. Neurosci.* **2016**, *7*, 1255–1263.
[15] a) E. Atrián-Blasco, E. Cerrada, A. Conte-Daban, D. Testemale, P. Faller, M. Laguna, C. Hureau, *Metallomics* **2015**, *7*, 1229–1232; b) G. R. Walke, D. S. Ranade, S. N. Ramteke, S. Rapole, C. Satriano, E. Rizzarelli, G. A. Tomaselli, G. T. Sfrazzetto, P. P. Kulkarni, *Inorg. Chem.* **2017**, *56*, 3729–3732.
[16] a) G. Meloni, V. Sonois, T. Delaine, L. Guilloreau, A. Gillet, J. Teissié, P. Faller, M. Vasak, *Nat. Chem. Biol.* **2008**, *4*, 366–372; b) L. Perrone, E. Mothes, M. Vignes, A. Mockel, C. Figueroa, M. C. Miquel, M. L. Maddelein, P. Faller, *ChemBioChem* **2010**, *11*, 110–118.
[17] M. E. Rice, *Trends Neurosci.* **2000**, *23*, 209–216.
[18] N. D'Ambrosi, L. Rossi, *Neurochem. Int.* **2015**, *90*, 36–45.
[19] W. Goch, W. Bal, *PLoS One* **2017**, *12*, e0170749.
[20] S. K. Garg, V. Vitvitsky, R. Albin, R. Banerjee, *Antioxid. Redox Signaling* **2011**, *14*, 2385–2397.
[21] a) M. A. Telpoukhovskaia, C. Orvig, *Chem. Soc. Rev.* **2013**, *42*, 1836–1846; b) M. Nguyen, L. Rechignat, A. Robert, B. Meunier, *ChemistryOpen* **2015**, *4*, 27–31.
[22] T. T. Chen, X. Y. Wang, Y. F. He, C. L. Zhang, Z. Y. Wu, K. Liao, J. J. Wang, Z. J. Guo, *Inorg. Chem.* **2009**, *48*, 5801–5809.
[23] a) C. Hureau, V. Balland, Y. Coppel, P. L. Solari, E. Fonda, P. Faller, *J. Biol. Inorg. Chem.* **2009**, *14*, 995–1000; b) J. Shearer, V. A. Szalai, *J. Am. Chem. Soc.* **2008**, *130*, 17826–17835.
[24] R. A. Cherny, J. T. Legg, C. A. McLean, D. P. Fairlie, X. Huang, C. S. Atwood, K. Beyreuther, R. E. Tanzi, C. L. Masters, A. I. Bush, *J. Biol. Chem.* **1999**, *274*, 23223–23228.
[25] a) A. M. Pujol, C. Gateau, C. Lebrun, P. Delangle, *Chem. Eur. J.* **2011**, *17*, 4418–4428; b) A. M. Pujol, C. Gateau, C. Lebrun, P. Delangle, *J. Am. Chem. Soc.* **2009**, *131*, 6928–6929; c) A.-S. Jullien, C. Gateau, I. Kieffer, D. Testemale, P. Delangle, *Inorg. Chem.* **2013**, *52*, 9954–9961; d) A. M. Pujol, C. Lebrun, C. Gateau, A. Manceau, P. Delangle, *Eur. J. Inorg. Chem.* **2012**, 3835–3843.
[26] a) A. S. Jullien, C. Gateau, C. Lebrun, P. Delangle, *Eur. J. Inorg. Chem.* **2015**, 3674–3680; b) A.-S. Jullien, C. Gateau, C. Lebrun, I. Kieffer, D. Testemale, P. Delangle, *Inorg. Chem.* **2014**, *53*, 5229–5239.
[27] A. S. Jullien, C. Gateau, C. Lebrun, P. Delangle, *Inorg. Chem.* **2015**, *54*, 2339–2344.
[28] A. Dancs, N. V. May, K. Selmeczi, Z. Darula, A. Szorcsik, F. Matyuska, T. Pali, T. Gajda, *New J. Chem.* **2017**, *41*, 808–823.
[29] R. M. Smith, A. E. Martell, R. J. Motekaitis, NIST Critically Selected Stability Constants of Metal Complexes Database, NIST Standard Reference Database 46, **2001**.
[30] E. Q. Adams, *J. Am. Chem. Soc.* **1916**, *38*, 1503–1510.
[31] C. J. Siddons, R. D. Hancock, *Chem. Commun.* **2004**, 1632–1633.
[32] a) C. Kállay, K. Várnagy, G. Malandrinos, N. Hadjiliadis, D. Sanna, I. Sóvágó, *Dalton Trans.* **2006**, 4545–4552; b) D. La Mendola, A. Magrì, A. M. Santoro, V. G. Nicoletti, E. Rizzarelli, *J. Inorg. Biochem.* **2012**, *111*, 59–69; c) A. Fragoso, R. Delgado, O. Iranzo, *Dalton Trans.* **2013**, *42*, 6182–6192.
[33] a) C. S. Bonnet, P. H. Fries, S. Crouzy, O. Sénèque, F. Cisnetti, D. Boturyn, P. Dumy, P. Delangle, *Chem. Eur. J.* **2009**, *15*, 7083–7093; b) A. Fragoso, P. Lamosa, R. Delgado, O. Iranzo, *Chem. Eur. J.* **2013**, *19*, 2076–2088; c) C. Lebrun, M. Starck, V. Gathu, Y. Chenavier, P. Delangle, *Chem. Eur. J.* **2014**, *20*, 16566–16573; d) M. Starck, N. Sisommay, F. A. Laporte, S. Oros, C. Lebrun, P. Delangle, *Inorg. Chem.* **2015**, *54*, 11557–11562; e) M. Starck, F. A. Laporte, S. Oros, N. Sisommay, V. Gathu, P. L. Solari, G. Creff, J. Roques, C. Den Auwer, C. Lebrun, P. Delangle, *Chem. Eur. J.* **2017**, *23*, 5281–5290.
[34] L. Alderighi, P. Gans, A. Ienco, D. Peters, A. Sabatini, A. Vacca, *Coord. Chem. Rev.* **1999**, *184*, 311–318.
[35] J. Peisach, W. E. Blumberg, *Arch. Biochem. Biophys.* **1974**, *165*, 691–708.
[36] a) U. Sakaguchi, A. W. Addison, *J. Chem. Soc. Dalton Trans.* **1979**, 600–608; b) F. Jiang, J. McCracken, J. Peisach, *J. Am. Chem. Soc.* **1990**, *112*, 9035–9044; c) R. M. Rasia, C. W. Bertoncini, D. Marsh, W. Hoyer, D. Cherny, M. Zweckstetter, C. Griesinger, T. M. Jovin, C. O. Fernández, *Proc. Natl. Acad. Sci. USA* **2005**, *102*, 4294–4299; d) P. Manikandan, B. Epel, D. Goldfarb, *Inorg. Chem.* **2001**, *40*, 781–787.
[37] L. S. Kau, D. J. Spira-Solomon, J. E. Penner-Hahn, K. O. Hodgson, E. I. Solomon, *J. Am. Chem. Soc.* **1987**, *109*, 6433–6442.
[38] a) Z. Xiao, L. Gottschlich, R. van der Meulen, S. R. Udagedara, A. G. Wedd, *Metallomics* **2013**, *5*, 501–513; b) B. Alies, B. Badei, P. Faller, C. Hureau, *Chem. Eur. J.* **2012**, *18*, 1161–1167.
[39] J. T. Rubino, M. P. Chenkin, M. Keller, P. Riggs-Gelasco, K. J. Franz, *Metallomics* **2011**, *3*, 61–73.
[40] N. Le Poul, Y. Le Mest, I. Jabin, O. Reinaud, *Acc. Chem. Res.* **2015**, *48*, 2097–2106.
[41] a) N. Le Poul, M. Campion, B. Douzieh, Y. Rondelez, L. Le Clainche, O. Reinaud, Y. Le Mest, *J. Am. Chem. Soc.* **2007**, *129*, 8801–8810; b) N. Le Poul, M. Campion, G. Izzet, B. Douzieh, O. Reinaud, Y. Le Mest, *J. Am. Chem. Soc.* **2005**, *127*, 5280–5281.
[42] a) A. Conte-Daban, V. Borghesani, S. Sayen, E. Guillon, Y. Journaux, G. Gontard, L. Lisnard, C. Hureau, *Anal. Chem.* **2017**, *89*, 2155–2162; b) T. Kowalik-Jankowska, M. Ruta, K. Wiśniewska, L. Łankiewicz, *J. Inorg. Biochem.* **2003**, *95*, 270–282; c) B. Alies, E. Renaglia, M. Rozga, W. Bal, P. Faller, C. Hureau, *Anal. Chem.* **2013**, *85*, 1501–1508.
[43] a) N. E. Wezynfeld, E. Stefaniak, K. Stachucy, A. Drozd, D. Płonka, S. C. Drew, A. Krężel, W. Bal, *Angew. Chem. Int. Ed.* **2016**, *55*, 8235–8238; *Angew. Chem.* **2016**, *128*, 8375–8378; b) M. Mital, N. E. Wezynfeld, T. Frączyk, M. Z. Wiloch, U. E. Wawrzyniak, A. Bonna, C. Tumpach, K. J. Barnham, C. L. Haigh, W. Bal, S. C. Drew, *Angew. Chem. Int. Ed.* **2015**, *54*, 10460–10464; *Angew. Chem.* **2015**, *127*, 10606–10610.
[44] M. Newville, Data Processing with IFFEFIT, ATHENA & ARTEMIS, consortium for advanced radiation sources, July 24, 2007, University of Chicago.
[45] A. Conte-Daban, A. Day, P. Faller, C. Hureau, *Dalton Trans.* **2016**, *45*, 15671–15678.
[46] J. T. Pedersen, S. W. Chen, C. B. Borg, S. Ness, J. M. Bahl, N. H. Heegaard, C. M. Dobson, L. Hemmingsen, N. Cremades, K. Teilum, *J. Am. Chem. Soc.* **2016**, *138*, 3966–3969.
[47] B. Alies, I. Sasaki, O. Proux, S. Sayen, E. Guillon, P. Faller, C. Hureau, *Chem. Commun.* **2013**, *49*, 1214–1216.
[48] S. Noël, F. Perez, J. T. Pedersen, B. Alies, S. Ladeira, S. Sayen, E. Guillon, E. Gras, C. Hureau, *J. Inorg. Biochem.* **2012**, *117*, 322–325.
[49] a) A. M. Pujol, M. Cuillel, A.-S. Jullien, C. Lebrun, D. Cassio, E. Mintz, C. Gateau, P. Delangle, *Angew. Chem. Int. Ed.* **2012**, *51*, 7445–7448; *Angew. Chem.* **2012**, *124*, 7563–7566; b) A. M. Pujol, M. Cuillel, O. Renaudet, C. Lebrun, P. Charbonnier, D. Cassio, C. Gateau, P. Dumy, E. Mintz, P. Delangle, *J. Am. Chem. Soc.* **2011**, *133*, 286–296.
[50] A. E. Martell, R. J. Motekaitis, *Determination and use of stability constants*, VCH, New York, **1992**.
[51] P. Gans, A. Sabatini, A. Vacca, *Talanta* **1996**, *43*, 1739–1753.
[52] O. Proux, X. Biquard, E. Lahera, J. J. Menthonnex, A. Prat, O. Ulrich, Y. Soldo, P. Trévisson, G. Kapoujyan, G. Perroux, P. Taunier, D. Grand, P. Jeantet, M. Deleglise, J.-P. Roux, J.-L. Hazemann, *Phys. Scr.* **2005**, *115*, 970–973.
[53] O. Proux, V. Nassif, A. Prat, O. Ulrich, E. Lahera, X. Biquard, J. J. Menthonnex, J.-L. Hazemann, *J. Synchrotron Radiat.* **2006**, *13*, 59–68.
[54] A. Michalowicz, J. Moscovici, D. Muller-Bouvet, K. Provost, *J. Phys. Conf. Ser.* **2009**, *190*, 012034.
[55] a) B. Lengeler, P. Eisenberg, *Phys. Rev. B* **1980**, *21*, 4507–4520; b) E. Guillon, P. Merdy, M. Aplincourt, *Chem. Eur. J.* **2003**, *9*, 4479–4484.
[56] S. I. Zabinsky, J. J. Rehr, A. L. Ankudinov, R. C. Albers, M. J. Eller, *Phys. Rev. B* **1995**, *52*, 2995–3009.

Manuscript received: July 24, 2017
Accepted manuscript online: August 28, 2017
Version of record online: November 9, 2017

II-C.iii Supporting information

A trishistidine pseudopeptide with ability to remove both Cu(I) and Cu(II) from the amyloid-β peptide and to stop the associated ROS formation

A. Conte-Daban,[a,b]§ B. Boff,[c]§ A. Candido Matias,[c,d] C. N. Montes Aparicio,[a,b] C. Gateau,[c] C. Lebrun,[c] G. Cerchiaro,[d] I. Kieffer,[e,f] S. Sayen,[g] E. Guillon,[g] P. Delangle,[c]* and C. Hureau[a,b]*

[a.] *CNRS, LCC (Laboratoire de Chimie de Coordination), 205 route de Narbonne, BP 44099 31077 Toulouse Cedex 4, France.*
[b.] *University of Toulouse, UPS, INPT, 31077 Toulouse Cedex 4, France.*
[c.] *Univ. Grenoble Alpes, CEA, CNRS, INAC, SyMMES (UMR 5819), CIBEST, 17 rue des martyrs, F-38 000 Grenoble, France.*
[d.] *Center for Natural Sciences and Humanities, Federal University of ABC – UFABC, 09210-580, Santo André, SP, Brazil*
[e.] *BM30B/FAME beamline, ESRF, F-38043 Grenoble cedex 9, France*
[f.] *Observatoire des Sciences de l'Univers de Grenoble, UMS 832 CNRS Université Grenoble Alpes, F-38041 Grenoble, France*
[g.] *Institut de Chimie Moléculaire de Reims (ICMR, UMR CNRS 7312), Université de Reims Champagne-Ardenne, F-51687 Reims Cedex 2, France*

§ These two authors contributed equally to the work.

Supplementary Information

Content

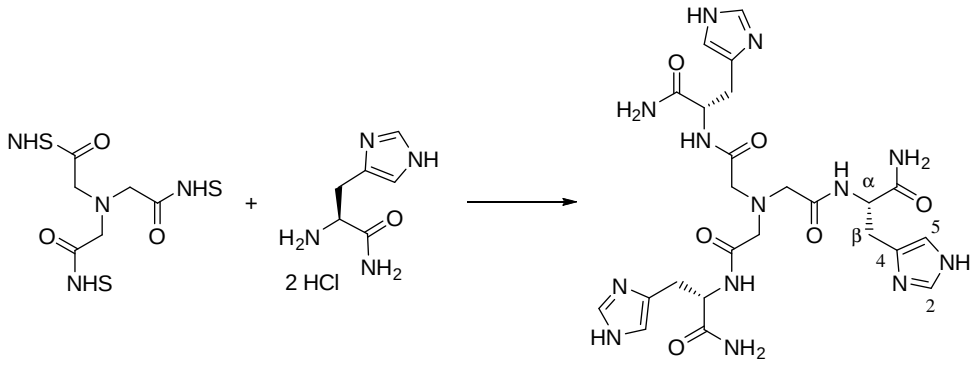

Scheme S1. Synthesis of **L** ≈ NTA(HisNH$_2$)$_3$ – reagents and conditions: DIEA, CH$_3$CN/DMF, 11 %

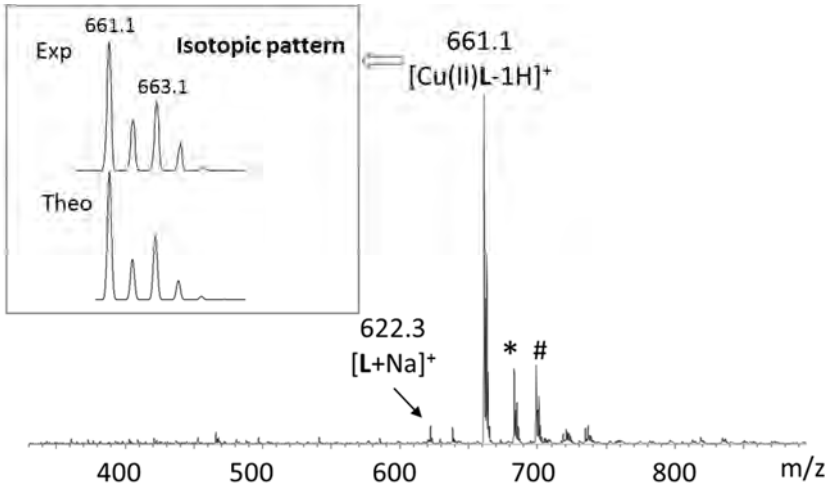

Figure S1. (+)ESI-MS spectrum of **L** (100 µM) with equimolar Cu(II)SO$_4$, in ammonium acetate buffer (20 mM, pH 6.9). * Sodium adducts. # Potassium adducts.

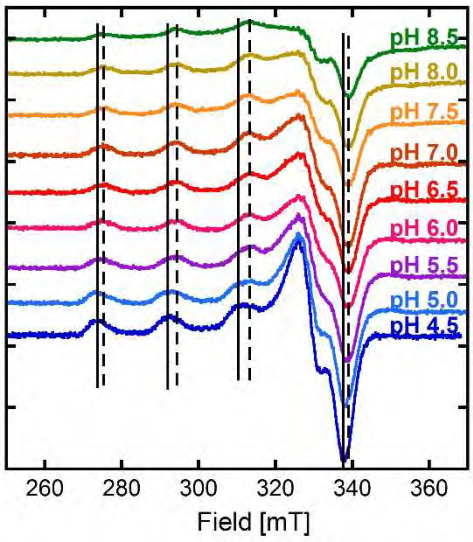

Figure S2. EPR signatures of Cu(II)**L** at different pH values. [**L**] = 200 µM, [^{65}Cu(II)] = 180 µM. 10% of glycerol was used as cryoprotectant. *T* = 110 K.

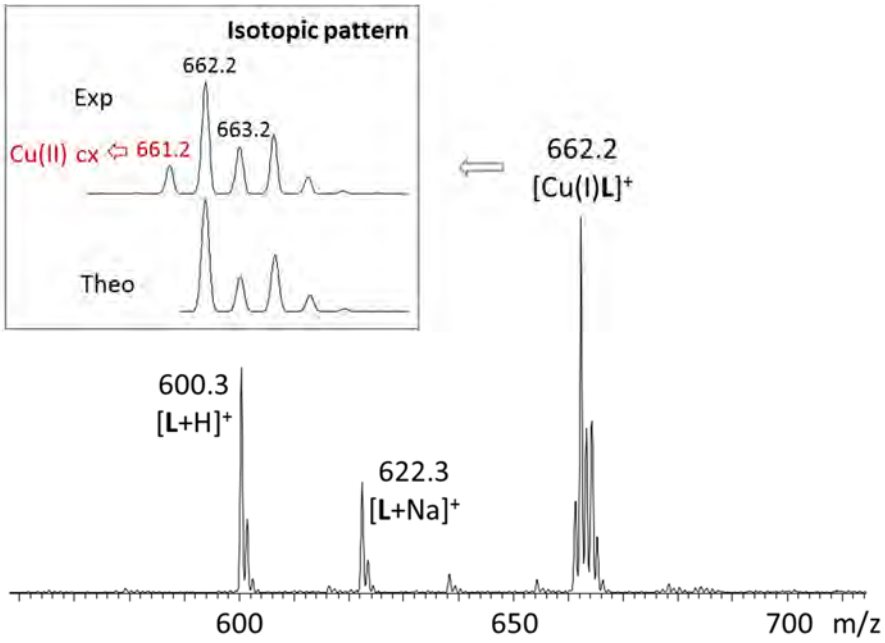

Figure S3. (+)ESI-MS spectrum of **L** (100 µM) with equimolar Cu(I)$(CH_3CN)_4PF_6$, in ammonium acetate buffer (20 mM, pH 6.9).

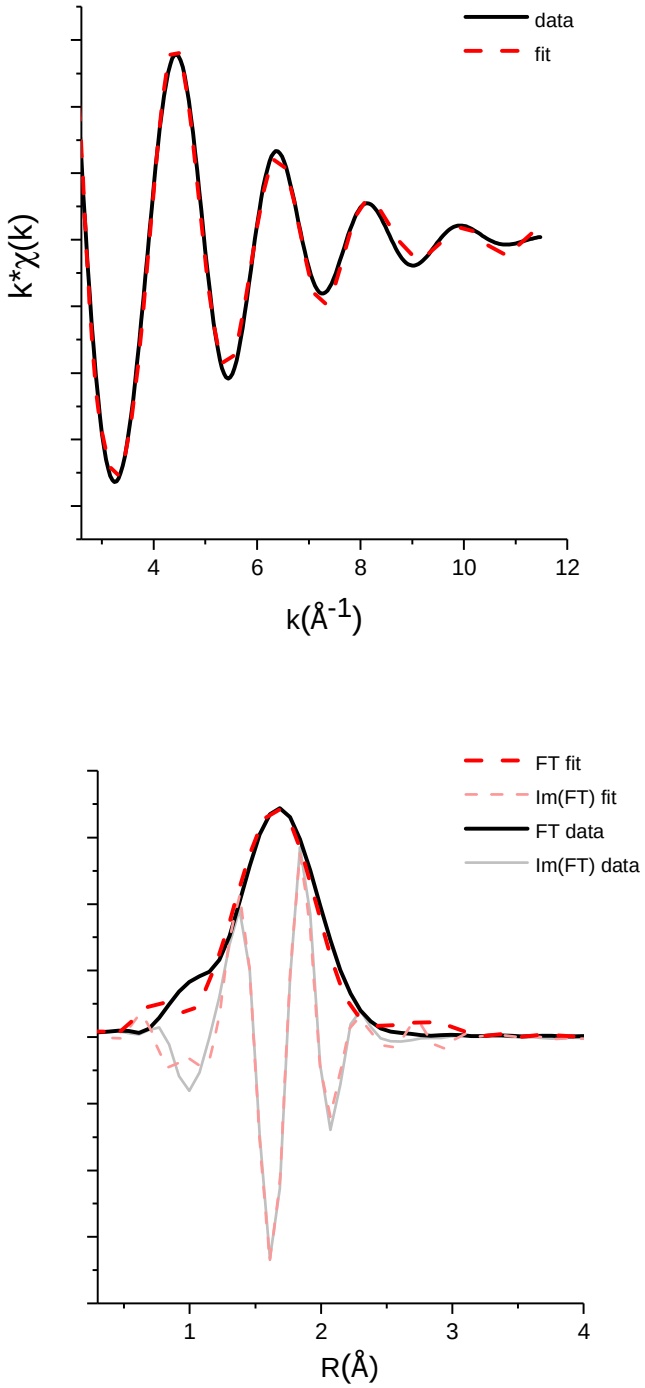

Figure S4. EXAFS data for the Cu(I)**L** complex. Top. Experimental data (solid black curve) and simulated fit (dotted red line) of the filtered first shell of the EXAFS function and Down. the corresponding radial structure functions (RSF, not corrected phase shift). FT and Im(FT) are the magnitude and imaginary part of Fourier transforms, respectively.

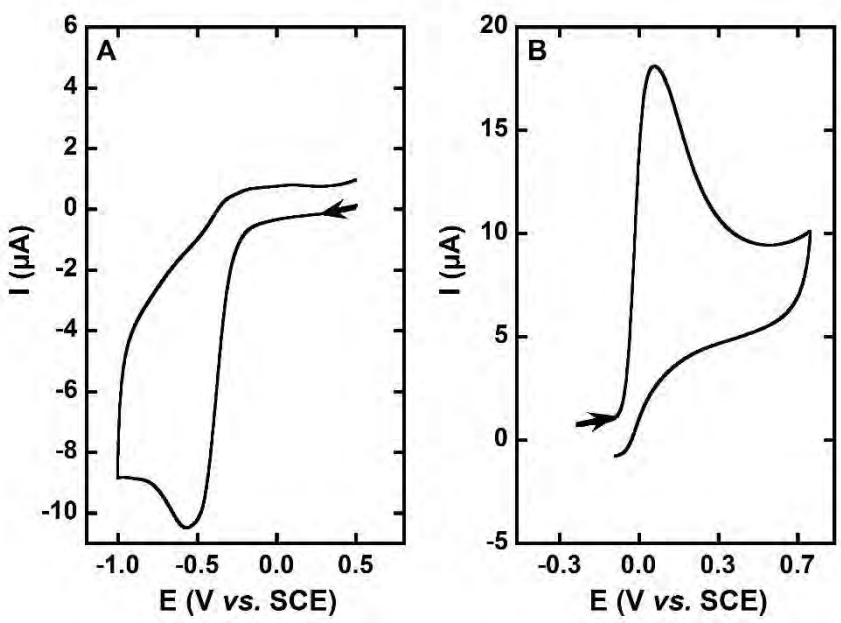

Figure S5. Cyclic voltamograms of O_2 (*Panel A*) and ascorbate (*Panel B*). [O_2] = ~ 0.2 mM, [Asc] = 1 mM in [phosphate buffer] = 100 mM at pH 7.1. Scan rate = 100 mV.s^{-1}; WE = Glassy carbon, Ref = SCE, CE = Pt wire.

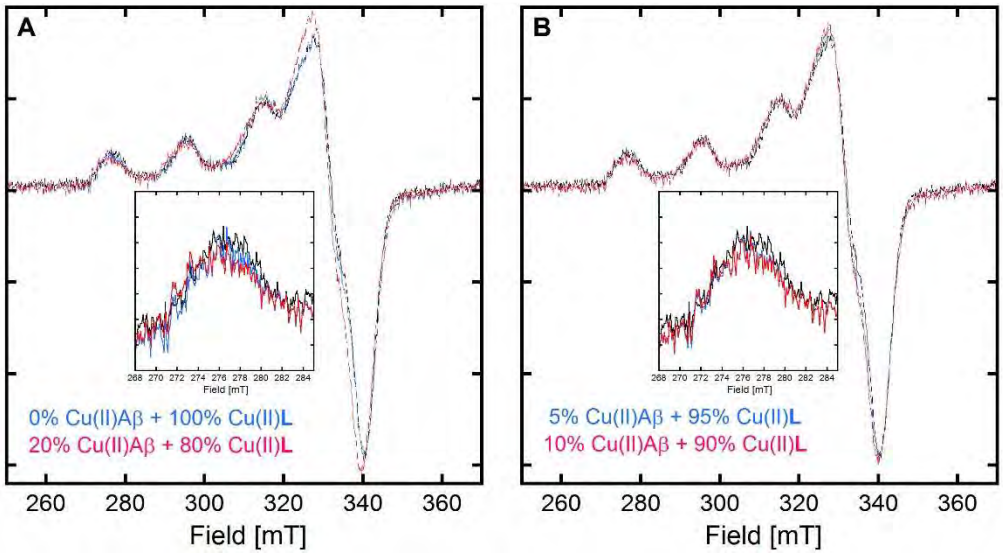

Figure S6. *Panel A*. EPR experiments of Cu(II)A$\beta_{1\text{-}16}$ + Cu(II)**L** (black curve), linear combination: 0% Cu(II)A$\beta_{1\text{-}16}$ + 100% Cu(II)**L** (blue curve), linear combination: 20% Cu(II)A$\beta_{1\text{-}16}$ + 80% Cu(II)**L** (pink curve). The inset corresponds to a zoom of the first band. *Panel B*. EPR experiments of Cu(II)A$\beta_{1\text{-}16}$ + Cu(II)**L** (black curve), linear combination: 5% Cu(II)A$\beta_{1\text{-}16}$ + 95% Cu(II)**L** (blue curve), linear combination: 10% Cu(II)A$\beta_{1\text{-}16}$ + 90% Cu(II)**L** (pink curve). The inset corresponds to a zoom of the first band. [**L**] = [A$\beta_{1\text{-}16}$] = [^{65}Cu(II)] = 200 µM, [HEPES] = 50 mM, pH 7.1. 10% of glycerol was used as cryoprotectant. *T* = 110 K.

Only insignificant difference can be observed in the reproduction of the experimental competition spectrum using 0 -100 % ; 5 – 95 % and 10 % - 90 % as Cu(II)A$\beta_{1\text{-}16}$– Cu**L**H$_{-1}$ ratio. We thus propose that in the competition spectrum there is 5 % +/- 5% of Cu(II)A$\beta_{1\text{-}16}$.

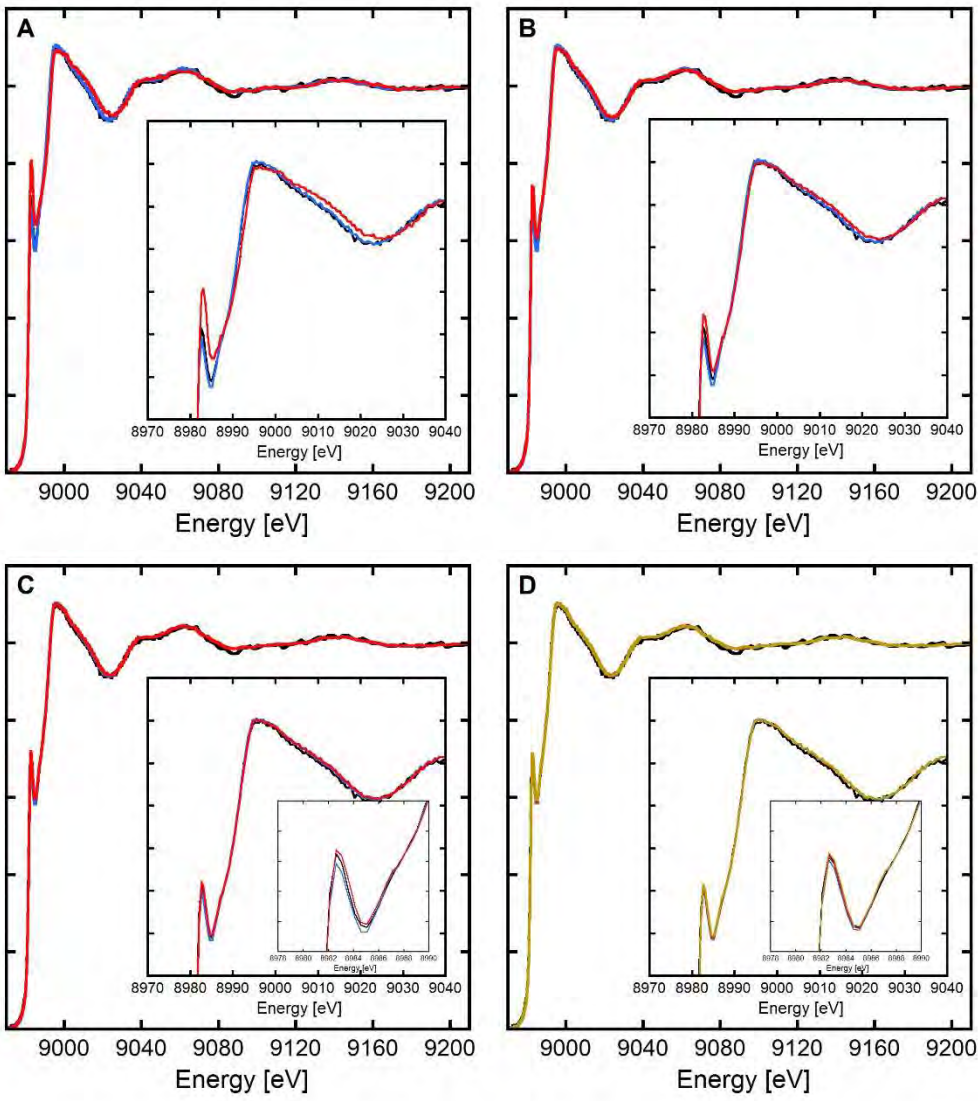

Figure S7. *Panel A*. XANES spectra of Cu(I)A$\beta_{1\text{-}16}$ + Cu(I)**L** (black line), linear combination: 0% Cu(I)A$\beta_{1\text{-}16}$ + 100% Cu(I)**L** (blue line), linear combination: 100% Cu(I)A$\beta_{1\text{-}16}$ + 0% Cu(I)**L** (red line). *Panel B*. XANES spectra of Cu(I)A$\beta_{1\text{-}16}$ + Cu(I)**L** (black line), linear combination: 0% Cu(I)A$\beta_{1\text{-}16}$ + 100% Cu(I)**L** (blue line), linear combination: 50% Cu(I)A$\beta_{1\text{-}16}$ + 50% Cu(I)**L** (red line). *Panel C*. XANES spectra of Cu(I)A$\beta_{1\text{-}16}$ + Cu(I)**L** (black line), linear combination: 10% Cu(I)A$\beta_{1\text{-}16}$ + 90% Cu(I)**L** (blue line), linear combination: 30% Cu(I)A$\beta_{1\text{-}16}$ + 70% Cu(I)**L** (red line). *Panel D*. XANES spectra of Cu(I)A$\beta_{1\text{-}16}$ + Cu(I)**L** (black line), linear combination: 15% Cu(I)A$\beta_{1\text{-}16}$ + 85% Cu(I)**L** (blue line), linear combination: 20% Cu(I)A$\beta_{1\text{-}16}$ + 80% Cu(I)**L** (red line), linear combination: 25% Cu(I)A$\beta_{1\text{-}16}$ + 75% Cu(I)**L** (green line). The insets correspond to a zoom of the absorption. [**L**] = [A$\beta_{1\text{-}16}$] = 1.00 mM, [Cu(II)] = 0.95 mM, [dithionite] = 10 mM, [HEPES] = 100 mM, pH 7.1. 10% of glycerol was used as cryoprotectant.

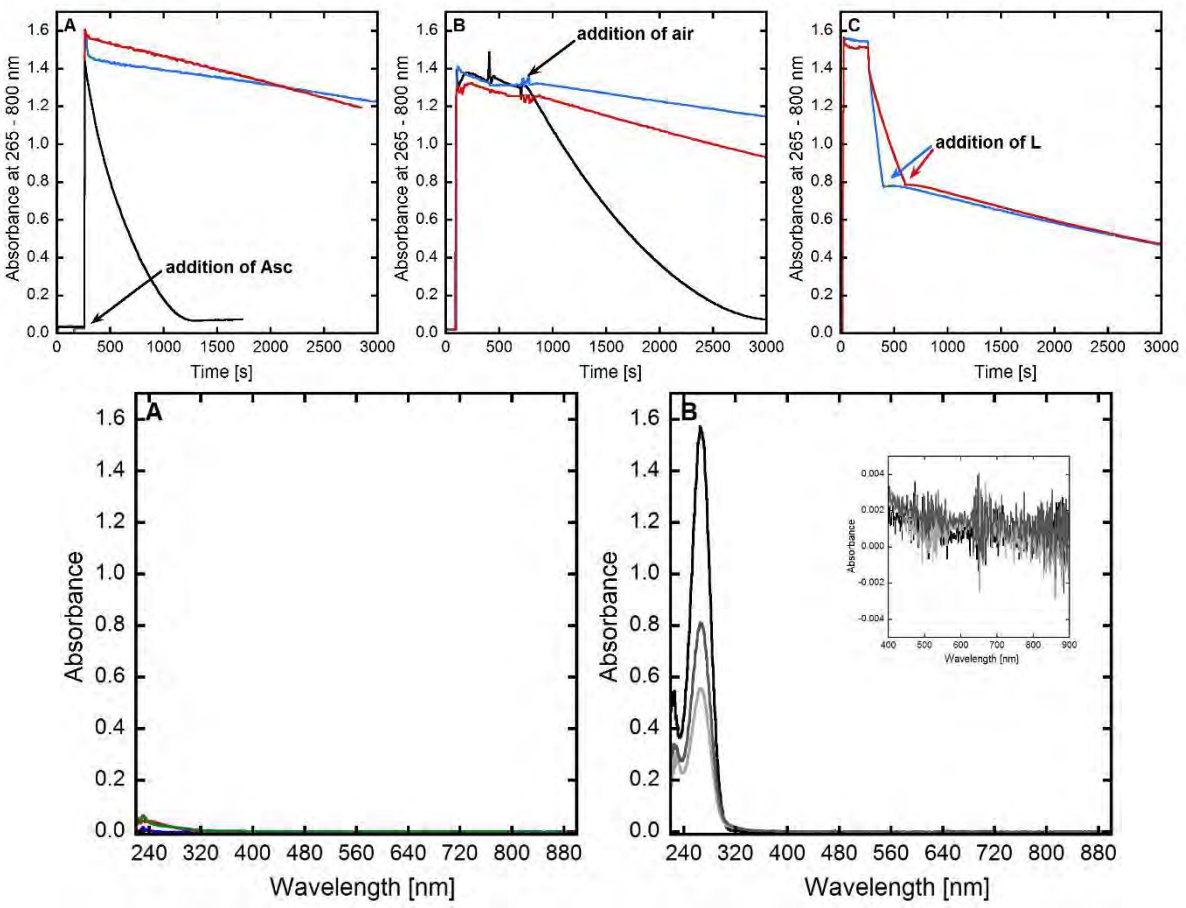

Figure S8. **Top:** Kinetics of ascorbate consumption, followed by UV-visible spectroscopy at 265 with subtraction of the background signal at 800 nm. *Panel A*. $A\beta_{1\text{-}16}$ + Cu(II) + Asc (black curve), **L** + Cu(II) + Asc (blue curve), $A\beta_{1\text{-}16}$ + Cu(II) + **L** + Asc (red curve). *Panel B*. Cu(II) + Asc + $A\beta_{1\text{-}16}$ + air (black curve), Cu(II) + Asc + **L** + air (blue curve), Cu(II) + Asc + $A\beta_{1\text{-}16}$ + **L** + air (red curve). *Panel C*. Asc + Cu(II) + **L** (blue curve), Asc + $A\beta_{1\text{-}16}$ + Cu(II) + **L** (red curve). [**L**] = [$A\beta_{1\text{-}16}$] = 12 µM, [Cu(II)] = 10 µM, [Asc] = 100 µM, [HEPES] = 100 mM, pH 7.1. For the experiments from Panel B, all the solutions were deoxygenated by bubbling Argon and were added under a little overpressure of Argon in order to keep Cu under its +I oxidation state. **Bottom:** *Panel A*. UV-vis spectra of **L** (blue curve), **L** + Cu(II) (red curve), **L** + Cu(I) (green curve). [**L**] = 100 µM, [Cu(II)] = [Cu(I)] = 100 µM, [HEPES] = 100 mM, pH 7.1. To ease direct comparison, the absorbance intensity has been divided by a factor of ten since data were recorded at a ten-fold higher concentration to improve the signal over noise ratio. *Panel B*. Spectra corresponding to the experiment shown in Figure 7. Asc + $A\beta_{40}$ (black curve), Asc + $A\beta_{40}$ + Cu(II) at 720 s, just before the addition of **L** (dark grey curve), Asc + $A\beta_{40}$ + Cu(II) + **L** at the end of the kinetic (light grey curve). [**L**] = [$A\beta_{1\text{-}16}$] = 12 µM, [Cu(II)] = 10 µM, [Asc] = 100 µM, [HEPES] = 100 mM, pH 7.1.

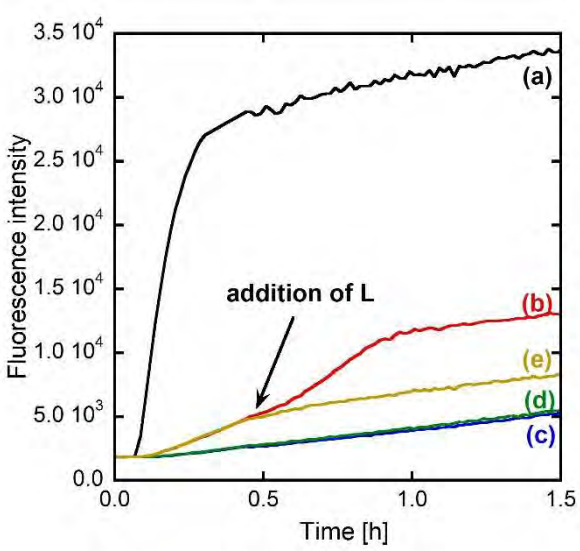

Figure S9. Fluorescence kinetics of CCA experiments of (a) Cu(II) + Asc, (b) $A\beta_{1-16}$ + Cu(II) + Asc, (c) **L** + Cu(II) + Asc, (d) $A\beta_{1-16}$ + Cu(II) + **L** + Asc, (e) $A\beta_{1-16}$ + Cu(II) + Asc + L at 20 min. Asc was added 5 min after the beginning of the measurement. [**L**] = [$A\beta_{1-16}$] = 12 µM, [Cu(II)] = 10 µM, [CCA] = 500 µM, [Asc] = 500 µM, [phosphate buffer] = 50 mM, pH 7.1.

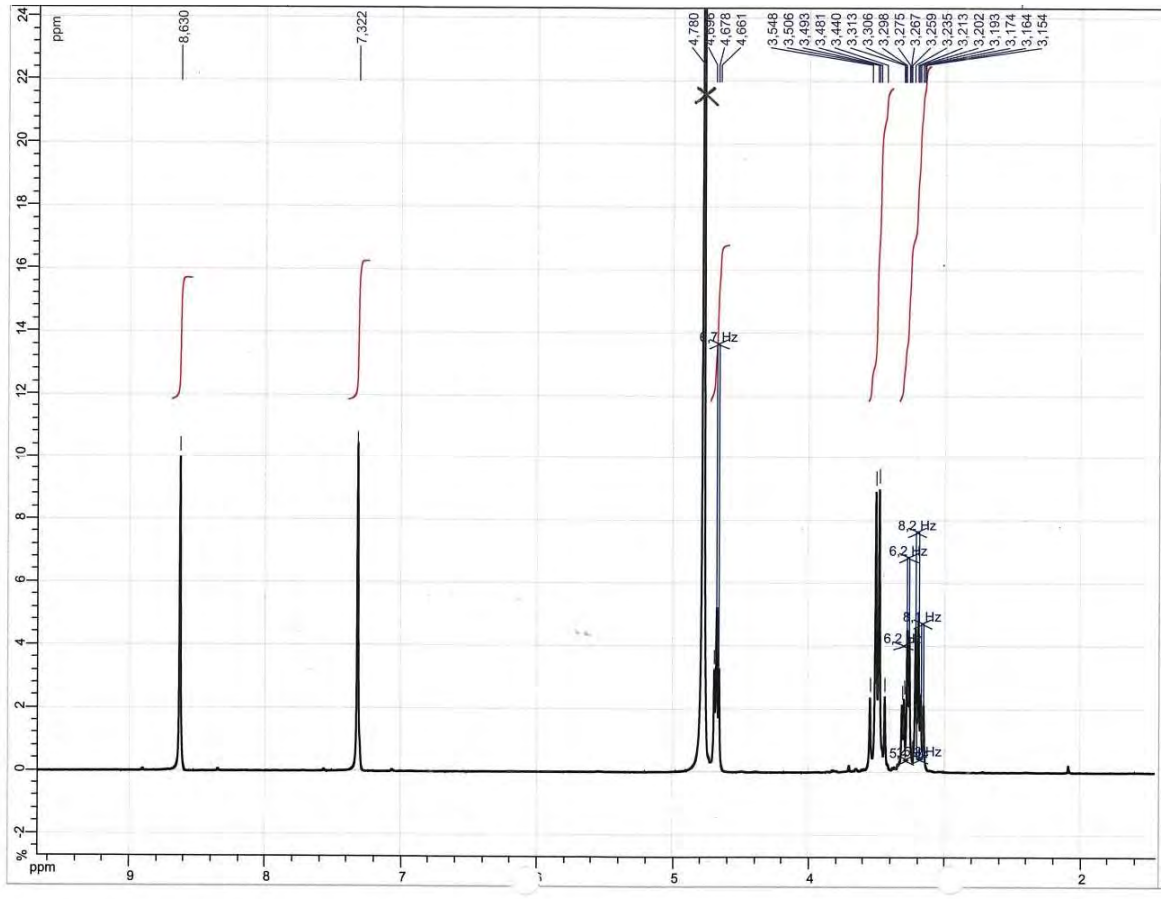

Figure S10. 400 MHz ^{1}H NMR spectrum in D_2O at 300 K.

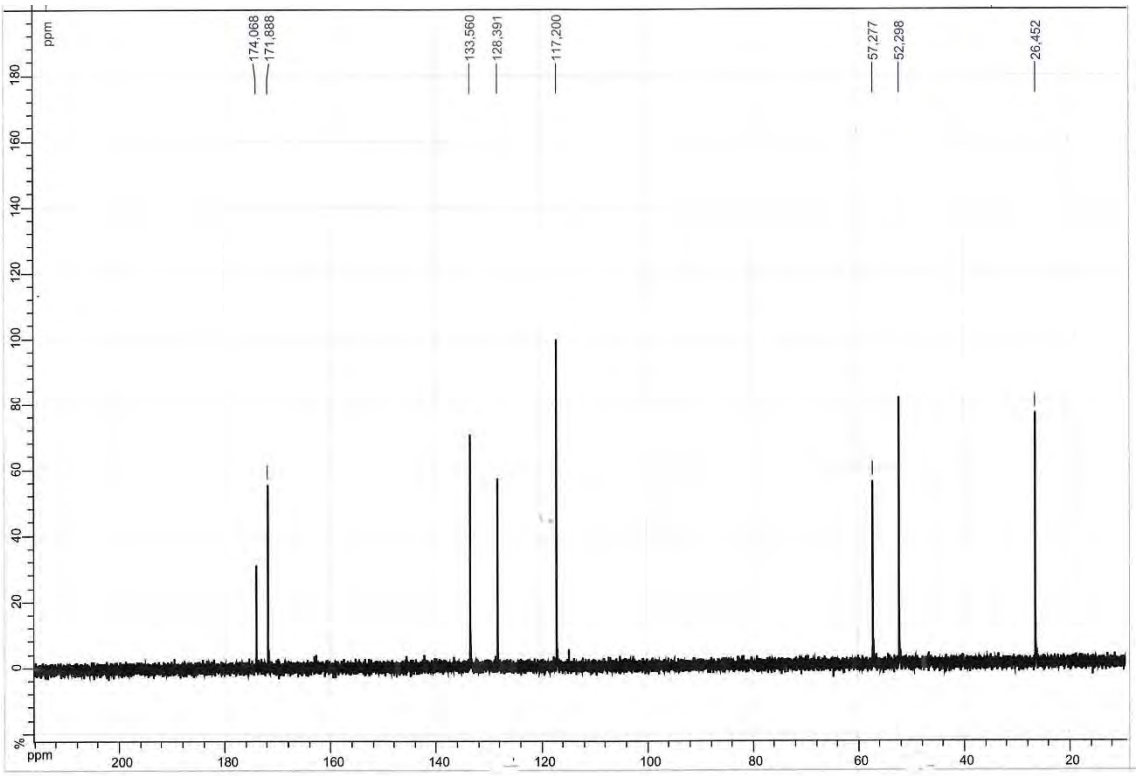

Figure S11. 100 MHz ^{13}C NMR spectrum decoupled from ^{1}H in D_2O at 300 K.

II-D Conclusion

In this part regarding the Cu chelation in the AD context, two proofs of concept have been detailed. The importance of the kinetic in the Cu removal from the Aβ peptide has been illustrated with two series of macrocyclic ligands. Indeed, if the redox process switching from Cu(II)-Aβ to Cu(I)-Aβ is faster than the Cu removal by the ligand, Cu ions stay bound to Aβ, leading to the production of ROS and the stabilisation of species such as the toxic oligomers. Then, the importance of targeting Cu(I) and Cu(II) ions in the chelatotherapy has been shown using the ligand **L**. As the redox state of Cu ions in the synaptic cleft is still unknown, it could be more useful to target both redox states. A caution has to be paid on the redox silencing of the ROS production by the Cu complex formed. A more secure approach in the chelatotherapy could be the use of a ligand with a fast kinetic in the removal of Cu ions from Aβ and able to chelate both Cu(I) and Cu(II). As it could chelate Cu ions faster than the redox process and as it could chelate both Cu(I) and Cu(II), it should be able to remove Cu ions from Aβ *in vivo*.

Nevertheless, one can wonder if a ligand, with a fast Cu chelation kinetic, *in vivo*, could not remove Cu ions after its administration and before reaching the synaptic cleft. This could have severe negative effects. *In vivo*, another issue for a Cu(I)/Cu(II) ligand can be the removal of Cu(I) from important metalloproteins found inside the cells, as the ligand is able to remove Cu(I). It is important that the ligand does not exhibit a too high affinity for Cu(I) (as for the Cu(II) affinity constant), compared to the affinity constant of the intra-cellular metalloproteins such as the metallothioneins or the Cu-chaperons. Furthermore, adding a targeting Aβ moiety to such a ligand could help in the removal of the “AD Cu ions”.

Another important point could be the metallophoric capabilities of a Cu(I)/Cu(II) ligand. Indeed, as previously explained, there is a dyshomeostasis of Cu ions the brain. The final idea of the chelatotherapy is not only the removal of Cu ions from Aβ but also their intra-cellular redistribution. In the literature, the metallophores are Cu(II) ligands which, under a reducing medium as the intra-cellular medium, get reduced and release the Cu(I). However, a Cu(I) and Cu(II) ligand will form quite stable Cu(II) but also Cu(I) complexes. It can be more difficult to release the Cu(I) from such a stable complex. The design of such a ligand has to take into account that a Cu-protein in the intra-cellular medium has to be able to remove Cu(I) from the Cu(I)-L formed, in order to re-equilibrate the Cu homeostasis.

References

1. Rowinska-Zyrek, M.; Salerno, M.; Kozlowski, H., Neurodegenerative diseases – Understanding their molecular bases and progress in the development of potential treatments. *Coord. Chem. Rev.* **2015,** *284*, 298–312.
2. Xia, N.; Liu, L., Metallothioneins and Synthetic Metal Chelators as Potential Therapeutic Agents for Removal of Aberrant Metal Ions from Metal-AB Species. *Mini Rev. Med. Chem.* **2014,** *14* (3), 271-281.
3. Robert, A.; Liu, Y.; Nguyen, M.; Meunier, B., Regulation of copper and iron homeostasis by metal chelators: a possible chemotherapy for Alzheimer's disease. *Acc. Chem. Res.* **2015,** *48* (5), 1332-1339.
4. Santos, M. A.; Chand, K.; Chaves, S., Recent progress in multifunctional metal chelators as potential drugs for Alzheimer's disease. *Coord. Chem. Rev.* **2016,** *327 –328*, 287–303.
5. Scott, L. E.; Orvig, C., Medicinal inorganic chemistry approaches to passivation and removal of aberrant metal ions in disease. *Chem. Rev.* **2009,** *109* (10), 4885-4910.
6. Hung, L. W.; Barnham, K. J., Modulating metals as a therapeutic strategy for Alzheimer's disease. **2012,** *4* (8), 955-969.
7. Gnjec, A.; Fonte, J. A.; Atwood, C.; Martins, R. N., Transition metal chelator therapy – A potential treatment for alzheimer's disease? *Front. Biosci.* **2002,** *7*, 1016-1023.
8. Budimir, A., Metal ions, Alzheimer's disease and chelation therapy. *Acta Pharm.* **2011,** *61*, 1-14.
9. Rodríguez-Rodríguez, C.; Telpoukhovskaia, M.; Orvig, C., The art of building multifunctional metal-binding agents from basic molecular scaffolds for the potential application in neurodegenerative diseases. *Coord. Chem. Rev.* **2012,** *256* (19), 2308-2332.
10. Cuajungco, M. P.; Fagét, K. Y.; Huang, X.; Tanzi, R. E.; Bush, A. I., Metal chelation as a potential therapy for Alzheimer's disease. *Ann. N.Y. Acad. Sci.* **2000,** *920*, 292-304.
11. Bolognin, S.; Drago, D.; Messori, L.; Zatta, P., Chelation therapy for neurodegenerative diseases. *Med Res Rev.* **2009,** *29* (4), 547-570.
12. Wezynfeld, N. E.; Stefaniak, E.; Stachucy, K.; Drozd, A.; Płonka, D.; Drew, S. C.; Krężel, A.; Bal, W., Resistance of Cu(Aβ4-16) to Copper Capture by Metallothionein-3 Supports a Function for the Aβ4-42 Peptide as a Synaptic Cu(II) Scavenger. *Angew. Chem. Int. Ed.* **2016,** *55* (29), 8235-8238.
13. Mital, M.; Wezynfeld, N. E.; Fraczyk, T.; Wiloch, M. Z.; Wawrzyniak, U. E.; Bonna, A.; Tumpach, C.; Barnham, K. J.; Haigh, C. L.; Bal, W.; Drew, S. C., A Functional Role for Aβ in Metal Homeostasis? N-Truncation and High-Affinity Copper Binding. *Angew. Chem. Int. Ed.* **2015,** *54* (36), 10460-10464.
14. Gabathuler, R., Approaches to transport therapeutic drugs across the blood–brain barrier to treat brain diseases. *Neurobiol. Dis.* **2010,** *37* (1), 48-57.
15. Lipinski, C. A.; Lombardo, F.; Dominy, B. W.; Feeney, P. J., Experimental and computational approaches to estimate solubility and permeability in drug discovery and development settings. *Adv. Drug Deliv. Rev.* **2001,** *46* (1), 3-26.
16. Savelieff, M. G.; DeToma, A. S.; Derrick, J. S.; Lim, M. H., The Ongoing Search for Small Molecules to Study Metal-Associated Amyloid-β Species in Alzheimer's Disease. *Acc. Chem. Res.* **2014,** *47* (8), 2475–2482.
17. Bush, A. I.; Tanzi, R. E., Therapeutics for Alzheimer's Disease Based on the Metal Hypothesis. *Neurotherapeutics* **2008,** *5*, 421–432.
18. Gaeta, A.; Hider, R. C., The crucial role of metal ions in neurodegeneration: the basis for a promising therapeutic strategy. *Br. J. Pharmacol.* **2005,** *146* (8), 1041-1059.
19. Derrick, J. S.; Lim, M. H., Tools of the Trade: Investigations into Design Strategies of Small Molecules to Target Components in Alzheimer's Disease. *ChemBioChem* **2015,** *16* (6), 887-898.
20. Masui, H., Metalloaromaticity. *Coord. Chem. Rev.* **2001,** *219*, 957-992.

21. Rimola, A.; Alí-Torres, J.; Rodríguez-Rodríguez, C.; Poater, J.; Matito, E.; Solà, M.; Sodupe, M., Ab Initio Design of Chelating Ligands Relevant to Alzheimer's Disease: Influence of Metalloaromaticity. *J. Phys. Chem. A.* **2011,** *115* (45), 12659-12666.
22. Perez, L. R.; Franz, K. J., Minding metals: Tailoring multifunctional chelating agents for neurodegenerative disease. *Dalton Trans.* **2010,** *39* (9), 2177-2187.
23. Beck, M. W.; Pithadia, A. S.; DeToma, A. S.; Korshavn, K. J.; Lim, M. H., Ligand Design to Target and Modulate Metal–Protein Interactions in Neurodegenerative Diseases. In *Ligand Design in Medicinal Inorganic Chemistry*, Storr, T., Ed. Wiley: 2014; pp 256-286.
24. Sahni, J. K.; Doggui, S.; Ali, J.; Baboota, S.; Dao, L.; Ramassamy, C., Neurotherapeutic applications of nanoparticles in Alzheimer's disease. *J. Controlled Release* **2011,** *152* (2), 208-231.
25. Liu, G.; Men, P.; Kudo, W.; Perry, G.; Smith, M. A., Nanoparticle–chelator conjugates as inhibitors of amyloid-β aggregation and neurotoxicity: A novel therapeutic approach for Alzheimer disease. *Neurosci. Lett.* **2009,** *455* (3), 187-190.
26. Cui, Z.; Lockman, P. R.; Atwood, C. S.; Hsu, C. H.; Gupte, A.; Allen, D. D.; Mumper, R. J., Novel D-penicillamine carrying nanoparticles for metal chelation therapy in Alzheimer's and other CNS diseases. *Eur. J. Pharm. Biopharm.* **2005,** *59* (2), 263-272.
27. Berk, C.; Paul, G.; Sabbagh, M., Investigational drugs in Alzheimer's disease: current progress. *Expert Opin. Investig. Drugs* **2014,** *23* (6), 837-846.
28. Guzior, N.; Więckowska, A.; Panek, D.; Malawska, B., Recent Development of Multifunctional Agents as Potential Drug Candidates for the Treatment of Alzheimer's Disease. *Curr. Med. Chem.* **2015,** *22* (3), 373-404.
29. Braymer, J. J.; DeToma, A. S.; Choi, J.-S.; Ko, K. S.; Lim, M. H., Recent Development of Bifunctional Small Molecules to Study Metal-Amyloid-β Species in Alzheimer's Disease. *Int. J. Alzheimers Dis.* **2011,** *2011*, 1-9.
30. Dickens, M. G.; Franz, K. J., A Prochelator Activated by Hydrogen Peroxide Prevents Metal-Induced Amyloid β Aggregation. *ChemBioChem* **2010,** *11* (1), 59-62.
31. Folk, D. S.; Franz, K. J., A Prochelator Activated by β–Secretase Inhibits Aβ Aggregation and Suppresses Copper-Induced Reactive Oxygen Species Formation. *J. Am. Chem. Soc.* **2010,** *132*, 4994–4995.
32. Hung, Y. H.; Bush, A. I.; Cherny, R. A., Copper in the brain and Alzheimer's disease. *J. Biol. Inorg. Chem.* **2010,** *15*, 61–76.
33. Squitti, R.; Salustri, C., Agents complexing copper as a therapeutic strategy for the treatment of Alzheimer's disease. *Curr. Alzheimer Res.* **2009,** *6* (6), 476-487.
34. Barnham, K. J.; Bush, A. I., Biological metals and metal-targeting compounds in major neurodegenerative diseases. *Chem. Soc. Rev.* **2014,** *43* (19), 6727-6749.
35. Ayton, S.; Lei, P.; Bush, A. I., Biometals and their therapeutic implications in Alzheimer's disease. *Neurotherapeutics* **2015,** *12* (1), 109-120.
36. Bush, A. I., Drug Development Based on the Metals Hypothesis of Alzheimer's Disease. *J. Alzheimers Dis.* **2008,** *15*, 223-240.
37. Crouch, P. J.; Barnham, K. J., Therapeutic Redistribution of Metal Ions To Treat Alzheimer's Disease. *Acc. Chem. Res.* **2012,** *45* (9), 1604–1611.
38. Bareggi, S. R.; Cornelli, U., Clioquinol: Review of its Mechanisms of Action and Clinical Uses in Neurodegenerative Disorders. *CNS Neurosci Ther* **2012,** *18*, 41-46.
39. Bush, A. I., Metal complexing agents as therapies for Alzheimer's disease. *Neurobiol. Aging* **2002,** *23*, 1031-1038.
40. Zatta, P.; Drago, D.; Bolognin, S.; Sensi, S. L., Alzheimer's disease, metal ions and metal homeostatic therapy. *Trends Pharmacol. Sci.* **2009,** *30* (7), 346-355.
41. Cahoon, L., The curious case of clioquinol. *Nat. Med.* **2009,** *15* (4), 356-359.
42. Bolognin, S.; Zatta, P.; Drago, D.; Tognon, G.; Parnigotto, P. P.; Ricchelli, F., Mutual stimulation of beta-amyloid fibrillogenesis by clioquinol and divalent metals. *Neuromol. Med.* **2008,** *10* (4), 322-332.

43. Di Vaira, M.; Bazzicalupi, C.; Orioli, P.; Messori, L.; Bruni, B.; Zatta, P., Clioquinol, a drug for Alzheimer's disease specifically interfering with brain metal metabolism: structural characterization of its zinc(II) and copper(II) complexes. *Inorg. Chem.* **2004,** *43* (13), 3795-3797.
44. Budimir, A.; Humbert, N.; Elhabiri, M.; Osinska, I.; Birus, M.; Albrecht-Gary, A. M., Hydroxyquinoline based binders: promising ligands for chelatotherapy? *J. Inorg. Biochem.* **2011,** *105* (3), 490-496.
45. Pushie, M. J.; Nienaber, K. H.; Summers, K. L.; Cotelesage, J. J. H.; Ponomarenko, O.; Nichol, H. K.; Pickering, I. J.; George, G. N., The solution structure of the copper clioquinol complex. *J. Inorg. Biochem.* **2014,** *133*, 50-56.
46. Raman, B.; Ban, T.; Yamaguchi, K.-i.; Sakai, M.; Kawai, T.; Naiki, H.; Goto, Y., Metal Ion-dependent Effects of Clioquinol on the Fibril Growth of an Amyloid β Peptide. *J. Biol. Chem.* **2005,** *280* (16), 16157-16162.
47. Mancino, A. M.; Hindo, S. S.; Kochi, A.; Lim, M. H., Effects of Clioquinol on Metal-Triggered Amyloid-β Aggregation Revisited. *Inorg. Chem.* **2009,** *48* (20), 9596-9598.
48. Padmanabhan, G.; Becue, I.; Smith, J., Analytical profiles of drug substances. Academic Press, New York: 1989; pp 57-90.
49. Cherny, R. A.; Atwood, C. S.; Xilinas, M. E.; Gray, D. N.; Jones, W. D.; McLean, C. A.; Barnham, K. J.; Volitakis, I.; Fraser, F. W.; Kim, Y.-S.; Huang, X.; Goldstein, L. E.; Moir, R. D.; Lim, J. T.; Beyreuther, K.; Zheng, H.; Tanzi, R. E.; Masters, C. L.; Bush, A. I., Treatment with a copper-zinc chelator markedly and rapidly inhibits beta-amyloid accumulation in Alzheimer's disease transgenic mice. *Neuron* **2001,** *30* (3), 665-676.
50. Grossi, C.; Francese, S.; Casini, A.; Rosi, M. C.; Luccarini, I.; Fiorentini, A.; Gabbiani, C.; Messori, L.; Moneti, G.; Casamenti, F., Clioquinol decreases amyloid-beta burden and reduces working memory impairment in a transgenic mouse model of Alzheimer's disease. *J. Alzheimers Dis.* **2009,** *17* (2), 423-440.
51. Schafer, S.; Pajonk, F. G.; Multhaup, G.; Bayer, T. A., Copper and clioquinol treatment in young APP transgenic and wild-type mice: effects on life expectancy, body weight, and metal-ion levels. *Journal of molecular medicine* **2007,** *85* (4), 405-413.
52. Regland, B.; Lehmann, W.; Abedini, I.; Blennow, K.; Jonsson, M.; Karlsson, I.; Sjogren, M.; Wallin, A.; Xilinas, M.; Gottfries, C. G., Treatment of Alzheimer's disease with clioquinol. *Dement. Geriatr. Cogn. Dis.* **2001,** *12* (6), 408-14.
53. Ibach, B.; Haen, E.; Marienhagen, J.; Hajak, G., Clioquinol treatment in familiar early onset of Alzheimer's disease: a case report. *Pharmacopsychiatry* **2005,** *38* (4), 178-179.
54. Ritchie, C. W.; Bush, A. I.; Mackinnon, A.; Macfarlane, S.; Mastwyk, M.; MacGregor, L.; Kiers, L.; Cherny, R. A.; Li, Q.-X.; Tammer, A.; Carrington, D.; Mavros, C.; Volitakis, I.; Xilinas, M. E.; Ames, D.; Davis, S.; Beyreuther, K.; Tanzi, R. E.; Masters, C. L., Metal-protein attenuation with iodochlorhydroxyquin (clioquinol) targeting Aβ amyloid deposition and toxicity in alzheimer disease: A pilot phase 2 clinical trial. *Arch. Neurol.* **2003,** *60* (12), 1685-1691.
55. Ritchie, C. W.; Bush, A. I.; Masters, C. L., Metal-protein attenuating compounds and Alzheimer's disease. *Expert Opin. Investig. Drugs* **2004,** *13* (12), 1585-1592.
56. Rosenberg, R. N., Translational research on the way to effective therapy for Alzheimer disease. *Arch. Gen. Psychiatry* **2005,** *62* (11), 1186-1192.
57. Kenche, V. B.; Barnham, K. J., Alzheimer's disease & metals: therapeutic opportunities. *Br. J. Pharmacol.* **2011,** *163*, 211-219.
58. Treiber, C.; Simons, A.; Strauss, M.; Hafner, M.; Cappai, R.; Bayer, T. A.; Multhaup, G., Clioquinol Mediates Copper Uptake and Counteracts Copper Efflux Activities of the Amyloid Precursor Protein of Alzheimer's Disease. *J. Biol. Chem.* **2004,** *279* (50), 51958–51964.
59. Mital, M.; Zawisza, I. A.; Wiloch, M. Z.; Wawrzyniak, U. E.; Kenche, V.; Wróblewski, W.; Bal, W.; Drew, S. C., Copper Exchange and Redox Activity of a Prototypical 8-Hydroxyquinoline: Implications for Therapeutic Chelation. *Inorg. Chem.* **2016,** *55* (15), 7317-7319.
60. Barnham, K. J.; Gautier, E. C. L.; Kok, G. B.; Krippner, G., 8-hydroxy quinoline derivatives. In *WO 2004007461 A1*, Google Patents: 2004.

61. Fu, C. L.; Hsu, L. S.; Liao, Y. F.; Hu, M. K., New Hydroxyquinoline-Based Derivatives as Potent Modulators of Amyloid-beta Aggregations. *Arch. Pharm.* **2016,** *349* (5), 327-341.
62. Adlard, P. A.; Cherny, R. A.; Finkelstein, D. I.; Gautier, E.; Robb, E.; Cortes, M.; Volitakis, I.; Liu, X.; Smith, J. P.; Perez, K.; Laughton, K.; Li, Q.-X.; Charman, S. A.; Nicolazzo, J. A.; Wilkins, S.; Deleva, K.; Lynch, T.; Kok, G.; Ritchie, C. W.; Tanzi, R. E.; Cappai, R.; Masters, C. L.; Barnham, K. J.; Bush, A. I., Rapid restoration of cognition in Alzheimer's transgenic mice with 8-hydroxy quinoline analogs is associated with decreased interstitial Abeta. *Neuron* **2008,** *59* (1), 43-55.
63. Lannfelt, L.; Blennow, K.; Zetterberg, H.; Batsman, S.; Ames, D.; Harrison, J.; Masters, C. L.; Targum, S.; Bush, A. I.; Murdoch, R.; Wilson, J.; Ritchie, C. W., Safety, efficacy, and biomarker findings of PBT2 in targeting Aβ as a modifying therapy for Alzheimer's disease: a phase IIa, double-blind, randomised, placebo-controlled trial. *Lancet Neurol.* **2008,** *7* (9), 779-786.
64. Faux, N. G.; Ritchie, C. W.; Gunn, A.; Rembach, A.; Tsatsanis, A.; Bedo, J.; Harrison, J.; Lannfelt, L.; Blennow, K.; Zetterberg, H.; Ingelsson, M.; Masters, C. L.; Tanzi, R. E.; Cummings, J. L.; Herd, C. M.; Bush, A. I., PBT2 rapidly improves cognition in Alzheimer's Disease: additional phase II analyses. *J. Alzheimers Dis.* **2010,** *20* (2), 509-516.
65. Relkin, N. R., Testing the mettle of PBT2 for Alzheimer's disease. *The Lancet. Neurology* **2008,** *7* (9), 762-763.
66. Oliveri, V.; Vecchio, G., 8-Hydroxyquinolines in medicinal chemistry: A structural perspective. *Eur. J. Med. Chem.* **2016,** *120*, 252-274.
67. Hindo, S. S.; Mancino, A. M.; Braymer, J. J.; Liu, Y.; Vivekanandan, S.; Ramamoorthy, A.; Lim, M. H., Small Molecule Modulators of Copper-Induced Aβ Aggregation. *J. Am. Chem. Soc.* **2009,** *131* (46), 16663-16665.
68. Martínez, A.; Alcendor, R.; Rahman, T.; Podgorny, M.; Sanogo, I.; McCurdy, R., Ionophoric polyphenols selectively bind Cu^{2+}, display potent antioxidant and anti-amyloidogenic properties, and are non-toxic toward *Tetrahymena thermophila*. *Biorg. Med. Chem.* **2016,** *24* (16), 3657-3670.
69. Barcia, E.; Salama, A.; Fernández-Carballido, A.; Negro, S., Protective effects of clioquinol on human neuronal-like cells: a new formulation of clioquinol-loaded PLGA microspheres for Alzheimer's disease. *Journal of Drug Targeting* **2011,** *19* (8), 637-646.
70. Gomes, L. M.; Vieira, R. P.; Jones, M. R.; Wang, M. C.; Dyrager, C.; Souza-Fagundes, E. M.; Da Silva, J. G.; Storr, T.; Beraldo, H., 8-Hydroxyquinoline Schiff-base compounds as antioxidants and modulators of copper-mediated Aβ peptide aggregation. *J. Inorg. Biochem.* **2014,** *139*, 106-116.
71. Crouch, P. J.; Savva, M. S.; Hung, L. W.; Donnelly, P. S.; Mot, A. I.; Parker, S. J.; Greenough, M. A.; Volitakis, I.; Adlard, P. A.; Cherny, R. A.; Masters, C. L.; Bush, A. I.; Barnham, K. J.; White, A. R., The Alzheimer's therapeutic PBT2 promotes amyloid-β degradation and GSK3 phosphorylation via a metal chaperone activity. *J. Neurochem.* **2011,** *119*, 220–230.
72. Nguyen, M.; Robert, A.; Soumia-Saquet, A.; Vendier, L.; Meunier, B., Characterization of new specific copper chelators as potential drugs for the treatment of Alzheimer's disease. *Chem. Eur. J.* **2014,** *20* (22), 6771-6785.
73. Nguyen, M.; Rechignat, L.; Robert, A.; Meunier, B., The Necessity of Having a Tetradentate Ligand to Extract Copper(II) Ions from Amyloids. *ChemistryOpen* **2015,** *4* (1), 27-31.
74. Nguyen, M.; Bijani, C.; Martins, N.; Meunier, B.; Robert, A., Transfer of Copper from an Amyloid to a Natural Copper-Carrier Peptide with a Specific Mediating Ligand. *Chem. Eur. J.* **2015,** *21* (47), 17085-17090.
75. Ceccom, J.; Coslédan, F.; Halley, H.; Francès, B.; Lassalle, J. M.; Meunier, B., Copper Chelator Induced Efficient Episodic Memory Recovery in a Non-Transgenic Alzheimer's Mouse Model. *PLoS One* **2012,** *7* (8), e43105.
76. Deraeve, C.; Boldron, C.; Maraval, A.; Mazarguil, H.; Gornitzka, H.; Vendier, L.; Pitié, M.; Meunier, B., Preparation and Study of New Poly-8-Hydroxyquinoline Chelators for an anti-Alzheimer Strategy. *Chem. Eur. J.* **2008,** *14* (2), 682-696.
77. Kenche, V. B.; Zawisza, I. A.; Masters, C. L.; Bal, W.; Barnham, K. J.; Drew, S. C., Mixed ligand Cu^{2+} complexes of a model therapeutic with Alzheimer's amyloid-β peptide and monoamine neurotransmitters. *Inorg. Chem.* **2013,** *52* (8), 4303-4318.

78. Choi, J.-S.; Braymer, J. J.; Nanga, R. P. R.; Ramamoorthy, A.; Lim, M. H., Design of small molecules that target metal-Aβ species and regulate metal-induced Aβ aggregation and neurotoxicity. *PNAS* **2010,** *107* (51), 21990-21995.
79. Beck, M. W.; Oh, S. B.; Kerr, R. A.; Lee, H. J.; Kim, S. H.; Kim, S.; Jang, M.; Ruotolo, B. T.; Lee, J.-Y.; Lim, M. H., A rationally designed small molecule for identifying an in vivo link between metal–amyloid-β complexes and the pathogenesis of Alzheimer's disease. *Chemical Science* **2015,** *6* (3), 1879-1886.
80. Beck, M. W.; Derrick, J. S.; Kerr, R. A.; Oh, S. B.; Cho, W. J.; Lee, S. J. C.; Ji, Y.; Han, J.; Tehrani, Z. A.; Suh, N.; Kim, S.; Larsen, S. D.; Kim, K. S.; Lee, J.-Y.; Ruotolo, B. T.; Lim, M. H., Structure-mechanism-based engineering of chemical regulators targeting distinct pathological factors in Alzheimer's disease. *Nat. Commun.* **2016,** *7*, 13115-13127.
81. Lee, S.; Zheng, X.; Krishnamoorthy, J.; Savelieff, M. G.; Park, H. M.; Brender, J. R.; Kim, J. H.; Derrick, J. S.; Kochi, A.; Lee, H. J.; Kim, C.; Ramamoorthy, A.; Bowers, M. T.; Lim, M. H., Rational Design of a Structural Framework with Potential Use to Develop Chemical Reagents That Target and Modulate Multiple Facets of Alzheimer's Disease. *J. Am. Chem. Soc.* **2014,** *136* (1), 299-310.
82. Geng, J.; Li, M.; Wu, L.; Ren, J.; Qu, X., Liberation of Copper from Amyloid Plaques: Making a Risk Factor Useful for Alzheimer's Disease Treatment. *J. Med. Chem.* **2012,** *55*, 9146−9155.
83. Rodríguez-Rodríguez, C.; Sánchez de Groot, N.; Rimola, A.; Álvarez-Larena, Á.; Lloveras, V.; Vidal-Gancedo, J.; Ventura, S.; Vendrell, J.; Sodupe, M.; González-Duarte, P., Design, Selection, and Characterization of Thioflavin-Based Intercalation Compounds with Metal Chelating Properties for Application in Alzheimer's Disease. *J. Am. Chem. Soc.* **2009,** *131* (4), 1436-1451.
84. Harford, C.; Sarkar, B., Amino Terminal Cu(II)- and Ni(II)-Binding (ATCUN) Motif of Proteins and Peptides: Metal Binding, DNA Cleavage, and Other Properties. *Acc. Chem. Res.* **1997,** *30* (3), 123-130.
85. Lakatos, A.; Gyurcsik, B.; Nagy, N. V.; Csendes, Z.; Weber, E.; Fulop, L.; Kiss, T., Histidine-rich branched peptides as Cu(ii) and Zn(ii) chelators with potential therapeutic application in Alzheimer's disease. *Dalton Trans.* **2012,** *41* (6), 1713-1726.
86. Jensen, M.; Canning, A.; Chiha, S.; Bouquerel, P.; Pedersen, J. T.; Østergaard, J.; Cuvillier, O.; Sasaki, I.; Hureau, C.; Faller, P., Inhibition of Cu-Amyloid-β by using Bifunctional Peptides with β-Sheet Breaker and Chelator Moieties. *Chem. Eur. J.* **2012,** *18* (16), 4836-4839.
87. Conte-Daban, A.; Boff, B.; Candido, A.; Montes Aparicio, C.; Gateau, C.; Lebrun, C.; Cerchiaro, G.; Kieffer, I.; Sayen, S.; Guillon, E.; Delangle, P.; Hureau, C., A trishistidine pseudopeptide with ability to remove both Cu(I) and Cu(II) from the amyloid-beta peptide and to stop the associated ROS formation. *Chem. Eur. J.* **2017**, In press.
88. Caballero, A. B.; Terol-Ordaz, L.; Espargaró, A.; Vázquez, G.; Nicolás, E.; Sabaté, R.; Gamez, P., Histidine-Rich Oligopeptides To Lessen Copper-Mediated Amyloid-β Toxicity. *Chem. Eur. J.* **2016,** *22* (21), 7268-7280.
89. Hu, X.; Zhang, Q.; Wang, W.; Yuan, Z.; Zhu, X.; Chen, B.; Chen, X., Tripeptide GGH as the Inhibitor of Copper-Amyloid-β-Mediated Redox Reaction and Toxicity. *ACS Chem. Neurosci.* **2016,** *7* (9), 1255-1263.
90. Quintanova, C.; Keri, R. S.; Chaves, S.; Santos, M. A., Copper(II) complexation of tacrine hybrids with potential anti-neurodegenerative roles. *J. Inorg. Biochem.* **2015,** *151*, 58-66.
91. Chen, T.; Wang, X.; He, Y.; Zhang, C.; Wu, Z.; Liao, K.; Wang, J.; Guo, Z., Effects of Cyclen and Cyclam on Zinc(II)- and Copper(II)-Induced Amyloid β-Peptide Aggregation and Neurotoxicity. *Inorg. Chem.* **2009,** *48* (13), 5801-5809.
92. Wu, W.-h.; Lei, P.; Liu, Q.; Hu, J.; Gunn, A. P.; Chen, M.-s.; Rui, Y.-f.; Su, X.-y.; Xie, Z.-p.; Zhao, Y.-F.; Bush, A. I.; Li, Y.-m., Sequestration of Copper from β-Amyloid Promotes Selective Lysis by Cyclen-Hybrid Cleavage Agents. *J. Biol. Chem.* **2008,** *283* (46), 31657-31664.
93. Yang, Y.; Chen, T.; Zhu, S.; Gu, X.; Jia, X.; Lu, Y.; Zhu, L., Two macrocyclic polyamines as modulators of metal-mediated Aβ40 aggregation. *Integr. Biol.* **2015,** *7* (6), 655-662.
94. Kaden, D.; Bush, A. I.; Danzeisen, R.; Bayer, T. A.; Multhaup, G., Disturbed Copper Bioavailability in Alzheimer's Disease. *Int. J. Alzheimers Dis.* **2011,** *2011*.

95. Storr, T.; Merkel, M.; Song-Zhao, G. X.; Scott, L. E.; Green, D. E.; Bowen, M. L.; Thompson, K. H.; Patrick, B. O.; Schugar, H. J.; Orvig, C., Synthesis, Characterization, and Metal Coordinating Ability of Multifunctional Carbohydrate-Containing Compounds for Alzheimer's Therapy. *J. Am. Chem. Soc.* **2007,** *129*, 7453-7463.
96. Conte-Daban, A.; Day, A.; Faller, P.; Hureau, C., How Zn can impede Cu detoxification by chelating agents in Alzheimer's disease: a proof-of-concept study. *Dalton Trans.* **2016,** *45* (39), 15671-15678.
97. Noël, S.; Perez, F.; Pedersen, J. T.; Alies, B.; Ladeira, S.; Sayen, S.; Guillon, E.; Gras, E.; Hureau, C., A new water-soluble Cu(II) chelator that retrieves Cu from Cu(amyloid-β) species, stops associated ROS production and prevents Cu(II)-induced Aβ aggregation. *J. Inorg. Biochem.* **2012,** *117*, 322-325.
98. Lakatos, A.; Zsigo, E.; Hollender, D.; Nagy, N. V.; Fulop, L.; Simon, D.; Bozso, Z.; Kiss, T., Two pyridine derivatives as potential Cu(ii) and Zn(ii) chelators in therapy for Alzheimer's disease. *Dalton Trans.* **2010,** *39* (5), 1302-1315.
99. Atrian-Blasco, E.; Cerrada, E.; Conte-Daban, A.; Testemale, D.; Faller, P.; Laguna, M.; Hureau, C., Copper(i) targeting in the Alzheimer's disease context: a first example using the biocompatible PTA ligand. *Metallomics* **2015,** *7* (8), 1229-1232.
100. Donnelly, P. S.; Caragounis, A.; Du, T.; Laughton, K.; Volitakis, I.; Cherny, R. A.; Sharples, R. A.; Hill, A. F.; Li, Q.-X.; Masters, C. L.; Barnham, K. J.; White, A. R., Selective intracellular release of copper and zinc ions from bis(thiosemicarbazonato) complexes reduces levels of Alzheimer disease amyloid-beta peptide. *J. Biol. Chem.* **2008,** *283* (8), 4568-4577.
101. Crouch, P. J.; Hung, L. W.; Adlard, P. A.; Cortes, M.; Lal, V.; Filiz, G.; Perez, K. A.; Nurjono, M.; Caragounis, A.; Du, T.; Laughton, K.; Volitakis, I.; Bush, A. I.; Li, Q. X.; Masters, C. L.; Cappai, R.; Cherny, R. A.; Donnelly, P. S.; White, A. R.; Barnham, K. J., Increasing Cu bioavailability inhibits Aβ oligomers and tau phosphorylation. *PNAS* **2009,** *106* (2), 381-386.
102. Sanabria-Castro, A.; Alvarado-Echeverría, I.; Monge-Bonilla, C., Molecular Pathogenesis of Alzheimer's Disease: An Update. *Ann. Neurosci.* **2017,** *24* (1), 46-54.
103. Savelieff, M. G.; Lee, S.; Liu, Y.; Lim, M. H., Untangling Amyloid-β, Tau, and Metals in Alzheimer's Disease. *ACS Chem. Biol.* **2014,** *8*, 856-865.
104. Atrian-Blasco, E.; Gonzalez, P.; Santoro, A.; Alies, B.; Faller, P.; Hureau, C., Cu and Zn coordination to amyloids: a chemistry of pathological importance ? *Coord. Chem. Rev.* **2017**.
105. Ono, K., Alzheimer's disease as oligomeropathy. *Neurochem. Int.* **2017,** *17*, 30331-30335.
106. Solomon, E. I.; Heppner, D. E.; Johnston, E. M.; Ginsbach, J. W.; Cirera, J.; Qayyum, M.; Kieber-Emmons, M. T.; Kjaergaard, C. H.; Hadt, R. G.; Tian, L., Copper active sites in biology. *Chem. Rev.* **2014,** *114* (7), 3659-3653.
107. Hureau, C., Coordination of redox active metal ions to the APP and to the amyloid-β peptides involved in AD. Part 1: an overview. *Coord. Chem. Rev.* **2012,** *256* (19-20), 2164-2174.
108. Cheignon, C.; Tomas, M.; Bonnefont-Rousselot, D.; Faller, P.; Hureau, C.; Collin, F., Oxidative stress and the amyloid beta peptide in Alzheimer's Disease. *Redox Biology* **2017,** *accepted*.
109. Santos, M. A.; Chand, K.; Chaves, S., Recent progress in multifunctional metal chelators as potential drugs for Alzheimer's disease. *Coord. Chem. Rev.* **2016,** *327-328*, 287-303.
110. Barnham, K. J.; Bush, A. I., Biological metals and metal-targeting compounds in major neurodegenerative diseases. *Chem. Soc. Rev.* **2014,** *43*, 6727-6749.
111. Atrian-Blasco, E.; Conte-Daban, A.; Hureau, C., Mutual interference of Cu and Zn ions in Alzheimer's disease: perspectives at the molecular level. *Dalton Transactions* **2017,** *in press*.
112. Chen, T.; Wang, X.; He, Y.; Zhang, C.; Wu, Z.; Liao, K.; Wang, J.; Zijian, G., Effects of Cyclen and Cyclam on Zinc(II)- and Copper(II)-Induced Amyloid β-Peptide Aggregation and Neurotoxicity. *Inorg. Chem.* **2009,** *48* (13), 5801-5809.
113. Banerjee, S. R.; Pullambhatla, M.; Foss, C. A.; Nimmagadda, S.; Ferdani, R.; Anderson, C. J.; Mease, R. C.; Pomper, M. G., ^{64}Cu-Labeled Inhibitors of Prostate-Specific Membrane Antigen for PET Imaging of Prostate Cancer. *J. Med. Chem.* **2014,** *57* (6), 2657-2669.

114. Stasiuk, G. J.; Long, N. J., The ubiquitous DOTA and its derivatives: the impact of 1,4,7,10-tetraazacyclododecane-1,4,7,10-tetraacetic acid on biomedical imaging. *Chem. Commun.* **2013,** *49* (27), 2732-2746.
115. Wong, E. H.; Weisman, G. R.; Hill, D. C.; Reed, D. P.; Rogers, M. E.; Condon, J. S.; Fagan, M. A.; Calabrese, J. C.; Lam, K.-C.; Guzei, I. A.; Rheingold, A. L., Synthesis and Characterization of Cross-Bridged Cyclams and Pendant-Armed Derivatives and Structural Studies of Their Copper(II) Complexes. *J. Am. Chem. Soc.* **2000,** *122* (43), 10561-10572.
116. Terreno, E.; Castelli, D. D.; Viale, A.; Aime, S., Challenges for Molecular Magnetic Resonance Imaging. *Chem. Rev.* **2010,** *110* (5), 3019-3042.
117. Izatt, R. M.; Pawlak, K.; Bradshaw, J. S.; Bruening, R. L., Thermodynamic and kinetic data for macrocycle interaction with cations, anions, and neutral molecules. *Chem. Rev.* **1995,** *95* (7), 2529-2586.
118. Delgado, R.; Felix, V.; Lima, L. M. P.; Price, D. W., Metal complexes of cyclen and cyclam derivatives useful for medical applications: a discussion based on thermodynamic stability constants and structural data. *Dalton Trans.* **2007,** (26), 2734-2745.
119. Burai, L.; Fabian, I.; Kiraly, R.; Szilagyi, E.; Brucher, E., Equilibrium and kinetic studies on the formation of the lanthanide(III) complexes, $[Ce(dota)]^-$ and $[Yb(dota)]^-$ (H4dota[space]=[space]1,4,7,10-tetraazacyclododecane-1,4,7,10-tetraacetic acid). *J. Chem. Soc., Dalton Trans.* **1998,** (2), 243-248.
120. Lima, L. M. P.; Esteban-Gómez, D.; Delgado, R.; Platas-Iglesias, C.; Tripier, R., Monopicolinate Cyclen and Cyclam Derivatives for Stable Copper(II) Complexation. *Inorg. Chem.* **2012,** *51* (12), 6916-6927.
121. Rodriguez-Rodriguez, A.; Garda, Z.; Ruscsak, E.; Esteban-Gomez, D.; de Blas, A.; Rodriguez-Blas, T.; Lima, L. M. P.; Beyler, M.; Tripier, R.; Tircso, G.; Platas-Iglesias, C., Stable Mn2+, Cu2+ and Ln3+ complexes with cyclen-based ligands functionalized with picolinate pendant arms. *Dalton Trans.* **2015,** *44* (11), 5017-5031.
122. Peisach, J.; Blumberg, W. E., Structural implications derived from the analysis of electron paramagnetic resonance spectra of natural and artificial copper proteins. *Arch. Biochem. Biophys.* **1974,** *165* (2), 691-708.
123. Hancock, R. D.; Salim Shaikjee, M.; Dobson, S. M.; Boeyens, J. C. A., The Stereochemical activity or non-activity of the 'Inert' pair of electrons on lead(II) in relation to its complex stability and structural properties. Some considerations in ligand design. *Inorg. Chim. Acta* **1988,** *154* (2), 229-238.
124. Kodama, M.; Kimura, E., A thermodynamic and kinetic interpretation of the macrocyclic effect. Polarographic studies on copper(II) 1,4,7,10-tetraazacyclododecane complexation. *J. Chem. Soc., Chem. Commun.* **1975,** (9), 326-327.
125. Kodama, M.; Kimura, E., Equilibria of complex formation between several bivalent metal ions and macrocyclic tri- and penta-amines. *Dalton Trans.* **1978,** (9), 1081-1085.
126. Motekaitis, R. J.; Rogers, B. E.; Reichert, D. E.; Martell, A. E.; Welch, M. J., Stability and Structure of Activated Macrocycles. Ligands with Biological Applications. *Inorg. Chem.* **1996,** *35* (13), 3821-3827.
127. Alies, B.; Sasaki, I.; Proux, O.; Sayen, S.; Guillon, E.; Faller, P.; Hureau, C., Zn impacts Cu coordination to Amyloid-ß, the Alzheimer's peptide, but not the ROS production and the associated cell toxicity. *Chem. Commun.* **2013,** *49* (12), 1214-1216.
128. Royal, G.; Dahaoui-Gindrey, V.; Dahaoui, S.; Tabard, A.; Guilard, R.; Pullumbi, P.; Lecomte, C., New Synthesis of trans-Disubstituted Cyclam Macrocycles – Elucidation of the Disubstitution Mechanism on the Basis of X-ray Data and Molecular Modeling. *Eur. J. Org. Chem.* **1998,** *1998* (9), 1971-1975.
129. Mato-Iglesias, M.; Roca-Sabio, A.; Pálinkás, Z.; Esteban-Gómez, D.; Platas-Iglesias, C.; Tóth, É.; de Blas, A.; Rodríguez-Blas, T., Lanthanide Complexes Based on a 1,7-Diaza-12-crown-4 Platform Containing Picolinate Pendants: A New Structural Entry for the Design of Magnetic Resonance Imaging Contrast Agents. *Inorg. Chem.* **2008,** *47* (17), 7840-7851.
130. Oxford Diffraction Ltd, A., U.K. *Crysalis software system, version 1.171.28 cycle 4 beta*, 2005.
131. Sheldrick, G., A short history of SHELX. *Acta Cryst. A* **2008,** *64* (1), 112-122.

132. Glasoe, P. K.; Long, F. A., Use of glass electrodes to measure acidities in deuterium oxide. *J. Phys. Chem.* **1960,** *64* (1), 188-190.
133. Rossotti, F. J. C.; Rossotti, H., Potentiometric titrations using Gran plots: A textbook omission. *J. Chem. Educ.* **1965,** *42* (7), 375-378.
134. Schwarzenbach, G.; Flaschka, H. A., *Complexometric titrations*. Methuen: London, 1969.
135. Delgado, R.; do Carmo Figueira, M.; Quintino, S., Redox method for the determination of stability constants of some trivalent metal complexes. *Talanta* **1997,** *45* (2), 451-462.
136. Gans, P.; Sabatini, A.; Vacca, A., Investigation of equilibria in solution. Determination of equilibrium constants with the HYPERQUAD suite of programs. *Talanta* **1996,** *43* (10), 1739-1753.
137. Alderighi, L.; Gans, P.; Ienco, A.; Peters, D.; Sabatini, A.; Vacca, A., Hyperquad simulation and speciation (HySS): a utility program for the investigation of equilibria involving soluble and partially soluble species. *Coord. Chem. Rev.* **1999,** *184* (1), 311-318.

Chapter III. Impact of Zn(II) on the Cu(II) chelation

This chapter focuses on the impact of Zn(II) ion on the Cu(II) chelation within the Alzheimer's disease context. This work is biologically relevant since Zn(II) is present in very high concentrations in the synaptic cleft compared to the Cu ions. Furthermore, Cu and Zn ions are found co-localised with the Aβ peptide in the senile plaques. That is the reason why it is biologically relevant to investigate the interplay between Cu and Zn ions with the Aβ peptide and the drug-candidates that are based on the chelation of Cu from Aβ.

A first part describes the state of the art regarding the impact of Zn(II) on the interaction between Cu ions and Aβ peptide. Metal ions coordination, ROS production and aggregation of the peptide are under focus. Moreover, the impact of Zn ions on the Cu ion chelation is reported and developed in the III-B section. A second part focuses on the Cu(II) chelation from a thermodynamic point of view. Studies regarding the removal of Cu(II) by different chelators from Aβ in the presence of Zn(II) have been performed by EPR, UV-Visible and XANES spectroscopies. The impact of this removal on the arrest of ROS production and on the aggregation have then been studied by fluorescence and UV-Visible spectroscopies. Aggregates have been imaged by AFM. The last part describes another proof of concept: the "pull-push" effect. For some ligands, Zn ions are necessary in order to remove Cu ions from Aβ. Zn(II) pulls Cu ions out from the peptide et pushes them into the chelator. This concept is described and experimentally illustrated by EPR, XANES and UV-Vis spectroscopies.

III-A State of the art: the mutual interactions of Cu and Zn ions on the Aβ peptide

This part summarises the state of the art about the interactions of Zn(II) on the interplay between Cu ions and Aβ peptide. It is composed of a perspective article published in *Dalton Transactions* in 2017 and a summary of this perspective. I have co-written this review.

III-A.i Summary

This perspective summarises the different investigations published until now on the mutual interactions of Cu ions and Zn(II) with the Aβ peptide.

In AD brains, a dyshomeostasis of Cu and Zn ions is reported: extracellular Cu(II) level is too high while the intracellular concentrations of Cu(I) are too low. Regarding Zn(II) concentrations, the tendency is not so clear. Indeed, some groups have found Zn ions in concentrations too high, and other ones, in concentrations too low. Furthermore, Cu and Zn ions have been found in the senile plaques and *in vitro* studies have shown that not only Cu ions but also Zn ions can interact with the Aβ peptide. These metal ions can also modulate the aggregation of Aβ, but again no tendency *in vitro* has been reached yet. Aggregation is important because oligomeric forms of Aβ are considered to be the most toxic species to cells. All the studies agree on the importance of the metal:peptide ratio and the fact that Cu(II) and Zn(II) ions both have an effect on the aggregation but that effect differs between Cu(II) and Zn(II). Another potential toxic mechanism is the ROS production catalysed by the Cu-Aβ complex, which can attack and degrade the surrounding biomolecules. That is why Cu(II) chelation is an important part of the Alzheimer's therapeutic investigations since the last years. It has been reported that not only removing the Cu(II) from Aβ and redox silencing the Cu ions by the chelator might be important, but also the subsequent transport of Cu into the cell and its release as Cu(I) (such chelators are often called metallophores). Some of the chelators, such as clioquinol and then PBT2, have been under clinical trials but failed in phase II. Nowadays, one of the hypothesis for these failures is that the selectivity (*i.e*. the ratio between the affinity constant for Cu(II) and the one for Zn(II)) of the chelators between Cu(II) and Zn(II) is not high enough: the ligand removes Zn ions which then precludes removal of Cu ions. This could indicate that Cu(II) is a therapeutic target but that the interactions of Zn(II) (or other factors) has to be taken into account as well. In this perspective, the coordination of the homometallic (Cu(II) or Cu(I) or Zn(II)) and of the hetero-bimetallic (Zn(II) and Cu(II) or Cu(I)) complexes are reported, then the impact of Zn ions on the ROS production by Cu-Aβ and on the Cu-Aβ aggregation is described, and finally the impact of the presence of Zn(II) on the Cu ion removal by different chelators is discussed.

III.A.i.1.1 Coordination

The first part of this perspective reports the most accepted coordinations of the monometallic and hetero-bimetallic complexes (Figure III-1). The coordination sites of the monometallic complexes are described in the part I-B.iii.1. The coordination of the hetero-bimetallic complexes has been probed by different spectroscopic and potentiometric techniques. Regarding the Cu(II) coordination, Zn ions have an impact on it since Cu and Zn binding sites share some amino acids as ligands. Zn(II) coordination keeps the His6 as ligand, leading to the displacement of the Cu(II) binding site from component I to component II at physiological pH. The other ligands for the Zn(II) coordination are not yet been described, but the other His residue should be removed to this coordination at lower pH. Regarding

Cu(I), Cu(I) keeps the same coordination than in the monometallic Cu(I)-Aβ and it imposes its coordination to the Zn ions, which loose the second His residue in its coordination. In brief, Cu(I/II) and Zn(II) have a mutual interference in their binding site to Aβ. It would be interesting to know the impact of this mutual interaction on the affinity constant of the metal ions for Aβ.

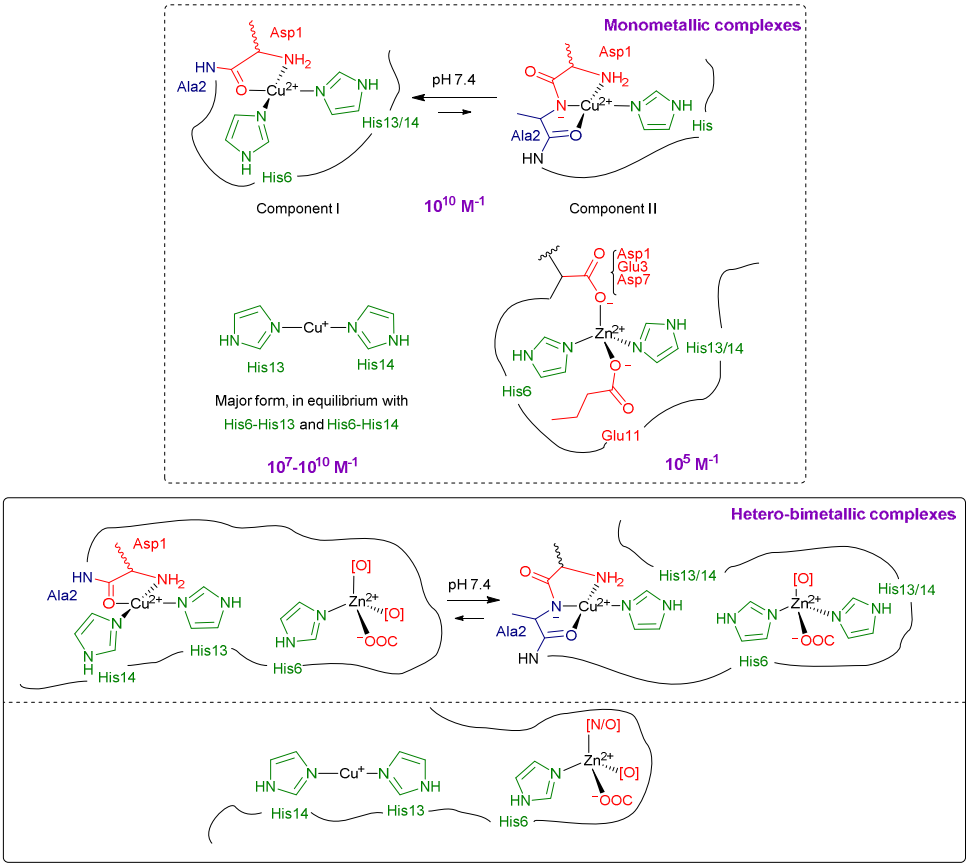

Figure III-1. Proposed models for the Cu(I), Cu(II) and Zn(II) coordination sites to Aβ as well as the hetero-bimetallic coordination..

III.A.i.1.2 ROS production and aggregation

The second part of this perspective focuses on the impact of Zn(II) on the aggregation and the ROS production by the complex Cu-Aβ. First of all, the aggregation of the Aβ peptide is modulated by Cu and Zn ions and these aggregations are highly dependent on the metal:peptide ratio, on the pH, on the temperature, etc. In the case of the Cu-Aβ aggregation, the metal:peptide ratio is very important. Indeed, in a sub-stoichiometric ratio of Cu ions compare to Aβ, fibrils are formed, whereas in at least a stoichiometric ratio, toxic oligomers are formed. Zn(II) impacts the Aβ aggregation even at a very low ratio, and at a stoichiometric ratio, fibrils as well as amorphous aggregates are formed. Note that the Zn(II)-induced fibrils are different from the apo-fibrils. The aggregation in the presence of both Cu(II) and Zn(II) has been reported to be the same than the aggregation with Zn ions only. Then, the ROS

production by monomeric species in the presence of Zn(II) is reported. Indeed, there is a mutual interference of Cu and Zn ions in the coordination of the metal, in the aggregation of the peptide; it is biologically relevant to determine whether there is an impact of Zn(II) on the ROS production. Nevertheless, the tendency is not clear. Some studies show that Zn(II) has a protective effect towards the ROS production, increasing the survival of cells and decreasing the H_2O_2 production. This effect would be due to the displacement of the binding site of Cu(II) from component I to component II. Nevertheless, other studies confirm that Cu(II) is displaced at another site upon Zn(II)-binding, but they disagree on the fact that component II is redox silent. The presence of Zn(II) do not change the ROS production. This result is in line with a recent study explaining that the Cu(II) coordination is not the key parameter of the ROS production at all. Finally, the ROS production by aggregated species is reported in this perspective. One study describes that for a 0.5:1 Cu:Aβ ratio, the monomeric complex produces more ROS than the aggregate one. Another study shows that for a stoichiometric ratio, Cu-Aβ complex aggregates produce more ROS than the Cu,Zn-Aβ complex aggregates. In other words, the aggregated species should produce less ROS than the monomeric ones, and the presence of Zn should have a protective role on the ROS production by aggregates. In brief, nowadays, there are not enough studies with both Cu and Zn ions on the ROS production and/or the aggregation. No clear tendency can be reached with these few investigations, except that Zn(II) has not a dramatic effect on Cu-Aβ ROS production, for the monomeric species.

III.A.i.1.3 Cu(II) chelation

The last part of this perspective focuses on the impact of the presence of Zn(II) on the withdrawal of Cu(II) from Aβ by a chelator. The Cu(II) chelation in the AD context has been developed in the last years. A ligand needs a higher affinity constant for Cu(II) than the Aβ peptide, but its affinity constant has also to be lower than the one of essential metalloproteins, in order to not remove the essential Cu(II). As previously shown, Zn(II) impacts the Cu ion coordination, the ROS production and the aggregation. Therefore, it is an important parameter to take into account in the Cu chelation. The first studies regarding the impact of Zn(II) on the Cu chelation have been performed with the metallothionein Zn_7-MT-3 (Figure III-2, left). There is a swap of metal ions between Cu(II) bound to Aβ and Zn(II) bound to Zn_7-MT-3, removing Cu(II) from Aβ and forming an air stable $Cu(I)_4$-thiolate cluster inside the metallothionein. This cluster silences the ROS production. Then the same results are shown with the MT-2A. Moreover, with the MT-2A, the same experiments with the apo-MT-2A are performed: Cu(II) stays bound to Aβ and the ROS production is not reduced. This sheds light on the importance of the presence of Zn(II). Then this kind of experiments is performed with synthetic ligands (Figure III-2, right). The two studied ligands, with a higher affinity constant for Cu(II) than the one of

Aβ, are able to remove Cu(II) from Aβ. Nevertheless, in the presence of Zn(II), only one of them removes Cu(II) from the peptide. Indeed, they need a selectivity for Cu(II) towards Zn(II), *i.e*. a ratio between the affinity constant for Cu(II) and the one for Zn(II), and this is the case for both of them. They need also that this selectivity is higher than the selectivity of Aβ; if not they are not able to remove Cu(II) from Aβ. Note that this part is detailed in part III-B. Some future work or ideas to take into account are then given. All of these studies prove that the Cu chelation has to be performed in a Zn(II)-rich environment, even for Cu(I). Then, if Zn(II) can impact the Cu-chelation in the AD context, other biologically relevant ions such as Fe, Ca, Mg, etc. may also have an important role. Finally, as the thermodynamics are important in the Cu ion removal, the kinetics of removal of Cu ions from Aβ can also be an important parameter and should be studied next.

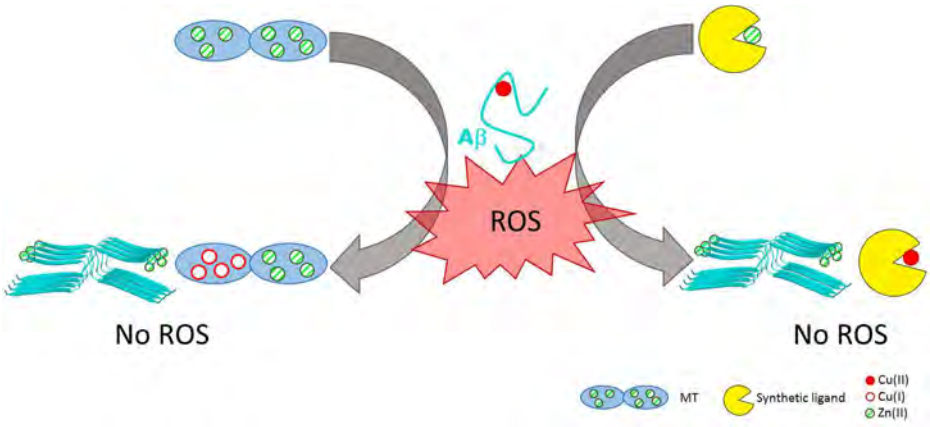

Figure III-2. Scheme representing the swap of metallic ions between metallothioneins or chelators and the Aβ peptide. The impact on the ROS production is also illustrated.

In this perspective, the mutual interactions of Cu and Zn ions with the Aβ peptide are described. Zn(II) has an important impact on the relationship between Cu ions and Aβ peptide. Zn(II) displaces Cu(II) from a binding site to another one. Moreover, it influences the ROS production of the Cu-Aβ complex. The aggregation of the peptide is also influenced by the presence of Zn(II): it appears that Zn(II) should impose its metal-induced aggregation. All of these studies shed light on the high impact of Zn(II) on the Cu-Aβ complex and its properties. Zn(II) also impacts the Cu chelation. In order to remove Cu ions from Aβ in the presence of Zn(II), the ligand needs not only a higher affinity constant for Cu than Aβ, but also a higher selectivity of Cu over Zn than the Aβ. This selectivity issue has to be taken into account also for the Cu(I) removal.

III-A.ii Perspective

Volume 46 | Number 38 14 October 2017 Pages 12735–13146

Dalton Transactions

An international journal of inorganic chemistry

rsc.li/dalton

ISSN 1477-9226

ROYAL SOCIETY OF CHEMISTRY

PERSPECTIVE
Christelle Hureau *et al.*
Mutual interference of Cu and Zn ions in Alzheimer's disease: perspectives at the molecular level

Dalton Transactions

PERSPECTIVE

View Article Online
View Journal | View Issue

Cite this: *Dalton Trans.*, 2017, **46**, 12750

Mutual interference of Cu and Zn ions in Alzheimer's disease: perspectives at the molecular level

Elena Atrián-Blasco, †[a,b] Amandine Conte-Daban†[a,b] and Christelle Hureau *[a,b]

Received 13th April 2017,
Accepted 22nd June 2017

DOI: 10.1039/c7dt01344b

rsc.li/dalton

While metal ions such as copper and zinc are essential in biology, they are also linked to several amyloid-related diseases, including Alzheimer's disease (AD). Zinc and copper can indeed modify the aggregation pathways of the amyloid-β (Aβ) peptide, the key component encountered in AD. In addition, the redox active copper ions do produce Reactive Oxygen Species (ROS) when bound to the Aβ peptide. While Cu(I) or Cu(II) or Zn(II) coordination to the Aβ has been extensively studied in the last ten years, characterization of hetero-bimetallic Aβ complexes is still scarce. This is also true for the metal induced Aβ aggregation and ROS production, for which studies on the mutual influence of the copper and zinc ions are currently appearing. Last but not least, zinc can strongly interfere in therapeutic approaches relying on copper detoxification. This will be exemplified with a biological lead, namely metallothioneins, and with synthetic ligands.

Introduction

Alzheimer's disease (AD) is the most common neurodegenerative disease, with a prevalence of around 35 million patients worldwide.[1] This number is expected to triple within the next 35 years, making AD a current major global public health problem. In the brain, one of the hallmarks of the disease is the extracellular accumulation of Amyloid-β (Aβ) peptides into senile plaques. The amyloid cascade hypothesis describes this process: Aβ is present in healthy brains in soluble and monomeric forms. In contrast, in AD brains, these peptides aggregate into oligomers and then fibrils which assemble themselves into so-called senile plaques.[2,3] In the last few years,

[a]CNRS, LCC (Laboratoire de Chimie de Coordination), 205 route de Narbonne, BP 44099 31077 Toulouse Cedex 4, France. E-mail: christelle.hureau@lcc-toulouse.fr
[b]University of Toulouse, UPS, INPT, 31077 Toulouse Cedex 4, France
†These authors contributed equally.

Elena Atrián-Blasco (right), Amandine Conte-Daban (left) and Christelle Hureau (middle)

Elena Atrián-Blasco (right) was born in Zaragoza (Spain) in 1988, where she obtained her BSc degree in 2011 after an Erasmus stay at Queen's University Belfast (UK) in 2009–2010, and her MSc in Chemistry in 2012. After obtaining her PhD diploma at the ISQCH (Univ. Zaragoza-CSIC) under the supervision of Prof. Mariano Laguna and Dr Elena Cerrada, she joined Christelle's team in Toulouse for her postdoctoral stay. Amandine Conte-Daban (left) was born in Tarasteix (France) in 1991 and obtained her BSc degree in Physical Chemistry at Université Paris-Sud, and obtained her MSc degree in Medicinal Chemistry from the Université Paul Sabatier in Toulouse in 2014. She is currently performing her PhD in the "Alzheimer and amyloids" team with Christelle. Christelle Hureau (middle) was born in Charleville-Mézières (France) in 1976. She has a background in physical inorganic chemistry with a focus on EPR and electrochemistry. She is interested in chemistry in link with the biological world. In 2015, she became the group leader of the "Alzheimer and amyloids" team at the Laboratoire de Chimie de Coordination (UPR 8241 – CNRS). There, she investigates the structural and dynamic aspects of metal ion coordination to the amyloid-β peptide and new chelating concepts against Alzheimer's disease.

therapies based on inhibiting the aggregation of the Aβ peptides have failed clinical trials and, as a consequence, attention has been paid to other factors.[4] Indeed, AD has been linked to the dyshomeostasis of both Cu(I/II) and Zn(II) ions.[5] Regarding Zn(II) ions, both increased and decreased concentrations have been measured in AD brains compared to healthy brains.[6] Similarly, Cu ions are present in a 2-fold higher concentration in the CNS[6] and in higher concentrations in the hippocampus while intra-neuronal Cu(I) deficiency has been reported to be a key factor in AD.[7,8] Important levels of these metal ions have also been found in the senile plaques: 0.4 mM of Cu and 1 mM of Zn(II).[9,10] Consequently, these metal ions are supposed to play a key role in the aggregation of the Aβ peptides *in vivo* and thus in the associated amyloid cascade process.[11,12] In addition, the literature reveals the impact of metal ions on the Aβ aggregation *in vitro*, although contradictory effects have been reported.[11,12] They can modify either the kinetics of aggregation or the morphology of the aggregates. While there are many divergent reports on the impact of metal ions, two main consensual features are described: (i) the importance of the ratio between metal ions and peptides,[11–13] and (ii) the different effects produced by Cu and Zn ions.[11] Metal-induced aggregation is also described for other neurodegenerative diseases such as Parkinson's and Prion diseases, all characterized by misfolding of amyloidogenic proteins and metal ion dyshomeostasis.[6,14]

In AD, another important consequence of this dyshomeostasis is the production of Reactive Oxygen Species (ROS) by the Cu–Aβ complex, which catalyses the reduction of O_2, in the presence of a reductant such as ascorbate.[9,15] Indeed, it has been proposed that superoxide, hydrogen peroxide and hydroxyl radicals, which are the resulting species of the incomplete reduction of O_2, attack the surrounding biomolecules, thus participating in the global oxidative stress observed in AD.[16]

Within this context, metal chelation (using chelators)‡ or metal redistribution (using metallophores)‡ therapeutic approaches against AD have been under focus during the past few years.[8,17] In general, Cu is considered as the most pertinent target due to the ROS related toxicity of this redox competent ion.[8] The first generations of ligands‡ were capable of removing Cu(II) from Aβ peptides, stopping ROS production and favouring the disaggregation of Aβ senile plaques.[8] Clioquinol and PBT2 have shown to be the best candidates and have gone under clinical trials, however, both have failed in phase II.[18] To explain such unsuccessful results, it has first been proposed that these ligands cannot differentiate between the toxic Cu bound to Aβ and the Cu bound to essential metalloproteins. A new hypothesis relies on a too weak discrimination between the Cu(II) target and the Zn ions.[19,20] In fact, the significance of the selectivity in the development of ligands in the wide context of the chelation therapy has already been reviewed.[21,22] Particularly, the need for selectivity between the targeted toxic metal ion and other biological metal ions has been discussed for actinide decorporation,[23] and the need for Cu/Zn selectivity in the case of Wilson's disease.[24]

Therefore, different approaches are under focus to find new generations of ligands:[17,25] (i) prochelators,[26] which can be activated by H_2O_2 [27] or β-secretase[28] directly in the brain; (ii) multi-target compounds, *e.g.* those with an Aβ recognition moiety and a chelating moiety;[29,30] (iii) Cu(II)-chelators with a glucose moiety[31] or nanoparticles[32] as transporters through the Blood Brain Barrier.

It seems clear that the brain is a highly complex system, which also makes AD an intricate illness. There are many factors that could be implicated in the development of the disease, such as the different metal ions present in the synaptic cleft altogether with a wide range of biomolecules. The interaction of all of them could be relevant for the etiology, but trying to understand the basis requires starting by the simplest systems. For example, from a bio-inorganic chemistry approach of the disease, the effort was put on monometallic systems *i.e.* Cu–Aβ,[10,33] or Zn–Aβ.[34–36] Nevertheless, this is partially representative of the reality. Hence, a first step toward a more realistic picture would be to study the mutual influence of both metal ions in their interaction with the peptide at the molecular level, in order to understand the fundamental aspects of AD and to improve the development of ligands.

In this review, we report first the coordination chemistry of Aβ peptides with Cu(II), Cu(I) or Zn(II) and also of hetero-bimetallic species. The impact of the co-presence of Cu and Zn ions on the metal-induced Aβ aggregation and/or on the ROS production by the Cu–Aβ complex is then described. Finally, the importance of considering Zn in Cu-based chelation therapy is discussed. Personal points of view are also given about future research lines with respect to these three aspects.

Coordination chemistry of Cu and Zn to Aβ

Monometallic complexes

The amyloid-β (Aβ) peptide is a 40–42 amino-acid residue long peptide, of which the more hydrophobic region, the C-terminal, is prone to aggregation. The high affinity metal binding site of Aβ peptides is found at residues 1–16. For this reason, Aβ1–16 is proposed as a model for the coordination and redox properties of the full-length peptides. Coordination of Cu(II), Cu(I) and Zn(II) to the amyloid-β peptides has been extensively studied and probed by many different techniques. The most accepted coordination spheres for these metal ions, as well as their corresponding affinities, are summarized in Fig. 1. In the case of Cu(II), two different binding modes can be found at physiological pH, known as components I and II.

‡ Chelators: molecules capable of binding Cu ions with a high affinity constant, which then cannot release them rapidly. Metallophores: molecules capable of binding Cu ions and releasing them in another place. Ligands: molecules capable of binding Cu ions, with no precision on their releasing ability (a ligand can keep the metal ions or can release them, *i.e.* a ligand can either be a chelator or a metallophore).

They both show a distorted square-planar geometry and share the terminal amine as a ligand. Component I, which is predominant at lower pH, binds to Cu(II) through the N-terminal amine, the carbonyl from the amide bond of Asp1–Ala2, and the imidazole nitrogen (N_{im}) from two His residues, His6 and His13 or His14 in equilibrium. In component II, predominant at higher pH values, the nitrogen atom from the Asp1–Ala2 amide bond is deprotonated and binds to the Cu(II) ion, together with the N-terminal amine, the CO from the Ala2–Glu3 peptide bond and one imidazole group from a His residue.[10,37] A second site has been described for the Aβ1–28 peptide but its low affinity would make it a biologically irrelevant coordination site.[38] Cu(I) is bound in a linear fashion by two among the three possible N_{im} of His6, His13 and His14 in an equilibrium, in which the His13–His14 pair seems to be the preferred ligands.[39–41] The first 16 amino acids are also involved in the coordination of Zn(II). Previous studies stated the involvement of the three histidine residues in the coordination site.[42–48] The N-terminal amine and the Glu11 residue (among others) would be also involved in the coordination.[34–36] A more recent study proposes a different coordination sphere deduced from the study by ^{1}H-NMR and X-ray absorption spectroscopy of Aβ1–16 and a range of modified peptides.[34] The Zn(II) ion has a tetrahedral binding to two histidine residues (His6 and His13 or His14), and two carboxylate residues (Glu11 and Asp1 or Glu3 or Asp7, with a preference for Asp1). In this case, the N-terminal amine does not coordinate to Zn(II) at physiological pH. This proposition is in line with previously reported affinity studies on the very same series of modified peptides.[19]

Hetero-bimetallic complexes

A seminal competition study observed that Cu(II) displaced more than 95% of Zn(II) bound to Aβ.[50] The first research regarding the simultaneous binding of Cu(II) and Zn(II) to Aβ peptides was performed by Damante *et al.*[51] where they used the polyethylene glycol (PEG) conjugated peptide, which has enhanced water solubility and could aid in the spectroscopic studies. By using potentiometric measurements altogether with UV-Vis, CD and EPR spectroscopy studies, they shed light on the mutual interference of the metal ions. At pH >7, a hetero-bimetallic complex of Cu(II), Zn(II) and Aβ at a ratio of 1 : 1 : 1 is formed. Addition of up to 4-fold equivalents of Zn(II) to a Cu(II)–Aβ solution shifts the copper binding mode from

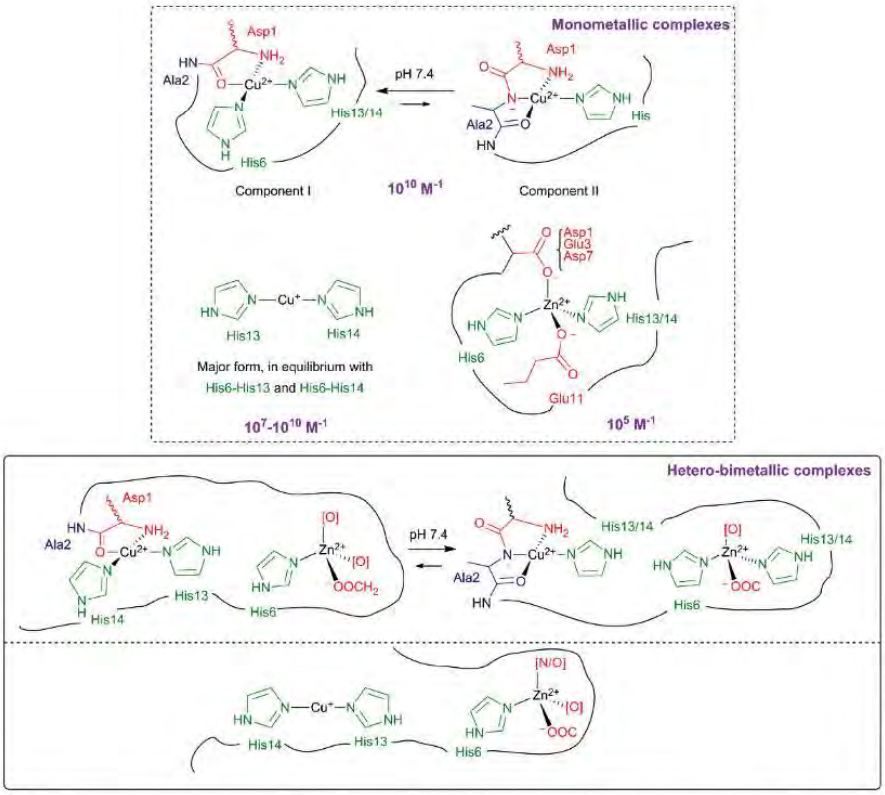

Fig. 1 Proposed coordination modes of Cu(II),[10] Cu(I),[10] Zn(II)[34] and the mixed metal Cu(II),Zn(II) or Cu(I),Zn(II) complexes[52,53] based on experimental results and bibliographic data. Affinity constant values (K_a) at pH 7.4 for Cu(II),[57] Cu(I)[58,59] and Zn(II)[49] are given in M^{-1} (bold, purple).

component I to component II (Fig. 1), while His13 and His14 would be involved in Zn(II) binding. The addition of Zn(II) would not release Cu(II), probably due to the high affinity of the peptide for Cu(II), but would modify its distribution in the available binding sites. Spectroscopic data obtained by Alies *et al.*[52] support this hypothesis. Furthermore, Silva *et al.*[53] have also corroborated the shift of components for Cu(II) bound to Aβ upon addition of increasing equivalents of Zn(II) (see Table 1). Contrary to the study of Damante *et al.*,[51] they also probed a more important contribution of His13 and His14 as ligands for Cu(II) in the presence of Zn(II).[53] In a further study, they proposed that Zn(II) and Cu(II) do compete for one binding site.[54] However, this is in disagreement with the respective affinity values of Cu(II) and Zn(II) for the Aβ peptide that differ by at least three orders of magnitude (Fig. 1). The most likely explanation for such unexpected observation is linked to the experimental procedure that may force precipitation of either Zn(II)–Aβ or Cu(II)–Aβ and modify the associated thermodynamic equilibria.[54] Indeed, with other sample preparation, only the formation of the hetero-bimetallic complex was observed.[52] Alies *et al.*[52] have investigated as well the Cu(I)/Zn(II) system which could be highly relevant *in vivo*. They used NMR spectroscopy and XANES to study the co-presence of Cu(I) and Zn(II). Indeed, XANES allows to distinguish the different oxidation states of the Cu ion and to observe the environments of Cu and Zn simultaneously since Cu and Zn K-edges are close enough to be recorded on the very same sample. While Zn(II) only slightly impacts the Cu(II) binding site (inducing a weak shift from component I to component II), both Cu(I) and Cu(II) influence the coordination sphere of Zn(II). Notably, in the case of the mixed Cu(I)/Zn(II) complex, Cu(I) remains coordinated to two histidine residues, leaving only one available for Zn(II) binding (Fig. 1).

Kinetics of metal binding by Aβ peptides

Another important parameter to take into account would be the kinetics of the interaction between metal ions and Aβ peptides. A pioneering study by Pedersen *et al.*[55] investigated the rate of the binding of Cu(II) to Aβ, and its impact on the aggregation. In the same context, a recent study by Branch *et al.*[56] has measured the rate of Cu(II)–Aβ complex formation. The component I binding mode is very rapidly formed, while component II forms through component I as an intermediate. The association rates of Cu(II) and Aβ reported vary between 1 and 100 ms. As a consequence, the association between Aβ and Cu(II) is fast and is thus of biological relevance.

Table 1 Approximate proportions of the Cu(II) binding modes (component I/component II) in the mixed Cu,Zn–Aβ complexes formed at different Cu : Zn : Aβ ratios, at pH 7.4

Ref.	1 : 0 : 1	1 : 1 : 1	1 : 2 : 1	1 : 4 : 1	1 : ≥8 : 1
52	~80/20	55/45	40/60	—	—
53	65/35	53/47	40/60	35/65	31/61

Table 2 Summary of the studies on the coordination of mixed Cu,Zn–Aβ complexes: used techniques and peptides

Ref.	Techniques	Peptides
51	Potentiometry; CD, UV-Vis, EPR; LC-ESI-MS	Aβ1–16-PEG; Aβ1–6; Ac-Aβ8–16-(Y10A)
52	XANES, EPR, NMR	Aβ1–16
53	CW-ESR, ESEEM	Aβ1–16; ^{15}N His-enriched Aβ1–40
54	XANES, EXAFS, CW-ESR	Aβ1–16

Concluding remarks and prospective

All the studies (summarized in Table 2) agree on the mutual influence of Zn(II) and Cu(II) on their coordination. Zn(II) impacts the binding mode of Cu(II) at physiological pH as observed by the shift from component I to component II, whereas Cu(I) maintains its bis-His coordination sphere in the presence of Zn(II). Moreover, Zn(II) coordination is affected by the presence of both Cu(I) and Cu(II).

Further studies would be needed to evaluate how the affinities of Cu(I/II) and Zn(II) are influenced by the co-presence of the metal ions and to determine the exact nature of the coordination spheres of Zn(II) in the Cu(I/II),Zn(II) hetero-bimetallic complexes. In addition, probing hetero-bimetallic species of other biologically relevant Aβ peptides (truncated peptides, murine Aβ and Familial Alzheimer's Disease mutants) is also of interest as well as the kinetics of interactions of Aβ with Cu(I), Aβ with Zn(II), and the mutual influence of Cu and Zn.

Aggregation and ROS production

Aggregation

Aβ aggregation is the catalytic auto-assembly of the monomeric peptide (mathematically described by a sigmoid-shape curve).[11] Metal-induced aggregation has been widely studied: different pH conditions, temperature, concentration, metal : peptide ratio, *etc.* seem to have an influence on the aggregation rate and species formed. The influence of Cu(II) on the Aβ aggregation seems to be mainly dependent on its ratio (see Fig. 2, left),[61] and may lead to the production of highly cytotoxic oligomers.[55,62,63] In the case of aggregation in the presence of Zn(II), even small sub-stoichiometric quantities of the metal ion have an important influence on the aggregation of the Aβ peptides (see Fig. 2, right).[60,63–68]

Intra and inter-molecular Zn(II) binding promotes a fast aggregation of species different from apo-fibrils. In the pioneering work by Mayes *et al.*[69], incubation of Aβ1–42 with equimolar quantities of Cu(II) and Zn(II) showed the coexistence of both small amorphous (non-fibrillar) aggregates and fibrils. Later, Matheou *et al.*[60] showed that Zn(II) has a greater influence on the aggregation as, at even a quarter less of Zn(II) than Cu(II), the ThT aggregation curve was strongly affected and typical Zn(II)-induced aggregates could be observed by TEM (see Fig. 2, bottom). At the suprastoichiometric ratio of Cu(II)

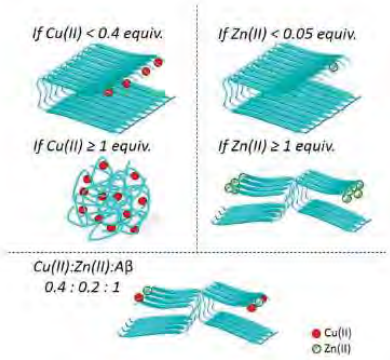

Fig. 2 This figure resumes the aggregation with different Cu(II) : Zn(II) : Aβ ratios.[60] Zn is the ion that dominates the Aβ metal-induced assembly even in the presence of Cu. For all of these aggregation experiments, metal ions have been added at the beginning, *i.e.* these are metal-induced aggregations.

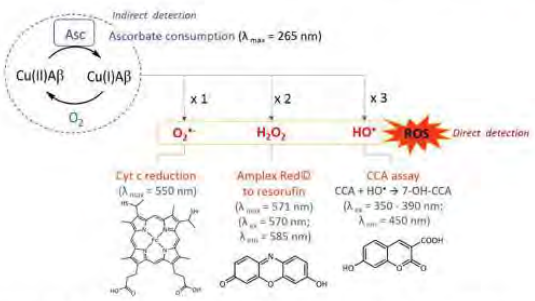

Fig. 3 ROS production from Cu–Aβ complexes and the classical assays for the detection of ROS produced[15] ($O_2^{\bullet-}$,[72] H_2O_2,[52] $HO^{\bullet}$,[73]) and indirect monitoring of Asc consumption.[74]

and/or Zn(II), Attanasio *et al.*[70] reported the formation of non-fibrillar aggregates.

ROS production by monomeric species

Since Zn(II) and Cu(I/II) have a clear mutual influence on their coordination to the Aβ peptides and on the metal-induced aggregation, Zn(II) could also have an impact on the ROS production by the Cu–Aβ complex. In this sense, a few studies have taken into account the co-presence of these metal ions and some of them have even indicated a protective role of Zn(II).[71] The first studies on the protective role of Zn(II) in Cu(II)–Aβ-induced ROS production were carried out by Bush and co-workers.[71] They found that the co-presence of Zn(II) improved the survival of cells incubated with Cu(II) and Aβ1–42 altogether with a decrease of the level of H_2O_2 production. They proposed a shift of the Cu ion in the peptide apart from its redox-active binding site as the origin of the redox-silencing properties associated with Zn(II). As it has been reported later, Zn(II) effectively displaces Cu(II) to its component II binding mode (see the previous paragraph); however, Alies *et al.*[52] showed that this has no impact on the ROS production as monitored by ascorbate consumption and H_2O_2 production (two of the most used methods to probe the production of ROS by Cu–peptide systems, see Fig. 3). In other words, while Zn(II) impacts the coordination of Cu(II) to Aβ, its addition at the stoichiometric ratio has no effect on the Cu–Aβ-induced ROS production and associated cellular toxicity (Fig. 4A). This is in line with a recent study proposing that, in contrast to what can be expected based on the redox potential of Cu(II) in component I or II,[75] the coordination mode of Cu(II) is not the predominant factor in ROS production.[76] Other factors such as the metal ion ratio or aggregation states might influence the

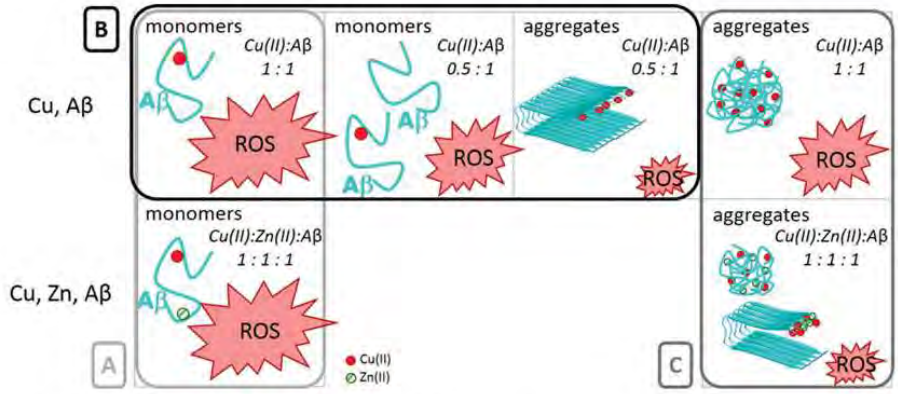

Fig. 4 Panel A. This part represents the identical ROS production of a monomeric monometallic Cu–Aβ complex and of a monomeric hetero-bimetallic Cu,Zn–Aβ complex.[52] Panel B. This part represents the ROS production by different Cu(II) : Aβ ratios and by different states of aggregation of the peptide: fibrils produce less ROS than monomers, for the 0.5 : 1 ratio.[52,78] Panel C. This last part compares the ROS production by amorphous aggregates of Cu(II)–Aβ to the ROS production of aggregates in the presence of Zn(II).[69] Note that for all of the aggregation experiments, metal ions have been added at the beginning, *i.e.* these are metal-induced aggregations.

ROS production by mixed metal complexes and it may be of interest to further investigate them as well.

ROS-production by aggregated species

The relationship between the aggregation states of the Cu–Aβ complexes and their ROS production *in vitro* has been described in the literature. Cu–Aβ aggregated species are able to produce ROS,[69] but at a lower level than the Cu–Aβ monomeric complex (see Fig. 4B).[77,78] Mayes *et al.*[69] have also incorporated into their research the ROS production of mixed metal Cu,Zn–Aβ aggregates (see Fig. 4C). They studied the degradation of H_2O_2 and the consequent HO˙ production by different Cu–Aβ and Cu,Zn–Aβ aggregated species. They observed that Aβ aggregates are capable of degrading H_2O_2 both when they have been formed in the presence of Cu(II) and when the metal has been added after fibril formation. In addition, increasing the ratio of Zn(II) over Cu(II) : Aβ diminished the quantity and the rate at which H_2O_2 was degraded. They also corroborate the "antioxidant" effect associated with Zn(II) with less intense oxidation of the peptides, followed by carbonyl group formation indicative of peptide oxidation.

Concluding remarks

In this part, studies have shown that metal-induced aggregation and/or ROS production are already complex in monometallic systems for which there are many studies reported (see reviews:[11,12,79]). There are still not enough reported data on hetero-bimetallic systems to reach any kind of general conclusion about the mutual influence of Cu and Zn ions on aggregation and/or ROS production. Future studies should address this issue and include more detailed investigations on the impact of different factors such as Cu to Zn ratios, metal to peptide ratios, pH, mixture of Aβ peptides (Aβ1–40, Aβ4–40, Aβ11–40, *etc.*)... In this context, pioneering aggregation studies performed in CSF mimicking media[70] or in CSF from AD patients are worth noting.[80]

Besides, kinetic aspects may also be extremely important for aggregation. This includes determining how the metal (Zn(II) or Cu(II)) addition during the aggregation matters both for the kinetics of the aggregation process and for the morphology of the aggregates. Knowing the rate of Zn and/or Cu-induced structural rearrangement to aggregation prone species would also be of significance.

Metal ion-based therapy

Due to the important toxicity shown by Cu ions within the context of AD, many Cu(II) ligands have been developed in the past few years.[17,25] They all can remove Cu(II) from Aβ peptides, and reduce its associated toxicity. One of the requirements for the design of ligands is their affinity towards Cu(II) compared to Aβ: it should be higher than that of the peptide (see Fig. 5, left). Nevertheless, their affinity should be lower than that of important metalloproteins, in order to avoid deleterious side effects. Furthermore, as previously mentioned, Zn(II) is present

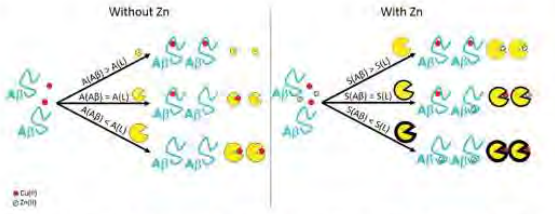

Fig. 5 Left panel. Representation of the importance of the affinity constant (written A) of the chelator in order to remove Cu from the Aβ peptide. Higher the affinity constant of the ligand is, higher is its efficiency in the removal of the metal ion from the peptide. Right panel. Representation of the importance of the selectivity (written S) of the ligand compared to the peptide one. Higher the selectivity of the ligand is compared to the peptide one, higher is its efficiency in the removal of Cu(II) ion from the peptide in the presence of Zn(II).

in high concentrations in the synaptic cleft and in the senile plaques and has an important impact on the Cu(II) coordination and the associated ROS production and Aβ aggregation. For this reason, some researchers have studied the impact of Zn(II) on the Cu(II) chelation therapy.

Metallothioneins: a biological model

Vašák and co-workers have studied the impact of metallothionein 3 (Zn_7-MT-3) on the toxicity of the Cu(II)–Aβ complex.[81,82] There is a swap of metallic ions between the Aβ peptides and Zn_7-MT-3 (see Fig. 6, left). The mechanism proposed includes the dissociation of the Cu(II)–Aβ complex and the chelation of the free metal ion by the metallothionein.[83] Also, the formation of two disulphide bonds triggers the reduction of Cu(II) into Cu(I), forming an air-stable $Cu(I)_4$-thiolate cluster inside the $Cu(I)_4Zn_4$MT-3 protein. The removal of Cu ions from the Aβ peptides and its consequent binding as an air-stable Cu(I)-complex silence the redox capability of Cu. Therefore, this swap has a protective effect against Cu(II)–Aβ toxicity.[82] Another study by West's group[84] focused on the metallothionein 2A (MT-2A) which is the major human-expressed subtype of metallothionein and, under stressful situations, it can be secreted near the synaptic cleft where aggregation of Aβ pep-

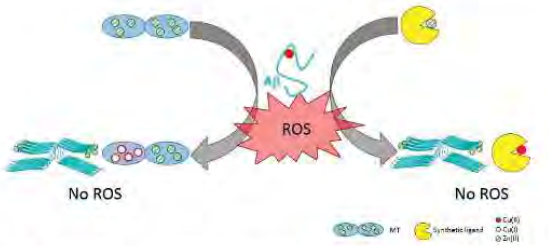

Fig. 6 Representation of the swap of metallic ions (Cu(II) in red and Zn(II) in green) between Aβ peptide and Zn_7-MT-3 (left) or a synthetic chelator, preloaded with Zn(II) (right). The impact on the ROS production is also illustrated.

tides occurs. West and his colleagues have demonstrated that under physiological conditions, Zn_7-MT-2A can also remove Cu ions from Aβ, stop the ROS production and prevent changes in the metallic balance within neurons. When the same experiments were performed with the apo metallothionein, no impact on the Cu removal or on the diminution of the neurotoxicity was detected. Recently, Bal and co-workers have also studied the metal swap between Zn_7-MT-3 and the truncated peptide Aβ4–16. In this case, the high affinity of the peptide prevents the sequestration of Cu(II) by the metallothionein.[85] Besides, the impact of the Zn_7-MT-3 has also been studied for the α-synuclein and the Prion proteins and the swap of metallic ions is observed. Cu(II) is sequestered by the metallothionein, silencing its redox activity and preventing the metal-induced aggregation of the protein.[86,87]

Synthetic ligands and selectivity issue

Later, our group has highlighted the impact of the presence of Zn(II) within the Cu(II)-chelation context.[19] Two synthetic chelators were tested, and while both are able to retrieve Cu(II) from Aβ, only one removes Cu(II) from Aβ in the presence of Zn(II). For the latter one and as in the case of Zn_7-MT-3, there is a swap of metallic ions between the peptide and the chelator, and the resulting species cannot produce ROS (see Fig. 6, right). We propose the following explanation (based on thermodynamics only): a good chelator needs not only a high affinity constant for Cu(II) (see Fig. 5, left) but also high Cu(II) over Zn(II) selectivity, that corresponds to the ratio between its affinity constant for Cu(II) and for Zn(II) (see Fig. 5, right). Actually, the Cu(II) over Zn(II) selectivity of the chelator should overcome that of the Aβ peptides themselves, which is high (about 4 orders of magnitude, see Fig. 1).

There are several studies reported in the literature that address the removal of Cu(II) *or* Zn(II) from Aβ,[88–91] and some introduce the importance of having a high Cu(II) over Zn(II) selectivity for the ligand.[92–94] However, to the best of our knowledge, the importance of overcoming the Cu(II) over Zn(II) selectivity of Aβ was not taken into account. In other words, the removal of Cu(II) from Aβ by a chelator in the presence of Zn(II) was not thoroughly described except in ref. 19. Nevertheless, Zn(II) interference in Cu(II) removal from Aβ should be taken into account as it can either promote protective effects when the metal swap occurs[19,82,84] or be detrimental if not.[19]

Prospective

Importance of the selectivity issue for other metal-based therapeutic approaches. All of these different studies prove that within the chelation therapy context, not only the toxic Cu(II) ion has to be taken into account but also other metal ions in the environment of the peptides such as Zn(II). The same kind of study should be applied to the removal of Cu(I) in the presence of Zn(II). Indeed, the oxidation state of Cu in the synaptic cleft is not well defined. It would also be interesting to design Cu(I) chelators within the AD context, as recently reported in the literature.[95,96] However, there are no studies about Cu(I) chelation against AD in a Zn(II)-rich environment. The same selectivity issue may also apply for metallophores, such as clioquinol, PBT2,[18] and gtsm,[97] and for multi-target ligands as well.[17]

Selectivity issues regarding other peptides. The selectivity of the ligands may take into account the intrinsic selectivity of the peptide of interest as there are many forms of Aβ peptides. In the case of Aβ4–40 and Aβ11–40 peptides, which are N-terminally truncated, an extremely high Cu(II) over Zn(II) selectivity is expected based on the formation of the high Cu(II)-affinity ATCUN motif,[98] while Zn(II) affinity may remain mostly unchanged. This will imply having ligands with even higher Cu(II) over Zn(II) selectivity than the one required in the case of Aβ1–40. The same would also be true for the murine peptide for which higher Cu(II) affinity has been reported,[99] as well as weaker Zn(II) affinity.[100] This might be important as murine peptides are co-secreted along with human peptides in AD model mice.

Influence of other biological components. As probed here for Zn(II) and Cu(I/II), interference of other biological components might also be of importance. Iron, for example, is also present in concentrations that would legitimate this kind of investigation. Indeed, iron is also responsible for ROS production, and might modulate the aggregation of the Aβ peptides.[10,101,102] The removal of this metal ion is likewise important and some groups are working on specific iron chelators for AD (for review, see ref. 101). Recently, Youdim's group has studied the ability of new Fe chelators to improve memory loss in rats.[103] However, in contrast to Zn(II), much effort is required to decipher the Fe(II/III) binding ability to Aβ, since only a very preliminary study has been reported until now.[104] Moreover, other metal ions, despite having a lower affinity constant for the peptides, can also interfere since they are highly concentrated. Thus, it would be important to investigate different metal chelation/redistribution therapeutic approaches in the presence of all the biologically relevant ions (Mg(II), Ca(II), Na(I), K(I)...).

Kinetic issues. Another key parameter is the rate of Cu ion removal from the Aβ peptides,[56,105] including in the presence of Zn(II). In other words, the kinetic aspect has to be taken into account as well as the thermodynamic one, as previously detailed.

Conclusions

In this review, we have focused on the mutual influence of Cu and Zn regarding their coordination to Aβ peptides, as well as the resulting impact on the aggregation and ROS production. We have also highlighted the importance of the co-presence of both Cu(II) and Zn(II) for the metal ion chelation/redistribution therapeutic approaches.

As detailed through the present manuscript, future chemical work will undoubtedly include studies of the interaction of both metal ions with the peptide in the presence of other biologically relevant components, such as glutamate, acetyl-

choline, other metal ions, metallothioneins... This will bridge the gap between *in vitro* and *in vivo* studies, probing metal ion–peptide interactions under more complex conditions but still at the molecular level.

Abbreviations

Aβn–m	Amyloid-β starting from the amino acid residue number n to the number m.
AD	Alzheimer's disease
Ala	Alanine
Asc	Ascorbate
Asp	Aspartic acid
ATCUN	Amino-terminal copper and nickel
CCA	Coumarin-3-carboxylic acid
CD	Circular dichroism
CNS	Central nervous system
CW-ESR	Continuous-wave electron spin resonance
Cyt c	Cytochrome c
EPR	Electronic paramagnetic resonance
ESEEM	Electron spin echo envelope modulation
EXAFS	Extended X-ray absorption fine structure
Glu	Glutamic acid
His	Histidine
LC-ESI-MS	Liquid chromatography–electro spray ionization-mass spectrometry
MT-2A	Metallothionein-2A
MT-3	Metallothioncin-3
N_{im}	Nitrogen from the imidazole ring
NMR	Nuclear magnetic resonance
PBT2	5,7-Dichloro-2-[(dimethylamino)methyl]quinolin-8-ol
PEG	Polyethylene glycol
ROS	Reactive oxygen species
TEM	Transmission electron microscopy
ThT	Thioflavin T
UV-Vis	UV-Visible
XANES	X-ray absorption near edge structure

Acknowledgements

The ERC aLzINK grant (ERC-StG-638712) is acknowledged for financial support. We thank warmly Prof. Peter Faller for inspiring discussions.

Notes and references

1 C. Ising, M. Stanley and D. M. Holtzman, *Clin. Pharmacol. Ther.*, 2015, **98**, 469–471.
2 R. Riek and D. S. Eisenberg, *Nature*, 2016, **539**, 227–235.
3 R. Roychaudhuri, M. Yang, M. M. Hoshi and D. B. Teplow, *J. Biol. Chem.*, 2009, **284**, 4749–4753.
4 D. A. Drachman, *Alzheimers Dement.*, 2014, **10**, 372–380.
5 K. J. Barnham and A. I. Bush, *Curr. Opin. Chem. Biol.*, 2008, **12**, 222–228.
6 H. Kozłowski, M. Luczkowski, M. Remelli and D. Valensin, *Coord. Chem. Rev.*, 2012, **256**, 2129–2141.
7 P. S. Donnelly, Z. Xiao and A. G. Wedd, *Curr. Opin. Chem. Biol.*, 2007, **11**, 128–133.
8 K. J. Barnham and A. I. Bush, *Chem. Soc. Rev.*, 2014, **43**, 6727–6749.
9 A. S. Pithadia and M. H. Lim, *Curr. Opin. Chem. Biol.*, 2012, **16**, 67–73.
10 C. Hureau, *Coord. Chem. Rev.*, 2012, **256**, 2164–2174.
11 P. Faller, C. Hureau and O. Berthoumieu, *Inorg. Chem.*, 2013, **52**, 12193–12206.
12 J. H. Viles, *Coord. Chem. Rev.*, 2012, **256**, 2271–2284.
13 V. Togu, A. Tiiman and P. Palumaa, *Metallomics*, 2011, **3**, 250–261.
14 M. Rowińska-Żyrek, M. Salerno and H. Kozłowski, *Coord. Chem. Rev.*, 2015, **284**, 298–312.
15 S. Chassaing, F. Collin, P. Dorlet, J. Gout, C. Hureau and P. Faller, *Curr. Top. Med. Chem.*, 2012, **12**, 2573–2595.
16 H. W. Querfurth and F. M. LaFerla, *N. Engl. J. Med.*, 2010, **362**, 329–344.
17 M. A. Santos, K. Chand and S. Chaves, *Coord. Chem. Rev.*, 2016, **327–328**, 287–303.
18 A. Robert, Y. Liu, M. Nguyen and B. Meunier, *Acc. Chem. Res.*, 2015, **48**, 1332–1339.
19 A. Conte-Daban, A. Day, P. Faller and C. Hureau, *Dalton Trans.*, 2016, **45**, 15671–15678.
20 M. Nguyen, L. Vendier, J.-L. Stigliani, B. Meunier and A. Robert, *Eur. J. Inorg. Chem.*, 2017, 600–608.
21 O. Andersen, *Chem. Rev.*, 1999, **99**, 2683–2710.
22 L. E. Scott and C. Orvig, *Chem. Rev.*, 2009, **109**, 4885–4910.
23 A. E. V. Gorden, J. Xu, K. N. Raymond and P. Durbin, *Chem. Rev.*, 2003, **103**, 4207–4282.
24 P. Delangle and E. Mintz, *Dalton Trans.*, 2012, **41**, 6335–6370.
25 N. Xia and L. Liu, *Mini-Rev. Med. Chem.*, 2014, **14**, 271–281.
26 Q. Wang and K. J. Franz, *Acc. Chem. Res.*, 2016, **49**, 2468–2477.
27 M. G. Dickens and K. J. Franz, *ChemBioChem*, 2010, **11**, 59–62.
28 D. S. Folk and K. J. Franz, *J. Am. Chem. Soc.*, 2010, **132**, 4994–4995.
29 C. Rodríguez-Rodríguez, M. Telpoukhovskaia and C. Orvig, *Coord. Chem. Rev.*, 2012, **256**, 2308–2332.
30 S. Noël, S. Cadet, E. Gras and C. Hureau, *Chem. Soc. Rev.*, 2013, **42**, 7747–7762.
31 T. Storr, L. E. Scott, M. L. Bowen, D. E. Green, K. H. Thompson, H. J. Schugar and C. Orvig, *Dalton Trans.*, 2009, 3034–3043.
32 Z. Cui, P. R. Lockman, C. S. Atwood, C. H. Hsu, A. Gupte, D. D. Allen and R. J. Mumper, *Eur. J. Pharm. Biopharm.*, 2005, **59**, 263–272.
33 S. C. Drew and K. J. Barnham, *Acc. Chem. Res.*, 2011, **44**, 1146–1155.

34 B. Alies, A. Conte-Daban, S. Sayen, F. Collin, I. Kieffer, E. Guillon, P. Faller and C. Hureau, *Inorg. Chem.*, 2016, **55**, 10499–10509.
35 V. Tõugu and P. Palumaa, *Coord. Chem. Rev.*, 2012, **256**, 2219–2224.
36 C. Migliorini, E. Porciatti, M. Luczkowski and D. Valensin, *Coord. Chem. Rev.*, 2012, **256**, 352–368.
37 C. Hureau and P. Dorlet, *Coord. Chem. Rev.*, 2012, **256**, 2175–2187.
38 L. Guilloreau, L. Damian, Y. Coppel, H. Mazarguil, M. Winterhalter and P. Faller, *J. Biol. Inorg. Chem.*, 2006, **11**, 1024–1038.
39 J. Shearer and V. A. Szalai, *J. Am. Chem. Soc.*, 2008, **130**, 17826–17835.
40 C. Hureau, V. Balland, Y. Coppel, P.-L. Solari, E. Fonda and P. Faller, *J. Biol. Inorg. Chem.*, 2009, **14**, 995–1000.
41 R. A. Himes, G. Y. Park, G. S. Siluvai, N. J. Blackburn and K. D. Karlin, *Angew. Chem., Int. Ed.*, 2008, **47**, 9084–9087.
42 Y. Mekmouche, Y. Coppel, K. Hochgräfe, L. Guilloreau, C. Talmard, H. Mazarguil and P. Faller, *ChemBioChem*, 2005, **6**, 1663–1671.
43 C. D. Syme and J. H. Viles, *Biochim. Biophys. Acta, Proteins Proteomics*, 2006, **1764**, 246–256.
44 S. Zirah, S. A. Kozin, A. K. Mazur, A. Blond, M. Cheminant, I. Segalas-Milazzo, P. Debey and S. Rebuffat, *J. Biol. Chem.*, 2006, **281**, 2151–2161.
45 J. Danielsson, R. Pierattelli, L. Banci and A. Gräslund, *FEBS J.*, 2007, **274**, 46–59.
46 E. Gaggelli, A. Janicka-Klos, E. Jankowska, H. Kozłowski, C. Migliorini, E. Molteni, D. Valensin, G. Valensin and E. Wieczerzak, *J. Phys. Chem. B*, 2008, **112**, 100–109.
47 C. A. Damante, K. Ősz, Z. Nagy, G. Pappalardo, G. Grasso, G. Impellizzeri, E. Rizzarelli and I. Sóvágó, *Inorg. Chem.*, 2009, **48**, 10405–10415.
48 P. O. Tsvetkov, A. A. Kulikova, A. V. Golovin, Y. V. Tkachev, A. I. Archakov, S. A. Kozin and A. A. Makarov, *Biophys. J.*, 2010, **99**, L84–L86.
49 S. Noël, S. Bustos Rodriguez, S. Sayen, E. Guillon, P. Faller and C. Hureau, *Metallomics*, 2014, **6**, 1220–1222.
50 A. Clements, D. Allsop, D. M. Walsh and C. H. Williams, *J. Neurochem.*, 1996, **66**, 740–747.
51 C. A. Damante, K. Ösz, Z. Nagy, G. Grasso, G. Pappalardo, E. Rizzarelli and I. Sóvágó, *Inorg. Chem.*, 2011, **50**, 5342–5350.
52 B. Alies, I. Sasaki, O. Proux, S. Sayen, E. Guillon, P. Faller and C. Hureau, *Chem. Commun.*, 2013, **49**, 1214.
53 K. I. Silva and S. Saxena, *J. Phys. Chem. B*, 2013, **117**, 9386–9394.
54 E. De Santis, V. Minicozzi, O. Proux, G. C. Rossi, K. I. Silva, M. J. Lawless, F. Stellato, S. Saxena and S. Morante, *J. Phys. Chem. B*, 2015, **119**, 15813–15820.
55 J. T. Pedersen, K. Teilum, N. H. H. Heegaard, J. Østergaard, H.-W. W. Adolph and L. Hemmingsen, *Angew. Chem., Int. Ed.*, 2011, **50**, 2532–2535.
56 T. Branch, P. Girvan, M. Barahona and L. Ying, *Angew. Chem., Int. Ed.*, 2015, **54**, 1227–1230.
57 B. Alies, E. Renaglia, M. Rózga, W. Bal, P. Faller and C. Hureau, *Anal. Chem.*, 2013, **85**, 1501–1508.
58 B. Alies, B. Badei, P. Faller and C. Hureau, *Chem. – Eur. J.*, 2012, **18**, 1161–1167.
59 T. R. Young, A. Kirchner, A. G. Wedd and Z. Xiao, *Metallomics*, 2014, **6**, 505–517.
60 C. J. Matheou, N. D. Younan and J. H. Viles, *J. Mol. Biol.*, 2016, **428**, 2832–2846.
61 S. Jun and S. Saxena, *Angew. Chem., Int. Ed.*, 2007, **46**, 3959–3961.
62 C. J. Matheou, N. D. Younan and J. H. Viles, *Biochem. J.*, 2015, **466**, 233–242.
63 A. K. Sharma, S. T. Pavlova, J. Kim, J. Kim and L. M. Mirica, *Metallomics*, 2013, **5**, 1529–1536.
64 L. Pan and J. C. Patterson, *PLoS One*, 2013, **8**, e70681.
65 P. Giannozzi, K. Jansen, G. La Penna, V. Minicozzi, S. Morante, G. C. Rossi and F. Stellato, *Metallomics*, 2012, **4**, 156–165.
66 B. Alies, P.-L. Solari, C. Hureau and P. Faller, *Inorg. Chem.*, 2012, **51**, 701–708.
67 Y. Miller, B. Ma and R. Nussinov, *Proc. Natl. Acad. Sci. U. S. A.*, 2010, **107**, 9490–9495.
68 A. I. Bush, W. H. Pettingell, G. Multhaup, M. D. Paradis, J.-P. Vonsattel, J. F. Gusella, K. Beyreuther, C. L. Masters and R. E. Tanzi, *Science*, 1994, **265**, 1464–1467.
69 J. Mayes, C. Tinker-Mill, O. Kolosov, H. Zhang, B. J. Tabner and D. Allsop, *J. Biol. Chem.*, 2014, **289**, 12052–12062.
70 F. Attanasio, P. De Bona, S. Cataldo, M. F. M. Sciacca, D. Milardi, B. Pignataro and G. Pappalardo, *New J. Chem.*, 2013, **37**, 1206–1215.
71 M. P. Cuajungco, L. E. Goldstein, A. Nunomura, M. A. Smith, J. T. Lim, C. S. Atwood, X. Huang, Y. W. Farrag, G. Perry and A. I. Bush, *J. Biol. Chem.*, 2000, **275**, 19439–19442.
72 K. Reybier, S. Ayala, B. Alies, J. V. Rodrigues, S. Bustos Rodriguez, G. La Penna, F. Collin, C. M. Gomes, C. Hureau and P. Faller, *Angew. Chem., Int. Ed.*, 2016, **55**, 1085–1089.
73 C. Cheignon, F. Collin, P. Faller and C. Hureau, *Dalton Trans.*, 2016, **45**, 12627–12631.
74 C. Cheignon, P. Faller, D. Testemale, C. Hureau and F. Collin, *Metallomics*, 2016, **8**, 1081–1089.
75 L. G. Trujano-Ortiz, F. J. González and L. Quintanar, *Inorg. Chem.*, 2015, **54**, 4–6.
76 C. Cheignon, M. Jones, E. Atrián-Blasco, I. Kieffer, P. Faller, F. Collin and C. Hureau, *Chem. Sci.*, 2017, **8**, 5107–5118.
77 R. C. Nadal, S. E. J. Rigby and J. H. Viles, *Biochemistry*, 2008, **47**, 11653–11664.
78 J. T. Pedersen, S. W. Chen, C. B. Borg, S. Ness, J. M. Bahl, N. H. H. Heegaard, C. M. Dobson, L. Hemmingsen, N. Cremades and K. Teilum, *J. Am. Chem. Soc.*, 2016, **138**, 3966–3969.
79 P. Faller and C. Hureau, *Chem. – Eur. J.*, 2012, **18**, 15910–15920.

80 E. R. Padayachee, H. Zetterberg, E. Portelius, J. Borén, J. L. Molinuevo, N. Andreasen, R. Cukalevski, S. Linse, K. Blennow and U. Andreasson, *Brain Res.*, 2016, **1651**, 11–16.
81 G. Meloni, P. Faller and M. Vašák, *J. Biol. Chem.*, 2007, **282**, 16068–16078.
82 G. Meloni, V. Sonois, T. Delaine, L. Guilloreau, A. Gillet, J. Teissie, P. Faller and M. Vašák, *Nat. Chem. Biol.*, 2008, **4**, 366–372.
83 J. T. Pedersen, C. Hureau, L. Hemmingsen, N. H. H. Heegaard, J. Østergaard, M. Vašák and P. Faller, *Biochemistry*, 2012, **51**, 1697–1706.
84 R. S. Chung, C. Howells, E. D. Eaton, L. Shabala, K. Zovo, P. Palumaa, R. Sillard, A. Woodhouse, W. R. Bennett, S. Ray, J. C. Vickers and A. K. West, *PLoS One*, 2010, **5**, e12030.
85 N. E. Wezynfeld, E. Stefaniak, K. Stachucy, A. Drozd, D. Płonka, S. C. Drew, A. Krężel and W. Bal, *Angew. Chem., Int. Ed.*, 2016, **55**, 8235–8238.
86 G. Meloni and M. Vašák, *Free Radical Biol. Med.*, 2011, **50**, 1471–1479.
87 G. Meloni, A. Crameri, G. Fritz, P. Davies, D. R. Brown, P. M. H. Kroneck and M. Vašák, *ChemBioChem*, 2012, **13**, 1261–1265.
88 A. K. Sharma, S. T. Pavlova, J. Kim, D. Finkelstein, N. J. Hawco, N. P. Rath, J. Kim and L. M. Mirica, *J. Am. Chem. Soc.*, 2012, **134**, 6625–6636.
89 A. Lakatos, É. Zsigó, D. Hollender, N. V. Nagy, L. Fülöp, D. Simon, Z. Bozsó and T. Kiss, *Dalton Trans.*, 2010, **39**, 1302–1315.
90 C. Deraeve, C. Boldron, A. Maraval, H. Mazarguil, H. Gornitzka, L. Vendier, M. Pitié and B. Meunier, *Chem. – Eur. J.*, 2008, **14**, 682–696.
91 T. Chen, X. Wang, Y. He, C. Zhang, Z. Wu, K. Liao, J. Wang and Z. Guo, *Inorg. Chem.*, 2009, **48**, 5801–5809.
92 T. Storr, M. Merkel, G. X. Song-Zhao, L. E. Scott, D. E. Green, M. L. Bowen, K. H. Thompson, B. O. Patrick, H. J. Schugar and C. Orvig, *J. Am. Chem. Soc.*, 2007, **129**, 7453–7463.
93 S. Lee, X. Zheng, J. Krishnamoorthy, M. G. Savelieff, H. M. Park, J. R. Brender, J. H. Kim, J. S. Derrick, A. Kochi, H. J. Lee, C. Kim, A. Ramamoorthy, M. T. Bowers and M. H. Lim, *J. Am. Chem. Soc.*, 2014, **136**, 299–310.
94 J.-S. Choi, J. J. Braymer, R. P. R. Nanga, A. Ramamoorthy and M. H. Lim, *Proc. Natl. Acad. Sci. U. S. A.*, 2010, **107**, 21990–21995.
95 E. Atrián-Blasco, E. Cerrada, A. Conte-Daban, D. Testemale, P. Faller, M. Laguna and C. Hureau, *Metallomics*, 2015, **7**, 1229–1232.
96 G. R. Walke, D. S. Ranade, S. N. Ramteke, S. Rapole, C. Satriano, E. Rizzarelli, G. A. Tomaselli, G. Trusso Sfrazzetto and P. P. Kulkarni, *Inorg. Chem.*, 2017, **56**, 3729–3732.
97 P. J. Crouch, L. W. Hung, P. A. Adlard, M. Cortes, V. Lal, G. Filiz, K. A. Perez, M. Nurjono, A. Caragounis, T. Du, K. Laughton, I. Volitakis, A. I. Bush, Q.-X. Li, C. L. Masters, R. Cappai, R. A. Cherny, P. S. Donnelly, A. R. White and K. J. Barnham, *Proc. Natl. Acad. Sci. U. S. A.*, 2009, **106**, 381–386.
98 W. Bal, M. Sokołowska, E. Kurowska and P. Faller, *Biochim. Biophys. Acta, Gen. Subj.*, 2013, **1830**, 5444–5455.
99 H. Eury, C. Bijani, P. Faller and C. Hureau, *Angew. Chem., Int. Ed.*, 2011, **50**, 901–905.
100 B. Alies, V. Borghesani, S. Sayen, I. Kieffer, E. Guillon, P. Faller and C. Hureau, manuscript in preparation.
101 A. A. Belaidi and A. I. Bush, *J. Neurochem.*, 2016, **139**, 179–197.
102 N. Singh, S. Haldar, A. K. Tripathi, K. Horback, J. Wong, D. Sharma, A. Beserra, S. Suda, C. Anbalagan, S. Dev, C. K. Mukhopadhyay and A. Singh, *Antioxid. Redox Signaling*, 2014, **20**, 1324–1363.
103 M. Salkovic-Petrisic, A. Knezovic, J. Osmanovic-Barilar, U. Smailovic, V. Trkulja, P. Riederer, T. Amit, S. Mandel and M. B. H. Youdim, *Life Sci.*, 2015, **136**, 108–119.
104 F. Bousejra-ElGarah, C. Bijani, Y. Coppel, P. Faller and C. Hureau, *Inorg. Chem.*, 2011, **50**, 9024–9030.
105 P. Girvan, T. Miyake, X. Teng, T. Branch and L. Ying, *ChemBioChem*, 2016, **17**, 1732–1737.

III-B The thermodynamic study

This section focuses on the thermodynamic aspect of the Cu(II) withdrawal from Cu(II)-Aβ by a chelator in the presence of Zn(II). It is composed of a summary of the article published in *Dalton Transactions* in 2016, the article itself and finally the supporting information. Note that this article is part of the review above.

III-B.i Summary

This article describes the impact of Zn(II) ions on the Cu(II) chelation from Aβ. The first step of the chelation therapy, meaning the removal of Cu ions from Aβ in AD brains, was to understand how a ligand can sequester Cu(II) ion from the Aβ peptide and how it can stop the ROS production. Many studies have proposed organic as well as peptidic ligands in order to remove Cu(II) from the Aβ peptide. But, as previously explained, Zn(II) ion is present in high concentrations in the synaptic cleft, and in the senile plaques. Some works have shown that Zn(II) has an influence on the Cu(II) coordination with Aβ, on the ROS production by the Cu(II)-Aβ complex, and on the metal-induced aggregation of the peptide. Thus, the second step of the chelation therapy studies before going to more complex systems like studies *in cellulo*, has been the understanding of the 4-partner system, namely Cu(II), Zn(II), Aβ and a chelator. This four-partner system has two metal ions and two ligands: it is important to know if the chelator can remove Cu ions from Aβ in the presence of Zn ions or if it will chelate Zn ions. The following equilibrium is considered:

$$\text{Cu(II)-A}\beta + \text{Zn(II)} + \text{L} \rightleftharpoons \text{Zn(II)-A}\beta + \text{Cu(II)-L}$$

In order to determine if this equilibrium is on the right or on the left, spectroscopic techniques are used to distinguish if Zn(II) and/or Cu(II) is bound to Aβ or to the chelator.

A good chelator needs a higher affinity constant for Cu(II) than Aβ: the metal ion is chelated by the ligand. Nevertheless, in the presence of Zn(II) ion, this parameter is not enough for the removal of Cu(II) from Aβ. In this article, two Cu(II) chelators, L2 and Lc, have been studied: both have an affinity constant for Cu(II) higher than Aβ and they both sequester the metal ion in the absence of Zn(II).

The study of the swap of metal ions, Cu(II) and Zn(II), between these two chelators and Aβ is the first part of this work (see equilibrium above). UV-Visible, EPR and XANES are used in order to perform this experiment. For the L2 ligand, all the results lead towards the swap of metal ions (equilibrium on the right), whereas not for the Lc ligand (equilibrium on the left). For the latter, in the presence of

Zn(II), Cu(II) stays bound to Aβ: Lc is not able to remove Cu(II) from the peptide whereas L2 can, altough both have a higher affinity constant for Cu(II) than Aβ. A thermodynamic explanation is proposed for this phenomenon. The main difference between these two chelators is their selectivity. The selectivity of a ligand is the ratio between its affinity for Cu(II) and its affinity for Zn(II). Moreover, a high affinity constant for Cu(II) does not mean that the corresponding selectivity is high, and *vice versa*. In order to remove Cu(II) from Aβ in the presence of Zn(II), the chelator needs not only a higher affinity constant for Cu(II) than Aβ, but also a higher selectivity, which is already relatively high for Aβ (about $10^{4.2}$ at pH 7.1). The Cu(II) over Zn selectivities of L2 and Lc are about $10^{7.7}$ and $10^{2.0}$, respectively, at pH 7.1. Thermodynamically, only L2 is able to sequester Cu(II) in the presence of Zn(II).

A second part of the study is dedicated to the efficiency of these two chelators in preventing the ROS production. This work is performed *via* two different experiments: the first one consists in the following of the kinetic of ascorbate consumption mirroring the ROS production and the second one is the kinetic of formation of 7-OH-CCA, a fluorescent compound formed *via* the reaction between the coumarin carboxylic acid (CCA) and the $HO^{\bullet}$. Without Zn(II), both ligands stop the formation of these toxic species, at least reduce considerably their production, meaning that when Cu(II) is bound to L2 or Lc, the associated complexes do not produce ROS. Then, in order to mimic the high concentrations of Zn(II) in the synaptic cleft, Zn(II) is preloaded to the ligands: in a rich Zn(II)-environment, the probability of the ligand to not chelate first Zn(II) is very low. When Zn(II) is preloaded to the L2 ligand, there is more or less no effect of Zn(II) on the ROS production, contrary to the Lc ligand. In the presence of Zn(II), Lc is not able to stop the ROS production anymore. This result is relatively obvious since in the presence of Zn(II), Cu(II) is chelated by the Aβ peptide and not by Lc (equilibrium above on the left), and so, the Cu-Aβ complex can produce ROS.

The last study of this work focuses on the aggregation of the Aβ peptide with the L2 ligand. Note that the aggregation with Lc has not been performed because in the presence of Zn(II), Cu stays bound to Aβ and the aggregation would be the same than without the ligand. The aggregation of Aβ is followed by the ThT fluorescence, and the samples have then been visualized by AFM. The hypothesis of this thesis is that apo-Aβ and Zn(II)-Aβ aggregate into fibrils, whereas Cu(II)-Aβ aggregates into oligomers or protofibrils. If the L2 ligand is added to Cu(II)-Aβ before the starting of the aggregation, L2 chelates Cu(II) and Aβ peptide can aggregate into fibrils, as an apo-peptide. The same result is obtained if Zn(II)-L2 is added to Cu(II)-Aβ. This confirms that L2 is able to withdraw Cu(II) from Aβ even when preloaded with Zn(II).

This article proposes a thermodynamic criterion for a Cu(II) chelator in a rich Zn(II)-environment: the selectivity of Cu(II) over Zn ions. It has to be higher than Aβ, already important (about $10^{4.2}$ at pH 7.1), due to the different binding site of Cu(II) and Zn(II). When a ligand satisfies this criterion, Cu(II) can be withdrawn from Aβ even in the presence of Zn(II). This leads to a stop of the ROS production (in case of Cu(II)-ligand does not produce ROS itself) and to a fibrillary Zn(II)-induced aggregation, aggregates which are proposed to be less toxic than oligomers. Figure III-3 illustrates the thermodynamic issue described in this part.

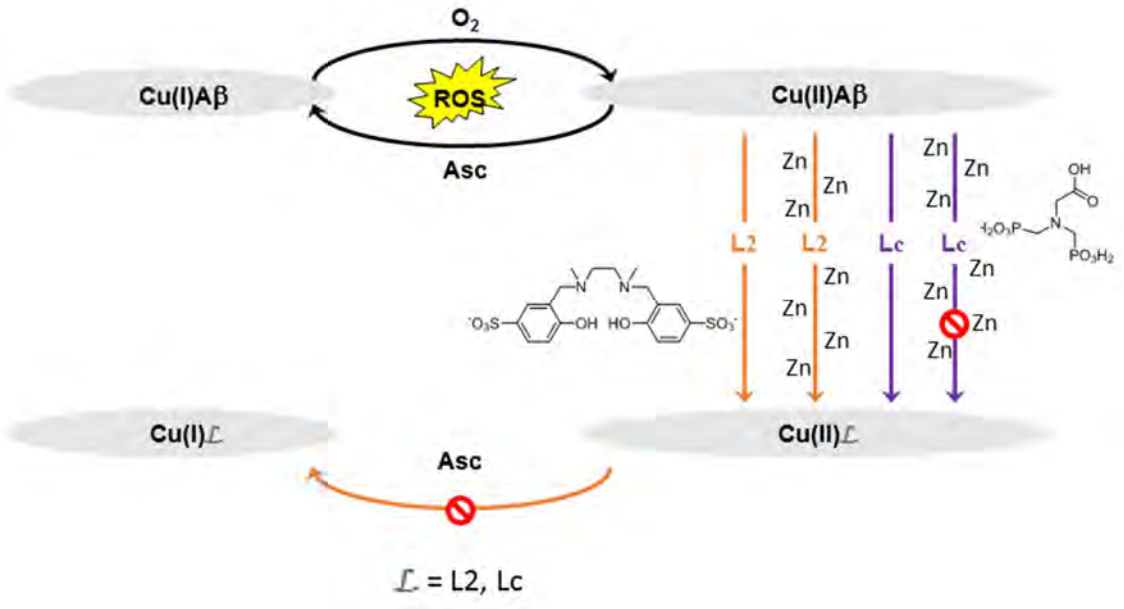

Figure III-3. Scheme of the possible approach on the chelatotherapy describes in this part. While without Zn(II), L2 and Lc are able to remove Cu(II) from Aβ and stop the ROS production, in the presence of Zn(II) only L2 is able to remove Cu(II) and stop the ROS production. This is due to the fact that L2 and Lc have both an affinity constant for Cu(II) higher than the one of Aβ, but only L2 has a Cu(II) over Zn(II) selectivity higher than the one of Aβ.

This study is a first step before a more elaborate system. Indeed, it would be interesting to investigate the impact of the surrounding biomolecules within the synaptic cleft and also other metal ions on the Cu(II) chelation. Moreover, this parameter can be applied to the Cu(I) therapy, but also to other amyloidogenic diseases such as Parkinson or Amyotrophic Lateral Sclerosis, in which a dyshomeostasis of metal ions is involved.

III-B.ii Article

Dalton Transactions

PAPER

View Article Online
View Journal

Cite this: DOI: 10.1039/c6dt02308h

How Zn can impede Cu detoxification by chelating agents in Alzheimer's disease: a proof-of-concept study†

Amandine Conte-Daban,[a,b] Adam Day,[a,b] Peter Faller‡[a,b] and Christelle Hureau*[a,b]

The role of Cu and Zn ions in Alzheimer's disease is linked to the consequences of their coordination to the amyloid-β (Aβ) peptide, *i.e.* to the modulation of Aβ aggregation and to the production of Reactive Oxygen Species (ROS), two central events of the so-called amyloid cascade. The role of both ions in Aβ aggregation is still controversial. Conversely the higher toxicity of the redox competent Cu ions (compared to the redox inert Zn ions) in ROS production is acknowledged. Thus the Cu ions can be considered as the main therapeutic target. Because Zn ions are present in higher quantity than Cu ions in the synaptic cleft, they can prevent detoxification of Cu by chelators unless they have an unusually high Cu over Zn selectivity. We describe a proof-of-concept study where the role of Zn on the metal swap reaction between two prototypical ligands and the Cu(Aβ) species has been investigated by several complementary spectroscopic techniques (UV-Vis, EPR and XANES). The first ligand has a higher Cu over Zn selectivity relative to the one of Aβ peptide while the second one exhibits a classical Cu over Zn selectivity. How Zn impacts the effect of the ligands on Cu-induced ROS production and Aβ aggregation is also reported.

Received 10th June 2016,
Accepted 23rd August 2016

DOI: 10.1039/c6dt02308h

www.rsc.org/dalton

Introduction

Alzheimer's disease (AD) is the most common cause of dementia in the elderly population with an estimated prevalence of 30 million people worldwide early in the decade.[1] AD is a multi-factorial neurodegenerative disease in which many features are involved. This may be the reason why only symptomatic drugs with limited effect are currently available.[2] Hence the development of curative treatments is urgently needed. This requires a right understanding of the trafficking between the drug candidate and the biological partners.

In AD, aggregation of the amyloid-β peptide (Aβ), a 40 to 42 amino-acid residue peptide, forming amyloid plaques has been considered to be a central process and an early event in the pathology, known as the amyloid cascade.[1,3,4] Indeed, while amyloid plaques are observed post-mortem in AD patients' brains, the monomeric soluble Aβ peptide is present in healthy patients. Metal ions, mainly Cu(I/II) and Zn(II), have been related to alteration of the Aβ aggregation process[5,6] and both metal ions are bound to the Aβ peptide within the amyloid plaques.[7] It is generally assumed that these metal ions are bound to Aβ under AD conditions, but not in healthy subjects.[8] This makes zinc and copper potential therapeutic targets, and hence chelators to remove these metal ions have been developed (for recent reviews, see ref. 8–13). A milestone article concerning the use of chelators to target metal ions bound to Aβ was the work of Cherny *et al.* in 2001.[14] It was shown that the chelator clioquinol (5-chloro-7-iodo-quinolin-8-ol) inhibits the accumulation of Aβ in AD model mice. Later the same group showed that a clioquinol derivative named PBT2 also improved the cognitive performance in AD model mice.[15] More recent studies on the impact of chelators on AD model mice include the studies of bis-8-aminoquinoline derivatives[16] and of the so-called metamorphosizers.[17] However, these seminal studies did not address the question of which metal is targeted by the chelators. Until now, whether the key target is Cu(I/II) or Zn(II) or both is still uncertain, because the effect of these metal ions on the Aβ aggregation process is dependent on conditions. Indeed, while the impact of Cu(II) and Zn(II) on the aggregation of Aβ and cell toxicity has been studied by different groups and reported in a multitude of publications (see *e.g.* ref. 18–22 and for recent reviews, see ref. 5 and 23), there is no clear trend as results are dependent on conditions (concentration, stoichiometry, pH, peptide

[a]CNRS, LCC (Laboratoire de Chimie de Coordination), 205 route de Narbonne, BP 44099 31077 Toulouse Cedex 4, France. E-mail: christelle.hureau@lcc-toulouse.fr
[b]University of Toulouse, UPS, INPT, 31077 Toulouse Cedex 4, France

†Electronic supplementary information (ESI) available. See DOI: 10.1039/c6dt02308h

‡Present address: Institute de Chimie (UMR 7177), 4 rue B. Pascal, F-67000 Strasbourg, France.

preparation, *etc.*). However, it is very well established that Zn(II) and Cu(II) do not have the same impact on the aggregation process. Thus it makes a large difference whether the chelator targets both metal ions or only one, and if only one whether it is Zn(II) or Cu(II).

In addition, several other factors play a role, like oxidative stress including overproduction of Reactive Oxygen Species (ROS).[3] In this context, only Cu(I/II) can directly catalyse the production of ROS, because Zn(II) is redox inert. As a direct consequence, Cu(I/II) ions in contrast to Zn(II) can be considered as the most pertinent biological target in the so-called chelation therapy in the context of oxidative stress.[8,24–27]

Zn(II) is the most common metal ion involved in neuronal signal transduction being released by some glutamatergic neurons. Although concentration values reported for Zn(II) vary between studies, they are 10–100 fold higher than those for Cu(I/II).[3,8,28] Aβ peptide, Cu(I/II) and Zn(II) ions are thus all present in the synaptic cleft and both ions can bind to Aβ in its N-terminal part.[5] Because Cu(II) and Zn(II) can be bound to the same amino-acid residues of the Aβ peptide, they are in competition for binding to Aβ (see Scheme S1†).[5,29,30] Likewise, they also compete for any other ligands, including chelating drug candidates. This could have a double deleterious impact: (i) assuming that Cu(II) is the target of choice, Zn(II) can impede its detoxification if the chelator binds Zn(II) instead of Cu(II); and (ii) considering that Zn(II) is involved in neurotransmission process,[31–33] its removal could be detrimental.

In the present article, we investigate the problem of which metal ion binds to which ligand in a 4-partner system with two metal ions (Cu(II) and Zn(II)) and two ligands (Aβ and chelator) in the test tube only. Such metal selectivity issue is an important parameter for chelators to bind the wanted metal ion and is well established in a 3-partner system (the chelator and the two metal ions) for different applications in biology, including in AD as discussed in ref. 23. This issue has also been discussed concerning the chelation of metal ions bound to Aβ in a 3-partner system (Aβ and the two metal ions)[22,34,35] and sometimes inferred for the 4-partner system (see *e.g.* ref. 12, 25 and 36), but no experiments on the 4-partner system have been provided and the question of how specific a chelator has to be has not been treated quantitatively. This is the aim of the present report.

In the past, removal of Cu(II) and Zn(II) ions from Aβ has been widely studied but never discussed in terms of mutual interference. More precisely, the capacity to remove Cu(II) only OR Zn(II) only from Aβ was researched even when the two metal ions were studied.[25,27,36–43] Such chelator formally corresponds to a situation where either $K_{Cu} \gg 1$ or $K_{Zn} \gg 1$, where K_M is defined in eqn (1). Several typical studied chelators, for which the affinities for Cu and Zn are known, are shown in Table 1. They include examples of the bis(8-aminoquinoline) series from Meunier's group,[25,27] the various ligands from Lim's group[36–38] and the Schiff base derivatives from Orvig's group.[39] As can be seen from their K_{Cu} values (higher than 1), all of them can remove Cu(II) from Aβ in the absence of Zn(II). However, in the presence of Zn(II), most of them mainly extract Zn(II) but not Cu(II) from the peptide; in other words, despite having a stronger affinity for Cu(II), they are rather selective for Zn(II). Only Schiff base derivatives[39] such as the L_2 ligand described here[44] have the ability to remove Cu(II) despite the presence of Zn(II). Indeed, to remove Cu(II) from Aβ in the presence of Zn(II), it is not enough that the chelator has a higher Cu(II) affinity than the Aβ. The Cu(II) over Zn(II) selectivity (*i.e.* affinity of Cu(II) compared to affinity of Zn(II) for a given ligand, S_L, eqn (3)) is crucial. The chelator must have a higher Cu(II) over Zn(II) selectivity than Aβ ($S_L \gg S_{A\beta}$, eqn (3)). In other words, this formally corresponds to a situation where $K \gg 1$ where K is defined in eqn (2) and describes the relative Cu(II) over Zn(II) selectivity of a ligand compared to that of Aβ. Having $K \gg 1$ is not that easy to achieve (Tables 1 and S1†) as the Cu(II) over Zn(II) selectivity of Aβ is very high ($\log(S_{A\beta}) = 4.2$, Table 1). The high value of $S_{A\beta}$ is due to a different coordination sphere for Cu(II) and Zn(II) when bound to the Aβ peptide (Scheme S1†). Near physiological pH, Cu(II) is bound to Aβ *via* the N-terminal amine, the adjacent Asp1-Ala2 carbonyl function, and two imidazole rings from His6 and His13 or 14 (so called component I). Another minor species is also present, where the Cu is bound to Aβ *via* the N-terminal amine, the deprotonated Asp1-Ala2 amide function, a carbonyl function and one imidazole ring from His6, His13 or His14 (so called component II).[45] While the Zn binding site into Aβ is more debated in the literature,[29,30] recent data support the non-involvement of the N-terminal amine in Zn coordination, a main difference compared to Cu.[46]

Table 1 Apparent affinity values at pH 7.1 for Cu and Zn, for Aβ and representative ligands and corresponding K_{Cu} and K values in log unit. *: in those cases, the Cu(II) removal from Aβ is partial. For the other ligands studied in the AD context, see Table S1. Scheme of ligands are given in the ESI (Scheme S2). Only 1 : 1 M : L complexes were considered here

		Aβ16	L_2	L1	ENDIP	ML	12[a]	Lc	L2′
	$\log(K_L^{Cu})^b$	9.2	13.8	17.3	15.4	12.6	15.7	11.6	12.9
	$\log(K_L^{Zn})^b$	5.0	6.1	12.0	10.1	8.6	12.6	9.6	11.6
	$\log(S_L)^b$	4.2	7.7	5.3	5.3	4.0	3.1	2.0	1.3
Without Zn	$\log(K_{Cu})^b$		4.6	8.1	6.2	3.4	6.5	2.4	2.7
	Complete Cu removal from Aβ		✓	✓	✓	✓	✓	✓	✓
With Zn	$\log(K)^b$		3.5	1.1	1.1	0.2	−1.1	−2.2	−2.9
	Complete Cu removal from Aβ		✓	✗*	✗*	✗	✗	✗	✗
	Ref.	46–48	44 and 46	42	43	38	27	49	42

[a] Value at pH 7.4. [b] Apparent constant value.

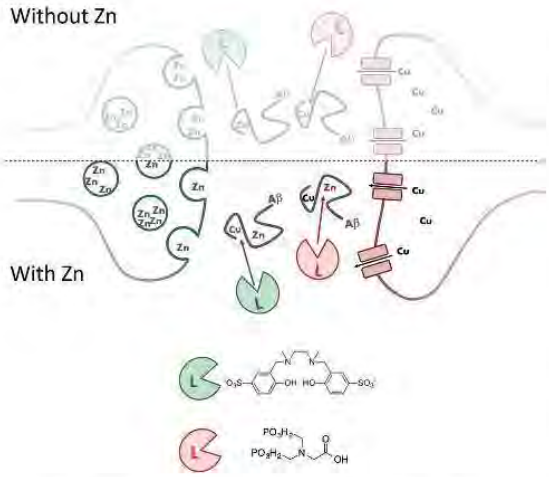

Scheme 1 Top: Classical strategy where Zn is not considered corresponding to a situation with low biological relevance. Bottom: Present strategy where Zn is considered in the exchange reaction. Cu removal by a ligand with $S_L > S_{A\beta}$ is shown in green and by a ligand with $S_L < S_{A\beta}$ in red. In the present study, the Cu : Zn : Aβ : L stoichiometry was fixed to 1 : 1 : 1 : 1. The complete set of equations describing this situation is detailed in the ESI.†

A schematic situation within the synaptic cleft is shown in Scheme 1 and is described by the equations and notations given below (with M = Cu(II) or Zn(II)).

Without Zn:

$$M(A\beta) + (L) \rightleftharpoons A\beta + M(L) \text{ is defined by } K_M \quad (1)$$

where $K_M = \frac{K_L^M}{K_{A\beta}^M}$ and K_L^M corresponds to the M + L ⇌ M(L) equilibrium

With Zn:

$$Cu(A\beta) + Zn(L) \rightleftharpoons Zn(A\beta) + Cu(L) \text{ is defined by } K \quad (2)$$

where $K = \frac{K_L^{Cu}}{K_{A\beta}^{Cu}} \frac{K_{A\beta}^{Zn}}{K_L^{Zn}} = \frac{S_L}{S_{A\beta}}$

$$\text{where } S_L = \frac{K_L^{Cu}}{K_L^{Zn}} \text{ and corresponds to } Cu(L) + Zn \rightleftharpoons Zn(L) + Cu \quad (3)$$

Results and discussion

In the present communication, we illustrate the importance of Zn(II) interference into Cu(II) targeting by ligands, including removing from Aβ and the impact on associated events, *i.e.* ROS production and Aβ aggregation. As a prototypical ligand with an appropriate Cu(II) over Zn(II) selectivity ($\log(S_{L_2}) = 7.7$, *i.e.* $S_{L_2} > S_{A\beta}$)[44,46] we have used a water-soluble Schiff base derivative noted as L_2 (in green in Scheme 1) and compare its properties to those of a control ligand noted as Lc (in red in Scheme 1) having an appropriate Cu(II) affinity ($\log(K_{Cu}) = 2.4$) but an inappropriate selectivity ($\log(S_{Lc}) = 2.0$, *i.e.* $S_{Lc} < S_{A\beta}$).[49] The peptides used here are either the N-terminal part of the full-length peptide encompassing the residues involved in metal ions coordination (sequence DAEFRHDSGYEVHHQK noted as Aβ16) and considered as a valuable and more soluble model of the Aβ40 [3,50] or the full length Aβ40 peptide, noted as Aβ in the following. This is a proof-of-concept study in the sense that the ligands used are not suitable for direct use *in vivo* due to a probable bad Blood Brain Barrier (BBB) penetration ability. Indeed, the main objective is to illustrate the impact of Zn(II) in Cu(II) removal from Aβ, an issue that has been overlooked. It might seem evident to anticipate the outcome of the experiments, since all the affinities of the four complexes are known. However, Zn(II) and Cu(II) bind to several binding sites in fast equilibrium and the main Zn(II) and Cu(II) sites do partially overlap.[51] This is not a classical situation and it is worth confirming the expected results by a set of complementary experiments. In addition, the approach developed here would also be very useful for other ligands with potential as drug candidates when the affinity constants cannot be determined (for instance due to solubility issue).

First, Cu(II) removal from Aβ in the presence of Zn(II) has been monitored for both L_2 and Lc ligands by UV-Vis (Fig. 1, left and Fig. S1, S2†) and EPR (Fig. 1, right and Fig. S3†). UV and EPR signatures show that: (i) for L_2, the Cu(II) ion is chelated by the ligand and not by the peptide (compare traces

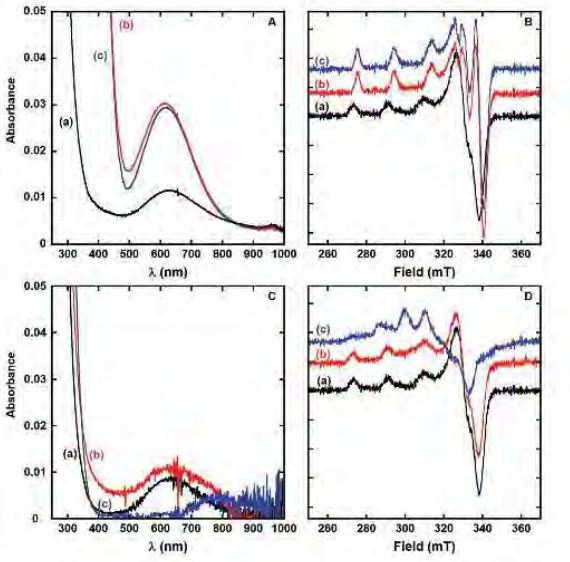

Fig. 1 UV-Vis absorption spectra (left) and EPR signatures (right) of (a) Cu(Aβ16), (b) Cu(Aβ16) + Zn(L) and (c) Cu(L), L = L_2 (top, panels A and B) or Lc (bottom, panels C and D). For UV-vis experiments: [Aβ16] = [L] = 0.1 mM, [M] = 0.1 mM (M = Cu(II) or Zn(II)), [hepes] = 0.1 M, pH 7.1, T = 25 °C, l = 1 cm; for EPR experiments: [Aβ16] = [L] = [Zn] = 0.20 mM, [Cu] = 0.18 mM, [hepes] = 50 mM, pH 7.1, T = 110 K.

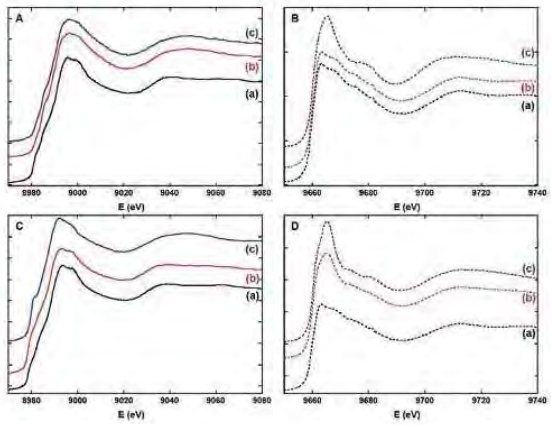

Fig. 2 Normalized Cu (left, panels A and C) and Zn (right, panels B and D, dotted lines) K-edges X-ray absorption near edge structure (XANES) spectra of (a) M(Aβ16) (M = Cu(II) or Zn(II)), (b) Cu(Aβ16) + Zn(L) and (c) M(L), (M = Cu(II) or Zn(II), L = L_2 (top, panels A and B) or Lc (bottom, panels C and D); [Aβ16] = [L] = 1.0 mM, [M] = 1.0 mM, [hepes] = 0.1 M, pH 7.1, T = 20 K.

(b) to traces (a) and (c) in Fig. 1, top) and (ii) for Lc, Cu(II) mainly remains bound to Aβ (compare traces (b) to traces (a) and (c) in Fig. 1, bottom). To confirm these conclusions by probing both metal centres, XANES (X-ray Absorption Near Edge Structure) measurements were performed. This spectroscopy is the most appropriate: (i) Zn(II) is silent in most of classical techniques and (ii) Cu and Zn K-edges are close enough to be recorded during the same beam-time session. The Cu- and Zn-edges XANES signatures show that: (i) for L_2, the Cu(II) is bound to the ligand (compare trace (b) to traces (a) and (c) in Fig. 2, panel A) and the Zn(II) to the Aβ peptide (compare trace (b) to traces (a) and (c) in Fig. 2, panel B). This is evidence of the complete metal exchange between Cu(Aβ) and Zn(L_2) and (ii) for Lc, the Cu(II) remains mainly bound to the Aβ peptide (compare trace (b) to traces (a) and (c) in Fig. 2, panel C) and Zn(II) to the ligand (compare trace (b) to traces (a) and (c) in Fig. 2, panel D). This is in line with the absence of metal exchange between Cu(Aβ) and Zn(Lc), although Cu(II) can be removed from Aβ by the control ligand Lc in the absence of Zn(II) (Fig. S1–S3†). Note that the results described here are also obtained when Zn(II) is pre-incubated with Cu(Aβ) instead of the ligand.

The ability to stop the Cu(Aβ) ROS production is a prerequisite of any Cu(II) chelator in the context of oxidative stress linked to AD. Such ROS production can be studied by proven methods (Scheme S3†)[35,44,52] that rely either on the UV monitoring of consumption of ascorbate (Asc) (Fig. 3) or on the detection of the fluorescent 7-OH-CCA formed by a reaction between the HO˙ produced and the 3-CCA (Fig. S5†). Fig. 3, curves (a), (b) and (b′) show the ascorbate consumption by Cu, Cu(Aβ) and Cu,Zn(Aβ) species. In the presence of Aβ, regardless the co-presence of Zn(II), Asc consumption is decreased com-

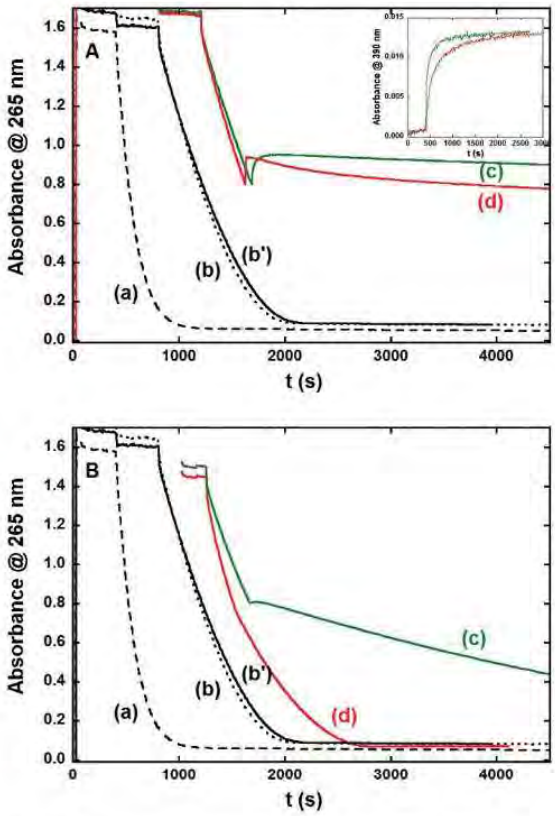

Fig. 3 Ascorbate consumption as a function of time. Time of experiments starts has been arbitrarily shifted for the sake of clarity. (a) Cu; (b, b′) Cu(Aβ) or Cu,Zn(Aβ), (c) Cu(Aβ) + L, (d) Cu(Aβ) + Zn(L), avec L = L_2 (top, panel A) and L = Lc (bottom, panel B). Ascorbate is added as the first reactant. The ligands are added when the absorbance at 265 nm ≈ 0.8. [Aβ] = [L] = 12 μM, [Zn] = 12 μM; [Cu] = 10 μM, [Asc] = 100 μM, [hepes] = 0.1 M, pH 7.1, T = 25 °C. Inset: monitoring of the Cu(L_2) complex formation during the ascorbate consumption experiments corresponding to curves (c) (green line) and (d) (red line).

pared to free Cu(I/II), as previously observed and discussed.[35,44] Curves (c) in panels A and B recorded in the absence of Zn(II) show that L_2 (panel A) is able to stop Asc consumption by Cu (Aβ) while Lc (panel B) can slow it down. Note that just after the addition of the L_2 (curve (c), panel A), there is an increase in the absorbance due to the formation of the Cu(L_2) complex that absorbs at 265 nm, the wavelength where the Asc consumption is monitored. Curves (d) in panels A and B show that in the presence of Zn(II), L_2 (panel A) is able to stop Asc consumption by Cu,Zn(Aβ) whereas Lc (panel B) has no impact on it, the same trend being observed if Zn(II) is first incubated with the ligand instead of Cu(Aβ) (Fig. S6†) and if Asc is added in the last chemical reaction step (Fig. S7†). Note that the Asc consumption experiments are confirmed by the CCA experiments (Fig. S5†). In the case of L_2, the arrest of Asc consumption is immediate while for Zn(L_2) a lag phase does

exist during which there is a weak Asc consumption. After this lag phase, slopes of the Asc consumption are similar for L_2 and $Zn(L_2)$. This indicates that the pre-loading of L_2 with Zn(II) slightly slows down the arrest of Asc consumption in line with a slowdown of Cu(II) removal from Aβ by $Zn(L_2)$ compared to L_2, as monitored by formation of the $Cu(L_2)$ complex (inset in Fig. 3, panel A). In summary, these results show that L_2 can arrest ROS production of Cu(Aβ) even in the presence of Zn(II), whereas Lc can slow it down only in the absence of Zn(II). This is linked to the ability of the $Zn(L_2)$ but not of the Zn(Lc) to remove Cu(II) from Cu(Aβ). In addition, in the course of this experiment, kinetic effects appear when the L_2 ligand is preloaded with Zn(II), although not problematic.

Finally, the impact of L_2 or $Zn(L_2)$ on the Cu(II) modulated Aβ aggregation was monitored by using the classical amyloid reporter fluorophore Thioflavin T (ThT) (Fig. 4, top). Under the present conditions, aggregation of Aβ in the absence or presence of Zn(II) is both characterized by sigmoid-like curves (curves (a) and (d), Fig. 4, top), with a first phase corresponding to nucleation, a second one to the elongation and the third one to the plateau. However, the two curves have different kinetic profiles ($t_{1/2} \approx 50$ h for apo-Aβ and $t_{1/2} \approx 100$ h for Zn(Aβ)), where $t_{1/2}$ is the time where the ThT fluorescence equals half the value of the maximum fluorescence. In addition, the maximal ThT fluorescence value is twice as higher for the apo-peptide compared to its Zn complex, but numerous fibrils are detected by AFM for both systems (Fig. 4, bottom), suggesting that Aβ and Zn(Aβ) both form amyloid fibrils but with different morphologies and ThT interactions. The Cu(Aβ) aggregation kinetic curve exhibits a less defined process leading to a weaker maximal fluorescence and a longer nucleation phase ($t_{1/2} \approx 120$ h), in line with the detection of oligomers and protofibrils by AFM. When performed at the beginning of the aggregation process, addition of L_2 or $Zn(L_2)$ on Cu(Aβ) induces the formation of apo-type fibrils or Zn-type fibrils, respectively (Fig. 4, top, curves c and e). This indicates Cu(II) removal from Aβ or Cu(II) and Zn(II) exchange between Aβ and L_2, respectively. When L_2 or $Zn(L_2)$ is added later on, similar trends are observed only if addition is done before the elongation phase (Fig. S8†). Else if L_2 or $Zn(L_2)$ addition is performed on the plateau phase, no modification of the ThT fluorescence is observed although Cu(II) is readily removed from the fibrils as probed by UV-Vis (Fig. S9†). Deeper investigations are foreseen to delineate the impact of adding the chelator after the formation of the fibrils regardless the presence of Zn(II) and are thus beyond the scope of the present study.

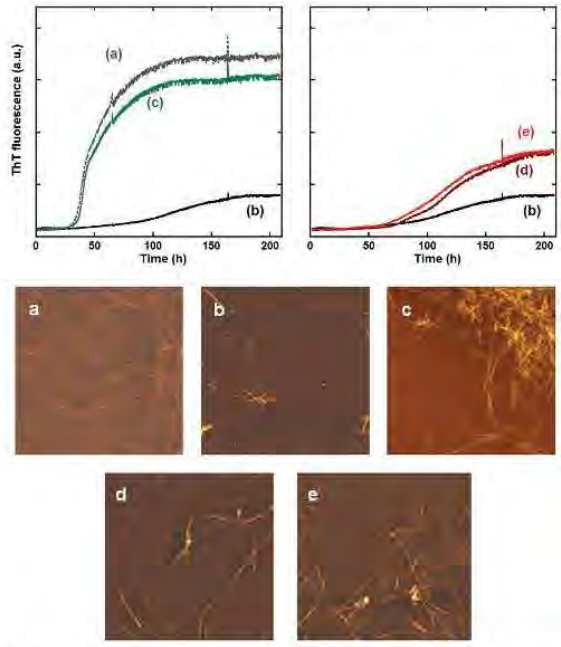

Fig. 4 Top: Kinetic measurement of Aβ aggregates formation using ThT fluorescence. Left: (a) Aβ; (b) Cu(Aβ) and (c) Cu(Aβ) + L_2; right: (d) Zn(Aβ); (b) Cu(Aβ) and (e) Cu(Aβ) + $Zn(L_2)$. [Aβ] = $[L_2]$ = $[L_2$-Zn] = 20 μM, [Cu] = 18 μM, [phosphate buffer] = 0.05 M, pH 7.1, T = 37 °C. Bottom: AFM images corresponding to ThT curves (a–e), 5 μm × 5 μm pictures.

Concluding remarks

In the present study, we have demonstrated the importance of taking Zn(II) into account when designing Cu(II) chelators against AD. The impact of Zn(II) on the ability to remove Cu(II) from Aβ and to impede related effects on ROS production and peptide aggregation have been investigated. It was shown that in addition to other requirements, such as being able to redox silence the Cu(II) ions and cross the BBB, the ligand has to display a high Cu(II) over Zn(II) selectivity (*i.e.* higher than the one of Aβ). This condition has been overlooked in the literature and is not so easy to satisfy because Aβ is itself very selective for Cu(II) compared to Zn(II), which is linked to the different binding sites adopted by the two metal centres when bound to Aβ. This suggests that several chelators designed and used in this context (Tables 1 and S1†) would chelate only Zn(II) in a synapse, where the high Zn(II) : Cu(II) stoichiometry will enhance the effects of the concept described in the present work with a 1 : 1 Cu(II) : Zn(II) ratio. Indeed, the stoichiometric ratio used here represents "the least unfavourable" condition. This is illustrated by the loss of the arrest of ROS production by the L_2 ligand in the presence of five equivalents of Zn(II) while in the presence of one equivalent of Zn(II) the L_2 was able to completely stop the ROS production (Fig. S6 and S7†).

Taking Zn(II) into account when designing a Cu(II) chelator is a first step towards studies under biologically pertinent conditions, and on-going studies include additional impact of pH, the presence of amino-acids and of other ions to be as close as possible to the biological medium. In addition, in the course of the ROS experiments shown here, kinetic issues appear. Indeed, removal of Cu(II) by L_2 preloaded with Zn(II) is slower than that for the ligand only when the Cu(Aβ) is producing ROS. In the case of the L_2 that was not a problem, but similar

kinetic effects could preclude the arrest of ROS production in the case of other ligands.

The proof-of-concept shown here for Cu(II) can also apply (i) for Cu(I) chelation, a quite unexplored target,[52] and (ii) for ligands with a redistribution ability. The capacity to re-distribute the Cu(I/II) ions rather than to eliminate them from Aβ seems important since it has been proposed that metal deregulation rather than metal overload is a key parameter in AD.[8,23,53] Strategies to go further towards potential therapeutic applications include: (i) improving the BBB penetration ability, for instance by addition of sugar moieties,[11,39] or (ii) moving towards multi-functional ligands able to target specific aggregation states, for instance.[11,54] Lastly, it is worth mentioning that most if not all amyloid related pathologies (such as Parkinson, ALS, *etc.*) also involved several metal ions (Fe, Cu and Zn) with various toxicities.[55] Hence the metal ions selectivity of a chelator relative to peptides or proteins of interest and described here for Cu(II), Zn(II) and Aβ is also relevant for other biomolecules and metal ions involved in these diseases.

Experimental section

Chemicals

Reagents were commercially available and were used as received.

Hepes buffer (sodium salt of 2-[4-(2-hydroxyethyl)piperazin-1-yl]ethanesulfonic acid) was bought from Fluka (bioluminescence grade).

Phosphate buffer was prepared from K_2HPO_4 and KH_2PO_4 bought from Fluka.

The Cu(II) and Zn(II) sources were $Zn(SO_4)(H_2O)$ and $Cu(SO_4)(H_2O)_5$ and purchased from Sigma.

A stock solution (5 mM) of ascorbate was prepared in Milli-Q water at room temperature just before beginning the experiment. Because ascorbate degrades quickly, a fresh solution was prepared each day.

A stock solution of coumarin-3-carboxylic acid (CCA, 5 mM) was prepared in phosphate buffer (500 mM, pH 7.1) at room temperature. The stock solution was stored at 4 °C.

A stock solution of Thioflavin T (ThT) at 250 μM was prepared in water without any further purification with ThT bought from Acros Organics.

Peptides

Aβ16 peptide (sequence DAEFRHDSGYEVHHQK and referred to as Aβ16) and Aβ40 (sequence DAEFRHDSGYEVHHQK LVFFAEDVGSNKGAIIGLMVGGVV and referred to as Aβ) were bought from GeneCust (Dudelange, Luxembourg) with purity grade >98%.

Stock solutions of the Aβ16 peptide were prepared by dissolving the powder in Milli-Q water (resulting pH ~ 2) at approx. 10 mM. Peptide concentration was then determined by UV-visible absorption of Tyr10 considered as free tyrosine (at pH 2, $(\varepsilon_{276} - \varepsilon_{296}) = 1410\ M^{-1}\ cm^{-1}$). Stock solutions of the Aβ40 peptide were prepared by dissolving the powder in 50 mM NaOH at approx. 3 mM. Peptide concentration was then determined by UV-visible absorption of Tyr10 considered as free tyrosine (at pH 13, $(\varepsilon_{296} - \varepsilon_{360}) = 2400\ M^{-1}\ cm^{-1}$).[56] The solutions were diluted down to the appropriate concentration in the peptide. All pH values are given with a ±0.2 pH unit error.

Monomerization of Aβ40. After preparation of the stock solution (see above), Aβ40 peptide is monomerized by FPLC, with a Superdex 75 column. 500 μL of the Aβ40 peptide at ~3 mM are injected. 15 mM NaOH eluent is used, at 1 mL min^{-1}. The peptide is detected at 293 nm and at a retention time of approx. 10 min. All the fractions corresponding to the peptide are collected and their concentrations are determined by UV-visible spectroscopy.

X-ray absorption spectroscopy

Cu(II) and Zn(II) K-edge XANES (X-ray Absorption Near Edge Structure) spectra were recorded at the BM30B (FAME) beamline at the European Synchrotron Radiation Facility (ESRF, Grenoble, France).[57] The storage ring was operated in 7/8 + 1 mode at 6 GeV with a 200 mA current. The beam energy was selected using an Si(220) N_2 cryo-cooled double-crystal monochromator with an experimental resolution close to that which was theoretically predicted (namely ~0.5 eV FWHM at the Cu and Zn energy).[58] The beam spot on the sample was approximately 300 × 100 μm^2 (H × V, FWHM). Because of the low Cu(II) and Zn(II) concentrations, spectra were recorded in fluorescence mode with a 30-element solid state Ge detector (Canberra) in frozen liquid cells in a He cryostat. The temperature was kept at 20 K during data collection. The energy was calibrated with Cu and Zn metallic foils, such that the maximum of the first derivative was set at 8979 and 9659 eV. XANES Cu(II) data were collected from 8840 to 8960 eV using 5 eV step of 2 s, from 8960 to 9020 eV using 0.5 eV step of 3 s, and from 9020 to 9300 eV with a *k*-step of 0.05 $Å^{-1}$ and 3 s per step. XANES Zn(II) data were collected from 9510 to 9630 eV using 5 eV step of 3 s, from 9630 to 9700 eV using 0.5 eV step of 3 s, and from 9700 to 10 000 eV with a *k*-step of 0.05 $Å^{-1}$ and 3 s per step. For each sample, at least three scans recorded on different spots were averaged and spectra were background-corrected by a linear regression through the pre-edge region and a polynomial through the post-edge region and normalized to the edge jump. XANES samples were prepared from the stock solution of peptide, ligands and metallic ions diluted down to approx. 1.0 mM in a buffered solution. Samples were frozen in the sample holder after addition of 10% glycerol as a cryoprotectant and stored in liquid nitrogen until use. Cu(II) photoreduction was controlled by recording successive scans at the same spot. It was considered that during the first 20 minutes of recording the photoreduction is insignificant.

Electron paramagnetic resonance

Electron Paramagnetic Resonance (EPR) data were recorded using an Elexsys E 500 Bruker spectrometer, operating at a microwave frequency of approximately 9.5 GHz. All spectra

were recorded using a microwave power of 20 mW across a sweep width of 150 mT (centred at 310 mT) with a modulation amplitude of 0.5 mT. Experiments were carried out at 110 K using a liquid nitrogen cryostat.

EPR samples were prepared from the stock solution of peptide and/or ligand diluted down to 0.2 mM in H_2O. 0.9 equiv. of ^{65}Cu(II) was added from 25 mM $^{65}Cu(NO_3)_2$ stock solution prepared in house from a copper foil (Eurisotop). Concentration was determined by formation of the $Cu(BCS)_2^{3-}$ (BCS = bathocuproinedisulfonic acid, from Sigma-Aldrich) complex in the presence of an excess of ascorbate, using a molar extinction coefficient at 483 nm of 13 000 M^{-1} cm^{-1}. Samples were frozen in a quartz tube after addition of 10% glycerol as a cryoprotectant and stored in liquid nitrogen until use.

UV-Visible spectroscopy

UV-Vis experiments were performed on an Agilent 8453 UV-Vis spectrometer at 25 °C.

Fluorescence spectroscopy

Fluorescence spectra were recorded by using a Fluostar Optima (BMG Labtech) connected to a personal computer.

Thioflavin T measurements

Thioflavin T (ThT), Aβ, Cu(II), Zn(II) and ligands at respective concentrations of 10 μM, 20 μM, 18 μM, 18 μM and 20 μM were mixed in 50 mM phosphate buffer, pH 7.1 and placed in a 384-well microplate. The time course of ThT fluorescence was then measured (excitation 440 nm; emission 490 nm, bandwidth for emission and excitation 10 nm).

Atomic force microscopy

Tapping-mode AFM imaging was performed in air using a Smart SPM-1000 microscope (AIST-NT, Novato, USA) equipped with a 100 μm scanner. Sample solutions (20 μM) were deposited on freshly cleaved mica and left for adsorption on the substrate for 10–20 min. They were then rinsed three times with deionized water to remove salts and loosely bound peptide and dried under compressed air before imaging. Commercial Si cantilevers (NanoWorld, Switzerland) with an elastic modulus of ~42 N m^{-1} were used. All images were acquired as 512 × 512 pixel images at a typical scan rate of 1.0 kHz with a vertical tip oscillation frequency of 250–350 kHz. Representative images of samples were obtained by scanning at least 5 different locations on at least two different samples of the same chemical system.

Coumarin-3-carboxylic acid assay

3-CCA was used to detect HO˙. HO˙ reacts with 3-CCA to form 7-hydroxy-coumarin-3-carboxylic acid (7-OH-CCA), which is fluorescent at 452 nm upon excitation at 395 nm. Under the conditions used in the present study the intensity of the fluorescence signal is proportional to the number of 7-OH-CCA molecules formed. Performing the experiment in phosphate buffer is mandatory to detect formation of HO˙ since other buffers trap HO˙.

Ascorbate consumption assay

Ascorbate consumption was monitored by UV-Vis. Intensity of the Asc absorption band at λ = 265 nm (ε = 14 500 M^{-1} cm^{-1}) was monitored as a function of time, with the background signal at λ = 800 nm subtracted.

Acknowledgements

The authors acknowledge Prof. E. Guillon, Drs S. Sayen and F. Collin, and C. Cheignon for their help in the recording of the XANES data; Dr O. Berthoumieu and M. Tasse for their help in acquiring the AFM pictures; L. Rechignat for the recording of the EPR data and Dr S. Noël for the L_2 synthesis. The authors acknowledge the European Synchrotron Radiation Facility for provision of beamtime and the FAME staff for their support (20151029). CH thanks the ERC aLzINK – Contract no. 638712 for financial support.

References

1 D. M. Holtzman, J. C. Morris and A. M. Goate, *Sci. Transl. Med.*, 2011, **3**, 77sr1.
2 J. Godyń, J. Jończyk, D. Panek and B. Malawska, *Pharmacol. Rep.*, 2016, **68**, 127.
3 C. Hureau, *Coord. Chem. Rev.*, 2012, **256**, 2164.
4 S. H. Barage and K. D. Sonawane, *Neuropeptides*, 2015, **52**, 1.
5 P. Faller, C. Hureau and O. Berthoumieu, *Inorg. Chem.*, 2013, **52**, 12193.
6 A. Tiiman, P. Palumaa and V. Tõugu, *Neurochem. Int.*, 2013, **62**, 367.
7 L. M. Miller, Q. Wang, T. P. Telivala, R. J. Smith, A. Lanzirotti and J. Miklossy, *J. Struct. Biol.*, 2006, **155**, 30.
8 K. J. Barnham and A. I. Bush, *Chem. Soc. Rev.*, 2014, **43**, 6727.
9 A. Budimir, *Acta Pharm.*, 2011, **61**, 1.
10 J. S. Derrick and M. H. Lim, *ChemBioChem*, 2015, **16**, 887.
11 C. Rodriguez-Rodriguez, M. Telpoukhovskaia and C. Orvig, *Coord. Chem. Rev.*, 2012, **256**, 2308.
12 M. G. Savelieff, A. S. DeToma, J. S. Derrick and M. H. Lim, *Acc. Chem. Res.*, 2014, **47**, 2475.
13 A. Robert, Y. Liu, M. Nguyen and B. Meunier, *Acc. Chem. Res.*, 2015, **48**, 1332.
14 R. A. Cherny, C. S. Atwood, M. E. Xilinas, D. N. Gray, W. D. Jones, C. A. McLean, K. J. Barnham, I. Volitakis, F. W. Fraser, Y. Kim, X. Huang, L. E. Goldstein, R. D. Moir, J. T. Lim, K. Beyreuther, H. Zheng, R. E. Tanzi, C. L. Masters and A. I. Bush, *Neuron*, 2001, **30**, 665.
15 P. A. Adlard, R. A. Cherny, D. I. Finkelstein, E. Gautier, E. Robb, M. Cortes, I. Volitakis, X. Liu, J. P. Smith, K. Perez, K. Laughton, Q. X. Li, S. A. Charman, J. A. Nicolazzo,

S. Wilkins, K. Deleva, T. Lynch, G. Kok, C. W. Ritchie, R. E. Tanzi, R. Cappai, C. L. Masters, K. J. Barnham and A. I. Bush, *Neuron*, 2008, **59**, 43.
16 J. Ceccom, F. Coslédan, H. Halley, B. Francès, J. M. Lassalle and B. Meunier, *PLoS One*, 2012, **7**, e43105.
17 M. W. Beck, S. B. Oh, R. A. Kerr, H. J. Lee, S. H. Kim, S. Kim, M. R. Jang, T. Brandon, J.-Y. Lee and M. H. Lim, *Chem. Sci.*, 2015, **6**, 1879.
18 C. Opazo, X. Huang, R. A. Cherny, R. D. Moir, A. E. Roher, A. R. White, R. Cappai, C. L. Masters, R. E. Tanzi, N. C. Inestrosa and A. I. Bush, *J. Biol. Chem.*, 2002, **277**, 40302.
19 X. Huang, C. S. Atwood, M. A. Hartshorn, G. Multhaup, L. E. Goldstein, R. C. Scarpa, M. P. Cuajungco, D. N. Gray, J. Lim, R. D. Moir, R. E. Tanzi and A. I. Bush, *Biochemistry*, 1999, **38**, 7609.
20 Y. Yoshiike, K. Tanemura, O. Murayama, T. Akagi, M. Murayama, S. Sato, X. Sun, N. Tanaka and A. Takashima, *J. Biol. Chem.*, 2001, **276**, 32293.
21 M. P. Cuajungco and K. Y. Faget, *Brain Res. Rev.*, 2003, **41**, 44.
22 V. Tõugu, A. Karafin, K. Zovo, R. S. Chung, C. Howells, A. K. West and P. Palumaa, *J. Neurochem.*, 2009, **110**, 1785.
23 K. P. Kepp, *Chem. Rev.*, 2012, **112**, 5193.
24 G. Eskici and P. H. Axelsen, *Biochemistry*, 2012, **51**, 6289.
25 M. Nguyen, A. Robert, A. Sournia-Saquet, L. Vendier and B. Meunier, *Chem. – Eur. J.*, 2014, **20**, 6771.
26 M. P. Cuajungco, L. E. Goldstein, A. Nunomura, M. A. Smith, J. T. Lim, C. S. Atwood, X. Huang, Y. W. Farrag, G. Perry and A. I. Bush, *J. Biol. Chem.*, 2000, **275**, 19439.
27 C. Deraeve, C. Boldron, A. Maraval, H. Mazarguil, H. Gornitzka, L. Vendier, M. Pitié and B. Meunier, *Chem. – Eur. J.*, 2008, **14**, 682.
28 M. G. Savelieff, S. Lee, Y. Liu and M. H. Lim, *ACS Chem. Biol.*, 2014, **8**, 856.
29 V. Tõugu and P. Palumaa, *Coord. Chem. Rev.*, 2012, **256**, 2219.
30 C. Migliorini, E. Porciatti, M. Luczkowski and D. Valensin, *Coord. Chem. Rev.*, 2012, **256**, 352.
31 N. L. Bjorklund, V. M. Sadagoparamanujam and G. Taglialatela, *J. Neurosci. Methods*, 2012, **203**, 146.
32 S. Bohic, J. F. Ghersi-Egea, J. Gibon, P. Paoletti, J. Arnaud, S. Hunot, A. Boom and A. Bouron, *Rev. Neurol.*, 2011, **167**, 269.
33 C. J. Frederickson, J. Y. Koh and A. I. Bush, *Nat. Rev. Neurosci.*, 2005, **6**, 449.
34 C. A. Damante, K. Ösz, Z. Nagy, G. Grasso, G. Pappalardo, E. Rizzarelli and I. Sóvágó, *Inorg. Chem.*, 2011, **50**, 5342.
35 B. Alies, I. Sasaki, O. Proux, S. Sayen, E. Guillon, P. Faller and C. Hureau, *Chem. Commun.*, 2013, **49**, 1214.
36 M. G. Savelieff, Y. Liu, R. R. P. Senthamarai, K. J. Korshavn, H. J. Lee, A. Ramamoorthy and M. H. Lim, *Chem. Commun.*, 2014, **50**, 5301.
37 J.-S. Choi, J. J. Braymer, R. P. R. Nanga, A. Ramamoorthy and M. H. Lim, *Proc. Natl. Acad. Sci. U. S. A.*, 2010, **107**, 21990.
38 S. Lee, X. Zheng, J. Krishnamoorthy, M. G. Savelieff, H. M. Park, J. R. Brender, J. H. Kim, J. S. Derrick, A. Kochi, H. J. Lee, C. Kim, A. Ramamoorthy, M. T. Bowers and M. H. Lim, *J. Am. Chem. Soc.*, 2014, **136**, 299.
39 T. Storr, M. Merkel, G. X. Song-Zhao, L. E. Scott, D. E. Green, M. L. Bowen, K. H. Thompson, B. O. Patrick, H. J. Schugar and C. Orvig, *J. Am. Chem. Soc.*, 2007, **129**, 7453.
40 D. E. Green, M. L. Bowen, L. E. Scott, T. Storr, M. Merkel, K. Böhmerle, K. H. Thompson, B. O. Patrick, H. J. Schugar and C. Orvig, *Dalton Trans.*, 2010, **39**, 1604.
41 T. Storr, L. E. Scott, M. L. Bowen, D. E. Green, K. H. Thompson, H. J. Schugar and C. Orvig, *Dalton Trans.*, 2009, **16**, 3024.
42 A. K. Sharma, S. T. Pavlova, J. Kim, D. Finkelstein, N. J. Hawco, N. P. Rath, J. Kim and L. M. Mirica, *J. Am. Chem. Soc.*, 2012, **134**, 6625.
43 A. Lakatos, V. Zsigo, D. Hollender, N. V. Nagy, L. Fülöp, D. Simon, Z. Bozso and T. Kiss, *Dalton Trans.*, 2010, **39**, 1302.
44 S. Noël, F. Perez, S. Ladeira, S. Sayen, E. Guillon, E. Gras and C. Hureau, *J. Inorg. Biochem.*, 2012, **117**, 322.
45 C. Hureau and P. Dorlet, *Coord. Chem. Rev.*, 2012, **256**, 2175.
46 S. Noël, S. Bustos, S. Sayen, E. Guillon, P. Faller and C. Hureau, *Metallomics*, 2014, **6**, 1220.
47 T. Kowalik-Jankowska, M. Ruta, K. Wisniewska and L. Lankiewicz, *J. Inorg. Biochem.*, 2003, **95**, 270.
48 I. Zawisza, M. Rozga and W. Bal, *Coord. Chem. Rev.*, 2012, **256**, 2297.
49 A. P. Katkov, T. A. Matkovskaya, N. I. Krutikova, A. S. Monakhov and N. M. Dyatlova, *Russ. J. Inorg. Chem.*, 1991, **391**, 693.
50 V. Minicozzi, F. Stellato, M. Comai, M. Dalla Serra, C. Potrich, W. Meyer-Klaucke and S. Morante, *J. Biol. Chem.*, 2008, **283**, 10784.
51 P. Faller, C. Hureau and G. La Penna, *Acc. Chem. Res.*, 2014, **47**, 2252.
52 E. Atrian-Blasco, E. Cerrada, A. Conte-Daban, D. Testemale, P. Faller, M. Laguna and C. Hureau, *Metallomics*, 2015, **7**, 536.
53 D. J. Bonda, H.-g. Lee, J. A. Blair, X. Zhu, G. Perry and M. A. Smith, *Metallomics*, 2011, **3**, 267.
54 S. Noël, S. Cadet, E. Gras and C. Hureau, *Chem. Soc. Rev.*, 2013, **42**, 7747.
55 H. Kozlowski, M. Luczkowski, M. Remelli and D. Valensin, *Coord. Chem. Rev.*, 2012, **256**, 2129.
56 P. Faller, C. Hureau, P. Dorlet, P. Hellwig, Y. Coppel, F. Collin and B. Alies, *Coord. Chem. Rev.*, 2012, **256**, 2381.
57 O. Proux, X. Biquard, E. Lahera, J. J. Menthonnex, A. Prat, O. Ulrich, Y. Soldo, P. Trévisson, G. Kapoujvan, G. Perroux, P. Taunier, D. Grand, P. Jeantet, M. Deleglise, J.-P. Roux and J.-L. Hazemann, *Phys. Scr.*, 2005, **115**, 970.
58 O. Proux, V. Nassif, A. Prat, O. Ulrich, E. Lahera, X. Biquard, J. J. Menthonnex and J.-L. Hazemann, *J. Synchrotron Radiat.*, 2006, **13**, 59.

III-B.iii Supporting information

How Zn can impede Cu detoxification by chelating agents in Alzheimer's Disease: a proof-of-concept study

Amandine Conte-Daban,[a] Adam Day,[a] Peter Faller[a,b] and Christelle Hureau[a]

[a] A. Conte-Daban, A. Day, Prof. P. Faller, Dr. C. Hureau

CNRS, LCC (Laboratoire de Chimie de Coordination)

205 route de Narbonne, BP 44099, 31077 Toulouse Cedex 4 (France) and University of Toulouse, UPS, INPT, 31077 Toulouse Cedex 4 (France)

E-mail: christelle.hureau@lcc-toulouse.fr

[b] Prof. Dr. P. Faller

present address : Institute de Chimie (UMR 7177), 4 rue B. Pascal, F-67000 Strasbourg, France

SUPPORTING INFORMATION

Cu(II) and Zn(II) coordination sites to Aβ

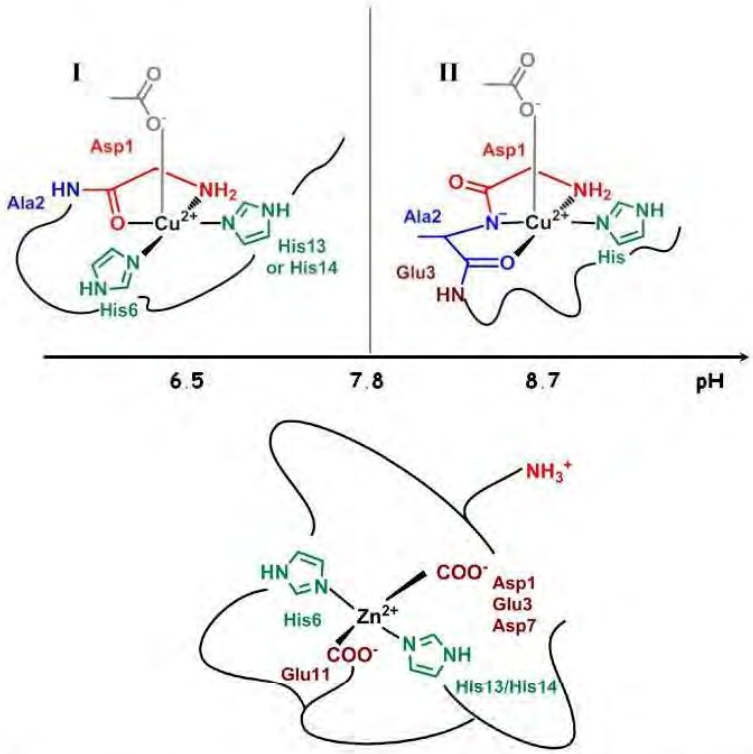

Scheme S1. Predominant coordination sites proposed for Cu(II) and Zn(II) to the Aβ peptide near physiological pH.

Ligands

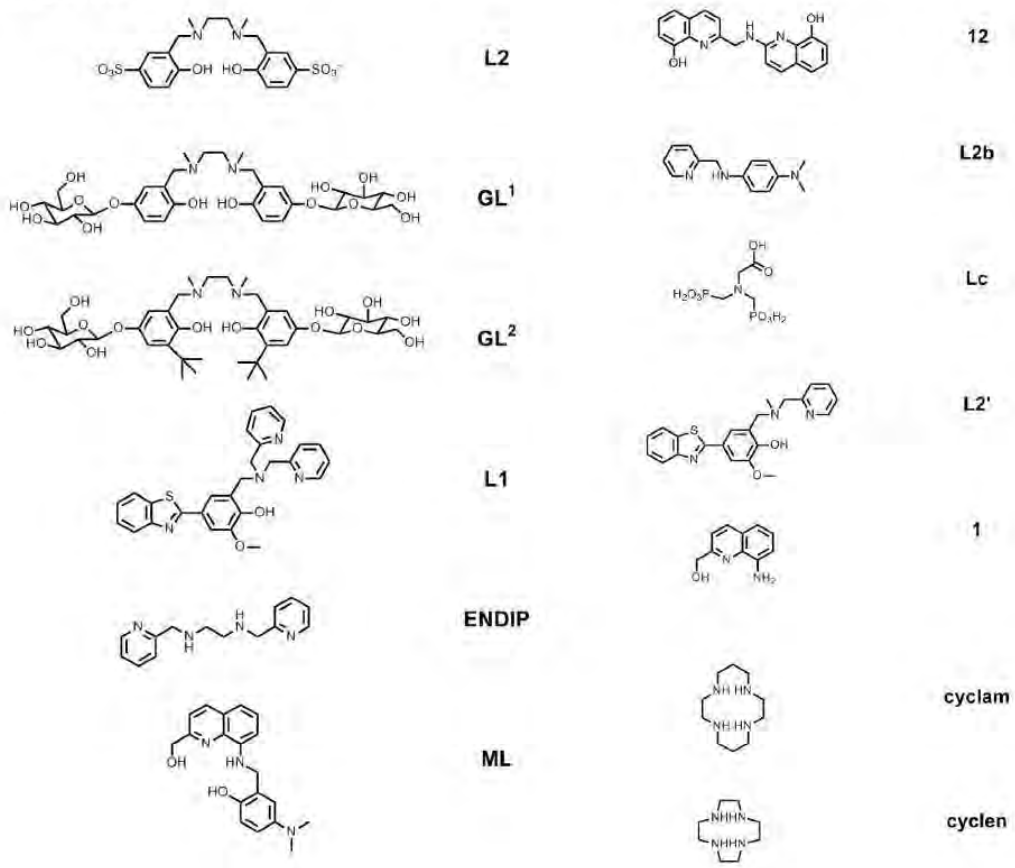

Scheme S2. Ligands corresponding to Table 1 and Table S1.

ROS detection methods.

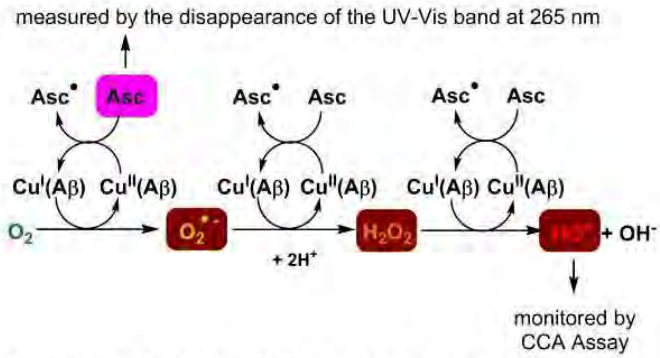

Scheme S3. Detection methods for ROS production based on the monitoring of ascorbate consumption by UV-Vis at 265 nm and HO° adduct formation with CCA observed at 450 nm by fluorescence.

Equations

The description of the situation (under thermodynamic control) within the synaptic cleft is represented by the equations and notations given in the box below, where Cu(II) and Zn(II) can both react with Aβ or L to form the four possible L-Cu(II), L-Zn(II), Aβ-Cu(II) and Aβ-Zn(II) complexes.

In absence of Zn(II) the condition to predominantly remove Cu(II) from Aβ is $K_{Cu} \gg 1$ while in presence of Zn(II), the condition is $K \gg 1$, using the following equations and corresponding reaction constants.

L	+	Cu(II)	⇌	L-Cu(II)	$K_L^{Cu} = \frac{[L - Cu(II)]}{[L][Cu(II)]}$
$1 - \alpha_{Cu} - \alpha_{Zn}$		$1 - \alpha_{Cu} - \beta_{Cu}$		α_{Cu}	
Aβ	+	Cu(II)	⇌	Aβ-Cu(II)	$K_{A\beta}^{Cu} = \frac{[A\beta - Cu(II)]}{[A\beta][Cu(II)]}$
$1 - \beta_{Cu} - \beta_{Zn}$		$1 - \alpha_{Cu} - \beta_{Cu}$		β_{Cu}	
L	+	Zn(II)	⇌	L-Zn	$K_L^{Zn} = \frac{[L - Zn]}{[L][Zn]}$
$1 - \alpha_{Cu} - \alpha_{Zn}$		$1 - \alpha_{Zn} - \beta_{Zn}$		α_{Zn}	
Aβ	+	Zn(II)	⇌	Aβ-Zn	$K_{A\beta}^{Zn} = \frac{[A\beta - Zn]}{[A\beta][Zn]}$
$1 - \beta_{Cu} - \beta_{Zn}$		$1 - \alpha_{Zn} - \beta_{Zn}$		β_{Zn}	

where α_{Cu} corresponds to the proportions in L-Cu(II), β_{Cu} in Aβ-Cu(II), α_{Zn} in L-Zn(II), and β_{Zn} in Aβ-Zn(II). We can then define $K_{Cu} = \frac{K_L^{Cu}}{K_{A\beta}^{Cu}}$; $K_{Zn} = \frac{K_L^{Zn}}{K_{A\beta}^{Zn}}$ and $K = \frac{K_L^{Cu} K_{A\beta}^{Zn}}{K_L^{Zn} K_{A\beta}^{Cu}} = \frac{K_{Cu}}{K_{Zn}}$,

where K_M (with M = Cu(II) or Zn) corresponds formally to the :

Aβ-M	+	L	⇌	L-M + Aβ

and σ to the "exchange reaction"

Aβ-Cu	+	L-Zn	⇌	L-Cu + Aβ-Zn

It comes that $\alpha_{Cu} = \frac{\sqrt{K}}{1 + \sqrt{K}}$.

To have a Cu(II) removal from the Aβ, the condition is $\alpha_{Cu} \geq 0.5 \leftrightarrow K \geq 1$.

Apparent affinity and selectivity values of the chelators

Table S1. Apparent affinity values at pH 7.1 for Cu and Zn, for Aβ and representative ligands and corresponding K_{Cu} and K values. Only 1:1 metal:ligand complexes are considered.

		Aβ16	L-2	GL1	GL2	L1	ENDIP	ML	12	L2b	Lc	L2'	1	Cyclam[c]	Cyclen[c]
	$log(K_L^{Cu})_{[a]}$	9.2	13.8	12.1	11.5	17.3	15.4	12.6	15.7	10.6	11.6	12.9	8.7	23.8	21.1
	$log(K_L^{Zn})_{[a]}$	5.0	6.1	4.6	4.2	12.0	10.1	8.6	12.6	8.4	9.6	11.6	8.1	12.6	12.7
	$log(S_L)$	4.2	7.7	7.5	7.3	5.3	5.3	4.0	3.1	2.2	2.0	1.3	0.6	11.1	8.4
Without Zn	$log(K_{Cu})$		4.6	2.9	2.3	8.1	6.2	3.4	6.5	1.4	2.4	2.7	-0.5	14.6	11.9
	Complete Cu removal from Aβ		▶	▶	▶	▶	▶	▶	▶	[illegible]	▶	▶	[illegible]	▶	▶
With Zn	$log(K)$		3.5	3.3	3.1	1.1	1.1	0.2	-1.1	-2.0	-2.2	-2.9	-3.6	6.9	4.2
	Complete Cu removal from Aβ		▶	▶	▶	[illegible]	[illegible]	[illegible]	[illegible]	[illegible]	[illegible]	[illegible]	[illegible]	▶	▶
	Ref.	1-3	2, 4	5	5	6	7	8	9	10	11	6	8	12	12

[a] value at pH 7.4

[b] Apparent binding constant.

[c] The cyclen and cyclam ligands have the correct selectivity but do not stop the production of ROS.[12]

UV-Vis, EPR and XANES monitoring of Cu(II) removal form Aβ in presence of Zn(II)

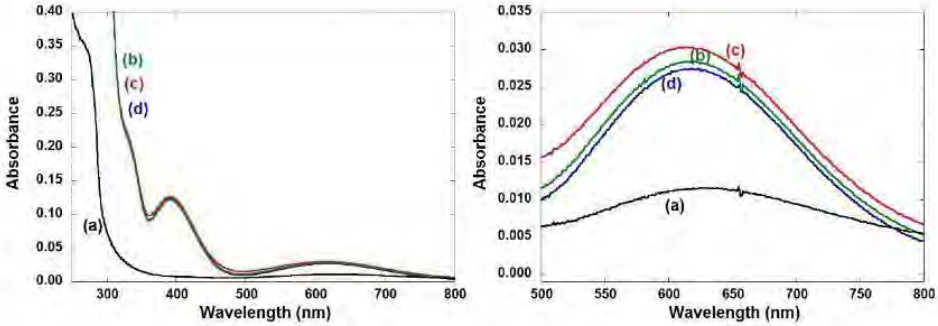

Figure S1. UV-Vis absorption spectra of Cu(Aβ16) (black, a) ; Cu(Aβ16) + L_2 (green, b) ; Cu(Aβ16) + Zn(L_2) (red, c) ; Cu(L_2) (blue, d). [Aβ16] = [L_2] = 0.1 mM, [M] = 0.1 mM, [hepes] = 0.1 M, pH 7.1, T = 25 °C, ℓ=1 cm.

Regardless the presence of Zn, the removal of Cu(II) from Aβ by L_2 is total as can be seen by comparison between curves (b, c and d), in line with the data described previously EPR and XANES.

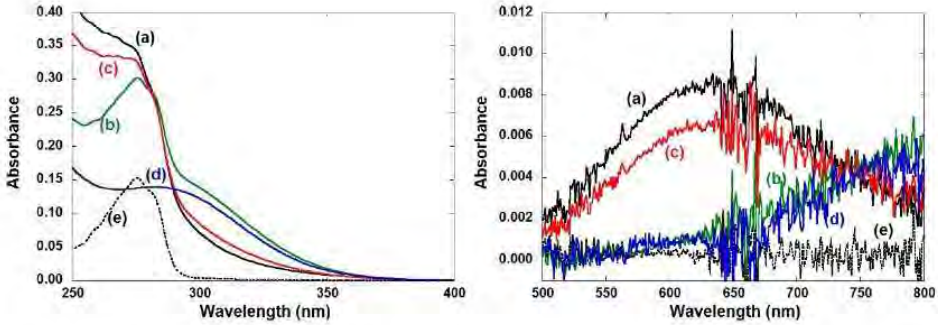

Figure S2. UV-Vis absorption spectra Cu(Aβ16) (black, a); Cu(Aβ16) + L_c (green, b); Cu(Aβ16) + Zn(L_c) (red, c); Cu(L_c) (blue, d) ; (Aβ16) (e, dotted black line). [Aβ16] = [L_c] = 0.1 mM, [M] = 0.1 mM, [hepes] = 0.1 M, pH 7.1, T = 25 °C, ℓ=1 cm.

In absence of Zn, the removal of Cu(II) from Aβ by L_c is almost total as can be seen by comparison between curves (b, d and e). Indeed, curve (b) corresponds to the addition of curves (d) and (e), in line with the presence of Cu(II) bound to L_c and free Aβ in the solution. In presence of Zn, the removal of Cu(II) from Aβ by L_c is hampered and the ratio of Cu(II) bound to L_C is approx. 25% in line with the data described previously EPR and XANES.

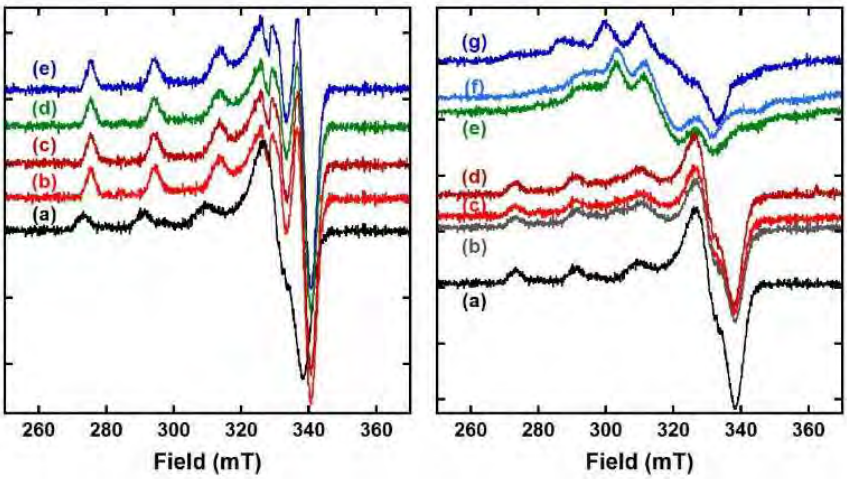

Figure S3. Left panel: EPR signatures of Cu(Aβ16) (a) ; Cu(Aβ16) + Zn(L_2) (b) ; Cu,Zn(Aβ16) + L_2 (c) ; Cu(Aβ16) + L_2 (d) ; Cu(L_2) (e). Right panel: EPR signatures of Cu(Aβ16) (a) ; calculated spectrum according to 0.3 spectrum (d) + 0.7 spectrum (a) (b) ; Cu(Aβ16) + Zn(L_C) (c) ; Cu,Zn(Aβ16) + L_C (d) ; Cu(L_C) + Aβ16 (e) ; Cu(L_C) + 1 equiv. of imidazole (f) ; Cu(L_C) (g). [Cu(II)] = 0.18 mM in 50 mM hepes buffer at pH 7.1. ν = 9.5 GHz, amplitude modulation = 0.5 mT, microwave power = 20 mW. T = 110 K.

Cu(II) extraction from the Aβ peptide is observed with L_2 in all the conditions tested, regardless of the absence or presence of Zn.

In the case of L_C, the situation is a little bit more complex, due to the formation of a ternary species between Cu(II), L_C and the Aβ peptide. Indeed, at this high concentration, the peptide can complete the Cu sphere in the Cu(L_C) complex, very likely via the coordination of the imidazole ring from one of the three His, as recently observed for Cu(II), Aβ and alpha-synuclein.[13, 14] This is further confirmed by the high similarity between the EPR signatures of the Cu(L_C) species in presence of Aβ or of one equiv. of imidazole. Anyway, in presence of Zn, the removal of Cu(II) from Aβ is hampered and the ratio of Cu(II) bound to L_C is only approx. 30% as expected based on the relative Cu over Zn selectivity of Aβ ($10^{4.2}$) and L_C (10^2) (compare spectra (b) and (c) and see Table S1).

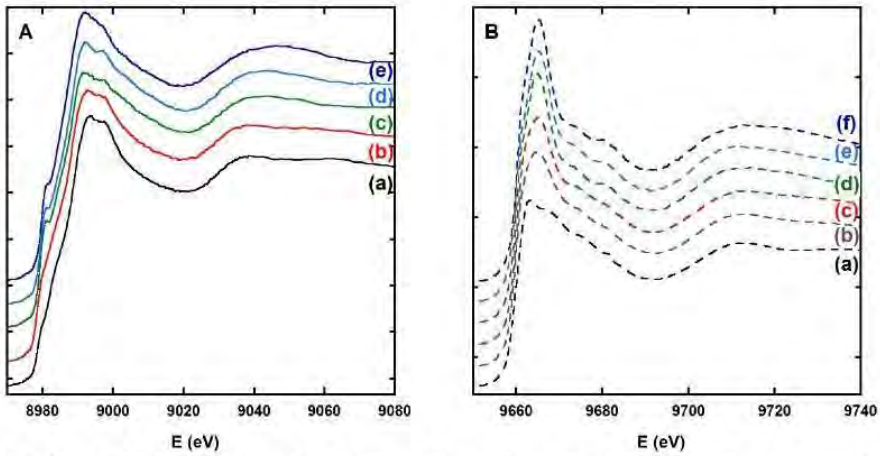

Figure S4. Panel A: Normalized Cu K-edge X-ray absorption near edge structure (XANES) spectra of Cu(Aβ16) (a) ; Cu(Aβ16) + Zn(L_C) (b) ; Cu(L_C) + Aβ16 (c) ; Cu(L_C) + 1 equiv. of imidazole (d) ; Cu(L_C) (e). Panel B: Normalized Zn K-edge XANES spectra of Zn(Aβ16) (a) ; calculation spectrum according to 0.4 spectrum (a) + 0.6 spectrum (d)) (b) ; Cu(Aβ16) + Zn(L_C) (c) ; Zn(L_C) + Aβ16 (d) ; Zn(L_C) + 1 equiv. of imidazole (e) ; Zn(L_C) (f). [Aβ] = [L] = 1 mM, [M] = 1 mM, [hepes] = 0.1 M, pH 7.1, T = 20 K.

The evaluation of the distribution of Cu(II) between the peptide and the L_C ligand in the exchange experiment by XANES is difficult due to the high similarity between the various signatures (and to a lesser extent by the presence of Cu(II) photoreduction). EPR is more appropriate (see next paragraph).

In contrast, the evaluation of the distribution of Zn(II) between the peptide and the L_C ligand in the exchange experiment by XANES at the Zn K-edge is possible. This leads to approx. 60% of Zn bound to the L_C (compare spectra (b) and (c)) in line with the proportion of Cu(II) bound to the ligand found by EPR (see next paragraph).

ROS production assays

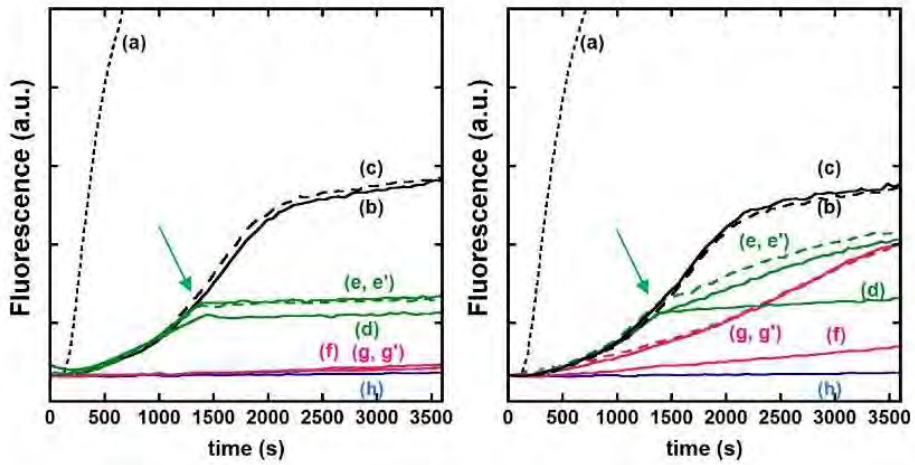

Figure S5. Cu(II) induced 7-OH-CCA formation. Cu(II) (a), Cu(Aβ16) (b), Cu,Zn(Aβ16) (c), Cu(Aβ16) + L added @ t = 20 min (d) ; Cu(Aβ16) + Zn(L) added @ t = 20 min (e) ; Cu,Zn(Aβ16) + L added @ t = 20 min (e', dotted line) ; Cu(Aβ16) + L (f) ; Cu(Aβ16) + Zn(L) (g) ; Cu,Zn(Aβ16) + L (g', dotted line) ; control experiment (without Cu) (h). Ascorbate is added to trigger the reaction. Left panel L = L_2 ; Right panel : L = L_C. [Cu(II)] = 10 µM, 1.2 equiv of Aβ, L and Zn. λ_{em} = 452 nm, [Asc] = 0.5 mM, [PO_4] = 50 mM, pH 7.1, [CCA] = 0.5 mM, T = 25°C.

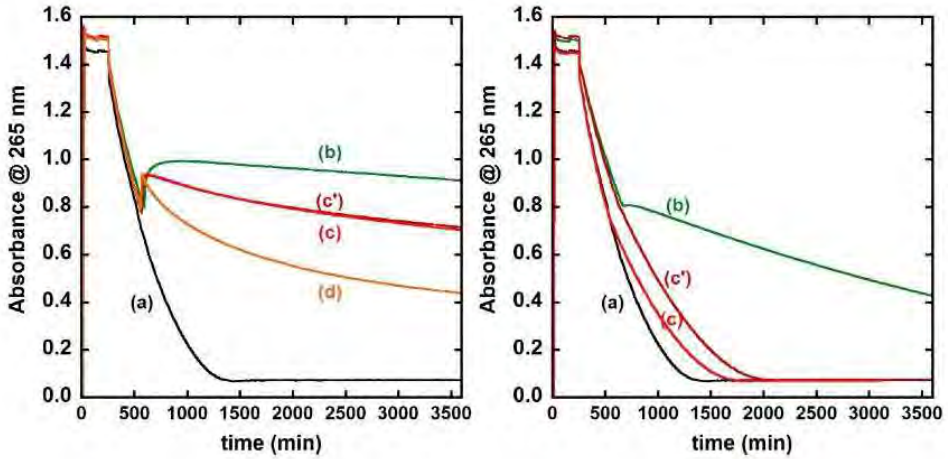

Figure S6. Cu(II) induced ascorbate consumption. Cu(Aβ16) (a), Cu(Aβ16) + L added @ t = 590 s (b) ; Cu(Aβ16) +Zn(L) added @ t = 560 s (c) ; Cu,Zn(Aβ16) + L added @ t = 570 s (c') ; Cu(Aβ16) + 5eq. Zn + L added @ t = 560 s (d). Left panel L = L_2 ; Right panel : L = L_C. [Cu(II)] = 10 µM, 1.2 equiv of Aβ, L and Zn. [Asc] = 0.1 mM, [hepes] = 100 mM, pH 7.1, T = 25°C.

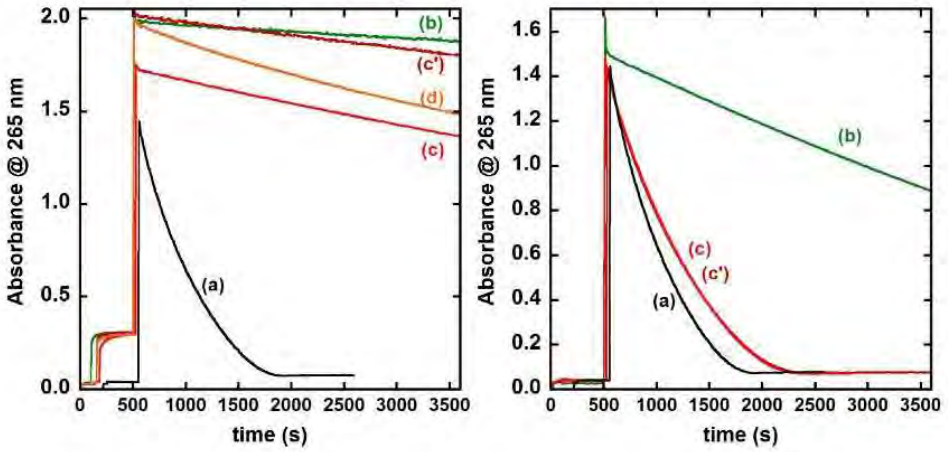

Figure S7. Cu(II) induced ascorbate consumption. Cu(Aβ16) (a), Cu(Aβ16) + L (b) ; Cu(Aβ16) +Zn(L) (c) ; Cu,Zn(Aβ16) + L (c') ; Cu(Aβ16) + 5eq. Zn + L (d). Ascorbate is added to trigger the reaction. Left panel L = L_2 ; Right panel : L = L_C. [Cu(II)] = 10 µM, 1.2 equiv of Aβ, L and Zn. [Asc] = 0.1 mM, [hepes] = 100 mM, pH 7.1, T = 25°C. Ascorbate is added at t ≈ 500 s.

Aggregation assay

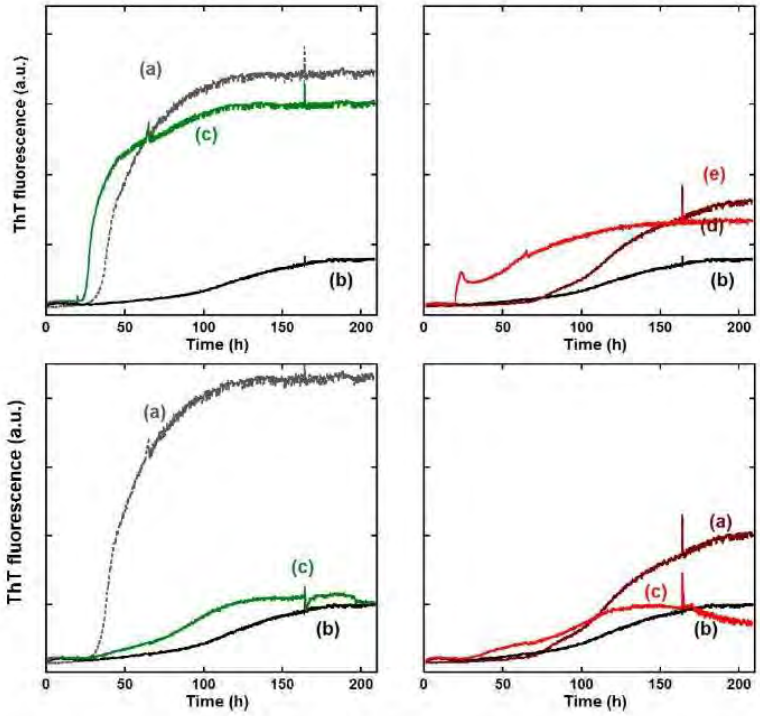

Figure S8. Kinetic measurement of amyloid fibrils formation using ThT Fluorescence. Left panel: (a) Aβ; (b) Cu(Aβ) and (c) Cu(Aβ) + L_2 added @ t = 20 h (top) and 162 h (bottom) ; Right panel: (a) Zn(Aβ); (b) Cu(Aβ) and (c) Cu(Aβ) + Zn(L_2) added @ t= 20 h (top) and 162 h (bottom). [Aβ] = [L_2] = [L_2-Zn] = 20 µM, [Cu] = [Zn] = 18 µM, [phosphate buffer] = 50mM, [ThT] = 10 µM, pH 7.1, T = 37°C.

When L_2 or Zn(L_2) addition is performed before the elongation phase, a trend similar to the one observed with an addition at t_0 is observed. The abrupt step in trace (c) of the top, right panel coincides with the addition of the Zn(L_2). In contrast, when L_2 or Zn(L_2) addition is performed later on, i.e. on the plateau phase, no modification of the ThT fluorescence is observed on the time scale of the experiment (two days), although Cu(II) is readily removed from the fibrils (Figure S9). This indicates that the transformation of Cu-induced oligomers, into fibrils is extremely slow in line with aggregation energetic profile.[15, 16]

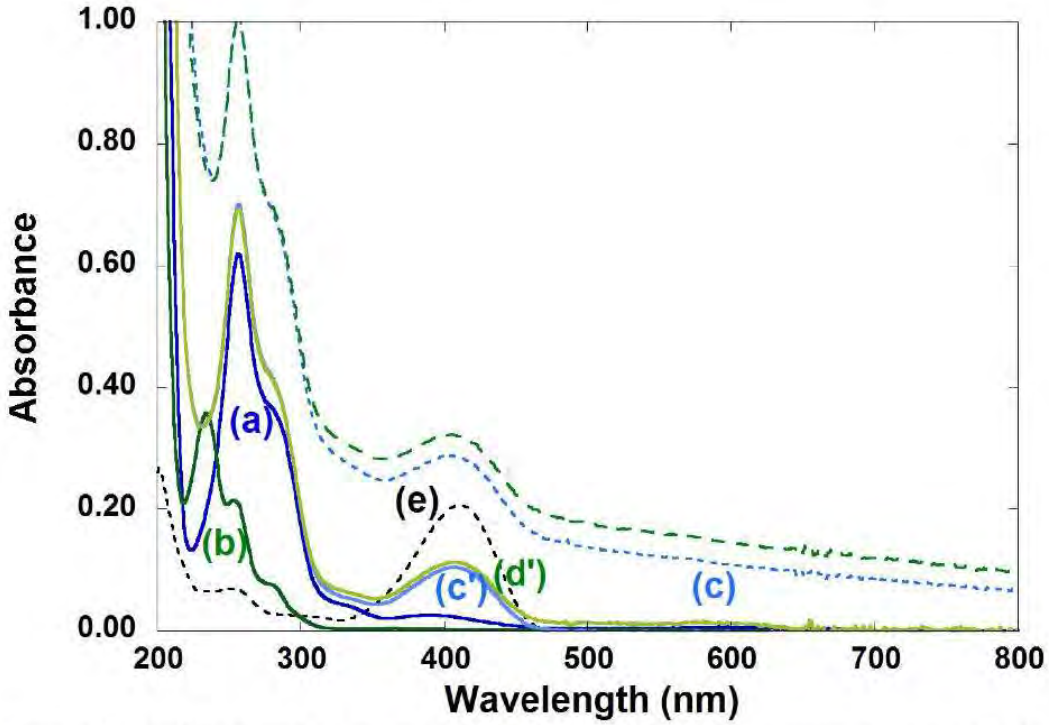

Figure S9. UV-Vis absorption spectra of $Cu(L_2)$ (blue, a) ; $Zn(L_2)$ (green, b) ; $Cu(A\beta)$ after aggregation and addition of L_2 @ t = 162 h (dotted light blue line, c) ; in the supernatant of $Cu(A\beta)$ after aggregation and addition of L_2 @ t = 162 h (plain light blue line, c') ; $Cu(A\beta)$ after aggregation and addition of $Zn(L_2)$ @ t = 162 h (dotted light green line, d) ; in the supernatant of $Cu(A\beta)$ after aggregation and addition of $Zn(L_2)$ @ t = 162 h (plain light green line, d') and free ThT (dotted black line, e); $[L_2] = [A\beta] = 20$ µM, [M] = 18 µM, [phosphate buffer] = 0.05 M, pH 7.1, [ThT] = 10 µM, T = 25 °C, ℓ=1 cm.

References.

1. T. Kowalik-Jankowska, M. Ruta, K. Wisniewska and L. Lankiewicz, *J. Inorg. Biochem.*, 2003, **95**, 270.
2. S. Noël, S. Bustos, S. Sayen, E. Guillon, P. Faller and C. Hureau, *Metallomics*, 2014, **6**, 1220.
3. I. Zawisza, M. Rozga and W. Bal, *Coord. Chem. Rev.*, 2012, **256**, 2297.
4. S. Noël, F. Perez, S. Ladeira, S. Sayen, E. Guillon, E. Gras and C. Hureau, *J. Inorg. Biochem.*, 2012, **117**, 322.
5. T. Storr, M. Merkel, G. X. Song-Zhao, L. E. Scott, D. E. Green, M. L. Bowen, K. H. Thompson, B. O. Patrick, H. J. Schugar and C. Orvig, *J. Am. Chem. Soc.*, 2007, **129**, 7453.
6. A. K. Sharma, S. T. Pavlova, J. Kim, D. Finkelstein, N. J. Hawco, N. P. Rath, J. Kim and L. M. Mirica, *J. Am. Chem. Soc.*, 2012, **134**, 6625.
7. A. Lakatos, v. Zsigo, D. Hollender, N. V. Nagy, l. Fülöp, D. Simon, Z. Bozso and T. Kiss, *Dalton Trans.*, 2010, **39**, 1302.
8. S. Lee, X. Zheng, J. Krishnamoorthy, M. G. Savelieff, H. M. Park, J. R. Brender, J. H. Kim, J. S. Derrick, A. Kochi, H. J. Lee, C. Kim, A. Ramamoorthy, M. T. Bowers and M. H. Lim, *J. Am. Chem. Soc.*, 2014, **136**, 299.
9. C. Deraeve, C. Boldron, A. Maraval, H. Mazarguil, H. Gornitzka, L. Vendier, M. Pitié and B. Meunier, *Chemistry- A European Journal*, 2008, **14**, 682.
10. J.-S. Choi, J. J. Braymer, R. P. R. Nanga, A. Ramamoorthy and M. H. Lim, *Proc. Natl. Acad. Sci. U. S. A.*, 2010, **107**, 21990.
11. A. P. Katkov, T. A. Matkovskaya, N. I. Krutikova, A. S. Monakhov and N. M. Dyatlova, *Russ. J. Inorg. Chem.*, 1991, **391**, 693.
12. T. Chen, X. Wang, Y. He, C. Zhang, Z. Wu, K. Liao, J. Wang and G. Zijian, *Inorg. Chem.*, 2009, **48**, 5801.
13. R. De Ricco, D. Valensin, S. Dell'Acqua, L. Casella, P. Dorlet, P. Faller and C. Hureau, *Inorg. Chem.*, 2015, **54**, 4744.
14. R. De Ricco, D. Valensin, S. Dell'Acqua, L. Casella, C. Hureau and P. Faller, *ChemBioChem*, 2015, **16**, 2319.
15. S. S. Leal, H. M. Botelho and C. M. Gomes, *Coord. Chem. Rev.*, 2012, **256**, 2253.
16. P. Faller, C. Hureau and O. Berthoumieu, *Inorg. Chem.*, 2013, **52**, 12193.

III-C The Cu(II) "pull-push" effect

This part focuses on a new concept: the "pull-push". It is composed on a theoretical explanation of the concept, an experimental section and the results obtained with three ligands.

III-C.i Theoretical concept

As previously explained, chelatotherapy is one of the therapeutic approach against AD. It exists different kind of chelators (for more details, see II-A.). Some of them have an affinity constant for Cu ions too high, meaning that they could remove essential Cu ions from other metalloproteins. Other chelators have a too low affinity constant for Cu ions; therefore they are likely not efficient against AD since Cu ions stay bound to the Aβ peptide. Lastly, some chelators have an affinity constant for Cu ions in the range of the one of the Aβ peptide. Thus, there is an equilibrium between Cu ions bound to Aβ and Cu ions bound to the chelator.

The importance of Zn ions on the Cu chelation has been demonstrated in III-B. Chelators with a higher affinity for Cu(II) than Aβ such as Lc are not yet able to remove Cu ions from Aβ in the presence of Zn ions. The thermodynamic explanation is the selectivity of Cu over Zn ions: to be an efficient Cu(II)-chelator in the presence of Zn ions, a selectivity of Cu(II) ions over Zn ions higher than the one for Aβ, which is of 4 orders of magnitude at pH 7.1, is needed (Table III-1, L >> Aβ). The following equilibria illustrate this phenomenon.

Equilibrium 1:

$M(II) + A\beta \leftrightarrow M(II) - A\beta$, with

$$K_M^{A\beta} = \frac{[M(II) - A\beta]}{[M(II)].[A\beta]}$$

Equilibrium 2:

$M(II) + L \leftrightarrow M(II) - L$, with

$$K_M^{L} = \frac{[M(II) - L]}{[M(II)].[L]}$$

Equilibrium 3:

$Cu(II) - A\beta + L \leftrightarrow A\beta + Cu(II) - L$, with

$$K_1 = \frac{[A\beta].[Cu(II) - L]}{[Cu(II) - A\beta].[L]} = \frac{K_{Cu}^{L}}{K_{Cu}^{A\beta}}$$

Equilibrium 4:

$Cu(II) - A\beta + Zn(II) - L \leftrightarrow Zn(II) - A\beta + Cu(II) - L$, with

$$K_2 = \frac{[Zn(II) - A\beta].[Cu(II) - L]}{[Cu(II) - A\beta].[Zn(II) - L]} = \frac{K_{Zn}^{A\beta}.K_{Cu}^{L}}{K_{Cu}^{A\beta}.K_{Zn}^{L}}$$

Equilibria 1 and 2 reflect the affinity constants of Aβ peptide or a ligand for a metal ion M, such as Cu or Zn ions. Equilibrium 3 is the equilibrium for the Cu removal from Aβ by a chelator L. Equilibrium 4 is the equilibrium for the Cu removal in the presence of Zn ions. K_1 and K_2 are the associated equilibrium constants. The following Table III-1 shows some examples of the impact of the selectivity of the chelator on the equilibrium 4. Note that the affinity constants of Aβ for Cu(II) and Zn(II) at pH 7.1 are approximately 10^9 and 10^5 M^{-1} respectively. The ideal chelator must have a selectivity at least equal to 7 order of magnitude in order to remove all Cu ions from Aβ in the presence of Zn ions. Note that the hypothesis is that all Cu ions are removed from Aβ when it stay 1/1000 of Cu ions bound to Aβ; the equilibrium constant being 10^3.

Table III-1. Table illustrating different cases for the equilibria 3 and 4. The percentages of Cu bound to L are also reported.

Cu(II) affinity constant of L	**K_1**	**% Cu(II)-L**	**Selectivity of L**	**K_2**	**% Cu(II)-L**
L >> Aβ $10^{11} >> 10^9$	10^2	90 %	10^1	10^{-3}	3 %
			10^4	1	50 %
			10^7	10^3	97 %
L = Aβ $10^9 = 10^9$	1	50 %	10^1	10^{-3}	3 %
			10^4	1	50 %
			10^7	10^3	97 %
L << Aβ $10^7 << 10^9$	10^{-2}	10 %	10^1	10^{-3}	3 %
			10^4	1	50 %
			10^7	10^3	97 %

The “pull-push” concept takes into account the fact that the addition of Zn ions can pull Cu ions out of the Aβ peptide and push it into the chelator. The chelator becomes more efficient in the removal of Cu ions in the presence of Zn ions than without. There are two main approaches for the “pull-push”.

The first one applies to chelators with an affinity constant close to the one for Aβ (10^9 M^{-1} at pH 7.1, see Table III-1, L = Aβ). This means that half of Cu ions is bound to Aβ peptide without Zn ions. Ideally, the addition of Zn ions should move the equilibrium 4 from about 50 % to near 100 % of Cu-L. This is the case if the selectivity of the chelator is at least 7 orders of magnitude (see Table III-1, L = Aβ); $K_{Cu}^{L} = 10^{8-9}$ M^{-1} and $K_{Zn}^{L} = 10^{1-2}$ M^{-1} at pH 7.1. The second approach applies to chelators with a very low affinity constant for Cu(II) (Table III-1, , L << Aβ). Note that if the affinity constant of the chelator for Cu ions is low, the selectivity cannot be equal to 7 orders of magnitude because the affinity constant for Zn ions is already very low and this is difficult to reach such affinities for only one molecule (the case of an affinity for Cu(II) at 10^7 and a selectivity at 10^7 is probably impossible to reach). In this second case, the addition of Zn(II) should move the equilibrium from about 10 % to 50 % of Cu(II) bound to L. The first approach is illustrated with three ligands and the experimental part is described in the following section.

III-C.ii Experimental section

Chemicals. Reagents were commercially available and were used as received. All the solutions were prepared in milliQ water (resistance: 18.2 MΩ.cm).

The Cu(II) ion source was $CuSO_4.5H_2O$, bought from Sigma-Aldrich. A stock solution was prepared at 25 mM. The Zn(II) ion source was $ZnSO_4.H_2O$, bought from Sigma-Aldrich. A stock solution was prepared at 100 mM.

HEPES buffer (sodium salt of 2-[4-(2-hydroxyethyl)piperazin-1-yl]ethanesulfonic acid) was bought from Sigma-Aldrich. A stock solution was prepared at 500 mM, pH = 7.1.

Ascorbate was bought from Sigma-Aldrich. A 5 mM stock solution was prepared in Milli-Q water just before beginning the experiments. Because ascorbate can be oxidized by air, a fresh solution was prepared every day.

Ligand and peptides. The 3,4-bis(oxamato)benzoic acid ligand L (see Figure III-2) was obtained from a collaboration with L. Lisnard (University Pierre et Marie Curie, Paris). For the synthesis, see ref.[1] A 8.5 mM stock solution was prepared, increasing the pH until solubilization, determined by UV-Vis titration with a titrated Cu(II) solution following the absorption band at 330 nm of the complex according to ref.[2].

Aβ16 (DAEFRHDSGYEVHHQK) and Aβ28 (DAEFRHDSGYEVHHQKLVFFAEDVGSNK) were bought from GeneCust (Dudelange, Luxembourg) with purity grade > 95 %. Stock solutions of the peptides

were prepared by dissolving powder in milliQ water (resulting pH ~ 2) and were titrated by UV-Vis absorption of Tyr10 considered as free tyrosine (at pH ~ 2.0, ε_{276} - ε_{296} = 1410 $cm^{-1}.M^{-1}$).[3]

ABH and BAH where B corresponds to the β-alanine amino acid were bought from Protéogenix (Strasbourg, France). The stock solutions were prepared by solubilizing the peptides in milliQ water and were titrated by UV-Vis with a titrated Cu(II) solution following the d-d band absorption of the complex at 545 nm and 536 nm respectively,[4] according to ref. [2]

Methods.

Electron Paramagnetic Resonance. Electron Paramagnetic Resonance (EPR) data were recorded using an Elexsys E 500 Bruker spectrometer, operating at a microwave frequency of approximately 9.5 GHz. Spectra were recorded using a microwave power of 5 mW across a sweep width of 120 mT (centred at 310 mT) with modulation amplitude of 0.5 mT. Experiments were carried out at 120 K using a liquid nitrogen cryostat.

EPR samples were prepared from stock solution of ligand diluted down to 0.2 mM in H_2O. 190 µM of $^{65}Cu(II)$ were added from 25 mM $^{65}Cu(NO_3)_2$ home-made stock solution from a ^{65}Cu foil. Samples were frozen in quartz tube after addition of 10% glycerol as a cryoprotectant and stored in liquid nitrogen until used.

X-ray Absorption Near–Edge Structure (XANES) spectra were recorded at the BM30B (FAME) beamline at the European Synchrotron Radiation Facility (ESRF, Grenoble, France).[5] The storage ring was operated in 7/8+1 mode at 6 GeV with a 200 mA current. The beam energy was selected using a Si(220) N_2 cryo-cooled double-crystal monochromator with an experimental resolution close to that theoretically predicted (namely ~ 0.5 eV FWHM at the Cu energy). The beam spot on the sample was approximately 300 x 100 μm^2 (H x V, FWHM). Because of the low Cu(II) concentration, spectra were recorded in fluorescence mode with a 30-element solid state Ge detector (Canberra) in frozen liquid cells in a He cryostat. The temperature was kept at 20 K during data collection. The energy was calibrated with Cu metallic foil, such that the maximum of the first derivative was set at 8979 eV. At least three scans recorded on different spots were averaged. The samples were prepared from stock solutions of ligand and Cu(II) diluted down to approx. 1.0 mM or 200 µM in buffered solution. Samples were frozen in the sample holder after addition of 10% glycerol as a cryoprotectant and stored in liquid nitrogen until used. Cu(II) photoreduction was avoided by changing the position of the beam between each scan. It was considered that during the first 20 minutes of recording (more or less one scan) the photoreduction is insignificant.

UV-Visible spectrophotometry. UV-vis spectra were recorded on a spectrophotometer Agilent 8453 at 25°C in 1 cm path length quartz cuvette, with stirring at 800 rpm.

Experiment illustrating the impact of Zn(II) on the Cu(II) removal from Aβ by the ligand L. The experiments have been monitored by UV-Vis in HEPES buffer 0.1 M at a resulting pH = 7.1. Aβ and Cu(II) (50 or 20 µM) were mixed and the ligand L (50 or 20 µM) was added. When the equilibrium is reached, successive additions of Zn(II) (0 to 20 equiv. in total) were added. Each addition of Zn(II) is made once the thermodynamic equilibrium of the previous reaction is reached.

ROS production experiment followed by Ascorbate consumption. The experiments have been monitored by UV-Vis in HEPES buffer 0.1 M at a resulting pH = 7.1. Ascorbate is diluted down 100 µM, the peptide and the ligands are at 12 µM and Cu(II) at 10 µM.

III-C.iii Illustration of the "pull-push" concept

To illustrate the "pull-push" concept, three chelators were used. Their structures are shown in Figure III-4. Note that L* stands for one of these ligands. The Cu(II) affinity constants of L, ABH and BAH are 3.2 10^9 M^{-1}, 3.0 10^8 M^{-1} and 3.7 10^9 M^{-1} at pH 7.1, respectively.[6] Note that these affinity constants are in the same range than the one of Aβ which is 1.6 10^9 M^{-1}.[1, 7] The calculations of the Equilibrium 3 give the K_1 values of 2.0, 0.2 and 2.3, respectively. These values indicate that in the absence of Zn(II), L and BAH removes ~ 60 % of Cu(II) from Aβ and ABH removes only 30 % of Cu(II). Note that the affinity constants for Zn ions of these three ligands is not known (but should be very low based on the structures of the ligands). The predictive calculations of Equilibrium 4 are not possible without these values. During this thesis, different experiments have been performed in order to know if these ligands are able to remove Cu(II) from Aβ, if the removal is in good agreement with the theory and what is the behavior of these ligands in the presence of Zn(II). First, EPR, then XANES and finally UV-Vis experiments are described.

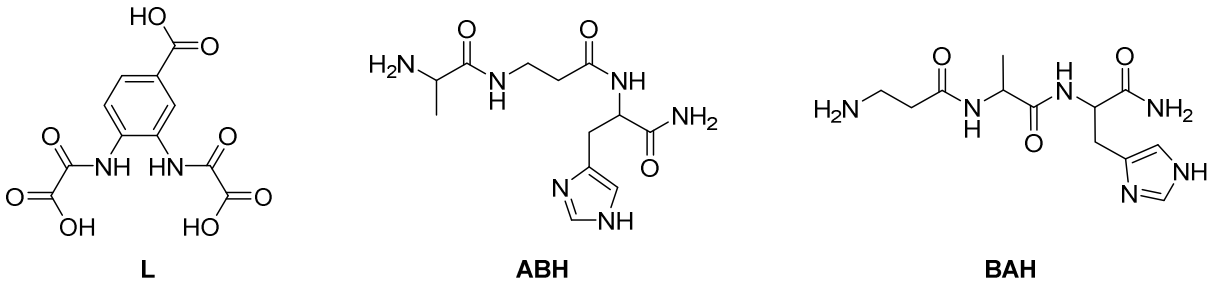

L **ABH** **BAH**

Figure III-4. Structures of the three ligands used in the "pull-push" concept. L is a synthetic ligand, ABH and BAH are synthetic peptides. B stands for the β-alanine.

III-C.iii.1 EPR experiments

Several EPR experiments have been performed. Figure III-5 shows one of them. A competition between Aβ and the ligands with or without Zn ions were carried out. For L, ABH and BAH, there is a good agreement with the thermodynamic calculations. Indeed, linear combinations of the EPR experiments shown in the Figure III-5 reveales that L removes 60 % of Cu(II) from Aβ, ABH 25 % and BAH 50 % (Table III-2). When Zn ions are also in competition, the percentages of the Cu(II) removal change. Using the calculations of the Equilibrium 4 and linear combinations of the EPR experiments (Figure III-5), the percentage in the presence of Zn(II) are 80 % of Cu(II) removed by L from Aβ, 45 % by ABH and 70 % by BAH (Table III-2). These experiments illustrate the "pull-push" effect. Note that there is a kinetic effect in the Cu(II) chelation. At t_0, meaning without incubation, ABH and BAH remove only 10 % of Cu(II) from Aβ, not consistent with the thermodynamic calculations. After t_1 (64 h in the fridge) ot t_2 (7h at room temperature), the percentages of Cu(II) removed from Aβ are consistent with the thermodynamic caluclations (Table III-2). Furthermore, the percentages obtained for Equilibria 3 and 4 change between the different experiments, but stay by less than 10 %.

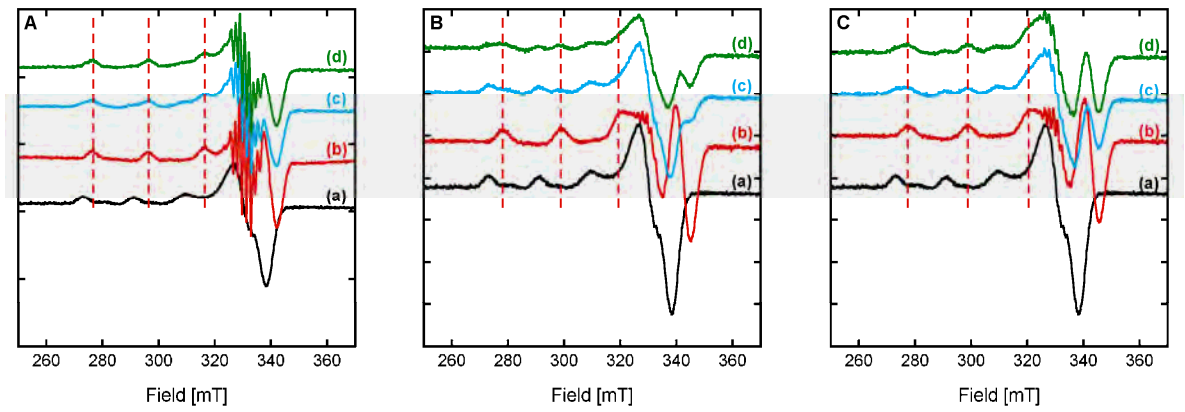

Figure III-5. EPR experiments of competition between Aβ and L (Panel A), ABH (Panel B) or BAH (Panel C). (a) Aβ + Cu(II), (b) L + Cu(II), (c) Aβ + Cu(II) + L*, (d) Aβ + Cu(II) + Zn(II)-L*. (L* = L, ABH or BAH). [L*] = [Aβ] = [Zn(II)] = 200 µM, [^{65}Cu(II)] = 190 µM, [HEPES] = 50 mM. pH = 7.1. T = 110 K. 10 % of glycerol was used as gryoprotectant. The incubation time for experiments for L and ABH is 64 h in the fridge, 7 h at room temperature for BAH.*

Table III-2. Table reporting the percentages of Cu(II) removed by the ligands from Aβ without and with Zn(II).

	Without Zn(II)	**With Zn(II)**
L	60 %	80 %
ABH	25 %	45 %
BAH	50 %	70 %

III-C.iii.2 XANES experiments

XANES is a very appropriate technique to probe the environment of Zn ions since they are silent in most of the classical spectroscopic techniques. XANES allows to follow Cu and Zn ion chelation in the same time and with the very same sample. Therefore, in order to illustrate the "pull-push" effect, XANES appears to be a very well appropriate technique.

Different experiments have been performed. The first two ones have been monitored with ligand, metal ions and the Aβ28 peptide at approximately 1 mM, minimal concentration required for our XANES conditions. Note that Aβ16 has not been used in order to limit the precipitation of Zn(II)-Aβ. The same experiments than for the EPR are carried out: Aβ + Cu(II) + L* and Aβ + Cu(II) + Zn(II)-L*. In the presence of Zn(II), even if Aβ28 was used, there was an issue with the precipitation. The "pull-push" effect was visible for the three ligands, leading to more or less 100 % of Cu(II) bound to the ligand in the presence of Zn(II). The "pull-push" effect worked well, maybe too well and was not consistent with the EPR experiments. The precipitation of Zn(II)-Aβ displaces the equilibrium through the formation of Zn(II)-Aβ (see Equilibrium 5 below). This implicates that the equilibrium goes towards the chelation of Cu(II) by L*. This is the reason why Cu ions are removed from Aβ by L* but this is not due to the "pull-push" effect only.

Equilibrium 5:

$$\text{Cu(II)-A}\beta + \text{Zn(II)} + \text{L*} \Longrightarrow \underline{\text{Zn(II)-A}\beta} + \text{Cu(II)-L*}$$

The other experiment was performed with Aβ16 at 200 µM; a concentration at which Zn(II)-Aβ does not precipitate. Nevertheless, 200 µM being a too low concentration for the beamline and detectors used; 1 mM is more or less the lower limit. To overcome this problem, 12 scans were accumulated instead of 3 when the concentration was around 1 mM. However, the spectra obtained were not exploitable. The noise of the spectra is too important, precluding any kind of calculations. In the ESRF at Grenoble where XANES was carried out, a new beamline for highly diluted samples has just opened. It could be interesting to perform these competition experiments in this beamline. However, all the current XANES results are useless.

III-C.iii.3 UV-Vis experiment for L

As previously described in ref.[1], Cu(II)-L exhibits an important absorbance at 330 nm, ε = 18 000$cm^{-1}.M^{-1}$. Therefore, the "pull-push" effect can be follow by the detection of Cu(II)-L. This is a preliminary experiment. First, Aβ is complexed with Cu(II). Then, one equivalent of L is added. When

the equilibrium is reached, one by one equivalent of Zn(II) is added, until 5 equivalents. Figure III-6 shows the kinetic of the formation of Cu(II)-L at 330 nm. Table III-3 exhibits the absorbance and the experimental percentages of Cu(II) bound to L, as a function of the number of equivalents of Zn(II). Without Zn(II), the percentage of Cu(II) bound to Aβ is quite high compare to what is expected based on the K_a values (78 % vs. 60 %). This may be due to a too high concentration of L in the cuve. The addition of each equivalent of Zn(II) until 5 equivalents increases the quantity of Cu(II) bound to Aβ until 100 %. For L, 4 or 5 equivalents of Zn(II) are needed to push all Cu(II) in the chelator.

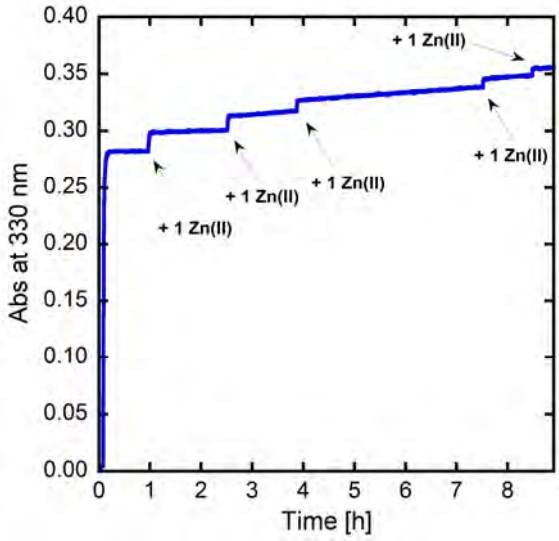

Figure III-6. Kinetic of formation of Cu(II)-L, followed by UV-Vis spectroscopy at 330 nm. [Aβ] = [L] = [Cu(II)] = 20 µM, Zn(II) is added equivalent by equivalent. [HEPES] = 100 mM, pH = 7.1, 25°C.

Table III-3. Table bringing together the values of absorbance of Cu(II)-L as a function of the number of added equivalent of Zn(II). The percentages of Cu(II) bound to L compared to the total Cu(II) are given.

Number of equivalents	0	1	2	3	4	5
Abs (330 nm)	0,28	0,30	0,32	0,34	0,35	0,36
% Cu(II)-L	78 %	83 %	89 %	94 %	97 %	100 %

This experiment is not possible for the other two ligands ABH and BAH because they do not exhibit an important absorbance when bound to Cu(II). Nevertheless, a fluorescence experiment could be carried out. Indeed, it is possible to add an extrinsic fluorophore to the ligand (strategy A) or to use the fluorescence of the tyrosine residue of Aβ (strategy B)[8] and, as the paramagnetism of Cu(II) quenches the fluorescence, it is possible to determine if Cu(II) is bound to Aβ or to the ligand. For the strategy A, if Cu(II) is bound to the ligand, there will be exctinction of the fluorescence contrary to if Cu(II) is bound to Aβ (detection of the fluorescence from the ligand). For the strategy B, this is the opposite.

III-C.iii.4 ROS production experiments

As previously explained, the ligands have to stop the ROS production. To monitor this, Ascorbate consumption assay has been performed. The results are shown in the Figure III-7. Cu(II)-L* produces ROS. Different kind of experiments have been monitored: a pre-incubation of Cu(II) and L* before adding Ascorbate, use of 10 equivalents of L* to preclude the free Cu (the used concentrations are very low), but Cu(II)-L* produces ROS. Up to now, it is very difficult to understand why these complexes catalyse the ROS production. Note that the "pull-push" concept cannot be seen with the ROS production experiments since Cu(II)-L* doesn't stop the ROS production.

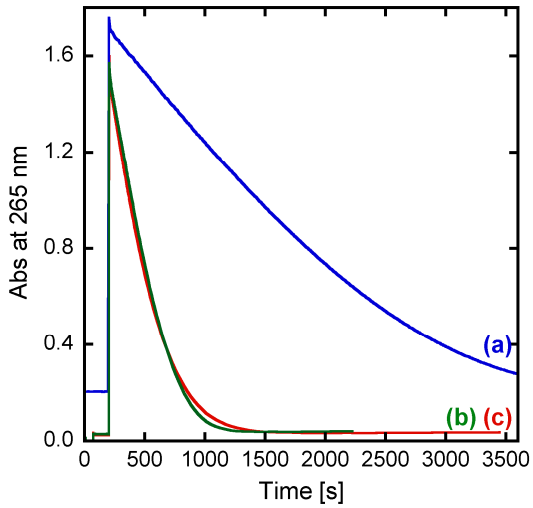

Figure III-7. ROS production followed by the consumption of Ascorbate by UV-Vis spectroscopy, at 265 nm with a background correction at 800 nm. (a) L + Cu(II) + Asc, (b) ABH + Cu(II) + Asc, (c) BAH + Cu(II) + Asc. [L] = 12 µM, [Cu(II)] = 10 µM, [Asc] = 100 µM, [HEPES] = 100 mM, pH = 7.1, T = 25°C.*

III-C.iv Conclusion

In this part, the "pull-push" concept is described (Figure III-8). It consists in pulling Cu(II) out from the Aβ by the presence of Zn(II) and pushing Cu(II) into the chelator. The ligands able to do the "pull-push" have an affinity constant for Cu(II) in the same range or below than the one of Aβ. Their selectivity for Cu over Zn ions has to be higher than the one of Aβ in order to remove almost all Cu(II) from Aβ in the presence of Zn(II). Three ligands (L* = L, ABH and BAH) have been probed for the "pull-push" concept by EPR, XANES and UV-Vis spectroscopies. One equivalent of Zn(II) increases the quantity of Cu(II) removed from Aβ and chelated by L*. In the case of L, 5 equivalents of Zn(II) are needed to remove all Cu(II) from Aβ. For the other two ligands, fluorescence experiments would have to be carried out in order to know the number of equivalents of Zn(II) to remove «all» Cu(II) from Aβ. Note that it is quite difficult to monitor the "pull-push" experiments due to precipitation issues of Zn(II)-Aβ.

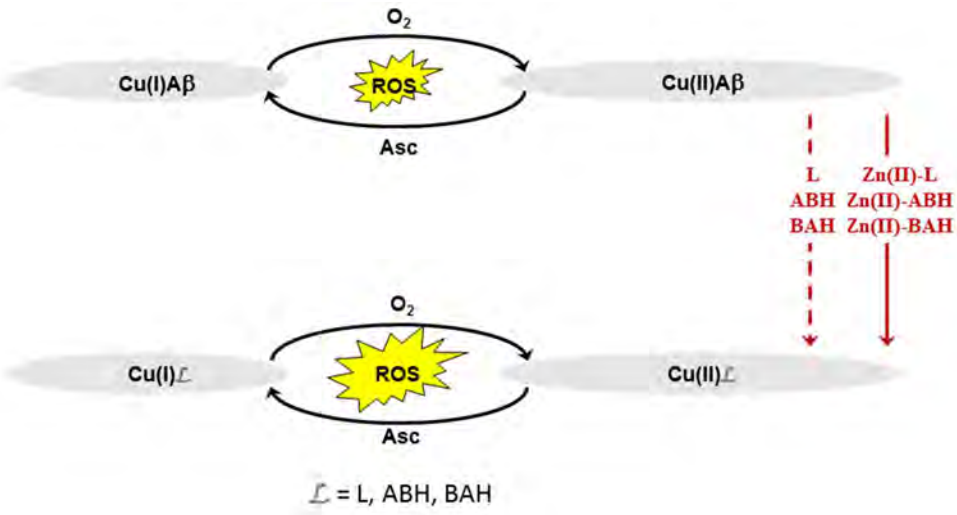

Figure III-8. Scheme representing the "pull-push" concept, with the three ligands studied here.

L, ABH and BAH are good "pull-push" ligands. The problem is that they are not able to stop the ROS production; but they illustrate quite well the "pull-push" concept. It would be interesting to determine their affinity constant for Zn(II). Indeed, for example, in case of L, 5 equivalents and not only one are needed to remove all Cu(II) from Aβ, the Cu over Zn ion selectivity of L should be too low. Nevertheless, Zn(II) concentration in the synaptic cleft is 10 to 100 times higher than Cu ions, the need of 5 equivalents might not be a problem *in vivo*.

Note that the "pull-push" concept is a thermodynamic concept. It does not take into account kinetic issues. Furthermore, it is difficult to understand why the Cu(II)-L* complexes are not able to stop the ROS production. Maybe the conditions needed to fulfill the criteria of the affinity and selectivity for a "pull-push" ligand preclude it to stop the ROS production (geometry and kinetic issues?).

Studying ligands with a very low affinity constant for Cu(II) to illustrate the second approach of the "pull-push" concept would be also interesting.

III-D Conclusion

This part focuses on the impact of Zn ions on the Cu(II) chelatotherapy against AD. It has been proposed that depending on the Cu(II) affinity constant and on the Cu(II) over Zn selectivity of the ligand, Zn ions can preclude the Cu(II) removal from Aβ or can trigger it. Both of these parameters are very important in the design of ligands against AD.

Maybe the better strategy would be the pro-drug one described with the “pull-push” concept. Indeed, for this strategy, the ligands have a low Cu(II) affinity constant, meaning that they could not be able to remove Cu(II) *in vivo* from any protein. Nevertheless, with a Cu(II) over Zn(II) selectivity around 10^5-10^6 (or higher if possible), the ligand is able to remove Cu(II) from Aβ only in the presence of Zn ions, as for example in the Zn(II)-rich synaptic cleft.

Zn ions are ejected from the neuron to the synaptic cleft and are re-taken very rapidly, meaning that Zn levels fluctuate constantly up and down. One can wonder if the important parameter of the kinetic of Cu(II) removal (detailed in the section II-2) is also important in the presence of Zn ions. It seems that it is always very important. The ligand needs a very important selectivity of Cu(II) over Zn to not chelate Zn ions during the ejection of these pools of Zn(II). Furthermore, the ligand needs to chelate Cu(II) very fast, as not to chelate Zn ions instead of Cu(II) ions. Some preliminary experiments have been performed, showing that, *in vitro*, even with a fast Cu(II) chelation, a ligand can chelate first Zn ions, leaving Cu(II) ions bound to Aβ. More studies are needed to understand how this issue could be resolved.

Another important parameter to take into account is the impact of other ions such as Ca or Fe ions or other biomolecules on the Cu(II) chelation. Indeed, Zn has been studied first because it is present in very high concentrations in the synaptic cleft. Nevertheless, as the impact of Zn is not insignificant, other molecules could also have an effect and it could be of interest to study the importance of this.

References

1. Conte-Daban, A.; Borghesani, V.; Sayen, S.; Guillon, E.; Journaux, Y.; Gontard, G.; Lisnard, L.; Hureau, C., Link between Affinity and Cu(II) Binding Sites to Amyloid-beta Peptides Evaluated by a New Water-Soluble UV-Visible Ratiometric Dye with a Moderate Cu(II) Affinity. *Anal. Chem.* **2017,** *89* (3), 2155-2162.
2. Hureau, C.; Eury, H.; Guillot, R.; Bijani, C.; Sayen, S.; Solari, P. L.; Guillon, E.; Faller, P.; Dorlet, P., X-Ray and solution structures of CuGHK and CuDAHK complexes. Influence on their redox propertieS**.** *Chem. Eur. J.* **2011,** *17* (36), 10151-10160.
3. Faller, P.; Hureau, C.; Dorlet, P.; Hellwig, P.; Coppel, Y.; Collin, F.; Alies, B., Methods and techniques to study the bioinorganic chemistry of metal-peptide complexes linked to neurodegenerative diseases. *Coord. Chem. Rev.* **2012,** *256* (19-20), 2381-2396.
4. Nagaj, J.; Stokowa-Sołtys, K.; Zawisza, I.; Jeżowska-Bojczuk, M.; Bonna, A.; Bal, W., Selective control of Cu(II) complex stability in histidine peptides by β-alanine. *J. Inorg. Biochem.* **2013,** *119*, 85-89.
5. Proux, O.; Biquard, X.; Lahera, E.; Menthonnex, J. J.; Prat, A.; Ulrich, O.; Soldo, Y.; Trévisson, P.; Kapoujvan, G.; Perroux, G.; Taunier, P.; Grand, D.; Jeantet, P.; Deleglise, M.; Roux, J.-P.; Hazemann, J.-L., FAME: A new beamline for X-ray absorption investigations of very-diluted systems of environmental, material and biological interests. *Phys. Scr.* **2005,** *115*, 970-973.
6. Nagaj, J.; Stokowa-Sołtys, K.; Zawisza, I.; Jeżowska-Bojczuk, M.; Bonna, A.; Bal, W., Selective control of Cu(II) complex stability in histidine peptides by β-alanine. *J. Inorg. Biochem.* **2013,** *119*, 85–89.
7. Kowalik-Jankowska, T.; Ruta, M.; Wiśniewska, K.; Łankiewicz, L., Coordination abilities of the 1–16 and 1–28 fragments of β-amyloid peptide towards copper(II) ions: a combined potentiometric and spectroscopic study. *J. Inorg. Biochem.* **2003,** *95* (4), 270-282.
8. Alies, B.; Renaglia, E.; Rózga, M.; Bal, W.; Faller, P.; Hureau, C., Cu(II) Affinity for the Alzheimer's Peptide: Tyrosine Fluorescence Studies Revisited. *Anal. Chem.* **2013,** *85* (3), 1501-1508.

General conclusion

Along this thesis, different proofs of concept regarding the Cu chelatotherapy against AD are described. The studies are split into two main parts: on one hand, the Cu chelation by a ligand from the Cu-Aβ complex and on the other hand the impact of Zn ions on this Cu chelation. Several questions were outlined in the introduction and the answers are given below.

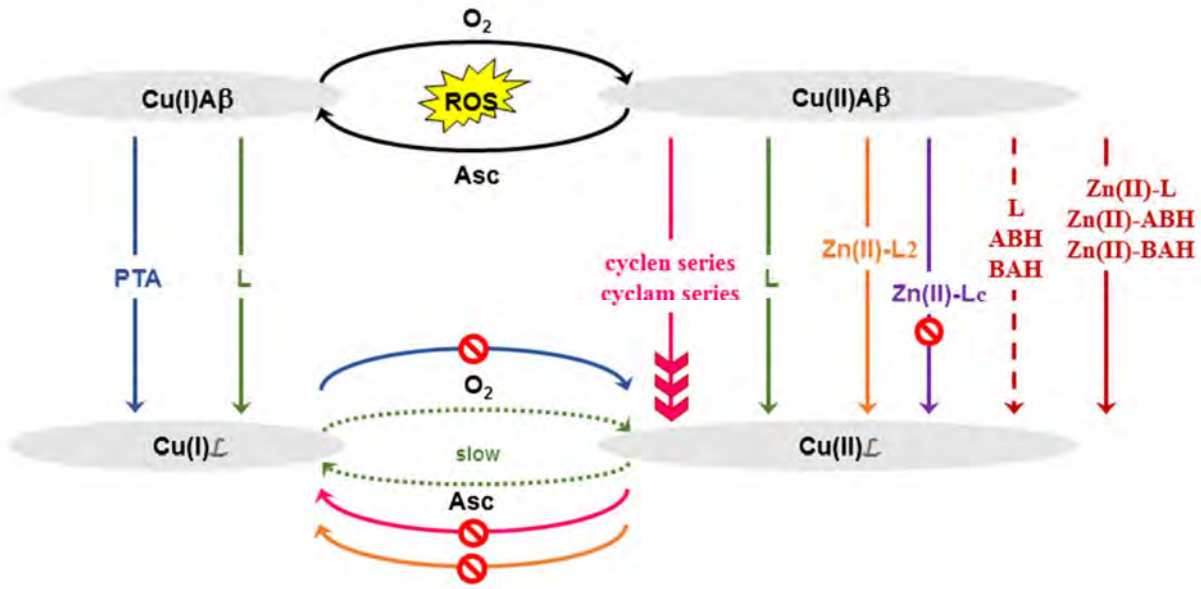

Figure 1. Summary scheme of the different ligands studied in this thesis. Note that the blue part (PTA) is described in Annexe 1 and focuses on a Cu(I) chelator. Solid arrows describe a quasi-total Cu ion removal by the ligand from Aβ. A dotted line describes an equilibrium. An arrow with special arrow head describes a fast kinetic in the Cu removal from Aβ by a ligand.

The first proof of concept detailed in this thesis is about the possible kinetic issue in the Cu chelation (Figure 1, pink). The first question was:

- Does the kinetic of Cu chelation by a ligand have an impact on the ROS production catalysed by Cu-Aβ complex?

To address this question, cyclen and cyclam macrocyclic ligands have been studied. The production of ROS has been monitored. Indeed, they can stop the ROS production only if they are pre-incubated with Cu(II)-Aβ (allowing formation of the Cu(II)-complex with the macrocyclic ligands) before the addition of the reductant since the Cu chelation by these ligands is too slow. Thus, this demonstrates the impact of the Cu(II) chelation kinetic on the arrest of the ROS production by Cu-Aβ.

- How is it possible to avoid that the ligands fail in the removal of Cu ions due to kinetic reasons (despite thermodynamically favoured) when designing a ligand against AD?

One of the possible answers is the addition of chelating arms. Indeed, cyclen and cyclam have been substituted with one or two picolinate arms. The following of the ROS production has also been performed with the substituted ligands. They are able to chelate Cu(II), even when it is found redox cycling during the ROS production, meaning that even in the presence of a mixture of Cu(I)/Cu(II), the substituted ligands are able to remove Cu from Aβ and stop the ROS production associated. In this case, there is no more need of incubation. Note that in the present case, the addition of chelating arms increases the Cu(II) chelation kinetic. Nevertheless, this strategy of adding chelating arms should not be efficient for all the ligands with Cu(II) chelation kinetic issues. Indeed, the addition of arms on linear ligands or macrocyclic ligands with another kind of cavity for example should not change the kinetics.

- *Does the complex geometry have an impact on the kinetic of the Cu chelation?*

Based on the results, as cyclam and cyclen complexes do not have the same geometry and present different behaviours regarding the Cu(II) removal from Aβ, the geometry of the complex could have an impact on the kinetic of the Cu chelation. Indeed, the Cu ion is found outside the cavity of the macrocycle for cyclen whereas it is inside the cavity for the cyclam. It should take more time to enter the cavity than to stay upon the cavity. Indeed, the Cu chelation by the cyclam is slower than for the cyclen.

We have been able to, by this first proof of concept, describe the importance of the kinetic on the Cu chelation approach.

The second proof of concept on the Cu chelatotherapy is about the choice of the target (Figure 1, green). Indeed, Cu is the target, but the redox state of the Cu to target is not defined. The issue is that the redox state of Cu in the synaptic cleft is not known. Therefore, using a Cu(II) or Cu(I) chelator should be useless, meaning that a Cu(I) chelator is not able to remove Cu(II) from Aβ and *vice versa*. The first two questions were:

- *Which redox state of Cu ions should be targeted by the ligand to efficiently remove Cu ions from Aβ? Cu(I), Cu(II) or both?*

As the redox state of Cu is not known, the ligand should target both of them. Thus, it would be interesting to compare the *in vivo* efficiency of a Cu(II), a Cu(I) and a Cu(I/II) chelator.

- *Is it possible to target both redox states? If yes, is there a risk that the Cu-complex formed with the ligand itself can produce efficiently ROS by cycling between Cu(I) and Cu(II)? What parameters should be considered?*

It can be possible to chelate both redox states and there is a risk to produce ROS, but this is not mandatory. Note that chelating both redox states could also be done by a mixture of a Cu(II) and a Cu(I) chelator. In this part, a ligand L has been studied. It is able to chelate both Cu(II) and Cu(I) and there is no more production of ROS when L is added to Cu-Aβ. The hypothesis to explain this

phenomenon is the difference between the Cu(I) coordination and geometry and the Cu(II) ones. Indeed, the coordinating ligands are not exactly the same as well as the geometry. It takes time to switch from one Cu complex (*e.g.* Cu(I) complex) to the other one (*e.g*. Cu(II) complex).
This can explain the fact that the ligand can chelate both redox states without producing ROS. This shed light also the importance of the design of the ligand.

The last part of this thesis focuses on the impact of Zn ions on the Cu chelation since the concentration of Zn ions in the synaptic cleft is much higher than the one of Cu ions. The third proof of concept focuses on the thermodynamics (Figure 1, orange and purple). In the absence of Zn(II), a higher affinity constant for Cu of the ligand than Aβ is sufficient to remove Cu ions from Aβ (if the kinetic is favourable).

- *Is it also the case in the presence of Zn ions?*

Based on the results obtained with the ligands L2 and Lc, Zn(II) can preclude the Cu(II) removal from Aβ while in the absence of Zn(II), the Cu(II) removal by the ligand was possible. Both L2 and Lc have higher affinity constants for Cu and Zn than the ones of Aβ. The difference between themselves is the selectivity of Cu(II) over Zn ions (with the selectivity being the ratio between the affinity constant for Cu(II) and the one for Zn(II)). The selectivity for L2 is higher than the one for Aβ while the selectivity for Lc is lower than the one for Aβ. Both L2 and Lc can remove Cu(II) from Aβ, while in the presence of Zn ions, only L2 is able.
This part highlights the importance of the selectivity of Cu over Zn ions on the Cu chelation. Not only the affinity constant is important, but also the selectivity compared to one for Aβ.

Finally, the last proof of concept describes the “pull-push” effect (Figure 1, red). The pull-push effect is the fact that for a category of ligand, Zn ions pull Cu ions out from the Aβ and push them inside the ligand.

- *Is a ligand with an affinity constant for Cu in the same range than A*β *able to remove totally Cu from A*β*? Can Zn(II) help the ligand to chelate Cu ions from A*β *in this case?*

The “pull-push” concept illustrates that a Cu chelator, with an affinity constant around the one of Aβ, can remove almost all Cu(II) bound to Aβ, only in the presence of Zn(II). Indeed, the ligands for the “pull-push” need an affinity constant for Cu in the same range than the one for Aβ and a selectivity of Cu over Zn ions higher than the one for Aβ. Without Zn(II), Cu ions are bound to Aβ and to the ligand in an equilibrium. In the presence of Zn(II), when the “pull-push” effect occurs, more Cu ions are bound to L than to Aβ, for the same ligand.
This can be useful in the AD context: le ligand is not able to remove « healthy » Cu ions except in a Zn-rich environment such as the synaptic cleft, where Cu ions are toxic.

Then, it would be interesting to investigate the impact of the selectivity regarding Cu(I) on the Cu removal from Aβ. Indeed, as Zn ions impact the Cu(II) chelation by a ligand, they could also impact the chelation of Cu(I). Furthermore, the impact of Zn(II) on the kinetic of Cu binding is also an important parameter to study. Preliminary experiments have been performed and show that *in vitro*, Zn can preclude the Cu chelation. Indeed, Zn ions can be first chelated by the ligand and the dissociation time is very long, meaning that Cu will stay bound to Aβ. Other studies on the kinetic issue are the addition of arms on chelators such as ABH. Indeed, with this kind of ligands, Cu(II) needs to deprotonate an amide to be chelated. This takes time and the addition of chelating arms can be of help in the Cu removal from Aβ. Regarding the "pull-push" concept, the study of the second approach, i.e. the ligand with a very weak affinity constant for Cu(II) and a quite good selectivity, would be interesting as well as the study of the "pull-push" Cu(I)-Zn. Another investigation regarding the Cu chelation is the use of a Mn-complex as a pro-chelator. The idea is to use a superoxide dismutase mimic complex able to stop the ROS production as a ligand against AD. Preliminary experiments show that a swap of metallic ions, Cu and Mn, between Aβ and the complex occurs, stopping the associated deleterious events of Cu-Aβ. Furthermore, the metallophoric capabilities of the ligand should also be studied in order to re-equilibrate the homeostasis in the brain.

Later, the idea would be to gather these criteria in only one ligand with the already known criteria (BBB permeability, the intrinsic toxicities of the ligand and the Cu-complex): a fast Cu(I) and Cu(II) chelation, quite low affinity constants for Cu(I) and Cu(II) in order to not remove "healthy" Cu(II) and Cu(I), a Cu over Zn selectivity allowing the Cu(I) and Cu(II) chelation only in the presence of Zn ions. Then, it will be interesting to understand if other criteria are needed or not. Actually, the answer would be yes, it is needed more criteria for an efficient ligand *in vivo*. For example, the Cu(II)-complex BBB permeability, its metabolism and finally its excretion have to be studied. Furthermore, as Zn ions have an important impact on the Cu chelation, other biomolecules or cations can also alter it. It would interesting to study the impact of Ca(II), Fe(II/III) for example or also some amino acids, the acetylcholine, etc., on the Cu chelation from thermodynamic and kinetic aspects.

Annexes

A- Determination of the affinity constant of Aβ peptide for Cu(II)

This section focused on the determination of the affinity constant of Aβ peptide for Cu(II), using a new water soluble UV-Visible dye. It is composed of a summary of the article published in *Analytical Chemistry* in 2017, the publication itself and finally the supporting information. The results reported have been obtained in collaboration with two groups. The organic and inorganic synthesises as well as the crystallographic characterisation of the water-soluble dye have been performed by Laurent Lisnard and his colleagues (at the University *Pierre et Marie Curie*, in Paris), and the fitting of the EXAFS experiment by Stéphanie Sayen and Emmanuel Guillon (at *Institut de chimie moléculaire*, in Reims). I have co-written the first draft of the paper with Valentina Borghesani.

A-i. Summary

This article reports the use of a new water soluble UV-Visible dye **L** (Figure 1) to determine the affinity constant of Aβ peptide for Cu(II). This is an important parameter for the design of ligands in a therapeutic approach relying on chelation because the chelators need an affinity constant for Cu(II) higher than Aβ. Many works were previously reported and the affinity constant values obtained ranged from 10^{6} M^{-1} to 10^{19} M^{-1} at pH 7.4. More recently, a consensual have been proposed by our group around 10^{10} M^{-1} at pH 7.4. Most of these studies used potentiometric titrations, isothermal calorimetry, and fluorescence or competition experiments. In the present article we describe the use of a competition experiment with a new UV-Visible dye that confirms the previous value. In addition, the affinity constants for Cu(II) of mutated Aβ peptides are determined with this method; the results obtained are consistent with the coordination site of Cu(II) to Aβ at pH 7.1.

The first part of the study focuses on the organic and inorganic synthesises of the UV-Visible competitor **L** (Figure 1), with a crystallographic characterisation of the Cu(II) complex. EXAFS and EPR experiments are performed to define the Cu(II) coordination in solution. Both in crystals and in solution, this complex has the same coordination mode: two nitrogens and two oxygens bind the metal ion. The Cu(II)-**L** complex exhibit an intense absorbance band at 330 nm.

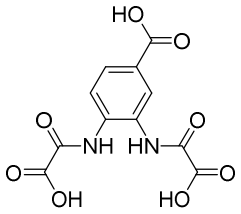

*Figure 1. Scheme of the ligand **L**.*

A second part is dedicated to the determination of the affinity constant of the UV-Visible dye **L** for Cu(II), at pH 7.1. Two three-amino-acid peptides, ABH and BAH (B stands for β-alanine) which affinity constant for Cu(II) are known, are used for a competition experiment. **L** is first added in the solution, then Cu(II), and after around 30 minutes, one of the peptides is added. When the thermodynamic equilibrium is reached, another equivalent of the peptide is added, and this until 10 equivalents of peptides. During the experiment, the absorbance of the Cu(II)-**L** complex is followed, and plotted as a function of the number of added equivalent of peptides. Then, with an home-made fitting, the affinity constant of **L** for Cu(II) is determined and the average value is $3.2 \pm 1.0 \times 10^9$ M^{-1} at pH 7.1.

A third part of this article focuses on the main issue of this work: the determination of the affinity constant of Aβ for Cu(II). Because the first sixteen amino-acids are responsible of the metal ions chelation, the competition experiment is performed with the Aβ16. The same competition, changing the ABH and BAH peptides by the Aβ peptide, and the same home-made fitting than for the determination of the affinity constant for Cu(II) of **L** are performed. The average value is 1.6×10^9 M^{-1}. This value is in line with previous report proposed by Kowalik-Jankowska *et al*. where potentiometric titration was used. Then, the affinity constants of Aβ28 and Aβ40 have been evaluated. As they are closed to the one of Aβ16, Aβ16 is a good model of the entire peptide with respect to Cu(II) coordination.

The last part is about the coordination of Cu(II) with Aβ. A wide series of Aβ16 mutants is used to determine which amino acid is involved in the Cu(II) coordination (if the affinity constant of the mutant changes, this is because the amino acid mutated is involved in the coordination). Note that the Cu(II) coordination is already well known. Therefore, if with this technique, the same Cu(II) coordination is proposed, this competition method with **L** can be claimed as a robust method. A first kind of mutant is studied: the N-terminal amine involved in the Cu(II) coordination is acetylated, preventing its Cu(II) binding ability. The impact of this mutation on the affinity constant is very important and the value cannot be determined precisely by the competition with **L** due to its too low value. This impact confirms that the N-terminal amine is strongly involved in the Cu(II) coordination. A second class of mutants is the carboxylate to amide change, carboxylate residues coordinating the metal ion in an

apical position. The affinity constants obtained for these mutants are lower than those of the wild-type Aβ, but higher than the acetylated peptide. This result is consistent with the literature: the apical position is less important in the Cu(II) coordination than the equatorial position. Furthermore, for the apical position, 4 ligands are in exchange, thus one mutation of a carboxylate group affects the Cu(II) coordination but not in an important way because three other ones remain. A last type of mutations is the Histidine to Alanine or to Arginine mutations. Cu(II) is coordinated by His6 and His13 or His14, in a dynamic exchange. The affinity constants measured with the competition experiment are in line with this coordination binding: the values for the peptides with the mutation H6A or H6R are close to each other and lower than those of the peptide with H13A and H14A. His6 has a stronger impact on the Cu(II) coordination with Aβ. Another study is performed with the murine Aβ. This peptide has 3 mutations compared to the human one: R5G, Y10F and H13R. The affinity constant for Cu(II) of the human mutants of Aβ corresponding to the mutations involved in the murine peptide are also evaluated with this method. Consistent results are also obtained. Indeed, the affinity constant of the murine peptide is twice stronger than the one of the human Aβ, as proposed in the literature. The R5G mutation is the most important one and the affinity constant of the associated mutant is the same than the murine. This is due to the formation of the 6-membered metallacycle between the peptidic bond Gly5-His6 and the His6. This formation of metallacyle stabilizes the Cu(II) complex, increasing its affinity constant.

These experiments allow to propose that **L** is a good competitor to determine the affinity constant of peptides or proteins with a moderate affinity constant for Cu(II). The validation of the Cu(II) coordination using different mutants also supports the reliability of **L**. This method is easy to handle do to the important absorbance of the Cu(II)-L complex. Indeed, only a UV-Vis spectrophotometer is required and a small quantity of **L** and peptide is needed. Furthermore, by UV-Vis, there is no bleaching of the dye, no inner filter effect, etc. Note that for the determination of the affinity constant of a peptide at another pH than pH 7.1, the affinity constant for the competitor **L** has to be determined previously. For peptides or proteins with lower or higher affinity constants, modifications of **L** are needed to adapt its affinity constant in the appropriate range.

This article proposes a consistent affinity constant of Aβ for Cu(II), at 1.6×10^{9} M^{-1}. This is an important parameter to know, for the development of new ligands able to remove Cu(II) from Aβ in a therapeutic approach based on chelation.

A-ii. Article

analytical chemistry

Article

pubs.acs.org/ac

Link between Affinity and Cu(II) Binding Sites to Amyloid-β Peptides Evaluated by a New Water-Soluble UV−Visible Ratiometric Dye with a Moderate Cu(II) Affinity

Amandine Conte-Daban,[†,‡,▽] Valentina Borghesani,[†,‡,▽] Stéphanie Sayen,[§] Emmanuel Guillon,[§] Yves Journaux,[∥,⊥] Geoffrey Gontard,[∥,⊥] Laurent Lisnard,[∥,⊥] and Christelle Hureau*[,†,‡]

[†]CNRS; LCC (Laboratoire de Chimie de Coordination); 205, route de Narbonne, F-31077 Toulouse, France

[‡]Université de Toulouse; UPS, INPT ; LCC; F-31077 Toulouse, France

[§]Université de Reims Champagne Ardenne, Institut de Chimie Moléculaire de Reims (ICMR), UMR 7312 CNRS-URCA, Moulin de la Housse, BP 1039, 51687 Reims Cedex 2, France

[∥]Sorbonne Universités, UPMC Univ. Paris 06, UMR 8232, IPCM, F-75005 Paris, France

[⊥]CNRS, UMR 8232, Institut Parisien de Chimie Moléculaire, F-75005 Paris, France

Supporting Information

ABSTRACT: Being able to easily determine the Cu(II) affinity for biomolecules of moderate affinity is important. Such biomolecules include amyloidogenic peptides, such as the well-known amyloid-β peptide involved in Alzheimer's disease. Here, we report the synthesis of a new water-soluble ratiometric Cu(II) dye with a moderate affinity (10^9 M^{-1} at pH 7.1) and the characterizations of the Cu(II) corresponding complex by X-ray crystallography, EPR, and XAS spectroscopic methods. UV−vis competition was performed on the Aβ peptide as well as on a wide series of modified peptides, leading to an affinity value of 1.6×10^9 M^{-1} at pH 7.1 for the Aβ peptide and to a coordination model for the Cu(II) site within the Aβ peptide that agrees with the one mostly accepted currently.

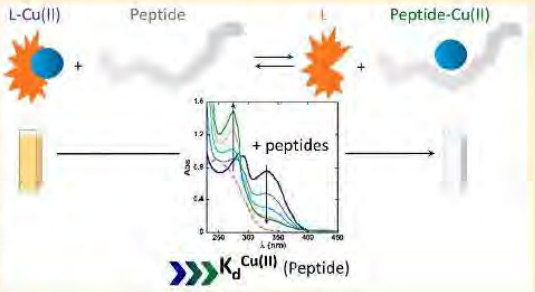

Copper ions play key biological roles.[1] They are essential metal ions that play an important role as catalytic centers in several processes, including very fundamental ones, such as energy production.[1] They have also been linked to several diseases. Dyshomeostasis of Cu is very dangerous and is well documented by two lethal genetic diseases, called Wilson's and Menkes' diseases, linked to an overload of Cu and to a depletion of Cu, respectively.[2−5] Cu imbalance has also been involved in the etiology of most neurological disorders,[6] such as Alzheimer's disease (AD),[7−9] Parkinson's disease (PD),[10,11] and Prion diseases.[10,12]

At a molecular scale, two parameters are important regarding Cu and the peptides or proteins involved in the above-mentioned diseases: (i) the metal environment, i.e. the nature of the atoms surrounding the metal center and (ii) the affinity of the peptides for the metal center. In the context of AD, which is under focus in the present article, there are many reports on the coordination sites of the Cu(II) center to the amyloid-β peptide (Aβ) (for recent reviews, see refs 8 and 13−15) and on the Cu(II) affinity for Aβ (see refs 16−18 and references therein). Some studies also aim at relating the Cu(II) affinity of modified Aβ peptides with the coordination sites.[19−21]

Determining the affinity of Cu(II) for peptides is thus of interest, first because this is intrinsically an important parameter that mirrors the possibility to have the metal ion−peptide interaction under biological conditions, and second because it give insights into the coordination sphere of the metal center when a series of modified peptides is studied. As a direct consequence, the straightforward and accurate determination of the Cu affinity for peptides is an important objective. However, this is an intricate task, since it necessitates appropriate analytical tools. The complexity of such studies is well illustrated by the abundant and differing reports on the evaluation of Cu(II) affinities for the Aβ peptide (see refs 16−20 and references therein). This is also true for the + I redox state of Cu,[18,22−24] which is however not under focus in the present study. While Cu(II) affinity values ranging from 10^6 M^{-1} to 10^{19} M^{-1} have been proposed,[25] a relative consensus has recently been reached around a value of 10^{10} M^{-1} at pH 7.4[17,18] (this value corresponds to the conditional affinity value,

Received: December 15, 2016
Accepted: January 12, 2017
Published: January 12, 2017

DOI: 10.1021/acs.analchem.6b04979
Anal. Chem. 2017, 89, 2155−2162

i.e. the absolute affinity value at a given pH; the interaction with buffer is not considered and will lead to a weaker so-called apparent affinity value).[25] Hence, the objective of the present study is to define a new tool appropriate for the rapid, easy, and accurate evaluation of Cu(II) binding affinities to peptides.

There are mainly two ways of determining affinity values.[16] The first one relies on potentiometric titrations that lead to absolute constants, from which an apparent affinity value can be calculated at any pH value.[16,26] The second one consists in measurements at a given pH either (i) by isothermal calorimetry (ITC), fluorescence when a fluorophore is natively present in the peptide sequence or added for a purpose and when the fluorescence is quenched by the addition of the metal ion of interest, or (ii) by competition experiments with a ligand of known affinity followed by the appropriate method. Potentiometry is likely the most powerful technique, since it gives access to the affinity value at any pH value but could be extremely difficult to implement in the case of biomolecules and requires an important quantity of the biological material. Results from ITC are far from straightforward, although additional data apart from the affinity can be evaluated (enthalpy, entropy, ...) (reviewed in ref 16). Competition experiments appear to be a well-suited method. With respect to Cu(II), UV−vis and fluorescent spectroscopic tools are of interest. In a seminal paper, Wedd and co-workers have designed four peptide-based fluorophores of various Cu(II) affinities ranging from 10^8 M^{-1} to 10^{14} M^{-1}. They were further used to probe the affinity of Cu(II) for different peptides and proteins by competition monitored by fluorescence.[27] While Cu(II) quenches the fluorescence of the competitor, the addition of the peptide of interest restores it, removing the Cu(II) from the probe.

In the present paper, we propose an alternative strategy that relies on a UV−visible competition experiment against an easy to synthesize Cu(II) dye with moderate affinity (3.2×10^9 M^{-1} at pH 7.1) that is anticipated to be perfectly appropriate for evaluation of Cu(II) affinity to weakly structured peptide, such as Aβ, at physiological pH. By UV−vis, the addition of the peptide of interest in the colored Cu(II) complex solution induces the disappearance of the absorption bands.

Using this new dye, we have investigated more than 17 peptidic sequences derived from the human Aβ peptide, including murine, N-terminally modified peptides, and biologically relevant mutants. Their Cu(II) affinities were evaluated and discussed with respect to the coordination models previously proposed in the literature.[13,21,28−30]

EXPERIMENTAL SECTION

Chemicals. Reagents were commercially available and were used as received. All the solutions were prepared in Milli-Q water (resistance: 18.2 MΩ·cm).

The Cu(II) ion source was $CuSO_4 \cdot 5H_2O$, bought from Sigma-Aldrich. A stock solution was prepared at 25 mM.

HEPES buffer (sodium salt of 2-[4-(2-hydroxyethyl)-piperazin-1-yl]ethanesulfonic acid) was bought from Sigma-Aldrich. A stock solution was prepared at 500 mM, pH = 7.3 in order to reach a resulting pH 7.1, and the same buffer stock solution was used over the course of the present study.

Peptides. Aβ_{16} (DAEFRHDSGYEVHHQK) and the mutants Ac-Aβ_{16}, **Ac**-DAEFRHDSGYEVHHQK; D1N-Aβ_{16}, **N**AEFRHDSGYEVHHQK; E3Q-Aβ_{16}, DA**Q**FRHDSGYEVHHQK; D7N-Aβ_{16}, DAEFRH**N**SGYEVHHQK; E11Q-Aβ_{16}, DAEFRHDSGY**Q**VHHQK; H6R-Aβ_{16}, DAEFR**R**DSGYEVHHQK; H6A-Aβ_{16}, DAEFR**A**DSGYEVHHQK; H13A-Aβ_{16}, DAEFRHDSGYEV**A**HQK; H14A-Aβ_{16}, DAEFRHDSGYEVH**A**QK; mAβ_{16}, DAEF**G**HDSGF**E**V**R**HQK; R5G-Aβ_{16}, DAEF**G**HDSGYEVHHQK; Y10F-Aβ_{16}, DAEFRHDSG**F**EVHHQK; H13R-Aβ_{16}, DAEFRHDSGYEV**R**HQK; R5G-H13R-Aβ_{16}, DAEF**G**HDSGYEV**R**HQK; Aβ_{28}, DAEFRHDSGYEVHHQKLVFFAEDVGSNK; Aβ_{40}, DAEFHDSGYEVHHQKLVFFAEDVGSNKGAILGLMVGGVV were bought from GeneCust (Dudelange, Luxembourg) with purity grade >95%.

Stock solutions of the peptides were prepared by dissolving powder in Milli-Q water (resulting pH ∼ 2), except for the Aβ_{28} and Aβ_{40} peptides, which were dissolved in NaOH 50 mM. Peptide concentration was determined by UV−vis absorption of Tyr10 considered as free tyrosine (at pH ∼ 2.0, $\varepsilon_{276} - \varepsilon_{296} = 1410$ $cm^{-1} \cdot M^{-1}$; at pH ∼ 12.5, $\varepsilon_{293} - \varepsilon_{360} = 2400$ $cm^{-1} \cdot M^{-1}$).[31] For the mutants without Tyr10, the absorption of the two Phe was used ($\varepsilon_{258} - \varepsilon_{280} = 390$ $cm^{-1} \cdot M^{-1}$).[32]

As the Cu(II) coordination sites in the Aβ peptide are localized in the first 16 amino acids residues,[8] the Aβ_{16} and its counterparts were used as a model of the full-length peptides.

ABH and BAH, where B corresponds to the β-alanine, were bought from Protéogenix (Strasbourg, France), and stock solutions were prepared by solubilizing the peptides in Milli-Q water. Their concentrations were determined by UV−vis titration with a titrated Cu(II) solution following the d-d band absorption of the complex,[33] according to ref .34.

Ligand. The 3,4-bis(oxamato)benzoic acid ligand, L (see Scheme S1), was synthesized as described below and used in its sodium salt form. A 8.5 mM stock solution was prepared, increasing the pH until solubilization, determined by UV−vis titration with a titrated Cu(II) solution following the band absorption at 330 nm of the complex (see text below and Figure 3), according to ref 34.

Synthesis of H_5L. H_3Et_2L: 3,4-(Diethyloxamate)benzoic acid. The ester form of the L ligand was prepared following the known procedure for oxamate ligands[35,36] instead of the previously reported synthesis.[37] To 5 g of 3,4-diaminobenzoic acid (32.8 mmol) in THF (200 mL) is added with strong stirring 8.25 mL of ethyl oxalyl chloride (72 mmol, 2.2 equiv). The mixture is refluxed for 2 h, filtered while hot, and let to cool down to room temperature. Removal of the solvent leads to a brown precipitate. The solid is abundantly washed with water, filtered, washed with 50% vol. ethanol and then with a minimum of cold 96% vol. ethanol, and dried in air. Yield: 8.9 g (77%). See Supporting Information for elemental analysis, NMR, and IR characterizations.

$Na_{1.5}H_{3.5}L \cdot 2.2H_2O$. Aqueous NaOH (2 M, 57 mL) was added dropwise to a suspension of H_3Et_2L (8 g, 22.7 mmol) in water (400 mL). The solution was stirred for 30 min and filtered. Addition of 4 M HCl (28 mL) to the resulting solution leads to the rapid formation of a brown precipitate. After 10 min the precipitate is collected on a sintered glass filter, washed with cold water, then with 96% vol. EtOH, and finally with ether before being dried for several hours in air and overnight at 45 °C in an oven. Yield: 5.4 g (64%). See Supporting Information for elemental analysis, NMR, and IR characterizations.

Synthesis of $Li_3[Cu(L)]$. Suitable crystals of the copper dye, Cu(L), were obtained as follows: A suspension of H_3Et_2L (0.100 g, 0.28 mmol) in water (10 mL) was treated with 0.71 mL of LiOH 2 M (1.42 mmol) and stirred at room temperature

DOI: 10.1021/acs.analchem.6b04979
Anal. Chem. 2017, 89, 2155−2162

until complete dissolution of the ligand. An aqueous solution of $Cu(NO_3)_2{\cdot}3H_2O$ (0.068 g, 0.28 mmol, 5 mL) was then added dropwise to the oxamate solution, resulting in a deep blue solution of the copper complex that was stirred for 30 min at room temperature and filtered. Slow diffusion of acetone yields crystals of $Li_3[Cu(L)]{\cdot}5.5H_2O$ in 15 days. Yield: 0.054 g (41% based on Cu). See Supporting Information for elemental analysis and IR characterizations.

METHODS

X-ray Structure. Crystallographic data were collected on a Bruker Kappa-APEX II CCD diffractometer (Cu Kα, λ = 1,54178). Crystal data: purple plates, monoclinic *C2/c*, a = 26.3214(15), b = 6.7217(4), c = 20.4183(11) Å, β = 112.590(3)°, V = 3335.3(3) Å^3, Z = 8, T = 200(1) K, ρ = 1.567 g·cm^{-3}, F(000) = 1560, μCu Kα = 2.293 mm^{-1}. Crystals were mounted on a Hamilton cryoloop using Paratone-N oil and placed in the cold flow produced with an Oxford Cryocooling device. Partial hemispheres of data, preselected with the APEX II software,[38] were collected using φ and ω scans. Integrated intensities were obtained with SAINT+ and were corrected for absorption with SADABS;[38,39] the structure was solved with SIR92[40] and refined with SHELXL-2014/7[41] (WinGX software package).[42] Data refinement gives (using 271 parameters and 6 restraints) *wR2* = 0.2432 (2923 unique reflections), R_1 = 0.0720 (2514 reflections with $I > 2\sigma(I)$), GOF = 1.128. Crystallographic details are available in CIF format, free of charge via www.ccdc.cam.ac.uk/conts/retrieving.html (or from the Cambridge Crystallographic Data Centre, 12 Union Road, Cambridge CB2 1EZ, UK; fax: (+44) 1223 336 033; or deposit@ccdc.cam.ac.uk). CCDC number 1516020.

NMR, IR, and Elemental Analysis. ^{1}H and ^{13}C NMR spectra were collected on a 400 MHz Bruker Avance spectrometer at 298 K.

ATR/FT-IR spectra were collected on a Bruker TENSOR 27 equipped with a simple reflection ATR diamond plate of the Harrick MPV2 series.

Elemental analysis was performed at the ICSN, CNRS UPR 2301, in Gif-sur-Yvette, France.

Electron Paramagnetic Resonance. Electron paramagnetic resonance (EPR) data were recorded using an Elexsys E 500 Bruker spectrometer, operating at a microwave frequency of approximately 9.5 GHz. Spectra were recorded using a microwave power of 20 mW across a sweep width of 150 mT (centered at 310 mT) with a modulation amplitude of 0.5 mT. Experiments were carried out at 110 K using a liquid nitrogen cryostat.

EPR samples were prepared from a stock solution of ligand diluted down to 0.2 mM in H_2O. ^{65}Cu(II) (0.9 equiv) was added from 25 mM $^{65}Cu(NO_3)_2$ stock solution homemade from a ^{65}Cu foil. Samples were frozen in quartz tubes after addition of 10% glycerol as a cryoprotectant and stored in liquid nitrogen until used.

X-ray Absorption Spectroscopy (XAS). Cu(II) K-edge EXAFS (extended X-ray absorption fine structure) and XANES (X-ray Absorption near-edge structure) spectra were recorded at the BM30B (FAME) beamline at the European Synchrotron Radiation Facility (ESRF, Grenoble, France).[43] The storage ring was operated in 7/8 + 1 mode at 6 GeV with a 200 mA current. The beam energy was selected using a Si(220) N_2 cryo-cooled double-crystal monochromator with an experimental resolution close to that theoretically predicted (namely ~0.5 eV fwhm at the Cu energy). The beam spot on the sample was approximately 300 × 100 μm^2 (H x V, fwhm). Because of the low Cu(II) concentration, spectra were recorded in fluorescence mode with a 30-element solid state Ge detector (Canberra) in frozen liquid cells in a He cryostat. The temperature was kept at 20 K during data collection. The energy was calibrated with Cu metallic foil, such that the maximum of the first derivative was set at 8979 eV. EXAFS Cu(II) data were collected from 8840 to 8960 eV using a 5 eV step of 2 s, from 8960 to 9020 eV using a 0.5 eV step of 3 s, and from 9020 to 9300 eV with a k-step of 0.05 Å^{-1} and 3 s per step. At least six scans recorded on different spots were averaged. XAS samples were prepared from stock solutions of ligand and Cu(II) diluted down to approximately 1.0 mM in buffered solution. Samples were frozen in the sample holder after addition of 10% glycerol as a cryoprotectant and stored in liquid nitrogen until used. Cu(II) photoreduction was controlled by recording successive scans at the same spot. It was considered that during the first 20 min of recording the photoreduction is insignificant.

The data analysis was performed using the "Multi-Plateform Applications for X-ray Absorption" package, including Cherokee and Roundmidnight programs,[44] according to the standard and previously reported data analysis procedures.[45,46]

Spectra were background-corrected by a linear regression through the pre-edge region and a polynomial through the postedge region. The backscattering phase, $\Phi_i(k, R_i)$, and amplitude, $A_i(k, R_i)$, functions were obtained using the ab initio FEFF7 code.[47] Since theoretical phase shifts were used, it is necessary to fit the energy threshold E_0 by adding an extra fitting parameter, ΔE_0. Moreover, the FEFF7 code was used to check if the multiple scattering of our reference compounds of known crystallographic structure is negligible in the 0−3 Å range. The estimated errors for distances and coordination numbers are ±0.02 Å and ±20%, respectively.

UV−Visible Spectrophotometry. UV−vis spectra were recorded on a spectrophotometer SPECORD S600 Analytik Jena at 25 °C in a 1 cm path length quartz cuvette.

Competition Experiments between the Ligand and the Peptides. The experiments have been monitored by UV−vis in HEPES buffer 0.1 M (at a resulting pH = 7.1). The ligand (50 μM in theory) and Cu(II) (45 μM in theory) were mixed, and successive additions of the different peptides (0 to 500 μM in total) were added. Each addition of the peptide is made once the thermodynamic equilibrium of the previous reaction is reached (this takes about 20 min). To be reproducible with respect to pH condition, the same stock buffer solution (pH = 7.3 to reach a resulting pH of 7.1) was used for all the experiments. The competition experiments were performed at 25 °C in triplicate.

Analysis of the Data. The data analysis was performed with a 2-step procedure for each experiment (corresponding to a given peptide).

Step 1. The theoretical concentrations of the ligand L and the Cu(II) were adjusted using the absorbance of ligand at 246 nm ($\varepsilon_{246} - \varepsilon_{450}$ = 18000 cm$^{-1}{\cdot}$M^{-1}) and the absorbance of the Cu(L) complex at 330 nm ($\varepsilon_{330} - \varepsilon_{450}$ = 18000 cm$^{-1}{\cdot}$M^{-1}), respectively.

Step 2. The absorbance of the competition experiments measured at 330 nm after completion of the reaction was plotted as a function of the number of peptides equivalents recalculated with respect to the real ligand concentration (see step 1). Then these data were fitted with an in-house procedure using the adjusted concentrations as starting parameters.

DOI: 10.1021/acs.analchem.6b04979
Anal. Chem. 2017, 89, 2155−2162

Absorbance was calculated according to

$$Abs = \varepsilon^{L}_{330nm}\cdot[L] + \varepsilon^{CuL}_{330nm}\cdot[CuL] + \varepsilon^{P}_{330nm}\cdot[P] + \varepsilon^{CuP}_{330nm}\cdot[CuP]$$

where P stands for peptide, L for the ligand, and CuP and CuL for the complex between Cu(II) and peptide and the ligand, respectively. l = 1 cm.

The same equation can be expressed as

$$Abs = \varepsilon^{L}_{330nm}\cdot([L]_0 - [Cu]_0 + [\alpha]) + \varepsilon^{CuL}_{330nm}\cdot([Cu]_0 - [\alpha]) + \varepsilon^{P}_{330nm}\cdot([P]_0 - [\alpha]) + \varepsilon^{CuP}_{330nm}\cdot[\alpha]$$

where α stands for the progression of the following reaction: peptide + Cu(II) → peptide-Cu(II) and the $[\ ]_0$ correspond to the starting values in which the dilution due to addition of the peptide has been taken into account when required.

Cu(II) is supposed to be chelated by the peptide or by L; there is no free Cu(II).

$$\frac{K_d^{CuP}}{K_d^{CuL}} = \frac{[P]\cdot[Cu]}{[\alpha]}\cdot\frac{[CuL]}{[L]\cdot[Cu]}$$

With the starting concentrations:

$$\frac{K_d^{CuP}}{K_d^{CuL}} = \frac{[P]_0 - [\alpha]}{[\alpha]}\cdot\frac{[Cu]_0 - [\alpha]}{[L]_0 - [Cu]_0 + [\alpha]}$$

This is a quadratic equation having the form

$$a\alpha^2 + b\alpha + c = 0, \text{ with}$$

$$\alpha = \frac{-b + \sqrt{\Delta}}{2a}, \text{ with}$$

$$b = \frac{K_d^{CuP}}{K_d^{CuL}}\cdot([L]_0 - [Cu]_0) + [P]_0 + [Cu]_0$$

$$\Delta = b^2 - 4\cdot a\cdot c$$

$$a = \frac{K_d^{CuP}}{K_d^{CuL}} - 1$$

$$c = -[P]_0\cdot[Cu]_0$$

Then, the K_d^{CuP} value was adjusted to obtain the best reproduction of the experimental data.

NB: Although K_d/K_a are dimensionless values, they are given here in M or M^{-1}, respectively, for convenience. Indeed for the 1:1 system, the K_d value in M gives a direct idea at which the concentration of the complex is predominantly formed.

NB: in a preliminary experiment, K_d^{CuL} was evaluated by competition with ABH and BAH knowing $K_d^{CuL(ABH)}$ and $K_d^{CuL(BAH)}$[33] with the similar procedure.

RESULTS

The competitor used in the present work to evaluate the Cu(II) affinity of a wide series of Aβ derived peptides by UV−vis competition experiments is an oxamate ligand (H_5L, Scheme S1; for the sake of clarity L^{5-} will be written L. Similarly, the $[Cu(L)]^{3-}$ will be noted Cu(L)). Oxamate ligands have largely proved their appeal for the design of metalloligands and the subsequent preparation of multidimensional compounds with controlled architectures and properties.[48] In particular, the use of oxamate ligands and the multistep assembly of oxamate-based complexes have successfully led to relevant objects in molecular magnetism: switchable molecules, high nuclearity coordination complexes, single-chain magnets, and porous magnets.[49,50] Recently, oxamate-based systems have also shown attractiveness in broader coordination chemistry fields, such as catalysis.[51,52] Here, we will take advantage of the mild Cu(II) affinity and of the presence of an intense UV−visible band for the complex with Cu(II) (λ = 330 nm, ε = 18000 $cm^{-1}\cdot M^{-1}$).

The X-ray structure of Cu(L) is shown in Figure 1, and the crystallographic parameters are given in Table 1, top, and in the Supporting Information. The complex adopts a square-planar geometry where the L ligand coordinates the Cu(II) ion via its two oxamate groups each binding the metal center through one nitrogen and one oxygen atom. The square-planar geometry is fairly regular with a 2.4° dihedral angle between the oxamate groups and a 3.1° dihedral angle between the Cu(II) coordination plane and the phenyl plane of the ligand. The carboxylate group of the ligand remains uncoordinated. Supramolecular arrangements of the complexes are described in the Supporting Information (Figure S1).

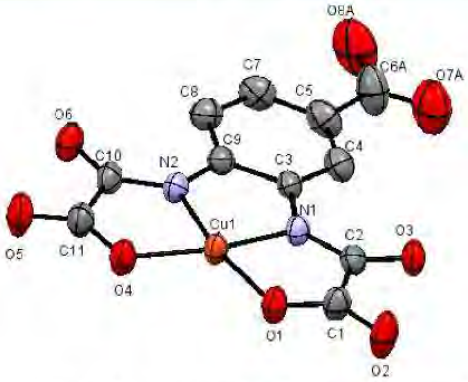

Figure 1. Ellipsoid plot (H and disorders atoms are omitted for clarity) of Cu(L).

Table 1. Crystallography Distances between Cu(II) and Their Neighbours (top) and EXAFS Parameters (bottom): N = Number of Neighbors, R = Absorber−Neighbour Distance, σ = Debye−Waller Factor

N	Distance (Å)
Cu−N_1	1.9061(55)
Cu−N_2	1.9127(37)
Cu−O_4	1.9588(34)
Cu−O_4	1.9642(51)
N	**Distance (Å)**
2 Cu−N	1.92
2 Cu−O	1.97
σ^2 (Å²)	**R factor**
0.00471	0.18%

The persistence of the structure in aqueous solution has been probed by several complementary techniques. The most appropriate one is EXAFS, by which the Cu−N and Cu−O distances have been determined in solution and are in perfect agreement with those obtained for the crystal structure (for

DOI: 10.1021/acs.analchem.6b04979
Anal. Chem. 2017, 89, 2155−2162

crystallography, see Table 1, bottom and Figure S1; for EXAFS fitting, see Figure S2).

The parameters estimated from the EPR signature (Figure 2A) are also in line with the Cu(L) solid-state structure. Indeed,

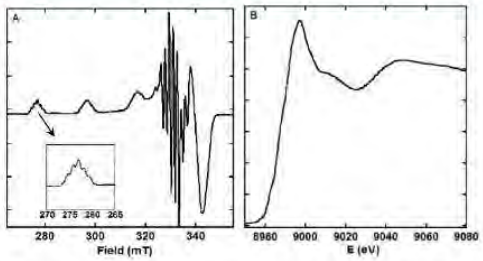

Figure 2. *Panel A.* EPR signature of Cu(L). [L] = 200 μM, [^{65}Cu(II)] = 180 μM, [HEPES] = 50 mM, pH = 7.1, T = 120 K. Inset: superhyperfine structure on the first parallel line. *Panel B.* Normalized Cu K-edge X-ray absorption near edge structure (XANES) spectrum of Cu(L). [L] = 1 mM, [Cu(II)] = 0.9 mM, [HEPES] = 0.1 M, pH = 7.0, T = 20 K.

the $g_{//}$ and $A_{//}(^{65}Cu)$ values equal 2.22 and 212 × 10^{4} cm^{-1}, respectively, and are thus in line with a 2N2O equatorial binding mode according to the Peisach and Blumberg correlation.[53] A weak rhombicity linked to the presence of four nonequivalent equatorial ligands is at the origin of the complex features observed in the $g_{\perp}$ region (coupling between I_{Cu} = 3/2 and S_{Cu} = 1/2 for the two g_x and g_y transitions). The presence of two equivalent nitrogen atoms is consistent with the five superhyperfine lines observed on the first parallel transition, arising from the coupling between I_N = 1 and S_{Cu} = 1/2. The XANES spectrum of Cu(L) is given in Figure 2B. It is in line with Cu(II) complexes where the Cu(II) center lies in a square planar environment.[1]

The other important parameter of this ligand is its affinity constant for Cu(II). This affinity was evaluated by the same type of competition experiments as those detailed below, performed first between L and two short peptides, namely ABH and BAH (B stands for β-alanine).[33] These peptides were studied by potentiometry to determine the impact of the 5-membered versus 6-membered metallacycles with regard to the Cu(II) affinity in an ATCUN-like (Amino Terminal CU and Nickel) site.[54] Their conditional Cu(II) affinity values calculated at pH 7.1 from the potentiometric data equal 3.0 × 10^{8} and 3.7 × 10^{9} M^{-1}, respectively. Competition experiments with the ABH (*respectively* BAH) lead to a Cu(II) affinity value of 2.2 × 10^{9} M^{-1} (*respectively* 4.1 × 10^{9} M^{-1}) for L. The average value of K_a' = 3.2 ± 1.0 × 10^{9} M^{-1} was used in the rest of the study.

The competition experiments between L and the Aβ peptides for Cu(II) binding were performed by using the peptides to remove the Cu(II) from the colored Cu(L) complex, leading to a disappearance of the signature at 330 nm characteristic of the Cu(L) complex. Figure 3A shows the typical series of spectra obtained for a given peptide (here Aβ_{16}). L was first added (dotted line), then Cu(II) (solid line), and then successive additions of the peptide were performed (gray lines; see Experimental Section for more details). Note that the increase at 276 nm is due to Tyr10 absorbance and perfectly matches the amount of peptide added.

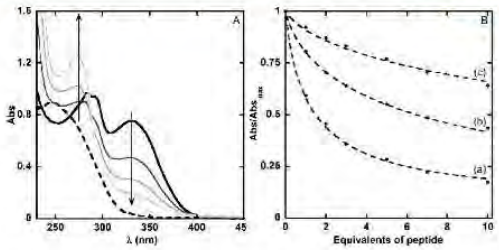

Figure 3. *Panel A.* UV−vis spectra of a solution of L (dotted line), in the presence of 0.9 equiv of Cu(II) (solid line) and after addition of increasing amounts (approx. 1, 3, 7, and 10 equiv) of Aβ_{16} peptide (gray lines). The arrows indicate the variation of the UV−vis spectra upon addition of the peptide. The increase at 276 nm is due to Tyr10 absorption. *Panel B.* Experimental absorbance at 330 nm (dots) and the best fits (dashed lines) of the Cu(L) system upon addition of peptides (Aβ_{16} (a), H6A-Aβ_{16} (b), and Ac-Aβ_{16} (c)). [L] = 50 μM, [Cu(II)] = 45 μM, [peptides] = 0 to 500 μM, [HEPES] = 0.1 M, pH = 7.1, T = 25 °C.

The absorbance at λ = 330 nm of the mixture was plotted as a function of the equivalent numbers of peptide added (dots in Figure 3B). Then, these data were fitted with an in-house procedure (dashed lines; for more details see Experimental Section).

Experimental absorbance values and their fits are shown in Figure 3B as a matter of illustration for Aβ_{16}, H6A-Aβ_{16}, and Ac-Aβ_{16} (curves a, b, and c, respectively). Qualitative analysis indicates that the Cu(II) affinity of the three peptides follows the trend: Aβ_{16} > H6A-Aβ_{16} > Ac-Aβ_{16}. All the Cu(II) affinity values obtained in the present study are gathered in Table 2 while the corresponding reproductions of the experimental data are given in the Supporting Information (Figure S3). The accuracy of the fitting procedure is shown in Figure S4. All the calculated Cu(II) affinity values were normalized with respect

Table 2. Cu(II) Affinity Values of the Aβ Peptides Studied Here[a]

Peptide	K_a (10^{9} M^{-1})[b]	K_a(peptide)/K_a(hAβ_{16})
Aβ_{16}	1.6	1.0
Aβ_{28}	1.8	1.1
Aβ_{40}	2.2	1.4
Ac-Aβ_{16}	<0.1	<0.1
D1N-Aβ_{16}	1.1	0.7
E3Q-Aβ_{16}	1.0	0.6
D7N-Aβ_{16}	1.1	0.7
E11Q-Aβ_{16}	1.3	0.8
H6R-Aβ_{16}	0.3	0.2
H6A-Aβ_{16}	0.3	0.2
H13A-Aβ_{16}	0.9	0.6
H14A-Aβ_{16}	0.8	0.5
mAβ_{16}	3.0	1.9
R5G-Aβ_{16}	3.1	1.9
Y10F-Aβ_{16}	1.2	0.8
H13R-Aβ_{16}	0.7	0.4
R5G-H13R-Aβ_{16}	2.7	1.7

[a]The reference for the normalization is the Aβ_{16}. A Cu(II) affinity value of 3.2 ± 1.0 × 10^{9} M^{-1} for the competing ligand L was taken. [b]The error bars are evaluated in the Supporting Information (see Figure S4). [c]The K_a value for Ac−Aβ_{16} is too weak to be thoroughly determined by this method. Only a higher value can be given.

DOI: 10.1021/acs.analchem.6b04979
Anal. Chem. 2017, 89, 2155−2162

to the value of Aβ_{16} for an easier comparison, as shown in Table 2 and in Figure 4.

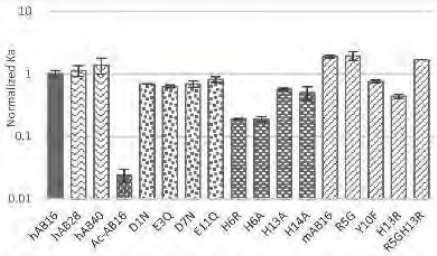

Figure 4. Bar graph of the normalized affinity constants in log units of the Aβ peptides and some of their mutants for Cu(II). The reference for the normalization is the hAβ_{16}. The error bars indicate the standard deviation. [L] = 50 μM, [Cu(II)] = 45 μM, [peptides] = 0 to 500 μM, [HEPES] = 0.1 M, pH = 7.1, T = 25 °C. The affinity constant of the ligand is $K_a = 3.2 \pm 1.0 \times 10^9$ M^{-1}.

DISCUSSION

The Aβ peptides used in this study were modified with respect to the human sequence on any potential binding amino-acids, namely the carboxylate containing amino-acid residues, the His residues, and the N-terminal amine. The mutations involved between the human and murine sequences were also studied.

Human-Derived Peptides. The first modification is the acetylation of the N-terminal amine (Asp1) precluding the possibility of Cu(II) binding. The affinity constant of Cu(II) for this modified peptide is at least 10 times weaker than that of the Aβ_{16} peptide, in line with an important contribution of the N-terminal amine in Cu(II) binding to Aβ_{16}, as discussed in the literature.[28,55,56] In the second group of modified peptides, the impact of the carboxylate function is evaluated. The carboxylate group of each of the amino acid residues Asp1, Glu3, Asp7, and Glu11 is mutated with an amide function. Only a very weak impact is observed with a decrease in the affinity upon modification that does not exceed a factor of 2. In the Aβ_{16} there are 4 carboxylate groups available for the Cu(II) coordination. Therefore, if one carboxylate is mutated, 3 other ones remain to complete the coordination sphere. This is in perfect agreement with the possibility of having an equilibrium between the four carboxylate groups for one binding position.[57] The high similarity of affinity values for the four carboxylate-modified peptides also suggests that there is no preference for one given carboxylate group. The last group of modified peptides consists in the His mutants (His6, His13, and His14). While the His6 mutation (H6A or H6R) has a significant impact (a 5-fold decrease of the affinity value), the His13 or His14 mutation has a lesser effect (with a maximal 2-fold decrease of the affinity value). This indicates that (i) none of the His is essential but (ii) the His13 and His14 can more easily exchange for the binding position on the peptide than His6 and His13 or than His6 and His14 do. This is in line with the proposition that in the main coordination site His13 and His14 exchange for one binding position while His6 is constantly bound.[13,30,58] It is worth mentioning that similar differences have been previously determined by ITC.[19,20] All together, these data fit very well with the coordination site of Cu(II) proposed based on spectroscopic data (reviewed in refs 13 and 30) and reminded in Scheme 1. In such a proposition,

Scheme 1. Predominant Forms at pH 7.1 of the Cu(II) Coordination with Human (left) and Murine (right) Aβ Peptides

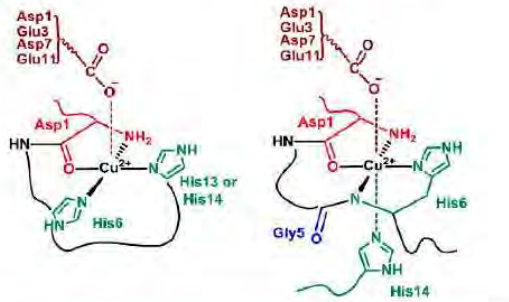

the Cu(II) ion is equatorially bound to the N-terminal amine, the adjacent carbonyl group from the Asp1−Ala2 bond, the imidazole group from His 6 and from His13 or 14 in equilibrium (see Scheme S2, top).[8] A carboxylate-containing residue has been proposed to occupy the apical position.[57] Last, the Cu(II) affinity seems to weakly increase with the length of the peptide, in line with previous reports,[17,59] but this result has to be taken with caution due to the increase in the error bar when working with the Aβ_{40} peptide. This confirms that the Aβ_{16} moiety is a good model with respect to the Cu(II) binding site within the full-length peptide.

Human versus Murine Peptides. The murine sequence differs from the human one by 3 mutations: R5G, Y10F, and H13R. With respect to Cu(II) affinity values, the murine peptide is twice stronger than the human one, in line with previous measurements by direct competition,[17,29] ITC,[19] and potentiometry.[55] The main mutation responsible for such a difference is the R5G mutation. This has been previously related to the formation of a 6-membered metallacycle between the side chain of His6 and the deprotonated Gly5-His6 peptide function for the murine peptide that is not observed in the human case (see Schemes 1 and S2 bottom).[29,30]

CONCLUSIONS

In the present study, a new ratiometric dye was synthesized and fully characterized. It was further used to determine the affinity constant of Cu(II) for several Aβ peptides by UV−vis competition experiments. This was made possible by the intense (18000 $cm^{-1}\cdot M^{-1}$) LMCT band displayed at λ = 330 nm by the Cu(L) complex. The affinity values obtained in this study for the various modified peptides agree perfectly with published coordination sites, thus validating the proposed strategy that relies on the determination of affinity constants of a wide series of modified peptides to extrapolate a coordination model for a given peptide. In addition, the designed dye could be further used to straightforwardly determine Cu(II) affinity for other flexible peptides such as α-synuclein, involved in Parkinson's disease,[11] or Prion protein,[12] for which the Cu(II) affinities are proposed to lie in the 10^8−10^{10} M^{-1} range. However, outside this range, competition with L will not give reliable values. In addition, the molar extinction coefficient is relatively low, implying the use of quite a large biomolecule concentration. As a consequence, to generalize this approach to the evaluation of Cu(II) affinity for any other (bio)molecules relies on the ability to modulate the Cu(II) affinities and to

DOI: 10.1021/acs.analchem.6b04979
Anal. Chem. 2017, 89, 2155−2162

increase the molar extinction coefficient of oxaloamino-benzoic acid derivatives by playing with the scaffold.

■ ASSOCIATED CONTENT

Supporting Information

The Supporting Information is available free of charge on the ACS Publications website at DOI: 10.1021/acs.analchem.6b04979.

Characterization of the ligand and of the Cu(L) complex, EXAFS parameters, competition data, error bar, and Cu coordination model (PDF)

■ AUTHOR INFORMATION

Corresponding Author

*E-mail: christelle.hureau@lcc-toulouse.fr.

Author Contributions

▽A.C.D. and V.B. contributed equally to this work.

Notes

The authors declare no competing financial interest.

■ ACKNOWLEDGMENTS

C.H. thanks the ERC aLzINK, Contract n° StG 638712, for financial support. The authors thank the European Synchrotron Radiation Facility for provision of beamtime (experiment 30-02-1060), the FAME staff for their support, and F. Collin and C. Cheignon for their help in recording the XANES and EXAFS data. P. Faller is acknowledged for interesting discussions.

■ REFERENCES

(1) Solomon, E. I.; Heppner, D. E.; Johnston, E. M.; Ginsbach, J. W.; Cirera, J.; Qayyum, M.; Kieber-Emmons, M. T.; Kjaergaard, C. H.; Hadt, R. G.; Tian, L. *Chem. Rev.* **2014**, *114*, 3659−3653.
(2) Sarkar, B. *Chem. Rev.* **1999**, *99*, 2535−2544.
(3) Delangle, P.; Mintz, E. *Dalton Trans.* 2012, *41*.
(4) Lalioti, V.; Muruais, G.; Tsuchiya, Y.; Pulido, D.; Sandoval, I. V. *Front. Biosci., Landmark Ed.* **2009**, *14*, 4878−4903.
(5) Scheiber, I. F.; Mercer, J. F. B.; Dringen, R. *Prog. Neurobiol.* **2014**, *116*, 33−57.
(6) Kozlowski, H.; Luczkowski, M.; Remelli, M.; Valensin, D. *Coord. Chem. Rev.* **2012**, *256*, 2129−2141.
(7) Ayton, S.; Lei, P.; Bush, A. I. *Free Radical Biol. Med.* **2013**, *62*, 76−89.
(8) Hureau, C. *Coord. Chem. Rev.* **2012**, *256*, 2164−2174.
(9) Barnham, K. J.; Bush, A. I. *Chem. Soc. Rev.* **2014**, *43*, 6727−6749.
(10) D'Ambrosi, N.; Rossi, L. *Neurochem. Int.* **2015**, *90*, 36−45.
(11) Binolfi, A.; Quintanar, L.; Bertoncini, C. W.; Griesinger, C.; Fernández, C. O. *Coord. Chem. Rev.* **2012**, *256*, 2188−2201.
(12) Arena, G.; La Mendola, D.; Pappalardo, G.; Sóvágó, I.; Rizzarelli, E. *Coord. Chem. Rev.* **2012**, *256*, 2202−2218.
(13) Drew, S. C.; Barnham, K. J. *Acc. Chem. Res.* **2011**, *44*, 1146−1155.
(14) Faller, P.; Hureau, C.; Berthoumieu, O. *Inorg. Chem.* **2013**, *52*, 12193−12206.
(15) Telpoukhovskaia, M. A.; Orvig, C. *Chem. Soc. Rev.* **2013**, *42*, 1836−1846.
(16) Zawisza, I.; Rozga, M.; Bal, W. *Coord. Chem. Rev.* **2012**, *256*, 2297−2307.
(17) Alies, B.; Renaglia, E.; Rozga, M.; Bal, W.; Faller, P.; Hureau, C. *Anal. Chem.* **2013**, *85*, 1501−1508.
(18) Young, T. R.; Kirchner, A.; Wedd, A. G.; Xiao, Z. *Metallomics* **2014**, *6*, 505−517.
(19) Hong, L.; Carducci, T. M.; Bush, W. D.; Dudzik, C. G.; Millhauser, G. L.; Simon, J. D. *J. Phys. Chem. B* **2010**, *114*, 11261−11271.
(20) Hong, L.; Simon, J. D. *Metallomics* **2011**, *3*, 262−266.
(21) Alies, B.; Bijani, C.; Sayen, S.; Guillon, E.; Faller, P.; Hureau, C. *Inorg. Chem.* **2012**, *51*, 12988−13000.
(22) Alies, B.; Badei, B.; Faller, P.; Hureau, C. *Chem. - Eur. J.* **2012**, *18*, 1161−1167.
(23) Feaga, H. A.; Maduka, R. C.; Foster, M. N.; Szalai, V. A. *Inorg. Chem.* **2011**, *50*, 1614−1618.
(24) Xiao, Z.; Gottschlich, L.; van der Meulen, R.; Udagedara, S. R.; Wedd, A. G. *Metallomics* **2013**, *5*, 501−513.
(25) Faller, P.; Hureau, C. *Dalton Trans.* **2009**, 1080−1094.
(26) Arena, G.; Papppalardo, G.; Sovago, I.; Rizzarelli, E. *Coord. Chem. Rev.* **2012**, *256*, 3−12.
(27) Young, T. R.; Wijekoon, C. J. K.; Spyrou, B.; Donnelly, P. S.; Wedd, A. G.; Xiao, Z. *Metallomics* **2015**, *7*, 567−578.
(28) Alies, B.; Eury, H.; Bijani, C.; Rechignat, L.; Faller, P.; Hureau, C. *Inorg. Chem.* **2011**, *50*, 11192−11201.
(29) Eury, H.; Bijani, C.; Faller, P.; Hureau, C. *Angew. Chem., Int. Ed.* **2011**, *50*, 901−905.
(30) Hureau, C.; Dorlet, P. *Coord. Chem. Rev.* **2012**, *256*, 2175−2187.
(31) Faller, P.; Hureau, C.; Dorlet, P.; Hellwig, P.; Coppel, Y.; Collin, F.; Alies, B. *Coord. Chem. Rev.* **2012**, *256*, 2381−2396.
(32) Fasman, G. D. H. o. B. a. M. B. *Proteins, I*, 3rd ed.; CRC: 1976; p 183.
(33) Nagaj, J.; Stokowa-Sołtys, K.; Zawisza, I.; Jeżowska-Bojczuk, M.; Bonna, A.; Bal, W. *J. Inorg. Biochem.* **2013**, *119*, 85−89.
(34) Hureau, C.; Eury, H.; Guillot, R.; Bijani, C.; Sayen, S.; Solari, P. L.; Guillon, E.; Faller, P.; Dorlet, P. *Chem. - Eur. J.* **2011**, *17*, 10151−10160.
(35) Stumpf, H. O.; Pei, Y.; Kahn, O.; Sletten, J.; Renard, J. P. *J. Am. Chem. Soc.* **1993**, *115*, 6738−6745.
(36) Cervera, B.; Sanz, J. L.; Ibanez, M. J.; Vila, G.; Lloret, F.; Julve, M.; Ruiz, R.; Ottenwaelder, X.; Aukauloo, A.; Poussereau, S.; Journaux, Y.; Munoz, M. C. *J. Chem. Soc., Dalton Trans.* **1998**, *5*, 781−790.
(37) Paul-Roth, C. O. *C. R. Chim.* **2005**, *8*, 1232−1236.
(38) Bruker AXS Inc. Madison, Wisconsin, USA, 1998.
(39) Blessing, R. H. *Acta Crystallogr., Sect. A: Found. Crystallogr.* **1995**, *51*, 33.
(40) Altomare, A.; Cascarano, G.; Giacovazzo, C.; Guagliardi, A.; Burla, M. C.; Polidori, G.; Camalli, M. *J. Appl. Crystallogr.* **1994**, *27*, 435.
(41) Sheldrick, G. M. *Acta Crystallogr., Sect. C: Struct. Chem.* **2015**, *71*, 3−8.
(42) Farrugia, L. J. *J. Appl. Crystallogr.* **2012**, *45*, 849−854.
(43) Proux, O.; Biquard, X.; Lahera, E.; Menthonnex, J. J.; Prat, A.; Ulrich, O.; Soldo, Y.; Trévisson, P.; Kapoujyan, G.; Perroux, G.; Taunier, P.; Grand, D.; Jeantet, P.; Deleglise, M.; Roux, J.-P.; Hazemann, J.-L. *Phys. Scr.* **2005**, *115*, 970−973.
(44) Michalowicz, A.; Moscovici, J.; Muller-Bouvet, D.; Provost, K. *J. Phys.: Conf. Ser.* **2009**, *190*, 012034−012035.
(45) Lengeler, B.; Eisenberg, P. *Phys. Rev. B: Condens. Matter Mater. Phys.* **1980**, *21*, 4507−4520.
(46) Guillon, E.; Merdy, P.; Aplincourt, M. *Chem. - Eur. J.* **2003**, *9*, 4479−4484.
(47) Zabinsky, S. I.; Rehr, J. J.; Ankudinov, A. L.; Albers, R. C.; Eller, M. J. *Phys. Rev. B: Condens. Matter Mater. Phys.* **1995**, *52*, 2995−3009.
(48) Pardo, E.; Ruiz-García, R.; Cano, J.; Ottenwaelder, X.; Lescouëzec, R.; Journaux, Y.; Lloret, F.; Julve, M. *Dalton Trans.* **2008**, *21*, 2780.
(49) Dul, M.-C.; Pardo, E.; Lescouëzec, R.; Journaux, Y.; Ferrando-Soria, J.; Ruiz-Garcia, R.; Cano, J.; Julve, M.; Lloret, F.; Cangussu, D.; Pereira, C. L. M.; Stumpf, H. O.; Pasan, J.; Ruiz-Perez, C. *Coord. Chem. Rev.* **2010**, *254*, 2281−2296.
(50) Grancha, T.; Ferrando-Soria, J.; Castellano, M.; Julve, M.; Pasán, J.; Armentano, D.; Pardo, E. *Chem. Commun.* **2014**, *50*, 7569−7585.
(51) Fortea-Pérez, F. R.; Schlegel, I.; Julve, M.; Armentano, D.; De Munno, G.; Stiriba, S.-E. *J. Organomet. Chem.* **2013**, *743*, 102−108.
(52) do Pim, W. D.; Oliveira, W. X. C.; Ribeiro, M. A.; Faria, É. N. d.; Teixeira, I. F.; Stumpf, H. O.; Lago, R. M.; Pereira, C. L. M.; Pinheiro, C. B.; Figueiredo-Júnior, J. C. D.; Nunes, W. C.; Souza, P. P. d.;

DOI: 10.1021/acs.analchem.6b04979
Anal. Chem. 2017, 89, 2155−2162

Pedroso, E. F.; Castellano, M.; Cano, J.; Julve, M. *Chem. Commun.* **2013**, *49*, 10778−10780.
(53) Peisach, J.; Blumberg, W. E. *Arch. Biochem. Biophys.* **1974**, *165*, 691−708.
(54) Bal, W.; Sokołowska, M.; Kurowska, E.; Faller, P. *Biochim. Biophys. Acta, Gen. Subj.* **2013**, *1830*, 5444−5455.
(55) Kowalik-Jankowska, T.; Ruta, M.; Wisniewska, K.; Lankiewicz, L. *J. Inorg. Biochem.* **2003**, *95*, 270−282.
(56) Syme, C. D.; Nadal, R. C.; Rigby, S. E.; Viles, J. H. *J. Biol. Chem.* **2004**, *279*, 18169−18177.
(57) Hureau, C.; Coppel, Y.; Dorlet, P.; Solari, P. L.; Sayen, S.; Guillon, E.; Sabater, L.; Faller, P. *Angew. Chem., Int. Ed.* **2009**, *48*, 9522−9525.
(58) Dorlet, P.; Gambarelli, S.; Faller, P.; Hureau, C. *Angew. Chem., Int. Ed.* **2009**, *48*, 9273−9276.
(59) Kowalik-Jankowska, T.; Ruta-Dolejsz, M.; Wisniewska, K.; Lankiewicz, L. *J. Inorg. Biochem.* **2001**, *86*, 535−545.

DOI: 10.1021/acs.analchem.6b04979
Anal. Chem. 2017, 89, 2155−2162

A-iii. Supporting information

Supplementary Information

Link Between Affinity and Cu(II) Binding Sites to Amyloid-β Peptides Evaluated by a New Water-Soluble UV-Visible Ratiometric Dye with a Moderate Cu(II) Affinity

Amandine Conte-Daban,[a,b‡] Valentina Borghesani,[a,b‡] Stéphanie Sayen,[c] Emmanuel Guillon,[c] Yves Journaux,[d,e] Geoffrey Gontard,[d,e] Laurent Lisnard[d,e] and Christelle Hureau[a,b]

[a,b] CNRS; LCC (Laboratoire de Chimie de Coordination) ; 205, route de Narbonne, F-31077 Toulouse, France. Université de Toulouse; UPS, INPT ; LCC ; F-31077 Toulouse, France

[c] Université de Reims Champagne Ardenne, Institut de Chimie Moléculaire de Reims (ICMR), UMR 7312 CNRS-URCA, Moulin de la Housse, BP 1039, 51687 Reims Cedex 2, France

[d] Sorbonne Universités, UPMC Univ. Paris 06, UMR 8232, IPCM, F-75005, Paris, France

[e] CNRS, UMR 8232, Institut Parisien de Chimie Moléculaire, F-75005, Paris, France

[†] These authors contribute equally to this work.

1- CHARACTERIZATION OF THE LIGAND AND OF THE Cu(L) COMPLEX

Characterization of H_3Et_2L. 3,4-(diethyloxamate)benzoic acid

^{1}H NMR (400 MHz, DMSO) δ 13.06 (s, 1H), 10.50 (d, J = 18.9 Hz, 2H), 8.12 (d, J = 2.0 Hz, 1H), 7.85 (dd, J = 8.5, 2.0 Hz, 1H), 7.78 (d, J = 8.5 Hz, 1H), 4.32 (qd, J = 7.1, 1.5 Hz, 4H), 1.32 (td, J = 7.1, 1.9 Hz, 6H). ^{13}C NMR (101 MHz, DMSO) δ 166.26, 160.00, 155.77, 155.57, 133.88, 129.13, 128.23, 127.26, 126.99, 124.96, 62.61, 62.53, 13.79, 13.77. IR (cm^{-1}): 3300(m), 3215(w), 1760(m), 1690(s), 1611(w), 1595(m), 1530(m), 1491(w), 1444(w), 1410(w), 1388(m), 1370(w), 1312(w), 1257(w), 1225(m), 1175(s), 1125(w), 1014(m), 945(w), 900(w), 862(m), 845(w), 820(w), 809(w), 774(s), 745(w), 707(w), 640(w), 608(w), 561(w), 542(m), 496(w), 458(m), 378(w), 328(m). Elemental analysis (%) calculated for $C_{15}H_{16}N_2O_8$ (Mr = 352.29 g mol^{-1}): C 51.13, H 4.57, N 7.95. Found: C 51.14, H 4.43, N 8.00.

Characterization of $Na_{1.5}H_{3.5}L{\cdot}2.2H_2O$

^{1}H NMR (400 MHz, DMSO) δ 10.48 (d, J = 18.1 Hz, 2H), 8.14 (d, J = 1.7 Hz, 1H), 7.88 – 7.75 (m, 1H). ^{13}C NMR (101 MHz, DMSO) δ 166.45, 161.67, 161.65, 158.74, 158.62, 134.31, 129.16, 127.71, 127.01, 126.72, 124.22. IR (cm^{-1}): 3272(w), 3194(s), 1659(s), 1607(w), 1529(m), 1492(w), 1442(w), 1359(m), 1292(s), 1226(w), 1183(m), 1098(w), 928(w), 904(w), 841(w), 819(w), 757(m), 727(w), 707(w), 506(w), 452(m). Elemental analysis (%) calculated for $C_{11}H_{10.9}N_2Na_{1.5}O_{10.2}$ (M_r = 368.79 g mol^{-1}): C 35.82, H 2.97, N 7.59. Found: C 35.89, H 3.02, N 7.50.

Characterization of $Li_3[Cu(L)]{\cdot}5.5H_2O$, Cu(L).

IR (cm^{-1}): 3298(bd), 1611(s), 1577(s), 1539(m), 1444(w), 1369(s), 1319(s), 1256(w), 1210(w), 1086(w), 981(w), 875(w), 787(m), 557(w), 448(w). Elemental analysis (%) calculated for $C_{11}H_{14}CuLi_3N_2O_{13.5}$ (M_r = 474.6 g mol^{-1}): C 27.83; H 2.97; N 5.90. Found: C 27.95; H 2.45; N 5.86.

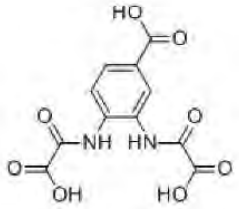

Scheme S1. Acidic form of the ligand, H_5L

Supramolecular arrangement/Crystal packing. On the oxamate groups, the remaining carbonyl functions chelate lithium ions. As a result, these ions link two adjacent complexes, generating thus a corrugated chain of complexes along the crystallographic *c* axis. The chains are further stacked along the crystallographic *b* axis (see Figure S1). See Table S1 and S2 for crystallographic data and for selected bond lengths and angles.

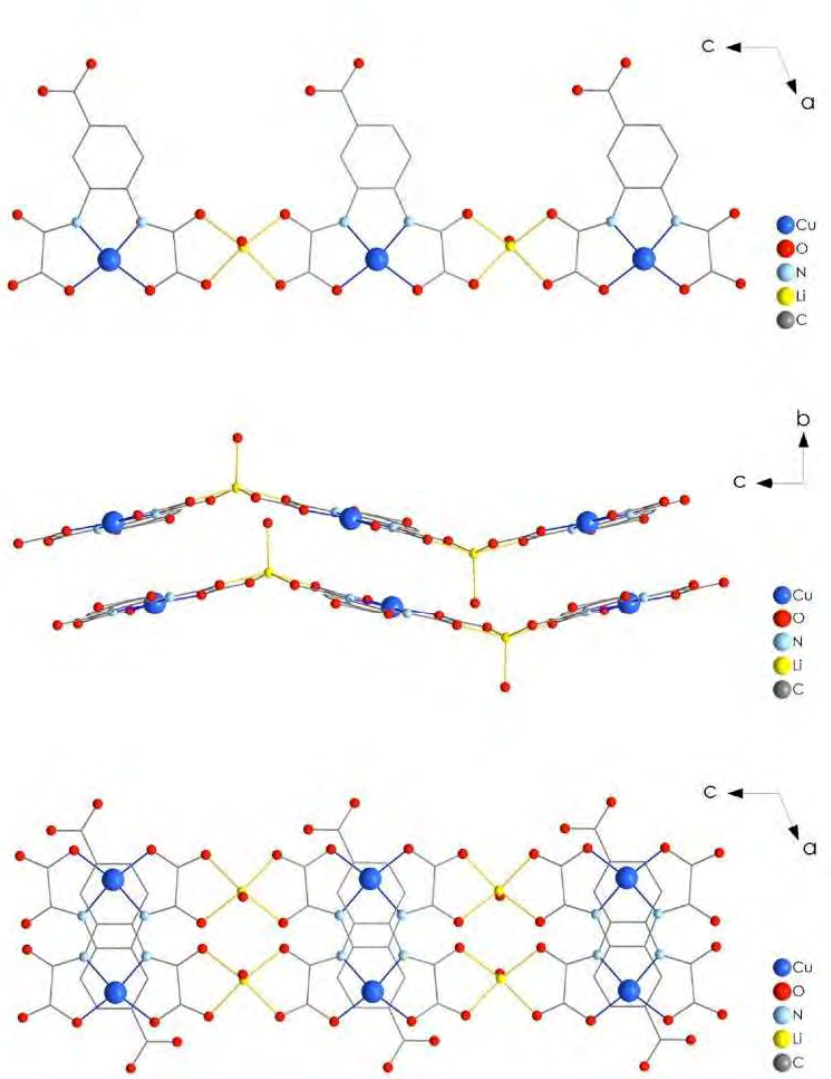

Figure S1. Crystal packing of Cu(L).

Table S1. Crystallographic data.

Formula[a]	$C_{11}H_5CuLi_3N_2O_9$
F.W. [g mol^{-1}]	393.53
Crystal system	Monoclinic
Space group	*C 2/c*
a [Å]	26.3214(15)
b [Å]	6.7217(4)
c [Å]	20.4183(11)
α [°]	90
β [°]	112.590(3)
γ [°]	90
V [Å^3]	3335.3(3)
Z	8
T [K]	200(1)
λ [Å]	1,54178
ρ_{calc} [g cm^{-3}]	1,567
μ ($Cu_{K\alpha}$) [mm^{-1}]	2,293
Measured reflections	16560
Unique reflections	2923
R_{int}	0.0216
Reflections I>2σ(I)	2514
Parameters	271
Restraints	6
R_1[b] [I>2σ(I)]	0.0720
wR_2[c] [I>2σ(I)]	0.2432
GOF	1.128
Largest residuals [eÅ^3]	-0.626 ; 1.658

[a] *Including solvate molecules.*

[b] $R_1 = \sum||F_0| - |F_C||/\sum|F_0|$

[c] $\omega R_2 = [\sum(\omega(F_0^2 - F_c^2)^2)/\sum(\omega(F_0^2)^2)]^{1/2}$

Table S2. Selected bond lengths (Å) and angles (°).

Cu1—O1	1.9588(34) Å	Cu1—N1	1.9061(55) Å
Cu1—O4	1.9642(51) Å	Cu1—N2	1.9127(37) Å
N1—Cu1—N2	83.35 (20) °	O1—Cu—O4	106.26(16) °
N1—Cu1—O1	85.28(17) °	N2—Cu1—O4	85.13(18) °

2- EXAFS PARAMETERS

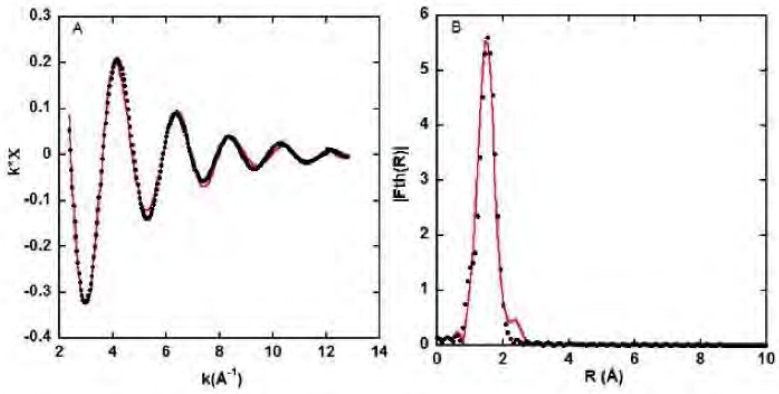

Figure S2. Cu K-edge EXAFS data fitting. Experimental data (dotted black points) and best fit (red lines) of the Cu(L) EXAFS signal, before and after the Fourier Transform, panels A and B respectively. [L] = 1 mM, [Cu(II)] = 0.9 mM, [HEPES] = 0.1 M, pH = 7.0, T = 20K.

3- COMPETITION DATA

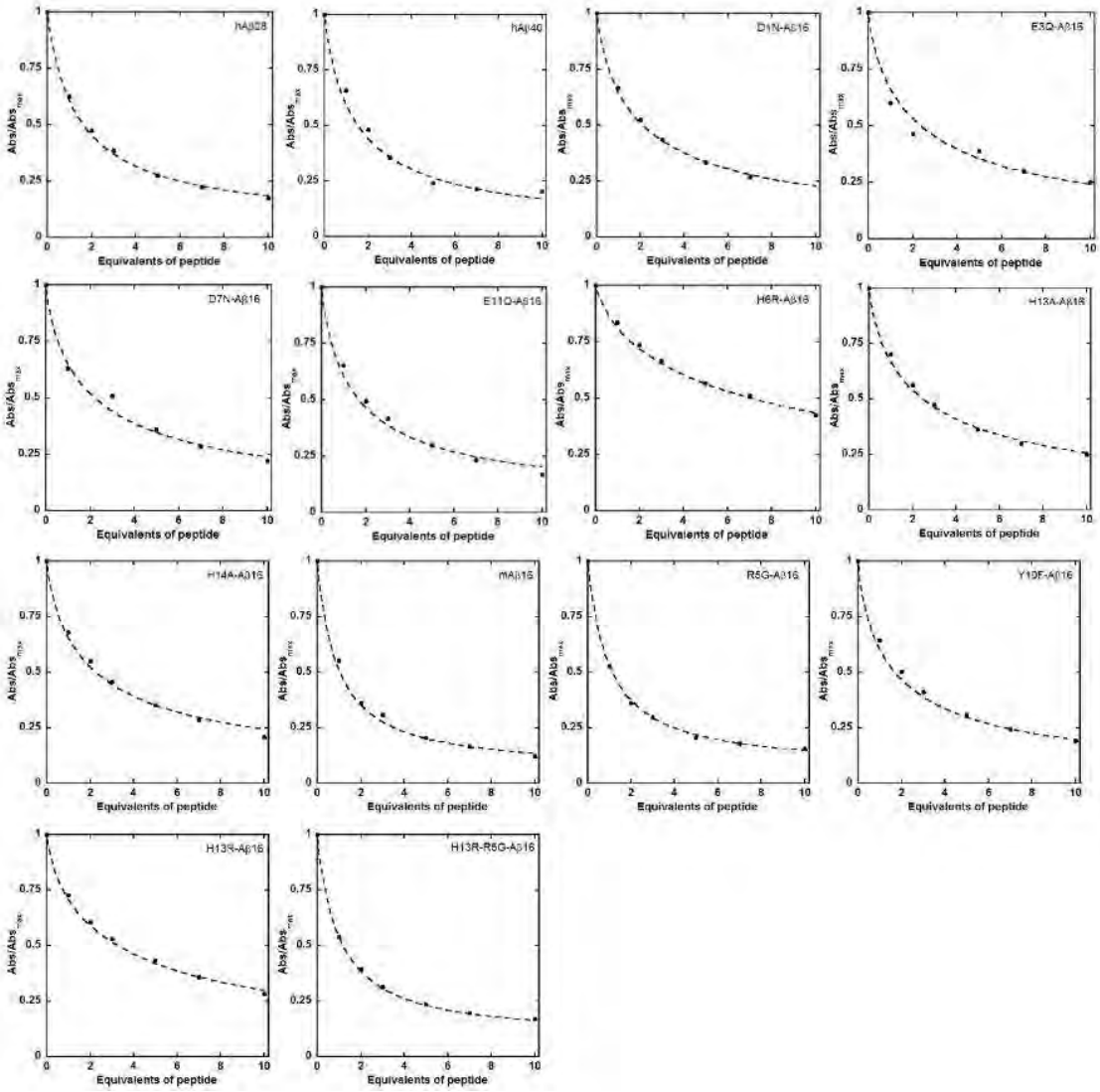

Figure S3. Experimental absorbance (points) and the best fits (dotted lines) of the Cu(L) system upon addition of peptides. |L| = 50 µM, |Cu(II)| = 45 µM, |peptides| = 0 to 500 µM, |HEPES| = 0.1 M, pH = 7.1, T = 25°C (where mentioned).

4- ERROR BAR

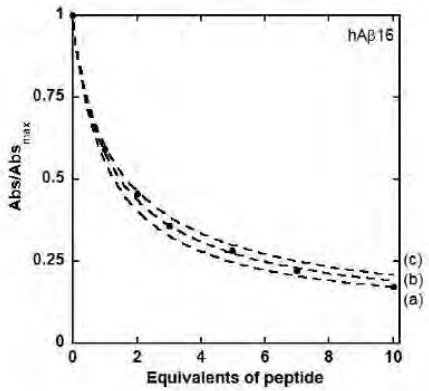

Figure S4. Experimental absorbance (points) and its fits (dotted lines) of the Cu(II) system upon addition of increasing equivalents of $hA\beta_{16}$, with (a) $K_a = 2.04\ 10^9$, (b) $K_a = 1.61\ 10^9$, (c) $K_a = 1.34\ 10^9$. [T] = 50 µM, [Cu(II)] = 45 µM, $[hA\beta_{16}]$ = 0 to 500 µM, [HEPES] = 0.1 M, pH = 7.1, T = 25°C.

The accuracy of the fitting procedure is shown in the Fig. S4. The best fit is the (b) one and the curves (a) and (c) are calculated with ± 20 % of difference in the K_a value. The fits (a) and (c) are not so closed to the best reproduction of the experimental data, so the error bar on the K_a value is below 20 %.

5- Cu COORDINATION MODEL

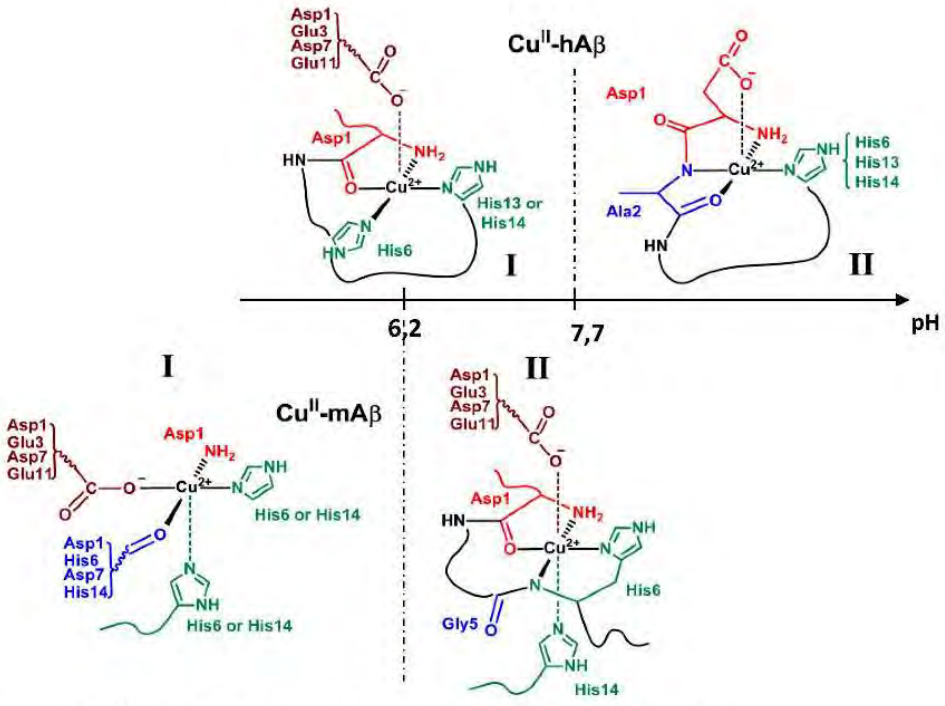

Scheme S2. Cu(II) coordination model for the human and the murine Aβ peptides.

B- Zn(II) coordination to Aβ peptide

This section focuses on the Zn(II) coordination to the Aβ peptide. It is composed of a summary of the article published in *Inorganic Chemistry* in 2016, the publication itself and finally the supporting information. My contribution to this work has been some NMR experiments and the analysis of the NMR results and participation in the writing.

B-i. Summary

This article describes the Zn(II) coordination to the Aβ peptide at pH 7.4. The study of the interaction between Zn(II) and Aβ peptide is biologically relevant since Zn(II) is the most common transition metal ion involved in the neurotransmission signal. It is present in higher concentrations in the synaptic cleft than Cu. In addition, important concentrations of Zn(II) have been found in the senile plaques, evidencing the interactions between Zn(II) and Aβ. Previous works have described a possible protective role of Zn(II) ion, such as the precipitation of Aβ in excess into redox-silent species. Moreover, as previously explained, Zn(II) has also an impact on the Cu(II) coordination, on the ROS production by the Cu-Aβ complex and on the aggregation of the peptide; it is thus important to understand its interaction with the peptide in order to understand its impact in the disease. Zn(II) coordination models already exist, but are still debated. Investigation of Zn(II) coordination is a difficult task since Zn(II) is silent in most of the spectroscopic technics and the flexibility of Aβ peptide precludes X-Ray characterization. In this work, XAS and NMR studies are paralleled; a first EXAFS study determines the number of ligands coordinating the metal ion. Then NMR and XANES studies with a wide series of mutated Aβ peptides allow the characterization of the amino acids involved in Zn(II) binding. The affinity constant is also discussed.

The first part of this work focuses on the characterisation of the Zn(II) binding site to Aβ. An EXAFS study allows to determine the number and the nature of the atoms involved in the metal ion coordination and also the distance between the metal centre and the coordinating atoms. However, due to the ill-defined coordination sphere of Zn(II), only the first shell can be solved. The fitting of the experimental data proposes a 4N/O shell at an average 1.98 Å distance from Zn(II). A complementary NMR study investigates also the binding site of Zn(II), using comparisons between the spectrum of Aβ and the one of the Zn(II)-Aβ complex. Two kind of modifications of the spectra are observed due to the addition of Zn(II) to Aβ: the broadening of some protons and their up- and down-field shift. Protons in the close vicinity of the atom bound to Zn(II) due to Lewis acidity of Zn ion have their signal modified. In addition, remote protons can also be impacted since chelation of Zn(II) by Aβ leads to modifications

in the “folding” of the peptide, and the protons, even not involved in the coordination, exhibit different signals than the ones for Aβ. Hence, signals associated to more than four different amino-acid residues, are affected by the presence of Zn(II) and so the coordination site cannot be straightforwardly characterized.

The second part of this article presents the XANES and NMR studies of a wide series of Aβ modified peptides. For the XANES experiment, comparison of the Zn(II)-Aβ spectrum and of the Zn(II)-mutant spectrum allows to identify the amino acids involved in the coordination of the metal ion. First of all, the white line intensity of the XANES data is in good agreement with the four-coordination of Zn(II). Furthermore, the data are consistent with biological systems, with a four-coordination including two Histidine, except for the Zn(II)-E11Q complex. If one Histidine is mutated, it is replaced by another one; two Histidine being always involved in the Zn(II) coordination. For the E11Q mutant, the carboxylate group is replaced by a Histidine, leading to a four-coordination with three Histidine. In summary, the XANES data describe a four-coordination system, involving two Histidine for the native peptide. The main amino acids inducing changes in the XANES fingerprints are the mutations of the Histidine (H6A, H13A and H14A) and the mutation E11Q. Some weak changes upon the Zn(II) addition are induced by the N-terminal acetylation and by the D1N, E3Q and D7N mutations.

NMR study is needed to gain more insights in the coordination of Zn(II) to Aβ. The NMR spectra are compared between each other and there are two possibilities: (i) if the changes induced by Zn(II) on Aβ fingerprint and on the mutant one are the same, the amino acid mutated is not involved in the Zn(II) coordination, (ii) if these changes are different, the amino acid is important for the coordination. The first important point of this study is the determination of which Histidine is involved in the binding of the metal ion. H13A and H14A have shown the broadening of R5 (mutants in which H6 can coordinate the metal ion), which disappeares for the H6A, evidencing the importance of H6 in the coordination. Moreover, the affinity constant of H6A for Zn(II) is lower than H13A and H14A. Regarding H13, there is no important broadening upon Zn(II) addition for the mutation H13A while for the wild type Aβ there is. H13 should be involved in the Zn(II) coordination. In addition, V12 signal is affected for H6A and H14A (mutants in which H13 can coordinate the metal ion) but is not for H13A. This evidences the implication of H13 in the Zn(II) coordination. All of these data lead to the conclusion that H6 is involved in the Zn(II) coordination, but H13 and H14 are in a dynamic exchange (Figure 2). The other important point of this part is the determination of the importance of the carboxylate groups. The carboxylate groups of Asp1, Glu3 and Asp7 are in a dynamic exchange for the binding of Zn(II), whereas the carboxylate of Glu11 binds Zn(II) independently (Figure 2). The last important point of this part is the importance of the N-terminal amine. The changes induced by the addition of Zn(II) for the

Aβ peptide and for the N-terminal acetylated are identical, meaning that the changes are due to the involvement of the carboxylate side chain the Asp1. This is in line with the weak decrease of the affinity constant for Zn(II) of the N-terminal acetylated peptide. Contrary to what is previously proposed in the literature, the N-terminal amine is not involved in the Zn(II) coordination at pH 7.4 (Figure 2), but seems to be involved at higher pH (around 9).

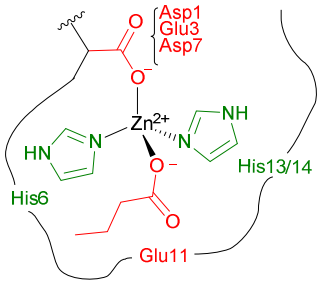

Figure 2. Scheme of the Zn(II) coordination site to Aβ16.

In conclusion, this article describes the Zn(II) coordination mode to Aβ at pH 7.4. His6 and Glu11 bind Zn(II). The carboxylate group of Asp1, Glu3 and Asp7 are in a dynamic exchange for one binding position, as well as the His13 and the His14 for another one. This binding site is different from the Cu(II) one. This is in line with a largely stronger affinity for Cu(II) compared to Zn(II) (4 order of magnitude) This impacts also the global charge of these complexes, since Cu(II) is bound to the deprotonated N-terminal amine whereas Zn(II) is not bound and the amine is protonated. This difference could participate in the distinct behaviour of Cu and Zn-induced Aβ aggregation.

B-ii. Article

Inorganic Chemistry

Article

pubs.acs.org/IC

Zinc(II) Binding Site to the Amyloid-β Peptide: Insights from Spectroscopic Studies with a Wide Series of Modified Peptides

Bruno Alies,[†,‡,§] Amandine Conte-Daban,[†,‡] Stéphanie Sayen,[∥] Fabrice Collin,[†,‡,⊥] Isabelle Kieffer,[#,¶] Emmanuel Guillon,[*,∥] Peter Faller,[†,‡,□] and Christelle Hureau[*,†,‡]

[†]CNRS, LCC (Laboratoire de Chimie de Coordination), 205 Route de Narbonne, BP 44099, F-31077 Toulouse Cedex 4, France

[‡]Université de Toulouse, UPS, INPT, F-31077 Toulouse Cedex 4, France

[∥]Université Reims Champagne Ardenne, Institut de Chimie Moléculaire de Reims (ICMR), UMR 7312 CNRS-URCA, Moulin de la Housse, BP 1039, 51687 Reims Cedex 2, France

[⊥]Université de Toulouse, UPS, UMR 152 PHARMA-DEV, Université Toulouse 3, and Institut de Recherche pour le Développement (IRD), UMR 152 PHARMA-DEV, F-31062 Toulouse Cedex 09, France

[#]Observatoire des Sciences de l'Univers de Grenoble (OSUG), CNRS UMS 832, 414 Rue de la Piscine, 38400 Saint Martin d'Hères, France

[¶]BM30B/FAME, ESRF, The European Synchrotron, 71 Avenue des Martyrs, 38000 Grenoble, France

S *Supporting Information*

ABSTRACT: The Zn(II) ion has been linked to Alzheimer's disease (AD) due to its ability to modulate the aggregating properties of the amyloid-β (Aβ) peptide, where Aβ aggregation is a central event in the etiology of the disease. Delineating Zn(II) binding properties to Aβ is thus a prerequisite to better grasp its potential role in AD. Because of (i) the flexibility of the Aβ peptide, (ii) the multiplicity of anchoring sites, and (iii) the silent nature of the Zn(II) ion in most classical spectroscopies, this is a difficult task. To overcome these difficulties, we have investigated the impact of peptide alterations (mutations, N-terminal acetylation) on the Zn(Aβ) X-ray absorption spectroscopy fingerprint and on the Zn(II)-induced modifications of the Aβ peptides' NMR signatures. We propose a tetrahedrally bound Zn(II) ion, in which the coordination sphere is made by two His residues and two carboxylate side chains. Equilibria between equivalent ligands for one Zn(II) binding position have also been observed, the predominant site being made by the side chains of His6, His13 or His14, Glu11, and Asp1 or Glu3 or Asp7, with a slight preference for Asp1.

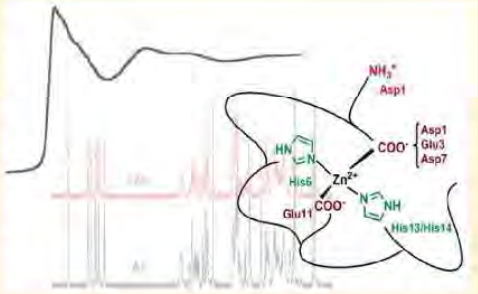

INTRODUCTION

Alzheimer's disease (AD) is the most common cause of dementia in the elderly population, accounting for 50−80% of dementia cases. The worldwide prevalence of AD is approximately 30 million, a number that is expected to quadruple within the next 40 years.[1] As a direct consequence, AD currently represents a major global public health problem with increased impacts of AD over a short time scale.

AD shares some molecular features with other neurodegenerative diseases such as Parkinson's disease, prion diseases, and amyotrophic lateral sclerosis. This includes, in addition to the presence in diseased brains of proteinaceous aggregates, the role of metal ions, mainly copper and zinc, which are directly involved in the degeneration. Indeed, several studies have shown abnormalities in brain homeostasis and in metabolism of copper and zinc ions in neurodegenerative diseases.[2] In AD, the neurohistological hallmarks detected post-mortem are extracellular amyloid plaques, also called senile plaques, and intracellular neurofibrillary tangles of hyperphosphorylated Tau protein. It has been proposed that the apparition of the amyloid plaques precedes, and thus likely induces, the hyperphosphorylation of Tau protein and the associated neuronal degeneration.[1] According to the amyloid cascade hypothesis, the mismetabolism of a peptide, called amyloid-β (Aβ), its accumulation, and aggregation in insoluble forms in the senile plaques are thus key early events in AD pathogenesis. In addition, soluble monomeric forms are found in healthy brains, while the amyloid plaques, rich in Aβ aggregates and copper and zinc ions, are detected in AD patient's brains.[3,4]

The Aβ peptide is mainly a 40/42-residue peptide with a N-terminal hydrophilic part containing potential ligands of metal ions (from positions 1 to 16) and a C-terminal hydrophobic part (from positions 17 to 42). Aβ is able to bind metal ions using several residues including the N-terminal amine, the side

Received: July 19, 2016
Published: September 26, 2016

DOI: 10.1021/acs.inorgchem.6b01733
Inorg. Chem. 2016, 55, 10499−10509

Scheme 1. Aβ Peptide in the Protonation State Predominant at pH 7.4[a]

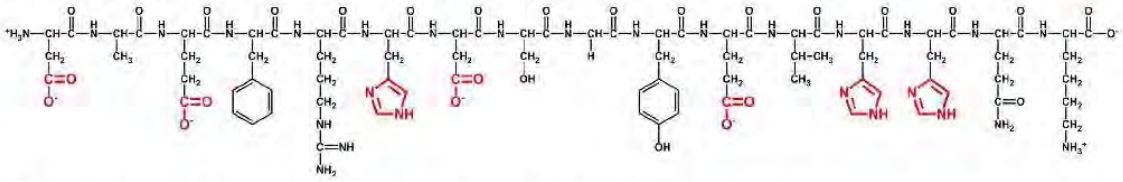

[a]The functional groups of the amino acid residues potentially involved in Zn(II) binding are highlighted in red.

chains of the carboxylic acid residues at positions 1 (Asp), 3 (Glu), 7 (Asp), and 11 (Glu), and the side chains of the three His residues at positions 6, 13, and 14. These residues are all located in the 1−16 region, which is located near the central hydrophobic core (residues 17 to 21) involved in Aβ dimerization (first step of the aggregation), and thus binding of metal ions can modulate the aggregating properties of Aβ.[3,5,6] Analyses by different NMR techniques and other means showed that adding Zn(II) to Aβ40 affected predominantly the first 16 amino acids.[7,8] Thus, it is well established that the first coordination sphere of Zn binding lies in the first 16 amino acids sequence (peptide noted Aβ16), which is a correct model of the first coordination sphere on Zn(II) binding to the soluble monomeric Aβ40/42. However, it is not excluded that the other part of the peptide (amino acids 17−40/42) could contribute to the second or third coordination sphere and hence modulate slightly the coordination.

In line with the previous statements and supported by studies in vitro, in cell cultures, and in AD model animals, metal ions have been proposed to play key roles in the development of AD via their intervention in the amyloid cascade process.[1−3] In contrast to redox-active Cu ions, for which the deleterious impact in AD is linked to oxidative stress[3,9−11] and to a lesser extent to formation of oligomeric and fibrillar aggregates[5] is acknowledged, the impact of the redox-silent Zn ion is less obvious.[12,13] A positive impact of Zn(II) has mainly been proposed, with modes of action that include the precipitation of Aβ in excess into a redox-inert form, precipitation of toxic aggregates, formation of nontoxic aggregates,[12,14−16] and chaperone mimicking,[17] while negative effects of Zn were mainly attributed to the promotion of oligomeric forms.[18,19] Additionally, Zn(II) is the most common transition metal ion involved in neuronal signal transmission being released by certain glutamatergic neurons and can be present in high amounts in the synaptic cleft.[20−22] Both Cu and Zn(II) ions can bind Aβ in the synaptic cleft since the dissociation constants of Aβ for Cu(II) and Zn(II) are ~10^{-10} M[23,24] and ~10^{-5} M,[24,25] respectively, while their respective concentration can reach ~10 μM[26,27] and 300 μM.[20] Note that the dissociation constant of Aβ for Cu(I) is still under debate, with the most relevant propositions spanning from 10^{-7} M[28] to 10^{-10} M.[29] In addition, Zn(II) is found at higher concentration (~1 mM) than Cu (~400 μM) in the senile plaques.[30−32] Most of the current chemical studies on the influence of metal ions in the amyloid cascade are mainly dedicated to the role of Cu, because it seems to be the most pertinent therapeutic target for chelation therapy. However, Zn(II) is also important since it can have a direct impact in the amyloid cascade according to the elements discussed above but also because it can interfere with the deleterious role of Cu. As a consequence, there is a need for better understanding of how Zn(II) intervenes in the amyloid cascade. The first step to reach this long-term objective is to decipher the coordination site of Zn(II) in the N-terminal part of the peptide. This is highly difficult because there is no direct way to investigate Zn(II) interactions with the multiple possible anchoring sites (due to the spectroscopically silent nature of Zn(II)). In addition, the flexibility of the peptide precludes any characterizations by X-ray diffraction studies. As a consequence, there are currently several coordination models debated in the literature (refs 13 and 33 and Table S1). To circumvent these limitations, we investigate Zn(II) binding to Aβ16 (a well-accepted model for Zn coordination to the full-length Aβ40/42)[7,8,34] and a wide series of its modified counterparts by NMR and XAS (X-ray absorption spectroscopy) spectroscopies. Throughout the description of the present work, Aβ16 will be noted Aβ for convenience reasons. EXAFS (extended X-ray absorption fine structure) is useful to determine the number of surroundings atoms, while the impact of peptide modifications on Zn(II)−peptide species can be monitored by XANES (X-ray absorption near-edge structures). The evaluation of Zn(II)-induced alterations of the NMR signatures of Aβ and its modified counterparts also brings new insights into the Zn(II) binding site to Aβ. In addition, the results of affinity measurements of Zn to Aβ and its modified counterparts were also integrated.[25] Hence, the strength and robustness of the present study lie in the use of several complementary techniques and samples, which is unparalleled in the literature.

RESULTS

Zn(II) Coordination to the Aβ Peptide. *EXAFS.* Due to its d^{10} electronic configuration, the Zn(II) ion is "silent" in most of the classical spectroscopic techniques (UV−vis, EPR, etc.). Hence, its coordination sphere can mainly be directly probed by X-ray absorption spectroscopy, either XANES or EXAFS. The XANES signature carries a lot of structural information that has been analyzed qualitatively. The analysis is described below since not only the Aβ peptide but also modified peptides have been studied (see paragraph Zn(II) Coordination to Modified Aβ Peptides: XANES). More quantitative data can be obtained only after simulation of the spectrum. Development of simulation approaches that can be applied to the study of biological systems are currently emerging but still require a starting structural dataset, provided for instance by X-ray crystallography.[35] Since such structural data are not available in the present case, exploration of XANES simulations has been considered to be outside the scope of our study.

EXAFS data can give access to the nature, number, and distance of the coordinating atoms. However, in the case of the Aβ peptides, the data recorded suffer from the ill-defined coordination sphere of the Zn(II) ions, and in line with previous observations,[34,36,37] the number of useful oscillations is limited. This is a common feature of such peptidic species that

DOI: 10.1021/acs.inorgchem.6b01733
Inorg. Chem. 2016, 55, 10499−10509

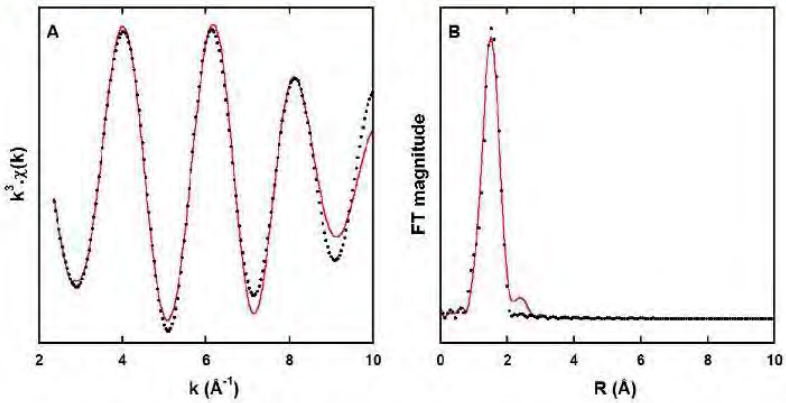

Figure 1. k^3-Weighted experimental (black dots) and least-squares fitted (red line) first coordination shell EXAFS spectra of the Zn(Aβ) at pH 6.9 (A) and the corresponding non-phase-shift-corrected Fourier transforms (B). Recording conditions: [Aβ] = 1.0 mM, [Zn(II)] = 0.9 mM in Hepes buffer 50 mM, T = 20 K.

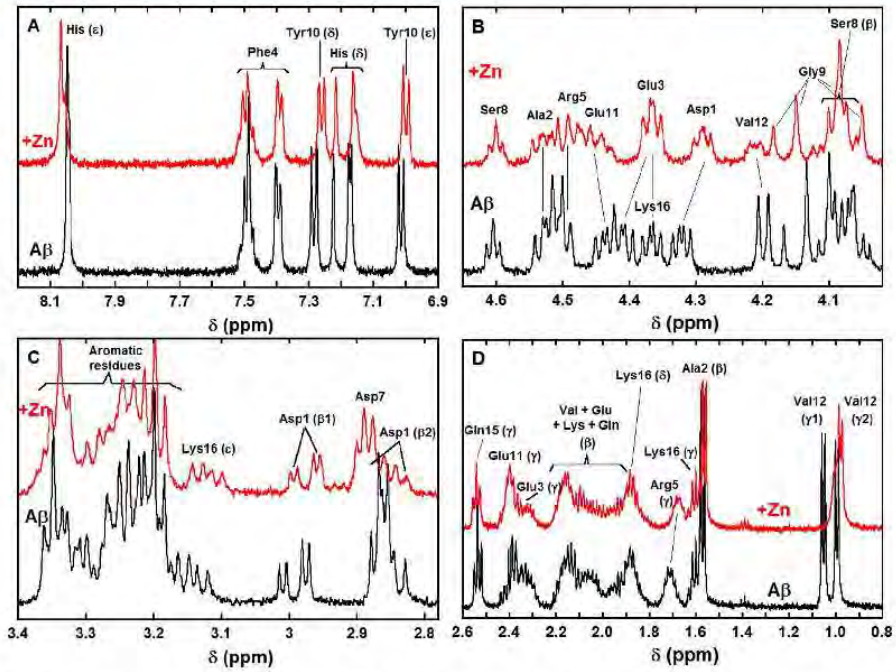

Figure 2. ^{1}H NMR spectra of Aβ (bottom black lines) and of Aβ in the presence of 0.9 equiv of Zn(II) (top red lines) in selected regions (A: aromatic, B: Hα, C: Hβ, D: Hβ and Hγ, unless otherwise specified). [Aβ] = 300 μM, [Zn(II)] = 270 μM in d_{11}-TRIS buffer 50 mM, pH = 7.4, T = 318 K, ν = 500 MHz. δ(His6 Hδ) > δ(His14 Hδ) > δ(His13 Hδ). For the details of the amino acid residue nomenclature, see Scheme S1.

differ from either Zn metalloprotein[38] or inorganic complexes,[39] for which more insights can be obtained due to a higher number of well-resolved oscillations. Hence, only the first coordination sphere can be determined in the present case. Experimental and fitted first coordination shell EXAFS spectra and their corresponding Fourier transform of Zn(II) bound to Aβ at pH 6.9 are shown in Figure 1 (and the corresponding unfiltered data are shown in Figure S1). The EXAFS oscillations are best reproduced with a 4N/O shell at an average distance of 1.98 Å from the metallic center (see all parameters in Table S2). In addition, to confirm the four-coordination of the Zn center, the bond-valence sum (BVS) theory was applied.[40,41] The bond valence calculated using the equation reported by Thorp[40] is equal to 0.52, in line with the corresponding calculated Zn oxidation state of 2.08 in the case of a four-coordinated Zn, while a five-coordination environment would have led to an unrealistic value (2.60) for the Zn oxidation state. This strongly supports a tetrahedrally bound Zn(II), in line with the most widespread environment for this ion in biological systems.[42]

DOI: 10.1021/acs.inorgchem.6b01733
Inorg. Chem. 2016, 55, 10499−10509

NMR. Another way to investigate the coordination sphere of the Zn(II) is to determine how its binding impacts the NMR signature of potential coordinating groups from the Aβ peptide. The impact can be either a broadening of some protons or their up- or downfield shift. Such modifications of the NMR spectrum can witness (i) the direct binding of the Zn(II) ion in the close vicinity of protons affected by the Zn(II)-induced change of Lewis acidity or (ii) the indirect changes in the folding of the peptide upon Zn(II) binding, which affected protons more distant from the Zn(II) binding site, while shifts arise from a different chemical environment of the proton of interest; broadening finds its origin in a fast equilibrium between Zn-bound and free peptide. However, we could not find any direct correlation between the type of Zn(II)-induced modifications (broadening versus chemical shift changes) and the involvement of residues as direct Zn(II) ligands or structural changes. This might be due to the overall very high flexibility of the peptide ligand in which all Zn(II) binding groups can exchange on a fast time scale.

Zn(II) coordination models from published NMR studies are not fully convergent. This could be due to different experimental conditions (length of peptides (Aβ16, Aβ28, Aβ40), buffer, temperature, etc.)[43,44] and/or means used for increasing the solubility of the Aβ peptide (use of PEGylated counterpart of the peptide,[45] N-terminal acetylation of Aβ,[46] or study in water-micelle environment).[47] However, such modifications (of the peptide or of the medium) can alter the native Zn(II) binding coordination to the peptide.

In the present study, we performed ^{1}H NMR because the peptide concentration is limited to a maximal value in the low millimolar range, above which precipitation occurs in the presence of Zn(II). Such low concentration precludes the use of ^{13}C or 2D NMR unless ^{13}C- and ^{15}N-labeled peptide is used,[7] but in contrast to ^{13}C- or 2D-labeled Aβ40, the modified counterparts are not commercially available. Several recording conditions were tested and conditions under which the Zn(II)-induced broadening of the peptide protons is the most specific, i.e., the effect is clearly observed (not too weak as in ref 43) but the broadening is not too strong (so that it becomes weakly specific, as observed in ref 44 for a Zn(II):peptide ratio of 1:1), were used. Only the formation of 1:1 Zn(Aβ) as predominant species was detected under those conditions (see Figure S4), in line with previous reports relying on either NMR titration[43,44] or determination of the hydrodynamic radius by NMR or gel filtration studies.[17,48] Note that proton attributions are based on previous works.[49,50]

In the aromatic region (panel A in Figure 2), protons of the three His residues are impacted by the addition of Zn(II). The three His Hδ (respectively Hε; for nomenclature of the protons, see Scheme S1) are slightly down-shifted (respectively up-shifted). Only one out of the three His Hδ is significantly broadened upon Zn(II) addition. Both the Hδ and Hε protons from the Tyr10 are down-shifted, with a stronger shift for the Hδ. In the Hα region (panel B in Figure 2), the most obvious modifications induced by Zn(II) are (i) strong broadening of the Val12 Hα, (ii) down-shift of the Asp1 Hα, and (iii) down-shift (respectively up-shift) of the Glu3 and Glu11 Hα, with a relatively intense broadening for the latter one. In the Hβ region (panel C in Figure 2), the two diastereotopic Asp1 Hβ_1 and Hβ_2 are brought closer and the Asp7 Hβ are up-shifted. Lastly, in the low-field region (panel D in Figure 2), broadening of Val12 Hγ_1 is clearly observed as well as a slight broadening and down-shift of the Arg5 Hγ and a weak down-shift of the Ala2 Hβ. The impact of Zn(II) addition on other protons is more difficult to unambiguously detect due to the superimposition or closeness of signals. The various effects of Zn(II) addition on pertinent protons from Aβ amino acid residues are summarized in Table S3, entry 1. Note that for convenience reasons the XAS and NMR data shown in Figures 1 and 4 and in Figures 2, 5, 6, and 7 have been recorded at pH 6.9 and 7.4, respectively (for further details, see the Supporting Information). The pH 7.4 and 6.9 counterparts of Figures 1, S1, 2, and 4 are given in the Supporting Information (Figures S2, S3, S5, and S6).

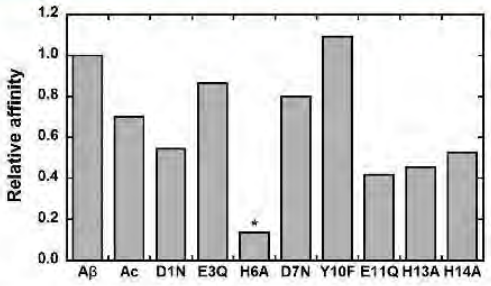

Figure 3. Zn(II) binding affinity values for the various modified peptides relative to Aβ. For the H6A mutant (*), the given value corresponds to a maximum value.

Zn(II) Coordination to Modified Aβ Peptides. *Affinity Values.* From the data obtained with the sole peptide, it is difficult to determine the Zn(II) binding site. In particular, the NMR study is not sufficient since more than four coordinating groups are impacted by Zn(II) addition. As previously pointed out,[13,33,43] this strongly suggests the presence of several possible sites in equilibrium, in line with what has already been evidenced for Cu(I),[3,51,52] Cu(II),[3,49,51] and Fe(II)[3,50,51] ions bound to Aβ peptide. This is the reason that we use here an indirect strategy relying on the use of pertinent modified Aβ peptides. In a previous publication, we have reported the impact of nine Aβ modifications on the Zn(II) binding affinity.[25] Evaluation of the affinity is another indirect way to probe the amino acid residues important for Zn(II) binding. The results are recounted in Figure 3, which shows the relative Zn(II) affinity of each altered peptide (namely, Ac-Aβ, D1N-Aβ, E3Q-Aβ, H6A-Aβ, D7N-Aβ, Y10F-Aβ, E11Q-Aβ, H13A-Aβ, and H14A-Aβ) with respect to Aβ. The impact of acetylation and His6 and Glu11 mutation were in line with previous data obtained by calorimetry.[53]

Here, we have performed XANES and NMR studies of Zn(II) binding to the same nine altered peptides. [Note that preliminary EXAFS data were recorded with all modified peptides, but they do not show any significant differences with the Aβ peptide. Trying to obtain more insightful data would have required too much time than the beam-time allocated.] Monitoring how sequence alteration impacts the XANES signature of the Zn(II)−peptides species helps to identify the amino acids key for Zn(II) binding. By NMR, changes induced by Zn(II) binding on the peptides will be compared between the Aβ and the modified peptides. Two possibilities can be foreseen: (i) if the changes induced by Zn(II) to the NMR spectrum of the Aβ peptide and its modified counterparts are identical, then the modified amino acid residue is not strongly involved in Zn(II) binding; (ii) if the changes induced by

DOI: 10.1021/acs.inorgchem.6b01733
Inorg. Chem. 2016, 55, 10499−10509

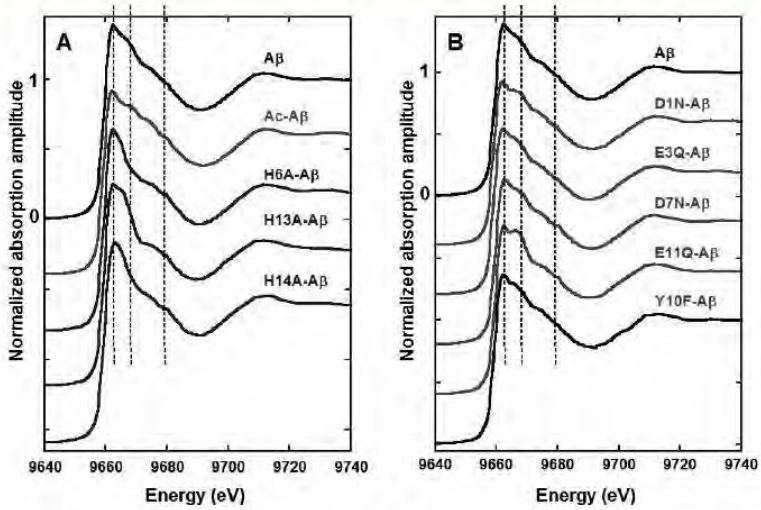

Figure 4. Zn(II) K-edge XANES spectra of Zn(II) bound to Aβ (black line) and to N mutants (panel A) and O mutants (panel B), Hepes buffer 50 mM pH 6.9, [Zn(II)] = 1.0 mM, [peptide] = 1.1 mM, T = 20 K. Normalization of the amplitude is given for the reference Zn(Aβ) complex.

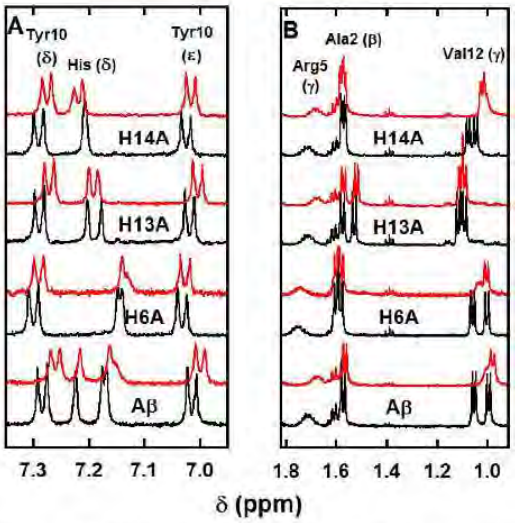

Figure 5. ^{1}H NMR spectra of Aβ peptide and His-Ala mutants (bottom black lines) and of Aβ peptide and His-Ala mutants in the presence of 0.9 equiv of Zn(II) (top red lines) in selected regions (panel A: aromatic, panel B: Hβ and Hγ). [peptide] = 300 μM, [Zn(II)] = 270 μM in d_{11}-TRIS buffer 50 mM, pH = 7.4, T = 318 K, ν = 500 MHz.

Zn(II) to the NMR spectrum of the Aβ peptide and its modified counterparts are different (Zn(II) can have either a weaker or a stronger impact), then the modified amino acid residue is involved in Zn(II) binding. Because insights gained into Zn(II) binding site using spectroscopic studies obtained with modified peptides are indirect, use of complementary techniques is required to get reliable insights and data analysis has to be performed very carefully.

XANES. Figure 4 shows the XANES patterns of Zn(II) bound to Aβ peptide and altered counterparts on the N (panel A) and O (panel B) amino acid residues with coordinating abilities (to compare with the XANES signature of free Zn(II), see Figure S7). As a general trend, the white line intensity of the XANES spectra of all Zn(II)−peptides complexes is in line with a four-coordination of the metal center,[38] thus (i) strengthening the EXAFS data for the Zn(Aβ) species and (ii) indicating that when a residue is modified and made unable to bind the Zn(II) ion, it is replaced by another equivalent one keeping the coordination number to four in the Zn(II) complexes of modified peptides. In addition, the pattern of the white line of all peptidic complexes except the Zn(E11Q-Aβ) is reminiscent of the signature of biological systems with two His residues bound (and a coordination number of four).[38] In line with the previous statement, this suggests that when one His is mutated, preventing its Zn(II) binding, it is replaced by another one. Regarding the E11Q mutation, the spectrum of the Zn(II) complex resembles more a system with three His bound.[38] Hence, this would imply that in this particular case the binding of the carboxylate group from Glu11 is replaced by the third available His. With the desire not to overinterpret the XANES data, we have mainly focused on the comparison of the impact of mutations of the Aβ peptide on the XANES signatures of the Zn(II) complexes to decipher the most important residues for Zn(II) binding. While some mutations, namely, H13A, H6A, H14A, and E11Q, induce significant differences in the XANES fingerprints by comparison to Zn(Aβ), other modifications, namely, N-terminal acetylation, and D1N, E3Q and D7N mutations induce weaker changes. Finally, the Y10F mutation has no impact.

NMR. Histidine Residues. To identify from which His the Hδ that is strongly broadened in the presence of Zn(II) comes from, the impact of Zn(II) binding to the three His-Ala mutants was studied (Figure 5, panel A, Figures S8−S10, and Table S3, entries 3−5). With the H6A-Aβ and to a lesser extent the H14A-Aβ mutants but not with the H13A-Aβ, the broadening is maintained. This agrees with the NMR of the Aβ peptide, in which the His13 Hδ signal undergoes a strong broadening in the presence of Zn(II). This is in line with the examination of the Val12 Hγ resonance plotted in Figure 5,

DOI: 10.1021/acs.inorgchem.6b01733
Inorg. Chem. 2016, 55, 10499−10509

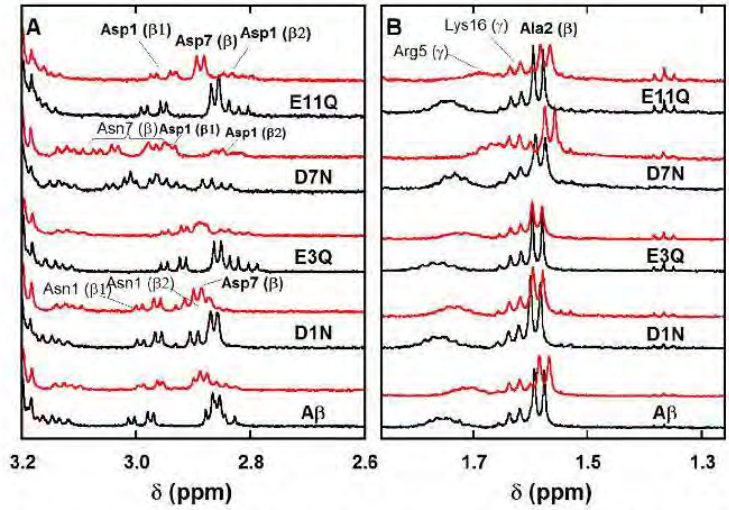

Figure 6. ^{1}H NMR spectra of Aβ peptide and Asp-Asn and Glu-Gln mutants (bottom black lines) and of Aβ peptide and Asp-Asn and Glu-Gln mutants in the presence of 0.9 equiv of Zn(II) (top red lines) in selected regions (panel A: aromatic, panel B: Hβ and Hγ). [peptide] = 300 μM, [Zn(II)] = 270 μM in d_{11}-TRIS buffer 50 mM, pH = 7.4, T = 318 K, ν = 500 MHz.

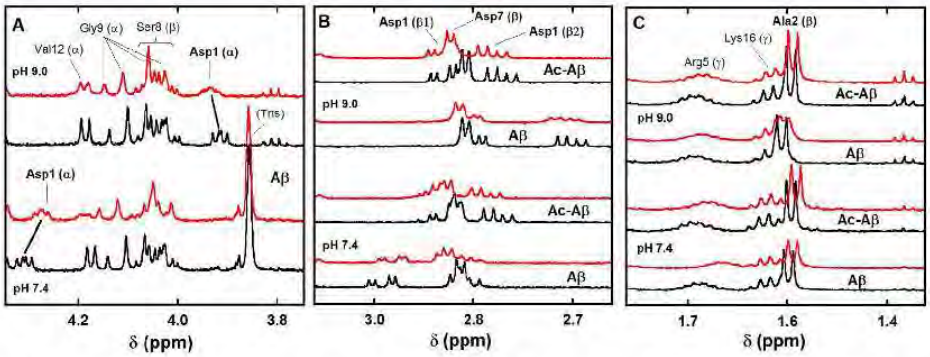

Figure 7. ^{1}H NMR spectra of Aβ and Ac-Aβ peptides (bottom black lines) and of Aβ and Ac-Aβ peptides in the presence of 0.9 equiv of Zn(II) (top red lines) in selected regions as a function of pH (panel A: Hα, panel B: Asp Hβ, * stands for Asp7 protons, and panel C: Ala 2 Hβ). [peptide] = 300 μM, [Zn(II)] = 270 μM in d_{11}-TRIS buffer 50 mM, pH = 7.4 or pH = 9.0, T = 318 K, ν = 500 MHz.

panel B, which is affected (both broadened and shifted) by Zn(II) addition for the Aβ peptide and the H6A-Aβ and H14A-Aβ mutants, but not for H13A-Aβ. Here, we can also note that the Arg5 Hγ is down-shifted upon addition of Zn(II) to the Aβ peptide and the H13A-Aβ and H14A-Aβ mutants but not to the H6A-Aβ mutant, indicating that this Zn(II)-induced shift is due to Zn(II) binding to the nearby His6 rather than to Arg5 itself as previously proposed.[13] These observations point to the involvement of the three His residues in the Zn(II) binding, but with various contributions. In particular, the roles of His13 and His6 are probed by broadening on the Val12 and Arg5 resonances, respectively, which are not observed with the H13A-Aβ and H6A-Aβ mutants.

Carboxylate-Containing Residues. The effect of Zn(II) on the carboxylate groups was evaluated by comparison of the impact of Zn(II) on the Aβ peptide and on the D1N-Aβ, E3Q-Aβ, D7N-Aβ, and E11Q-Aβ mutants. Analysis of the Asp1 Hβ region (Figure 6, panel A, Figures S11–S14, and Table S3, entries A, 6–9) and of the adjacent Ala2 Hβ region (Figure 6, panel B, Figures S11–S14, and Table S3 entries B, 6–9) indicates that (i) when the carboxylate group from D1 is amidated, Zn(II) has no more impact, thus suggesting that the carboxylate group from D1 is involved, at least partially, in Zn(II) binding by the Aβ peptide; (ii) in contrast, a similar Zn(II) effect on the Aβ peptide and on the E11Q-Aβ mutant is observed, meaning that when Glu11 binding to Zn(II) is precluded, this has no direct impact on Zn(II) binding by Asp1; (iii) with the other two mutants, E3Q-Aβ and D7N-Aβ, an intermediate situation is observed. Zn(II) impacts the Asp1 and Ala2 Hβ but in a different way than it does for the Aβ peptide. This suggests that Zn(II) binds to Glu3 and Asp7 in Aβ. From these data, it is proposed that Asp1, Glu3, and Asp7 side chains compete for one Zn(II) binding position, while Glu11 binds to Zn(II) independently to other carboxylate residues.

N-Terminal Amine. Modifications on the Asp1 Hα of the Aβ (panel A in Figure 7) and on the Asp1 Hβ of the Aβ and Ac-Aβ

DOI: 10.1021/acs.inorgchem.6b01733
Inorg. Chem. 2016, 55, 10499−10509

peptides (panel B in Figure 7 and Figure S15) upon Zn(II) binding have been investigated as a function of pH. On the Asp1 Hα of the Aβ, there is a down-shift and a weak broadening at pH 7.4, while the broadening is more intense at pH 9.0, along with an up-shift upon Zn(II) addition. The impact of Zn(II) on the Asp1 Hβ1 and Hβ2 at pH 7.4 is equivalent in the presence (Aβ) or absence (Ac-Aβ) of the free N-terminal amine, while a striking difference was observed with the D1N-Aβ peptide, for which Zn(II) addition has no impact on both Asp1 Hβ (panel A, Figure 6). Hence, the Zn(II)-induced modification detected on the Aβ peptide is mainly due to Zn(II) binding by the side chain of Asp1 rather than by the N-terminal amine. At pH 9.0, the situation is different since the broadening observed on the Aβ is no longer detected with the Ac-Aβ. In addition, the Ala2 Hβ is also a sensitive probe of Zn(II) binding in the N-terminal region (panel C in Figure 7). When the pH is increased from 7.4 to 9.0, broadening of the Ala2 Hβ of the Aβ peptide is strongly reinforced, whereas this effect is not observed with the acetylated counterpart. This suggests that the broadening of the Ala2 Hβ originates from the Zn(II) binding to the N-terminal amine, which is strongly (respectively weakly) observed at pH 9.0 (respectively 7.4). In brief, Zn(II) induces a stronger broadening of the Asp1 Hβ_2 and of the Ala2 Hβ of the Aβ peptide at pH 9 compared to pH 7.4, an effect that is not observed with the Ac-Aβ (Figure 7, panels B and C, top versus bottom), suggesting that the N-terminal amine is not bound to Zn(II) binding at pH 7.4.

DISCUSSION

On the basis of the various results described above, we propose the unprecedented model shown in Scheme 2 regarding Zn(II) binding to Aβ. Near pH 7, the main Zn(II) coordination sphere is [2N2O], made of two His residues and two carboxylate groups. The tetrahedral coordination is deduced from the EXAFS data (Table S2) and is in line with what is reported for Zn(II) preferred binding geometry in biological systems.[42] On the basis of NMR, XANES, and affinity data, an equilibrium between His13 and His14 for one binding position is anticipated, while His6 remains constantly bound. Regarding the carboxylate groups, binding by Glu11 is predominant, while the other three carboxylate side chains share the fourth coordination position, with a preference for Asp1.

Scheme 2. Proposed Zn(II) Binding Site in Aβ (Predominant Species at pH 7.4)

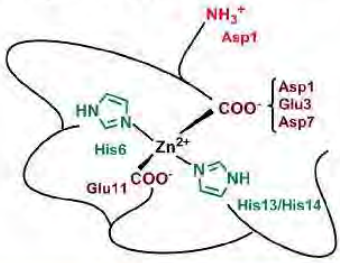

The present study has ruled out the possibility of having the Arg5 or the Tyr10 residues involved in Zn(II) binding as still recently proposed (reviewed in ref 13) by evidencing that the Zn(II)-induced modification of their NMR signatures is due to the binding of adjacent residues (His6 and Glu11, respectively) and not to their direct binding. In particular the NMR signature of the Y10F-Aβ mutant undergoes the very same Zn(II)-induced modification as the Aβ (compare entries 1 and 10 in Table S3 and see Figure S16).

More importantly, the present proposition differs from previous ones (see Table S1) regarding several points discussed below.

The N-Terminal Amine Is NOT Bound to Zn(II) in the Predominant Species at pH 7.4. The coexistence of two Zn(Aβ) species at pH 7.4 has been evidenced in the present study. The N-terminal amine has not been considered as a ligand in the predominant species at pH 7.4 because acetylation of the Aβ peptide does not induce strong alteration in comparison to Aβ neither in the NMR data nor in the XANES signatures of the Zn(II)−peptides complexes. This is in line with previous affinity data (Figure 3), in which acetylation of the N-terminal amine induces only a weak decrease in the Zn(II) affinity. In contrast, at pH 9, acetylation induces important changes with respect to Zn(II) binding as probed by NMR (Figure 7). A similar trend is observed by XANES, where differences between Zn(Aβ) and Zn(Ac-Aβ) are more obvious at higher pH (Figure S6). This strongly supports that the coordination change occurring when the pH is increased is the binding of the N-terminal amine to the Zn(II). This is in line with previous pH-dependent studies.[43,45] Taking into account the pH dependence is a prerequisite to sort out the possibility of having the N-terminal amine bound to Zn(II), this feature has thus been overlooked when only one pH value (near the physiological pH) was investigated (entries 2, 3, and 5 in Table S1). Misinterpretation of previous NMR data leading to the conclusion that the N-terminal amine is bound to Zn(II) in the main species present at pH 7.4[7,44,47] is probably due to (i) the involvement of the Asp1 side chain in Zn(II) binding, (ii) the presence of a mixture of two Zn(Aβ) complexes at pH 7.4 with the N-terminal amine linked to Zn(II) although in the minor species, and (iii) changes in the speciation of the two complexes due to different experimental conditions. In the present study, several consistent insights have been obtained by combining the use of the acetylated peptide, a pH-dependent study, and XANES data (in addition to NMR). Whether the proposed binding of the N-terminal amine in the predominant form at higher pH induces other changes in the Zn(II) coordination sphere is beyond the scope of the present paper.

It is worth noting that the nonbinding of the N-terminal amine to the Zn(II) ion has two main direct consequences: (i) Ac-Aβ is a correct model regarding Zn(II) binding in the main species present at physiological pH, thus strengthening the pertinence of previous studies with the Ac-Aβ peptide[46,53−56] and more recent studies of the H6R mutation and Ser8 phosphorylation impact on Zn(II) binding, both performed with acetylated peptides,[57,58] and (ii) the better solubility of the Zn(Ac-Aβ) compared to the Zn(Aβ) (as mentioned above) may be due to a change in the charge of the system since the N-terminal amine remains protonated in Zn(Aβ)[46] while being neutral when acetylated.

Two Histidine Residues Are Bound to the Zn(II) Center. The simultaneous coordination of the three His side chains is not considered here to be the most pertinent configuration. Indeed, it seems from literature data on truncated peptides (EVHH N-terminally protected or not) that coordination of the His13 is not favored. When the peptides start at position 11 (with or without acetylation), then the carboxylate group from Glu11 and the imidazole ring of

DOI: 10.1021/acs.inorgchem.6b01733
Inorg. Chem. 2016, 55, 10499−10509

His14 are involved in Zn(II) coordination.[54,59] Here the involvement of His13 is also proposed based on the strong broadening observed on Val12 protons that are no longer observed with the H13A-Aβ mutant (Figure S17). In addition, in contrast to the H6A mutation, H13A and H14A mutations have no strong impact on the affinity values, indicating that His13 or His14 could be exchanged. We thus propose that there is an equilibrium between Glu11-His13 and Glu11-His14 as binding couples for Zn(II). This coordination feature seems to be important, since both H13A and H14A mutation impact the Zn(II)-modulated Aβ aggregation.[16] The previous proposition of simultaneous binding of the three His may be due to the fact that indeed all three His are involved in Zn(II) binding and that quantification of their relative implication by NMR is difficult.[7,43,44,46,47]

Involvement of Two Carboxylate Side Chains. Taking into account the four-coordination of the Zn(II) center determined by EXAFS, the involvement of two His in Zn(II) binding and the noninvolvement of the N-terminal, two positions remained to be occupied by O-ligands. While Glu11 has a predominant role in Zn(II) binding as previously observed,[46,47,54] the second position may be occupied by Asp1 with only a slight preference with respect to other carboxylate residues (i.e., Glu3 and Asp7). The possibility of having one bidendate carboxylate bound to the Zn(II) is ruled out based on the EXAFS data, which are correctly reproduced with four equal distances, while having the bidentate coordination of the carboxylate would impose a longer distance (2.4 Å).[42,60] We cannot (completely) exclude that a water molecule is the fourth ligand, because effects on Asp1, Glu3, and Asp7 upon Zn(II) binding observed by NMR and XANES could be explained via H-bonding of these residues with the coordinating water.

Comparison with the Cu(II) Binding Site. The here-proposed model of the predominant Zn(II) binding site to Aβ shows that the site differs from the Cu(II) binding site. In the case of Cu(II), the predominant site (called component I) is composed of the N-terminal amine from Asp1, the carbonyl group from the peptide bond between Asp1−Ala2, and the imidazole groups from His6 and His13 or His14 in an almost square planar geometry.[3,61] Thus, a main difference between the Cu(II) and Zn(II) site is the involvement of the N-terminal amine, a main ligand for Cu(II), but not Zn(II). In contrast the His are involved in a very similar way in the binding site of both metal ions. In general, the Cu(II) and Zn(II) binding sites are different, but partially overlapping. This is in line with the analysis of the simultaneous binding of Cu(II) and Zn(II), i.e., in the bimetallic Cu(II),Zn(II)-Aβ species, in which both sites are partially different compared to the sites in the monometallic complexes (Cu(II)-Aβ and Zn(II)-Aβ).[62]

CONCLUDING REMARKS

In the present paper, we have reported a very complete study of Zn(II) binding to the Aβ peptide based on investigations of the impact of peptide modifications on the spectroscopic (NMR and XAS) signatures of the Zn(peptides) complexes. Although indirect, the large quantity of data obtained allows us to propose a new Zn(II) coordination site to Aβ. Some key features, such as the noncoordination of the N-terminal amine and the exchange of equivalent ligands for one binding position, have been revealed.

Since the N-terminal amine of Aβ is involved in Cu(II) binding, coordination of Zn(II) and Cu(II) differ at physiological pH. This is anticipated to impact their respective binding properties to physiologically relevant N-truncated[1,61,63−66] or N-elongated[67,68] Aβ. Indeed the Zn(II) binding site would not be strongly altered within the N-truncated[1,61,63−66] or N-elongated Aβ, whereas Cu(II) binding is strongly influenced by both N-truncation or N-elongation due to coordination of the N-terminal amine.

The coordination results obtained in the present study also impact the current view on the respective role of Zn(II) and Cu(II) in Aβ aggregation. Although there is no consensus in the literature on how Zn(II) modulates Aβ aggregation,[19] all reports agree that the impacts of Zn(II) and Cu(II) are different. This could be linked to an overall charge of the Zn(Aβ) and Cu(Aβ) complexes that differs by +1 unit at about neutral pH, due to the protonation of the free N-terminal amine in the case of Zn(II), while it is deprotonated and bound to the Cu(II). For the full-length Aβ40/42 peptides, the overall charge is thus −1 for the Zn(Aβ) and −2 for the Cu(Aβ), a difference that could be responsible for the higher tendency of the Zn(II) ion to induce aggregation and formation of amorphous aggregates.[59]

Ongoing studies include the determination of the high pH binding site of Zn(II) to Aβ and of the pK_a between the two species present at physiological pH, evaluation of the impact of some familial mutations, and more importantly how biologically relevant peptide modifications impact the Zn(II)-induced Aβ aggregation, one key parameter in Alzheimer's disease.

MATERIALS AND METHODS

Chemicals. Reagents were commercially available and were used as received. Hepes buffer (sodium salt of 2-[4-(2-hydroxyethyl)piperazin-1-yl]ethanesulfonic acid) was bought from Fluka (bioluminescence grade). d_{11}-TRIS (tris(hydroxymethyl)aminomethane) and d_{19}-BIS-TRIS (2-bis(2-hydroxyethyl)amino-2-(hydroxymethyl)-1,3-propanediol) were bought from Sigma-Aldrich. The Zn(II) ion source was $Zn(SO_4)(H_2O)_7$.

Peptides. Aβ16 peptide (sequence DAEFRHDSGYEVHHQK and referred to as Aβ in the following) and the modified counterparts (Ac-Aβ, Ac-DAEFRHDSGYEVHHQK; H6A-Aβ, DAEFRADSGYEVHHQK; H13A-Aβ, DAEFRHDSGYEVAHQK; H14A-Aβ, DAEFRHDSGYEVHAQK; D1N-Aβ, NAEFRHDSGYEVHHQK; E3Q-Aβ, DAQFRHDSGYEVHHQK; D7N-Aβ, DAEFRHNSGYEVHHQK; E11Q-Aβ, DAEFRHDSGYQVHHQK; and Y10F-Aβ, DAEFRHDSGFEVHHQK) were bought from GeneCust (Dudelange, Luxembourg) with purity grade >98%.

Stock solutions of the peptides were prepared by dissolving the powder in Milli-Q water (resulting pH ~2). Peptide concentration was then determined by UV−visible absorption of Tyr10 considered as free tyrosine (at pH 2, $(\varepsilon_{276}-\varepsilon_{296}) = 1410\ M^{-1}\ cm^{-1}$). For the Y10F-A$\beta$ mutant, the absorption of the two Phe ($(\varepsilon_{258}-\varepsilon_{280}) = 390\ M^{-1}\ cm^{-1}$) was used.

X-ray Absorption Spectroscopy. Zn(II) K-edge XANES and EXAFS spectra were recorded at the BM30B (FAME) beamline at the European Synchrotron Radiation Facility (ESRF, Grenoble, France).[69] The storage ring was operated in 7/8 + 1 mode at 6 GeV with a 200 mA current. The beam energy was selected using a Si(220) N_2 cryo-cooled double-crystal monochromator with an experimental resolution close to that theoretically predicted (namely, ~0.5 eV FWHM (full width at half maximum) at the Zn energy).[70] The beam spot on the sample was approximately 300 × 100 μm^2 ($H \times V$, FWHM). Because of the low Zn(II) concentrations, spectra were recorded in fluorescence mode with a 30-element solid-state Ge detector (Canberra) in frozen liquid cells in a He cryostat. The temperature was kept at 20 K during data collection. The energy was calibrated with Zn metallic foil, such that the maximum of the first derivative was set at 9659 eV. XANES Zn(II) data were collected from 9510 to 9630

DOI: 10.1021/acs.inorgchem.6b01733
Inorg. Chem. 2016, 55, 10499−10509

eV using 5 eV steps of 3 s, from 9630 to 9700 eV using 0.5 eV steps of 3 s, and from 9700 to 10 000 eV with a k-step of 0.05 $Å^{-1}$ and 3 s per step. For each sample three scans were averaged, and spectra were background-corrected by a linear regression through the pre-edge region and a polynomial through the postedge region and normalized to the edge jump. EXAFS Zn(II) data were collected from 9510 to 9630 eV using 5 eV steps of 3 s, from 9630 to 9700 eV using 0.5 eV steps of 3 s, and from 9700 to 10 500 eV with a k-step of 0.05 $Å^{-1}$ and an increasing time of 4−10 s per step. Samples for XAS measurements were prepared in the presence of 10% glycerol as cryoprotectant.

NMR. NMR experiments were realized on a Avance 500 Bruker NMR spectrometer. Several solutions of the buffer deuterated tris(hydroxymethyl)aminomethane (d_{11}-TRIS or d_{19}-BISTRIS) at different pH were prepared by solubilization of the buffer powder in D_2O and acidification or basification with D_2SO_4 or NaOD. Peptide samples were freshly prepared from a D_2O stock solution (see above peptide stock solution preparation). Peptides (final concentration 300 μM) were added to several TRIS/BIS-TRIS solutions at a given pH (final concentration 50 mM). The residual water signal was suppressed by a presaturation procedure. Zn(II) was directly added into the NMR tube.

Note that studies were performed in H_2O (XAS) or in D_2O (NMR). However, for clarity and consistency, we decided to use the notation pH even when the measurements were made in D_2O. pD was measured using a classical glass electrode according to pD = pH* + 0.4, and the apparent pH value was adjusted according to ref 71, pH = (pD − 0.32)/1.044, or equivalently to ref 72, pH = 0.929pH* + 0.41, to be in ionization conditions equivalent to those in H_2O.

■ ASSOCIATED CONTENT

Supporting Information

The Supporting Information is available free of charge on the ACS Publications website at DOI: 10.1021/acs.inorgchem.6b01733.

Scheme of the Aβ16 peptide sequence, models of Zn binding to Aβ proposed in the literature, first coordination shell structural data of Zn(Aβ) at pH 7.4 and 6.9 obtained from EXAFS fits, unfiltered experimental EXAFS data of Zn(Aβ) at pH 6.9, unfiltered and k^3-weighted experimental EXAFS data of Zn(Aβ) at pH 7.4, XANES spectra of Zn(Aβ) complexes for all the modified peptides described in the text at pH 7.4, XANES spectra of Zn in buffer, NMR spectra of Zn(Aβ) at pH 6.9 and 7.4, NMR spectra of Zn(Aβ) complexes for all the modified peptides described in the text, Zn-induced NMR broadenings and shifts of the Aβ peptides (PDF)

■ AUTHOR INFORMATION

Corresponding Authors

*E-mail: emmanuel.guillon@univ-reims.fr.
*E-mail: christelle.hureau@lcc-toulouse.fr.

Present Addresses

§(B.A.) Université de Bordeaux, ChemBioPharm INSERM U1212 CNRS UMR 5320, Bordeaux, France.
□(P.F.) Institut de Chimie, UMR 7177 CNRS-Université de Strasbourg, 4 Rue Blaise Pascal, Institut Le Bel, 67081 Strasbourg, France.

Notes

The authors declare no competing financial interest.

■ ACKNOWLEDGMENTS

The authors acknowledge the European Synchrotron Radiation Facility for provision of beamtime (experiment 30-02-1060), the FAME staff for their support, and Pier-Lorenzo Solari (synchrotron SOLEIL) for fruitful discussions. The ERC aLzINK grant (ERC-StG-638712) is acknowledged for financial support.

■ REFERENCES

(1) Holtzman, D. M.; Morris, J. C.; Goate, A. M. Alzheimer's disease: the challenge of the second century. *Sci. Transl. Med.* **2011**, *3*, 77sr1.
(2) Kozlowski, H.; Luczkowski, M.; Remelli, M.; Valensin, D. Copper, Zinc and iron in neurodegenerative diseases (Alzheimer's disease, Parkinson's disease and prion diseases). *Coord. Chem. Rev.* **2012**, *256*, 2129−2141.
(3) Hureau, C. Coordination of redox active metal ions to the APP and to the amyloid-β peptides involved in AD. Part 1: an overview. *Coord. Chem. Rev.* **2012**, *256*, 2164−2174.
(4) Noël, S.; Cadet, S.; Gras, E.; Hureau, C. The benzazole scaffold: a SWAT to combat Alzheimer's Disease. *Chem. Soc. Rev.* **2013**, *42*, 7747−7762.
(5) Viles, J. H. Metal ions and amyloid formation in neurodegenerative diseases. *Coord. Chem. Rev.* **2012**, *256*, 2271−2284.
(6) Alies, B.; Hureau, C.; Faller, P. Role of Metallic Ions in Amyloid Formation: General Principles from Model Peptides. *Metallomics* **2013**, *5*, 183−192.
(7) Danielsson, J.; Pierattelli, R.; Banci, L.; Graslund, A. High-resolution NMR studies of the zinc-binding site of the Alzheimer's amyloid beta-peptide. *FEBS J.* **2007**, *274*, 46−59.
(8) Rezaei-Ghaleh, N.; Giller, K.; Becker, S.; Zweckstetter, M. Effect of zinc binding on β-amyloid structure and dynamics: implications for Aβ aggregation. *Biophys. J.* **2011**, *101*, 1202−1211.
(9) Hureau, C.; Faller, P. Aβ-mediated ROS production by the Cu ions: structural insights, mechanisms and relevance to Alzheimer's disease. *Biochimie* **2009**, *91*, 1212−1217.
(10) Chassaing, S.; Collin, F.; Dorlet, P.; Gout, J.; Hureau, C.; Faller, P. Copper and heme-mediated Abeta toxicity: redox chemistry, Abeta oxidations and anti-ROS compounds. *Curr. Top. Med. Chem.* **2012**, *12*, 2573−2595.
(11) Barnham, K. J.; Masters, C. L.; Bush, A. I. Neurodegenerative diseases and oxidative stress. *Nat. Rev. Drug Discovery* **2004**, *2004*, 205−214.
(12) Cuajungco, M. P.; Faget, K. Y. Zinc takes the center stage: its paradoxical role in Alzheimer's disease. *Brain Res. Rev.* **2003**, *41*, 44−56.
(13) Tôugu, V.; Palumaa, P. Coordination of Zinc to the Aβ, APP, α-synuclein, PrP. *Coord. Chem. Rev.* **2012**, *256*, 2219−2224.
(14) Cuajungco, M. P.; Goldstein, L. E.; Nunomura, A.; Smith, M. A.; Lim, J. T.; Atwood, C. S.; Huang, X.; Farrag, Y. W.; Perry, G.; Bush, A. I. Evidence that the beta -amyloid plaques of Alzheimer's disease represent the redox-silencing and entombment of Aβ by zinc. *J. Biol. Chem.* **2000**, *275*, 19439−19442.
(15) Garai, K.; Sahoo, B.; Kaushalya, S. K.; Desai, R.; Maiti, S. Zinc Lowers Amyloid-β Toxicity by Selectively Precipitating Aggregation Intermediates. *Biochemistry* **2007**, *46*, 10655−10663.
(16) Tõugu, V.; Karafin, A.; Zovo, K.; Chung, R. S.; Howells, C.; West, A. K.; Palumaa, P. Zn(II)- and Cu(II)-induced non-fibrillar aggregates of amyloid-beta (1−42) peptide are transformed to amyloid fibrils, both spontaneously and under the influence of metal chelators. *J. Neurochem.* **2009**, *110*, 1785−1795.
(17) Abelein, A.; Gräslund, A.; Danielsson, J. Zinc as chaperone-mimicking agent for retardation of amyloid-β peptide fibril formation. *Proc. Natl. Acad. Sci. U. S. A.* **2015**, *112*, 5407−5412.
(18) Solomonov, I.; Korkotian, E.; Born, B.; Feldman, Y.; Bitler, A.; Rahimi, F.; Li, H.; Bitan, G.; Sagi, I. Zn2+-Aβ40 complexes form metastable quasi-spherical oligomers that are cytotoxic to cultured hippocampal neurons. *J. Biol. Chem.* **2012**, *287*, 20555−20564.
(19) Faller, P.; Hureau, C.; Berthoumieu, O. Role of Metal Ions in the Self-assembly of the Alzheimer's Amyloid-β Peptide. *Inorg. Chem.* **2013**, *52*, 12193−12206.

DOI: 10.1021/acs.inorgchem.6b01733
Inorg. Chem. 2016, 55, 10499−10509

(20) Frederickson, C. J. Neurobiology of zinc and zinc-containing neurons. *Int. Rev. Neurobiol.* **1989**, *31*, 145−238.
(21) Frederickson, C. J.; Giblin, L. J.; Krezel, A.; McAdoo, D. J.; Muelle, R. N.; Zeng, Y.; Balaji, R. V.; Masalha, R.; Thompson, R. B.; Fierke, C. A.; Sarvey, J. M.; de Valdenebro, M.; Prough, D. S.; Zornow, M. H. Concentrations of extracellular free zinc (pZn)e in the central nervous system during simple anesthetization, ischemia and reperfusion. *Exp. Neurol.* **2006**, *198*, 285−293.
(22) Frederickson, C. J.; Koh, J. Y.; Bush, A. I. The neurobiology of zinc in health and disease. *Nat. Rev. Neurosci.* **2005**, *6*, 449−462.
(23) Alies, B.; Renaglia, E.; Rozga, M.; Bal, W.; Faller, P.; Hureau, C. Cu(II) affinity for the Alzheimer's Peptide: Tyrosine fluorescence studies revisited. *Anal. Chem.* **2013**, *85*, 1501−1508.
(24) Zawisza, I.; Rozga, M.; Bal, W. Affinity of peptides (Aβ, APP, α-synuclein, PrP) for metal ions (Cu, Zn). *Coord. Chem. Rev.* **2012**, *256*, 2297−2307.
(25) Noël, S.; Bustos, S.; Sayen, S.; Guillon, E.; Faller, P.; Hureau, C. Use of a new water-soluble Zn sensor to determine Zn affinity for the amyloid-β peptide and relevant mutants. *Metallomics* **2014**, *6*, 1220−1222.
(26) Smith, D. G.; Cappai, R.; Barnham, K. J. The redox chemistry of the Alzheimer's disease amyloid beta peptide. *Biochim. Biophys. Acta, Biomembr.* **2007**, *1768*, 1976−1990.
(27) Stuerenburg, H. J. CSF copper concentrations, blood-brain barrier function, and coeruloplasmin synthesis during the treatment of Wilson's disease. *J. Neural Transm.* **2000**, *107*, 321−329.
(28) Alies, B.; Badei, B.; Faller, P.; Hureau, C. Reevaluation of Copper(I) affinity for amyloid-β peptides by competition with Ferrozine, an unusual Copper(I) indicator. *Chem. - Eur. J.* **2012**, *18*, 1161−1167.
(29) Xiao, Z.; Gottschlich, L.; van der Meulen, R.; Udagedara, S. R.; Wedd, A. G. Evaluation of quantitative probes for weaker Cu(i) binding sites completes a set of four capable of detecting Cu(i) affinities from nanomolar to attomolar. *Metallomics* **2013**, *5*, 501−513.
(30) Bush, A. I. The metallobiology of Alzheimer's disease. *Trends Neurosci.* **2003**, *26* (4), 207−214.
(31) Lovell, M. A.; Robertson, J. D.; Teesdale, W. J.; Campbell, J. L.; Markesbery, W. R. Copper, iron and zinc in Alzheimer's disease senile plaques. *J. Neurol. Sci.* **1998**, *158*, 47−52.
(32) Miller, L. M.; Wang, Q.; Telivala, T. P.; Smith, R. J.; Lanzirotti, A.; Miklossy, J. Synchrotron-based infrared and X-ray imaging shows focalized accumulation of Cu and Zn co-localized with β-amyloid deposits in Alzheimer's disease. *J. Struct. Biol.* **2006**, *155*, 30−37.
(33) Migliorini, C.; Porciatti, E.; Luczkowski, M.; Valensin, D. Structural characterization of Cu2+, Ni2+ and Zn2+ binding sites of model peptides associated with neurodegenerative diseases. *Coord. Chem. Rev.* **2012**, *256*, 352−368.
(34) Minicozzi, V.; Stellato, F.; Comai, M.; Dalla Serra, M.; Potrich, C.; Meyer-Klaucke, W.; Morante, S. Identifying the minimal Cu and Zn binding site sequence in amyloid-β peptides. *J. Biol. Chem.* **2008**, *283*, 10784−10792.
(35) Cui, P.; Wang, Y.; Chu, W.; Guo, X.; Yang, F.; Yu, M.; Zhao, H.; Dong, Y.; Xie, Y.; Gong, W.; Wu, Z. How water molecules affect the catalytic activity of hydrolases - A XANES study of the local structures of peptide deformylase. *Sci. Rep.* **2014**, *4* (7453), 1−6.
(36) Stellato, F.; Menestrina, G.; Serra, M. D.; Potrich, C.; Tomazzolli, R.; Meyer-Klaucke, W.; Morante, S. Metal binding in amyloid beta-peptides shows intra- and inter-peptide coordination modes. *Eur. Biophys. J.* **2006**, *35*, 340−351.
(37) De Santis, E.; Minicozzi, V.; Proux, O.; Rossi, G.; Silva, I.; Lawless, M. J.; Stellato, F.; Saxena, S.; Morante, S. Cu(II)−Zn(II) Cross-Modulation in Amyloid−Beta Peptide Binding: An X-ray Absorption Spectroscopy Study. *J. Phys. Chem. B* **2015**, *119*, 15813−15820.
(38) Giachini, L.; Veronesi, G.; Francia, F.; Venturolid, G.; Boscherinib, F. Synergic approach to XAFS analysis for the identification of most probable binding motifs for mononuclear zinc sites in metalloproteins. *J. Synchrotron Radiat.* **2010**, *17*, 41−52.
(39) Clark-Baldwin, K.; Tierney, D. L.; Govindaswamy, N.; Gruff, E. S.; Kim, C.; Berg, J.; Koch, S. A.; Penner-Hahn, J. E. The Limitations of X-ray Absorption Spectroscopy for Determining the Structure of Zinc Sites in Proteins. When Is a Tetrathiolate Not a Tetrathiolate? *J. Am. Chem. Soc.* **1998**, *120*, 8401−8409.
(40) Thorp, H. H. Bond valence sum analysis of metal-ligand bond lengths in metalloenzymes and model complexes. *Inorg. Chem.* **1992**, *31*, 1585−1588.
(41) Penner-Hahn, J. E. Characterization of "spectroscopically quiet" metals in biology. *Coord. Chem. Rev.* **2005**, *249*, 161−177.
(42) Alberts, I. L.; Nadassy, K.; Wodak, S. J. Analysis of zinc binding sites in protein crystal structures. *Protein Sci.* **1998**, *7*, 1700−1716.
(43) Mekmouche, Y.; Coppel, Y.; Hochgrafe, K.; Guilloreau, L.; Talmard, C.; Mazarguil, H.; Faller, P. Characterization of the Zn1I binding to the peptide amyloid-beta1−16 linked to Alzheimer's disease. *ChemBioChem* **2005**, *6*, 1663−1671.
(44) Syme, C. D.; Viles, J. H. Solution 1H NMR investigation of Zn^{2+} and Cd^{2+} binding to amyloid-beta peptide (Abeta) of Alzheimer's disease. *Biochim. Biophys. Acta, Proteins Proteomics* **2006**, *1764*, 246−256.
(45) Damante, C. A.; Osz, K.; Nagy, N. V.; Pappalardo, G.; Grasso, G.; Impellizzeri, G.; Rizzarelli, E.; Sovago, I. Metal Loading Capacity of Aβ N-Terminus: a Combined Potentiometric and Spectroscopic Study of Zinc(II) Complexes with Aβ(1−16), Its Short or Mutated Peptide Fragments and Its Polyethylene Glycol-ylated Analogue. *Inorg. Chem.* **2009**, *48*, 10405−10415.
(46) Zirah, S.; Kozin, S. A.; Mazur, A. K.; Blond, A.; Cheminant, M.; Ségalas-Milazzo, I.; Debey, P.; Rebuffat, S. Structural changes of region 1−16 of the Alzheimer disease amyloid β-peptide upon zinc binding and in vitro aging. *J. Biol. Chem.* **2006**, *281*, 2151−2161.
(47) Gaggelli, E.; Janicka-Klos, A.; Jankowska, E.; Kozlowski, H.; Migliorini, C.; Molteni, E.; Valensin, D.; Valensin, G.; Wieczerzak, E. NMR studies of the Zn2+ interactions with rat and human beta-amyloid (1−28) peptides in water-micelle environment. *J. Phys. Chem. B* **2008**, *112*, 100−109.
(48) Talmard, C.; Guilloreau, L.; Coppel, Y.; Mazarguil, H.; Faller, P. Amyloid-beta peptide forms monomeric complexes with Cu(II) and Zn(II) prior to aggregation. *ChemBioChem* **2007**, *8*, 163−165.
(49) Hureau, C.; Coppel, Y.; Dorlet, P.; Solari, P. L.; Sayen, S.; Guillon, E.; Sabater, L.; Faller, P. Deprotonation of the Asp1-Ala2 Peptide Bond Induces Modification of the Dynamic Copper(II) Environment in the Amyloid-β Peptide near Physiological pH. *Angew. Chem., Int. Ed.* **2009**, *48*, 9522−9525.
(50) Bousejra-El-Garah, F.; Bijani, C.; Coppel, Y.; Faller, P.; Hureau, C. Iron(II) Binding to Amyloid-β, the Alzheimer's Peptide. *Inorg. Chem.* **2011**, *50*, 9024−9030.
(51) Faller, P.; Hureau, C.; La Penna, G. Metal Ions and Intrinsically Disordered Proteins and Peptides: From Cu/Zn Amyloid-β to General Principles. *Acc. Chem. Res.* **2014**, *47*, 2252−2259.
(52) Hureau, C.; Balland, V.; Coppel, Y.; Solari, P. L.; Fonda, E.; Faller, P. Importance of dynamical processes in the coordination chemistry and redox conversion of copper amyloid-β complexes. *JBIC, J. Biol. Inorg. Chem.* **2009**, *14*, 995−1000.
(53) Tsvetkov, P. O.; Kulikova, A. A.; Golovin, A. V.; Tkachev, Y. V.; Archakov, A. I.; Kozin, S. A.; Makarov, A. A. Minimal Zn(2+) binding site of amyloid-β. *Biophys. J.* **2010**, *99*, L84−86.
(54) Kozin, S. A.; Mezentsev, Y. V.; Kulikova, A. A.; Indeykina, M. I.; Golovin, A. V.; Ivanov, A. S.; Tsvetkov, P. O.; Makarov, A. A. Zinc-induced dimerization of the amyloid-b metal-binding domain 1−16 is mediated by residues 11−14w. *Mol. BioSyst.* **2011**, *7*, 1053−1055.
(55) Kozin, S. A.; Zirah, S.; Rebuffat, S.; Hoa, G. H.; Debey, P. Zinc binding to Alzheimer's Abeta(1−16) peptide results in stable soluble complex. *Biochem. Biophys. Res. Commun.* **2001**, *285*, 959−964.
(56) Zirah, S.; Rebuffat, S.; Kozin, A.; Debey, P.; Fournier, F.; Lesage, D.; Tabet, J.-C. Zinc binding properties of the amyloid fragment Ab(1−16) studied by electrospray-ionization mass spectrometry. *Int. J. Mass Spectrom.* **2003**, *228*, 999−1016.
(57) Kulikova, A. A.; Tsvetkov, P. O.; Indeykina, M. I.; Popov, I. A.; Zhokhov, S. S.; Golovin, A. V.; Polshakov, V. I.; Kozin, S. A.; Nudler,

DOI: 10.1021/acs.inorgchem.6b01733
Inorg. Chem. 2016, 55, 10499−10509

E.; Makarov, A. A. Phosphorylation of Ser8 promotes zinc-induced dimerization of the amyloid-β metal-binding domain. *Mol. BioSyst.* **2014**, *10*, 2590−2596.
(58) Kozin, S. A.; Kulikova, A. A.; Istrate, A. N.; Tsvetkov, P. O.; Zhokhov, S. S.; Mezentsev, Y. V.; Kechko, O. I.; Ivanov, A. S.; Polshakov, V. I.; Makarov, A. A. The English (H6R) familial Alzheimer's disease mutation facilitates zinc-induced dimerization of the amyloid-β metal-binding domain. *Metallomics* **2015**, *7*, 422−425.
(59) Alies, B.; La Penna, G.; Sayen, S.; Guillon, E.; Hureau, C.; Faller, P. Insights into the Mechanisms of Amyloid Formation of ZnII-Ab11−28: pH-Dependent Zinc Coordination and Overall Charge as Key Parameters for Kinetics and the Structure of ZnII-Ab11−28 Aggregates. *Inorg. Chem.* **2012**, *41*, 7897−7902.
(60) Ryde, U. Carboxylate binding modes in zinc proteins: A theoretical study. *Biophys. J.* **1999**, *77*, 2777−2787.
(61) Hureau, C.; Dorlet, P. Coordination of redox active metal ions to the APP protein and to the amyloid-β peptides involved in Alzheimer disease. Part 2: How Cu(II) binding sites depend on changes in the Aβ sequences. *Coord. Chem. Rev.* **2012**, *256*, 2175−2187.
(62) Alies, B.; Sasaki, I.; Proux, O.; Sayen, S.; Guillon, E.; Faller, P.; Hureau, C. Zn impacts Cu coordination to Amyloid-ß, the Alzheimer's peptide, but not the ROS production and the associated cell toxicity. *Chem. Commun.* **2013**, *49*, 1214−1216.
(63) Jawhar, S.; Wirths, O.; Bayer, T. A. Pyroglutamate Amyloid-β (Aβ): A Hatchet Man in Alzheimer Disease. *J. Biol. Chem.* **2011**, *286*, 38825−38832.
(64) Schlenzig, D.; Rönicke, R.; Cynis, H.; Ludwig, H. H.; Scheel, E.; Reymann, K.; Saido, T.; Hause, G.; Schilling, S.; Demuth, H. U. N-terminal Pyroglutamate (pGlu) formation of Aβ38 and Aβ40 Enforces Oligomer Formation and Potency to Disrupt Hippocampal LTP. *J. Neurochem.* **2012**, *121*, 774−784.
(65) Wirths, O.; Breyhan, H.; Cynis, H.; Schilling, S.; Demuth, H. U.; Bayer, T. A. Intraneuronal pyroglutamate-Abeta 3−42 triggers neurodegeneration and lethal neurological deficits in a transgenic mouse model. *Acta Neuropathol.* **2009**, *118*, 487−496.
(66) Wittnam, J. L.; Portelius, E.; Zetterberg, H.; Gustavsson, M. K.; Schilling, S.; Koch, B.; Demuth, H. U.; Blennow, K.; Wirths, O.; Bayer, T. A. Pyroglutamate amyloid β (Aβ) aggravates behavioral deficits in transgenic amyloid mouse model for Alzheimer disease. *J. Biol. Chem.* **2012**, *287*, 8154−8162.
(67) Willem, M.; Tahirovic, S.; Busche, M. A.; Ovsepian, S. V.; Chafai, M.; Scherazad, K.; Hornburg, D.; Evans, L. D. B.; Moore, S.; Daria, A.; Hampel, H.; Müller, V.; Giudici, C.; Nuscher, B.; Wenninger-Weinzierl, A.; Kremmer, E.; Heneka, M. T.; Thal, D. R.; Giedraitis, V.; Lannfelt, L.; Müller, U.; Livesey, F. J.; Meissner, F.; Herms, J.; Konnerth, A.; Marie, H.; Haass, C. η-Secretase processing of APP inhibits neuronal activity in the hippocampus. *Nature (London, U. K.)* **2015**, *256*, 443−447.
(68) Portelius, E.; Olsson, M.; Brinkmalm, G.; Rüetschi, U.; Mattsson, N.; Andreasson, U.; Gobom, J.; Brinkmalm, A.; Hölttä, M.; Blennow, K.; Zetterberg, H. Mass spectrometric characterization of amyloid-β species in the 7PA2 cell model of Alzheimer's disease. *J. Alzheimers Dis.* **2013**, *33*, 85−93.
(69) Proux, O.; Biquard, X.; Lahera, E.; Menthonnex, J. J.; Prat, A.; Ulrich, O.; Soldo, Y.; Trévisson, P.; Kapoujyan, G.; Perroux, G.; Taunier, P.; Grand, D.; Jeantet, P.; Deleglise, M.; Roux, J.-P.; Hazemann, J.-L. FAME: A new beamline for X-ray absorption investigations of very-diluted systems of environmental, material and biological interests. *Phys. Scr.* **2005**, *115*, 970−973.
(70) Proux, O.; Nassif, V.; Prat, A.; Ulrich, O.; Lahera, E.; Biquard, X.; Menthonnex, J. J.; Hazemann, J.-L. Feedback system of a liquid nitrogen cooled double-crystal monochromator: design and performances. *J. Synchrotron Radiat.* **2006**, *13*, 59−68.
(71) Delgado, R.; Da Silva, J. J. R. F.; Amorim, M. T. S.; Cabral, M. F.; Chaves, S.; Costa, J. Dissociation constants of Brempty setnsted acids in D2O and H2O: studies on polyaza and polyoxa-polyaza macrocycles and a general correlation. *Anal. Chim. Acta* **1991**, *245*, 271−282.
(72) Krezel, A.; Bal, W. A formula for correlating pKa values determined in D_2O and H_2O. *J. Inorg. Biochem.* **2004**, *98*, 161−166.

DOI: 10.1021/acs.inorgchem.6b01733
Inorg. Chem. 2016, 55, 10499−10509

B-iii. Supporting information

Zn(II) binding site to the amyloid-β peptide: insights from spectroscopic studies with a wide series of modified peptides.

Bruno Alies,[a,b,c] Amandine Conte-Daban,[a,b] Stéphanie Sayen,[d] Fabrice Collin,[a,b,c] Isabelle Kieffer,[f,g] Emmanuel Guillon,[d,*] Peter Faller,[a,b,h] and Christelle Hureau[a,b,*]

[a] CNRS, LCC (Laboratoire de Chimie de Coordination), 205 route de Narbonne, BP 44099, F-31077 Toulouse Cedex 4, France

[b] Université de Toulouse, UPS, INPT, F-31077 Toulouse Cedex 4, France

[c] *Current address*: Université de Bordeaux, ChemBioPharm INSERM U1212 CNRS UMR 5320, Bordeaux, France

[d] Université Reims Champagne Ardenne, Institut de Chimie Moléculaire de Reims (ICMR), UMR 7312 CNRS-URCA, Moulin de la Housse, BP 1039, 51687 Reims Cedex 2, France

[e] Université de Toulouse, UPS, UMR 152 PHARMA-DEV, Université Toulouse 3, F-31062 Toulouse Cedex 09 (France) and Institut de Recherche pour le développement (IRD), UMR 152 PHARMA-DEV, F-31062 Toulouse Cedex 09 (France)

[f] Observatoire des Sciences de l'Univers de Grenoble (OSUG), CNRS UMS 832, 414 rue de la piscine, 38400 Saint Martin d'Hères, France

[g] BM30B/FAME, ESRF, The European Synchrotron, 71 avenue des Martyrs, 38000 Grenoble, France

[h] *Current address*: Institut de Chimie, UMR 7177 CNRS-Université de Strasbourg, 4 rue Blaise Pascal, Institut Le Bel, 67008 Strasbourg (France)

SUPPORTING INFORMATION

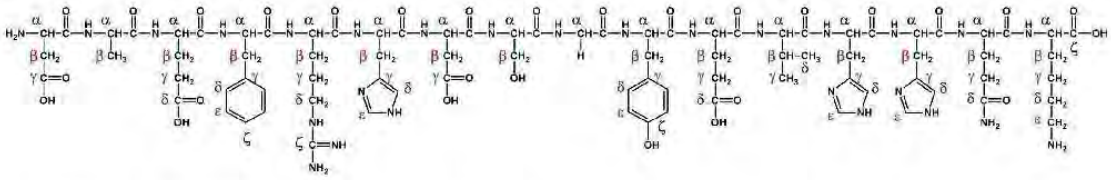

Scheme S1. Aβ16 (referred to as Aβ) peptide sequence with the atom identifiers of each amino-acid residue.

Table S1. Models of Zn(II) binding to Aβ previously proposed form NMR studies.

peptide used	conditions	Binding site proposed	Refs.	entry
Aβ16	1 mM in phosphate buffer 50 mM,[a] pH 7.1 (H_2O/D_2O, 9/1), 293 K.	His6, His13, His14, ?	[1]	1
Aβ16, Aβ28	~ 0.1 mM in D_2O, pH 7.8, 293 K.	NH_2[b], His6, His13, His14	[2]	2
Aβ40[c]	50 µM in phosphate buffer 10mM, pH 7.4 , 286 K.	NH_2[b], His6, His13, His14	[3]	3
Ac-Aβ16[d]	2 mM in phosphate buffer 50mM, pH 6.5 (H_2O/D_2O, 9/1).	His6, Glu11, His13, His14	[4]	4
Aβ28	0.4 mM, 100 mM SDS, pH 7.5, D_2O, 298 K.	NH_2[b], His6, Glu11, His13, His14	[5]	5
Aβ16-PEG[e]	2 mM pH 7.0, D_2O, 300 K.	NH_2, His6, His13, His14	[6]	6
Aβ16	300 µM in TRIS buffer, pH 7.4, D_2O, 318 K	His6, His13 **or** His14, Glu11, COO^-	this work	7

[a] Impact of zinc in phosphate buffer is weaker than in other buffer (or in absence of buffer) due to partial precipitation of $Zn_3(PO_4)_2$.

[b] N-terminal amine from Asp1 residue.

[c] ^{15}N and ^{13}C-labelled peptide.

[d] Acetylation was used to avoid precipitation at high peptide concentration.

[e] PEGylation was used to avoid precipitation at high peptide concentration.

Table S2. First coordination shell structural data obtained from R-space fits of Zn(Aβ) in solution EXAFS spectra. N = number of neighbours, R = absorber-neighbour distance, σ = Debye-Waller factor.

pH	N	σ^2 (Å^{-2})	R (Å)	ΔE (eV)	R factor
6.9	4.33	0.00694	1.98	-0.12	0.26 %
7.4	4.20	0.0067	1.99	2.31	0.38 %

Impact of pH on the XAS and NMR data.

The reason why the XAS and NMR experiments have been performed at two pH values is based on the fact that at pH 7.4 two species may coexist. Indeed, as shown in the full text, the N-terminal amine is bound to the Zn(II) at higher pH (pH 9.0). In addition, from literature data,[7, 8] it is known that the N-terminal amine is deprotonated around pH 8.0 in the apo-peptide. Hence we have anticipated that the coordination of the N-terminal amine occurs partially at pH 7.4. Hence we have performed all studies (XAS and NMR) at the two pH values. (i) simulations of the pH 6.9 and 7.4 EXAFS data show comparable simulation parameters, this is in line with the replacement of a coordinating group by the N-terminal amine, keeping a coordination number equals to 4 ; (ii) in contrast, impact of Zn(II) on the NMR data is better observed at pH 7.4. This may be due to a partial loss of solubility of the Zn(Aβ) complex when the pH is decreased to 6.9, leading to a less specific broadening. The effects are however very similar to those observed at pH 7.4 and the presence of a second minor species at pH 7.4 doesn't disturb the analysis of the NMR data. While some insights on the nature of this second minor species is given in the full text, its full identification is beyond the scope of the present paper that aims at describing the structure of the main species in physiological conditions.

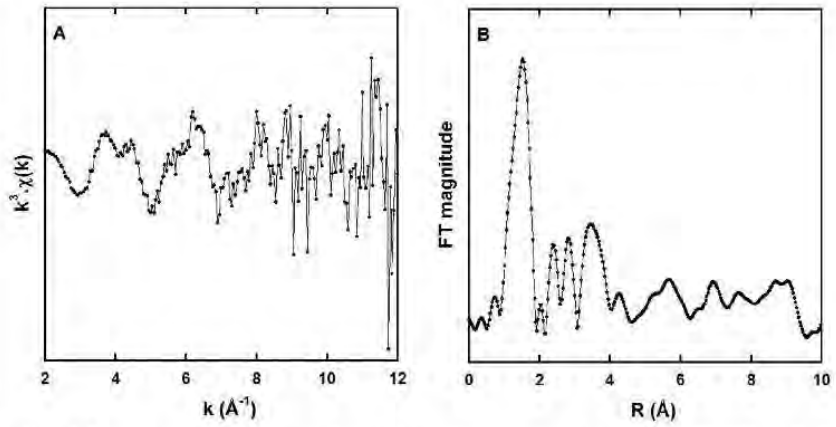

Figure S1. k^3-weighted experimental EXAFS spectrum of Zn(Aβ) at pH 6.9 and its corresponding non-phase-shift corrected Fourier transform. [Aβ] = 1.0 mM, [Zn(II)] = 0.9 mM in Hepes buffer 50 mM, T = 20 K.

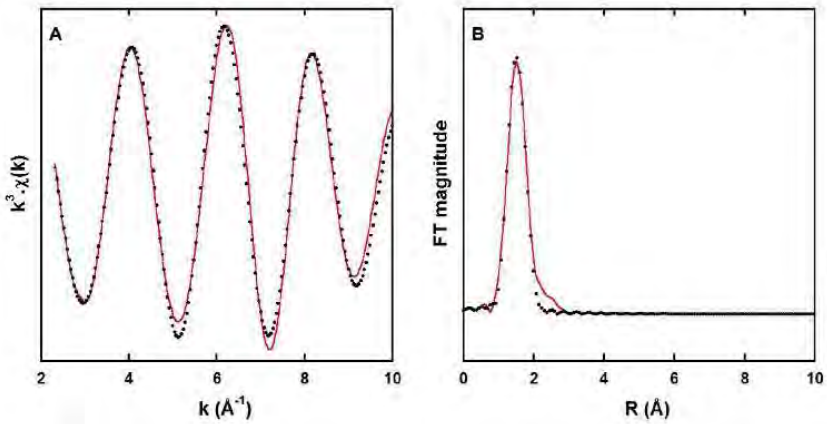

Figure S2. k^3-weighted experimental (black dots) and least-squares fitted (red line) first coordination shell EXAFS spectra of the Zn(Aβ) at pH 7.4 (A) and the corresponding non-phase-shift corrected Fourier transforms (B). Recording conditions: [Aβ] = 1 mM, [Zn(II)] = 0.9 mM in Hepes buffer 50 mM, T = 20 K.

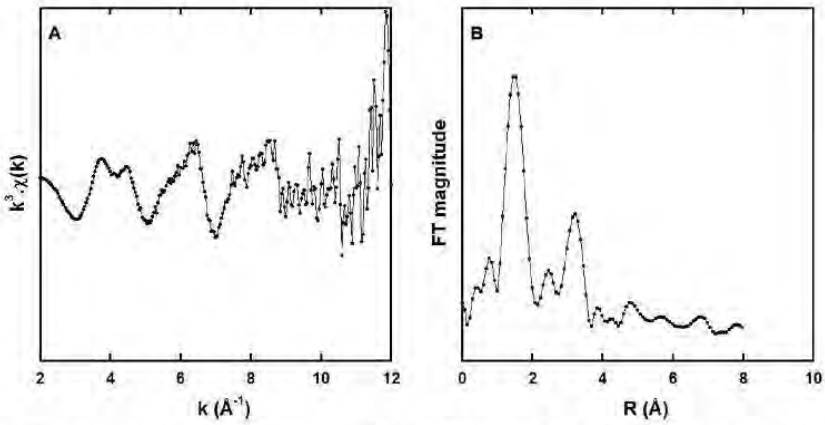

Figure S3. k^3-weighted experimental EXAFS spectrum of Zn(Aβ) at pH 7.4 and its corresponding non-phase-shift corrected Fourier transform. [Aβ] = 1.0 mM, [Zn(II)] = 0.9 mM in Hepes buffer 50 mM, T = 20 K.

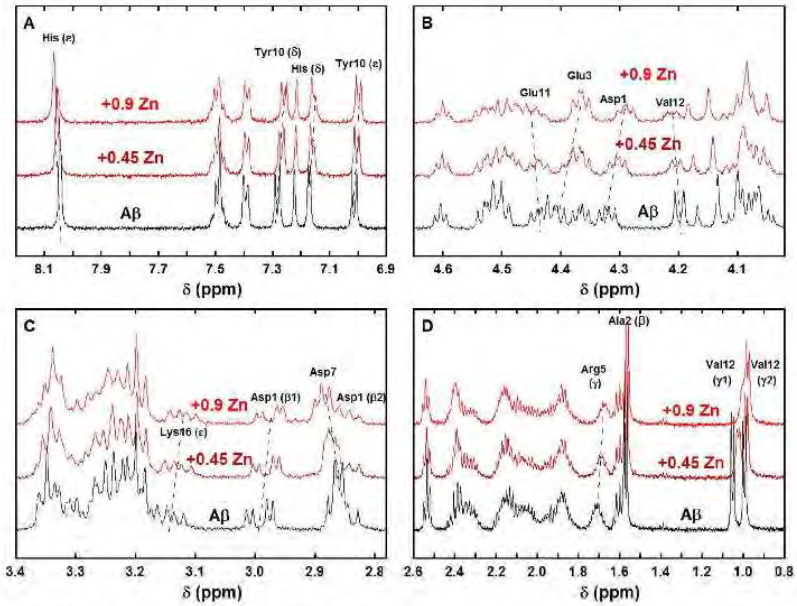

Figure S4. ^{1}H NMR spectra of Aβ (bottom black lines) and of Aβ in presence of 0.45 and 0.9 equiv. of Zn(II) in selected regions (A: aromatic, B: Hα, C: Hβ, D: Hβ and Hγ). [Aβ] = 300 μM, [Zn(II)] = 270 μM in d_{11}-TRIS buffer 50 mM, pH = 7.4, T = 318 K, ν = 500 MHz. δ(His6 Hδ) > δ(His14 Hδ) > δ(His13 Hδ). For the details of the amino-acid residues nomenclature, see Scheme S1.

Table S3. Zn(II) induced shifts and broadening of protons from Aβ peptide and modified counterparts. For nomenclature of protons, see Scheme S1.

	D1	A2	E3	F4	R5	H6	D7	E11	V12	H13	H14	entry
Aβ	α -33 2 β1 -16 2 β2 +12 2	α 3 2 β 6 1	α -42 2	δ -5 1 ε 1 ζ 1	α -9 1 γ -37 2	δ -8 1 ε >9 1	β +22 1	α +15 2	α +12 4 γ1 -60 4 γ2 -15 1	δ -16 3 ε > 1	δ -13 1 ε >9 1	**1**
Ac-Aβ	α β1 ~ 2 1 β2 +22 1	α 0 1 β -6 1	α β γ	δ -6 1 ε 0 2 ζ -5 2	α γ -20 1	δ 2 1 ε 2		α β γ	α 22 4 γ1 -55 5 γ2 -10 2	δ -18 3 ε 1	δ -14 1 ε 1	**2**
H6A-Aβ	α β1 +16 2 β2 +22 3	α β	α β γ	δ -13 0 ε -8 0 ζ -9 0	α γ -7 1		β +17 1	α β γ	α 4 γ1 -26 5 γ2 +2 1	δ 3 ε ~ 28 2	δ 1 ε ~ 28 2	**3**
H13A-Aβ	α β1 -9 3 β2 +8 1	α β -6 1	α -38 β γ	δ -1 1 ε 1 ζ 1	α γ -37 2	δ < 5 1 ε + 42 1	β +21 2	α >11 β γ	α -10 1 γ1 -9 1 γ2 0 1		δ <5 1 ε +42 1	**4**
H14A-Aβ	α +24 3 β1 -11 2 β2 +5 3	α β	α -50 > 3 β γ	δ -1 1 ε +10 1 ζ +4 1	α γ -35 1	δ +5 1 ε ~30 1	β +20 3	α β γ	α +39 4 γ1 -78 5 γ2 -26 1	δ +20 2 ε ~30 1		**5**
D1N-Aβ	α β1 0 1 β2 0 1	α +2 1 β -4 1	α -8 2 β γ	δ -5 1 ε -5 2 ζ 0 1	α 0 2 γ -23 2	δ +3 1 ε +6 1	β +29 2	α +21 3 β γ	α +2 4 γ1 -56 5 γ2 -10 2	δ -15 3 ε +6 1	δ -10 1 ε +6 1	**6**
E3Q-Aβ	α 3 β1 -4 2 β2 +14 3	α 3 β 0 1	α 3	δ -14 2 ε 0 2 ζ 3	α 3 γ -34 2	δ +2 2 ε >19 3	β +29 4	α 3 β γ	α 5 γ1 +54 5 γ2 -17 2	δ -10 4 ε >19 3	δ -7 2 ε >19 3	**7**
D7N-Aβ	α -30 1 β1 +23 1 β2 +18 3	α 0 1 β	α β γ	δ -2 1 ε +9 1 ζ +4 2	α γ -52 1	δ -13 1 ε >16 1		α β γ	α 0 4 γ1 -39 4 γ2 -17 1	δ -16 3 ε >16 1	δ -10 1 ε >16 1	**8**
E11Q-Aβ	α +29 2 β1 -18 1 β2 -1 3	α 0 1 β -10 1	α -75 5 β γ	δ -5 1 ε +6 1 ζ 2	α γ -48 2	δ -18 1 ε >3 2	β 26 1		α -13 2 γ1 -18 1 γ2 -18 2	δ -18 1 ε >3 2	δ -18 1 ε >3 2	**9**
Y10F-Aβ	α -14 2 β1 -12 1 β2 +1 2	α β -8 2	α -50 > 3 β γ	δ ε ζ	α γ -35 2	δ -30 1 ε >20 2	β +28 2	α +8 3 β γ	α +10 3 γ1 -46 4 γ2 -16 2	δ -8 3 ε >20 2	δ -7 1 ε >20 2	**10**
entry	**A**	**B**	**C**	**D**	**E**	**F**	**G**	**H**	**I**	**J**	**K**	

Chemical shifts are given in 10^{-3} ppm. Recording frequency is 500 MHz.
Broadening is characterized by a number ranging from 0 to 5, 0 corresponding to no change and 5 to complete disappearance of the peak.

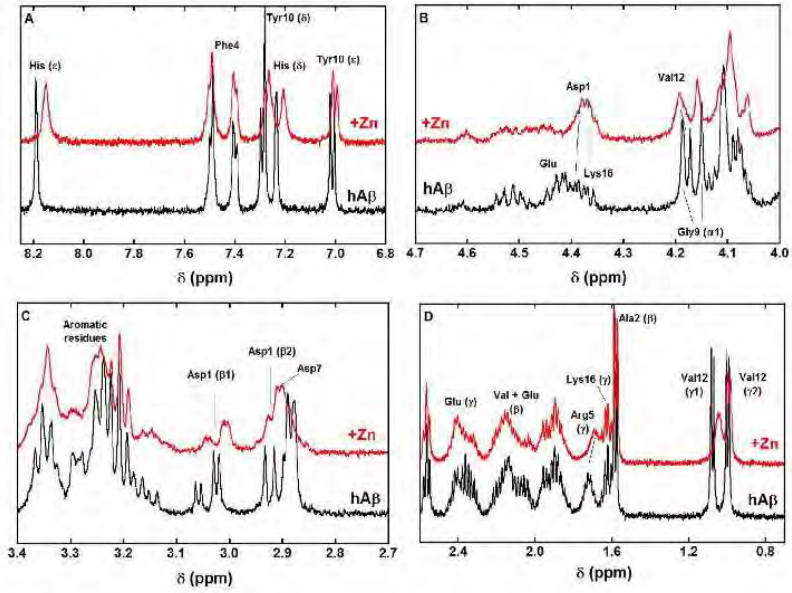

Figure S5. ^{1}H NMR spectra of Aβ (bottom black lines) and of Aβ in presence of 0.9 equiv. of Zn(II) (top red lines) in selected regions (A: aromatic, B: Hα, C: Hβ, D: Hβ and Hγ). [Aβ] = 300 μM, [Zn(II)] = 270 μM in d_{19}-BisTRIS buffer 50 mM, pH = 6.9, T = 318 K; ν = 500 MHz. For the details of the amino-acid residues nomenclature, see Scheme S1.

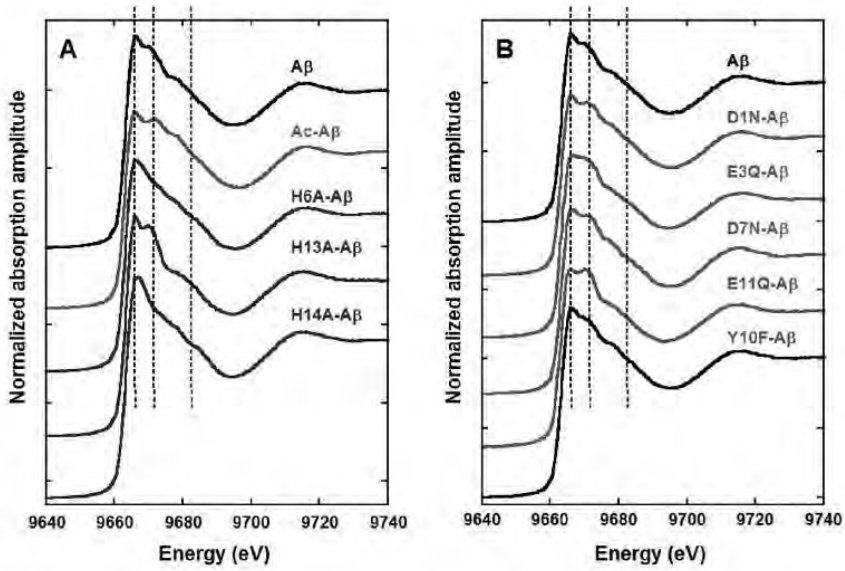

Figure S6. Zn(II) k-edge XANES spectra of Zn(II) bound to Aβ (black line) and to N mutants (panel A) and O mutants (panel B), hepes buffer 50 mM pH 7.4 [Zn(II)] = 1 mM, [peptide] = 1.1 mM. T = 20 K.

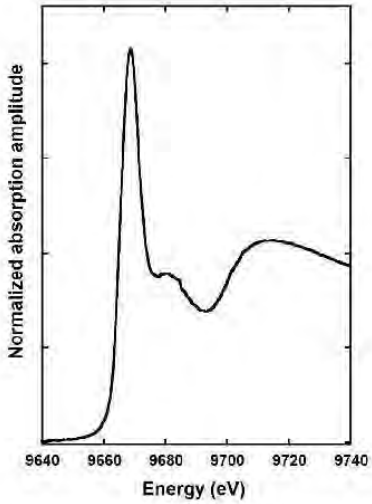

Figure S7. Zn(II) k-edge XANES spectra of Zn(II) in hepes buffer 50 mM pH 7.1 [Zn(II)] = 1 mM, T = 20 K.

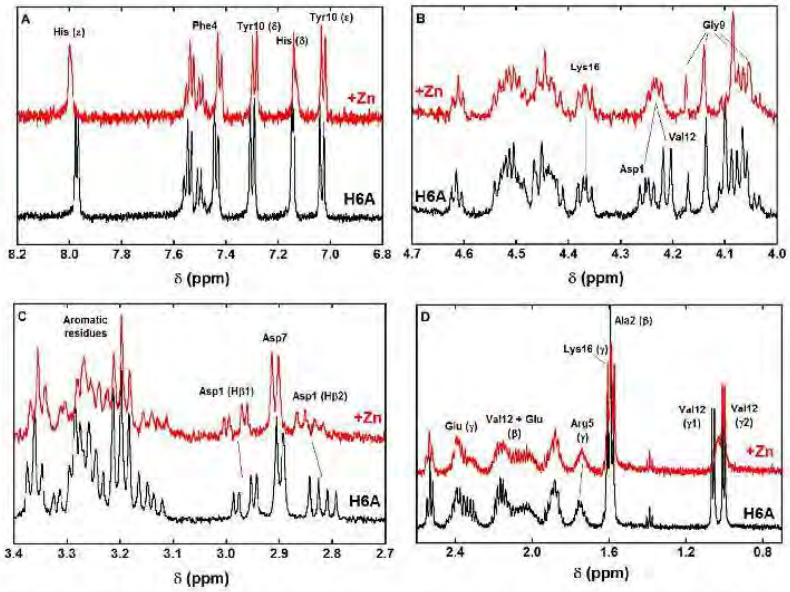

Figure S8. ^{1}H NMR spectra of H6A-Aβ (bottom black lines) and of H6A-Aβ in presence of 0.9 equiv. of Zn(II) (top red lines) in selected regions (A: aromatic, B: Hα, C: Hβ, D: Hβ and Hγ). [Aβ] = 300 µM, [Zn(II)] = 270 µM in d_{11}-TRIS buffer 50 mM, pH = 7.4, T = 318 K, ν = 500 MHz. For the details of the amino-acid residues nomenclature, see Scheme S1.

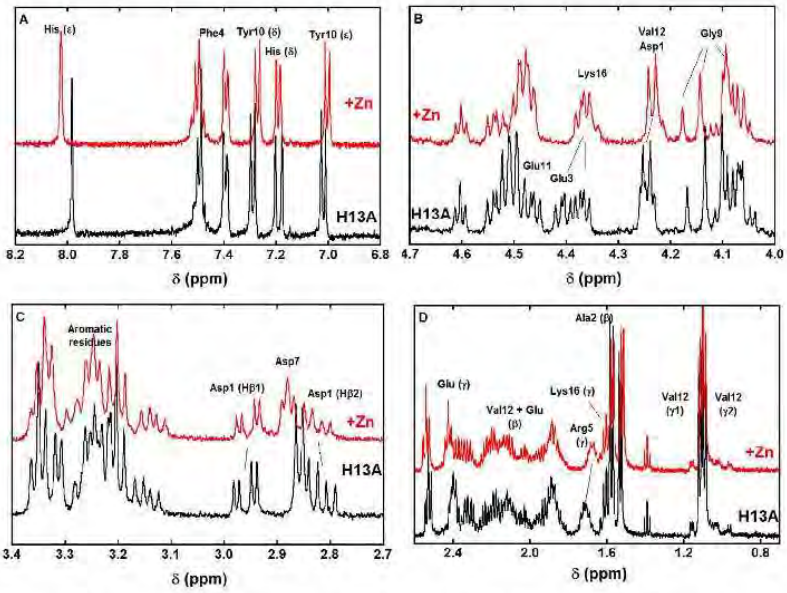

Figure S9. ^{1}H NMR spectra of H13A-Aβ (bottom black lines) and of H13A-Aβ in presence of 0.9 equiv. of Zn(II) (top red lines) in selected regions (A: aromatic, B: Hα, C: Hβ, D: Hβ and Hγ). [Aβ] = 300 µM, [Zn(II)] = 270 µM in d_{11}-TRIS buffer 50 mM, pH = 7.4, T = 318 K, ν = 500 MHz. For the details of the amino-acid residues nomenclature, see Scheme S1.

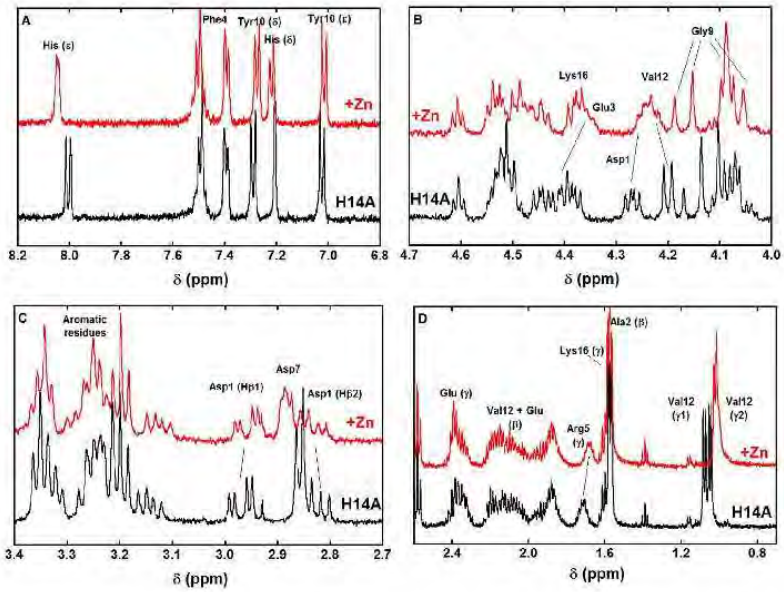

Figure S10. ^{1}H NMR spectra of H14A-Aβ (bottom black lines) and of H14A-Aβ in presence of 0.9 equiv. of Zn(II) (top red lines) in selected regions (A: aromatic, B: Hα, C: Hβ, D: Hβ and Hγ). [Aβ] = 300 μM, [Zn(II)] = 270 μM in d_{11}-TRIS buffer 50 mM, pH = 7.4, T = 318 K, ν = 500 MHz. For the details of the amino-acid residues nomenclature, see Scheme S1.

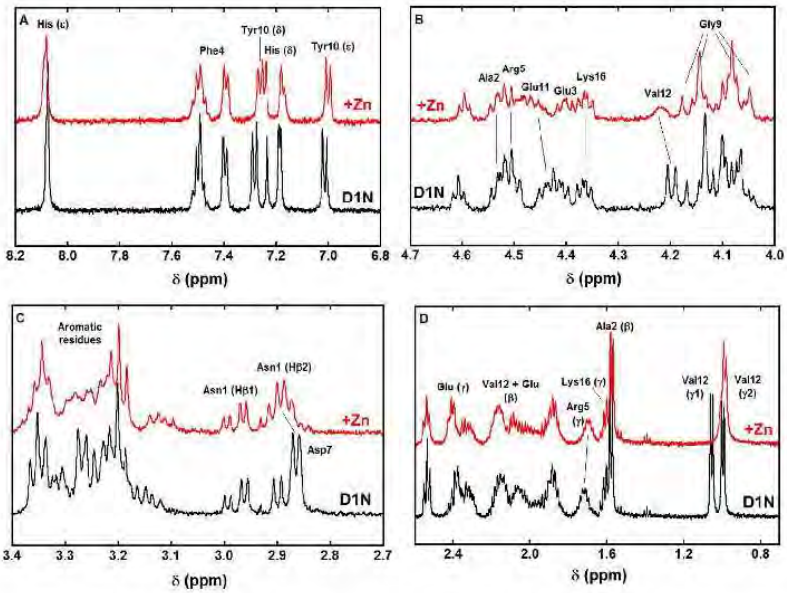

Figure S11. ^{1}H NMR spectra of D1N-Aβ (bottom black lines) and of D1N-Aβ in presence of 0.9 equiv. of Zn(II) (top red lines) in selected regions (A: aromatic, B: Hα, C: Hβ, D: Hβ and Hγ). [Aβ] = 300 μM, [Zn(II)] = 270 μM in d_{11}-TRIS buffer 50 mM, pH = 7.4,T = 318 K, ν = 500 MHz. For the details of the amino-acid residues nomenclature, see Scheme S1.

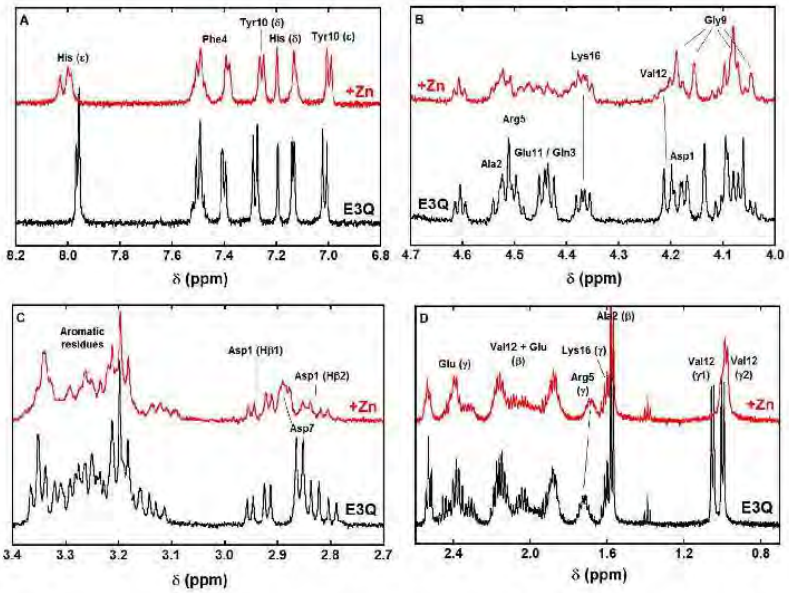

Figure S12. ^{1}H NMR spectra of E3Q-Aβ (bottom black lines) and of E3Q-Aβ in presence of 0.9 equiv. of Zn(II) (top red lines) in selected regions (A: aromatic, B: Hα, C: Hβ, D: Hβ and Hγ). [Aβ] = 300 µM, [Zn(II)] = 270 µM in d_{11}-TRIS buffer 50 mM, pH = 7.4, T = 318 K, ν = 500 MHz. For the details of the amino-acid residues nomenclature, see Scheme S1.

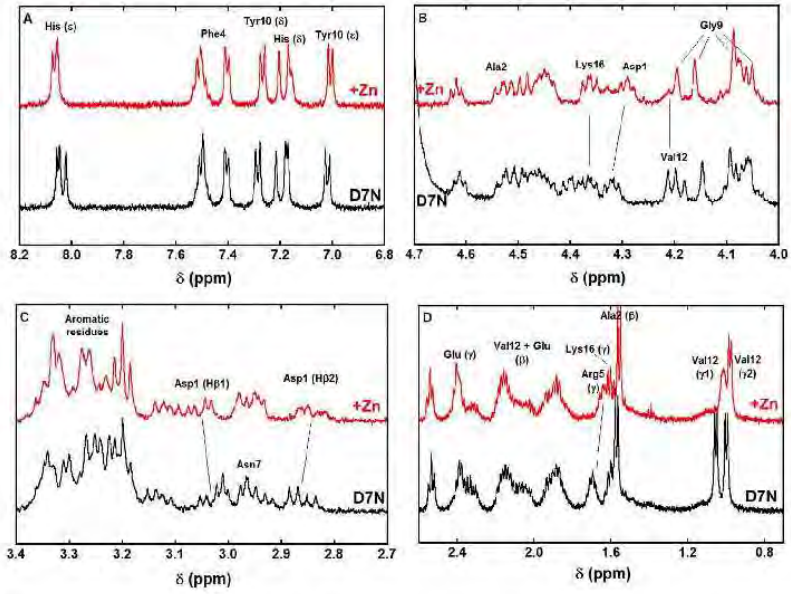

Figure S13. ^{1}H NMR spectra of D7N-Aβ (bottom black lines) and of D7N-Aβ in presence of 0.9 equiv. of Zn(II) (top red lines) in selected regions (A: aromatic, B: Hα, C: Hβ, D: Hβ and Hγ). [Aβ] = 300 µM, [Zn(II)] = 270 µM in d_{11}-TRIS buffer 50 mM, pH = 7.4, T = 318 K, ν = 500 MHz. For the details of the amino-acid residues nomenclature, see Scheme S1.

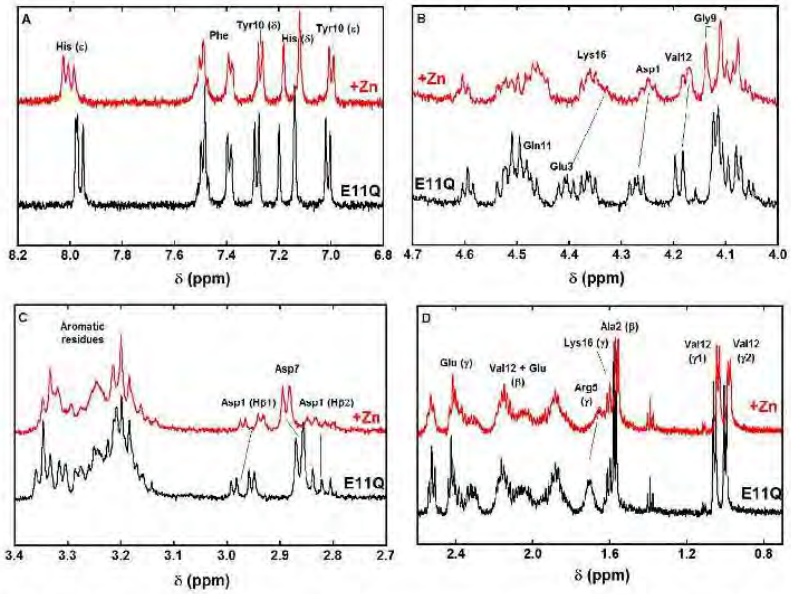

Figure S14. ^{1}H NMR spectra of E11Q-Aβ (bottom black lines) and of E11Q-Aβ in presence of 0.9 equiv. of Zn(II) (top red lines) in selected regions (A: aromatic, B: Hα, C: Hβ, D: Hβ and Hγ). [Aβ] = 300 μM, [Zn(II)] = 270 μM in d_{11}-TRIS buffer 50 mM, pH = 7.4, T = 318 K, ν = 500 MHz. For the details of the amino-acid residues nomenclature, see Scheme S1.

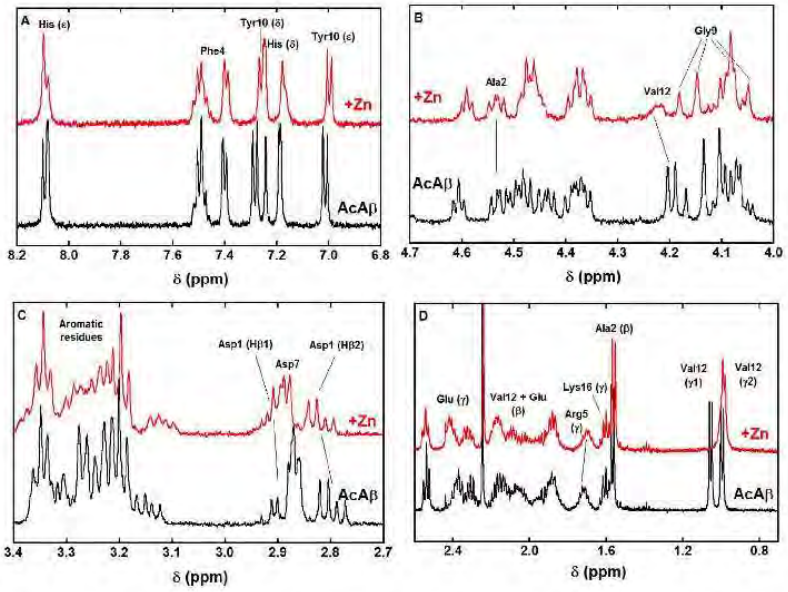

Figure S15. ^{1}H NMR spectra of Ac-Aβ (bottom black lines) and of Ac-Aβ in presence of 0.9 equiv. of Zn(II) (top red lines) in selected regions (A: aromatic, B: Hα, C: Hβ, D: Hβ and Hγ). [Aβ] = 300 μM, [Zn(II)] = 270 μM in d_{11}-TRIS buffer 50 mM, pH = 7.4, T = 318 K, ν = 500 MHz. For the details of the amino-acid residues nomenclature, see Scheme S1.

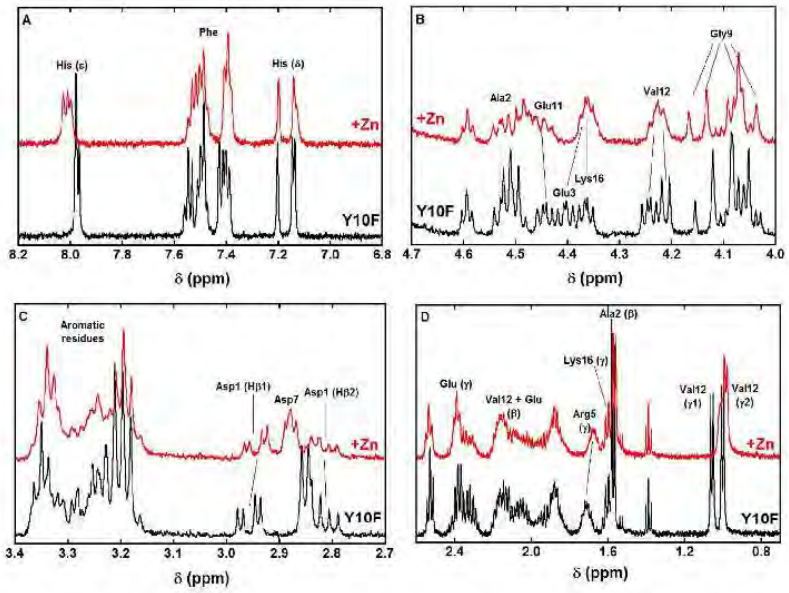

Figure S16. ^{1}H NMR spectra of Y10F-Aβ (bottom black lines) and of Y10F-Aβ in presence of 0.9 equiv. of Zn(II) (top red lines) in selected regions (A: aromatic, B: Hα, C: Hβ, D: Hβ and Hγ). [Aβ] = 300 µM, [Zn(II)] = 270 µM in d_{11}-TRIS buffer 50 mM, pH =7.4, T = 318 K, ν = 500 MHz. For the details of the amino-acid residues nomenclature, see Scheme S1.

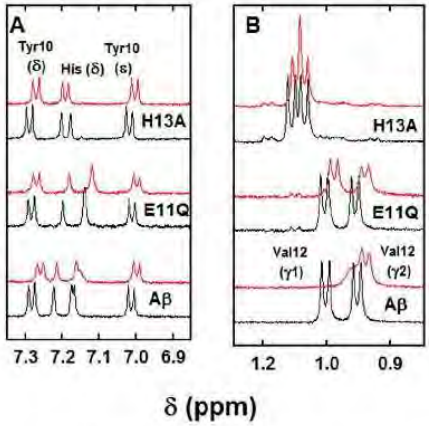

Figure S17. ^{1}H NMR spectra of Aβ, E11Q-Aβ and H13A-Aβ peptides (bottom black lines) and of Aβ, E11Q-Aβ and H13A-Aβ peptides in presence of 0.9 equiv. of Zn(II) (top red lines) in selected regions (A: aromatic, B: Val12 Hβ). [Aβ] = 300 μM, [Zn(II)] = 270 μM in d_{11}-TRIS buffer 50 mM, pH = 7.4, T = 318 K, ν = 500 MHz. For the details of the amino-acid residues nomenclature, see Scheme S1.

References

[1] Y. Mekmouche, Y. Coppel, K. Hochgrafe, L. Guilloreau, C. Talmard, H. Mazarguil and P. Faller, *ChemBioChem* **2005**, *6*, 1663-1671.
[2] C. D. Syme and J. H. Viles, *Biochim. Biophys. Acta* **2006**, *1764*, 246-256.
[3] J. Danielsson, R. Pierattelli, L. Banci and A. Graslund, *FEBS J.* **2007**, *274*, 46-59.
[4] S. Zirah, S. A. Kozin, A. K. Mazur, A. Blond, M. Cheminant, I. Ségalas-Milazzo, P. Debey and S. Rebuffat, *J. Biol. Chem.* **2006**, *281*, 2151-2161.
[5] E. Gaggelli, A. Janicka-Klos, E. Jankowska, H. Kozlowski, C. Migliorini, E. Molteni, D. Valensin, G. Valensin and E. Wieczerzak, *J. Phys. Chem. B.* **2008**, *112*, 100-109.
[6] C. A. Damante, K. Osz, N. V. Nagy, G. Pappalardo, G. Grasso, G. Impellizzeri, E. Rizzarelli and I. Sovago, *Inorg. Chem.* **2009**, *48*, 10405-10415.
[7] C. Hureau, Y. Coppel, P. Dorlet, P. L. Solari, S. Sayen, E. Guillon, L. Sabater and P. Faller, *Angew. Chem., Int. Ed. Engl.* **2009**, *48*, 9522-9525.
[8] T. Kowalik-Jankowska, M. Ruta, K. Wisniewska and L. Lankiewicz, *J. Inorg. Biochem.* **2003**, *95*, 270-282.

C- The first Cu(I) chelator against AD

This section is dedicated to the description of the first Cu(I) chelator reported within the context of Alzheimer's disease. It is composed of a summary of the article published in *Metallomics* in 2015, the publication itself and finally the supporting information. This work has mainly been performed by Elena Atrián-Blasco and her collegues in Spain. My contribution is the aggregation part and in the visualisation of the samples by AFM.

C-i. Summary

This article describes for the first time the use of a Cu(I) chelator in order to remove the metal ion from the Aβ peptide and to reduce the associated deleterious effects. As demonstrated in the section II-A, most of the researches on metal chelation or metal redistribution approaches focus on the Cu(II) ion. Nevertheless, until now, there is no evidence of the redox state of Cu ions in the synaptic cleft. In addition, some studies have proved that a Cu(II) ligand naturally present in the brain, Human Serum Albumin (HSA), protected less cells from Cu-Aβ complex toxicity in comparison with metallothionein 3 (MT-3), which is a Cu(I) ligand.

This work proposes a Cu(I) chelator, the Phosphane 1,3,5-Triaza-7-phosphaAdamantane (PTA), which is a phosphine based ligand strongly resistant to oxidation. Another advantage is its water solubility, usefull in the Alzheimer's disease studies. It is also biocompatible and has a low intrinsic toxicity.

The first step of this work is the removal of Cu ions from the Aβ peptide. For this study, XANES and EPR experiments were performed. XANES allows to follow Cu(II) and Cu(I) at the same time, and EPR is specific to Cu(II) ions, so in the presence of Cu(I), there is no signal. XANES experiments are used to monitor the removal of Cu(I) from Aβ by PTA. The ligand was added progressively and after 4.5 equiv. of PTA, Cu ion is totally chelated by the ligand and not by the peptide. 4 equiv. are needed for the Cu(I) chelation and 0.5 equiv. is required for the reduction of Cu(II) into Cu(I). EPR experiment confirms this result: with 6 equiv. of PTA, the signature of Cu(II)-Aβ becomes flat, in line with complete Cu(II) reduction. The results of the UV-Visible competition are consistent with that: the addition of PTA eliminates the d-d band of Cu(II)-Aβ; it is needed around 1 h to remove Cu(I) from Aβ. NMR experiments are in good agreement with these results of Cu ion removal. Indeed, upon Cu(I) addition, the spectrum of Aβ changes mainly for the Histidine signals. When PTA is added to Cu(I)-Aβ, the signal for apo Histidine are recovered. 4.5 equiv. of PTA are needed to remove Cu ion from the Aβ peptide,

reduce it and chelate it. Another aspect of this removal is the oxidation of PTA, but oxidised PTA cannot chelate the metal ion, that is why 4.5 equiv. of PTA are needed.

The second part of the work is the analysis of the impact of PTA on the ROS production. The following of the ascorbate consumption kinetic as well as the detection of the $HO^{\bullet}$ formed by the kinetic of fluorescence of 7-OH-CCA are used mirroring the ROS production. Experiments are performed with and without Aβ. For the Asc consumption experiments, for both cases, the first part of the curves shows an important decrease of their gradient upon addition of PTA, meaning that PTA is able to decrease if not stop the ROS production by Cu-Aβ complexes. Note that PTA has not a high enough affinity constant for Cu(I) to fully avoid free Cu. By fluorescence, for the experiments without Aβ, the more equiv. of PTA is added, the lower is the fluorescence at the plateau. This means that PTA has captured $HO^{\bullet}$ radicals instead of the 3-CCA, leading to a lower concentration of 7-OH-CCA at the end of the reaction. Thus, the phosphine group of PTA is oxidised into phosphoryl group, the phosphorous is not yet able to coordinate Cu(I) and there is a release of the metal ions. Free Cu ions can react with ascorbate and O_2 to trigger the $HO^{\bullet}$. This hypothesis is relevant due to the exactly same gradient of the fluorescence curve of Cu alone and of Cu in the presence of PTA. This PTA oxidative process is evidence by the increase of the lag phase: when the concentration of PTA increases, there are more PTA available for the Cu(I) chelation, and so, when PTA is oxidised, another PTA can chelate Cu(I) and increase the protection against the ROS production. In the presence of Aβ peptide, the same trend is observed: PTA induced less 7-OH-CCA formation and there is a delay due to oxidation of PTA itself. In conclusion, PTA is able to stop the ROS production but it is required a huge quantity of ligand to not forming ROS after a while. These results have also been confirmed by the ascorbate consumption experiments.

The last part of this work focuses on the aggregation of the Aβ peptide and the impact of PTA on it. ThT fluorescence experiments were performed and the samples were imaged by AFM. Apo Aβ peptide aggregates into fibrils whereas Cu(II)-Aβ aggregates into oligomers, non-fibrillar species. In the presence of PTA and Cu(II), the aggregation of Aβ looks like the apo aggregation: PTA sequesters the metal ions and the Aβ peptide can aggregate into fibrils. Nevertheless, 4.5 equiv. of PTA is not enough here. Indeed, Cu(I)-PTA_4 complex is not air-stable for a long time and can be oxidised by O_2. A release of Cu ions thus happens and a Cu(II) induced Aβ aggregation can occur. It is very important to use a super-stoichiometric ratio of Cu:PTA to keep the Cu(I)-PTA_4 during all the aggregation process. For this experiment, 20 equiv. of PTA are added. Thus, PTA is able to prevent the Cu(II)-Aβ oligomeric species, supposed to be the most toxic forms.

In conclusion, this article describes the first Cu(I) chelator able to remove Cu(II) and Cu(I) from Aβ, to reduce considerably the ROS production by Cu-Aβ complex (see Scheme below) and to avoid the formation of the toxic oligomeric species in a large excess of ligand. Moreover, as PTA can be easily modified by alkylation or arylation in the nitrogen atoms, it could be interesting to improve the PTA scaffold to be more resistant to oxidation, more air-stable, and to increase its affinity constant for Cu(I), making dimer of PTA for instance, in order to remove all the Cu ions from the Aβ peptide. Another improvement could be the coupling of PTA and an Aβ target moiety, in order to be more specific in the removal of Cu ions.

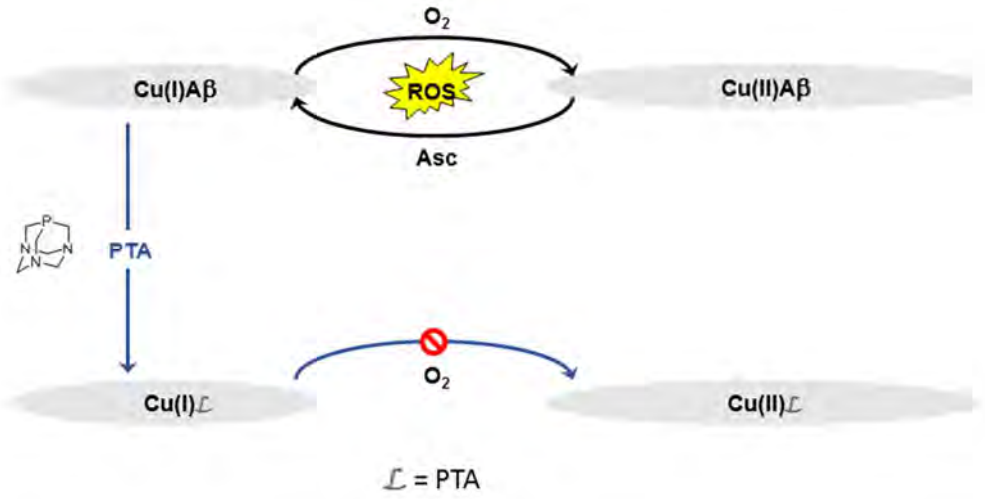

Scheme representing the strategy used in this publication: a Cu(I) chelator is used on order to remove Cu ions from Aβ and to stop the ROS production.

C-ii. Article

Volume 7 | Number 8 | August 2015 | Pages 1199–1292

Metallomics

www.rsc.org/metallomics

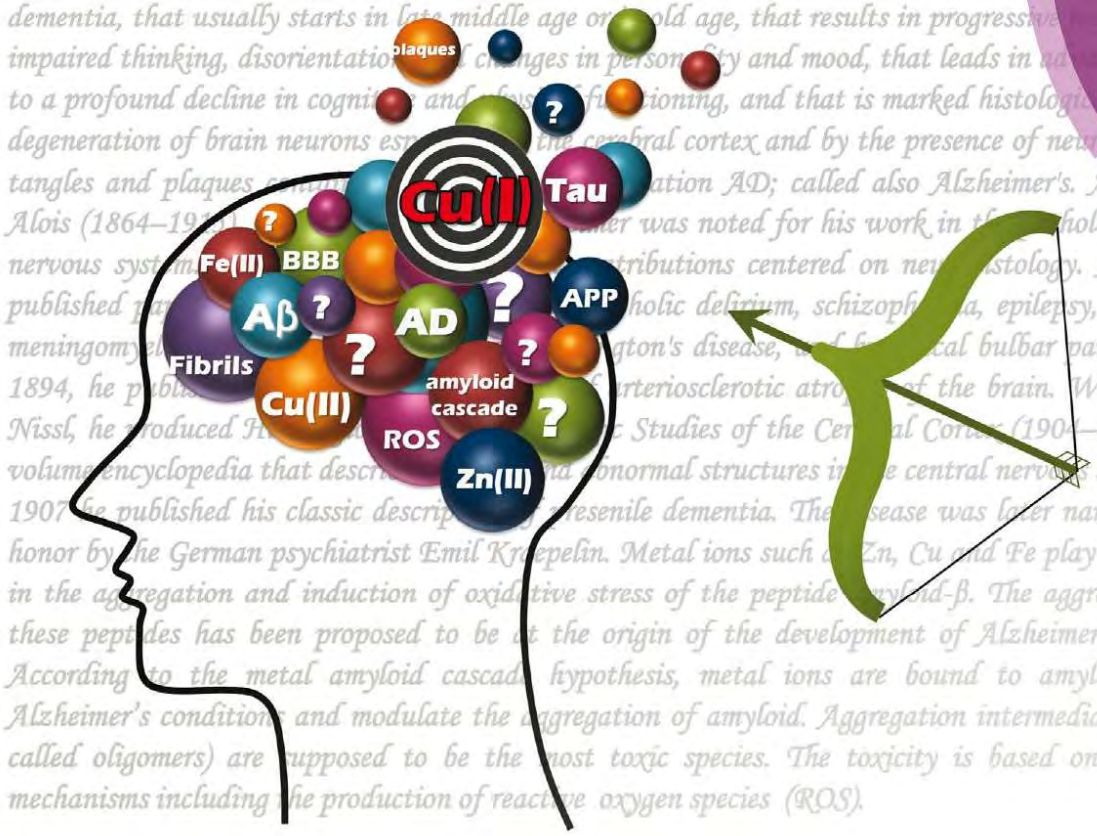

ISSN 1756-5901

ROYAL SOCIETY OF CHEMISTRY

COMMUNICATION
M. Laguna, C. Hureau *et al.*
Copper(I) targeting in the Alzheimer's disease context: a first example using the biocompatible PTA ligand

Indexed in Medline!

Metallomics

COMMUNICATION

View Article Online
View Journal | View Issue

Cite this: *Metallomics*, 2015, 7, 1229

Received 18th March 2015,
Accepted 9th April 2015

DOI: 10.1039/c5mt00077g

www.rsc.org/metallomics

Copper(I) targeting in the Alzheimer's disease context: a first example using the biocompatible PTA ligand†

E. Atrián-Blasco,[abc] E. Cerrada,[c] A. Conte-Daban,[ab] D. Testemale,[de] P. Faller,[ab] M. Laguna*[c] and C. Hureau*[ab]

Copper(I) coordinating ligands in the Alzheimer's disease context have remained unexplored, despite the biological relevance of this redox state of the copper ion. Here, we show that the PTA ligand can remove copper from Aβ, prevent reactive oxygen species production and oligomer formation, two deleterious events in the disease's etiology.

It is estimated that one out of twenty people over 65 years old suffers from Alzheimer's disease (AD). In the early stages the main symptom is memory loss but with time, AD patients lose other intellectual abilities, thus interfering with their daily life. As life expectancy has been generally growing in recent years, and keeps going up, AD is going to be an issue of paramount importance. Up to now there has been no cure for AD, the only medications approved by the U.S. Food and Drug Administration are indicated to palliate the symptoms.

At a physiological level, two noteworthy hallmarks have been observed in brains of AD patients:[1] extracellular amyloid plaques containing high amounts of the amyloid-β (Aβ peptide) in aggregated forms and of metal ions (mainly copper and zinc),[2] and neurofibrillary intracellular tangles. The soluble monomeric Aβ peptide is found in healthy brains and because amyloid plaques are found in AD patients, it is thought that formation of the plaques is a key process for the etiology of AD, known as the amyloid cascade.[3] According to this hypothesis, aggregation of Aβ has been proposed to be a key and early event in the AD progression inducing further events of the disease processes, including formation of neurofibrillary tau tangles, local inflammatory response, *etc.* leading to the death of the neuronal cells and finally to dementia. Despite senile plaques being very important in AD, it has been found that soluble oligomers of Aβ (low molecular weight aggregates) would be even more toxic.[4,5]

In addition, the brain is an organ rich in metal ions, and some of them (Zn and Cu) can be found in high levels in the hippocampus, the region of the brain related to memory.[6] They can bind to the Aβ peptide, impact its aggregation and also the production of reactive oxygen species (ROS),[2] a second crucial element in AD.[7] In this context, Cu due to its redox ability is the target of choice for therapeutic purpose based on removal of metal ions by chelators.[8]

As a consequence, an intensive field of research has recently developed following this approach. However, it is worth noting that molecules described to date in the literature are all competent to sequester the +II redox state of Cu[8] and sometimes to redox silence it[7] but that there are no data reported regarding ligands specific for Cu^{I}. However, the brain is a reducing environment and the extracellular ascorbate concentration can reach up to 300 μM.[9] In addition, during production of ROS, the Cu ion cycles between the +I and +II redox states. It has also been shown that the biological Cu(I) chelator MT-3 (metallothionein-3) was more efficient in protecting cells from Cu-Aβ toxicity compared to HSA (Human Serum Albumin), a Cu(II) chelator.[10,11] That is why the +I state of Cu is as much biologically relevant as the +II state.

The present study thus aims at evidencing that the use of Cu(I) ligands could be a prospective approach for the design of new therapeutic agents against AD. In this context, the ability of the phosphane 1,3,5-triaza-7-phosphaadamantane (PTA, Scheme 1) to reduce Cu(II) and stabilize Cu(I) as a tetrahedral coordinated compound[12] has been exploited. PTA presents some advantages such as its small cone angle, its resistance to oxidation compared to other phosphines, its solubility in water, its biocompatibility and low intrinsic toxicity.[13] Another important characteristic is that there are several positions through which the molecule can be modified by alkylation or arylation in the nitrogen atoms[14]

[a] *CNRS, LCC (Laboratoire de Chimie de Coordination), 205, route de Narbonne et Université de Toulouse, F-31077 Toulouse, France. E-mail: christelle.hureau@lcc-toulouse.fr; Tel: +33 5 61 33 31 62*
[b] *UPS, INPT, LCC, F-31077 Toulouse, France*
[c] *Instituto de Síntesis Química y Catálisis Homogénea, Universidad de Zaragoza-CSIC, Pza. San Francisco s/n, 50009 Zaragoza, Spain*
[d] *University of Grenoble Alpes, Institut NEEL, F-38000 Grenoble, France*
[e] *CNRS, Institut NEEL, F-38042 Grenoble, France*

† Electronic supplementary information (ESI) available: UV-vis and EPR monitoring of Cu^{II}(Aβ) reduction by PTA, NMR spectra of Cu(I) exchange between Aβ and PTA, of O=PTA formation, $HO^{\bullet}$ production and ascorbate consumption studies, details of speciation calculations, large AFM pictures of aggregation study and description of materials and methods. See DOI: 10.1039/c5mt00077g

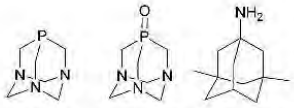

Scheme 1 From left to right: PTA and PTA-oxide (O=PTA) molecules and memantine.

among other examples. Coordination compounds of PTA and PTA derivatives have thus been studied for biomedical applications. In addition to the popular RAPTA complex, an organometallic species where a Ru(II) centre is bound to one PTA ligand, which has shown a promising activity against cancer cells,[15] Cu(I)–PTA complexes, has also been developed.[13,16]

In this communication, the (i) removal of Cu (Cu(I) and Cu(II)) from Aβ by PTA ligands and associated (ii) delay of ROS production and (iii) inhibition of formation of oligomeric Cu-Aβ species are reported.

As a starting point, Cu removal from the Aβ‡ peptide using the PTA ligands was investigated. Several techniques were used. The most appropriate one is XANES (X-ray Absorption Near Edge Structure) spectroscopy since it is possible to follow the entire reaction pictured in Scheme 2. Indeed, both Cu(II) and Cu(I) are active in XANES. Thus Fig. 1 shows the evolution of the signature of the $Cu^{II}(A\beta)$ species in the presence of increasing equivalent of PTA ligands. In the presence of 4.5 equiv. of PTA, the $Cu^{II}(A\beta)$ spectrum (a) is replaced by the fingerprint of the $[Cu^{I}(PTA)_4]^+$ complex (spectrum c). 0.5 equiv. of PTA are necessary for Cu(II) reduction and 4 equiv. for the Cu(I) capture from Aβ. Increasing the number of PTA equivalents helps to accelerate the completion of the process (see the footnote§).

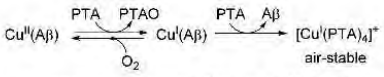

Scheme 2 Two-step process from $Cu^{II}(A\beta)$ to $[Cu^{I}(PTA)_4]^+$. Stoichiometry of the reaction is not given for the sake of clarity. [Cu] in the mM range.

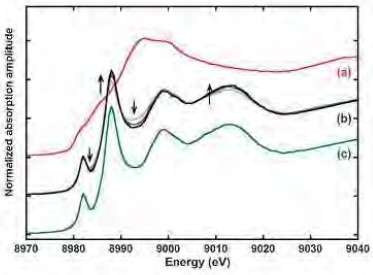

Fig. 1 XANES spectra of a mixture of [Aβ16] = 1 mM and $[Cu^{II}]$ = 0.9 mM (spectrum (a), red) and after addition of [PTA] from 4 to 6 mM after approx. 10 min of incubation time (spectra (b) from grey to black) and of [PTA] = 5 mM and $[Cu^{II}]$ = 0.9 mM leading to the *in situ* formation of $[Cu^{I}(PTA)_4]^+$ after approx. 10 min of incubation time (spectrum (c), green). Hepes buffer 50 mM pH 7.4, T = 20 K.

To ascertain the two-step process, we also recorded (i) the UV-vis and EPR signatures of $Cu^{II}(A\beta)$ after addition of 6 equiv. of PTA, which evidence the Cu(II) reduction (Fig. S1 and S2, ESI†) and (ii) the NMR spectra of a mixture of $Cu^{I}(A\beta)$ and 6 equiv. of PTA that shows the transfer of Cu(I) to the PTA ligands (Fig. S3, ESI†). Note that reduction of Cu(II) by PTA ligands leading to O=PTA is evidenced by the formation of the characteristic NMR peak in $^{31}P\{^1H\}$-NMR (Fig. S4, ESI†), in line with a similar redox process observed with other metallic ions.[17] However, in the present case, in contrast to what has been reported for Co(II),[18] Zn(II), Cd(II) and Hg(II)[19] complexes, no binding of the O=PTA to Cu(I) has been detected. Note also that quantitative formation of the $[Cu^{I}(PTA)_4]^+$ complex observed here by spectroscopy is in agreement with the respective affinity constants of Aβ and PTA ligands for Cu(I).[20–22]

Then, the impact of Cu removal from Aβ and sequestration as the air-stable $[Cu^{I}(PTA)_4]^+$ complex on ROS production was investigated by established methods.[23] Briefly, the ROS production can be seen as the reduction of dioxygen by ascorbate catalysed by the $Cu^{I/II}(A\beta)$ complex leading to $O_2^{\bullet-}$, H_2O_2 and $HO^{\bullet}$. Thus, either ascorbate consumption can be followed by UV-vis at 265 nm or $HO^{\bullet}$ formation can be monitored by the detection of the fluorescent 7-OH-CCA (7-hydroxycoumarin-3-carboxylic acid) dye formed by reaction of $HO^{\bullet}$ and the CCA (coumarin-3-carboxylic acid) molecule (see the Experimental part in the ESI‡ for details).[7]

In Fig. 2, formation of the fluorescent 7-OH-CCA dye is monitored as a function of time and of PTA equivalents with (panel B) and without Aβ (panel A). In the absence of the Aβ peptide, impact of PTA is double: (i) it diminishes the number of 7-OH-CCA formed, since the values of the fluorescence plateau decrease as the number of PTA added is increased. This indicates that PTA could be oxidized (in competition with CCA and ascorbate) by $HO^{\bullet}$; (ii) it slows down the production of 7-OH-CCA, with a lag phase that increases with the number of PTA equivalents. This means that oxidation of PTA induces the Cu release and subsequent $HO^{\bullet}$ production with a rate similar to what is observed in the absence of PTA and that PTA in excess delays the Cu release. Two mechanisms, a direct one and

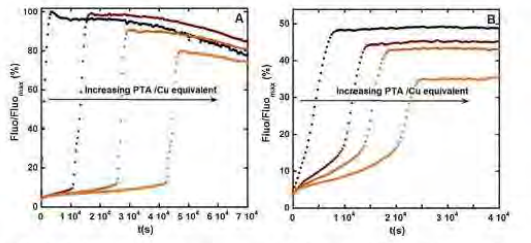

Fig. 2 7-OH-fluorescence spectra as a function of time of unbound Cu (panel A) and Cu(Aβ) (panel B) in the presence of increasing equivalent of PTA (no PTA added, black dots), 4 equiv. of PTA (brown dots), 5 equiv. of PTA (light brown dots) and 6 equiv. of PTA (orange dots). $[Cu^{II}]$ = 10 μM, [Aβ16] = 12 μM, [PTA] = 0, 42, 52, 63 μM, [CCA] = 500 μM, [ascorbate] = 1 mM, phosphate buffer, 50 mM, pH 7.4, T = 25 °C.

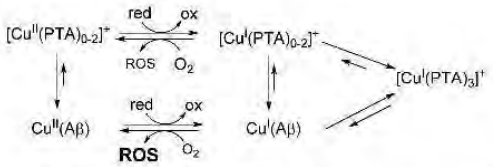

Scheme 3 Catalytic production of ROS in the presence of Cu and PTA or Cu plus Aβ plus PTA. Red = reductant, *i.e.* ascorbate or PTA. The ROS formed can attack PTA, Aβ and CCA. PTA and Aβ ligands are not mentioned in the equation for the sake of clarity. [Cu] in the 10 μM range.

an indirect one, can explain the oxidation of PTA: (ii) PTA reduces Cu(II) directly; (ii) $[Cu^{I}(PTA)_3]^+$, the main species present at low concentration, is in equilibrium with redox-active $[Cu^{I}(PTA)_{0-2}]^+$ species (see the ESI† for details). In the presence of ascorbate, the latter species produce ROS catalytically, leading to the predominant oxidation of PTA, in line with the reactions shown in Scheme 3.

In the presence of Aβ, the same trend is observed except that the slope of the lag phase is not as flat as that in the absence of Aβ. This is explained by the presence of a significant amount of Cu(I) bound to Aβ (see the ESI† for the calculation details) leading to a higher ROS production. For the same reason, the lag phases are shorter than in the absence of Aβ. Note also that the level of 7-OH-CCA formed at the plateau is lower than in the absence of Aβ. This is due to the oxidation of Aβ itself (*i.e.* HO• attacks Aβ instead of CCA).

Thus, PTA is highly efficient in stopping, at least for a period of time, ROS formation. This positive impact is observed regardless of the time of PTA addition during the ROS production process (Fig. S5 for HO• formation and Fig. S6 for ascorbate consumption experiments, ESI†). Hence, the PTA ligand is able to redox silence both the $Cu^{I}(A\beta)$ and $Cu^{II}(A\beta)$ species, which is a very important property if further therapeutic purposes are intended.

Finally, PTA propensity to modulate Aβ aggregation was determined by the classical ThT (Thioflavin-T) assay (Fig. 3, left) and the nature of the aggregates formed (oligomers or fibrils) was determined by AFM (Fig. 3, right).[24,25] Under our working

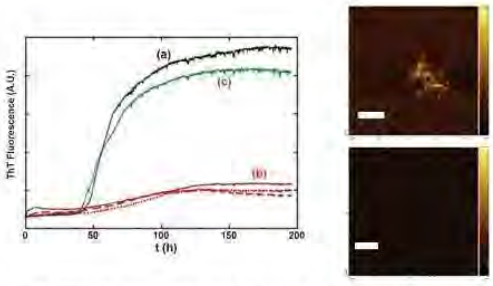

Fig. 3 Left: ThT-fluorescence spectra as a function of time of Aβ (a), $Cu^{II}(A\beta)$ (b) and $Cu^{II}(A\beta)$ in the presence of 20 equiv. of PTA (c). Dotted red curves are obtained in the presence of 5 and 10 equiv. of PTA. $[Cu^{II}]$ = 18 μM, [Aβ40] = 20 μM, [ThT] = 7 μM, phosphate buffer, 50 mM, pH 7.0, T = 37 °C. Right: AFM pictures corresponding to curve (a) (top) and (b) (bottom). Samples were withdrawn at t = 180 h. White scale corresponds to 2 nm.

conditions, Cu(II)-modulated aggregation of Aβ leads to the formation of oligomeric and small protofibril species (considered as the most toxic species in the aggregation process from the monomeric Aβ to the fibrils found in the senile plaques) exhibiting very low ThT fluorescence and characteristic AFM pictures (Fig. 3, left, (b) and right, bottom and Fig. S7, ESI†). In contrast, the Aβ-only peptide follows the classical aggregation pathway characterized by the sigmoid-shape curve of the ThT fluorescence (Fig. 3, left, a)[24,25] and forms amyloid-type fibrils (Fig. 3, right, top and Fig. S7, ESI†). Addition of 20 equiv. of PTA into a solution of $Cu^{II}(A\beta)$ results in the detection of a ThT fluorescence curve very similar to the one observed for aggregation of the apo-Aβ and to the AFM picture that resembles those of the apo-fibrils (Fig. S7, ESI†). This indicates that similar amyloids are formed. When less PTA equivalents are added, the ThT curves and AFM pictures resemble those of the $Cu^{II}(A\beta)$ sample (Fig. 3, dotted red line and Fig. S7, ESI†). This can be explained by reoxidation of the Cu(I) ion that occurs when there is not enough reductant in the medium (Scheme 2). Hence, here the excess of PTA is used to keep the PTA : Cu(I) ratio above 4 despite the loss of PTA due to oxidation. In summary, the PTA ligand is able to extract Cu from Aβ and preclude the formation of the oligomeric species.

Conclusions

In the present communication, we report the first Cu(I) ligand able to retrieve both Cu(I) and Cu(II) from the Aβ peptide, to redox silence them, thus retarding the formation of the toxic ROS species and finally to induce the formation of apo-type fibrils instead of toxic Cu(Aβ) oligomers. To the best of our knowledge this is the very first example of such a Cu(I) targeting ligand in a field where all the current research studies are focusing on Cu(II) as a target despite both redox states of Cu being biologically relevant. Although, PTA can hardly be used as such against AD, the present study proves that it is worth considering the Cu(I) targeting approach. In addition, the versatility of the PTA ligand could be further used to increase its Cu(I) affinity thus its resistance to ROS production and its resistance to oxidation, so that PTA can reach its biological target without prior oxidation. Sophistication can also include functionalization with the Aβ recognition moiety in a strategy similar to the one developed for Cu(II) chelators.[8,25] It will also be interesting to make some modifications to increase its structural similarity with the memantine scaffold (Scheme 1), a drug used to palliate some of the effects of AD and thus to propose a new kind of bi-functional therapeutic tool.

Acknowledgements

The authors acknowledge Emmanuel Guillon, Stéphanie Sayen and Fabrice Collin for their help in the recording of the XANES data and Olivia Berthoumieu for the AFM pictures. E. Atrián-Blasco would like to thank Campus Iberus for financial support for a short-term fellowship. The authors acknowledge the European Synchrotron Radiation Facility for provision of beamtime and the FAME staff for their support.

Notes and references

‡ Note that the Aβ peptide used in the coordination and ROS production experiments is the N-terminal part encompassing the first 16 amino-acid residues (one code letter sequence: DAEFRHDSGYEVHHQK) known to well reproduce the Cu^{I} and Cu^{II} binding sites but exhibiting no aggregation propensity (ref. 2). Hence for the aggregation study, the full-length Aβ40 peptide was used (see the ESI† for details).
§ This is due to the fact that when the XANES data were recorded, we did not pay attention to the time necessary for the Cu(II) reduction, which is quite long (see the ESI,‡ Fig. S1) and thus a higher PTA equivalent number accelerates the reduction reaction.

1 D. M. Holtzman, J. C. Morris and A. M. Goate, *Sci. Transl. Med.*, 2011, **3**, 77sr1.
2 C. Hureau, *Coord. Chem. Rev.*, 2012, **256**, 2164.
3 J. A. Hardy and G. A. Higgins, *Science*, 1992, **256**, 184.
4 R. Roychaudhuri, M. Yang, M. M. Hoshi and D. B. Teplow, *J. Biol. Chem.*, 2009, **284**, 4749.
5 C. Glabe, *J. Biol. Chem.*, 2008, **283**, 29639.
6 J. S. Becker, M. V. Zoriy, C. Pickhardt, N. Palomero-Gallagher and K. Zilles, *Anal. Chem.*, 2005, **77**, 3208.
7 S. Chassaing, F. Collin, P. Dorlet, J. Gout, C. Hureau and P. Faller, *Curr. Top. Med. Chem.*, 2012, **12**, 2573.
8 C. Rodriguez-Rodriguez, M. Telpoukhovskaia and C. Orvig, *Coord. Chem. Rev.*, 2012, **256**, 2308.
9 M. E. Rice, *Trends Neurosci.*, 2000, **23**, 209.
10 G. Meloni, V. Sonois, T. Delaine, L. Guilloreau, A. Gillet, J. Teissié, P. Faller and M. Vasak, *Nat. Chem. Biol.*, 2008, **4**, 366.
11 L. Perrone, E. Mothes, M. Vignes, A. Mockel, C. Figueroa, M. C. Miquel, M. L. Maddelein and P. Faller, *ChemBioChem*, 2010, **11**, 110.
12 A. M. Kirillov, P. Smoleński, M. F. C. G. da Silva and A. J. L. Pombeiro, *Eur. J. Inorg. Chem.*, 2007, 2686.
13 M. Porchia, F. Benetollo, F. Refosco, F. Tisato, C. Marzano and V. Gandin, *J. Inorg. Biochem.*, 2009, **103**, 1644.
14 E. García-Moreno, S. Gascón, E. Atrián-Blasco, M.-J. Rodriguez-Yoldi, E. Cerrada and M. Laguna, *Eur. J. Med. Chem.*, 2014, **79**, 164–172.
15 C. Scolaro, A. Bergamo, L. Brescacin, R. Delfino, M. Cocchietto, G. Laurenczy, T. J. Geldbach, G. Sava and P. J. Dyson, *J. Med. Chem.*, 2005, **48**, 4161.
16 C. Santini, M. Pellei, G. Papini, B. Morresi, R. Galassi, S. Ricci, F. Tisato, M. Porchia, M. P. Rigobello, V. Gandin and C. J. Marzano, *J. Inorg. Biochem.*, 2011, **105**, 232.
17 D. J. Darensbourg, J. B. Robertson, D. L. Larkins and J. H. Reibenspies, *Inorg. Chem.*, 1999, **38**, 2473.
18 B. J. Frost, J. L. Harkreader and C. M. Bautista, *Inorg. Chem. Commun.*, 2008, **11**, 580.
19 B. J. Frost, W.-C. Lee, K. Pal, T. H. Kim, D. VanDerveer and D. Rabinovich, *Polyhedron*, 2010, **29**, 2372.
20 B. Alies, B. Badei, P. Faller and C. Hureau, *Chem. – Eur. J.*, 2012, **18**, 1161.
21 Z. Xiao, L. Gottschlich, R. van der Meulen, S. R. Udagedara and A. G. Wedd, *Metallomics*, 2013, **5**, 501.
22 F. Endrizzi, PhD thesis, University of Padua, 2013.
23 S. Noël, F. Perez, S. Ladeira, S. Sayen, E. Guillon, E. Gras and C. Hureau, *J. Inorg. Biochem.*, 2012, **117**, 322.
24 P. Faller, C. Hureau and O. Berthoumieu, *Inorg. Chem.*, 2013, **52**, 12193.
25 S. Noël, S. Cadet, E. Gras and C. Hureau, *Chem. Soc. Rev.*, 2013, **42**, 7747.

C-iii. Supporting information

Electronic Supplementary Material (ESI) for Metallomics.

SUPPORTING INFORMATION

Copper(I) targeting in the Alzheimer's disease context: a first example using the biocompatible PTA ligand

E. Atrian-Blasco, E. Cerrada, A. Conte-Daban, D. Testemale, P. Faller, M. Laguna, and C. Hureau

Materials and methods.

Aβ16 peptide (sequence DAEFRHDSGYEVHHQK) was bought from GeneCust (Dudelange, Luxembourg) with a 95% purity grade.

Approx. 10 mM stock solution of peptide was prepared by dissolving the powder in milliQ water (resulting pH ~ 2). Peptide concentration was then determined by UV-visible absorption of Tyr10 considered as free tyrosine ($(\varepsilon_{276}-\varepsilon_{296}) = 1410\ M^{-1}cm^{-1}$).

Human Aβ40 peptide (DAEFRHDSGYEVHHQKLVFFAEDVGSNK-GAIIGLMVGGVV) was bought from GeneCust (Dudelange, Luxembourg) with a 95% purity grade. It was prepared by dissolving the powder in milliQ water and peptide concentration was then determined by UV-visible absorption of Tyr10 considered as free tyrosine ($(\varepsilon_{293}-\varepsilon_{360}) = 2400\ M^{-1}cm^{-1}$) in NaOH 0.1 M.[1]

Copper solutions: Cu(II) used was from $CuSO_4.5(H_2O)$ and purchased from Sigma. Stock solution of Cu(II) (~1M) was prepared in D_2O.

Hepes buffer (sodium salt of 2-[4-(2-hydroxyethyl)piperazin-1-yl]ethanesulfonic acid) was bought from Fluka (bioluminescence grade).

Phosphate buffer was prepared from K_2HPO_4 and KH_2PO_4 bought from Sigma-Aldrich.

Ascorbate: A stock solution (20 mM) of ascorbate was prepared in milli-Q water at room temperature just before beginning the experiment and was used immediately. Because ascorbate degrades very quickly, a new solution was prepared for each experiment.

CCA: A stock solution of coumarin-3-carboxylic acid (5 mM) was prepared in phosphate (20 mM), NaCl (100 mM) buffer at pH 9 at room temperature. The stock solution was stored at -20°C.

PTA was prepared according to procedures described in ref. [2].

UV-Vis spectroscopy: UV-Vis spectra were recorded on Agilent 8453 UV-Visible.

Fluorescence spectroscopy: Fluorescence spectra were measured by using a Fluostar Optima (BMG Labtech) connected to a personal computer. Thioflavin T, Aβ40, Cu(II) and PTA ligand were mixed in XXX buffer 100 mM pH 7.4 and placed in 96-well microplate. The time course of thioflavin T fluorescence was then measured (Excitation 440 nm ; Emission 490 nm, bandwidth for emission and excitation 10 nm).

NMR: 1D ^1H experiments were recorded on a Bruker Avance 500 spectrometer equipped with a 5 mm triple resonance inverse Z-gradient probe (TBI ^1H, ^{31}P, BB). All chemical shifts are relative to tetramethylsilane. Spectra were collected at 298 K in D_2O. NMR tubes were

prepared under Argon. The $Cu^{I}(A\beta)$ complex state was obtained from the Cu(II) counterpart by reduction with 1.5 equiv. of dithionite according to ref. [3]. Briefly, samples were prepared as follow: the Cu(I) was produced in situ, by direct addition (1.5 equiv.) of fresh made $Na_2S_2O_3$ stock solution (0.1M) into a NMR tube previously degassed with water-saturated Ar containing the peptide and Cu(II) at 1 mM concentration. NMR tube was sealed under Ar, measured as soon as possible to prevent possible oxidation. In such conditions, no broadening due to Cu(II) traces was observed and no significant pH drift due to the addition of $Na_2S_2O_3$ was measured.

EPR: Electron Paramagnetic Resonance (EPR) data were recorded using an Elexsys E 500 Bruker spectrometer, operating at a microwave frequency of approximately 9.5 GHz. All spectra were recorded using a microwave power of 20 mW across a sweep width of 150 mT (centred at 310 mT) with modulation amplitude of 0.5 mT. Experiments were carried out at 110 K using a liquid nitrogen cryostat.

EPR samples were prepared from stock solution of peptide diluted down to 0.2 mM in H_2O. 0.9 equiv. of Cu(II) was added from 0.1 M $Cu(NO_3)_2$ stock solution. Samples were frozen in quartz tube after addition of 10% glycerol as a cryoprotectant and stored in liquid nitrogen until used.

XANES: Cu K-edge XANES (X-ray absorption near edge structure) spectra were recorded at the BM30B (FAME) beamline at the European Synchrotron Radiation Facility (ESRF, Grenoble, France).[4] The storage ring was operated in 7/8+1 mode at 6GeV with a 200mA current. The beam energy was selected using an Si(220) N_2 cryo-cooled double-crystal monochromator with an experimental resolution close to that theoretically predicted (namely ~ 0.5 eV FWHM at the Cu energy).[5] The beam spot on the sample was approximately 300 x 200 μm^2 (H x V, FWHM). Because of the low Cu concentrations, spectra were recorded in fluorescence mode with a 30-element solid state Ge detector (Canberra) in frozen liquid cells in a He cryostat. The temperature was kept at 10 K during data collection to prevent sample damage and slow down possible beam-induced Cu photo-reduction. In addition, to limit this Cu photo-reduction even further, samples are moved at each scan in order for the radiation not to hit the same portion of the sample. The energy was calibrated with Cu metallic foils, such that the maximum of the first derivative was set at 8979. Cu data were collected from 8830 to 8960 eV using 3 eV step of 2 s, from 8960 to 9030 eV using 0.5 eV step of 3 s, and from 9030 to 9300 eV with a k-step of 0.05 $Å^{-1}$ and an increasing time of 2-10 s per step. For each sample three scans were averaged and spectra were background-corrected by a linear

regression through the pre-edge region and a polynomial through the post-edge region and normalized to the edge jump.

Samples for XANES measurements were prepared in presence of 10% of glycerol as cryoprotectant.

Coumarin-3-carboxylic acid assay. 3-CCA was used to detect HO•. HO• reacts with 3-CCA to form 7-hydroxy-coumarin-3-carboxylic acid (7-OH-CCA), which is fluorescent at 452 nm upon excitation at 395 nm. The intensity of the fluorescence signal is proportional to the number of 7-OH-CCA molecules formed.

Ascorbate consumption was monitored by UV-Vis. Intensity of the Asc absorption band at λ = 265 nm (ε = 14 500 M-1.cm-1) was monitored as a function of time, in 100 mM phosphate buffer, pH 7.4 containing 100 µM of Asc.

Atomic Force Microscopy (AFM)

Taping-mode AFM imaging was performed in air on a Smart SPM-1000 microscope (AIST-NT, Novato, USA) equipped with a 100µm scanner. Sample solutions (20µM) were deposited on freshly cleaved mica and left for adsorption on the substrate for 10 min. They were then rinsed three times with deionized water to remove salts and loosely bound peptide and dried with compressed N_2 before imaging. Commercial Si cantilevers (NanoWorld, Swizerland) with an elastic modulus of ~42 N m^{-1} were used. All images were acquired as 512 x 512 pixel images at a typical scan rate of 1.0 kHz with a vertical tip oscillation frequency of 250-350 kHz. Representative images of each chemical system (apo-Aβ, Cu^{II}(Aβ), Cu^{II}(Aβ) + 5PTA and Cu^{II}(Aβ) + 20PTA) were obtained by scanning at least 5 different locations on at least two different samples of the same chemical system.

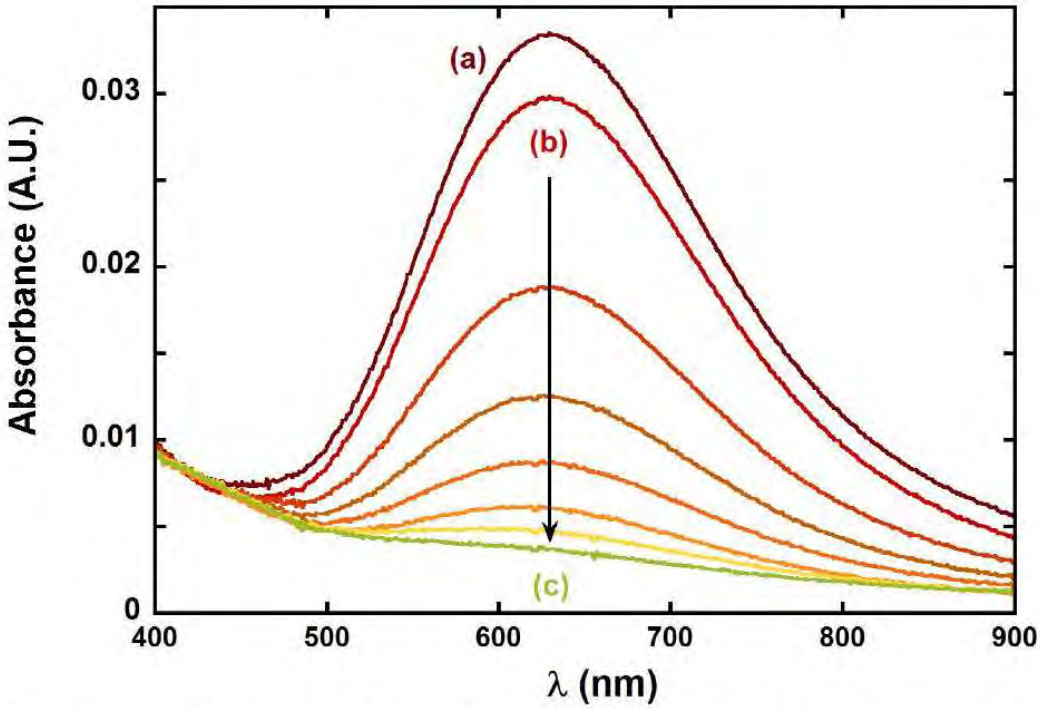

Figure S1. UV-Vis signature of $Cu^{II}(A\beta)$ complex before and after addition of 6 equiv. of PTA as a function of time. (a) before addition of the PTA ligands, and from t = 0 (b) to t = 60 min (c) after addition of the PTA ligands. [Aβ16] = 500 µM, [Cu] = 450 µM, [PTA] = 2.7 mM, Phosphate buffer 50 mM pH 7.4, T = 25°C, ℓ = 1 cm.

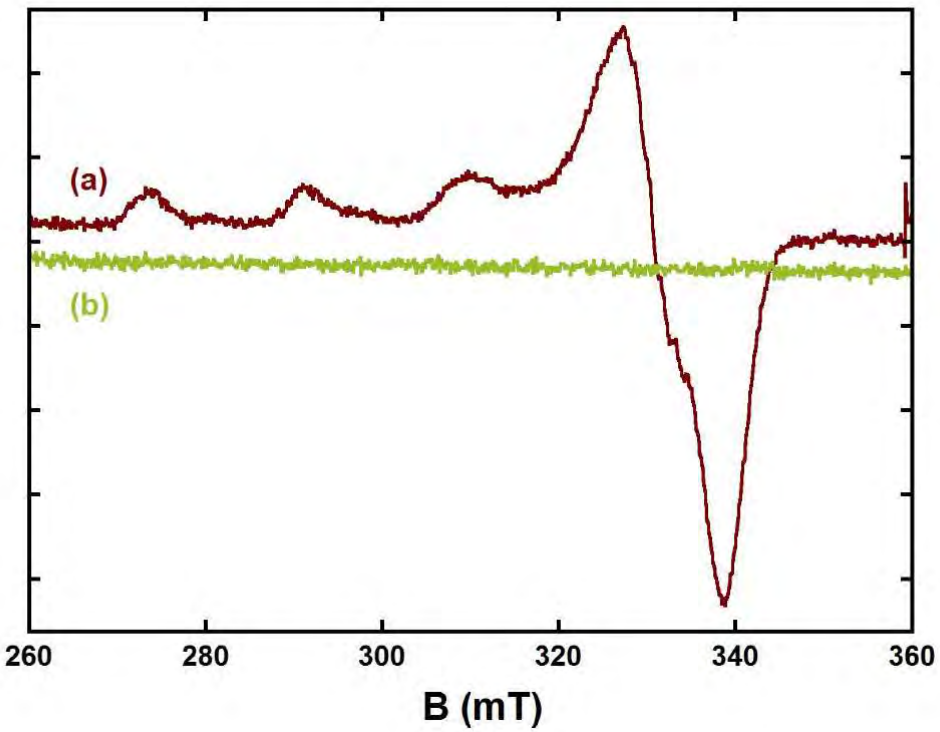

Figure S2. EPR signature of $Cu^{II}(A\beta)$ complex before (a) and after one hour of incubation with 6 PTA equivalents (b). [Aβ16] = 200 µM, [Cu] = 180 µM, [PTA] = 1.4 mM, pH 7.4, T = 120 K.

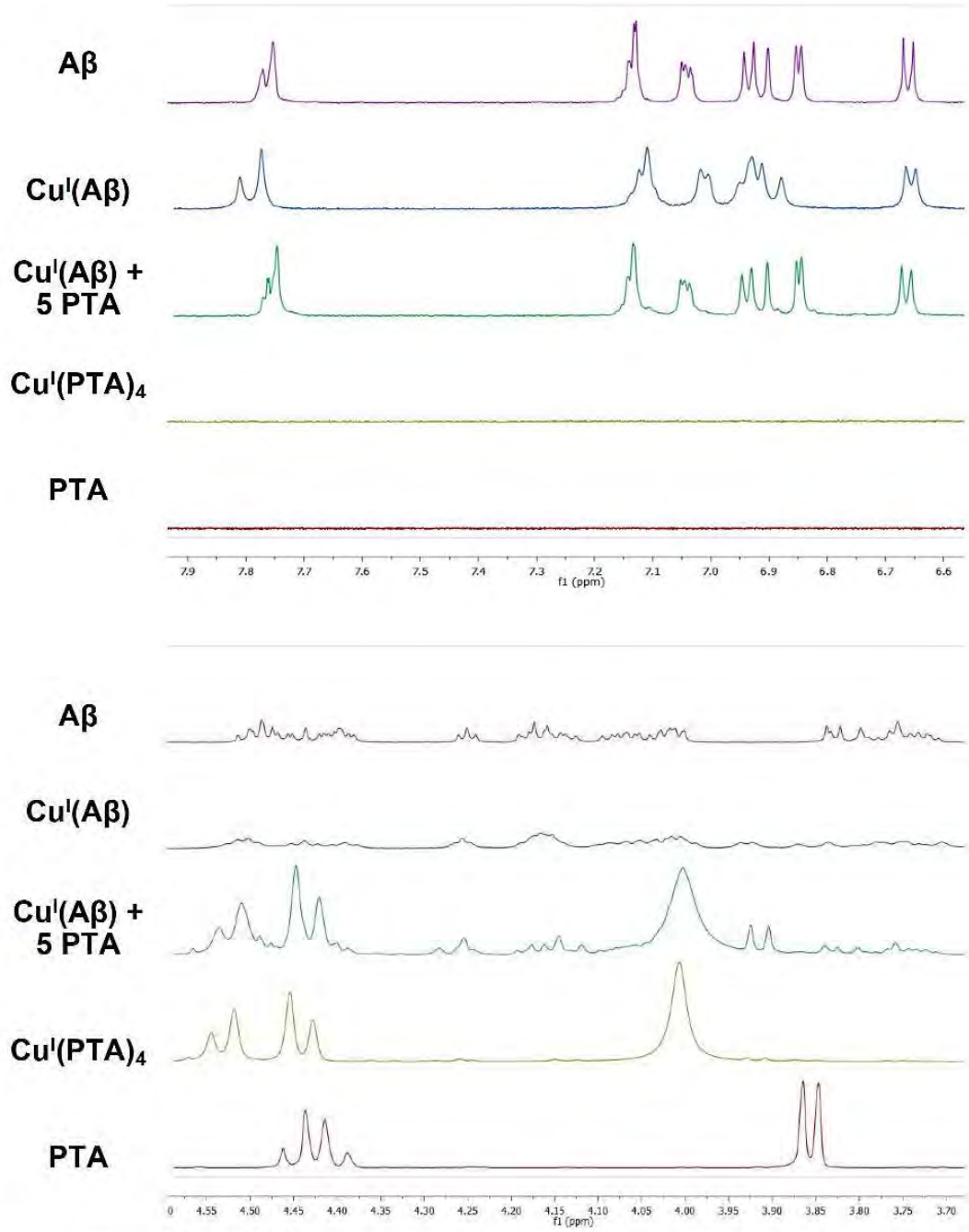

Figure S3. ^{1}H NMR Spectra. From top to bottom: spectra of the Aβ peptide, the Cu^{I}(Aβ) complex prepared as described in ref. [3] and Cu^{I}(Aβ) after addition of 5 equiv. of PTA ligand, of the Cu^{I}(PTA)$_4$ complex and of the PTA ligand. Top: aromatic regions; Bottom: aliphatic regions. [Aβ16] = 1 mM, [Cu^{T}] = 0.9 mM, [PTA] = 5 mM, Phosphate buffer 0.1M. υ = 500 MHz, T = 25°C.

After addition of the PTA ligands to the $Cu^{I}(A\beta)$ species, the NMR signature of both the unbound Aβ and the $Cu^{I}(PTA)_4$ complex are observed.

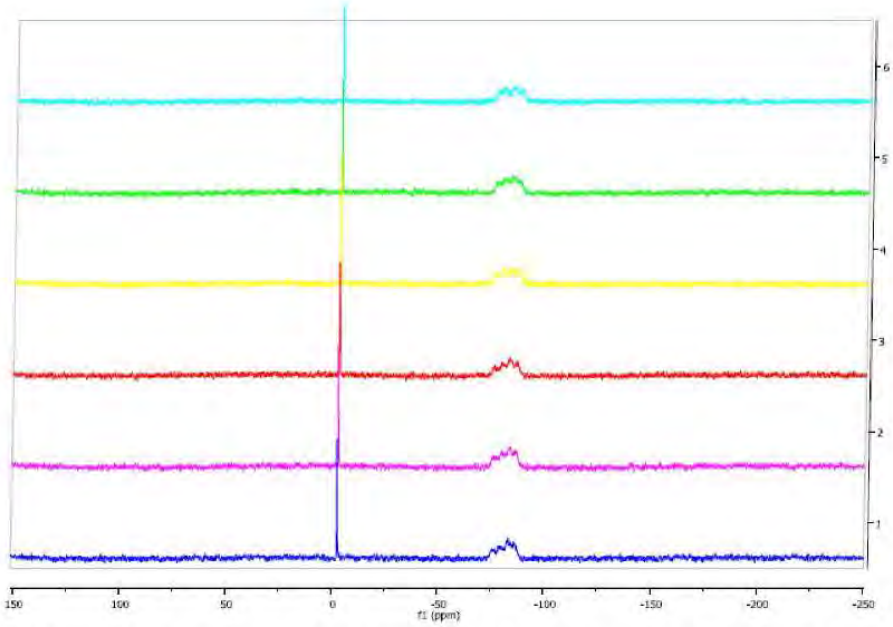

Figure S4. $^{31}P\{^{1}H\}$-NMR spectra of the PTA ligand after addition of Cu(II). [PTA] = 30 mM, [Cu(II)] = 6.7 mM, no buffer, pH = 6.5 (bottom) to 9.5 (top) adjusted by NaOD and D_2SO_4. υ = 500 MHz, T = 25°C.

The PTA oxide signal is at approx. -2 ppm, and the broad signal of $[Cu(PTA)_4]^{+}$ at -80 ppm. Note that if there is free PTA ligand, we could not see the corresponding singulet, as due to equilibria it would be included in the broad signal at -80 ppm. As it was not possible to buffer the solution using phosphate buffer, experiments were performed on a large pH range and show similar results.

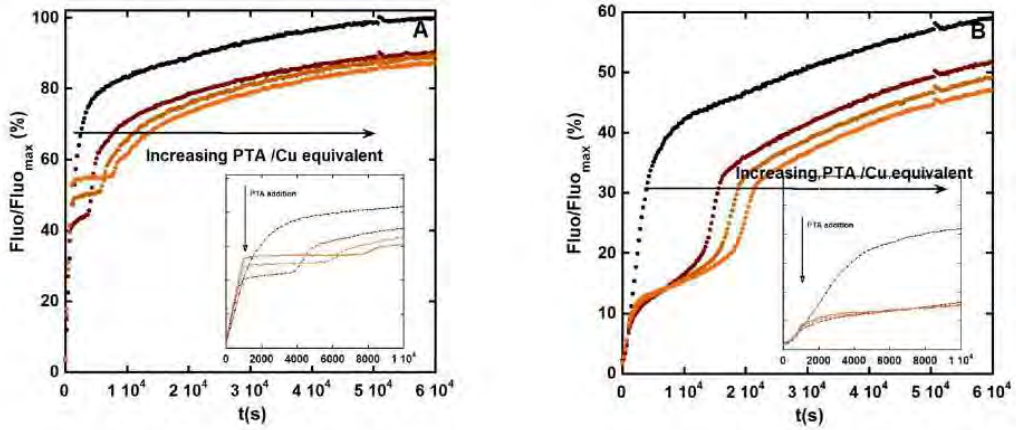

Figure S5. 7-OH-CCA Fluorescence spectra of unbound Cu (panel A) of Cu(Aβ) (panel B) in presence of increasing equivalent of PTA (no PTA added, black dots), 4 equiv. of PTA (brown dots), 5 equiv. of PTA (light brown dots) and 6 equiv. of PTA (orange dots) added at t ~15 min after the start of the ROS production. $[Cu^{II}]$ = 10μM, [Aβ16] = 12 μM, [PTA] = 0, 42, 52, 63 μM, [CCA] = 500 μM, [ascorbate] = 1mM, phosphate buffer, 50mM, pH 7.4, T= 25°C.

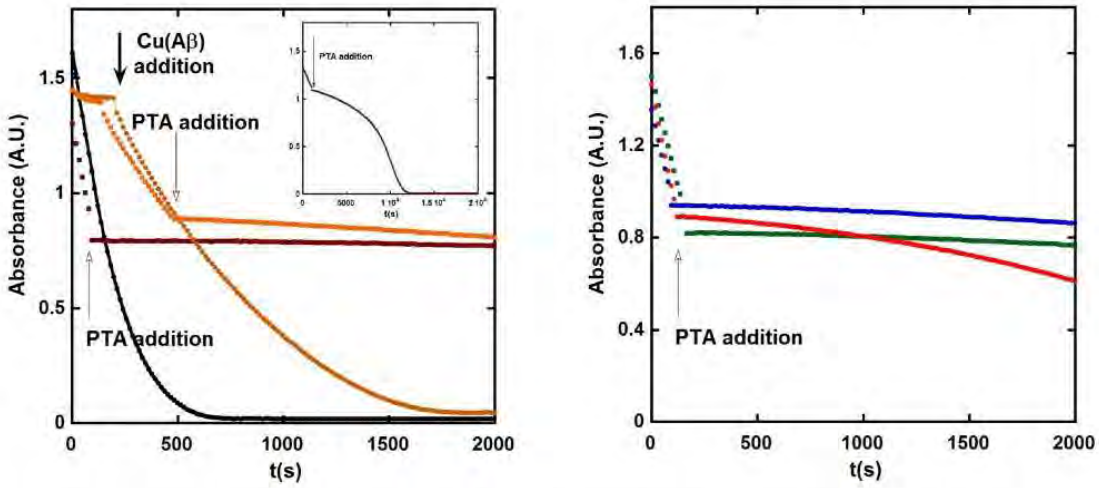

Figure S6. Left: UV-Vis absorption of ascorbate (at 265 nm) as a function of time in presence of unbound Cu before (solid lines, black dots) and after addition of 5 equiv. of PTA (dark brown squares) or of Cu(Aβ) before (solid lines, light brown dots) and after addition of 5 equiv. of PTA (orange squares). Inset: UV-Vis absorption of ascorbate (at 265 nm) as a function of time in presence of Cu(Aβ) after addition of 5 equiv. of PTA. [Cu^{II}] = 10µM, [Aβ16] = 12 µM, [PTA] = 60 µM, [ascorbate] = 100 µM, Hepes 50mM, pH 7.4, T= 25°C. Right: UV-Vis absorption of ascorbate (at 265 nm) as a function of time in presence of unbound Cu before and after addition of 2 (red line), 3 (blue line), and 4 equiv. of PTA (green line). [Cu^{II}] = 10µM, [Aβ16] = 12 µM, [PTA] = 24, 36 and 48 µM, [ascorbate] = 100 µM, Hepes 50mM, pH 7.4

In presence of the PTA ligands, the ascorbate consumption is dramatically slowed down. The same trend as in the HO° experiment is also observed here with a flattening of the slope after the PTA addition that is weaker in presence of Aβ (See full text, Figure 2). In the inset of Figure 5, the sigmoid-like curve observed in the HO° experiment is also present when time necessary to complete the reaction is allowed (Figure S6, left).

In presence of 3 and 4 PTA equivalents, the ascorbate consumption is highly slowed down, which is no more the case with 2 equivalents of PTA. This is in line with a $[Cu(PTA)_3]^+$ air-stable complex (Figure S6, right). Anyway, the $[Cu(PTA)_2]^+$ species remains less efficient in ascorbate consumption than Cu(Aβ).

Note that for experimental reasons (use of a multi-plate fluorimeter but of a single cuvette UV-Vis), it is possible to screen several conditions on long time scale by fluorescence but not by UV-Vis.

Speciation of Cu(I), $[Cu^{I}(PTA)_n]^+$ and $Cu^{I}(A\beta)$ as a function of the Cu concentration

By considering only the predominant species $[Cu^{I}(PTA)_n]^{+}$ at a given concentration, the following equations can be used to evaluate the species present in the experiments performed.

General equations:

(A) (i)

Cu^{I} +	n PTA	→	$[Cu^{I}(PTA)_n]$
1	m		0
1-x	m-nx		x

$$\beta_{PTA,n} = \frac{[Cu(PTA)n]}{[PTA]^n[Cu]} = \frac{x}{(1-x)\left(1-\frac{n}{m}x\right)^n m^n {C_0}^n}$$

(ii) equilibrium between $[Cu^{I}(PTA)_n]^{+}$ and $[Cu^{I}(PTA)_{n-1}]^{+}$ complexes

Cu^{I} +	n PTA	→	$[Cu^{I}(PTA)_n]^{-}$
1	m		0
1-x-y	m-nx-(n-1)y		x

Cu^{I} +	(n-1) PTA	→	$[Cu^{I}(PTA)_{n-1}]^{+}$
1	m		0
1-x-y	m-nx-(n-1)y		y

$$\frac{\beta_{PTA,n-1}}{\beta_{PTA,n}} = \frac{[Cu(PTA)_{n-1}][Cu][PTA]^n}{[PTA]^{n-1}[Cu][Cu(PTA)_n]} = \frac{y\,[PTA]}{x} = \frac{(1-x)\,(m-n+1-x)C_0}{x}$$

(B)

Cu^{I} +	n PTA	→	$[Cu^{I}(PTA)_n]^{-}$
1	m		0
1-x-y	m-nx		x

Cu^{I} +	Aβ	→	$Cu^{I}(A\beta)$
1	1+ε		0
1-x-y	1+ε-y		y

$$\frac{K_{A\beta}}{\beta_{PTA,n}} = \frac{[PTA]^n[Cu]\,[Cu(A\beta)]}{[Cu(PTA)n][Cu][A\beta]} = \frac{m^n\left(1-\frac{n}{m}x\right)^n(y){C_0}^{n-1}}{(x)(1+\varepsilon-y)} = \frac{m^n\left(1-\frac{n}{m}x\right)^n(1-x){C_0}^{n-1}}{(x)(x+\varepsilon)}$$

(1) Spectroscopic characterizations of metal capture by the PTA ligands, [Cu] = 0.9 mM, [Aβ] = 1mM, number of PTA equivalent: 4 (for the coordination), species mainly present: $[Cu^{I}(PTA)_4]^{+}$ and Cu(Aβ).

Equation (B) with: $C_0 = 0.9\ 10^{-3}$ M, ε=0.11, m=n=4, and

$\frac{K_{A\beta}}{\beta_{PTA,4}} = 10^{-15}$ based on refs. [4] and [5], $[Cu(PTA)_4]^{+}$ = 0.88 mM, Cu(Aβ) = 0.02 mM

$\frac{K_{A\beta}}{\beta_{PTA,4}} = 10^{-12}$ based on refs. [6] and [5], $[Cu(PTA)_4]^{+}$ = 0.82 mM, Cu(Aβ) = 0.08 mM.

(2) ROS production experiments without Aβ

Equation (A) with: $C_0 = 10^{-5}$ M, m=4, n=3

$\frac{\beta_{PTA,2}}{\beta_{PTA,3}} = 10^{-6}$ based on ref. [5], $[Cu(PTA)_3]^{+}$ = 9.1 µM, $[Cu(PTA)_2]$ = 0.9 µM

(3) ROS production experiments: with Aβ

Equation (B) with: $C_0 = 10^{-5}$ M, ε=0.2, m=4, n=3,

$\frac{K_{A\beta}}{\beta_{PTA,3}} = 10^{-11}$ based on refs. [4] and [5], $[Cu(PTA)_4]^{+}$ = 9.4 µM, Cu(Aβ) = 0.6 µM

$\frac{K_{A\beta}}{\beta_{PTA,3}} = 10^{-8}$ based on refs. [6] and [5], $[Cu(PTA)_4]^{+}$ = 3.3 µM, Cu(Aβ) = 6.7 µM

Depending on the values taken for the affinity of Cu(Aβ) in the literature reports, the speciation could be significantly different in case (3). Determination of the Cu(Aβ) affinity is beyond the scope of the present paper.

Note that for the above calculations, complexes with PTAH have not been taken into account since there only exist in acidic medium.

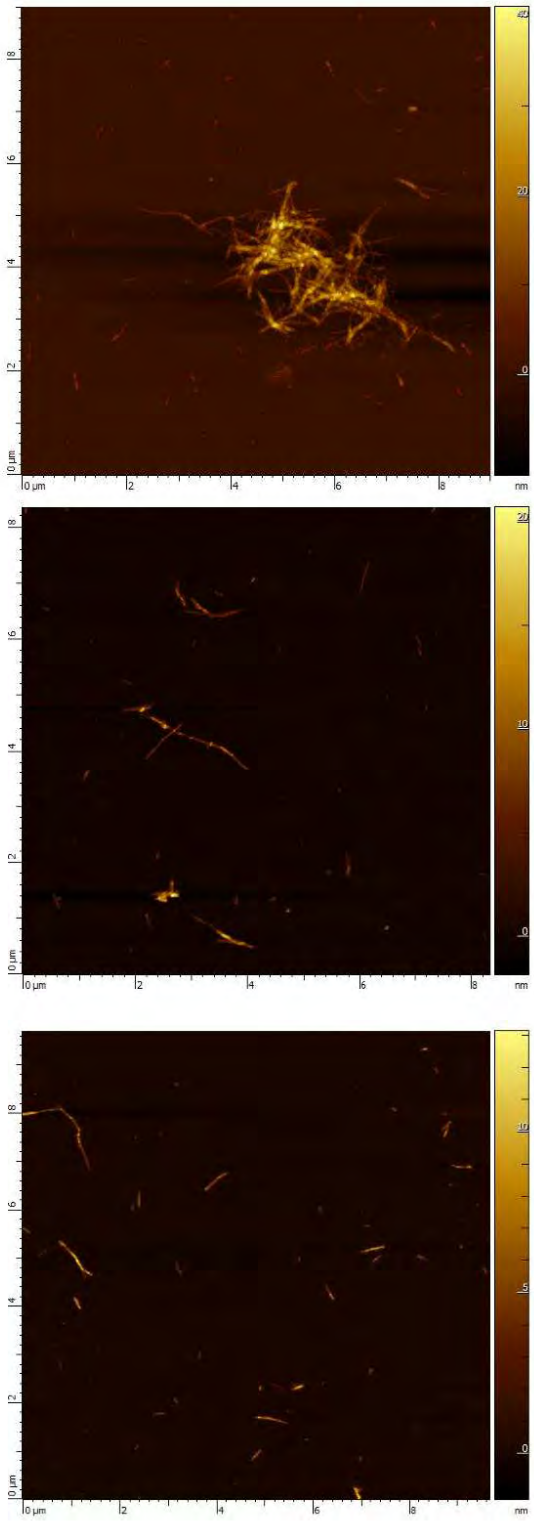

Cu^{II}-Aβ

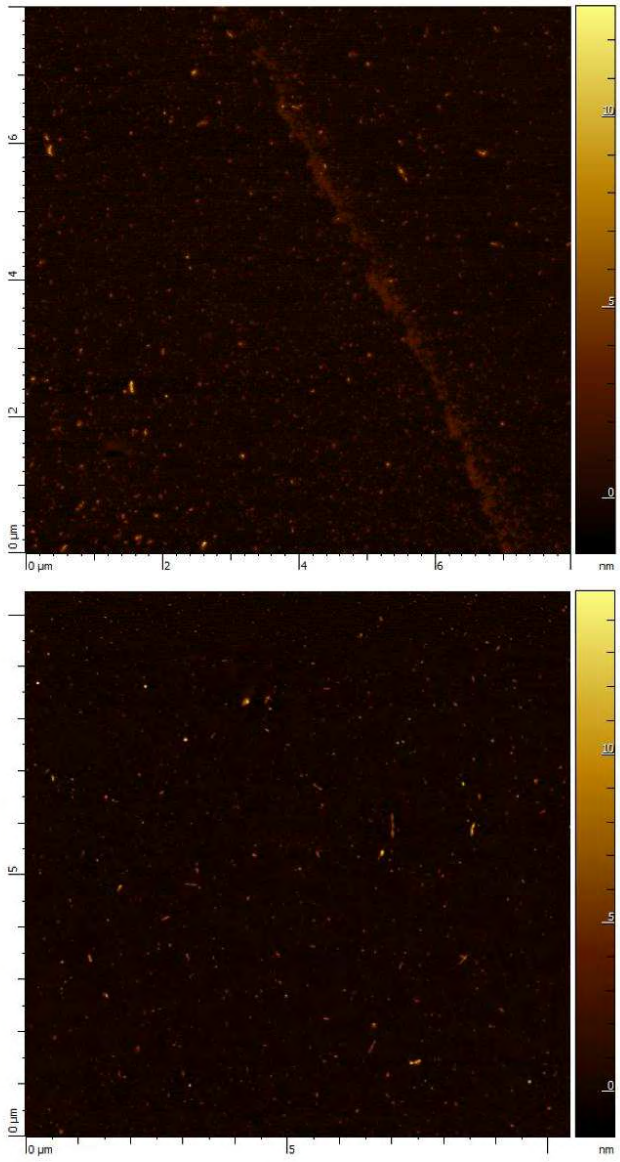

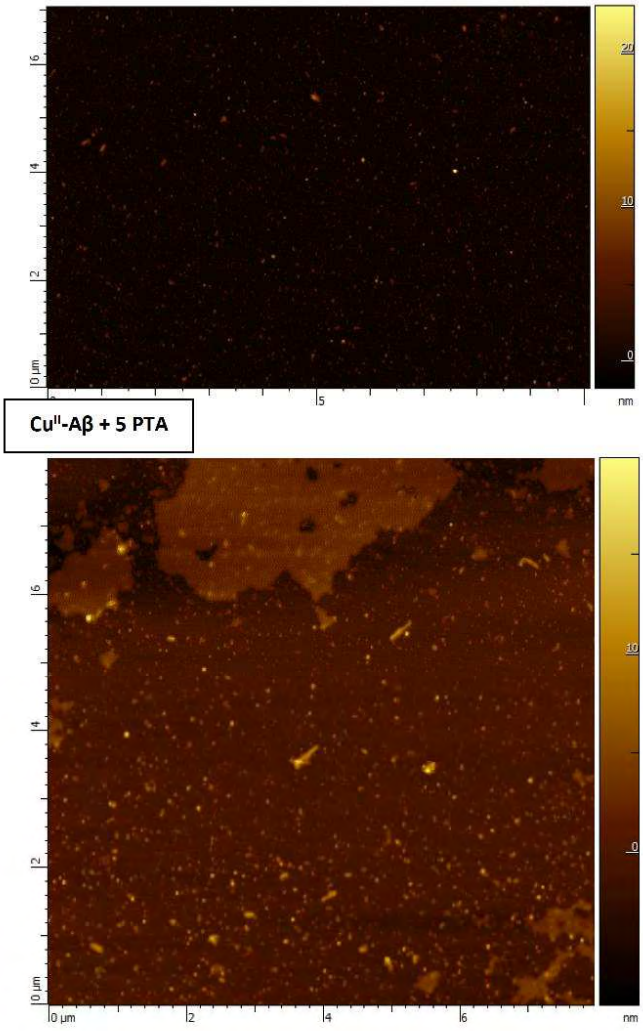
Cu^{II}-Aβ + 5 PTA
0 µm
2
4
6
5
nm
20
10
0

Cu^{II}-Aβ + 10 PTA

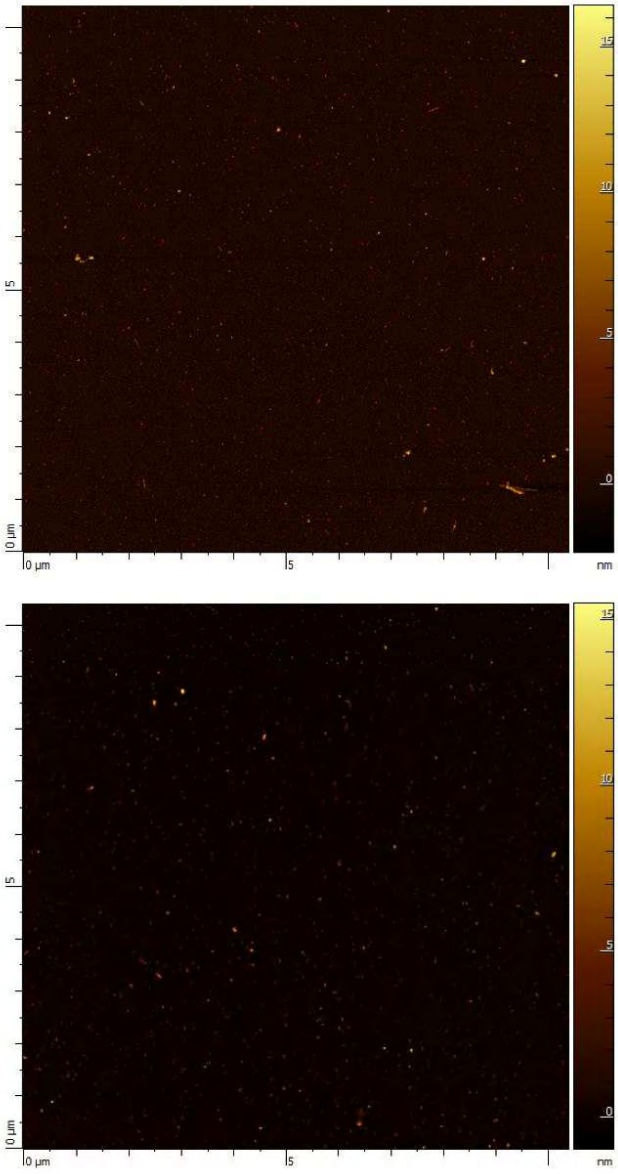

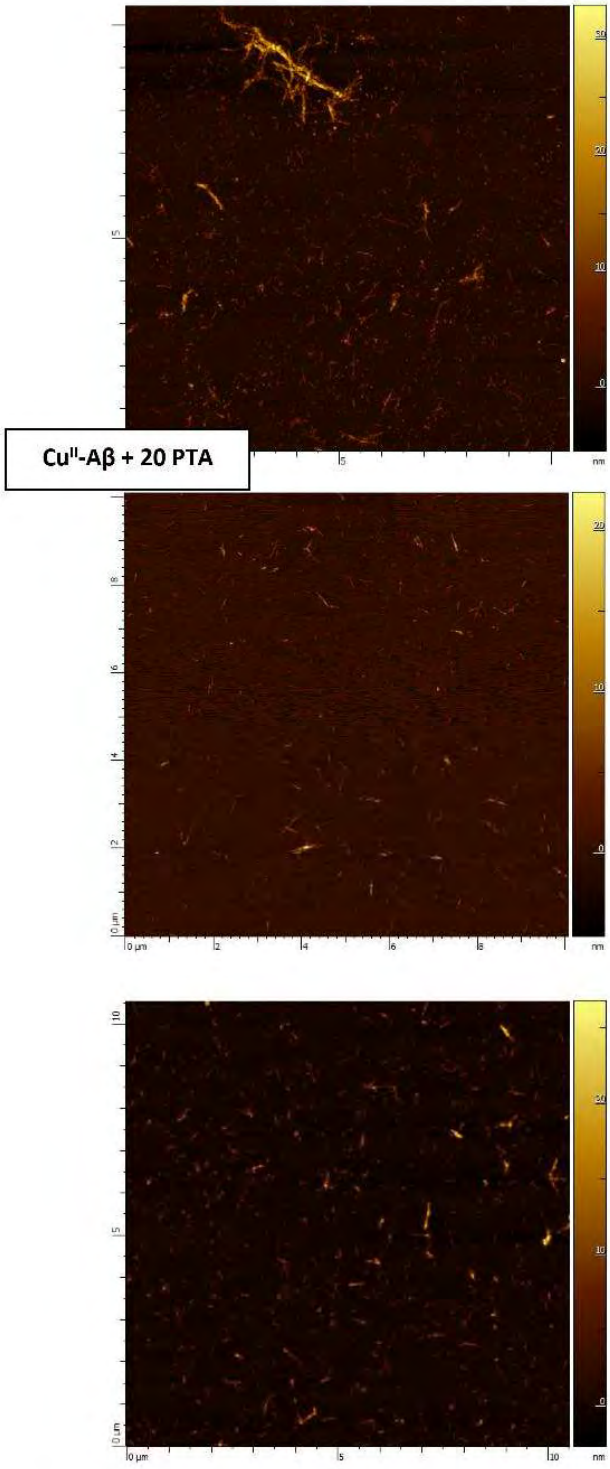

Figure S7. Selection of characteristic AFM pictures of 20µM Aβ40, Cu^{II}Aβ, Cu^{II}Aβ + 5 PTA, Cu^{II}Aβ + 10 PTA and Cu^{II}Aβ + 20 PTA following 180h of ThT fluorescence assay (T° = 37°C, pH = 7.0).

References.

1. P. Faller, C. Hureau, P. Dorlet, P. Hellwig, Y. Coppel, F. Collin and B. Alies, *Coord. Chem. Rev.*, 2012, **256**, 2381.
2. D. J. Daigle, T. J. Decuir, J. B. Robertson and D. J. Darensbourgh, *Inorg. Synth.*, 1998, **32**, 40.
3. C. Hureau, V. Balland, Y. Coppel, P. L. Solari, E. Fonda and P. Faller, *J. Biol. Inorg. Chem.*, 2009, 995.
4. B. Alies, B. Badei, P. Faller and C. Hureau, *Chem. Eur. J.*, 2012, **18**, 1161.
5. F. Endrizzi, *PhD thesis from the University of Padua*, 2013.
6. Z. Xiao, L. Gottschlich, R. van der Meulen, S. R. Udagedara and A. G. Wedd, *Metallomics*, 2013, **5**, 501.

Résumé

La maladie d'Alzheimer est une maladie neurodégénérative, touchant plus de 30 millions de personnes dans le monde. A ce jour, seules des thérapies symptomatiques sont disponibles ; aucun traitement curatif n'existe. Une des hypothèses concernant cette maladie propose une mauvaise régulation des quantités en ions métalliques, notamment les ions Cu et Zn, dans certaines zones du cerveau. Ils favoriseraient une accumulation de peptides appelés Amyloïdes-β (Aβ) dans les fentes synaptiques. Ces dépôts empêcheraient les connexions neuronales, entrainant les symptômes connus de la maladie, tels que la perte de mémoire ou les déficiences intellectuelles. Les ions Cu seraient également responsables d'un stress oxydant incontrôlé, dégradant entre autres les membranes neuronales. Les ions Cu sont donc une cible thérapeutique à privilégier. Les recherches se dirigent vers le développement de nouvelles molécules, dites chélateurs, en vue d'extraire sélectivement ces ions Cu (par rapport aux ions Zn), pour réguler leur quantité et limiter voire empêcher cette accumulation de peptides. Mon projet de recherche se place précisément dans ce contexte. Différents chélateurs des ions Cu(II) et Cu(I) sont étudiés, en présence ou non de Zn(II), pour comprendre les paramètres à prendre en compte pour le développement de chélateurs efficaces. La première partie de cette étude regroupe différentes preuves de concept concernant les chélateurs des ions Cu. L'aspect cinétique du retrait du Cu(II) du peptide Aβ par un chélateur est étudié grâce à des ligands macrocycliques. Ensuite, l'état d'oxydation des ions Cu dans les fentes synaptique n'étant pas connu à ce jour, deux chélateurs du Cu(I) ou du Cu(I/II) sont proposés. La seconde partie de l'étude prend en compte l'impact du Zn(II) dans la chélation des ions Cu. Le côté thermodynamique de la chélation du Cu en présence de Zn(II) est mis en évidence grâce à différents chélateurs aux caractéristiques différentes.

Abstract

Alzheimer's disease is a neurodegenerative disease, affecting more than 30 million people all over the world. Nowadays, only symptomatic therapies exist, there is no cure yet. A dyshomeostasis of metal ions such as Cu and Zn ions in some areas of the brain is one of the different hypothesis about this disease. They would promote an accumulation of peptides, the Amyloid-β (Aβ) peptides, in the synaptic cleft. These aggregates would prevent the neuronal connections, triggering known symptoms of the disease, such as memory loss or cognitive impairments. Cu ions would also be responsible for an important oxidative stress, destroying the neuronal membranes for example. Cu ions are an important therapeutic target to cure the disease. Investigations are currently focusing on the development of new molecules, called chelators, in order to remove selectively Cu ions (over Zn ions), to regulate their concentrations and avoid the accumulation of the peptides. My research project focuses precisely on such kind of investigations. Different Cu(II) and Cu(I) chelators are studied, in the presence or not of Zn(II), in order to understand the different criteria to take into account for the development of good chelators. Different proof-of-concepts are developed in the first part. The kinetic aspect of the removal of Cu(II) from the Aβ peptide by a chelator is studied with macrocyclic ligands Then, the redox state of Cu ions in the synaptic cleft staying unknown, two Cu(I) or Cu(I/II) chelators are proposed. The second part of the study takes into account the impact of Zn(II) in the Cu chelation. The thermodynamic part of the Cu(II) chelation in the presence of Zn(II) is evidenced with different chelators.